

Roman Szewczyk
Cezary Zieliński
Małgorzata Kaliczyńska *Editors*

Progress in Automation, Robotics and Measuring Techniques

Control and Automation

Advances in Intelligent Systems and Computing

Volume 350

Series editor

Janusz Kacprzyk, Polish Academy of Sciences, Warsaw, Poland
e-mail: kacprzyk@ibspan.waw.pl

About this Series

The series “Advances in Intelligent Systems and Computing” contains publications on theory, applications, and design methods of Intelligent Systems and Intelligent Computing. Virtually all disciplines such as engineering, natural sciences, computer and information science, ICT, economics, business, e-commerce, environment, healthcare, life science are covered. The list of topics spans all the areas of modern intelligent systems and computing.

The publications within “Advances in Intelligent Systems and Computing” are primarily textbooks and proceedings of important conferences, symposia and congresses. They cover significant recent developments in the field, both of a foundational and applicable character. An important characteristic feature of the series is the short publication time and world-wide distribution. This permits a rapid and broad dissemination of research results.

Advisory Board

Chairman

Nikhil R. Pal, Indian Statistical Institute, Kolkata, India
e-mail: nikhil@isical.ac.in

Members

Rafael Bello, Universidad Central “Marta Abreu” de Las Villas, Santa Clara, Cuba
e-mail: rbellop@uclv.edu.cu

Emilio S. Corchado, University of Salamanca, Salamanca, Spain
e-mail: escorchado@usal.es

Hani Hagras, University of Essex, Colchester, UK
e-mail: hani@essex.ac.uk

László T. Kóczy, Széchenyi István University, Győr, Hungary
e-mail: koczy@sze.hu

Vladik Kreinovich, University of Texas at El Paso, El Paso, USA
e-mail: vladik@utep.edu

Chin-Teng Lin, National Chiao Tung University, Hsinchu, Taiwan
e-mail: ctlin@mail.nctu.edu.tw

Jie Lu, University of Technology, Sydney, Australia
e-mail: Jie.Lu@uts.edu.au

Patricia Melin, Tijuana Institute of Technology, Tijuana, Mexico
e-mail: epmelin@hafsamx.org

Nadia Nedjah, State University of Rio de Janeiro, Rio de Janeiro, Brazil
e-mail: nadia@eng.uerj.br

Ngoc Thanh Nguyen, Wroclaw University of Technology, Wroclaw, Poland
e-mail: Ngoc-Thanh.Nguyen@pwr.edu.pl

Jun Wang, The Chinese University of Hong Kong, Shatin, Hong Kong
e-mail: jwang@mae.cuhk.edu.hk

More information about this series at <http://www.springer.com/series/11156>

Roman Szewczyk · Cezary Zieliński
Małgorzata Kaliczyńska
Editors

Progress in Automation, Robotics and Measuring Techniques

Control and Automation

Editors

Roman Szewczyk
Industrial Research Institute for Automation
and Measurements PIAP
Warsaw
Poland

Małgorzata Kaliczyńska
Industrial Research Institute for Automation
and Measurements PIAP
Warsaw
Poland

Cezary Zielinski
Industrial Research Institute for Automation
and Measurements PIAP
Warsaw
Poland

ISSN 2194-5357 ISSN 2194-5365 (electronic)
Advances in Intelligent Systems and Computing
ISBN 978-3-319-15795-5 ISBN 978-3-319-15796-2 (eBook)
DOI 10.1007/978-3-319-15796-2

Library of Congress Control Number: 2015931809

Springer Cham Heidelberg New York Dordrecht London

© Springer International Publishing Switzerland 2015

This work is subject to copyright. All rights are reserved by the Publisher, whether the whole or part of the material is concerned, specifically the rights of translation, reprinting, reuse of illustrations, recitation, broadcasting, reproduction on microfilms or in any other physical way, and transmission or information storage and retrieval, electronic adaptation, computer software, or by similar or dissimilar methodology now known or hereafter developed.

The use of general descriptive names, registered names, trademarks, service marks, etc. in this publication does not imply, even in the absence of a specific statement, that such names are exempt from the relevant protective laws and regulations and therefore free for general use.

The publisher, the authors and the editors are safe to assume that the advice and information in this book are believed to be true and accurate at the date of publication. Neither the publisher nor the authors or the editors give a warranty, express or implied, with respect to the material contained herein or for any errors or omissions that may have been made.

Printed on acid-free paper

Springer International Publishing AG Switzerland is part of Springer Science+Business Media
(www.springer.com)

Foreword

Control, automation, robotics and measuring techniques have been paramount to the development of industry in the last few decades. As currently the process of reindustrialization of European Union has gained importance, so have the mentioned disciplines. For this reason, both theoretical and application oriented developments in automation, robotics and measuring techniques are at the focus of interest of the scientific and engineering community.

It should be underscored that automation, robotics and measuring techniques have a significant innovative potential. In the case of automation and control, currently this potential is mainly connected with discrete systems, emergence of new actuators and sensors, new diagnostic methods, as well as modern design approaches exemplified by fuzzy logic, evolutionary computation, neural networks, probabilistic methods etc.

Development of field and service robots is still the most important part of theoretical and application development in widely perceived robotics. Crucial problems and challenges are associated with control of mechatronic systems in general, perception, navigation, manipulation and grasping, locomotion and reasoning.

Elements of measuring systems are recently developed on the base of such modern and advanced materials as graphene. Moreover, increase in computational power of modern computers fosters new approaches to advanced signal processing and experimental verification of sophisticated problems of the theory of metrology.

This book presents the recent progress in control, automation, robotics, and measuring techniques that are jointly trying to meet those challenges and to fulfil technological, economic and social needs of European Union. It presents the contributions of experts in those fields. Their work is concerned both with theory and industrial practice. Individual chapters present the theoretical analysis of specific technical problems, often supplemented by numerical analysis and simulation and real experiments on prototypes. The implementation of the research results in industrial practice is also reported.

We hope that the presented progress in theoretical analysis and practical solutions will be useful to both the researchers working in the area of engineering sciences and to practitioners solving industrial problems.

Warsaw, January 2015

Roman Szewczyk
Cezary Zieliński
Małgorzata Kaliczyńska

Contents

| | |
|---|----|
| Synchronization of the Chaotic Pandey-Baghel-Singh Systems of Fractional Order | 1 |
| <i>Mikołaj Busłowicz, Andrzej Ruszewski, Adam Makarewicz</i> | |
| Multiple Project Portfolio Scheduling Subject to Mass Customized Service | 11 |
| <i>Krzysztof Bzdyra, Zbigniew Banaszak, Grzegorz Bocewicz</i> | |
| Recurrent Polynomial and Neural Structures in Modelling of a Neutralisation Process | 23 |
| <i>Patryk Chaber, Maciej Ławryńczuk</i> | |
| Memory-Based Prediction of District Heating Temperature Using GPGPU | 33 |
| <i>Paweł D. Domański, Marcin Więctawski</i> | |
| The Architecture of an Embedded Smart Camera for Intelligent Inspection and Surveillance | 43 |
| <i>Michał Fularz, Marek Kraft, Adam Schmidt, Andrzej Kasiński</i> | |
| Nature-Inspired, Parallel Object Recognition | 53 |
| <i>Bogdan Harasymowicz-Boggio, Łukasz Chechliński, Barbara Siemiątkowska</i> | |
| Digraphs Minimal Realisations of State Matrices for Fractional Positive Systems | 63 |
| <i>Krzysztof Hryniów, Konrad Andrzej Markowski</i> | |
| Optimisation of Digraphs-Based Realisations for Polynomials of One and Two Variables | 73 |
| <i>Krzysztof Hryniów, Konrad Andrzej Markowski</i> | |

| | |
|--|-----|
| Analysis Thrust for Different Kind of Propellers | 85 |
| <i>Arkadiusz Jakubowski, Arkadiusz Kubacki, Bartosz Minorowicz, Amadeusz Nowak</i> | |
| SysML Modeling of Functional and Non-functional Requirements for IEC 61131-3 Control Systems | 91 |
| <i>Marcin Jamro</i> | |
| Fractional Standard and Positive Descriptor Time-Varying Discrete-Time Linear Systems | 101 |
| <i>Tadeusz Kaczorek</i> | |
| Decomposition and Parallelization of Linear Programming Algorithms | 113 |
| <i>Andrzej Karbowski</i> | |
| 45 Years of Mechatronics – History and Future | 127 |
| <i>Andrzej Milecki</i> | |
| Analysis and Modelling of Magnetic Circuits in Magnetic Shape Memory Alloy Actuators | 137 |
| <i>Bartosz Minorowicz, Cezary Jędryczka, Frederik Stefański, Amadeusz Nowak</i> | |
| Share Mode Magnetorheological Dampers for Vibration Attenuation in Domestic Washing Machines | 147 |
| <i>Bartosz Minorowicz, Frederik Stefański, Grzegorz Pittner, Roman Regulski</i> | |
| Immune Algorithm for Optimization of Membership Function in Fuzzy Models | 157 |
| <i>Bogumiła Mrozek</i> | |
| Characteristics of the Improved Magnetic Shape Memory Alloy Actuator Test Stand | 169 |
| <i>Amadeusz Nowak, Bartosz Minorowicz, Frederik Stefański, Zoran Pandilov</i> | |
| Control of an Oriented PV System with the Use of a Discrete, Robust, Fractional Order PID Controller | 177 |
| <i>Krzysztof Oprzedkiewicz</i> | |
| Production System Designing with the Use of Digital Factory and Augmented Reality Technologies | 187 |
| <i>Dariusz Plinta, Martin Krajčovič</i> | |
| Monitoring and Prediction of Time Series Based on Fuzzy Cognitive Maps with Multi-step Gradient Methods | 197 |
| <i>Katarzyna Poczęta, Alexander Yastrebov</i> | |
| Multichannel High Voltage Amplifier for Piezo Actuators | 207 |
| <i>Roman Regulski, Amadeusz Nowak, Bartosz Minorowicz, Frederik Stefański</i> | |

| | |
|---|-----|
| Modelling of Electrohydraulic Drive with a Valve Controlled by Synchronous Motor | 215 |
| <i>Dominik Rybarczyk, Dariusz Sędziak, Piotr Owczarek, Adam Owczarkowski</i> | |
| Object-Oriented Approach to I/O Handling in Control Programs | 223 |
| <i>Dariusz Rzońca, Jan Sadolewski, Bartosz Trybus</i> | |
| Solution of the State Equation of Descriptor Fractional Continuous-Time Linear Systems with Two Different Fractional | 233 |
| <i>Łukasz Sajewski</i> | |
| A Hybrid Approach to Sustainable Supply Chain Optimization | 243 |
| <i>Paweł Sitek</i> | |
| New Approach to Automation and Robotics Vocational Education in Support of Europe Reindustrialization | 255 |
| <i>Michał Smater, Jacek Zieliński</i> | |
| Ship Maneuvering Model for Autopilot Simulator | 265 |
| <i>Andrzej Stec</i> | |
| Research of Basic Parameters of Piezoelectric Tube Actuator | 275 |
| <i>Roman Regulski, Frederik Stefański, Bartosz Minorowicz, Dariusz Sędziak</i> | |
| Hysteresis Modelling of a Piezoelectric Tube Actuator | 283 |
| <i>Frederik Stefański, Bartosz Minorowicz, Amadeusz Nowak</i> | |
| Application of Jiles-Atherton Model for Modelling Magnetization Characteristics of Textured Electrical Steel Magnetized in Easy or Hard Axis | 293 |
| <i>Roman Szewczyk</i> | |
| Tuning Rules of Conventional and Advanced Ship Autopilot Controllers ... | 303 |
| <i>Leszek Trybus, Zbigniew Świder, Andrzej Stec</i> | |
| A Novel Approach to Optimization of Jobs in Groups | 313 |
| <i>Jarosław Wikarek</i> | |
| Multiple File Server with the Implemented Mechanism ACL | 323 |
| <i>Marian Wrzesień, Piotr Ryszawa</i> | |
| Predictive Control of a Multivariable Neutralisation Process Using Elman Neural Networks | 335 |
| <i>Antoni Wysocki, Maciej Ławryńczuk</i> | |
| Evaluation of Automatic Identification Systems According to ISO 50001: 2011 | 345 |
| <i>Paweł Zajac</i> | |
| Author Index | 357 |

About the Editors

Professor Roman Szewczyk received both his PhD and DSc in the field of mechatronics. He is specializing in the modelling of properties of magnetic materials as well as in sensors and sensor interfacing, in particular magnetic sensors for security applications. He is the leading the development of a sensing unit for a mobile robot developed for the Polish Police Central Forensic Laboratory and of methods of non-destructive testing based on the magnetoelastic effect. Professor Szewczyk was involved in over 10 European Union funded research projects within the FP6 and FP7 as well as projects financed by the European Defence Organization. Moreover, he was leading two regional and national scale technological foresight projects and was active in the organization and implementation of technological transfer between companies and research institutes. Roman Szewczyk is Secretary for Scientific Affairs in the Industrial Research Institute for Automation and Measurements (PIAP). He is also Associate Professor at the Faculty of Mechatronics, Warsaw University of Technology and a Vice-chairman of the Academy of Young Researchers of the Polish Academy of Sciences.

Professor Cezary Zieliński received his M.Sc./Eng. degree in control in 1982, Ph.D. degree in control and robotics in 1988, the D.Sc. (habilitation) degree in control and robotics in 1996, all from the Faculty of Electronics and Information Technology, Warsaw University of Technology, Warsaw, Poland, and Professorship in 2012. Currently he is Professor both in the Industrial Research Institute for Automation and Measurement (PIAP) and the Warsaw University of Technology, where he is Director of the Institute of Control and Computation Engineering. Since 2007 he has been a member of the Committee for Automatic Control and Robotics, the Polish Academy of Sciences. Professor Zieliński is Head of the Robotics Group in the Institute of Control and Computation Engineering working on robot control and programming methods. His research interests focus on robotics in general and in particular include: robot programming methods, formal approach to the specification of architectures of multi-effector and multi-receptor systems, robot kinematics, robot position-force control, visual servo control, and design of digital circuits. He is the author/coauthor of over 180 conference and journal papers as well as books concerned with the above mentioned research subjects.

Dr. Małgorzata Kaliczyńska received her M.Sc. Eng. degree in cybernetics from the Faculty of Electronics, Wrocław University of Technology, and her Ph.D. degree in the field of fluid mechanics from the Faculty of Mechanical and Power Engineering in this same university. Now she is Assistant Professor in the Industrial Research Institute for Automation and Measurement (PIAP) and Editor of the scientific and technological magazine “Measurements, Automation, Robotics”. Her areas of research interest include distributed control systems, Internet of Things, information retrieval and webometrics.

Synchronization of the Chaotic Pandey-Baghel-Singh Systems of Fractional Order

Mikołaj Busłowicz¹, Andrzej Ruszewski¹, and Adam Makarewicz²

¹ Bialystok University of Technology, Faculty of Electrical Engineering

² Doctoral Study, Faculty of Electrical Engineering, Bialystok University of Technology

Abstract. The paper considers the modified Pandey-Baghel-Singh system of fractional order. Chaotic behavior of the system is analyzed and the problem of synchronization of two modified Pandey-Baghel-Singh systems via master-slave configuration with linear coupling is considered. A simple sufficient condition for synchronization using the Lyapunov and Gershgorin stability theory is proposed. The considerations are illustrated by numerical simulations.

Keywords: chaos, fractional, Pandey-Baghel-Singh system, synchronization.

1 Introduction

Dynamical systems described by fractional order differential or difference equations have been investigated in several areas such as viscoelasticity, electrochemistry, diffusion processes, control theory, electrical engineering, etc. The problems of analysis and synthesis of dynamic systems described by fractional order differential (or difference) equations recently have considerable attention, see monographs [8, 13, 15, 17–19], for example.

Many non-linear dynamical systems have behavior known as chaos. Chaos is a very interesting non-linear phenomenon. Chaotic systems are deterministic and highly sensitive on initial condition and system parameters. There are many chaotic systems, e.g. in paper [16] was introduced Pandey-Baghel-Singh chaotic system of integer order. Synchronization of chaos is a very interesting problem, enjoying a wide interest, for example, in control technology, cryptography, communications [9, 20], etc. The problem of synchronization of chaos recently has been intensively studied in many papers, see for example [3, 4, 7, 10, 11, 25] for systems of integer order and [2, 6, 12, 14, 17, 21, 22] for system of fractional order. In the paper [2] the method of the synchronization of two coupled general chaotic fractional order Van der Pol-Duffing systems with a unidirectional linear error feedback coupling is presented.

In this paper we consider the modified Pandey-Baghel-Singh oscillator of fractional order. Chaotic behavior of this system will be analyzed for different values of fractional orders. Simple sufficient condition for synchronization of two such systems with non-commensurate fractional orders via master/slave configuration with linear coupling will be given. The proposed condition is obtained in a similar way as in the paper [2] using the Lyapunov and Gershgorin stability theory.

2 Preliminaries

The modified Pandey-Baghel-Singh oscillator is described by following normalized non-linear differential equation

$$\dot{X}(t) = f(X(t)) = \begin{bmatrix} y(t) \\ z(t) \\ -ax(t) - by(t) - cz(t) - dx^2(t) \end{bmatrix}, \quad X(t) = \begin{bmatrix} x(t) \\ y(t) \\ z(t) \end{bmatrix}. \quad (1)$$

The oscillator (1) with integer order recently was considered in [16] for $a = 1$, $b = 1.1$, $c = 0.42$ and $d = 1$. We assume the following values of parameters

$$a = 1.3, \quad b = 1.6, \quad c = 0.09 \quad \text{and} \quad d = 1. \quad (2)$$

In this paper we consider the modified Pandey-Baghel-Singh oscillator of fractional non-commensurate order, described by the state equation

$$D_t^{\bar{\alpha}} X(t) = f(X(t)) = \begin{bmatrix} y(t) \\ z(t) \\ -ax(t) - by(t) - cz(t) - dx^2(t) \end{bmatrix}, \quad D_t^{\bar{\alpha}} X(t) = \begin{bmatrix} D_t^{\alpha_1} x(t) \\ D_t^{\alpha_2} y(t) \\ D_t^{\alpha_3} z(t) \end{bmatrix}, \quad (3)$$

with parameters (2), where derivatives of fractional orders satisfy the inequality $0 < \alpha_i < 1$ for $i = 1, 2, 3$,

$$D_t^{\alpha_i} x(t) = \frac{1}{\Gamma(1 - \alpha_i)} \int_0^t \frac{x'(\tau) d\tau}{(t - \tau)^{\alpha_i}}, \quad 0 < \alpha_i < 1, \quad (4)$$

is the Caputo definition for derivative of fractional order α_i , where $x'(t) = dx(t)/dt$ and $\Gamma(\alpha_i) = \int_0^{\infty} e^{-t} t^{\alpha_i - 1} dt$ is the Euler gamma function.

3 Stability Analysis

The fractional order system (3), similarly as the natural order system (1), has two equilibrium points. These point are obtained by solution of the non-linear equation $f(X(t)) = 0$, i.e. the set of equations

$$0 = y(t), \quad 0 = z(t), \quad 0 = -ax(t) - by(t) - cz(t) - dx^2(t). \quad (5)$$

Solving the equations (5) for parameters (2) we obtain the following equilibrium points

$$E_0 = \begin{bmatrix} 0 \\ 0 \\ 0 \end{bmatrix}, \quad E_1 = \begin{bmatrix} -\frac{a}{d} \\ 0 \\ 0 \end{bmatrix} = \begin{bmatrix} -1.3 \\ 0 \\ 0 \end{bmatrix}. \quad (6)$$

Let

$$A_k = \left. \frac{\partial f(X)}{\partial X} \right|_{X=E_k} = \begin{bmatrix} 0 & 1 & 0 \\ 0 & 0 & 1 \\ -a-2x(t)d & -b & -c \end{bmatrix}_{X=E_k}, \quad k=0,1, \quad (7)$$

be the Jacobian matrix of the function $f(X)$ evaluated at $X = E_k$ ($k=0,1$).

Firstly, we assume that fractional orders of the system satisfy the condition $\alpha_1 = \alpha_2 = \alpha_3 = \alpha$. In this case the linearized system (3) about its the equilibrium point E_k ($k=0,1$) has the form

$$D_t^\alpha X(t) = A_k X(t), \quad (8)$$

where the matrix A_k is computed form (7) for parameters (2).

It is well known [1] that the fractional order system (8) is stable if and only if its characteristic polynomial of fractional degree has no zeros in the closed right-half of the Riemann complex surface, i.e.

$$w(s) = \det(s^\alpha I - A) \neq 0 \text{ for } \operatorname{Re} s \geq 0, \quad (9)$$

or equivalently, the following condition is satisfied

$$|\arg \lambda_i(A)| > \alpha\pi/2, \quad i=1,2,\dots,n, \quad (10)$$

where $\lambda_i(A)$ is the i -th eigenvalues of matrix A .

The condition (10) can be written in the form

$$\alpha < 2\phi/\pi, \quad \phi = \min_i |\arg \lambda_i(A)|. \quad (11)$$

Now, we check the stability of the equilibrium points (6). From (7) we have

$$A_0 = \begin{bmatrix} 0 & 1 & 0 \\ 0 & 0 & 1 \\ -a & -b & -c \end{bmatrix} = \begin{bmatrix} 0 & 1 & 0 \\ 0 & 0 & 1 \\ -1.3 & -1.6 & -0.09 \end{bmatrix}, \quad (12)$$

$$A_1 = \begin{bmatrix} 0 & 1 & 0 \\ 0 & 0 & 1 \\ -a+2.6 & -b & -c \end{bmatrix} = \begin{bmatrix} 0 & 1 & 0 \\ 0 & 0 & 1 \\ 1.3 & -1.6 & -0.09 \end{bmatrix}. \quad (13)$$

Computing eigenvalues of matrices (12) and (13) we obtain

- for A_0 : $\lambda_1 = -0.6585$; $\lambda_{2,3} = 0.2842 \pm j1.3761$
- for A_1 : $\lambda_1 = 0.6321$; $\lambda_{2,3} = -0.3611 \pm j1.3878$.

The matrix A_1 has real positive eigenvalue which lies in instability region. This means that the equilibrium point E_1 is unstable for all $\alpha \in (0, 1)$.

The matrices A_0 have two eigenvalues with positive real parts. From (11) it follows that the equilibrium point E_0 is locally stable for

$$\alpha < \frac{2}{\pi} \arctan \frac{1.3761}{0.2842} = 0.8703. \quad (14)$$

From the above it follows that the system (8) has a chaotic behavior for $\alpha > 0.88$.

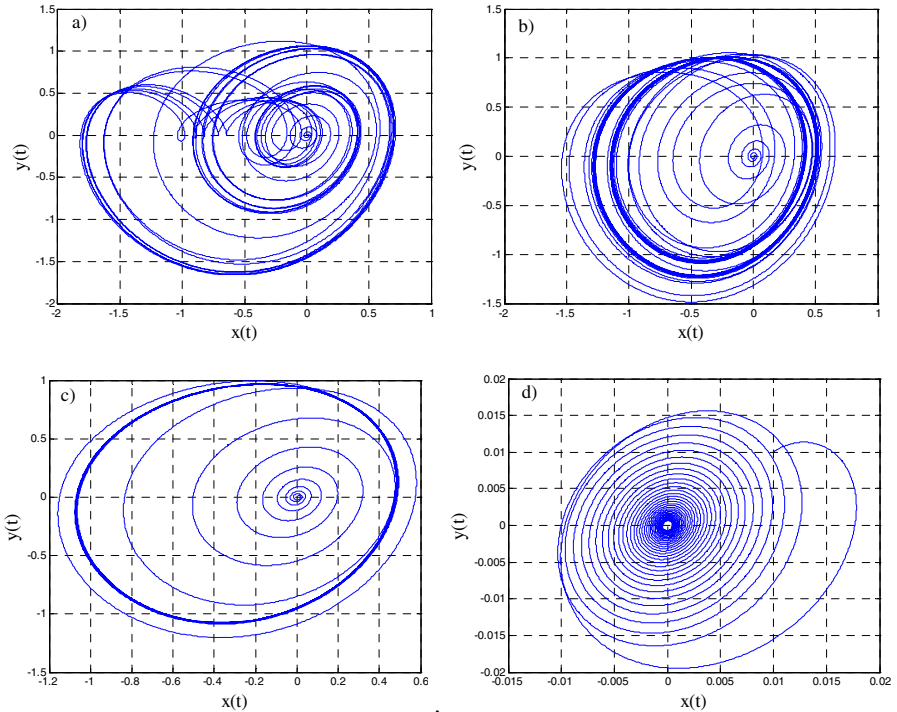


Fig. 1. Trajectories of the system (8): a) $\alpha=0.954$; b) $\alpha=0.94$; c) $\alpha=0.92$; d) $\alpha=0.86$

Plots of numerical simulations for $\alpha = 0.954$, $\alpha = 0.94$, $\alpha = 0.92$ and $\alpha = 0.86$ are shown in Fig. 1. From this figure it follows that for $\alpha = 0.954$ and $\alpha = 0.94$ one-band chaotic behavior is obtained. When $\alpha = 0.92$ the limit cycle is found and for $\alpha = 0.86$ asymptotically stable attractor exists.

Simulations were performed using the Ninteger Fractional Control Toolbox for MatLab [23]. In this toolbox exists a Simulink block *nid* for fractional derivative and integral. Order and method for rational approximation of fractional derivative/integral can be selected. In simulations we select the Oustaloup's approximation technique (CRONE) of order $n=7$. The block *nid* has the transfer function ks^v , where v is real number from the interval $(-1, 1)$. In simulations the fractional integrator $1/s^\alpha$ is modeled by series connection of the classical integrator and the block *nid*. Transfer function of this connection is k/s^{v-1} . It is easy to see that $v \in (0, 1)$ for $\alpha \in (0, 1)$.

Now, using numerical simulations we investigate chaotic behavior of the system (3) with non-commensurate fractional orders and we obtain that the system is chaotic for $\alpha_1 = \alpha_2 = 0.954$ and $\alpha_3 = 0.875$. Chaotic trajectories and the time domain plot of $x(t)$ are shown in Fig. 2.

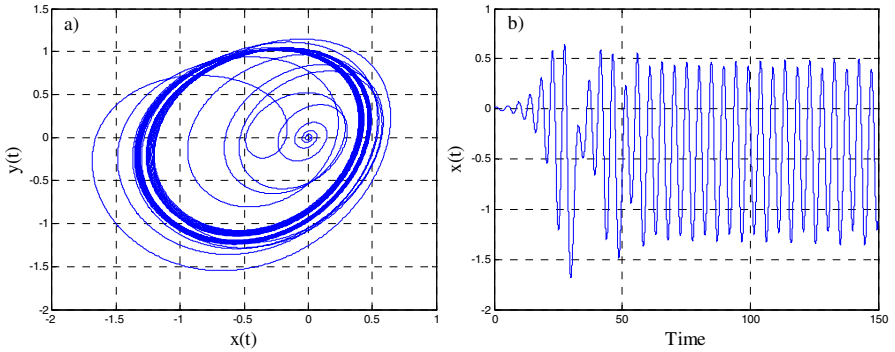


Fig. 2. The system (3) for $\alpha_1=\alpha_2=0.954$ and $\alpha_3=0.875$: a) chaotic trajectories, b) time domain plot of $x(t)$

4 Synchronization

Let the fractional system (3) with $\alpha_1 = \alpha_2 = 0.954$ and $\alpha_3 = 0.875$ be the Master system and the coupled Slave fractional-order system is described by

$$D_t^{\bar{\alpha}} \bar{X}(t) = \begin{bmatrix} \bar{y}(t) \\ \bar{z}(t) \\ -a\bar{x}(t) - b\bar{y}(t) - c\bar{z}(t) - d\bar{x}^2(t) \end{bmatrix} + KE(t), \quad D_t^{\bar{\alpha}} \bar{X}(t) = \begin{bmatrix} D_t^{\alpha_1} \bar{x}(t) \\ D_t^{\alpha_2} \bar{y}(t) \\ D_t^{\alpha_3} \bar{z}(t) \end{bmatrix}, \quad (15)$$

where $K = \text{diag}(k_1, k_2, k_3)$, $k_i \geq 0$, and

$$E(t) = \begin{bmatrix} e_x(t) \\ e_y(t) \\ e_z(t) \end{bmatrix} = X(t) - \bar{X}(t) = \begin{bmatrix} x(t) - \bar{x}(t) \\ y(t) - \bar{y}(t) \\ z(t) - \bar{z}(t) \end{bmatrix} \quad (16)$$

is the synchronization error.

We select a feedback gain K such that $\lim_{t \rightarrow \infty} \|E(t)\| = 0$, where $\|\cdot\|$ denotes the Euclidean norm.

Using (3) and (15), the error dynamics of coupled systems can be written in the form

$$D_t^{\bar{\alpha}} E(t) = \begin{bmatrix} e_y(t) \\ e_z(t) \\ -ae_x(t) - be_y(t) - ce_z(t) - de_x^2(t) \end{bmatrix} - KE(t). \quad (17)$$

Using the relation

$$x^2(t) - \bar{x}^2(t) = [x(t) - \bar{x}(t)][x(t) + \bar{x}(t)] = e_x(t)k_x, \quad (18)$$

where

$$k_x = x(t) + \bar{x}(t), \quad (19)$$

the equation (17) can be written in the form

$$D_t^{\bar{\alpha}} E(t) = (A - K + M_x)E(t), \quad (20)$$

with

$$A = \begin{bmatrix} 0 & 1 & 0 \\ 0 & 0 & 1 \\ -a & -b & -c \end{bmatrix}, \quad M_x = \begin{bmatrix} 0 & 0 & 0 \\ 0 & 0 & 0 \\ 0 & 0 & -dk_x \end{bmatrix}. \quad (21)$$

To select a feedback gain matrix K , we apply the method presented in [2], which is based on approach proposed in papers [7] (see also [3]). This method has been applied to the modified Van der Pol-Duffing system with fractional commensurate order [12] and non-commensurate order [2].

The system is a chaotic system with bounded values of state variables. We assume that the time-dependent parameter (19) is a interval parameter which values belong to interval, i.e. $k_x \in [g, h]$, where g and h are known bounds. From Fig. 3 it follows that $x(t) \in [-1.687, 0.6446]$ and (since the Slave system has the same dynamic as Master) $\bar{x}(t) \in [-1.687, 0.6446]$. Hence, from (19) we have that $k_x \in [0, 1.2892]$ for all $t > 0$.

Firstly, we consider the case of integer order system (20), i.e. the system (20) with $\alpha_1 = \alpha_2 = \alpha_3 = 1$. In this case the equation (21) takes the form

$$\dot{E}(t) = (A - K + M_x)E(t). \tag{22}$$

To select a feedback gain matrix K , we apply the Lyapunov stability theory to the system (22).

Let

$$V(t) = E^T(t)PE(t), \tag{23}$$

where P is a positive definite symmetric constant matrix, be the Lyapunov function for the system (22).

The derivative of (23) along solution of (22) is as follows

$$\dot{V}(t) = \dot{E}^T(t)PE(t) + E^T(t)P\dot{E}(t) = E^T(t)[A_c^T P + PA_c]E(t), \tag{24}$$

where $A_c = A - K + M_x$.

The equation (24) can be written in the form

$$\dot{V}(t) = E^T(t)QE(t), \tag{25}$$

where

$$Q = A_c^T P + PA_c = (A^T - K^T + M_x^T)P + P(A - K + M_x). \tag{26}$$

According to the Lyapunov stability theory, the system (22) is asymptotically stable if and only if $\dot{V}(t) < 0$ for $t \geq 0$, or equivalently, the symmetric matrix Q defined by (26) is negative definite (all eigenvalues have negative real parts).

To check when the matrix (26) has all eigenvalues with negative real parts, we apply the Gershgorin theorem [5, 24].

The matrix Q defined by (26) for (21) has the following form

$$Q = \begin{bmatrix} -k_1 & 0 & -a \\ 1 & -k_2 & -b \\ 0 & 1 & -c - k_3 - dk_x \end{bmatrix} P + P \begin{bmatrix} -k_1 & 1 & 0 \\ 0 & -k_2 & 1 \\ -a & -b & -c - k_3 - dk_x \end{bmatrix}. \tag{27}$$

If we choose $P = \text{diag}(p_1, p_2, p_3)$ with $p_i = 1 > 0$, then we obtain

$$Q = \begin{bmatrix} -2k_1 & 1 & -a \\ 1 & -2k_2 & 1-b \\ -a & 1-b & -2(k_3 + c + dk_x) \end{bmatrix}. \tag{28}$$

From the Gershgorin theorem we have that all eigenvalues of (28) have negative real parts if the following conditions are satisfied

$$-2k_1 + 1 - a < 0,$$

$$-2k_2 + 1 - b + 1 < 0,$$

$$-2(k_3 + c + dk_x) + 1 - a - b < 0.$$

Since $k_x \in [0, 1.2892]$, from the above and (2) we obtain

$$k_1 > 0.5(1 - a) = -0.15,$$

$$k_2 > 0.5(2 - b) = 0.2,$$

$$k_3 > 0.5(1 - a - b) - c + dk_x = 0.2492.$$

This means that the system (22) is asymptotically stable if we choose the values of gain matrix $K = \text{diag}(k_1, k_2, k_3)$, for example $k_1 = 0.09$, $k_2 = 0.3$, $k_3 = 0.5$. We perform numerical simulations to check stability of the fractional order system (20) for $\alpha_1 = \alpha_2 = 0.954$ and $\alpha_3 = 0.875$. We investigate the synchronization problem of two coupled chaotic the modified Pandey-Baghel-Singh systems (3), (15) for $k_1 = 0.09$, $k_2 = 0.3$, $k_3 = 0.5$ and for smaller feedback gain coefficients. From simulations we obtain that synchronization holds for $k_1 = 0.09$, $k_2 = 0.3$, $k_3 = 0.5$ and also for values of these coefficients smaller, for example, for $k_1 = -0.1$, $k_2 = 0.1$ and $k_3 = 0.5$. Results of simulations are shown in Fig. 3 with initial conditions for the system (3): $x(0) = 0.05$, $y(0) = 0.01$, $z(0) = 0$ and for the system (15): $\bar{x}(0) = 0.5$, $\bar{y}(0) = -0.2$, $\bar{z}(0) = -0.5$. From this figure it follows that synchronization is attained at about 30 second for $k_1 = 0.09$, $k_2 = 0.3$, $k_3 = 0.5$ and at about 60 second for $k_1 = -0.1$, $k_2 = 0.1$ and $k_3 = 0.5$.

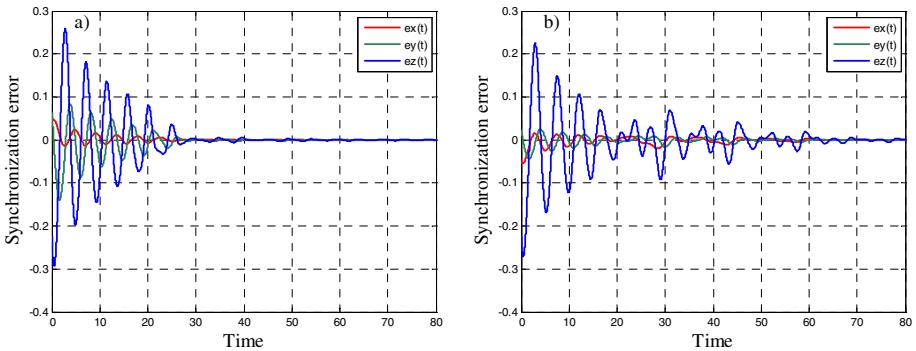


Fig. 3. Synchronization error: a) for $k_1=0.09$, $k_2=0.3$, $k_3=0.5$; b) for $k_1=-0.1$, $k_2=0.1$, $k_3=0.5$

5 Concluding Remarks

Chaotic behavior of the modified Pandey-Baghel-Singh oscillator of fractional order has been analyzed and the problem of synchronization of two such systems with linear coupling has been considered. A simple necessary condition for chaotic behavior of the system with commensurate orders of derivatives and a simple sufficient condition for synchronization of two coupled systems with non-commensurate orders have been proposed. Numerical simulations showed the effectiveness of theoretical considerations and the sensitivity to changes in synchronization gain $K = \text{diag}(k_1, k_2, k_3)$. The delay synchronization depends on the values of K . Simulations have been performed using Ninteger Fractional Control Toolbox for MatLab.

Acknowledgement. This work was supported by the Polish Ministry of Science and Higher Education under the work S/WE/1/11.

References

1. Busłowicz, M.: Stability of State-Space Models of Linear Continuous-time Fractional Order Systems. *Acta Mechanica et Automatica* 5, 15–22 (2011)
2. Busłowicz, M., Makarewicz, A.: Chaos Synchronization of the Modified Van der Pol-Duffing Oscillator of Fractional Order. In: Szewczyk, R., Zieliński, C., Kaliczyńska, M. (eds.) *Recent Advances in Automation, Robotics and Measuring Techniques*. AISC, vol. 267, pp. 33–44. Springer, Heidelberg (2014)
3. Deleanu, D.: On a Sufficient Criterion for Global Synchronization in Chaotic Systems. In: Kanarachos, A. (ed.) *Recent Advances in Telecommunications, Signals and Systems*, pp. 95–100. WSEAS Press (2013)
4. Dibakar, G.A., Chowdhury, R., Saha, P.: On the Various Kinds of Synchronization in Delayed Duffing-Van der Pol System. *Commun. Nonlinear Sci. Numer. Simulat.* 13, 790–803 (2008)
5. Gantmacher, F.R.: *The Theory of Matrices*. Nauka, Moscow (1966) (in Russian)
6. He, G.T., Luo, M.: Dynamic Behavior of Fractional Order Duffing Chaotic System and its Synchronization via Singly Active Control. *Appl. Math. Mech.* 33(5), 567–582 (2012)
7. Jiang, G.-P., Tang, W.K.-S., Chen, G.: A Simple Global Synchronization criterion for Coupled Chaotic Systems. *Chaos Solitons and Fractals* 15, 925–935 (2003)
8. Kaczorek, T.: *Selected Problems of Fractional Systems Theory*. LNCIS, vol. 411. Springer, Berlin (2011)
9. Kenfack, G., Tiedeu, A.: Secured Transmission of ECG Signals: Numerical and Electronic Simulations. *Journal of Signal and Information Processing* 4, 158–169 (2013)
10. Kimiaefar, A., Saidi, A.R., Sohoul, A.R., Ganji, D.D.: Analysis of Modified Van der Pol's Oscillator Using He's Parameter-Expanding Methods. *Current Applied Physics* 10, 279–283 (2010)
11. Mahmoud, G.M., Aly, S.A., Farghaly, A.A.: On Chaos Synchronization of a Complex Two Coupled Dynamical System. *Chaos, Solitons and Fractals* 33, 178–187 (2007)
12. Matouk, A.E.: Chaos, Feedback Control and Synchronization of a Fractional-Order Modified Autonomous Van der Pol–Duffing Circuit. *Commun. Nonlinear Sci. Numer. Simulat.* 16, 975–986 (2011)

13. Monje, C., Chen, Y., Vinagre, B., Xue, D., Feliu, V.: *Fractional-Order Systems and Controls*. Springer, London (2010)
14. Menacer, T., Hamri, N.: Synchronization of Different Chaotic Fractional-Order Systems via Approached Auxiliary System the Modified Chua Oscillator and the Modified Van der Pol-Duffing Oscillator. *Electronic Journal of Theoretical Physics*, EJTP 8(25), 253–266 (2011)
15. Ostalczyk, P.: *Epitome of the Fractional Calculus, Theory and its Applications in Automatics*. Publishing Department of Technical University of Łódź, Łódź (2008) (in Polish)
16. Pandey, A., Baghel, R.K., Singh, R.P.: Analysis and Circuit Realization of a New Autonomous Chaotic System. *International Journal of Electronics and Communication Engineering* 5(4), 487–495 (2012)
17. Petras, I.: *Fractional-Order Nonlinear Systems Modeling, Analysis and Simulation*. Higher Education Press, Beijing, Springer, Heidelberg (2011)
18. Podlubny, I.: *Fractional Differential Equations*. Academic Press, San Diego (1999)
19. Sabatier, J., Agrawal, O.P., Machado, J.A.T. (eds.): *Advances in Fractional Calculus, Theoretical Developments and Applications in Physics and Engineering*. Springer, London (2007)
20. Sheu, L.J., Chen, W.C., Chen, Y.C., Wenig, W.T.: A Two-Channel Secure Communication Using Fractional Chaotic Systems. *World Academy of Science, Engineering and Technology* 65, 1057–1061 (2010)
21. Suchorsky, M.K., Rand, R.H.: A Pair of Van der Pol Oscillators Coupled by Fractional Derivatives. *Nonlinear Dyn.* 69, 313–324 (2012)
22. Wang, Y., Yin, X., Liu, Y.: Control Chaos in System with Fractional Order. *Journal of Modern Physics* 3, 496–501 (2012)
23. Valério, D.: *Ninteger v. 2.3 - Fractional Control Toolbox for MatLab, User and Programmer Manual*, Technical University of Lisbona, Lisbona (2005), <http://web.ist.utl.pt/duarte.valerio/ninteger/ninteger.htm>
24. Varga, R.S.: *Gershgorin and His Circles*. Springer, Berlin (2004)
25. Vincent, U.E., Odunaike, R.K., Laoye, J.A., Gbindinnuola, A.A.: Adaptive Backstepping Control and Synchronization of a Modified and Chaotic Van der Pol-Duffing Oscillator. *J. Control Theory Appl.* 9(2), 273–277 (2011)

Multiple Project Portfolio Scheduling Subject to Mass Customized Service

Krzysztof Bzdrya¹, Zbigniew Banaszak², and Grzegorz Bocewicz¹

¹ Dept. of Computer Science and Management, Koszalin University of Technology
Śniadeckich 2, 75-453 Koszalin, Poland

krzysztof.bzdrya@tu.koszalin.pl

² Dept. of Business Informatics, Warsaw University of Technology
Narbutta 85, 02-524 Warsaw, Poland

Z.Banaszak@wz.pw.edu.pl

Abstract. Declarative framework enabling to determine conditions as well as to develop a decision making software supporting small and medium size enterprises aimed at unique, multi project-like and mass customized oriented production is discussed. The set of unique production orders grouped into portfolio orders is considered. To each production order treated as an activity network common shared resources operation times of which are known in advance are allotted. The problem concerns of scheduling of a newly inserted projects portfolio subject to constraints imposed by a multi-project environment The answer sought is: Whether a given portfolio can be completed within assumed time period in a manufacturing system in hand? The goal is to provide a declarative model enabling to state a constraint satisfaction problem aimed at multi project-like and mass customized oriented production scheduling. The attached calculation example illustrates the computational efficiency of the proposed solution.

Keywords: project portfolio, scheduling, declarative modeling.

1 Introduction

Current manufacturing environment can be characterized in terms of many factors but the key one for companies confronting the challenge of remaining competitive in an era of globalization is undoubtedly the capability of fast and accurate decision making, especially so in the mass customized production/services domain. An optimal assignment of available resources to production steps in a multi-product job shop (MPJS) is often economically indispensable. The goal is to generate a plan/schedule of production orders for a given period of time while minimize the cost that is equivalent to maximization of MPJS's profit. In that context executives want to know how much a particular production order will cost, what resources are needed, what resources allocation can guarantee due time production order completion, and so on. So, a manager needs might be formulated in a form of standard, routine questions, such as: Does the production order can be completed before an arbitrary given deadline? Is it possible to undertake a new production order under given (constrained in time) resources availability while guaranteeing disturbance-free execution of the already

executed orders? What values and of what variables guarantee the production order will be completed following assumed set of performance indexes?

In recent years, focus has come to be on the Resource-Constrained Project Scheduling Problem (RCPSp) which involves scheduling project activities subjected to temporal and resource constraints, while minimizing the total project duration. Two different approaches have been taken in solving the RCPSp. The first approach includes exact algorithms, which produce optimum solutions [6, 7]. The second approach is comprised of algorithms that provide admissible solutions refer to [3, 4, 8, 9]. These all demonstrate good results for the limited objective of resource allocation, but fail to truly support decision makers on all stages of project execution.

Very limited work focuses on the joint technological processes, transportation routing and financial [2]. Furthermore, there is another aspect of the addressed problem, namely multi-criteria decision making under uncertain conditions. Fuzzy multi-criteria decision making is primarily adopted for selecting, evaluating and ranking of alternative solutions to problems [3]. Studies conducted so far on declarative models implemented in fuzzy sets framework [1, 11], show that the proposed concept of *reverse* projects portfolio planning provides a promising alternative to commercially available ones. Therefore the new methods and techniques addressing the impact of real-life constraints on online decision making are of great importance [4]. To do this in a way compatible with real life settings necessitate the use of stochastic and fuzzy logic frameworks [6]. The fuzzy model of project portfolio online control can be specified as a declarative one and then implemented using constraint programming techniques and finally implemented as a decision support system [3].

Regardless of its character and scope of business activities a modern enterprise, has to build a project-driven development strategy in order to respond to challenges imposed by growing complexity and globalization. In that context this contribution can be seen as continuation of our former work aimed at multi-product production flow planning focused on coordination of processes and activities related to work order processing [1, 3, 4, 10].

Our main goal is to propose a new modeling framework enabling to evaluate and prototype alternative flows of production orders portfolio (POP) in the manufacturing systems disposing untapped potential in production capacity. The following questions are of main interest [5]: Can the assumed MPJS processing simultaneously set of production orders meet the deadlines imposed by a given, newly introduced POP? Does there exist MPJS enabling to perform assumed variety of POPs?

The rest of the paper is organized as follows: Section 2 introduces to a concept of POP through an illustrative example. Section 3 provides the declarative problem formulation focused at POPs prototyping. Computational experiments and conclusions are presented in Sections 4 and 5, respectively.

2 Illustrative Example

Considered MPJS consists of the set of machines $\mathbb{M} = \{m_1, \dots, m_i, \dots, m_{LM}\}$ (where m_i means the i -th machine and LM a number of machines in the system) required for execution of operations belonging to different Project Portfolios. In the system,

the family of project portfolios $Z^* = \{Z^1, \dots, Z^k, \dots, Z^v\}$, composed of production orders (tasks – for short) $Z^k = \{Z_1^k, \dots, Z_i^k, \dots, Z_n^k\}$ can be performed. Each task $Z_i^k \in Z^k$ is defined by the set of operations $O_i^k = \{o_{i,1}^k, \dots, o_{i,j}^k, \dots, o_{i,lo(i)}^k\}$, where $o_{i,j}^k$ means the j -th operation, while $lo(i)$ a number of task Z_i^k operations. Operations execution order is specified by digraph $G_i^k = (O_i^k, E_i^k)$, vertices of which refer to operations from the set O_i^k and arcs $(o_{i,a}^k, o_{i,b}^k) \in E_i^k$ represent relation: $o_{i,a}^k < o_{i,b}^k$ ($< \subseteq O_i^k \times O_i^k$) which means: " $o_{i,a}^k$ is executed before $o_{i,b}^k$ ". Exemplary activity networks encompassing digraphs G_1^1 and G_2^1 (representing Z_1^1 and Z_2^1 from Z^1) are shown in Fig. 1.

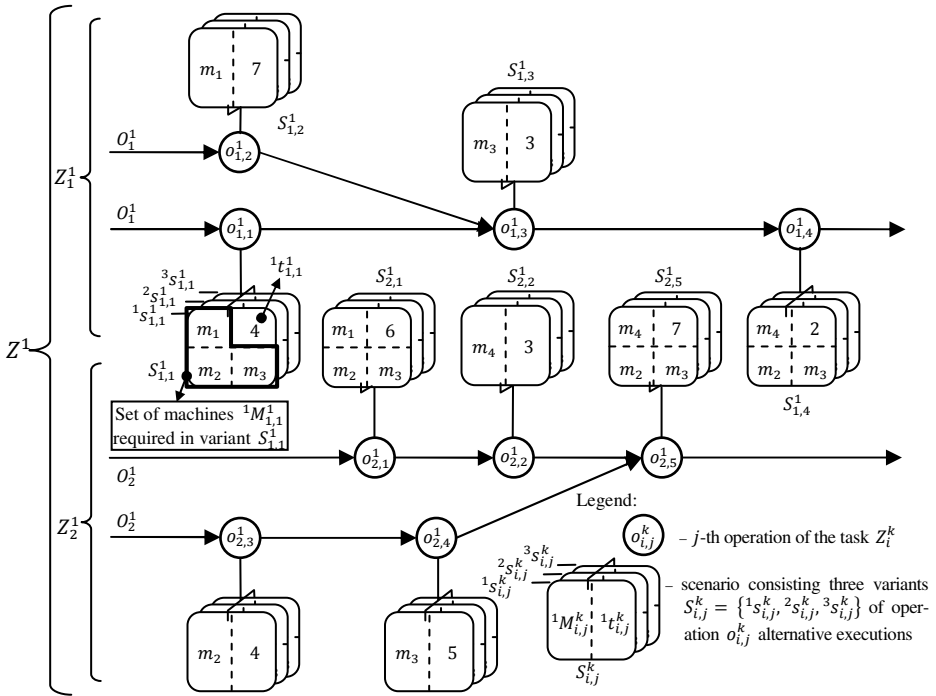


Fig. 1. Activity networks with distinguished scenarios of operation execution

To each operation $o_{i,j}^k$ the scenario $S_{i,j}^k \in \mathbb{S}$ of alternative executions of an operation is assigned (\mathbb{S} is a family of all MPJS scenarios). Scenario $S_{i,j}^k$ is the set of variants $S_{i,j}^k = \{^1s_{i,j}^k, \dots, ^b s_{i,j}^k, \dots, ^{ls(i,j,k)} s_{i,j}^k\}$, determining the way of operation $o_{i,j}^k$ execution. $^b s_{i,j}^k$ means the b -th variant of scenario $S_{i,j}^k$ while $ls(i,j,k)$ means a number of scenario $S_{i,j}^k$ variants.

Each variant $^b s_{i,j}^k = (^b M_{i,j}^k, ^b t_{i,j}^k)$, is specified by $^b M_{i,j}^k \in \mathbb{M}$ being the set of resources (e.g., machine tools) employed in course of operation $o_{i,j}^k$ execution, and $^b t_{i,j}^k \in \mathbb{N}^+$ being the time of $o_{i,j}^k$ execution following the variant $^b s_{i,j}^k$. The following assumptions are presupposed:

- each operation $o_{i,j}^k$ can be uniquely executed due to one of alternative variants following scenario $S_{i,j}^k$,
- at each moment only one operation $o_{i,j}^k$ can be executed on a resources from ${}^bM_{i,j}^k$,
- the resources belonging to ${}^bM_{i,j}^k$ are non-preemptable, that means the all resources of ${}^bM_{i,j}^k$ are reserved by operation $o_{i,j}^k$ until its completion, and cannot be used by other operations,
- resources from ${}^bM_{i,j}^k$ are released immediately after completion of actually executed operations.

Introduced assumptions takes into account cases when some operations (following assumed scenario) require simultaneous usage of a few different resources indispensable for their completion. For illustration consider operation $o_{1,1}^1$ from Fig. 1, requiring, due to assigned scenario, simultaneous usage of three machine to tools m_1 , m_2 and m_3 (distinguished by bold line in variant ${}^1S_{1,1}^1$, see Fig. 1).

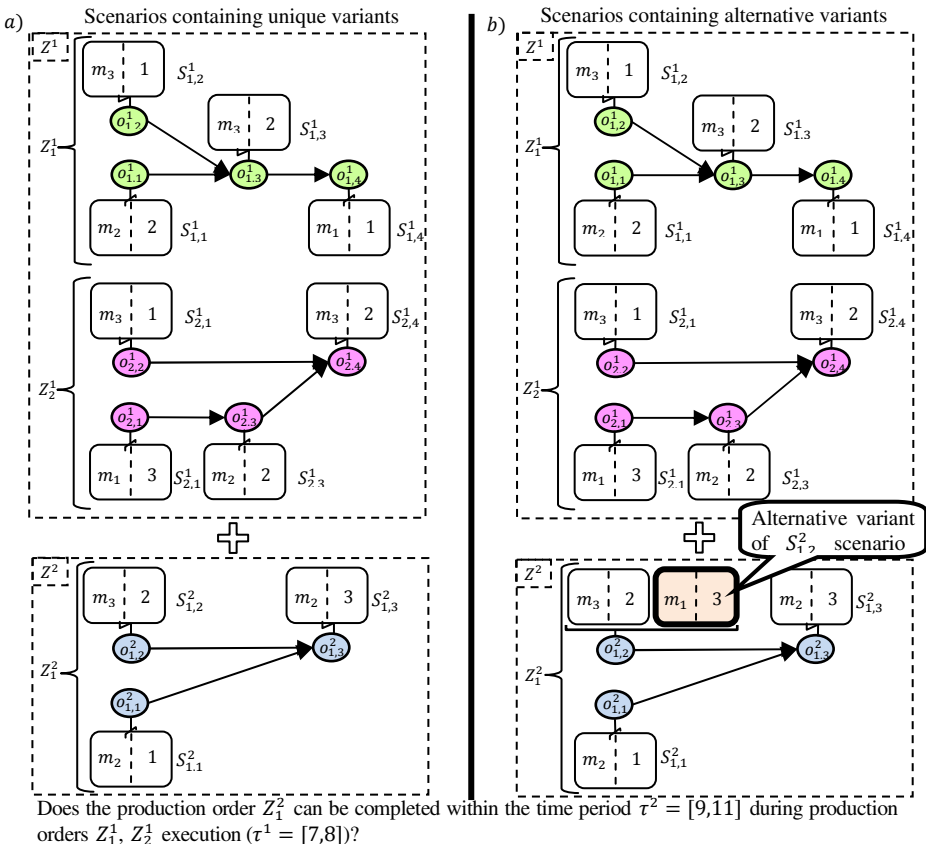


Fig. 2. Illustration of production orders portfolio assuming: scenarios containing unique variants a), scenarios containing alternative variants b)

Each operation $o_{i,j}^k$ can be specified by its two moments: start $x_{i,j}^k \in \mathbb{N}$, and termination $y_{i,j}^k = x_{i,j}^k + b_{i,j}^k$, respectively; where: $b_{i,j}^k$ – operation processing time depending on selected scenario $b_{i,j}^k$. The following set $X^k = \{x_{i,j}^k | i = 1 \dots n; j = 1 \dots l(i)\}$ is called a schedule of production orders portfolio Z^k .

Each Z^k portfolio makespan is calculated as $\max\{T_i^k = \max_{i=1 \dots n; j=1 \dots l(i)}\{y_{i,j}^k\}\}$. It is assumed that all production orders $Z_i^k \in Z^k$ have to be completed within an arbitrarily given period of time $\tau^k = [\tau a^k, \tau b^k]$: $T_i^k \in \tau^k$ for $i = 1 \dots n$.

In the above context one of possible ad-hoc managed, mass customized oriented production problems we are faced with can be stated as follows: Consider MPJS where simultaneously executed production orders $Z^* = \{Z^1, \dots, Z^q\}$ are processed (following arbitrarily given periods: $\tau^1 \dots \tau^q$). Given a newly added production orders portfolio Z^{q+1} , and associated period of time τ^{q+1} . What is the shortest portfolio makespan (schedule X^q) guaranteeing τ^{q+1} holds? That means the solution we are looking for has to guarantee that all production orders Z^{q+1} has to be accomplished not earlier than τa^{q+1} and not later than τb^{q+1} .

For illustration let us consider MPJS processing the portfolio Z^1 consisting two production orders Z_1^1, Z_2^1 , see Fig. 2 a), which should be completed within time period $\tau^1 = [7,8]$. Given portfolio Z^2 consisting only one production order Z_1^2 . What is the shortest portfolio makespan subject to $\tau^2 = [9,11]$ constraint? The possible solution is shown in Fig. 3a). From the relevant Gantt's chart it follows that both portfolios Z^1 and Z^2 (Fig. 3a) cannot be completed within assumed time periods $\tau^1 = [7,8]$ and $\tau^2 = [9,11]$, respectively.

Let us assume now that operation $o_{1,2}^2$ from Z_1^2 can be executed alternatively either on machine tool m_3 ($t_{1,2}^2 = 2$ t.u) or m_1 ($t_{1,2}^2 = 3$ t.u.), see Fig. 3b). Such solution follows assumed constraints $\tau^1 = [7,8]$, $\tau^2 = [9,11]$ see Gantt's chart from Fig. 3b).

Note that alternative scenarios treated as constraints limiting a number of possible solutions can be seen as constraints encompassing alternative and mutually excluding each other access to common shared system's resources.

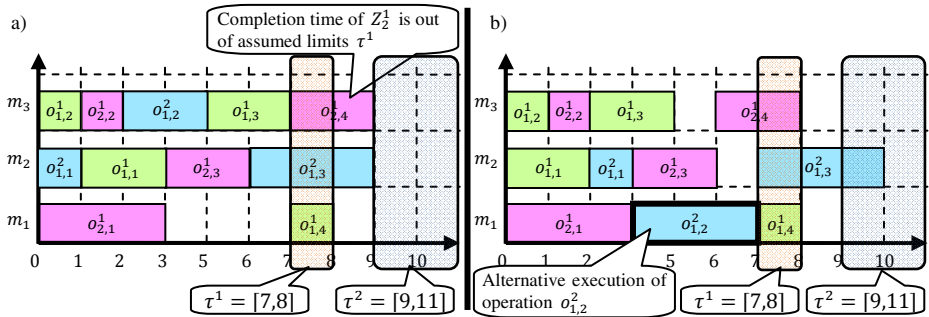


Fig. 3. Gantt's chart of executions of production order portfolios assuming: scenarios containing unique variants a), scenarios containing alternative variants b)

3 Declarative Problem Formulation

Considered assumptions imposing alternative and mutually excluding each other subsets of constraints lead to a new formulation of Constraints Satisfaction Problem (CSP) [12]:

$$CS = ((V, D), C) \tag{1}$$

where: V – the set of decision variables (in considered case the set of moments of operations beginning $x_{i,j}^k \in \mathbb{N}$), D – domain of admissible values of variables V , $C = C_S \cup C_A$ – the set of constraints describing relations between variables $x_{i,j}^k$: C_S – the set of basics constraints, $C_A = \{C_A^1, \dots, C_A^h, \dots, C_A^{lc}\}$ – the family of sets of constraints describing alternative scenarios, $C_A^h = \{Ca_1^h, \dots, Ca_i^h, \dots, Ca_{la(h)}^h\}$ – the set of mutually exclusive variants of scenario C_A^h .

The problem (1) can be treated as an extended version of classical constraint satisfaction problem CSP [12]. In opposition to this kind of problem the solution to proposed CS (1) is a set of variables value V following the all constrains C_S and all constraints, however from only one set Ca_i^h associated with scenario C_A^h . The examples of possible alternative constraints subsets are distinguished by green and orange lines.

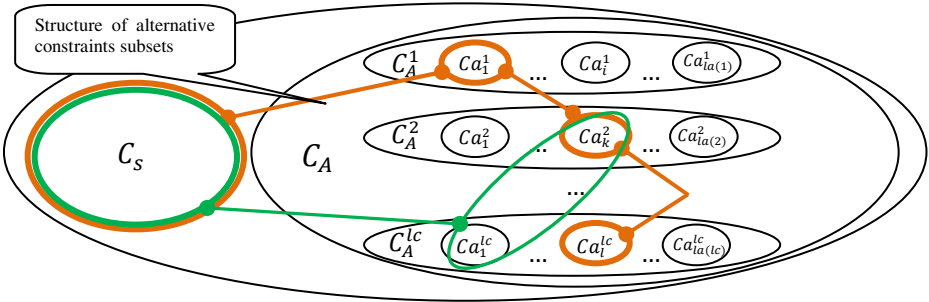


Fig. 4. Structure of constraints C defined by CSP (1)

In that context the considered problem of multiple Production Orders Portfolio (POP) scheduling can be treated as CS (1) where the set C consist of :

- the set C_S of constrains determining the order in which operations are executed:

$$x_{i,a}^k + h_{t,i,a}^k \leq x_{i,b}^k \text{ when } o_{i,a}^k < o_{i,b}^k \tag{2}$$

where: $x_{i,a}^k, x_{i,b}^k$ – moments of operations $o_{i,a}^k, o_{i,b}^k$ beginning; $h_{t,i,a}^k$ – execution time of operation $o_{i,a}^k$ following assigned scenario variant $h_{S_{i,a}^k}$.

- the family C_A of scenarios C_A^h specified by constraints guaranteeing the mutual exclusion of operations executed on common shared resources (machine tools):

$$(x_{i,j}^k + {}^h t_{i,j}^k \leq x_{a,b}^c) \vee (x_{a,b}^c + {}^l t_{a,b}^c \leq x_{i,j}^k) \text{ when } {}^h M_{i,j}^k \cap {}^l M_{a,b}^c \neq \emptyset \quad (3)$$

where: $x_{i,j}^k, x_{a,b}^c$ – moments of operations $o_{i,j}^k, o_{a,b}^c$ beginning; ${}^h t_{i,j}^k, {}^l t_{a,b}^c$ – execution times of operations $o_{i,j}^k, o_{a,b}^c$ following assigned scenario variants ${}^h S_{i,j}^k, {}^l S_{a,b}^c$; ${}^h M_{i,j}^k, {}^l M_{a,b}^c$ – sets of resources (machine tools) required for execution of operations $o_{i,j}^k, o_{a,b}^c$ (following assigned variants ${}^h S_{i,j}^k, {}^l S_{a,b}^c$).

Constraints C_S and C_A specifying POP from Fig. 2 are collected in Tab. 1 and graphically illustrated in Fig. 5. The sets distinguished by orange and green lines correspond to constraints specified in Fig. 2a) and Fig. 2b), respectively.

Table 1. The sets C_S and C_A specifying problem from Fig. 2

| | | C_S | | | | | |
|---------|----------|--|--------------------------------|--------------------------------|--|--|--|
| | | C_S^1 | C_S^2 | C_S^3 | C_S^4 | C_S^5 | |
| | | $x_{1,2}^1 + 1 \leq x_{1,3}^1$ $x_{1,1}^1 + 2 \leq x_{1,3}^1$ | $x_{1,3}^1 + 2 \leq x_{1,4}^1$ | $x_{2,1}^1 + 3 \leq x_{2,3}^1$ | $x_{2,2}^1 + 1 \leq x_{2,4}^1$ $x_{2,3}^1 + 2 \leq x_{2,4}^1$ | $x_{1,2}^2 + 2 \leq x_{1,3}^2$ $x_{1,1}^1 + 1 \leq x_{1,3}^2$ | |
| | | $x_{1,4}^1 + 1 \in \tau^1$ | | $x_{2,4}^1 + 2 \in \tau^1$ | | $x_{1,3}^2 + 3 \in \tau^2$ | |
| | | C_A | | | | | |
| C_A^1 | Ca_1^1 | $(x_{2,1}^1 + 3 \leq x_{1,4}^1) \vee (x_{1,4}^1 + 1 \leq x_{2,1}^1)$ | | | $(x_{2,1}^1 + 3 \leq x_{1,4}^1) \vee (x_{1,4}^1 + 1 \leq x_{2,1}^1)$ $(x_{2,1}^1 + 3 \leq x_{1,2}^2) \vee (x_{1,2}^2 + 3 \leq x_{2,1}^1)$ $(x_{1,4}^1 + 1 \leq x_{1,2}^2) \vee (x_{1,2}^2 + 3 \leq x_{1,4}^1)$ | | |
| | Ca_2^1 | $(x_{1,1}^1 + 2 \leq x_{1,2}^2) \vee (x_{1,2}^2 + 2 \leq x_{1,1}^1) \quad (x_{1,1}^1 + 2 \leq x_{2,3}^1) \vee (x_{2,3}^1 + 2 \leq x_{1,1}^1)$ $(x_{1,1}^1 + 2 \leq x_{1,1}^1) \vee (x_{1,1}^1 + 1 \leq x_{1,1}^1) \quad (x_{1,3}^2 + 3 \leq x_{2,3}^1) \vee (x_{2,3}^1 + 2 \leq x_{1,3}^2)$ $(x_{1,3}^2 + 3 \leq x_{1,1}^1) \vee (x_{1,1}^1 + 1 \leq x_{1,3}^2) \quad (x_{2,3}^1 + 2 \leq x_{1,1}^1) \vee (x_{1,1}^1 + 1 \leq x_{2,3}^1)$ | | | | | |
| C_A^3 | Ca_1^3 | $(x_{1,2}^1 + 1 \leq x_{2,2}^1) \vee (x_{2,2}^1 + 3 \leq x_{1,2}^1)$ $(x_{1,2}^1 + 1 \leq x_{1,3}^1) \vee (x_{1,3}^1 + 2 \leq x_{1,2}^1)$ $(x_{1,2}^1 + 1 \leq x_{2,4}^1) \vee (x_{2,4}^1 + 2 \leq x_{1,2}^1)$ $(x_{2,2}^1 + 3 \leq x_{1,3}^1) \vee (x_{1,3}^1 + 2 \leq x_{2,2}^1)$ $(x_{2,2}^1 + 3 \leq x_{2,4}^1) \vee (x_{2,4}^1 + 2 \leq x_{2,2}^1)$ $(x_{1,3}^1 + 2 \leq x_{2,4}^1) \vee (x_{2,4}^1 + 2 \leq x_{1,3}^1)$ $(x_{1,2}^1 + 2 \leq x_{1,2}^1) \vee (x_{1,2}^1 + 1 \leq x_{1,2}^1)$ $(x_{1,2}^2 + 2 \leq x_{2,2}^1) \vee (x_{2,2}^1 + 3 \leq x_{1,2}^2)$ $(x_{1,2}^2 + 2 \leq x_{1,3}^1) \vee (x_{1,3}^1 + 2 \leq x_{1,2}^2)$ $(x_{1,2}^2 + 2 \leq x_{2,4}^1) \vee (x_{2,4}^1 + 2 \leq x_{1,2}^2)$ | | | $(x_{1,2}^1 + 1 \leq x_{2,2}^1) \vee (x_{2,2}^1 + 3 \leq x_{1,2}^1)$ $(x_{1,2}^1 + 1 \leq x_{1,3}^1) \vee (x_{1,3}^1 + 2 \leq x_{1,2}^1)$ $(x_{1,2}^1 + 1 \leq x_{2,4}^1) \vee (x_{2,4}^1 + 2 \leq x_{1,2}^1)$ $(x_{2,2}^1 + 3 \leq x_{1,3}^1) \vee (x_{1,3}^1 + 2 \leq x_{2,2}^1)$ $(x_{2,2}^1 + 3 \leq x_{2,4}^1) \vee (x_{2,4}^1 + 2 \leq x_{2,2}^1)$ $(x_{1,3}^1 + 2 \leq x_{2,4}^1) \vee (x_{2,4}^1 + 2 \leq x_{1,3}^1)$ | | |

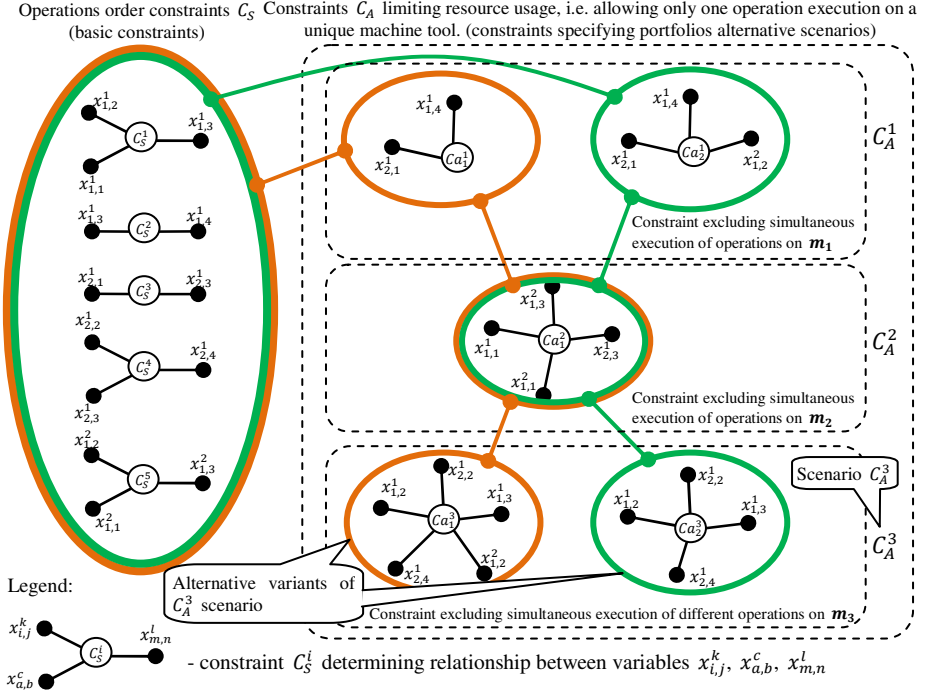


Fig. 5. Multi-graph illustration of alternative constraint structures

4 Calculation Example

Given MPJS where production orders portfolio Z^1 aimed at device A manufacturing is processed. The device should be completed within the time period $\tau^1 = [360,420]$ minutes. Consider newly submitted POP Z^2 containing the unique production order Z_1^2 . The activity networks encompassing operations order in considered POPs are show in Fig. 6. Possible assignment of operations and their operation times are collected in Tab. 2. Distinguished operations can be executed on shared resources m_1 - m_7 . The resources m_7, m_1 can replace each other, i.e. lead to alternative scenarios. The following question is considered: Is it possible to complete device B following the portfolio Z^2 within arbitrary assumed time period $\tau^2 = [420,480]$ minutes?

Aforementioned data fulfilling requirements imposed by CS (1) formulation have been implemented in constraints programming language Oz Mozart (Dual Core 2.67 GHz, 2.0 GB RAM). Three alternative scenarios following conditions (2), (3), have been considered.

The only admissible solution (admissible schedule $X = \{X^1, X^2\}$) obtained for unique scenario is show in Fig. 7. As it follows from the Gantt's chart the considered devices A and B are completed within assumed time periods, i.e. τ^1 and τ^2 , respectively. Due to the implemented scenario two operations among 22 others have to be realized on resource m_7 instead of m_1 . Since calculation time required by each

scenario is equal to 2 s, hence the overall time is greater than or equal to 6 s. In general case calculation complexity of the considered approach depends on a number of alternative scenarios and following them number of variants.

Finally it can be seen as a sum of time periods required for completeness evaluation of subsets of the set C_A constrains: $\sum_{h=1}^{lc} \sum_{i=1}^{la(h)} t_{CS}(i)$, where: lc – number of scenarios, $la(h)$ – number of variants of scenario C_A^h , $t_{CS}(i)$ – computation time of i -th iteration.

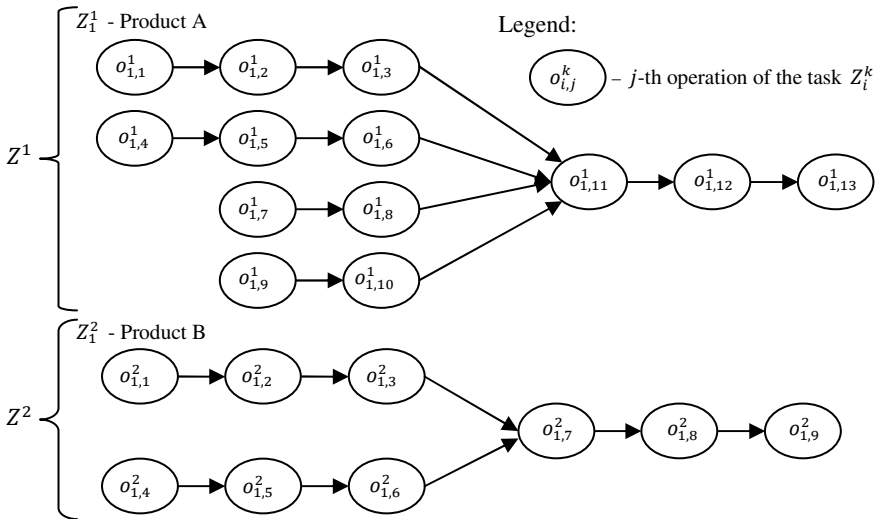


Fig. 6. Activity networks associated with devices A and B

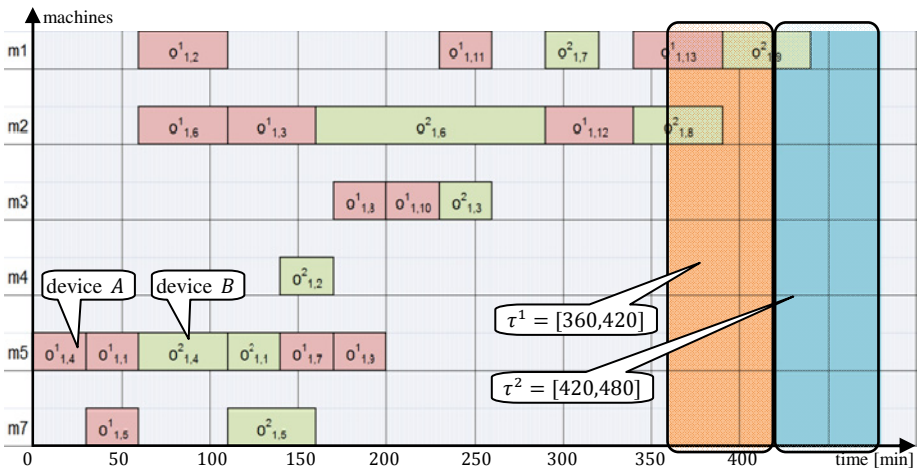


Fig. 7. Gantt's chart (schedule $X = \{X^1, X^2\}$) of executions of production order portfolios

Table 2. Operations alternative allocations and their operation times

| tasks | operations | variants | resources | time [min] |
|--------------|----------------------------------|----------------------------------|------------------|------------|
| Z_1^1 | $o_{1,1}^1$ | $^1s_{1,1}^1$ Cutting | m_5 Saw | 30 |
| | $o_{1,2}^1$ | $^1s_{1,2}^1$ Clearance | m_1 Workbench | 50 |
| | | $^2s_{1,2}^1$ Clearance | m_7 Workbench | 30 |
| | $o_{1,3}^1$ | $^1s_{1,3}^1$ Painting | m_2 Paint shop | 50 |
| | $o_{1,4}^1$ | $^1s_{1,4}^1$ Cutting | m_5 Saw | 30 |
| | $o_{1,5}^1$ | $^1s_{1,5}^1$ Clearance | m_1 Workbench | 50 |
| | | $^2s_{1,5}^1$ Clearance | m_7 Workbench | 50 |
| | $o_{1,6}^1$ | $^1s_{1,6}^1$ Painting | m_2 Paint shop | 50 |
| | $o_{1,7}^1$ | $^1s_{1,7}^1$ Cutting | m_5 Saw | 30 |
| | $o_{1,8}^1$ | $^1s_{1,8}^1$ Turing | m_3 Lathe | 30 |
| | $o_{1,9}^1$ | $^1s_{1,9}^1$ Cutting | m_5 Saw | 30 |
| | $o_{1,10}^1$ | $^1s_{1,10}^1$ Turing | m_3 Lathe | 30 |
| | | $^1s_{1,11}^1$ Assembly device A | m_1 Workbench | 30 |
| $o_{1,11}^1$ | $^2s_{1,11}^1$ Assembly device A | m_7 Workbench | 50 | |
| | $o_{1,12}^1$ | $^1s_{1,12}^1$ Lacquering | m_2 Paint shop | 50 |
| $o_{1,13}^1$ | $^1s_{1,13}^1$ Packaging | m_1 Workbench | 50 | |
| | $^2s_{1,13}^1$ Packaging | m_7 Workbench | 30 | |
| Z_1^2 | $o_{1,1}^2$ | $^1s_{1,1}^2$ Cutting | m_5 Saw | 30 |
| | $o_{1,2}^2$ | $^1s_{1,2}^2$ Clearance | m_4 Grinder | 30 |
| | $o_{1,3}^2$ | $^1s_{1,3}^2$ Turing | m_3 Lathe | 30 |
| | $o_{1,4}^2$ | $^1s_{1,4}^2$ Cutting | m_5 Saw | 50 |
| | $o_{1,5}^2$ | $^1s_{1,5}^2$ Clearance | m_1 Workbench | 90 |
| | | $^2s_{1,5}^2$ Clearance | m_7 Workbench | 50 |
| | $o_{1,6}^2$ | $^1s_{1,6}^2$ Painting | m_2 Paint shop | 130 |
| | $o_{1,7}^2$ | $^1s_{1,7}^2$ Assembly device B | m_1 Workbench | 30 |
| | | $^2s_{1,7}^2$ Assembly device B | m_7 Workbench | 30 |
| | $o_{1,8}^2$ | $^1s_{1,8}^2$ Varnishing | m_2 Paint shop | 50 |
| $o_{1,9}^2$ | $^1s_{1,9}^2$ Packaging | m_1 Workbench | 50 | |
| | $^2s_{1,9}^2$ Packaging | m_7 Workbench | 130 | |

5 Concluding Remarks

Better planning, in the manner supported by proposed approach, can improve companies' competitiveness through better utilization of resources and could be widely implemented in a number of production contexts, especially in mass customized production. A computer implementation of the proposed methodology should provide a new generation DSS supporting one in cases of online resource allocation and tasks scheduling as well as production orders routing. Such a tool should be especially helpful in cases when actually processed products portfolio do not spend all company's capability reserves, i.e. there is a room for additional work order considerations.

References

1. Bach, I., Bocewicz, G., Banaszak, Z., Muszyński, W.: Knowledge based and CP-driven approach applied to multi product small-size production flow. *Control and Cybernetics* 39(1), 69–95 (2010)
2. Badell, M., Romero, J., Huertas, R., Puigjaner, L.: Planning, scheduling and budgeting value-added chains. *Computers and Chemical Engineering* 28, 45–61 (2004)
3. Banaszak, Z.: CP-based decision support for project driven manufacturing. In: *Perspectives in Modern Project Scheduling*. International Series in Operations Research and Management Science, vol. 92, pp. 409–437. Springer, U.S. (2006)
4. Banaszak, Z.A., Zaremba, M.B.: Project-driven planning and scheduling support for virtual manufacturing. *Journal of Intelligent Manufacturing* 17, 641–651 (2006)
5. Bocewicz, G., Banaszak, Z.: Declarative approach to cyclic steady state space refinement: periodic process scheduling. *International Journal of Advanced Manufacturing Technology* 67, 137–155 (2013)
6. Dang, Q.-V., Nielsen, I., Steger-Jensen, K., Madsen, O.: Scheduling a single mobile robot for part-feeding tasks of production lines. *Journal of Intelligent Manufacturing* 25, 1–17
7. Groover, M.P.: *Automation, Production Systems and Computer-Integrated Manufacturing*, 3rd edn., p. 840. Prentice Hall, NJ (2007)
8. Khayat, G.E., Langevin, A., Riope, D.: Integrated Production and Material Handling Scheduling Using Mathematical Programming and Constraint Programming. *European Journal of Operational Research* 175(3), 1818–1832 (2006)
9. Krenczyk, D., Kalinowski, K., Grabowik, C.: Integration Production Planning and Scheduling Systems for Determination of Transitional Phases in Repetitive Production. In: Corchado, E., Snášel, V., Abraham, A., Woźniak, M., Graña, M., Cho, S.-B. (eds.) *HAIS 2012, Part II*. LNCS, vol. 7209, pp. 274–283. Springer, Heidelberg (2012)
10. Nielsen, I., Bocewicz, G., Dung, D.A.: Production and Resource Scheduling in Mass Customization with Dependent Setup Consideration. In: *Proceedings of the 7th World Conference on Mass Customization, Personalization, and Co-Creation (MCPC 2014)*. Lecture Notes in Production Engineering, pp. 461–472 (2014)
11. Relich, M., Jakabova, M.: A decision support tool for project portfolio management with imprecise data. In: *Proceedings of the 10th International Conference on Strategic Management and its Support by Information Systems*, pp. 164–172 (2013)
12. Sitek, P., Wikarek, J.: Hybrid Solution Framework for Supply Chain Problems. In: Omatu, S., Bersini, H., Corchado Rodríguez, J.M., González, S.R., Pawlewski, P., Bucciarelli, E. (eds.) *Distributed Computing and Artificial Intelligence*, 11th International Conference. AISC, vol. 290, pp. 11–18. Springer, Heidelberg (2014)

Recurrent Polynomial and Neural Structures in Modelling of a Neutralisation Process

Patryk Chaber and Maciej Ławryńczuk

Institute of Control and Computation Engineering, Warsaw University of Technology
ul. Nowowiejska 15/19, 00-665 Warsaw, Poland
P.Chaber@stud.elka.pw.edu.pl, M.Lawrynczuk@ia.pw.edu.pl

Abstract. This work discusses modelling of a neutralisation process by means of two recurrent modelling techniques: polynomials and neural networks. Model structures and training algorithms are shortly discussed. Two recurrent model classes are compared in terms of accuracy and complexity. Advantages of neural models are emphasised.

Keywords: recurrent dynamic models, multi layered perceptron, polynomial model, neural model, pH neutralisation.

1 Introduction

Advanced control algorithms [10] and fault detection methods [3] rely on models of dynamic systems. There are two main classes of models: fundamental (first-principle) [5] and empirical ones [6]. Fundamental models consist of systems of nonlinear differential and algebraic equations which describe all technological phenomena which take place. Such models, although potentially very precise, are very frequently not suitable for on-line control and fault detection. It is because they are usually very complicated, i.e. the total number of equation may be high and on-line solution of the equations may be difficult. Furthermore, numerical problems such as stiffness or ill-conditioning are likely. Finally, development of fundamental models needs specific knowledge and may be difficult.

Empirical models are alternatives to fundamental ones. In the empirical approach the technological phenomena taking place are not considered, input and output data sets recorded during process operation are used to find the model. Unlike fundamental models, the structure of empirical ones is chosen arbitrarily. A great number of different empirical models have been developed [6], e.g. Volterra series, piece-wise approximators, polynomial models, fuzzy systems and neural networks. The most important measures of model utility are: approximation accuracy, suitability for application and easiness of development [9].

Although numerous types of empirical models are possible, neural networks [2] have a particularly great importance. They are currently used in many applications, e.g. in fault detection methods [3], advanced control algorithms [4], medicine [7] and pattern recognition [8].

The objective of this work is to thoroughly compare properties of polynomial and neural structures in modelling of a neutralisation process. The recurrent

model configuration is considered. The neutralisation reactor [1] is used very frequently in chemical industry and it has a great technological importance. From the model identification perspective, it is a dynamic process whose properties are significantly nonlinear. This study considers selection of both model order of dynamics and model topology for polynomial and neural structures in terms of model accuracy and complexity (i.e. the number of parameters). Additionally, some remarks on model training concerning both structures are given.

2 Recurrent Dynamic Models

In the non-recurrent serial-parallel model [6] the output signal (for consecutive sampling instants $k = 1, 2, \dots$) is a function of the process input and output signals from previous instants

$$y^{\text{mod}}(k) = f(u(k - \tau), \dots, u(k - n_B), y(k - 1), \dots, y(k - n_A))$$

where $u(k - i)$ denotes the input signal for the discrete time $k - i$, $y(k - i)$ stands for the measured output signal for the discrete time $k - i$. In the recurrent parallel model [6], which is also called the simulation model, the past process outputs are replaced by the model outputs calculated at previous sampling instants

$$y^{\text{mod}}(k) = f(u(k - \tau), \dots, u(k - n_B), y^{\text{mod}}(k - 1), \dots, y^{\text{mod}}(k - n_A)) \quad (1)$$

where $y^{\text{mod}}(k - 1)$ denotes the output signal obtained the from model for the discrete time $k - i$. The parallel configuration is a natural choice when the model is used for long-range prediction in control or fault detection algorithms.

3 Recurrent Neural Network

3.1 Model Architecture

The structure of the Multi Layer Perceptron (MLP) neural network is shown in Fig. 1. Taking into account Eq. (1), the network has $N = n_B - \tau + n_A + 1$ input nodes, the input vector is

$$\begin{aligned} x(k) &= [x_0(k) \ \dots \ x_N(k)]^T \\ &= [1 \ u(k - \tau) \ \dots \ u(k - n_B) \ y^{\text{mod}}(k - 1) \ \dots \ y^{\text{mod}}(k - n_A)]^T \end{aligned} \quad (2)$$

The network has as many as K hidden nodes with the transfer function φ and one output node (adder). The output of the network is described by the equation

$$y^{\text{mod}}(k) = w_0^2 + \sum_{i=1}^K w_i^2 \varphi \left(\sum_{j=0}^N w_{i,j}^1 x_j(k) \right)$$

where $w_{i,j}^1$ ($i = 1, \dots, K$, $j = 0, \dots, N$) are weights of the first layer of the network, w_i^2 ($i = 0, \dots, K$) are weights of the second (hidden) layer of the network. All the weights forms a vector of parameters

$$\mathbf{w} = [w_{1,0}^1 \ w_{1,1}^1 \ \dots \ w_{K,N}^1 \ w_0^2 \ \dots \ w_K^2]^T$$

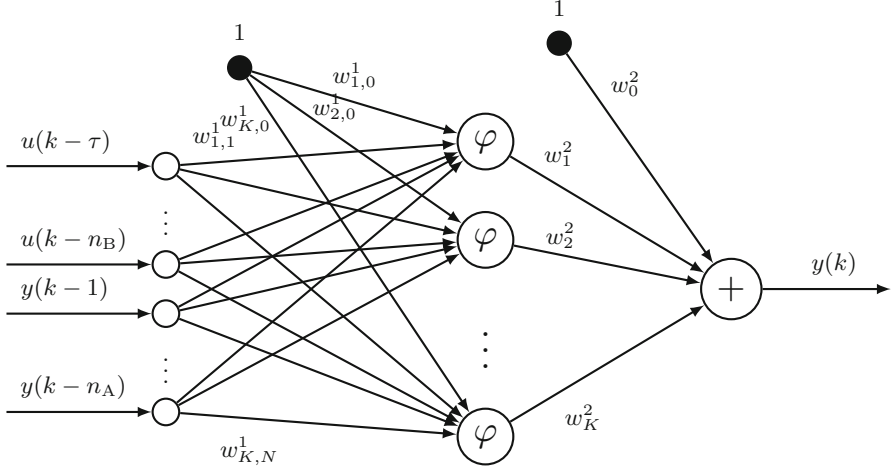


Fig. 1. Structure of Multi Layer Perceptron neural model

3.2 Model Training

Training of the neural model means finding such a vector of weights so that the value of the error function has an acceptable minimal value. The error function is

$$E(\mathbf{w}) = \sum_{k=S}^P (y^{\text{mod}}(k) - y(k))^2 \quad (3)$$

where $S = \max\{n_A, n_B\} + 1$, P is the number of training samples. Model training leads to minimisation of the error $E(k)$. The gradient vector $\nabla E(\mathbf{w})$ of the error function is calculated using analytic equations. Such an approach is much faster and precise in comparison with a numerically approximated gradient vector.

The current vector of model parameters is found as a function of the previous parameters (in the previous iteration $t - 1$)

$$\mathbf{w}_t = \mathbf{w}_{t-1} + \alpha_t p_t$$

where α_t is the step of minimisation – it is an argument which minimises the function $E_d(\alpha_t) = E(\mathbf{w}_{t-1} + \alpha_t p_t)$. The direction of minimisation is

$$p_t = -\mathbf{V}_t \nabla E(\mathbf{w}_t)$$

In the Broyden-Fletcher-Goldfarb-Shanno (BFGS) [2] algorithm approximation of the inverse hessian matrix \mathbf{V}_t is updated from

$$\mathbf{V}_t = \mathbf{V}_{t-1} + \left[1 + \frac{\mathbf{r}_t^T \mathbf{V}_{t-1} \mathbf{r}_t}{s_t^T \mathbf{r}_t} \right] \frac{s_t s_t^T}{s_t^T \mathbf{r}_t} - \frac{s_t \mathbf{r}_t^T \mathbf{V}_{t-1} + \mathbf{V}_{t-1} \mathbf{r}_t s_t^T}{s_t^T \mathbf{r}_t}$$

where $s_t = \mathbf{w}_t - \mathbf{w}_{t-1}$, $\mathbf{r}_t = \nabla E(\mathbf{w}_t) - \nabla E(\mathbf{w}_{t-1})$.

4 Recurrent Polynomial Model

4.1 Model Architecture

Taking into account Eq. (1), i.e. the input arguments of the model, given by Eq. (2), the polynomial model is described by the equation

$$y^{\text{mod}}(k) = w_0 x_0(k) + \sum_{i=1}^N w_i x_i(k) + \sum_{i_1=1}^N \sum_{i_2=i_1}^N w_{i_1, i_2} x_{i_1}(k) x_{i_2}(k) + \sum_{i_1=1}^N \dots \sum_{i_R=i_{R-1}}^N w_{i_1, \dots, i_R} x_{i_1}(k) \dots x_{i_R}(k)$$

where R is the degree of the polynomial model. Weights of the polynomial model $w_{i, \dots, j}$ form the parameters vector

$$\mathbf{w} = [w_0 \ w_1 \ \dots \ w_N \ w_{1,1} \ \dots \ w_{N,N} \ \dots \ \underbrace{w_{N, \dots, N}}_{R\text{-times}}]^T$$

4.2 Model Training

The BFGS optimisation algorithm is also used for training the polynomial model. The same actions as described in Section 3.2 are taken to achieve the goal, the model error function is given by Eq. (3). The gradient of the error function is also calculated using analytic equations.

It is necessary to emphasize that in both models, polynomial and neural ones, the inputs of models are exactly the same, but their internal structure is different. That is why it is interesting to compare their accuracy and complexity.

5 Simulation Results

5.1 Process Description

The process under consideration, shown on Fig. 2, is a pH neutralisation reactor [1]. A base (NaOH) stream q_1 , a buffer (NaHCO₃) stream q_2 and an acid (HNO₃) stream q_3 are mixed in a constant volume tank. The output pH is controlled by manipulating the base flow rate q_1 (ml/s). The buffer and acid streams are assumed to be constant ($q_2 = 0.55$ ml/s, $q_3 = 16.60$ ml/s).

The continuous-time fundamental model of the reactor is comprised of two nonlinear ordinary differential equations

$$\begin{aligned} \frac{dW_a(t)}{dt} &= \frac{q_1(t)(W_{a_1} - W_a(t))}{V} + \frac{q_2(t)(W_{a_2} - W_a(t))}{V} + \frac{q_3(t)(W_{a_3} - W_a(t))}{V} \\ \frac{dW_b(t)}{dt} &= \frac{q_1(t)(W_{b_1} - W_b(t))}{V} + \frac{q_2(t)(W_{b_2} - W_b(t))}{V} + \frac{q_3(t)(W_{b_3} - W_b(t))}{V} \end{aligned}$$

and one algebraic output equation

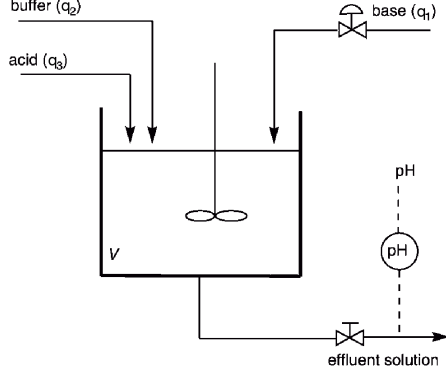


Fig. 2. Schematic representation of the pH neutralisation process [1]

$$W_a(t) + 10^{\text{pH}(t)-14} - 10^{-\text{pH}(t)} + W_b(t) \frac{1 + 2 \times 10^{\text{pH}(t)-\text{p}K_2}}{1 + 10^{\text{p}K_1-\text{pH}(t)} + 10^{\text{pH}(t)-\text{p}K_2}} = 0$$

State variables are reaction invariants: W_a is a charge-related quantity, W_b is the concentration of the carbonate ion. Parameters of the fundamental model are given in Table 1. Initial operating conditions are: $q_1 = 15.55$ ml/s, $q_2 = 0.55$ ml/s, $q_3 = 16.60$ ml/s, $\text{pH}=7$, $W_a = -4.32 \times 10^{-4}$ mol, $W_b = 5.28 \times 10^{-4}$ mol.

The fundamental model is simulated open-loop to obtain training, validation and test data sets. The sampling time is 10 s. The output signal contains small measurement noise. Input and output variables are scaled: $u = (q_1 - q_{10})/15$, $y = (\text{pH} - \text{pH}_0)/5$, where $q_{10} = 15.55$ ml/s, $\text{pH}_0 = 7$ correspond to the initial operating point.

5.2 Process Modelling

Neural models with different number of hidden neurons and polynomial models with different degree are found. Each model is trained 10 times starting from random weights, the best result is presented. The first and the second order of dynamics are considered. Three data sets are used. The training set is used only for training during which the validation error is monitored and training is terminated when it grows (due to overfitting). For model selection the validation error is used. For the chosen models the test error is also calculated.

Results of the experiments carried out are shown in Table 2 and Table 3. One may draw two conclusions. The first observation is that for the considered neutralisation process the models with the second order of dynamics are more accurate than the ones with the first order. Fig. 3 shows the influence of the number of model parameters on error of both model classes (for the second order of dynamics), the networks

Table 1. Constants of the neutralisation process

| | | |
|--------------------------------------|-------------------------------------|-----------------------|
| $W_{a_1} = -3.05 \times 10^{-3}$ mol | $W_{b_1} = 5.00 \times 10^{-5}$ mol | $V = 2900.00$ ml |
| $W_{a_2} = -3.00 \times 10^{-2}$ mol | $W_{b_2} = 3.00 \times 10^{-2}$ mol | $\text{p}K_1 = 6.35$ |
| $W_{a_3} = 3.00 \times 10^{-3}$ mol | $W_{b_3} = 0.00$ mol | $\text{p}K_2 = 10.25$ |

Table 2. Comparison of MLP neural models with K hidden neurons and polynomial models of degree R , the first order of dynamics; NP – number of parameters, E – model error

| Model | NP | E(training) | E(test) | E(validation) |
|----------------------|----|-------------|---------|---------------|
| MLP ($K=1$) | 5 | 17.1148 | – | 23.2655 |
| MLP ($K=2$) | 9 | 6.8523 | – | 8.4748 |
| MLP ($K=3$) | 13 | 4.1688 | – | 9.2880 |
| MLP ($K=4$) | 17 | 1.9640 | – | 11.2738 |
| MLP ($K=5$) | 21 | 1.8104 | – | 11.1847 |
| MLP ($K=6$) | 25 | 1.3555 | – | 9.8630 |
| MLP ($K=7$) | 29 | 1.0473 | – | 9.7711 |
| MLP ($K=8$) | 33 | 0.6861 | – | 4.8022 |
| MLP ($K=9$) | 37 | 0.5611 | 1.4845 | 1.7875 |
| Polynomial ($R=1$) | 2 | 51.9491 | – | 64.3449 |
| Polynomial ($R=2$) | 5 | 43.0225 | – | 59.8489 |
| Polynomial ($R=3$) | 9 | 8.2153 | – | 15.8497 |
| Polynomial ($R=4$) | 14 | 4.1837 | 10.9887 | 9.8154 |
| Polynomial ($R=5$) | 20 | 2.8962 | – | 5.9310 |
| Polynomial ($R=6$) | 27 | 2.6453 | – | 6.0533 |
| Polynomial ($R=7$) | 35 | 1.6315 | – | 3.6138 |
| Polynomial ($R=8$) | 44 | 1.5317 | – | 4.2552 |

Table 3. Comparison of MLP neural models with K hidden neurons and polynomial models of degree R , the second order of dynamics; NP – number of parameters, E – model error

| Model | NP | E(training) | E(test) | E(validation) |
|----------------------|----|-------------|---------|---------------|
| MLP ($K=1$) | 7 | 13.7367 | – | 20.4636 |
| MLP ($K=2$) | 13 | 6.0510 | – | 10.3906 |
| MLP ($K=3$) | 19 | 2.6126 | – | 4.5344 |
| MLP ($K=4$) | 25 | 1.2468 | – | 2.6950 |
| MLP ($K=5$) | 31 | 0.5378 | – | 1.9000 |
| MLP ($K=6$) | 37 | 0.2468 | 0.3087 | 0.2718 |
| MLP ($K=7$) | 43 | 0.2221 | – | 0.3556 |
| MLP ($K=8$) | 49 | 0.1518 | – | 0.1511 |
| MLP ($K=9$) | 55 | 0.1742 | 0.7059 | 0.9399 |
| Polynomial ($R=1$) | 4 | 46.0161 | – | 64.0808 |
| Polynomial ($R=2$) | 14 | 18.6045 | – | 25.8658 |
| Polynomial ($R=3$) | 34 | 3.6737 | – | 9.3822 |
| Polynomial ($R=4$) | 69 | 2.1597 | 5.5135 | 4.9911 |

with too many parameters have bad generalisation. The second observation is that neural models generally have much better accuracy than the polynomial ones and a lower number of parameters. Because of this, neural models of the second order of dynamics with $K = 6$ and $K = 9$ hidden neurons are chosen for further comparison. It is interesting to see that the neural model of the second order of dynamics but with as few as 6 hidden nodes gives better accuracy (for the validation data set) than the more complex ones (with 7 and 9 nodes).

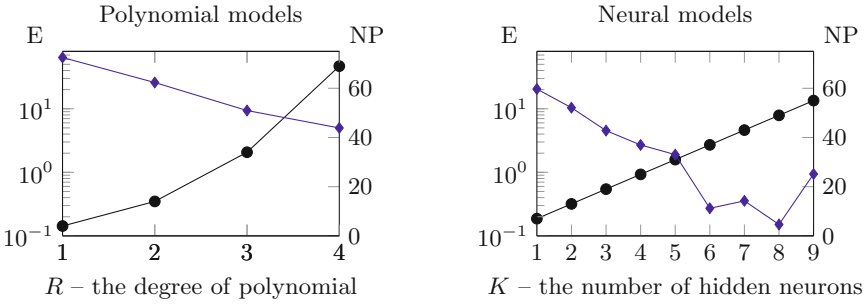


Fig. 3. Model errors E (for the validation data set) and the number of parameters NP for polynomial and neural model of the second order of dynamics

It is necessary to stress the fact that the number of parameters of the polynomial models heavily depends on their degree. For example, for the second order of dynamics, the polynomial of degree 2 is

$$\begin{aligned}
 y(k) = & w_0 + w_1 u(k-1) + w_2 u(k-2) + w_3 y(k-1) + w_4 y(k-2) \\
 & + w_{1,1} u(k-1)u(k-1) + w_{1,2} u(k-1)u(k-2) + w_{1,3} u(k-1)y(k-1) \\
 & + w_{1,4} u(k-1)y(k-2) + w_{2,2} u(k-2)u(k-2) + w_{2,3} u(k-2)y(k-1) \\
 & + w_{2,4} u(k-2)y(k-2) + w_{3,3} y(k-1)y(k-1) + w_{3,4} y(k-1)y(k-2) \\
 & + w_{4,4} y(k-2)y(k-2)
 \end{aligned}$$

whereas the polynomial of degree 3 is significantly more complicated

$$\begin{aligned}
 y(k) = & w_0 + w_1 u(k-1) + w_2 u(k-2) + w_3 y(k-1) + w_4 y(k-2) \\
 & + w_{1,1} u(k-1)u(k-1) + w_{1,2} u(k-1)u(k-2) + w_{1,3} u(k-1)y(k-1) \\
 & + w_{1,4} u(k-1)y(k-2) + w_{2,2} u(k-2)u(k-2) + w_{2,3} u(k-2)y(k-1) \\
 & + w_{2,4} u(k-2)y(k-2) + w_{3,3} y(k-1)y(k-1) + w_{3,4} y(k-1)y(k-2) \\
 & + w_{4,4} y(k-2)y(k-2) + w_{1,1,1} u(k-1)u(k-1)u(k-1) \\
 & + w_{1,1,2} u(k-1)u(k-1)u(k-2) + w_{1,1,3} u(k-1)u(k-1)y(k-1) \\
 & + w_{1,1,4} u(k-1)u(k-1)y(k-2) + w_{1,2,2} u(k-1)u(k-2)u(k-2) \\
 & + w_{1,2,3} u(k-1)u(k-2)y(k-1) + w_{1,2,4} u(k-1)u(k-2)y(k-2) \\
 & + w_{1,3,3} u(k-1)y(k-1)y(k-1) + w_{1,3,4} u(k-1)y(k-1)y(k-2) \\
 & + w_{1,4,4} u(k-1)y(k-2)y(k-2) + w_{2,2,2} u(k-2)u(k-2)u(k-2) \\
 & + w_{2,2,3} u(k-2)u(k-2)y(k-1) + w_{2,2,4} u(k-2)u(k-2)y(k-2) \\
 & + w_{2,3,3} u(k-2)y(k-1)y(k-1) + w_{2,3,4} u(k-2)y(k-1)y(k-2) \\
 & + w_{2,4,4} u(k-2)y(k-2)y(k-2) + w_{3,3,3} y(k-1)y(k-1)y(k-1) \\
 & + w_{3,3,4} y(k-1)y(k-1)y(k-2) + w_{3,4,4} y(k-1)y(k-2)y(k-2) \\
 & + w_{4,4,4} y(k-2)y(k-2)y(k-2)
 \end{aligned}$$

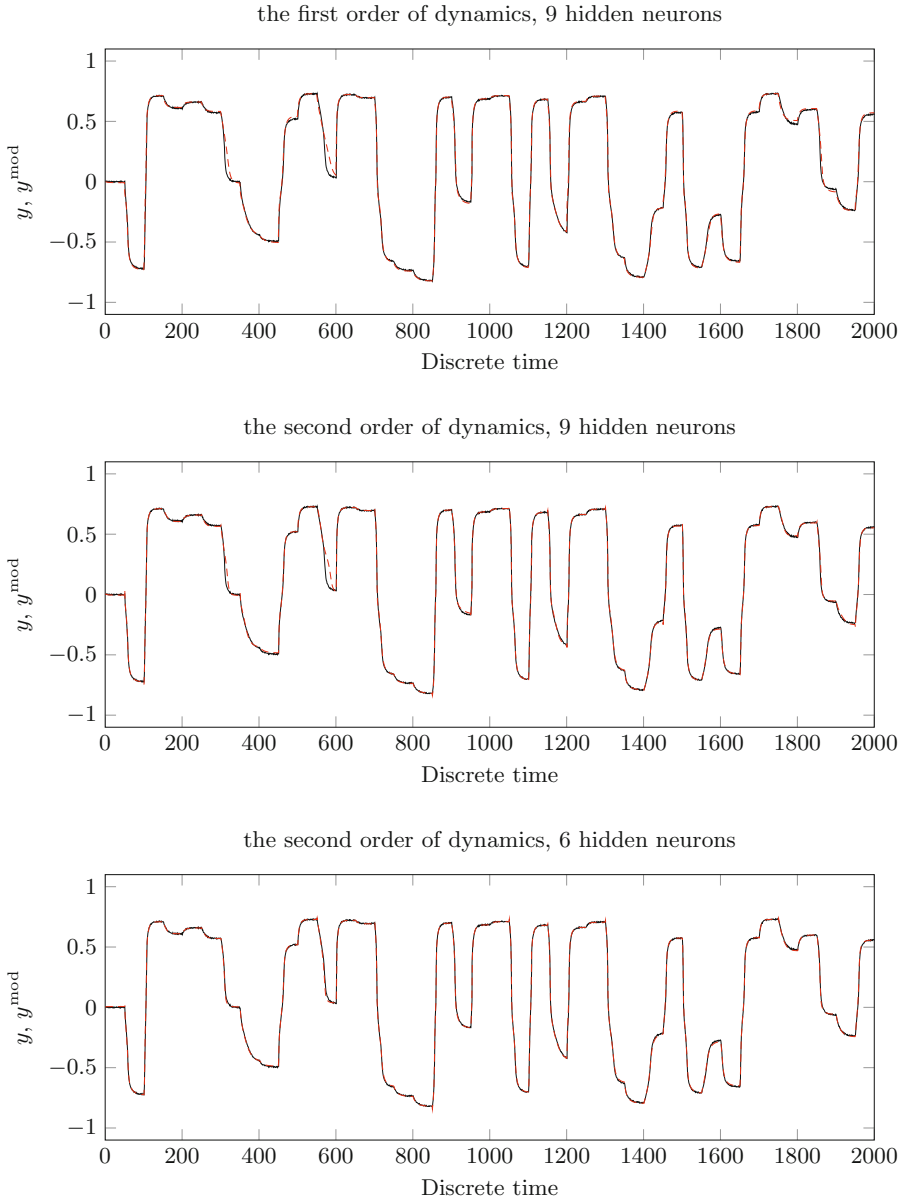


Fig. 4. The output signal of 3 chosen neural models (*dashed line*) vs. the validation data set (*solid line*)

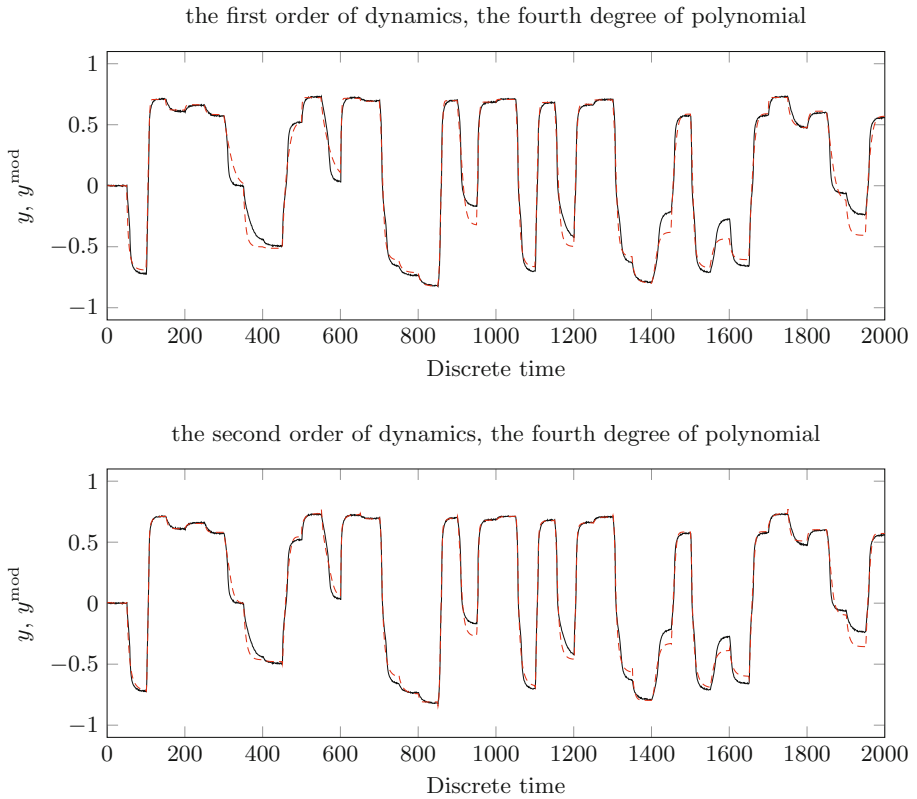


Fig. 5. The output signal of 2 chosen polynomial models (*dashed line*) vs. the validation data set (*solid line*)

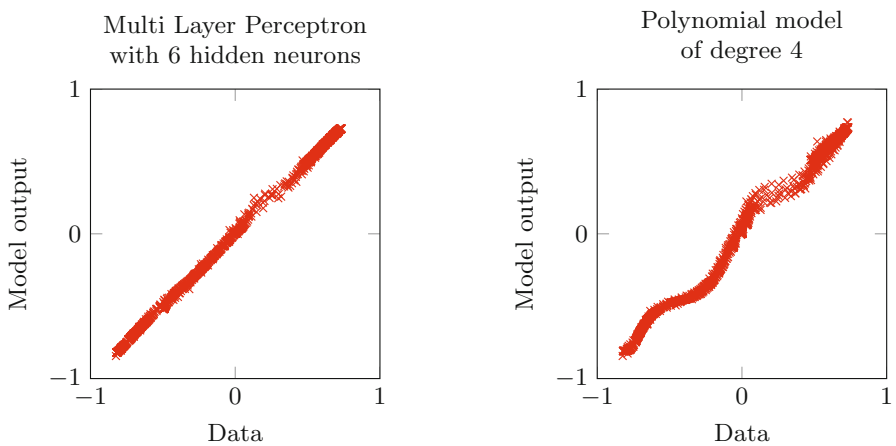


Fig. 6. Correlation between model output vs. the validation data set for the best neural and polynomial models of the second order of dynamics

Fig. 4 compares model outputs and the validation data set for three neural models: with the first order of dynamics and 9 hidden nodes (the best in its class) and two networks with the second order of dynamics as well as with 9 and 6 nodes, which is the best. Fig. 5 compares model outputs and the validation data set for two polynomials of the fourth degree, two orders of dynamics are considered. Unfortunately, the polynomials are characterised by significantly lower accuracy than the neural models. Fig. 6 depicts correlations of the best neural and polynomial structures.

6 Conclusions

Neural recurrent models of the neutralisation process outperforms the polynomial ones in terms in accuracy and complexity. The chosen model is of the second order dynamics and it has as few as 6 hidden nodes (37 parameters).

References

1. Gómez, J.C., Jutan, A., Baeyens, E.: Wiener model identification and predictive control of a pH neutralisation process. *IEE Proc. Part D, Control Theory and Appl.* 151, 329–338 (2004)
2. Haykin, S.: *Neural networks—a comprehensive foundation*, 2nd edn. Prentice-Hall, Inc., Upper Saddle River (1999)
3. Korbicz, J., Koscielny, J.M., Kowalczyk, Z., Cholewa, W.: *Fault Diagnosis: Models, Artificial Intelligence, Applications*. Springer, London (2004)
4. Ławryńczuk, M.: *Computationally Efficient Model Predictive Control Algorithms: A Neural Network Approach*. *Studies in Systems, Decision and Control*, vol. 3. Springer, Heidelberg (2014)
5. Marlin, T.E.: *Process control*. McGraw-Hill, New York (1995)
6. Nelles, O.: *Nonlinear system identification. From classical approaches to neural networks and fuzzy models*. Springer, Berlin (2001)
7. Ogiela, M., Tadeusiewicz, R.: *Modern computational intelligence methods for the interpretation of medical images*, *Studies in Computational Intelligence*. SCI, vol. 84. Springer, Heidelberg (2008)
8. Ripley, B.D.: *Pattern recognition and neural networks*. Cambridge University Press, Cambridge (1996)
9. Pearson, R.K.: Selecting nonlinear model structures for computer control. *Journal of Process Control* 13, 1–26 (2003)
10. Tatjewski, P.: *Advanced control of industrial processes, Structures and algorithms*. Springer, London (2007)

Memory-Based Prediction of District Heating Temperature Using GPGPU

Paweł D. Domański and Marcin Więclawski

Institute of Control and Computational Engineering,
Warsaw University of Technology,
ul. Nowowiejska 15/19, 00-665 Warszawa, Poland
p.domanski@ia.pw.edu.pl, wiecek1988@yahoo.co.uk

Abstract. The paper presents application of the memory-based prediction to the problem of the return water temperature prognosis in a district heating network. CHP (Combined Heating Plant) problem is defined as well as the algorithm based on the memory of the historical process realizations together with its novel, parallel implementation using CUDA on GPGPU. The use of the calculation extensive methods from one side enables to get good and reliable predictions, but in opposite the prognosis evaluation is done at high cost. An alternative application of the massively parallel version of the Memory-based time series prediction algorithm has been implemented and tested. The paper shows very good and promising improvement in comparison to the common applications. The algorithm is tested on the real process data.

1 Introduction

The time-series forecasting [1] is usually performed by means of well-known approach using mostly linear regression methods or non-linear (empirical) ones, like NARMAX, neural networks or fuzzy models. Most of the models, like neural networks or regression models, are short-memory systems so they use only a few past values of the series for making the prediction.

It seems that characteristics of the district heating datasets requires a very long memory, because the current data is correlated to some degree with all past data. We have to also take into consideration the statistical features of the data under consideration. It may happen that they cannot be well modelled through normal distribution functions but rather fits long-tail distributions [2]. Thus it is worth to verify whether alternative modelling approaches that are not biased by any assumptions on data distribution, i.e. Memory Based Reasoning - MBR.

Memory-based reasoning derives from the human ability to reason from experience, the ability to recognize appropriate examples from the past. It was successfully applied for classification and prediction purposes in many different fields [3], [4]. The big advantage of memory-based reasoning is that it gives good prediction results without the background knowledge of the process which makes it universal. The model requires only several parameters which optimal values

can be found experimentally or by using the evolutionary algorithms. The simplicity of the algorithms used in the model makes it possible to be computed in parallel what gives a significant decrease of computation time.

Memory-based reasoning is a very good method for time-series forecasting [5]. It is effective in calculations and straightforward in implementation. The aim of this work is to measure the prediction abilities of this method for the real-life example of time-series representing the process of heat distribution in the district heating network. The main stress is put on choosing the optimal algorithms and parameters of the model. The optimization of the implemented code (especially its parallelization) was one of the main aspects of the project.

For a very long time applications of MBR were limited, because of significant computational power necessary for the task. For a single prediction based on a moderate amount of historical data currently available computers will suffice, but for a problem involving hundreds of predictions, or a system where the prediction has to be made in real time, it is crucial to find a way to reduce algorithm's execution time.

The main subject considered in this paper is to apply and validate parallel GPGPU approach implemented on Nvidia CUDA technology to practical example of MBR in order to reduce the algorithm execution time.

2 Memory Based Reasoning

Memory-based reasoning, opposite to the other data mining techniques, does not care about the format of the records as long as the two operations are defined: distance function and combination function [6]. Another advantage of memory-based reasoning is that it easily adapts, it immediately takes into calculations the newly incorporated data. It produces good results without long training, without necessity of algorithm changing.

Memory-based reasoning requires a lot of historical data to give reliable prediction [7]. Insufficient data results in large prediction error because there are no records matching the pattern. All these data requires storage, which also must be considered. The classification process is very time consuming and requires big computational power. In the single classification all the historical data have to be processed [8].

Memory-based reasoning in time-series prediction have to consider the fact that a single record consist of several multi-field data points organized in time. All the calculations, distance calculation and combination of results, must be applied to a record as a whole. However the algorithms presented in the following chapters are valid and successfully applicable for the time-series prediction problems.

As we consider comparison between current frame and history several measure domains might be considered. The authors have tested different ones, e.g. pure time domain, variance benchmarking, comparison of the parameters of time polynomials and of weights of the Fast Fourier Transform [9] (in frequency domain). Below the main MBR notions are explained.

1. Window Size

Window is a set of data, a pattern, a state, that is compared in the process of matching. The window size, the number of consecutive data points that will be compared at each matching, is very important parameter in the memory-based reasoning application for time-series prediction. An empirical estimation of the window size is being used. A state of a minimal size is selected and the prediction is performed. The window size is incremented and the value is chosen for which the best accuracy of the forecast, the minimal prediction error, is obtained.

2. **Number of Nearest Neighbours** The notion derives from the name of the k nearest neighbour algorithm, which is most often used for classification, and is a part of memory-based reasoning systems. Instead of finding only one record that most closely matches the new one, several k nearest neighbours are found.

3. **Distance Function** Distance function is a measure of distance between any two records, i.e. of similarity between records. It is calculated for two records at the time.

4. **Combination Function** Combination function combines the results coming from several neighbours into one prediction. It is defined if the number of neighbours k is greater than one.

When MBR is used for classification, each neighbour votes for its own class. The proportion of votes decides if the unclassified record belongs to the corresponding class. If single class is to be assigned the one with the most votes wins. The rule of thumb is to use $c+1$ neighbours, where c is number of categories, to avoid ties among classifications. The unweighed voting means that the arithmetic mean from the k nearest neighbours is calculated and taken as a prediction.

5. Distance Measurement Algorithms

Distance measurement may be used in several places: between data points in time and frequency domain, between variances in time and frequency and between coefficients of algebraic polynomial in time. Three different algorithms are used for calculating distances with N being a number of data and x, y as data points, however Euclidean distance proved the best performance.

- Manhattan distance (absolute distance)
- Euclidean distance
- Infinity distance

6. Prediction Error Calculations [10]

The selection of appropriate error measurement is very important in estimating the forecasting abilities of the memory-based reasoning method. It is wise to use several statistical measures that have different properties. The following performance indices were tested, and RMSE with MAPE were finally applied in algorithm parallel version.

- Root Mean Square Error (RMSE)
- Mean Absolute Percentage Error (MAPE)
- Geometric Root Mean Square Error (GRMSE)
- Geometric Relative Absolute Error (GRAE)

3 GPGPU Parallel Computing

The first attempts to use the Memory Based Reasoning for time series prediction took place in the late *1980s* [10]. Although the idea was probably introduced earlier, the number of computations necessary for data analysis was so huge that even for a supercomputers available at this point of time it was not an easy task. Running a time series prediction algorithm on a PC was almost impossible until the middle *1990s*, because of insufficient memory resources. Even if the amount of accessible memory was sufficient, the computational power of any single CPU available at that point was too low.

3.1 Parallel Computations on a GPU

Until the end of the XX century increasing the number of CPU threads was the only reasonable solution which, with proper programming, could give an order of magnitude improvement in the speed of program execution [13]. At the beginning of the XXI century a group of programmers pointed out that in a modern Personal Computer (PC) the rapid development of Graphic Processing Units (GPU) may yield even greater potential than its CPU counterpart. The technology of redirecting part of the CPU load to the GPU is called GPGPU (General Purpose computing on Graphic Processing Unit) [14]. During these early attempts of GPU programming, there wasn't any specific API allowing the programmer to easily access the GPU to make computations. Even now the graphic card can be directly addressed only with Direct3D or OpenGL APIs.

In 2007 Nvidia Company made a major breakthrough in the field of GPU computations by introducing CUDA technology (Compute Unified Device Architecture) [15]-[17]. It was the first widely available high level API which enabled the programmer to access the computational power of the GPU with a high level C language, without the need to use Direct3D or OpenGL APIs. The whole task of translating the code into the API understood by the Graphic Card is done by a piece of hardware added to Nvidia products.

Before creating the first program in CUDA API it's important to understand that the CPU (host) and the GPU (device) are separated from each other. This distinction results in a series of advantages and disadvantages which have to be taken into account during the development of a program. To begin with the separation of the CPU and the GPU environments means that many tasks can only be done by one of those chips, in most cases the CPU, for example all the I/O operations.

Furthermore the fact that something can be run on the GPU not necessarily means that the achieved performance will be satisfactory. For example running a piece of code, which makes one arithmetical operation on a new data array and then returns the modified data to the host will most probably turn out to be slower on the GPU than on a CPU. A single task has to be executed on a reasonable big dataset (at least several hundred data points) in order to take full advantage of the GPU computational power.

The detached model of the GPU - CPU allows the programmer to load each of them with a different piece of code and execute those in an asynchronous mode. Before calling a kernel function we have to define the number and organization of threads which will be run on the GPU. Furthermore for each GPU function, all the input data have to be copied to the graphic cards global memory. Returning the data from the GPU also has to be done separately, because CUDA functions can operate only on the memory of the graphic card.

3.2 CUDA Technology Application to the Time Series Prediction

For the experiments in this project the Nvidia 9800GTX+ graphic card equipped with a G92 Graphic Processing Unit (GPU) is used. The 9xxx series of Nvidia graphic cards is an upgraded version of the first generation of GPUs supporting Nvidia CUDA technology. The G92 graphic chip has 8 blocks with two Streaming Multiprocessors (SM) each. A multiprocessor has 8 linked cores which gives us an overall number of 128 execution units, operating at the frequency of 1,8GHz.

Although there are 8 cores in a SM, there is only one instruction unit, so a Multiprocessor will execute the same instruction for all the threads. This architecture is often referred to as Single Instruction Multiple Threads (SIMT) [11]. During one clock cycles each Streaming Multiprocessor can make up to 24 Multiply And Add operations and 2 floating points operations with the Special Function Unit, so the overall pick performance of the GPU is ~ 748 GFLOPS.

Programming in CUDA involves a very highly multi-threaded environment, well suited for parallel computations. A G92 graphic processor can operate on up to 768 threads per each of 16 multiprocessors, which means that for a single GPU system its possible to operate on 12288 active threads. Threads on the GPU are organized in 1, 2 or 3 dimensional blocks, which then have to be organized in 1 or 2 dimensional grid of thread blocks. A GPU function (kernel) call creates a grid of parallel threads, which will execute the kernel function. Each thread block is assigned to a Multiprocessor and there divided into groups called warps.

CUDA programming API, as a parallel environment for processing huge data sets in SIMT mode, is highly dependent on the memory access speed and flexibility. The construction of the GPU comparing to the CPU, enforces some special changes in the way the data are accessed from the memory. In the case of the CPU, there are several processing units, the control block and a very big, extremely fast cache memory, which takes about half of the real chip size. Analysing the structure of a GPU chip, its clear that almost all the available space is used by the processing units, so there is very little space left for cache memory.

4 Experimental Results – District Heating Temperature Prediction

The basis for testing the effective speedup of a GPU in comparison to a CPU are two algorithms for calculating a time series prediction using Memory Based

Reasoning. Apart from checking the execution time of each function its also good to look for any differences between each algorithm results.

The data for which the experiment will be conducted are describing temperatures in a Combined Heating Plant (CHP), but for this algorithm, type of input data is irrelevant.

4.1 Process: CHP Plant

The task is to experimentally verify the prediction abilities of the memory-based reasoning implementation for the real-life time-series. The test data are representing the long delay process of heat supply and distribution in a district heating network (Figure 1). The process is represented by the following data: T_{in} , T_{out} (the input and output temperature of supplied water), T_{amb} (the ambient temperature disturbance).

Our goal is to predict T_{in} (input water coming back to the CHP plant from the district heating network) as a function of the CHP output temperature (input to the network) and ambient temperature.

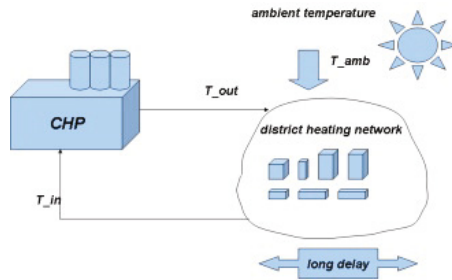


Fig. 1. Distribution of heat in a district heating network

The data were gathered during the 5 heating seasons in one of the central heating plants in large city. The data set consists of the disjoint sections, each collected approximately from the end of September till middle of April, which is connected with the specificity of the district heating process. The data were collected every hour during the heating periods (24 hours a day, 7 days per week), which gives the total of 21696 data points. The data are normalized and represented as a single precision floating-point numbers.

The study of the experimental results brings to the conclusion that memory-based reasoning might be very successful and effective model for prediction of a real-life process given in a task. The adjustment of model parameters enables to obtain the satisfactory quality of estimation at the level of mean absolute percentage error of below 1.2%.

The best choice of the window size is 24, it corresponds to the 24 hours periods, which is characteristic for the process. The calculations for longer windows are more time consuming without improvement in results. The optimal

prediction size is also 24 . It is the longest prediction size that can be used for window of length 24 and thus the most efficient. This length of prediction makes possible to performs forecasts only once per day. It is worth noticing that the results obtained for the window size equal to 12 are only slightly worse than for window size equal to 24 . The mean values of error measures for 100 different input frames are in both cases almost the same, but for the window size equal to 12 the maximum errors are higher. Moreover that the increase of window size from 12 through 16 and 20 gives small improvement of the prediction quality. It leads to the conclusion that 12 consecutive data points are sufficient to model the process of heat distribution in the district heating network. The above observation implies that the 24 hours periods are divided into two: day and night sub-periods, but the implication is not very strong.

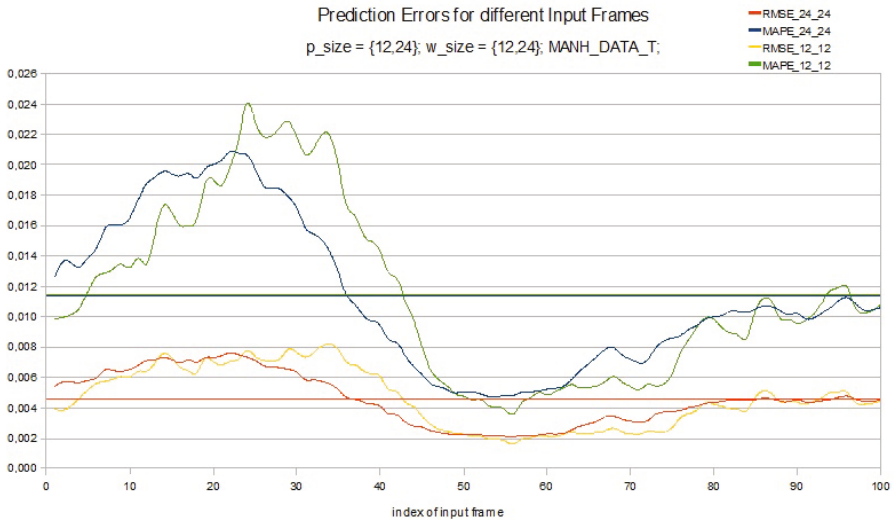


Fig. 2. Prediction errors for different input frames, prediction size = 24, window size = 24, algorithm: MANH_T

As far as algorithms including variance calculation, polynomial approximation and Fourier transformation turned out to gain no improvement in the results, the best choice is the simple Manhattan distance on the data in time domain. It's predicting abilities are very good, execution fast and implementation straightforward. The optimal number of nearest neighbours is one. The increase of this number makes the prediction quality to worsen. The impact of neighbours that are farther away from the input frame is significant, and negative.

Summing up, the best forecasting is obtained for prediction size and window size equal to 24, Manhattan distance on the data in time domain with one nearest neighbours. The maximum mean absolute percentage error obtained for

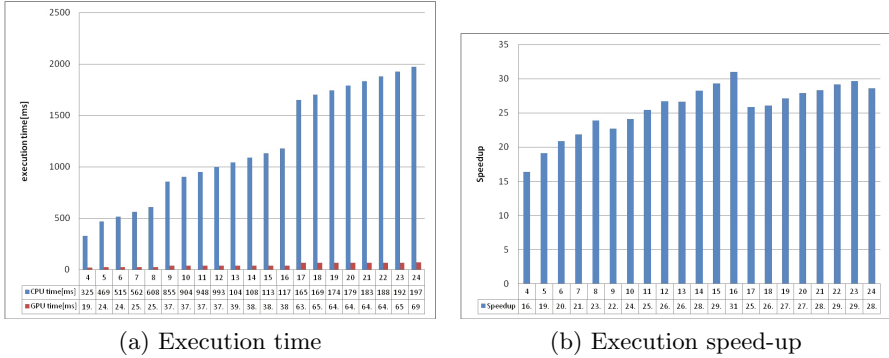


Fig. 3. Increase of the window size effect

a set of testing frames was slightly above 2%. The comparison between results for window and prediction size equal both to 12 and 24 for all testing frame are shown on Figure 2.

4.2 Execution Time Comparison

It was important to remember that even if an algorithm is using a GPU for the most difficult task, it also uses the CPU whenever possible. Every kernel call and most of the memory copy operations are run in an asynchronous way, which means that the CPU doesn't wait for those tasks to finish.

Looking at the Figure 3a it is clear that function, which for computations uses a GPU is much faster than a similar solution based only on a CPU. In both cases any non-critical pieces of code were removed. At this point it can be said that the difference in performance is very big. It can be observed in details on Figure 3b. The GPU speed-up of execution time is increasing for bigger prediction windows, which most probably means that the GPU doesn't work at its full potential for predictions window smaller then 24 .

4.3 Analyses of Each Calculation Performance

As for now we could find out how the overall performance speed-up changes for increasing size of prediction window. The second part of results analyses concerns the execution time of corresponding CPU and GPU functions. Comparing CPU and the GPU solution can give a row estimation how much faster is the GPU in terms of pure computations and what should be done to improve the overall speed of execution.

The results presented in table Table 1 give a bit more information about the program operation. Functions executed on the GPU consume only 16 – 21% of the overall GPU solution. In the case of the CPU those functions consume more than 70% of the overall solution execution time. The important difference is the speed of the remaining operations which are done apart from the functions

searching for the Memory Based Reasoning. In the case of CPU algorithm the execution of operations which are not included in the selected functions take even more than the execution of the whole GPU algorithm.

Basing on the results one can expect that the GPU solution may still hold hidden potential for a different time series with much bigger history of previous cases. On the other hand these results indicate that using a graphic card with more cores or operating at higher frequency will not yield a significant reduction in program execution time.

Table 1. Execution times for each function (in milliseconds)

| Window | GPU | | | | CPU | | | |
|----------------|-------|-------|-------|-------|--------|--------|---------|---------|
| | 4 | 8 | 16 | 24 | 4 | 8 | 16 | 24 |
| Distance[ms] | 0,56 | 0,68 | 1,11 | 1,46 | 12,13 | 21,63 | 40,25 | 58,69 |
| Variance[ms] | 0,43 | 0,33 | 1,92 | 0,48 | 58,18 | 116,22 | 229,11 | 337,63 |
| Polynomial[ms] | 3,54 | 3,68 | 4,24 | 4,72 | 127,46 | 250,94 | 487,02 | 729,12 |
| FFT[ms] | 0,63 | 0,99 | 2,26 | 4,81 | 38,65 | 73,91 | 151,32 | 319,15 |
| SUM[ms] | 5,16 | 5,68 | 9,53 | 11,47 | 236,42 | 462,7 | 907,7 | 1444,59 |
| Overall[ms] | 25,45 | 29,21 | 43,75 | 68,97 | 337,13 | 631,73 | 1206,63 | 2011,33 |

Both algorithms used in the experiment differ only with the API used, although final results are not identical. Despite the fact that differences are very small, the results should have been exactly the same. Different outputs of identical operations can be introduced either during the instruction execution or during the assignment to a floating point variable. As we can read in [12] there are several instructions for which the graphic card uses floating point rounding implementations, which are not IEEE-compliant. It is possible to use functions which follow the rounding procedures of IEEE-754 standard, but this will decrease the overall function performance. In the case of a difference smaller than 10^{-5} it is highly unlikely that it will cause any noticeable change in final results.

5 Conclusion

The Memory Based Reasoning as one of possible approaches to time series prediction is probably the most universal solution, yet it still has some disadvantages. The real problem of this approach is to supply a sufficiently big set of historical cases. Nonetheless even for a huge set of data points the algorithm may not necessarily find a good enough nearest neighbour. Furthermore for a growing set of historical data, the number of necessary computations is increasing.

On the other hand with using GPGPU, even an order of magnitude bigger set of historical cases shouldn't be a problem. The speed-ups which we were able to achieve for a single GPU and a CPU are impressive and the difference in the speed of computations would be even greater for a bigger number of data points to process.

At this point the algorithm for MBR is only a basis for further development. There are many possibilities for further improvements especially in terms of prediction errors. For example introducing a proper system of weights between each method, which with the CUDA implementation would find an acceptable value of each weight in a reasonable amount of time.

From a different perspective it's also possible to rewrite the current algorithm, so that it would operate on one of the open GPGPU programming techniques, which do not restrict the number of possible users to the owners of Nvidia graphic cards. For example DirectCompute or OpenCL.

References

1. Hamilton, J.D.: Time Series Analysis. Prentice Hall, New Jersey (1994); vol. SFB 373, pp. 837–900. Princeton University Press (1994)
2. Mandelbrot, B.B.: The (Mis) Behaviour of Markets: A Fractal View of Risk, Ruin and Reward, Building. Profile Books (2008)
3. Larose, D.T.: Discovering Knowledge in Data: An Introduction to Data Mining. Wiley-Interscience (2005)
4. Pedrycz, W.: Knowledge-Based Clustering: From Data to Information Granules. John Wiley & Sons, Hoboken (2005)
5. Zhang, X., Threling, K.: Non-Linear Time-Series Prediction by Systematic Data Exploration on a Massively Parallel Computer. Santa Fe Institute Technical Report 94-07-045 (1994)
6. Olson, D.L., Delen, D.: Advanced Data Mining Techniques, Part II, ch. 3. Springer, Heidelberg (2008)
7. Lan, Y., Neagu, D.: A New Time Series Prediction Algorithm Based on Moving Average of nth-Order Difference. In: Proc. of Sixth International Conference on Machine Learning and Applications, pp. 248–253 (2007)
8. Stanfill, C., Waltz, D.: Toward Memory-based Reasoning. Communications of the ACM 29(12) (December 1986)
9. Press, W.H., Teukolsky, S.A., Vetterling, W.T., Flannery, B.P.: Numerical Recipes in C: The Art of Scientific Computing. Cambridge University Press (2007)
10. Singh, S.: A long memory pattern modelling and recognition system for financial time-series forecasting. Springer-Verlag London Limited (1999)
11. Kirk, D., Hwu, W.: Programming Massively Parallel Processors: A Hands-on Approach. Morgan Kaufmann (2010)
12. Cheng, H., Tan, P.-N., Gao, J., Scripps, J.: Multistep-ahead time series prediction. In: Ng, W.-K., Kitsuregawa, M., Li, J., Chang, K. (eds.) PAKDD 2006. LNCS (LNAI), vol. 3918, pp. 765–774. Springer, Heidelberg (2006)
13. Gupta, G.G., Karypis, G., Kumar, V.: Introduction to Parallel Computing, 2nd edn. Addison-Wesley (2003)
14. Sanders, J., Kandrot, E.: CUDA by Example: An Introduction to General-Purpose GPU Programming, 1st edn. Addison-Wesley Professional (2010)
15. Nvidia Company, *NVIDIA_CUDA_C_ProgrammingGuide_3.1.pdf*, http://developer.download.nvidia.com/compute/cuda/3_1/toolkit/docs
16. Nvidia Company, CUDA training, http://developer.nvidia.com/object/cuda_training.html
17. Nvidia Company, *NVIDIA_CUDA_C_BestPracticesGuide_3.1.pdf*, http://developer.download.nvidia.com/compute/cuda/3_1/toolkit/docs/

The Architecture of an Embedded Smart Camera for Intelligent Inspection and Surveillance

Michał Fularz, Marek Kraft, Adam Schmidt, and Andrzej Kasiński

Institute of Control and Information Engineering, Poznań University of Technology,
Piotrowo 3A, 60-965 Poznań, Poland
`michal.fularz@put.poznan.pl`

Abstract. Real time video surveillance and inspection is complex task, requiring processing large amount of image data. Performing this task in each node of a multi-camera system requires high performance and power efficient architecture of the smart camera. Such solution, based on a Xilinx Zynq heterogeneous FPGA (Field Programmable Logic Array) is presented in this paper. The proposed architecture is a general foundation, which allows easy and flexible prototyping and implementation of a range of image and video processing algorithms. Two example algorithm implementations using the described architecture are presented for illustration – moving object detection and feature points detection, description and matching.

Keywords: Smart Camera, Embedded System, Computer Vision, Hardware Software Codesign, FPGA.

1 Introduction

Over the last years, an increased demand for vision-based inspection and monitoring can be observed. The most important reason behind this change is the fact, that visual data carries a lot of useful information. However, it also makes processing of visual data a non-trivial task. Extraction of desired information from such raw data requires significant computational power. At the same time, the number of cameras in a typical multi-camera system increases, to the point, at which human operators are unable to handle all the incoming information. A typical approach to the automated processing of data coming from a multi-camera system is the use of central server. However, such an approach is not without its limitations. The transfer of image data from the cameras to the central processing node requires appropriate infrastructure, which is oftentimes costly and may be cumbersome to deploy. Under extreme conditions, such as a very large number of cameras and/or the use of high resolution or high framerate video data, the bandwidth or processing power requirements may be impossible to satisfy. The most common way to deal with these limitations is to use more and more sophisticated compression algorithms. On the downside, the use of

such algorithms increases the computational power demand for video encoding and decoding, resulting in increased application cost and power consumption [15]. Furthermore, the compression degrades image quality which may impact the quality of processing results [18].

In the face of the problems and limitations given above, distributed smart camera networks are gaining more and more attention. The idea corresponds with the current Internet of Things trend[3]. In such networks, most of the processing is performed in the measurement node (a smart camera) with a certain degree of autonomy [5][2]. As only the information that is useful from the point of view of the application is transmitted to the central server or other cameras in the network, the load on communication infrastructure is reduced.

The autonomy of the smart camera allows to adjust the activity rate of the sensor to current conditions, which in turn reduces the power consumption. Furthermore, it also allows the collaborative, network-wide execution of designated tasks.

In this article, we present a smart camera architecture based on heterogeneous system-on-chip (SoC) Xilinx Zynq platform [27]. The device integrates a dual-core microprocessor, a pool of programmable logic resources and other peripherals in a single chip, enabling the implementation of highly integrated, low power, high performance embedded systems.

2 An Overview of the Existing Solutions

Depending on the perceived role of the smart camera in the network, existing solutions can be divided into three distinctive categories:

2.1 Semi-disposable, Widely Deployed Sensor Nodes

The main focus of the design of the smart cameras in this category is their low cost and low power consumption. As they are intended for possibly long battery operation, they are equipped with low power, yet relatively slow microprocessors or microcontrollers and rather slow communication interfaces. The processing power allows to perform simple operations on low resolution images (CIF, QCIF, QVGA) with the speed of a few frames per second or less. The interface is in most cases based on a low power, low bandwidth solution, e.g. ZigBee [14] or 6LoWPAN. The use of such an interface improves battery life, but on the other hand it is too slow for the transmission of images at high framerates. Moreover, the computational platform is usually not fast enough to compress the acquired images or video stream. The data transmitted in such sensor networks is usually constrained to observed scene metadata [22].

2.2 Application Processor and DSP-Based Smart Cameras

As the low power consumption is not always the primary concern and more sophisticated image and video processing requires more computational power,

smart camera designs are usually powered with application processors [9][10], digital signal processors (DSPs) [11][16] or a combinations of both for enhanced flexibility [25]. Such solutions are capable of performing video analysis in real-time. In many cases, they are also capable of on-the-fly video coding, so beside the scene metadata they can transmit the live video stream for viewing, logging and archiving. Video streaming requires a relatively high speed communication interface, contributing to the overall power consumption of the system [24]. The most common approach is using existing Ethernet or WiFi infrastructure.

2.3 Smart Cameras Using FPGAs

As shown in [4], computer vision algorithm implementations based on FPGAs can reach the performance beyond the capabilities of modern microprocessors. This is especially true for image processing operations based on pixel-level or neighbourhood-level access, as the FPGAs are inherently capable of massively parallel processing. Parallelism can also be achieved using GPUs, but such approach is usually not feasible for smart cameras because of the power constraints. Dedicated, application-specific integrated circuits like the one presented in [1] are another alternative. However, as the demands on computational power increase, the cost of development and implementation of specialised integrated circuits using state of the art fabrication process node becomes increasingly prohibitive. FPGAs are easily reconfigurable and offer the capability of connection with multiple external devices, e.g. CMOS imagers, other sensors, communication interfaces. However, dedicated programmable logic coprocessors are not well suited for high-level processing tasks that exhibit data-dependancy and irregular control flow. Thus, programmable processors are the prime choice for these tasks. On the other hand, the amount of logic resources in modern FPGAs is enough to implement a multicore microprocessor system along with specialised image processing hardware. In the light of the above, FPGAs are often viewed as an interesting computational platform for smart camera implementation, either standalone [7][6], or as a part of a system [19][23].

3 Architecture of the Proposed System

The opposing requirements of high computational capabilities and low power usage make choosing the platform for smart camera a complicated task. In our previous work [17], [13] we implemented image processing algorithms using FPGA devices (Xilinx Spartan 6 and Virtex 6) as the computational platform. These solutions were leveraging the reprogrammable logic for accelerating the image processing task while using soft processor cores (MicroBlaze) for communication and control functions. The algorithms that were difficult to implement in hardware had to be partitioned between many soft processors cores. The performed tasks required the implementation of a few of such processors due to their relatively low computational performance. This in turn resulted in the increased use of FPGA resources.

The advent of Xilinx Zynq devices, which combine high-performance dual ARM Cortex A9 microprocessor cores and a large pool of programmable logic resources, opens the way to the implementation of mixed, heterogeneous, integrated architectures, in which hardware accelerators can work alongside the general purpose processors. This provides a significant advantage over the solutions presented in section 2.3, as such architecture combines the best of microprocessor and programmable logic worlds in a single chip and provides mechanisms for high-throughput communication between these two domains. On the other hand, taking advantage of both parts of the device and dividing the workload to achieve the optimal performance is not an easy task.

The presented solution is a general framework for Xilinx Zynq devices, allowing seamless cooperation of the hardware coprocessors and the high level software-based algorithms (e.g. algorithms from the OpenCV library) running on the Cortex A9 cores. The architecture provides means for transporting the data between the processing elements in the system and the external memory. In addition, it offers an easy way of setting the parameters of hardware coprocessors. The schematic of proposed architecture is presented in Fig. 1.

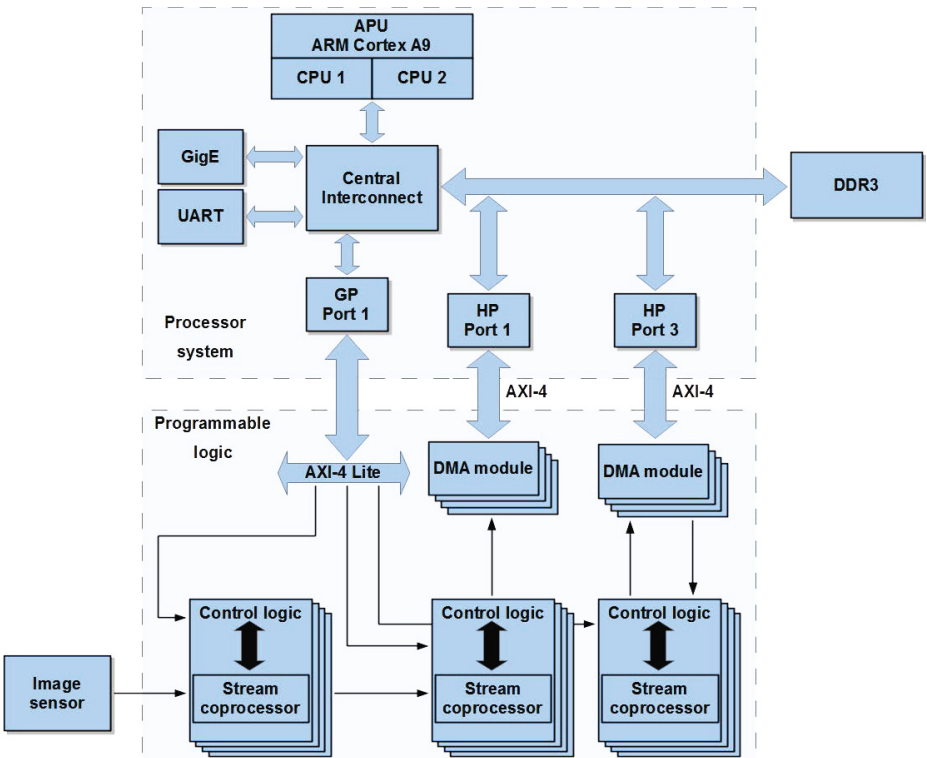


Fig. 1. The block diagram of the proposed system architecture

The architecture is based on the assumption that most of the computationally intensive operations should be performed by specialised coprocessors implemented in programmable logic. Such an approach is suitable for achieving high performance and low power as long as the algorithm being implemented is receptive to parallelization and operates on continuous stream of data instead of requiring random access to memory. Exemplary system presented in Fig. 1 acquires the input data directly from the image sensor or from a dedicated hardware block. Using such dedicated functional blocks, the data can be provided by e.g. GigE Vision IP camera connected to Ethernet port in the processor subsystem or read from the external memory. In each case, the image has to be converted to a stream of pixels encapsulated in AXI4-Stream interface [26]. Data in this format is provided to one or multiple processing elements (PE). Each PE consist of some control logic and stream coprocessor. The detailed structure of PE is shown in Fig. 2.

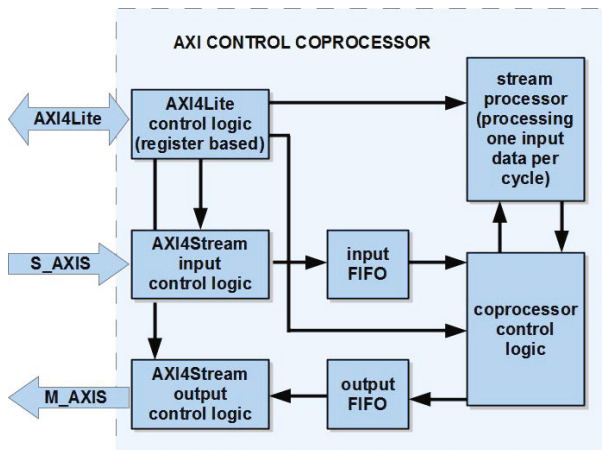


Fig. 2. The block diagram of the coprocessor control IP-core

The incoming data provided in AXI4-Stream format is buffered by input FIFO. The stream processor operates only when the input data (stored in input FIFO) is available and the output FIFO is not full. This design makes it possible to use different clock domains for the communication and the processing part, which is handy when e.g. the data is provided as 256-bit wide vectors while the stream processor input accepts 8-bit data. The provided coprocessor control logic block is very flexible, which makes it easy to implement various image processing algorithms without any concerns about communication and data transfers. In addition a dedicated AXI4-Lite interface is used for configuring parameters of stream processor (e.g. filter coefficients or threshold values).

As shown in Fig. 1, the PEs can be linked to each other provided the output of the preceding one is compatible with the input of the following PE. This can be

used for linking subsequent filtering or morphological operations or connecting the detector of feature points to the descriptor without storing the intermediate results in external memory. In each case, the final outcome of processing are transferred to external memory using DMA (Direct Memory Access) modules. Using the DMA modules is beneficial for the overall system performance, as it assures, that all the memory transfers from and to the PEs are handled by the memory controller exclusively. The processing results stored in in the memory can be fetched by other PE or by the software running on ARM cores. In such a solution, the processor cores act as a class of PE and can be used to implement algorithms that are otherwise difficult to implement in programmable logic. It should be noted, that unlike the PEs implemented with programmable logic, the ARM cores are limited to two instances and cannot be replicated. Additionally, in case of the smart camera, the processor is used for the communication with external world using the Ethernet or WiFi interface and for the control of the PEs.

The presented architecture of a smart camera can be applied in various use cases, such as automated surveillance or product inspection. The process of adapting the framework to the task should start with pure software implementation, followed by the transfer of the most computationally intensive parts to the hardware. Algorithms that perform pixel-level or neighbourhood-level operations are the best candidates for that, and can be placed in the system just after sensor acquisition module. Provided coprocessor controller simplifies the hardware implementation and hides the communication details from the user. The high level image processing algorithms (e.g. object recognition) can be converted to dedicated hardware coprocessors or, if it is not a viable solution, run on the processor cores. The standard ARM processor implemented in Zynq devices can allow the use of Linux operating system alongside popular image processing libraries (e.g. OpenCV). Modular architecture of the presented solution can be tailored to the application by replicating the PEs for higher degree of parallelism.

4 Example Results

To prove its feasibility and usefulness, the presented smart camera architecture was tested using two different vision applications. The first one was moving object detection and labelling [12], while the other one was point feature detection, description and matching. Schematics for both of this systems are shown in Fig. 3. In case of the solutions, only the coprocessor part was presented, as the processor subsystem was identical.

The moving object detection system uses approximate median algorithm presented in [20] with additional filtering and morphological operations implemented in hardware. The labelling operation is performed by ARM cores, which allows for parallel operation. The system achieves over 300 frames per second for VGA images and over 20 for frames per second for 1920x1080 images. The detailed information about processing speed and comparison to PC is presented in table 1, while resources usage is shown in table 2.

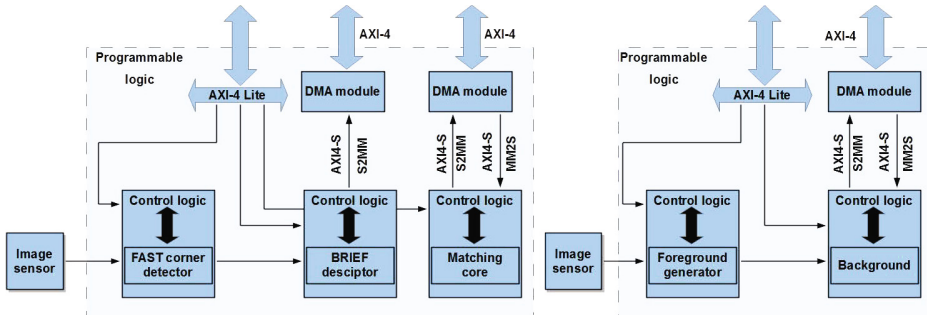


Fig. 3. On the left - block diagram of feature point detection, description and matching system. On the right - block diagram of moving object detection system.

The feature detection, description and matching system performs each of its primary operations in hardware. The image registered by the sensor is passed through AXI4-Stream interface to the first processing blocks - the FAST detector [21] and then to BRIEF descriptor [8]. For each incoming pixel, the coprocessors check if it is an interest point and calculate its descriptor. The descriptor is only saved if the pixel is considered to be a feature point. The results provided by this IP cores are sent to the external DDR RAM memory using the DMA engine. After two consecutive images are processed, the processor requests the matching module to find best matches between vectors of descriptors from both images. The appropriate data (descriptors) is send from DDR RAM memory to dedicated hardware matcher block and as a result, the best match for each interest point is found. Further processing can be done using general purpose ARM cores. The system can achieve over 300 VGA frames per second, while the matcher with four matching cores can keep up with detection and description of up to approximately 1100 feature points found in each matched image. Resources usage by this system is shown in table 2.

Table 1. Processing times for different resolutions and processing platforms given in milliseconds

| Resolution | | 640x480 | | 1920x1080 | |
|------------------|----------|---------|------|-----------|-------|
| Platform | | Zynq | PC | Zynq | PC |
| image processing | software | 42,45 | 2,80 | 285,53 | 18,15 |
| | hardware | 3,10 | N/A | 20,94 | N/A |
| labeling | software | 3,27 | 1,05 | 21,86 | 7,10 |

Table 2. Resource usage of the implemented design (designations: FFs - flip-flops, LUTs - lookup tables, BRAMs - block RAM memory blocks). The values in percent are given with respect to all corresponding resources available in XC7Z020 device.

| | FF | LUT | BRAMs |
|--------------------------|---------------|---------------|------------|
| approx. median system | 8612 (16,19) | 9745 (9,16) | 20 (14,29) |
| det. desc. match. system | 18314 (34,42) | 27422 (25,77) | 55 (39,29) |
| XC7Z020 | 53200 | 106400 | 140 |

Both of the described test systems were implemented using the low-cost Zed-board evaluation board. It hosts Xilinx Zynq-7000 SoC (XC7Z020-CLG484-1), 512 MB of DDR3 RAM, Gigabit Ethernet port, USB host, HDMI output and FMC connector for image sensor connection and has the ability to boot Linux from the SD card.

5 Conclusions and Future Work

Using hybrid heterogeneous reprogrammable devices allows for the integration of the low-level, pixel-based and neighbourhood-based image processing algorithms alongside the more complex and sophisticated ones (like object detection and matching) with a single device. Such solution offers high performance enabling real-time image processing with a relatively low power consumption. The presented architecture makes seamless integration of various processing elements and microprocessor cores in a single device possible. It is achieved by laying down the high-performance on-chip communication infrastructure based on the dedicated DMA channels and interfaces allowing the configuration of processing elements. The infrastructure was designed to use a standard streaming interface, which simplifies the implementation its components.

Future work will focus on broadening the range of available hardware coprocessors and analysing of performance in more complex applications.

Acknowledgment. This research was financed by the Polish National Science Centre grant funded according to the decision DEC-2011/03/N/ST6/03022, which is gratefully acknowledged.

References

1. Abbo, A., Kleihorst, R., Choudhary, V., Sevat, L., Wielage, P., Mouy, S., Vermeulen, B., Heijligers, M.: Xetal-II: A 107 GOPS, 600 mW massively parallel processor for video scene analysis. *IEEE Journal of Solid-State Circuits* 43(1), 192–201 (2008)

2. Aghajan, H., Cavallaro, A.: Multi-camera networks: principles and applications. Academic Press (2009)
3. Atzori, L., Iera, A., Morabito, G.: The internet of things: A survey. *Computer Networks* 54(15), 2787–2805 (2010)
4. Bailey, D.G.: Design for embedded image processing on FPGAs. John Wiley & Sons (2011)
5. Bhanu, B., Ravishankar, C., Roy-Chowdhury, A., Aghajan, H., Terzopoulos, D.: Distributed Video Sensor Networks. Springer (2011)
6. Birem, M., Berry, F.: DreamCam: A modular FPGA-based smart camera architecture. *Journal of Systems Architecture* 60(6), 519–527 (2014)
7. Bourrasset, C., Serot, J., Berry, F.: FPGA-based smart camera mote for pervasive wireless network. In: Proc. of International Conference on Distributed Smart Cameras (ICDSC), pp. 1–6 (October 2013)
8. Calonder, M., Lepetit, V., Ozuysal, M., Trzcinski, T., Strecha, C., Fua, P.: BRIEF: Computing a local binary descriptor very fast. *IEEE Transactions on Pattern Analysis and Machine Intelligence* 34(7), 1281–1298 (2012)
9. Chen, P., Ahammad, P., Boyer, C., Huang, S.I., Lin, L., Lobaton, E., Meingast, M., Oh, S., Wang, S., Yan, P., et al.: CITRIC: A low-bandwidth wireless camera network platform. In: Proc. of International Conference on Distributed Smart Cameras, pp. 1–10. IEEE (2008)
10. Chen, P., Hong, K., Naikal, N., Sastry, S.S., Tygar, D., Yan, P., Yang, A.Y., Chang, L.C., Lin, L., Wang, S., Lobatón, E., Oh, S., Ahammad, P.: A low-bandwidth camera sensor platform with applications in smart camera networks. *ACM Transactions on Sensor Networks* 9(2), 21:1–21:23 (2013)
11. Di Caterina, G., Hunter, I., Soraghan, J.: An embedded smart surveillance system for target tracking using a PTZ camera. In: 2010 4th European Education and Research Conference (EDERC), pp. 165–169 (December 2010)
12. Fularz, M., Kraft, M., Kasinski, A., Acasandrei, L.: A hybrid system on chip solution for the detection and labeling of moving objects in video streams. In: Signal Processing: Algorithms, Architectures, Arrangements, and Applications (SPA), pp. 94–99 (September 2013)
13. Fularz, M., Kraft, M., Schmidt, A., Kasiński, A.: FPGA implementation of the robust essential matrix estimation with RANSAC and the 8-point and the 5-point method. In: Keller, R., Kramer, D., Weiss, J.-P. (eds.) Facing the Multicore - Challenge II. LNCS, vol. 7174, pp. 60–71. Springer, Heidelberg (2012)
14. Hengstler, S., Prashanth, D., Fong, S., Aghajan, H.: Mesheye: A hybrid-resolution smart camera mote for applications in distributed intelligent surveillance. In: 6th International Symposium on Information Processing in Sensor Networks, IPSN 2007, pp. 360–369 (April 2007)
15. Jin, X., Goto, S.: Encoder adaptable difference detection for low power video compression in surveillance system. *Signal Processing: Image Communication* 26(3), 130–142 (2011)
16. Kandhalu, A., Rowe, A., Rajkumar, R.: Dspcam: A camera sensor system for surveillance networks. In: Third ACM/IEEE International Conference on Distributed Smart Cameras, ICDSC 2009, pp. 1–7 (August 2009)
17. Kraft, M., Fularz, M., Kasiński, A.: System on chip coprocessors for high speed image feature detection and matching. In: Blanc-Talon, J., Kleihorst, R., Philips, W., Popescu, D., Scheunders, P. (eds.) ACIVS 2011. LNCS, vol. 6915, pp. 599–610. Springer, Heidelberg (2011)

18. Ma, T., Hempel, M., Peng, D., Sharif, H.: A survey of energy-efficient compression and communication techniques for multimedia in resource constrained systems. *IEEE Communications Surveys Tutorials* 15(3), 963–972 (2013)
19. Maggiani, L., Salvadori, C., Petracca, M., Pagano, P., Saletti, R.: Reconfigurable FPGA architecture for computer vision applications in smart camera networks. In: 2013 Seventh International Conference on Distributed Smart Cameras (ICDSC), pp. 1–6 (October 2013)
20. McFarlane, N., Schofield, C.: Segmentation and tracking of piglets in images. *Machine Vision and Applications* 8(3), 187–193 (1995)
21. Rosten, E., Drummond, T.W.: Machine learning for high-speed corner detection. In: Leonardis, A., Bischof, H., Pinz, A. (eds.) *ECCV 2006, Part I*. LNCS, vol. 3951, pp. 430–443. Springer, Heidelberg (2006)
22. Seema, A., Reisslein, M.: Towards efficient wireless video sensor networks: A survey of existing node architectures and proposal for a Flexi-WVSNP design. *IEEE Communications Surveys Tutorials* 13(3), 462–486 (2011)
23. Tomasi, M., Pundlik, S., Luo, G.: FPGA–DSP co-processing for feature tracking in smart video sensors. *Journal of Real-Time Image Processing*, 1–17 (2014)
24. Winkler, T., Rinner, B.: Pervasive smart camera networks exploiting heterogeneous wireless channels. In: *IEEE International Conference on Pervasive Computing and Communications, PerCom 2009*, pp. 1–4 (March 2009)
25. Winkler, T., Rinner, B.: Trustcam: Security and privacy-protection for an embedded smart camera based on trusted computing. In: 2010 Seventh IEEE International Conference on Advanced Video and Signal Based Surveillance (AVSS), pp. 593–600 (August 2010)
26. Xilinx Inc.: AXI Reference Guide, Version 13.4 (2012)
27. Xilinx Inc.: Zynq-7000 all programmable SoC overview (August 2012)

Nature-Inspired, Parallel Object Recognition

Bogdan Harasymowicz-Boggio, Łukasz Chechliński,
and Barbara Siemiątkowska*

Institute of Automatic Control And Robotics,
Faculty of Mechatronics, Warsaw University of Technology, Poland
`rrg.mchtr.pw.edu.pl`

Abstract. In this article we present a massively parallel object recognition system designed to operate on-line, processing data acquired by indoor mobile robots equipped with 3D cameras. Inspired by the properties of the mammalian visual cortex, the proposed method incorporates a learned, selective use of features for the recognition of specific objects of interest, as well as a pre-processing stage of simultaneous localization and mapping (featuring Kinect Fusion) and a new parallel, heuristic scene segmentation algorithm. The benefits of applying class-specific feature spaces are demonstrated in an experiment carried using indoor scenes containing multiple common household objects.

Keywords: Object recognition, parallel, Kinect Fusion, nature-inspired, RGB-D features.

1 Introduction

Current research aims to develop companion and service mobile robots that operate in a complex human environment. In order for these robots to perform useful tasks, understanding the elements of the environment and thus, having some human-like perceptual capacities is an absolute necessity. However, for natural tasks such as image understanding, the processing power of current computers is incomparably smaller than that of the human brain. Perceptual tasks that are time consuming and difficult in computer vision are solved by people very quickly [3]. Many neurons of the retina, lateral geniculate nucleus (LGN) and visual cortex process optical information in parallel, which comes from over 100 million photoreceptors.

Nowadays, when due to physical constraints, the possibilities of further boosting clock rates of silicon-based CPUs is very limited, the use of graphics processing units (GPUs) – which are parallel and faster by several orders of magnitude – is essential for the further development of computer vision in robotics. However, the researchers developing 3D scene understanding methods rarely make use of this high computational power.

* The work described in this paper was partially conducted within the project 2012/05/B/ST6/03094 financed by the National Science Centre, which is gratefully acknowledged.

The popularization of fast and accessible depth cameras – the Kinect and PrimeSense sensors has opened wide application possibilities of 3D computer vision, including indoor mobile robotics. Compared to 2D cameras, these sensors provide much more information, which also requires much more computational power to be used. While modern CPUs are sufficient for most 2D on-line computer vision tasks, significantly lack the capacity to efficiently process large point clouds, taking up to several minutes to complete demanding algorithms on unorganized clouds.

State-of-the-art 3D object recognition methods, such as [13,11] consist in extracting low-level features from point clusters (3D image segments) and simplifying these clusters to single vectors (e.g. by calculating histograms). These methods rely on fixed feature spaces, meaning that the same features are used to classify every considered scene region. However, from a more intuitive point of view, we can conclude that different features are of different significance for recognition of particular objects (e.g. in human perception a specific rigid shape is an important quality of dishes, clothes are associated with texture and deformable shapes, and fruits may be linked to specific colors).

This intuition is backed by the findings of neurobiology. It is known that different qualities of the perceived objects [4,9,17], such as shape deduced from contours, shape deduced from shading, color properties and movement are processed in parallel and integrated in different regions of the brain. These features are processed hierarchically in several layers [8] of the visual cortex in a bottom-up process [16]. The signals flow from lower to higher levels. The higher the layer, the more complex and abstract the detected features of the image: higher layers associate multiple signals from the lower layers and combine them into higher-level features. However, the formation of specific features is conditioned by the repeated co-occurrence of specific stimuli in the presence of a perceived object at the learning stage. This feature learning involves both, bottom-up and top-down processes. Top-down processing is used in many other natural perception tasks, such as object tracking and prediction of an object's pose.

Another oversimplified aspect of current computer vision systems is the use of independent camera frames as input data. This approach is justified in many 2D vision systems, as modern high-definition cameras have very low noise levels and, detail and color quality. This is not the case, however, for depth sensors, which are much less accurate and provide significantly lower resolutions (e.g. 320x240 pixels for the Kinect sensor). Research on spatial memory [2] has confirmed that animals build spatial maps of their environment in a cumulative manner, using a continuous stream of input stimuli. This allows to possess and take advantage of a much wider range of useful information than is available in momentary sensory input and makes it possible to detect changes in the environment.

In this article we present a 3D object recognition system that uses massively parallel computing at each stage and comprises elements that resemble processes naturally occurring in the visual cortex of mammals. Our most important contribution is the object-dependent use of particular features for recognition – these feature spaces are learned in a top-down manner. Another quality of the

presented system is the cumulative integration of the perceived scene (by applying the Kinect Fusion SLAM algorithm), instead of independently processing individual frames. Furthermore, we describe a new parallel, heuristic segmentation method for point clouds. The following 3 sections concern these processing stages and the final section presents the experiments performed to validate the proposed system.

2 Pre-processing SLAM

Pre-processing techniques are very common in 2D object recognition, but rarely used and less developed for 3D scenes. Some examples of point cloud pre-processing for recognition algorithms are: voxel grid filtering, pass-through filtering, bilateral filtering, convex-hull calculation and outlier removal techniques [15]. These methods, however, are used to process data obtained from single sensor frames and intend to simplify surfaces mainly by removing statistically less significant details.

SLAM techniques (Simultaneous Localization and Mapping) can also be regarded as point cloud pre-processing, applied to obtain an augmented scene by aggregating data acquired by a moving sensor over a period of time. Such techniques are used to build 3D models of the environment that are not limited to a single viewpoint. The scenes resulting from advanced SLAM methods can be very large and even contain complete detailed models of buildings [7]. Besides often being the result of the operation of a mobile robot (in exploration and mapping tasks), in robotic systems scenes integrated with SLAM have such applications as 3D motion planning.

The introduction of such techniques as Kinect Fusion [10] has shown that SLAM techniques can provide not only larger, but significantly refined 3D scenes. Kinect Fusion is a massively parallel algorithm that builds a voxel-based scene model. For each frame this model is projected to the image plane and compared to the current depth map in order to localize the sensor. The incoming depth data is then aggregated to the model, which fills existing gaps and refines the details of the captured surfaces. As shown in figure 1, after a brief run of Kinect Fusion the level of visible details is much higher than for the input point clouds and the gaps are greatly reduced. Such result can be achieved only by using a moving sensor, which provides multiple frames of the same surfaces viewed from slightly different positions – this reduces both random and systematic errors.

As far as we know, Kinect Fusion has not yet been used for general purpose object recognition. The quality of the output scenes combined with high efficiency make it especially appealing to apply this method at a pre-processing stage for recognition on moving robots (as a moving sensor is required). Because the publicly available implementation of Kinect Fusion (in the PCL library), as most SLAM methods, is intended to register static environments, it cumulates errors when changing elements appear. To avoid this, we have adapted the algorithm for on-line use on a robot by cyclically re-initializing the voxel map building process. The on-line use of Kinect Fusion has enabled us to provide a

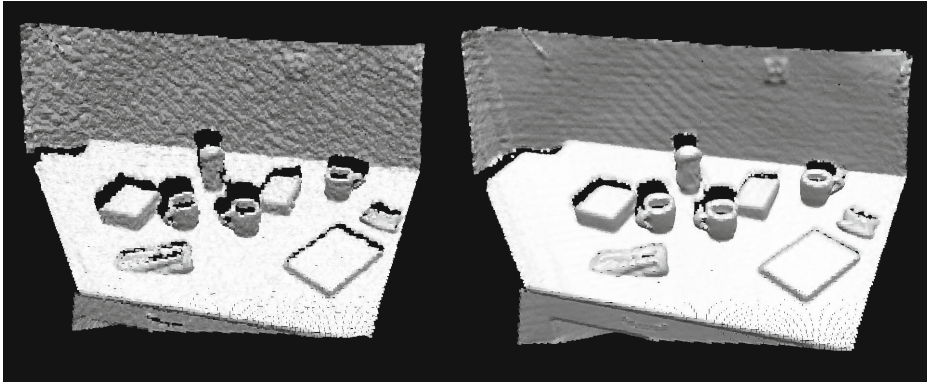


Fig. 1. 3D single Kinect frame enhanced with voxel grid and bilateral filtering (on the left) compared to the same scene obtained with Kinect Fusion after 3 seconds of SLAM with minimal camera movement (on the right)

mobile vision system with 3D input scenes of much higher quality than it would be achievable using simple pre-processing techniques.

3 Parallel Segmentation

The classic approach to the problem of 3D indoor scene segmentation is to detect and remove the largest planar surfaces (which represent structural elements of the building or furniture) and then apply euclidean clustering [14]. The flat surfaces are typically found iteratively, using a RANSAC (Random Sample Consensus) algorithm for matching a plane model to scene points. After a plane is successfully matched and removed, the fitting is repeated for the remaining points until no planes with the required minimal number of points are found. This procedure has important limitations: the RANSAC algorithm is very time-consuming and has not been parallelized yet in available implementations. For accurate fitting of a plane, the RANSAC output requires several post-processing steps of ICP (Iterative Closest Point) [1] and may leave undetected gaps if the surface is slightly curved. The number of times these methods need to be run is data-dependent (i.e. until there are no more large flat areas).

We propose a parallel form of plane-based segmentation, which we have implemented for CUDA architectures. Instead of using RANSAC, our method relies on unseeded region growth of a complexity that is not data-dependent. Each point of the cloud is assigned its own “seed”, which competes with other seeds in a parallel manner. Figure 2 presents the flowchart for a single thread.

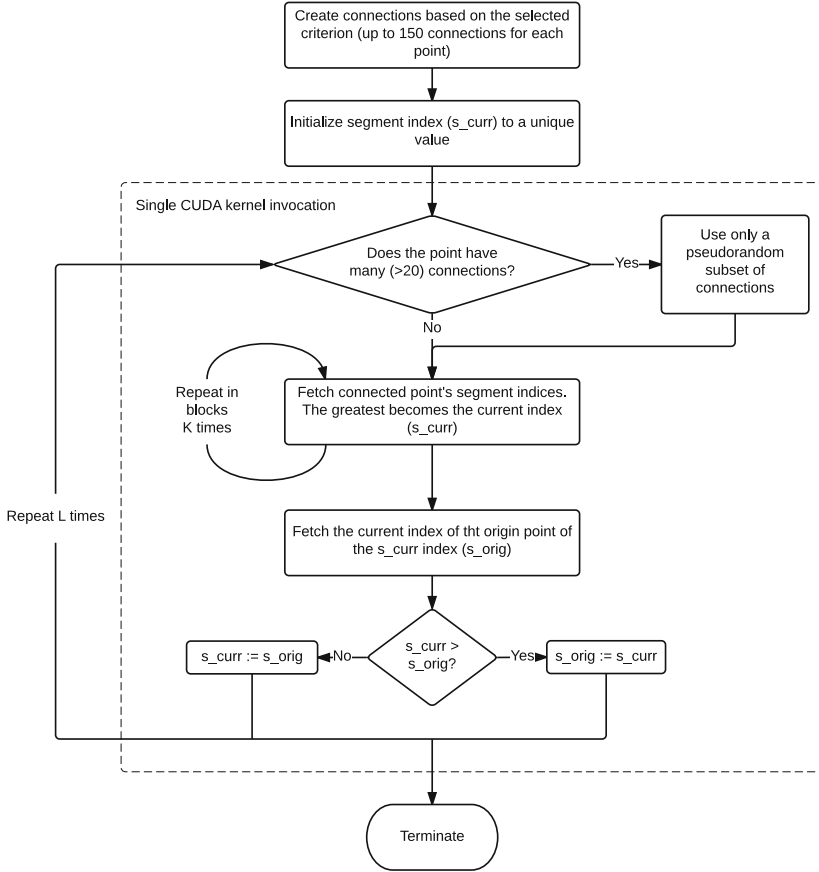


Fig. 2. Diagram of our parallel region growth algorithm for one thread. The conditional statements are heuristics that save unnecessary computation for well interconnected regions and speed up the segments' propagation.

In order to segment *props* (following the terminology used in [11], props are understood as objects that can be easily moved around), we use the presented parallel algorithm twice. In the first run we connect neighboring points with similar surface normal vectors (up to a given angle difference threshold). After the region growth completes, the resulting segments are projected into planes perpendicular to their average normal vectors, after which we threshold the dimensions of their 2D bounding boxes, obtaining *large* flat areas. For the second region growth step we interconnect all neighboring points, excluding only points belonging to the found *large* flat segments. The output for this step are spatially connected clusters separated from large flat surfaces, such as walls and furniture. The result for a test scene is presented in figure 3. For decent GPUs our segmentation algorithm achieves overall processing times of about 50 ms for scenes containing over 100000 points.

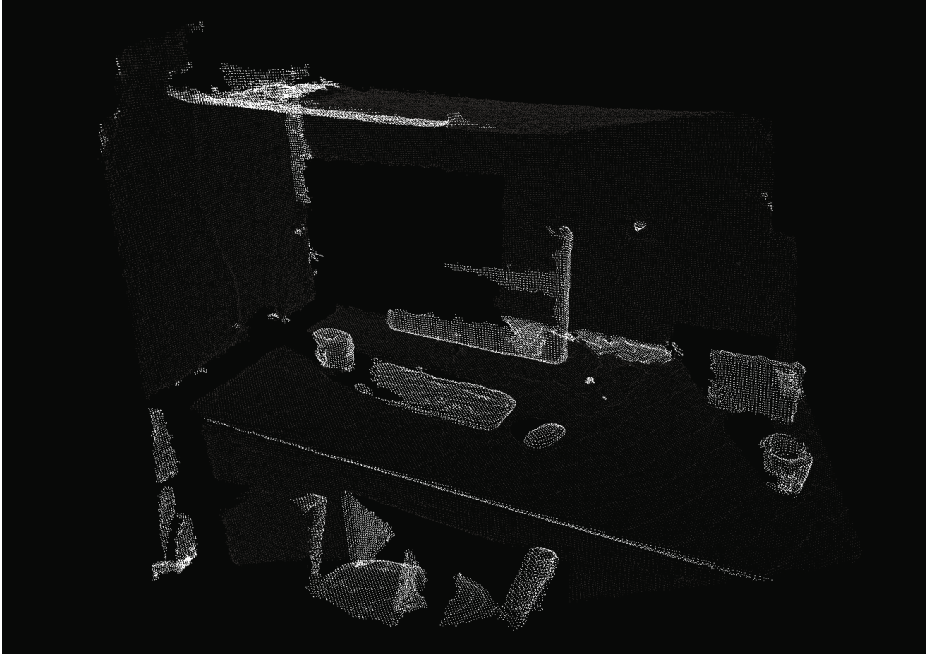


Fig. 3. Result of parallel props extraction performed in 51.17ms for 136765 points. The clusters segmented from large flat surfaces have been highlighted.

4 Feature Significance

As stated in the introduction, in the natural object recognition process, signals flow between layers of the mammal visual cortex both, in a bottom-up and top-down manner. Conventional object recognition methods apply only the former pattern, attempting to classify extracted scene segments in a fixed feature space. In the system presented in this article we also apply top-down-acquired information by selecting the features involved in the recognition process of each known object individually.

The applied methodology involves a mechanism to determine the significance of particular features relative to particular object classes at the learning stage. We have proposed such a methods in our previous works [6,5], which we briefly explain in this section.

We assume we are provided a training set, which consists of 3D views grouped in subsets representing semantic object classes. For any given feature, we simplify these views to equal length vectors. This can be achieved e.g. by calculating feature histograms. We obtain a 2D array of vectors \mathbf{V} , consisting of N class vectors \mathbf{C}_i , $i = 1, \dots, N$, each having M_i views.

$$\mathbf{V} = [\mathbf{C}_i], \mathbf{C}_i = [v_{ij}] \quad (1)$$

Using this representation, we define the *mean class similarity matrix* for a selected measure of vector similarity $s(x, y)$ (such as $L2$ distance or Person's correlation coefficient 4) for each histogram feature f as:

$$\mathbf{G} = [g_{ij}] = \left[\overline{s(v_{ip}, v_{jq})} \right], \quad (2)$$

$$v_{ip} \in \mathbf{C}_i, v_{jq} \in \mathbf{C}_j \vee v_{ip} \neq v_{jq}$$

Finally, we apply a Mahalanobis-like distance function to calculate a single-column matrix denoted as *class uniqueness*:

$$\mathbf{U} = [u_i] = \left[\frac{g_{ii} - \bar{g}_{ij}}{\sigma_i} \right], i \neq j \quad (3)$$

where σ_i represents the standard deviation of similarity for all the available view pairs which belong to class i . This quantity measures the capacity of a vector feature (or feature histogram) to differentiate each object class from other classes. If this capacity is high, the auto-similarity g_{ii} will be significantly higher than the mean similarity to other classes \bar{g}_{ij} . The variance normalization takes into consideration that the scale of these similarity values for the dataset is unknown.

In this work we present and test the application of knowledge obtained calculating this uniqueness measure for object recognition on real scenes. At the learning stage we calculate all the feature histograms for the objects of the training dataset in order to obtain the class uniqueness values for each semantic class. We apply a simple threshold to this parameter to determine which features are significant for particular objects, and thus should be considered in the recognition process. At the recognition stage the feature histograms for all the clusters obtained from segmentation are calculated and compared (using only significant features) with the corresponding histograms of model objects. For both stages in the experiment presented in the final section we have applied the known Pearson's correlation coefficient to compare histograms:

$$s_P(x, y) = \frac{\text{cov}(\mathbf{x}, \mathbf{y})}{\sigma_{\mathbf{x}}\sigma_{\mathbf{y}}} = \frac{E[(\mathbf{x} - \mu_{\mathbf{x}})(\mathbf{y} - \mu_{\mathbf{y}})]}{\sigma_{\mathbf{x}}\sigma_{\mathbf{y}}} \quad (4)$$

Multiple RGB-D features are considered by the presented system: *inclination, convexity, anisotropy of convexity, hue, saturation, D2-D4* histogram shape descriptors [12], as well as 2D histograms combining these features. The features' calculation algorithms are provided in [6,5]. The segments are classified using a *nearest neighbors* procedure, i.e. measuring their similarity to the model views for the relevant features. This similarity (or inverse distance) is calculated as:

$$D^{-1}(x, y) = \frac{\sum s_i(x, y)w_i}{\sum w_i} \quad (5)$$

where $s_i(x, y)$ is the applied vector similarity measure for the i -th feature histograms (in our case, Pearson's correlation) and w_i is a binary weight: 1 if the feature is significant and 0 otherwise.

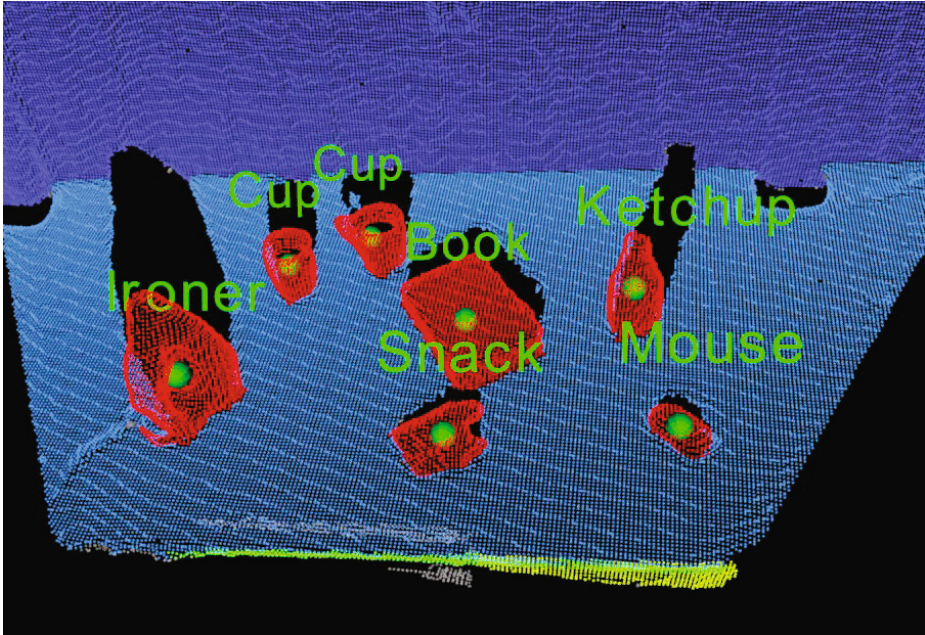


Fig. 4. Example recognition results

5 Experiments

The object recognition system featuring the algorithms described in this article has been implemented for GPU devices with CUDA architecture. The experiments were carried using a computer equipped with a *GTX Titan Black* graphics card with 2880 cuda cores. The scenes were acquired with a moving Kinect sensor and enhanced with the on-line adaptation of Kinect Fusion.

In order to validate the use of class uniqueness for class-dependent feature selection, we have built a training set consisting 28 different object views. The set was used to extract model histograms and calculate class uniqueness for particular semantic object classes. The semantic classes of these objects were: *cup*, *ketchup*, *mouse*, *book*, *ironer*, *snack*. A second, test set, consisting of 12 scenes containing various objects (including, but not limited to the training object instances and classes) was also collected and submitted to the full segmentation and recognition procedure. Figure 4 presents the output recognition visualization for an example scene.

We have compared the recognition quality for two methods of calculating class scores: a) using all the available features to compare the scene clusters to the model views and b) using only the features selected at the learning stage. In both cases the recognition score thresholds were tuned to maximize performance on the training set. Figure 5 summarizes the obtained results. As we can see, the

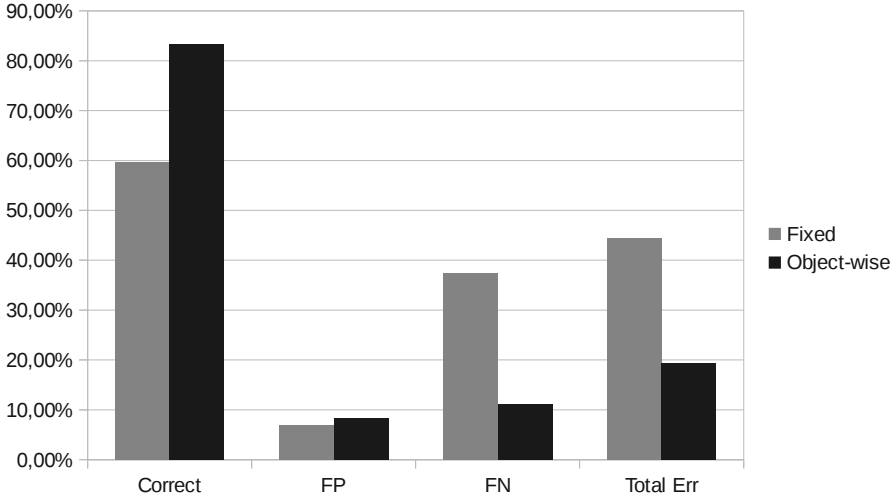


Fig. 5. Experiment results comparing the performance of the system using a fixed feature space with the system using object-wise features. The results of correct detection, false positive (FP), false negative (FN) and total error rates are relative to the total number of known object instances present on the test scenes.

overall error rates are significantly reduced when applying the learned, object-wise feature spaces. The false positive error has slightly increased, but is in both cases small. This is caused by the adjustment of recognition thresholds for both systems – the object-wise system could benefit from a higher tolerance, which produced much more false positive cases for the fixed-space system. To confirm this, a larger experiment involving more known and unknown objects should be performed.

6 Conclusion

We have proposed an object recognition method for mobile robots that learns the relevance of particular features for specific objects. It is computationally efficient (as the implementation is fully parallel) and takes advantage of the movement of mobile robots to perform pre-processing SLAM (using Kinect Fusion), which enhances the scenes' quality. In the experiment we have demonstrated the improvement of recognition rates associated with the introduction of object-wise features. However, larger experiments need to be performed, a.o. using different segmentation methods. Further improvement could be made by weighting the features according to the calculated uniqueness. Features that carry redundant information could be also detected and removed.

References

1. Besl, P., McKay, N.D.: A method for registration of 3-d shapes. *IEEE Transactions on Pattern Analysis and Machine Intelligence* 14(2), 239–256 (1992)
2. Derdikman, D., Moser, E.I.: A manifold of spatial maps in the brain. *Trends in Cognitive Sciences* 14(12), 561–569 (2010), <http://www.sciencedirect.com/science/article/pii/S1364661310002111>, special Issue: Space, Time and Number
3. Gerardin, P., Kourtzi, Z., Mamassian, P.: Prior knowledge of illumination for 3d perception in the human brain. *PNAS* 107, 16309–16314 (2010)
4. Goodale, M.A., Milner, A.D.: Separate visual pathways for perception and action. *Trends in Neurosciences* 15(1), 20–25 (1992)
5. Harasymowicz-Boggio, B., Chechliński, Ł., Siemiątkowska, B.: Significance of RGB-D features in object recognition. *International Journal of Applied Mathematics and Computer Science* (2014) (submitted for publication)
6. Harasymowicz-Boggio, B., Siemiątkowska, B.: Istotność cech RGB-D w rozpoznawaniu obiektów. *Prace Naukowe Politechniki Warszawskiej. Elektronika* pp. 235–244 (2014)
7. Hornung, A., Wurm, K.M., Bennewitz, M., Stachniss, C., Burgard, W.: OctoMap: An efficient probabilistic 3D mapping framework based on octrees. *Autonomous Robots* (2013), <http://octomap.github.com>
8. Hubel, D.H.: *Eye, Brain, and Vision* (Scientific American Library, No 22). W. H. Freeman, drugie edn. (May 1995)
9. Humphrey, G.K., Symons, L.A., Herbert, A.M., Goodale, M.A.: A neurological dissociation between shape from shading and shape from edges. *Behav. Brain Res.* 76(1-2), 117–125 (1996)
10. Izadi, S., Kim, D., Hilliges, O., Molyneaux, D., Newcombe, R., Kohli, P., Shotton, J., Hodges, S., Freeman, D., Davison, A., Fitzgibbon, A.: Kinectfusion: real-time 3D reconstruction and interaction using a moving depth camera. In: *Proceedings of the 24th Annual ACM Symposium on User Interface Software and Technology, UIST 2011*, pp. 559–568. ACM, New York (2011)
11. Silberman, N., Hoiem, D., Kohli, P., Fergus, R.: Indoor segmentation and support inference from RGBD images. In: *Fitzgibbon, A., Lazebnik, S., Perona, P., Sato, Y., Schmid, C. (eds.) ECCV 2012, Part V. LNCS, vol. 7576*, pp. 746–760. Springer, Heidelberg (2012)
12. Osada, R., Funkhouser, T., Chazelle, B., Dobkin, D.: Matching 3d models with shape distributions. In: *Shape Modeling International*, pp. 154–166 (2001)
13. Ren, X., Bo, L., Fox, D.: RGB-(D) scene labeling: Features and algorithms. In: *2012 IEEE Conference on Computer Vision and Pattern Recognition, Providence, RI, USA, June 16-21*, pp. 2759–2766 (2012), <http://dx.doi.org/10.1109/CVPR.2012.6247999>
14. Rusu, R.B., Cousins, S.: Plane model segmentation, http://www.pointclouds.org/documentation/tutorials/planar_segmentation.php#planar-segmentation
15. Rusu, R.B., Cousins, S.: 3D is here: Point Cloud Library (PCL). In: *IEEE International Conference on Robotics and Automation (ICRA), Shanghai, China, May 9-13* (2011)
16. Smith, E., Kosslyn, S.: *Cognitive psychology: mind and brain*. Pearson Education, Pearson Prentice Hall (2009), <http://books.google.pl/books?id=YIPSNwAACAAJ>
17. Treisman, A.M., Kanwisher, N.G.: Perceiving visually presented objects: recognition, awareness, and modularity. *Curr. Opin. Neurobiol.* 8(2) (1998)

Digraphs Minimal Realisations of State Matrices for Fractional Positive Systems

Krzysztof Hryniów and Konrad Andrzej Markowski*

Warsaw University of Technology, Faculty of Electrical Engineering
Institute of Control and Industrial Electronics
Koszykowa 75, 00-662 Warsaw, Poland
{Krzysztof.Hryniow,Konrad.Markowski}@ee.pw.edu.pl
<http://nas.isep.pw.edu.pl/repo>

Abstract. This paper presents a method of the determination of characteristic polynomial realisations of the fractional positive system. The algorithm finds a complete set of all possible realisations instead of only a few realisations. In addition, all realisations in the set are minimal. The proposed method uses a parallel computing algorithm based on a digraphs theory which is used to gain much needed speed and computational power for a numeric solution. The presented procedure has been illustrated with a numerical example.

Keywords: fractional systems, positive, digraphs, algorithm.

1 Introduction

In the recent years many researchers have been interested in positive linear systems [2, 4, 11, 12, 16]. In positive systems inputs, state variables and outputs take only non-negative values [3]. Positive linear systems are defined on cones and not on linear spaces. Therefore, the theory of positive systems is more complicated than standard systems [1, 2, 4, 11, 13, 14]. The realisation problem is a very difficult task. In many research studies, we can find a canonical form of the system, i.e. constant matrix form, which satisfies the system described by the transfer function. With the use of this form we are able to write only one realisation of the system, while there exists set of solutions. The state of the art in positive systems theory is given in the monographs [4, 12, 16]. In [8, 9, 10] a solution for finding set of possible realisations of the characteristic polynomial was proposed. This means that we can find many sets of matrices which fit into a system transfer function. In this paper, a new method of determination entries of the state matrices for the fractional system described by Roesser model will be proposed and the procedure for computation of the state matrices will be given. The procedure will be illustrated with a numerical example.

The first definition of the fractional derivative was introduced by Liouville and Riemann at the end of the 19th century [18]. Mathematical fundamentals of fractional calculus are given in the monographs [17, 18, 19].

* Research has been financed with the funds of the Statutory Research of 2015.

This work has been organised as follows: Section 2 presents some notation and basic definitions of positive fractional systems and the digraphs theory. In Section 3, we construct and discuss a method for determination of the set of polynomial realisations which are based on the digraphs theory. The proposed method is illustrated by a numerical example. Finally, we give some concluding remarks, present open problems and bibliography positions.

2 Preliminaries and Problem Formulation

Notation. In this paper the following notion will be used. The set $n \times m$ of real matrices will be denoted by $\mathbb{R}^{n \times m}$ and $\mathbb{R}^n = \mathbb{R}^{n \times 1}$. If $\mathbf{G} = [g_{ij}]$ is a matrix, we write $\mathbf{G} \gg 0$ (matrix \mathbf{G} is called strictly positive), if $g_{ij} > 0$ for all i, j ; $\mathbf{G} > 0$ (matrix \mathbf{G} is called positive), if $g_{ij} > 0$ for all i, j ; $\mathbf{G} \geq 0$ (matrix \mathbf{G} is called non-negative), if $g_{ij} \geq 0$ for all i, j . The set of $n \times m$ real matrices with non-negative entries will be denoted by $\mathbb{R}_+^{n \times m}$ and $\mathbb{R}_+^n = \mathbb{R}_+^{n \times 1}$. The $n \times n$ identity matrix will be denoted by \mathbf{I}_n . For more information about the matrix theory, an interested reader may be referred to, for instance: [3], [7].

Two-dimensional Model. Let be given fractional the two-dimensional Roesser model [15]

$$\begin{bmatrix} \Delta_\alpha^h x_{i+1,j}^h \\ \Delta_\beta^v x_{i,j+1}^v \end{bmatrix} = \begin{bmatrix} \mathbf{A}_{11} & \mathbf{A}_{12} \\ \mathbf{A}_{21} & \mathbf{A}_{22} \end{bmatrix} \begin{bmatrix} x_{ij}^h \\ x_{ij}^v \end{bmatrix} + \begin{bmatrix} \mathbf{B}_1 \\ \mathbf{B}_2 \end{bmatrix} u_{ij} \quad (1a)$$

$$y_{ij} = [\mathbf{C}_1 \ \mathbf{C}_2] \begin{bmatrix} x_{ij}^h \\ x_{ij}^v \end{bmatrix} + \mathbf{D}u_{ij} \quad (1b)$$

where $x_{ij}^h \in \mathbb{R}^{n_1}$ and $x_{ij}^v \in \mathbb{R}^{n_2}$ are horizontal and vertical state vectors at the point (i, j) , $u_{ij} \in \mathbb{R}^m$, $y_{ij} \in \mathbb{R}^p$ are input and output vectors at the point (i, j) and $\mathbf{A}_{kl} \in \mathbb{R}^{n_k \times n_l}$, $k, l = 1, 2$; $\mathbf{B}_1 \in \mathbb{R}^{n_1 \times m}$, $\mathbf{B}_2 \in \mathbb{R}^{n_2 \times m}$, $\mathbf{C}_1 \in \mathbb{R}^{p \times n_1}$, $\mathbf{C}_2 \in \mathbb{R}^{p \times n_2}$, $\mathbf{D} \in \mathbb{R}^{p \times m}$.

Definition 1. The fractional horizontal difference of α -order of the discrete function x_{ij} is defined by the relation

$$\Delta_\alpha^h x_{ij} = \sum_{k=0}^i c_\alpha(k) x_{i-k,j}, \quad (2)$$

where $\alpha \in \mathbb{R}$, $n-1 < \alpha < n$, $n \in \mathbb{N}$ and

$$c_\alpha(k) = \begin{cases} 1 & \text{for } k = 0 \\ (-1)^k \binom{\alpha}{k} = (-1)^k \frac{\alpha(\alpha-1)\dots(\alpha-k+1)}{k!} & \text{for } k > 0 \end{cases} \quad (3)$$

Definition 2. The fractional horizontal difference of β -order of the discrete function x_{ij} is defined by the relation

$$\Delta_\beta^v x_{ij} = \sum_{l=0}^j c_\beta(l) x_{i,j-l}, \quad (4)$$

where $\beta \in \mathbb{R}$, $n-1 < \beta < n$, $n \in \mathbb{N}$ and

$$c_\beta(l) = \begin{cases} 1 & \text{for } l = 0 \\ (-1)^l \binom{\beta}{l} = (-1)^l \frac{\beta(\beta-1)\dots(\beta-l+1)}{l!} & \text{for } l > 0 \end{cases} \quad (5)$$

Using Definitions 1 and 2 we can write equation (1a) in the following form:

$$\begin{bmatrix} x_{i+1,j}^h \\ x_{i,j+1}^v \end{bmatrix} = \begin{bmatrix} \mathbf{A}_\alpha & \mathbf{A}_{12} \\ \mathbf{A}_{21} & \mathbf{A}_\beta \end{bmatrix} \begin{bmatrix} x_{i,j}^h \\ x_{i,j}^v \end{bmatrix} - \begin{bmatrix} \sum_{k=2}^{i+1} c_\alpha(k) x_{i-k+1,j}^h \\ \sum_{l=2}^{j+1} c_\beta(l) x_{i,j-l+1}^v \end{bmatrix} + \begin{bmatrix} \mathbf{B}_1 \\ \mathbf{B}_2 \end{bmatrix} u_{ij}, \quad (6)$$

where

$$\mathbf{A}_\alpha = \mathbf{A}_{11} + \alpha \mathbf{I}_{n_1}, \quad \mathbf{A}_\beta = \mathbf{A}_{22} + \beta \mathbf{I}_{n_2}. \quad (7)$$

Definition 3. *The system (6) is called positive fractional 2D Roesser model if $x_{ij}^h \in \mathbb{R}_+^{n_1}$, $x_{ij}^v \in \mathbb{R}_+^{n_2}$ and $y_{ij} \in \mathbb{R}_+^p$, $i, j \in \mathbb{Z}_+$ for any boundary conditions $x_{0j}^h \in \mathbb{R}_+^{n_1}$, $j \in \mathbb{Z}_+$, $x_{i0}^v \in \mathbb{R}_+^{n_2}$, $i \in \mathbb{Z}_+$ and all inputs $u_{ij} \in \mathbb{R}_+^m$, $i, j \in \mathbb{Z}_+$.*

Theorem 1. *The fractional discrete-time linear system (6) with $0 < \alpha < 1$, $0 < \beta < 1$ is positive if and only if*

$$\begin{bmatrix} \mathbf{A}_\alpha & \mathbf{A}_{12} \\ \mathbf{A}_{21} & \mathbf{A}_\beta \end{bmatrix} \in \mathbb{R}_+^{n_1 \times n_2}, \quad \begin{bmatrix} \mathbf{B}_1 \\ \mathbf{B}_2 \end{bmatrix} \in \mathbb{R}_+^{n \times m}, \quad [\mathbf{C}_1 \ \mathbf{C}_2] \in \mathbb{R}_+^{p \times m}, \quad \mathbf{D} \in \mathbb{R}_+^{p \times m}. \quad (8)$$

The proof is given in [15].

When performing the zet transformation with zero initial conditions to system (6) we have:

$$\begin{bmatrix} X^h(z_1, z_2) \\ X^v(z_1, z_2) \end{bmatrix} = \begin{bmatrix} \mathbf{I}_{n_1}(z_1 - c_\alpha) - \mathbf{A}_\alpha & -\mathbf{A}_{12} \\ -\mathbf{A}_{21} & \mathbf{I}_{n_2}(z_2 - c_\beta) - \mathbf{A}_\beta \end{bmatrix}^{-1} \begin{bmatrix} \mathbf{B}_1 \\ \mathbf{B}_2 \end{bmatrix} U(z_1, z_2) \quad (9)$$

where:

$$c_\alpha = c_\alpha(k, z_1) = \sum_{k=2}^{i+1} c_\alpha(k) z_1^{-k+1}, \quad c_\beta = c_\beta(l, z_2) = \sum_{l=2}^{j+1} c_\beta(l) z_2^{-l+1}. \quad (10)$$

The transfer matrix of the system (1a)–(1b) is given by:

$$\begin{aligned} \mathbf{T}(z_1, z_2) &= \\ &= [\mathbf{C}_1 \ \mathbf{C}_2] \begin{bmatrix} \mathbf{I}_{n_1}(z_1 - c_\alpha) - \mathbf{A}_\alpha & -\mathbf{A}_{12} \\ -\mathbf{A}_{21} & \mathbf{I}_{n_2}(z_2 - c_\beta) - \mathbf{A}_\beta \end{bmatrix}^{-1} \begin{bmatrix} \mathbf{B}_1 \\ \mathbf{B}_2 \end{bmatrix} + \mathbf{D}. \end{aligned} \quad (11)$$

In this case, the transfer matrix (11) is the function of the operators $w_\alpha = z_1 - c_\alpha$ and $w_\beta = z_2 - c_\beta$. Function has the following form

$$T(w_\alpha, w_\beta) = \frac{\sum_{i=0}^{n_1} \sum_{j=0}^{n_2} b_{ij} w_\alpha^i w_\beta^j}{w_\alpha^{n_1} w_\beta^{n_2} - \sum_{\substack{i=0 \\ i+j \neq n_1+n_2}}^{n_1} \sum_{j=0}^{n_2} d_{i,j} w_\alpha^i w_\beta^j} \quad (12)$$

for single-input single-output system and for known α, β .

Multi-dimensional Digraphs. A two-dimensional digraphs $\mathfrak{D}^{(2)}$ is a directed graph with two types of arcs and input flows. For the first time, this type of digraph was presented in papers [5] and [6]. When we generalise this approach, we can define n -dimensional digraphs \mathfrak{D}^n in the following form.

Definition 4. An n -dimensional digraphs $\mathfrak{D}^{(n)}$ is a directed graph with q types of arcs and input flows. In detail, it is $(\mathbb{S}, \mathbb{V}, \mathfrak{A}_1, \mathfrak{A}_2, \dots, \mathfrak{A}_q, \mathfrak{B}_1, \mathfrak{B}_2, \dots, \mathfrak{B}_q)$, where $\mathbb{S} = \{s_1, s_2, \dots, s_m\}$ is the set of sources, $\mathbb{V} = \{v_1, v_2, \dots, v_n\}$ is the set of vertices, $\mathfrak{A}_1, \mathfrak{A}_2, \dots, \mathfrak{A}_q$ are the subsets of $\mathbb{V} \times \mathbb{V}$ which elements are called \mathfrak{A}_1 -arcs, \mathfrak{A}_2 -arcs, \dots , \mathfrak{A}_q -arcs respectively, $\mathfrak{B}_1, \mathfrak{B}_2, \dots, \mathfrak{B}_q$ are the subsets of $\mathbb{S} \times \mathbb{V}$ which elements are called \mathfrak{B}_1 -arcs, \mathfrak{B}_2 -arcs, \dots , \mathfrak{B}_q -arcs respectively.

There exists \mathfrak{A}_1 -arc (\mathfrak{A}_2 -arc, \dots , \mathfrak{A}_q -arc) from vertex v_j to vertex v_i if and only if the (i, j) -th entry of the matrix \mathbf{A}_1 ($\mathbf{A}_2, \dots, \mathbf{A}_q$) is non-zero. There exists \mathfrak{B}_1 -arc (\mathfrak{B}_2 -arc, \dots , \mathfrak{B}_q) from source s_l to vertex v_j if and only if the l -th entry of the matrix \mathbf{B}_1 ($\mathbf{B}_2, \dots, \mathbf{B}_q$) is non-zero.

Remark 1. \mathfrak{A}_q -arcs and \mathfrak{B}_q -arcs, are drawn by the other colour or line style. In this paper, \mathfrak{A}_1 -arc and \mathfrak{B}_1 -arc is drawn by the solid line, \mathfrak{A}_2 -arc and \mathfrak{B}_2 -arc is drawn by the dashed line and \mathfrak{A}_3 -arc and \mathfrak{B}_3 -arc is drawn by a dotted line.

Our Task Is the Following: For given characteristic polynomial

$$d(w_\alpha, w_\beta) = w_\alpha^{n_1} w_\beta^{n_2} - \sum_{\substack{i=0 \\ i+j \neq n_1+n_2}}^{n_1} \sum_{j=0}^{n_2} d_{i,j} w_\alpha^i w_\beta^j \quad (13)$$

determine entries of the state matrices \mathbf{A}_α and \mathbf{A}_β , \mathbf{A}_{12} and \mathbf{A}_{21} using multi-dimensional $\mathfrak{D}^{(n)}$ digraphs theory. The dimension of the state matrices must be the minimal among possible ones and cannot contain additional coefficients of the characteristic polynomial.

3 Problem Solution

By using the transfer matrix (11) we can write the characteristic polynomial of the system (1a)-(1b) in the following form:

$$\begin{aligned} d(w_\alpha, w_\beta) &= \det \begin{bmatrix} \mathbf{I}_{n_1} w_\alpha - \mathbf{A}_\alpha & -\mathbf{A}_{12} \\ -\mathbf{A}_{21} & \mathbf{I}_{n_2} w_\beta - \mathbf{A}_\beta \end{bmatrix} = \\ &= \det [\mathbf{I}_n w_\alpha w_\beta - \mathbf{A}_0 - \mathbf{A}_1 w_\beta - \mathbf{A}_2 w_\alpha], \end{aligned}$$

where

$$\mathbf{A}_0 = \mathbf{A}_\alpha \mathbf{A}_\beta + \mathbf{A}_{12} \mathbf{A}_{21}, \quad \mathbf{A}_1 = \mathbf{A}_\alpha, \quad \mathbf{A}_2 = \mathbf{A}_\beta. \quad (14)$$

By multiplying the nominator and the denominator of the transfer function (11) by $w_\alpha^{-n_1} w_\beta^{-n_2}$ we obtain the characteristic polynomial in the following form:

$$\begin{aligned} d(w_\alpha^{-1}, w_\beta^{-1}) &= \det \left[\mathbf{I}_n - \mathbf{A}_0 w_\alpha^{-1} w_\beta^{-1} - \mathbf{A}_1 w_\alpha^{-1} - \mathbf{A}_2 w_\beta^{-1} \right] = \\ &= 1 - \sum_{\substack{i=0 \\ i+j \neq n_1+n_2}}^{n_1} \sum_{j=0}^{n_2} d_{i,j} w_\alpha^{-i} w_\beta^{-j}. \end{aligned} \quad (15)$$

Proposed method finds state matrices \mathbf{A}_k , $k = 0, 1, 2$ using decomposition of the characteristic polynomial (15) into a set of simple monomials.

In the first step we decompose polynomial (15) into a set of the simple monomials. For each simple monomial we create a digraph representation. Then we can determine all possible characteristic polynomial (15) realisations using all combinations of the digraph monomial representation.

Theorem 2. *There exist positive state matrices of the discrete time linear system corresponding to the characteristic polynomial (15) if*

(C1) *the coefficients of the characteristic polynomial*

$$d_{i,j} \geq 0, \quad \text{for } i = 1, \dots, n_1; j = 1, \dots, n_2; \quad d_{n_1, n_2} = 1; \quad (16)$$

(C2) *the obtained digraph does not have additional cycles;*

(C3) *the A and B sets corresponding to two multidimensional digraphs are not disjoint.*

The proof is given in [10].

Remark 2. Each monomial is represented by one cycle. If after combining all digraphs (each corresponding to one monomial) we obtain an additional cycle, this means that in the polynomial additional simple monomial appears. If the created digraph is disjoint, this means that there is no intersection of A and B sets and created polynomial consists of additional simple monomial.

Using Theorem 2, we can construct the following algorithm.

Algorithm 1. *DetermineStateMatrix()*

```

1: monomial = 1;
2: Determine number of cycles in characteristic polynomial;
3: for monomial = 1 to cycles do
4:     Determine digraph  $\mathfrak{D}^{(n)}$  for all monomial;
5:     MonomialRealisation(monomial);
6: end for
7: for monomial = 1 to cycles do
8:     Determine digraph as a combination of the digraph monomial representation
9:     PolynomialRealisation(monomial);
10:    if PolynomialRealisation  $\neq$  cycles then
11:        Digraph contains additional cycles
12:        BREAK
13:    else if (C2) AND (C3) then
14:        Digraph satisfies characteristic polynomial;
15:        Determine weights of the arcs in digraph;
16:        Write state matrix  $\mathbf{A}_k$ ,  $k = 0, 1, 2$ ;
17:        return (PolynomialRealisation,  $\mathbf{A}_k$ ,  $k = 0, 1, 2$ );
18:    end if
19: end for

```

Example. Find a positive characteristic polynomial realisation

$$d(w_\alpha, w_\beta) = w_\alpha^2 w_\beta - 0.5w_\alpha^2 - 0.4w_\alpha w_\beta - 0.3w_\alpha - 0.2w_\beta - 0.1 \quad (17)$$

where $\alpha = \beta = 0.5$.

Multiplying the characteristic polynomial (17) by $w_\alpha^{-2} w_\beta^{-1}$ we obtain:

$$d(w_\alpha^{-1}, w_\beta^{-1}) = 1 - 0.5w_\beta^{-1} - 0.4w_\alpha^{-1} - 0.3w_\alpha^{-1} w_\beta^{-1} - 0.2w_\alpha^{-2} - 0.1w_\alpha^{-2} w_\beta^{-1} \quad (18)$$

where $\alpha = \beta = 0.5$.

To solve this problem, we can use Algorithm 1 based on parallel algorithm presented in paper [10]. In the first step we write the following initial conditions:

- number of colours in digraphs: *colours* = 3;
- monomials: $M_1 = 0.5w_\beta^{-1}$, $M_2 = 0.4w_\alpha^{-1}$, $M_3 = 0.3w_\alpha^{-1} w_\beta^{-1}$, $M_4 = 0.2w_\alpha^{-2}$, $M_5 = 0.1w_\alpha^{-2} w_\beta^{-1}$.

In the first step, we determine all possible realisations of the monomial M_1 (Figure 1). In the same way we follow with the monomials M_2 (Figure 2), M_3 (Figure 3), M_4 (Figure 4) and M_5 (Figure 5).

Remark 3. Aside from a number of possible combinations of monomial realisations, there is a number of variants of possible adding sub-digraphs. First monomial of the same size as the size of digraphs representing polynomial realisation will always have only 1 variant, as each other variant can be obtained by re enumerating vertices. For each other monomial realisation, there is a number of variants represented by the equation $variants = \prod_{i=0}^{n-1} (m - i)$, where: n is the size of sub-graph, and m is the size of polynomial digraphs realisation.

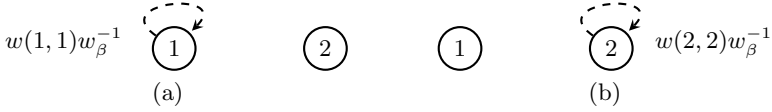


Fig. 1. $\mathfrak{D}^{(3)}$ digraphs with all possible minimal realisations of the monomial M_1

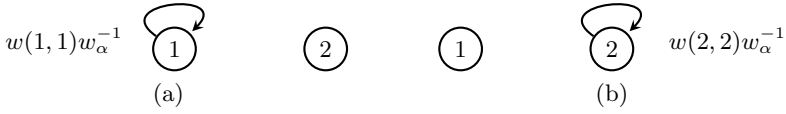


Fig. 2. $\mathfrak{D}^{(3)}$ digraphs with all possible minimal realisations of the monomial M_2

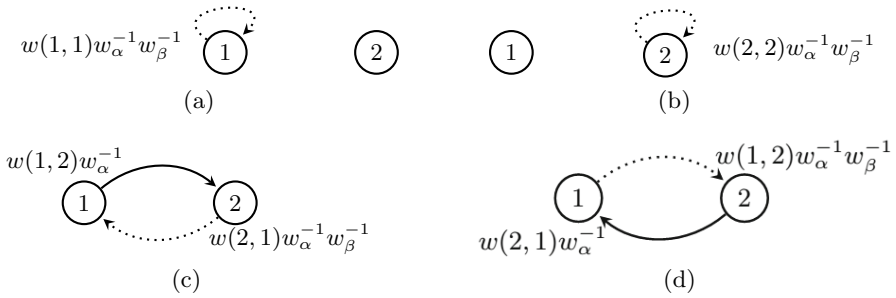


Fig. 3. $\mathfrak{D}^{(3)}$ digraphs with all possible minimal realisations of the monomial M_3

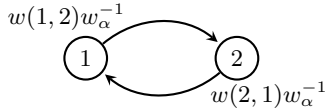


Fig. 4. $\mathfrak{D}^{(3)}$ digraphs with all possible minimal realisations of the monomial M_4

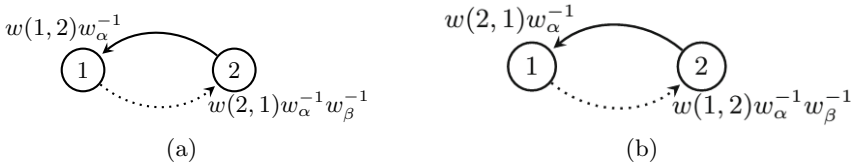


Fig. 5. $\mathfrak{D}^{(3)}$ digraphs with all possible minimal realisations of the monomial M_5

Subsequently, we determine all combinations of the digraph monomial representation and write matrices: \mathbf{A}_k , $k = 0, 1, 2$. In the defined problem we assume that dimension of the state matrices must be the minimal among possible. Taking into account this condition we have 16 ($variants = 2 \cdot 2 \cdot 4 \cdot 1$) possible

minimal polynomial realisations consisting of two vertices each. In the described example, we have only 4 minimal realisations which met our assumptions arisen from Theorem 2:

- Realisation 1 - consists of the following digraphs: Figure 1(a), 2(a), 3(a), 4 and 5(a);
- Realisation 2 - consists of the following digraphs: Figure 1(a), 2(a), 3(a), 4 and 5(b);
- Realisation 3 - consists of the following digraphs: Figure 1(b), 2(b), 3(b), 4 and 5(a);
- Realisation 4 - consists of the following digraphs: Figure 1(b), 2(b), 3(b), 4 and 5(b);

Consider the following two possible realisations. Realisation presented in Figure 6 consists of the following digraphs: Figure 1(a), 2(b), 3(b), 4 and 5. Using Theorem 2, we check the conditions:

- The coefficients of the characteristic polynomial (18) satisfy (16). **The condition (C1) is satisfied.**
- The obtained digraphs presented in Figure 6 do not have additional cycles. **The condition (C2) is satisfied.**
- To verify this condition, we must compare sets A and B corresponding to representation of simple monomial digraphs (we compare digraphs from Figures 1(a), 2(b), 3(b), 4 and 5). In this situation, we do not obtain intersection of sets. **Described realisation does not satisfy the condition (C3).**

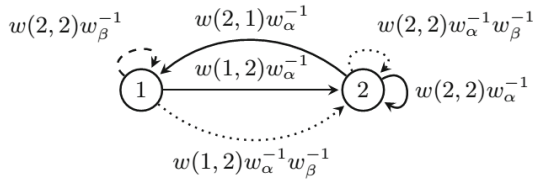


Fig. 6. Digraphs $\mathfrak{D}^{(3)}$ representing minimal realisation not satisfying Theorem 2

As the third condition is not satisfied, digraphs presented in Figure 6 are a wrong realisation of the polynomial (18).

The realisation presented in Figure 7 consists of the following digraphs: Figure 1(b), 2(b), 3(b), 4 and 5. Using Theorem 2, we check the conditions:

- The coefficients of the characteristic polynomial (18) satisfy the condition (16). **The Condition (C1) is satisfied.**
- The obtained digraphs presented in Figure 6 do not have additional cycles. **The Condition (C2) is satisfied.**

- To verify this condition, we must compare sets A and B corresponding to representation of simple monomial digraphs (we compare digraphs from Figures 1(b), 2(b), 3(b), 4 and 5). In this situation we obtain intersection of sets in form of the vertex with number 2. **Described realisation satisfies the Condition (C3).**

From digraphs we can write set of the equations

$$\begin{aligned} w(2, 2)_{\mathfrak{A}_1} &= 0.4, & w(2, 2)_{\mathfrak{A}_2} &= 0.5 & w(2, 2)_{\mathfrak{A}_0} &= 0.3 \\ w(1, 2)_{\mathfrak{A}_1} \cdot w(2, 1)_{\mathfrak{A}_1} &= 0.2, \\ w(1, 2)_{\mathfrak{A}_0} \cdot w(2, 1)_{\mathfrak{A}_1} &= 0.1. \end{aligned}$$

After solving them, we obtain weight coefficients, and we can write state matrices:

$$\begin{aligned} \mathbf{A}_0 &= \begin{bmatrix} 0 & 0 \\ w(1, 2)_{\mathfrak{A}_0} & w(2, 2)_{\mathfrak{A}_0} \end{bmatrix} = \begin{bmatrix} 0 & 0 \\ 0.1 & 0.3 \end{bmatrix}, \\ \mathbf{A}_1 &= \begin{bmatrix} 0 & w(2, 1)_{\mathfrak{A}_1} \\ w(1, 2)_{\mathfrak{A}_1} & w(2, 2)_{\mathfrak{A}_1} \end{bmatrix} = \begin{bmatrix} 0 & 1 \\ 0.2 & 0.4 \end{bmatrix}, \\ \mathbf{A}_2 &= \begin{bmatrix} 0 & 0 \\ 0 & w(2, 2)_{\mathfrak{A}_2} \end{bmatrix} = \begin{bmatrix} 0 & 0 \\ 0 & 0.5 \end{bmatrix}. \end{aligned} \tag{19}$$

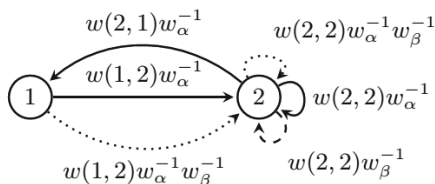


Fig. 7. Digraphs $\mathfrak{D}^{(3)}$ representing minimal realisation satisfying Theorem 2

In the last step, using (14) and (19) we can determine state matrices corresponding to the Roesser model (1a)–(1b) in the form:

$$\mathbf{A}_\alpha = \begin{bmatrix} 0 & 1 \\ 0.2 & 0.4 \end{bmatrix}, \mathbf{A}_\beta = \begin{bmatrix} 0 & 0 \\ 0 & 0.5 \end{bmatrix}, \mathbf{A}_{12} = \begin{bmatrix} 1 & 0 \\ 0 & 1 \end{bmatrix}, \mathbf{A}_{21} = \begin{bmatrix} 0 & 0.5 \\ 0.1 & 0.5 \end{bmatrix}. \tag{20}$$

4 Concluding Remarks

The paper includes a simple method based on digraph theory to determine minimal realisation of the characteristic polynomial of a positive two-dimensional fractional system describe by the Roesser model. By using this method, a fast algorithm for determination of all possible realisations of the characteristic polynomial was constructed. The effectiveness of the procedure has been illustrated

by a numerical example. Currently, the method of determining a positive polynomial realisation using GPU units and digraphs methods is being implemented in the memory-efficient way. At the same time, we are working on extension of the presented algorithm to solve realisation problems.

References

- [1] Benvenuti, L., Farina, L.: Positive and compartmental systems. *IEEE Transactions on Automatic Control* (47), 370–373 (2002)
- [2] Benvenuti, L., Farina, L.: A tutorial on the positive realization problem. *IEEE Transactions on Automatic Control* 49(5), 651–664 (2004)
- [3] Berman, A., Neumann, M., Stern, R.J.: *Nonnegative Matrices in Dynamic Systems*. Wiley, New York (1989)
- [4] Farina, L., Rinaldi, S.: *Positive linear systems: theory and applications*. Wiley-Interscience, Series on Pure and Applied Mathematics, New York (2000)
- [5] Fornasini, E., Valcher, M.E.: Directed graphs, 2D state models, and characteristic polynomials of irreducible matrix pairs. *Linear Algebra and Its Applications* 263, 275–310 (1997)
- [6] Fornasini, E., Valcher, M.E.: On the positive reachability of 2D positive systems. In: Benvenuti, L., De Santis, A., Farina, L. (eds.) *Positive Systems*. LNCIS, vol. 294, pp. 297–304. Springer, Heidelberg (2003)
- [7] Horn, R.A., Johnson, C.R.: *Topics in Matrix Analysis*. Cambridge Univ. Press (1991)
- [8] Hryniów, K., Markowski, K.A.: Parallel digraphs-building algorithm for polynomial realisations. In: *Proceedings of 2014 15th International Carpathian Control Conference (ICCC)*, pp. 174–179 (2014), <http://dx.doi.org/10.1109/CarpathianCC.2014.6843592>
- [9] Hryniów, K., Markowski, K.A.: Reachability index calculation by parallel digraphs-building. In: *19th International Conference on Methods and Models in Automation and Robotics (MMAR)*, Miedzyzdroje, Poland, September 2–5, pp. 808–813 (2014), <http://dx.doi.org/10.1109/MMAR.2014.6957460>
- [10] Hryniów, K., Markowski, K.A.: Digraphs-building of complete set of minimal characteristic polynomial realisations as means for solving minimal realisation problem of nD systems. *International Journal of Control* (Submitted to)
- [11] Kaczorek, T.: *Two-dimensional Linear Systems*. Springer, London (1985)
- [12] Kaczorek, T.: *Positive 1D and 2D systems*. Springer, London (2001)
- [13] Kaczorek, T.: Positive realization for 2D systems with delays. In: *Proceedings of 2007 International Workshop on Multidimensional (nD) Systems*, pp. 137–141. IEEE (2007)
- [14] Kaczorek, T.: Realization problem for positive 2D hybrid systems. *COMPEL* 27(3), 613–623 (2008)
- [15] Kaczorek, T.: *Selected Problems of Fractional Systems Theory*. Springer, Berlin (2011)
- [16] Luenberger, D.G.: *Positive linear systems*. In: *Introduction to Dynamic Systems: Theory, Models, and Applications*. Wiley, New York (1979)
- [17] Miller, K., Ross, B.: *An Introduction to the Fractional Calculus and Fractional Differential Equations*. Wileys, New York (1993)
- [18] Nishimoto, K.: *Fractional Calculus*. Decartess Press, Koriama (1984)
- [19] Podlubny, I.: *Fractional Differential Equations*. Academic Press, San Diego (1999)

Optimisation of Digraphs-Based Realisations for Polynomials of One and Two Variables

Krzysztof Hryniów and Konrad Andrzej Markowski*

Warsaw University of Technology, Faculty of Electrical Engineering
Institute of Control and Industrial Electronics
Koszykowa 75, 00-662 Warsaw, Poland
{Krzysztof.Hryniow,Konrad.Markowski}@ee.pw.edu.pl
<http://nas.isep.pw.edu.pl/repo>

Abstract. This paper proposes a set of modifications to the algorithm proposed earlier, that finds a complete set of minimal solutions for the characteristic polynomial on basis of digraphs theory and parallel computation. Changes proposed allow for parallelisation of previously sequential part of the algorithm, accurate estimation of number of solutions created and speed-up of both parts of the algorithm. Reduction of algorithm's complexity is greatest for monomials consisting of only one variable and for one-variable polynomial a complete set of minimal solutions can be found as fast as in linearithmic time.

Keywords: digraphs, parallel computation, characteristic polynomial, minimal realisation, positive systems.

1 Introduction

The realisation problem is a difficult task, that is solved commonly by the use of a canonical form of the system [2, 14], i.e. constant matrix form, which satisfies the system described by the transfer function. With the use of this form, we are able to write only one realisation out of many solutions that exist. The use of digraphs theory to the analysis of dynamical systems [6] is a new approach.

In this paper the set of $n \times m$ real matrices will be denoted by $\mathbb{R}^{n \times m}$ and $\mathbb{R}^n = \mathbb{R}^{n \times 1}$. If $\mathbf{G} = [g_{ij}]$ is a matrix, we write $\mathbf{G} \gg 0$ (matrix \mathbf{G} is called strictly positive), if $g_{ij} > 0$ for all i, j ; $\mathbf{G} > 0$ (matrix \mathbf{G} is called positive), if $g_{ij} > 0$ for all i, j ; $\mathbf{G} \geq 0$ (matrix \mathbf{G} is called non-negative), if $g_{ij} \geq 0$ for all i, j . The set of $n \times m$ real matrices with non-negative entries will be denoted by $\mathbb{R}_+^{n \times m}$ and $\mathbb{R}_+^n = \mathbb{R}_+^{n \times 1}$. The $n \times n$ identity matrix will be denoted by \mathbf{I}_n .

1.1 Realisation Problem

In this paper we will consider one-dimensional (1D) positive systems and two-dimensional (2D) positive systems.

* Research has been financed with the funds of the Statutory Research of 2015.

Let be given discrete one-dimensional system described by the equations:

$$\begin{aligned} x_{i+1} &= \mathbf{A}x_i + \mathbf{B}u_i, \\ y_i &= \mathbf{C}x_i + \mathbf{D}u_i, \end{aligned} \quad (1)$$

where $x_i \in \mathbb{R}^n$ is state vector in $i \in \mathbb{Z}_+$, $u_i \in \mathbb{R}^m$ is input vector, $y_i \in \mathbb{R}^p$ is output vector, $\mathbf{A} \in \mathbb{R}^{n \times n}$, $\mathbf{B} \in \mathbb{R}^{n \times m}$, $\mathbf{C} \in \mathbb{R}^{p \times n}$, $\mathbf{D} \in \mathbb{R}^{p \times m}$. Boundary condition for model (1) has the form: $x_0 \in \mathbb{R}^n$ [13].

Theorem 1. *The model (1) is internally positive if and only if*

$$\mathbf{A} \in \mathbb{R}_+^{n \times n}, \quad \mathbf{B} \in \mathbb{R}_+^{n \times m}, \quad \mathbf{C} \in \mathbb{R}_+^{p \times n}, \quad \mathbf{D} \in \mathbb{R}_+^{p \times m}. \quad (2)$$

The transfer matrix $T(z) \in \mathbb{R}_+^{p \times m}$ of the system (1) is given by

$$\mathbf{T}(z) = \mathbf{C}[\mathbf{I}_n z - \mathbf{A}]^{-1} \mathbf{B} + \mathbf{D} = \frac{\mathbf{N}(z)}{d(z)} \in \mathbb{R}^{p \times m}(z). \quad (3)$$

Consider the two-dimensional (2D) second Fornasini-Marchesini [4] model described by the equations:

$$\begin{aligned} x_{i+1,j+1} &= \mathbf{A}_1 x_{i+1,j} + \mathbf{A}_2 x_{i,j+1} + \mathbf{B}_1 u_{i+1,j} + \mathbf{B}_2 u_{i,j+1}, \\ y_{ij} &= \mathbf{C}x_{ij} + \mathbf{D}u_{ij}. \end{aligned} \quad (4)$$

where $x_{ij} \in \mathbb{R}^n$, $u_{ij} \in \mathbb{R}^m$ and $y_{ij} \in \mathbb{R}^p$ are state, input and output vectors, respectively at the point (i, j) , and $\mathbf{A}_k \in \mathbb{R}^{n \times n}$, $\mathbf{B}_k \in \mathbb{R}^{n \times m}$, $k = 0, 1, 2$, $\mathbf{C} \in \mathbb{R}^{p \times n}$, $\mathbf{D} \in \mathbb{R}^{p \times m}$ and $x_{i0} \in \mathbb{R}_+^n$, $i \in \mathbb{Z}_+$, $x_{0j} \in \mathbb{R}_+^n$, $j \in \mathbb{Z}_+$ [15].

Theorem 2. *The second Fornasini-Marchesini model (4) is internally positive if and only if*

$$\mathbf{A}_k \in \mathbb{R}_+^{n \times n}, \quad \mathbf{B}_k \in \mathbb{R}_+^{n \times m}, \quad k = 1, 2, \quad \mathbf{C} \in \mathbb{R}_+^{p \times n}, \quad \mathbf{D} \in \mathbb{R}_+^{p \times m}.$$

The proof of the Theorem 1 and Theorem 2 is given in [14].

The transfer matrix $T(z_1, z_2) \in \mathbb{R}_+^{p \times m}$ of the second Fornasini-Marchesini model (4) is given by:

$$\begin{aligned} T(z_1, z_2) &= \mathbf{C}[\mathbf{I}_{z_1 z_2} - \mathbf{A}_1 z_1 - \mathbf{A}_2 z_2]^{-1} (\mathbf{B}_1 z_1 + \mathbf{B}_2 z_2) + \mathbf{D} \\ &= \frac{\mathbf{C} \text{Adj} \mathbf{H}(z_1, z_2) (\mathbf{B}_1 z_1 + \mathbf{B}_2 z_2)}{\det \mathbf{H}(z_1, z_2)} + \mathbf{D} = \frac{\mathbf{N}(z_1, z_2)}{d(z_1, z_2)} + \mathbf{D}. \end{aligned} \quad (5)$$

For a one-dimensional system, the characteristic polynomial consists of one variable: s if we have a continuous time system or z if we have a discrete time system. For the discrete time system described by the equation (1), we have the following characteristic polynomial:

$$d(z) = \det [\mathbf{I}_n z - \mathbf{A}] = z^n - d_{n-1} z^{n-1} - d_{n-2} z^{n-2} - \dots - d_2 z^2 - d_1 z - d_0 \quad (6)$$

For a two-dimensional system, the characteristic polynomial consists of two variables: z_1 and z_2 if we have a discrete time system; s_1 and s_2 if we have a continuous time system. For the discrete time system described by the equation (4), we have the following characteristic polynomial:

$$\begin{aligned}
 d(z_1, z_2) &= \det [\mathbf{I}z_1 z_2 - \mathbf{A}_1 z - \mathbf{A}z_2] = z_1^n z_2^n - \sum_{i=0}^n \sum_{j=0}^n d_{ij} z_1^i z_2^j = \\
 &= z_1^n z_2^n - d_{n-1,n} z_1^{n-1} z_2^n - d_{n,n-1} z_1^n z_2^{n-1} - \dots - d_{10} z_1 - d_{01} z_2 - d_{00}
 \end{aligned}
 \tag{7}$$

for $n \leq i + j \leq 2n - 1$ and $i, j = 0, 1, \dots, n$.

For the one-dimensional system described by the equation (1) multiplying nominator and denominator by z^{-n} , we can rewrite the characteristic polynomial (6) in the following form:

$$d(z^{-1}) = 1 - d_{n-1} z^{-1} - d_{n-2} z^{-2} - \dots - d_2 z^{2-n} d_1 z^{1-n} - d_0 z^{-n}.
 \tag{8}$$

For the two-dimensional system described by the equation (4) multiplying nominator and denominator by $z_1^{-n} z_2^{-n}$, we can rewrite the characteristic polynomial (7) in the following form:

$$\begin{aligned}
 d(z_1^{-1}, z_2^{-1}) &= 1 - d_{n-1,n} z_1^{-1} - d_{n,n-1} z_2^{-1} - \dots - \\
 & d_{10} z_1^{1-n} z_2^{-n} - d_{01} z_1^{-n} z_2^{1-n} - d_{00} z_1^{-n} z_2^{-n}.
 \end{aligned}
 \tag{9}$$

1.2 Digraphs

A directed graph (called also digraph) \mathfrak{D} consists of a non-empty finite set $\mathbb{V}(\mathfrak{D})$ of elements called vertices and a finite set $\mathbb{A}(\mathfrak{D})$ of ordered pairs of distinct vertices called arcs. We call $\mathbb{V}(\mathfrak{D})$ the vertex set and $\mathbb{A}(\mathfrak{D})$ the arc set of \mathfrak{D} . The order of \mathfrak{D} is the number of vertices in \mathfrak{D} . The size of \mathfrak{D} is the number of arc in \mathfrak{D} . For an arc (v_1, v_2) , the first vertex v_1 is its tail and the second vertex v_2 is its head. More information about digraph theory is given in [1, 16].

Example 1. The digraph \mathfrak{D} in Figure 1 has order $\mathbb{V}(\mathfrak{D}) = \{v_1, v_2, v_3\}$ equal to 3 and size $\mathbb{A}(\mathfrak{D}) = \{(v_1, v_2), (v_2, v_3), (v_3, v_1), (v_3, v_2), (v_2, v_2)\}$ equal to 5.

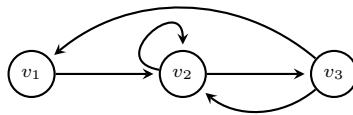


Fig. 1. A digraph \mathfrak{D}

A two-dimensional digraphs $\mathfrak{D}^{(2)}$ is a directed graph with two types of arcs and input flows. For the first time, this type of digraph was presented in [5, 6].

Definition 1. A two-dimensional digraph $\mathfrak{D}^{(2)}$ is sextuple $(s, V, \mathfrak{A}_1, \mathfrak{A}_2, \mathfrak{B}_1, \mathfrak{B}_2)$ where s is the source, $V = \{v_1, v_2, \dots, v_n\}$ is the set of vertices, \mathfrak{A}_1 and \mathfrak{A}_2 are subsets of $V \times V$ whose elements are called \mathfrak{A}_1 -arcs and \mathfrak{A}_2 -arcs respectively, meanwhile \mathfrak{B}_1 and \mathfrak{B}_2 are subsets of $s \times V$ whose elements are called \mathfrak{B}_1 -arcs and \mathfrak{B}_2 -arcs respectively. [6]

2 State-of-the-Art

There are some solutions for the problem of determination of entries of the state matrices \mathbf{A}_1 and $\mathbf{A}_2, \dots, \mathbf{A}_k$ for a given characteristic polynomial. Most of them are based on usage of the canonical forms of the system [2, 14], i.e. constant matrix form, which satisfies the system described by the transfer function. With the use of this form, we are able to write only one realisation of the system. Due to the complexity of the problem, such solutions are incapable of finding a set of all possible realisations for a given characteristic polynomial. Based on the multi-dimensional $\mathfrak{D}^{(n)}$ digraphs theory, a method that finds sets of solutions, which in addition are minimal, was proposed. First proposition of such method was given in [8] and [9], but the proposed method was only theoretical and extensive testing shown that it was not feasible for practical implementation as the problem of finding all possible realisations of a given polynomial is of such complexity that it cannot be solved in a reasonable time even by a brute-force GPGPU method [7].

In [7] and [11] an improved version of the algorithm was proposed. It creates digraphs for all monomials in the characteristic polynomial, then joins them by the use of a disjoint union to create all possible variants of digraphs representing polynomial realisation. The algorithm uses growth and prune steps to eliminate redundant solutions before the main computational step. The first part of the algorithm (growth and prune) is sequential, while polynomial digraphs realisations are computed during parallel part of the algorithm on multiple CUDA kernels.

The proposed method finds state matrix \mathbf{A} for 1D systems and state matrices \mathbf{A}_1 and \mathbf{A}_2 for 2D systems using decomposition of the characteristic polynomials (6) and (7) respectively. In the first step, we decompose a polynomial into a set of simple monomials. For each simple monomial, we create digraphs representations. Then we can determine all possible characteristic polynomial realisations using all combinations of the digraphs monomial representations. Finally, we combine received digraphs in one digraphs which is corresponding to a characteristic polynomial.

Remark 1. In [10] there is proposed an extension of the method for fractional positive systems in which state matrices $\mathbf{A}_\alpha, \mathbf{A}_\beta, \mathbf{A}_{12}$ and \mathbf{A}_{21} are used. Most of optimisation solutions proposed in this paper work also for fractional two-dimensional positive problems proposed in [10].

Theorem 3. *There exist positive state matrices of the discrete time linear system corresponding to the characteristic polynomial if*

(C₁) the coefficients of the characteristic polynomial

$$a_{i_1 i_2 \dots i_j} \geq 0, \quad \text{for } j = 1, 2 \dots, \infty, \quad a_{n_1, n_2, \dots, n_j} = 1; \quad (10)$$

(C₂) the obtained digraph does not have additional cycles;

(C₃) the set A and B corresponding to two multidimensional digraphs are not disjoint.

Proof for the Theorem 3 is presented in [11].

Recurrent function forms the core of growth part of the algorithm. It is executed for all possible combinations of monomial realisations for a given sub-graph size and number of colours. Some of the realisations obtained can be redundant and they will be removed by prune step of the algorithm. To achieve it fast, the algorithm checks control sums (hashes) that are unique – if two solutions have the same control sum, one is redundant as it can be obtained by classical shifting of rows and/or columns. A complete algorithm along with comprehensive explanation is presented in [11]. After creating and checking all monomial realisations, the algorithm creates all possible combinations of polynomial realisations by means of a disjoint union as proposed in [7]. Each possible combination is assigned to separate CUDA kernel on GPU for parallel computation. As each monomial is realised on sub-graph, for sub-graphs with size lower than the size of polynomial graph there are different possible variants of placement of a monomial (as explained in Remark 2).

Remark 2. Aside from a number of possible combinations of monomial realisations there is a number of variants of possible adding sub-digraphs. First monomial of the same size as the size of digraphs representing polynomial realisation will always have only 1 variant, as each other variant can be obtained by re enumerating vertices. For each other monomial realisation, there is a number of variants represented by the equation

$$\text{variants} = \prod_{i=0}^{n-1} (m - i), \quad (11)$$

where: n is the size of sub-graph, and m is the size of the polynomial digraphs realisation.

2.1 Complexity of the Problem

As many graph problems (like orientation, coverage, colouring, decomposition, disjunction, connection and finding both the shortest paths and cycles) are proposed or proven as NP-complete or NP-hard for 1D undirected graphs [1] and as method of creating digraphs realisations for characteristic polynomial includes many such operations, it is also a NP-hard problem. It can be assumed that its computational complexity will be very high as the proposed solution is based on operating on arbitrary multi-dimensional digraphs, making it more complicated than 1D undirected graphs and in [12] it is conjectured that for many

NP-complete problems there are no solutions that are capable of solving the problem under exponential time, and all well-known algorithms have at least exponential computational complexity. Because of the complexity of the proposed problem, there is a constant need of optimisation.

2.2 Complexity of the Algorithm

Sequential part (growth and prune steps, creation of monomial digraphs) of the algorithm creates a number of solutions that form a multiset permutation represented by the following equation:

$$s = \binom{m-1}{(x_1-1), x_2, \dots, x_c} = \frac{(m-1)!}{(x_1-1)!x_2!\dots x_c!}, \quad (12)$$

where x_i represents number of occurrences of i -th colour in monomial and $x_1 + x_2 + \dots + x_c = m$. In equation (12) decrementation of x_1 and m represents reduction of the number of the possible solutions by a fixed first choice as described in [3]. Sequential part of the algorithm needs

$$n[c^2(m-1) + (m-1)(s \log s + m)] \quad (13)$$

operations, where n is the number of monomials in polynomial.

In the worst-case scenario we can estimate computational complexity of the algorithm as:

$$n(V-1)(V^2 + (V-1)\log(V-1) + V), \quad (14)$$

so sequential part's computational complexity is factorial and can be presented as $\mathbf{T}(\mathbf{V}) = \mathbf{O}(V!)$ in big O notation.

Parallel part of the algorithm is executed on

$$\prod_1^n \left(s * \prod_{i=0}^m (V-i) \right) \quad (15)$$

kernels, where the number of solutions s is greatly reduced from the number presented in equation (12) by pruning, which is heavily dependent on x_i (where $i = 1, \dots, c$). Each kernel is performing

$$V(n(m+V)) + V^2 + m \log m + V \log V^n \quad (16)$$

operations. In the worst-case scenario parallel part's computational complexity can be presented as $\mathbf{T}(\mathbf{V}) = \mathbf{O}(V \log V^n)$, which makes parallel part solvable in linearithmic time, if there are enough kernels available.

3 Realisations Optimisation

As for larger polynomials, the number of kernels needed is greater than even an outfit of dedicated GPUs can provide. The reduction of kernels results in

the reduction of time needed for a parallel part (as when the number of threads executed is greater than the number of kernels on GPU, they need to be buffered and executed in batches – so if for example the number of threads exceeds 10 times the number of kernels available, the parallel part’s computational time will increase by an order of magnitude).

In the algorithm proposed in [11] first optimisations were performed in form of growth / prune steps, which restrict the number of solutions that are fully created and tested and in creating fixed solution start, which reduces the number of solutions created $\frac{m}{x_1}$ times, as can be seen in equation (12).

Candidate Growth and Pruning. Sequential part of the proposed algorithm can be optimised in three ways: optimisation of the growth step, optimisation of the prune step and parallelisation of the sequential part of the algorithm. To achieve a maximal reduction of the algorithm’s complexity, modifications based on all three methods proposed are presented below.

Parallelisation. For optimisation purposes it is important to be able to determine number of solutions that are created after the prune step of the algorithm, as it allows us to prepare number of kernels for each monomial in advance and it is essential for full parallelism of the algorithm.

Theorem 4. *There exist*

$$p = \binom{m-1}{x_1, x_2, \dots, x_c} = \frac{(m-1)!}{x_1! x_2! \dots x_c!}, \quad (17)$$

possible distinct digraphs solutions for given monomial, where x_i represents number of occurrences of i -th variable in monomial and $x_1 + x_2 + \dots + x_c = m$.

Proof. Number of distinct digraphs solutions is the same problem as determination of arrangement of n distinct objects along a fixed circle. As we have more than one variable, it is a case of a multi-set permutation which gives

$$\frac{n!}{m_1! m_2! \dots m_l!}$$

solutions. As the permutation is cyclic, $n!$ is reduced to $(n-1)!$ as the circle can be rotated [3].

Remark 3. Circle rotation used for digraphs representations of polynomials is synonymous with swapping columns / rows of \mathbf{A} matrix that is used in the control theory.

When we know the characteristic polynomial, we can determine at the start of the algorithm the number of solutions generated during the growth step (described by equation (12)) and the number of solutions generated after the prune step (described by equation (17)) for each of the monomials. With such information, we can compute different monomials that the characteristic polynomial consists of simultaneously by assigning each to a kernel block of precalculated size and preparing

memory blocks for each of the final solutions, which can be calculated independently of others, without incurring the synchronisation problem.

Omitting Prune Step. In [11] it was noted, based on experimental results, that for worst-case scenarios, when $x_1 = x_2 = \dots = x_c = 1$, the number of solutions created during growth step was always minimal. This quality can be proven as for such case equation (12) takes the form

$$s = \binom{m-1}{1, 1, \dots, 1} = \frac{(m-1)!}{1!1! \dots 1!} = (m-1)!, \quad (18)$$

which is synonymous with the number of solutions generated by cyclic permutation on fixed circle (and so is identical to the number of solutions generated after the prune step). In such cases, prune step can be omitted, which offsets additional computational complexity of such scenario.

Fixed Start Change. Introduction of fixed start in [11] allowed to reduce the number of redundant solutions created by $\frac{m}{x_1}$ as mentioned earlier. But it is not the best solution, as will be shown in a simple example below.

Example 2. Lets take two monomials, $z_1^{-1}z_2^{-2}$ and $z_1^{-2}z_2^{-1}$. For the first one growth and prune steps will generate

$$s = \binom{m-1}{(x_1-1), x_2} = \frac{(3-1)!}{(1-1)!2!} = 1; p = \binom{m-1}{x_1, x_2} = \frac{(3-1)!}{1!2!} = 1$$

solutions and for the second one

$$s = \binom{m-1}{(x_1-1), x_2} = \frac{(3-1)!}{(2-1)!1!} = 2; p = \binom{m-1}{x_1, x_2} = \frac{(3-1)!}{2!1!} = 1.$$

First results are clearly better than the second, as we do not generate a redundant candidate in the growth step. And it can be achieved for the second monomial just by swapping x_1 and x_2 . To generate a minimal number of redundant solutions during the growth step, we need to minimise s . That means we need to maximise the denominator, and to do this we need to choose as a fixed start (and decrease it by one) the variable that is minimal.

Complexity. These modifications will change the number of operations required for full candidate generation presented for the original algorithm in equation (13) to

$$c^2(m-1) + (m-1)(s \log s + m) \quad (19)$$

in case when enough kernels are available for full paralellisation of the part and

$$c^2(m-1) \quad (20)$$

for $x_1 = x_2 = \dots = x_c = 1$ scenarios, while parallel part of the algorithm will be executed on

$$\prod_1^n \left(\frac{(m-1)!}{x_1!x_2! \dots x_c!} * \prod_{i=0}^m (V-i) \right) \quad (21)$$

kernels. Algorithm will retain the factorial complexity ($\mathbf{T}(\mathbf{V}) = \mathbf{O}(V!)$), but will work much faster for previous worst-case scenario (as seen on equation (20)) and at least $2n$ times faster for all other scenarios.

3.1 One Variable Monomials

Growth / Prune Steps. For monomials consisting of only one variable (for example z_1^{-1} or s^{-3}) we can perform some additional optimisation of the algorithm to reduce the number of operations performed, as for 1D monomials (and polynomials) some steps of the algorithm are undue. First modification consist in the removal of both growth and prune steps for each one variable monomial, as in such cases there exists only one solution, as equation (12) for 1D monomials takes the form:

$$s = \binom{m-1}{x_1-1} = \frac{(m-1)!}{(x_1-1)!}, \quad (22)$$

and as $x_1 = m$ there always exists only one possible distinct solution (but many possible variants of placement of it on polynomial digraphs).

Reduction of Number of Variants. The number of variants (possible placements) is lower for 1D monomials, as for such monomials there are generated variants that are not distinct (as $(v_1, v_2)(v_2, v_1)$ cycle is identical to $(v_1, v_2)(v_2, v_1)$ cycle). Modification of the algorithm will change the equation (11) into:

$$variants = \frac{1}{n} \prod_{i=0}^{n-1} (m-i), \quad (23)$$

reducing number of variants and number of polynomial digraphs representations.

Complexity. For polynomial consisting only of 1D monomials, equation (13) will take the form

$$(m-1), \quad (24)$$

greatly reducing computational complexity of the first part of the algorithm from factorial to linear. While the second part will retain linearithmic complexity, the number of kernels needed to run the algorithm efficiently will be reduced

$$\sum_{i=0}^n n_i * \frac{(m-1)!}{(x_1-1)!x_2! \dots x_c!} \quad (25)$$

times, where n is the number of monomials and n_i is the size of i -th monomial.

4 Concluding Remarks

Modifications proposed in this article allow the parallelisation of the growth/prune part of the algorithm, due to the ability to accurately estimate the number of solutions created after pruning, and make algorithm perform much faster,

especially for characteristic polynomials of type which so far was the most problematic. Despite that, due to the complexity of the problem, the algorithm still retains very high computational complexity, but for some types of characteristic polynomials (especially 1D polynomials) complete set of minimal solutions can be found faster (as fast as in linearithmic time).

There is a need for further optimisation, both to reduce the complexity of the parallel part of the algorithm and of the growth/prune part. The second one can be done by adaptation of some kind of algorithm that will find only the results now obtained after the prune part, without the generation of undue solutions and loss of time needed for candidate testing. Adaptation of necklaces generation algorithms seems a viable solution, but additional work and experimental evaluation of such solutions are needed.

References

- [1] Bang-Jensen, J., Gutin, G.: *Digraphs: Theory, Algorithms and Applications*. Springer, London (2009)
- [2] Benvenuti, L., Farina, L.: A tutorial on the positive realization problem. *IEEE Transactions on Automatic Control* 49(5), 651–664 (2004)
- [3] Bona, M.: *Combinatorics of Permutations*, 2nd edn. Chapman Hall, CRC Press (2012)
- [4] Fornasini, E., Marchesini, G.: State-space realization theory of two-dimensional filters. *IEEE Trans. Autom. Contr.* 21, 481–491 (1976)
- [5] Fornasini, E., Valcher, M.E.: Directed graphs, 2D state models, and characteristic polynomials of irreducible matrix pairs. *Linear Algebra and Its Applications* 263, 275–310 (1997)
- [6] Fornasini, E., Valcher, M.E.: On the positive reachability of 2D positive systems. In: Benvenuti, L., De Santis, A., Farina, L. (eds.) *Positive Systems*. LNCIS, vol. 294, pp. 297–304. Springer, Heidelberg (2003)
- [7] Hryniów, K., Markowski, K.A.: Conditions for digraphs representation of the characteristic polynomial. In: *Young Scientists Towards the Challenges of Modern Technology*, pp. 77–80 (2014)
- [8] Hryniów, K., Markowski, K.A.: Parallel digraphs-building algorithm for polynomial realisations. In: *Proceedings of 2014 15th International Carpathian Control Conference (ICCC)*, pp. 174–179 (2014), <http://dx.doi.org/10.1109/CarpathianCC.2014.6843592>
- [9] Hryniów, K., Markowski, K.A.: Reachability index calculation by parallel digraphs-building. In: *19th International Conference on Methods and Models in Automation and Robotics (MMAR)*, Miedzyzdroje, Poland, September 2-5, pp. 808–813 (2014), <http://dx.doi.org/10.1109/MMAR.2014.6957460>
- [10] Hryniów, K., Markowski, K.A.: Digraphs minimal realisations of state matrices for fractional positive systems. In: *Szewczyk, Zieliński, Kaliczyńska (eds.) Progress in Automation, Robotics and Measuring Techniques*. AISC, vol. 350, pp. 63–72 (2015)
- [11] Hryniów, K., Markowski, K.A.: Digraphs-building of complete set of minimal characteristic polynomial realisations as means for solving minimal realisation problem of nD systems. *International Journal of Control* (Submitted to)

- [12] Impagliazzo, R., Paturi, R.: On the complexity of k-SAT. *Journal of Computer and System Sciences* 62, 367–375 (2001)
- [13] Kaczorek, T.: *Two-dimensional Linear Systems*. Springer, London (1985)
- [14] Kaczorek, T.: *Positive 1D and 2D systems*. Springer, London (2001)
- [15] Kurek, J.: The general state-space model for a two-dimensional linear digital system. *IEEE Trans. Autom. Contr.* 30, 600–602 (1985)
- [16] Wallis, W.D.: *A Beginner's Guide to Graph Theory*. Birkhäuser (2007)

Analysis Thrust for Different Kind of Propellers

Arkadiusz Jakubowski, Arkadiusz Kubacki, Bartosz Minorowicz,
and Amadeusz Nowak

Institute of Mechanical Technology
Poznan University of Technology
ul. Piotrowo 3, 61-138 Poznań, Poland
{arkadiusz.z.jakubowski,
arkadiusz.j.kubacki}@doctorate.put.poznan.pl,
{bartosz.minorowicz,nowak.amadeusz}@gmail.com

Abstract. The paper presents a design of test stand designed for thrust propellers measurements. There are shown results of the thrust for different propellers. The study thrust was made for six different propellers. Propellers differed in terms of diameter, pitch and material. For all of propellers used was the same drive and the same control parameters (voltage, current). During thrust measurements HBM force sensor was used. The propeller drive BLDC motor was used, which was controlled by a system of dSPACE. The following paper analyses indicates that propeller diameter is its most important parameter and in some range thrust is proportional to diameter.

Keywords: propeller, thrust, BLDC motor, balance of propeller, dSPACE.

1 Introduction

Propellers are one of the most important components in rotors design, which are used in aircrafts, helicopters, hovercrafts and other similar vehicles. Last two decades significant growth of military and civilian use of unmanned vehicles can be noticed. In a group of UAVs (Unmanned Aerial Vehicle) few remote controlled structures can be mentioned: quadcopters (four rotors), hexacopters (six rotors) and so on or mini helicopters and UAVs with co-axial rotor system [1]. Most common name for these objects are drone [2]. It is well known that these devices can be successfully used in areas where man is in not able to operate, they can be used as rescue, support or postal vehicles. What is more, these vehicles do not need runway and special techniques for landing [3]. On the other hand main disadvantage of drones is high power consumption, which leads in length and time of flight. Therefore that drive system should be optimized.

Most frequent rotor drive in these vehicles is based on BLDC (Brush Less Direct Current) motors where rotational speed is set by PWM signal (Pulse Width Modulation). Referring to the literature few different methods for propeller thrust measurement can be found. In paper [2] authors show results for lift force in relation with pulse width of PWM signal, but without experimental setup configuration. Interesting

method is presented in [4], where examined rotor is fixed to laboratory weight. Advanced experiments with wind tunnel are presented in [5]. Also simulations of propeller BLDC motor system are performed [6].

In this publication Authors built test rig for different propellers examinations to indicate which are the best. Reason for these studies is that horizontal rotor vehicles (different kind of copters), do not have lifting surface as wings in airplanes[7] whereby examinations for propellers are need.

2 The Experimental Setup

Test stand for thrust of propeller examination is presented in Fig. 3. The test stand consists: PC computer with Matlab-Simulink and dSPACE Control Desk (no. 15), which was used as control system for setting of PWM signal width (no. 9). BLDC motor (iPower iBM2212 Q, no. 2), was connected with ESC 20A controller (no. 13), which was powered by two laboratory DC power sources with range: 0–12 V, 0–10 A (no. 10). Parameters examined of BLDC (Fig. 1.), motor are placed in Table 1.



Fig. 1. iPower BLDC motor (<http://www.iflight-rc.com>)

Table 1. Parameters of BLDC motor

| Current max [A] | Supply voltage max [V] | Power max [W] | Mass [g] |
|-----------------|------------------------|---------------|----------|
| 12.2 | 14.8 | 135 | 77 |

Table 2. The list of examined propellers

| Ordinal | Diameter [inch] | Pitch [inch] | Material | Blades |
|---------|-----------------|--------------|----------|--------|
| 1 | 6 | 4 | Plastic | 3 |
| 2 | 8 | 6 | Plastic | 3 |
| 3 | 8 | 6 | Plastic | 2 |
| 4 | 10 | 6 | Plastic | 2 |
| 5 | 11 | 4 | Wood | 2 |
| 6 | 13 | 4.5 | Plastic | 2 |

ESC 20A controller was receiving PWM signal generated by dSPACE RapidPro system with filling range from 1 to 2 ms (no. 11). Frame (no. 5), was connected with base (no. 8), by means of screws. Movable frame (no. 4), was supported on roller bearings which provided free angular movements (no. 12). On the opposite side of BLDC motor steel plates for counterbalance were bolted (no. 3). Thus that solution

steel cable (no. 6) was pretensioned while rotor was not rotating, as a result measurement was free of backlash. Cable was a connector between frame and HBM U9N force transducer (no. 7), which was fixed to the base. Values of thrust force were displayed on measuring amplifier display HBM (no. 14). Parameters of tested propellers (no. 1) are placed in Table 2.

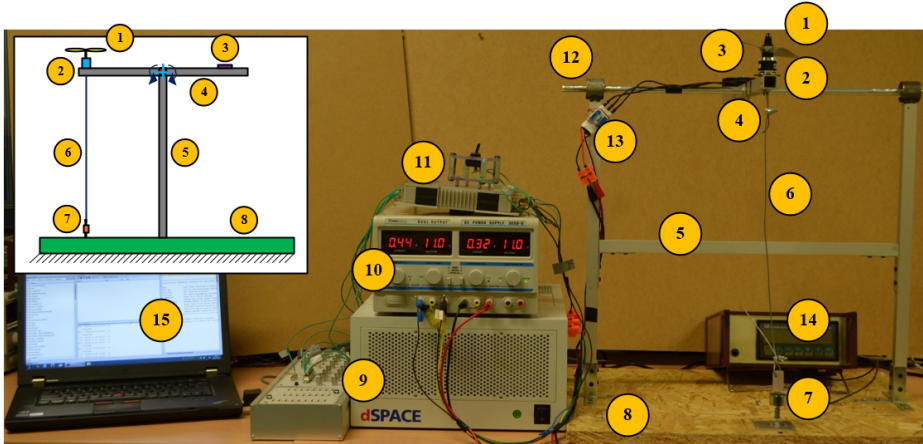


Fig. 2. Test stand configuration and schematic diagram

For propellers survey few copies were selected from group for hobby applications. Plastic propellers were made in injection moulding machine and delivered without final mechanical processing. Imperfections of molded propeller result in imbalance. Balancing is performed on special balancer (Fig. 3). The propeller is mounted on the pin (no. 2), and immobilized by two conical holders (no. 3). Pin is located between two permanent magnets (no. 1), with the possibility of free rotation. The next step is to set the propeller in a horizontal position. If the propeller remains in this position that means it is balanced properly. If it swings from the horizontal position it should be sanded of the surface so the propeller to the horizontal position it maintained.

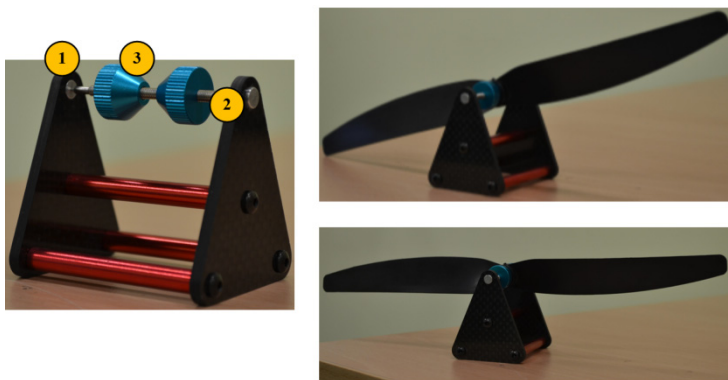


Fig. 3. Balancer for propeller (left), propeller before balancing (top) and the balance (bottom)

3 Experimental Results

Results for different propellers are shown in Fig. 4. Thrust is not proportional to pulse width of PWM signal for all tested propellers. Thrust variations for propeller 8×6 – 3 blades and 8×6 – 2 blades are similar. It indicates that number of blades does not have significant influence on the thrust. For smaller pulse width of PWM signal (up to 1.2 ms) the thrust for all tested propellers does not differ much. For maximum pulse width of PWM signal it can be seen large changes thrust for each propellers. Increased rotational speeds of propellers results in bigger differences in thrust values. Maximum recorded thrust at maximum rotational speed (actually maximum pulse width), is for propeller 13×4.5 – 2 blades and equals 7 N. Minimum thrust for maximum pulse width is obtained for propeller 6×4 – 3 blades, which is about 1.2 N. Diameter of propeller has the biggest influence on propeller thrust value. It is important to obtain highest available thrust and pitch. Comparison between propeller 8×6 – 2 blades and propeller 10×6 – 2 blades shows that thrust for propeller 10×6 – 2 blades is twice larger than 8×6 – 2 blades one. For the first one thrust is equal approximately 6 N and for the second one is equal approximately 3 N.

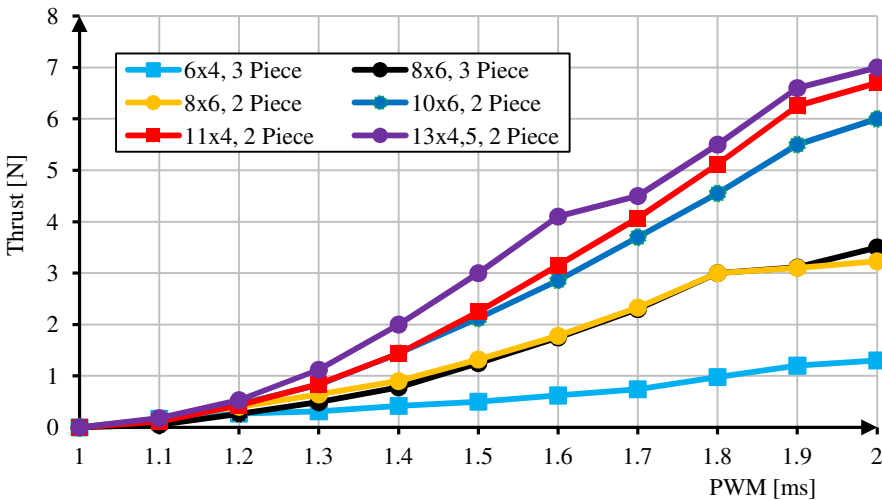


Fig. 4. Thrust of different propellers vs. filling PMW signal (legend: propeller size [inch], blades)

4 Discussion

In the Fig. 5 and 6 authors presented change of the thrusts for maximum set rotational speed, for chosen propellers. Noticeable is that for propellers with diameters smaller than 10 in, the thrust value changes proportionally to the diameter – see Fig. 5. Comparing almost all propellers in the Fig. 6 it can be seen that for diameters greater than 10 in the thrust change rate is smaller and decreases. The both variations could be approximated with accordingly linear and cubic functions.

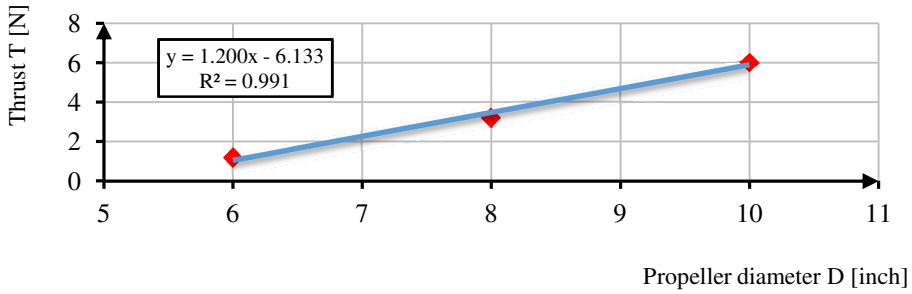


Fig. 5. Thrust values for maximum set rotational velocities, for different diameters of propellers (presented values from propellers: 6×4 – 3 blades, 8×6 – 2 blades, 10×6 – 2 blades, 11×4 – 2 blades, 13×4.5 – 2 blades)

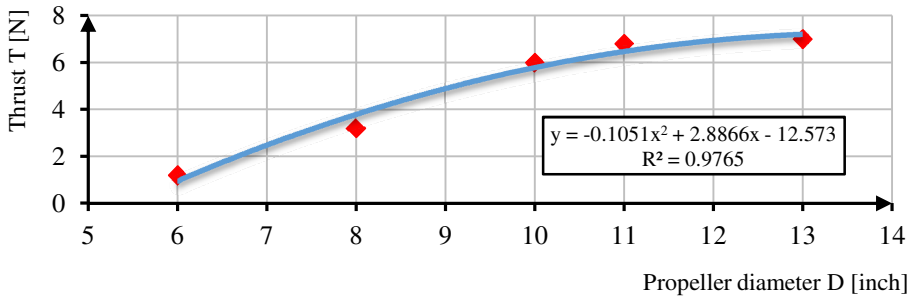


Fig. 6. Thrust values for maximum set rotational velocities, for different diameters of propellers (presented values from propellers: 6×4 – 3 blades, 8×6 – 2 blades, 10×6 – 2 blades)

5 Conclusion

The research proved that thrust rise with the increase of the propeller diameter and that this is the most important parameter. According to the acquainted data the maximum available thrust is proportional to propeller diameter. The comparison between two propellers with similar diameters but with different number of blades resulted with conclusion that number of blades does not have significant influence on thrust variations within tested velocity range. The test stand is useful to measure lift force of all available small size hobby propellers. The stand could be used also to check various control of propeller motors or even entire devices equipped with propeller drives, which should be the direction of the future studies.

References

1. Bell, J., Brazinskas, M., Prior, S.D., Erbil, M.A., Karamanoglu, M.: Development of a test-rig for exploring optimal conditions of small unmanned aerial vehicle co-axial rotor systems (2010)
2. Lee, K.U., Yun, Y.H., Chang, W., Park, J.B., Choi, Y.H.: Modeling and altitude control of quad-rotor UAV. In: International Conference on Control, Automation and Systems, pp. 1897–1902 (2011)
3. Cieślak, S.: Analiza wpływu czynników konstrukcyjnych oraz parametrów sterowania na czas trwania i wysokość bezrozbiegowego startu wiatrakowca. *Prace Instytutu Lotnictwa* 219, 39–46 (2011)
4. Gebauer, J., Koci, P., Sofer, P.: Multicopter potentialities. In: International Carpathian Control Conference, pp. 194–197 (2012)
5. Takahashi, K., Fujimoto, H., Hori, Y., Kobayashi, H., Nishizawa, A.: Modeling of propeller electric airplane and thrust control using advantage of electric motor. In: AMC 2014, Yokohama, pp. 482–487 (2014)
6. Martinez-Alvarado, R., Granda-Gutierrez, E.E., Sanchez-Orta, A., Ruiz-Sanchez, F.J.: Modeling and simulation of a propeller-engine system for Unmanned Aerial Vehicles, pp. 1–6 (2013)
7. Szafranski, G., Czyba, R., Blachuta, M.: Modeling and identification of electric propulsion system for multirotor unmanned aerial vehicle design. In: International Conference on Unmanned Aircraft Systems, pp. 470–476 (2014)

SysML Modeling of Functional and Non-functional Requirements for IEC 61131-3 Control Systems

Marcin Jamro

Rzeszow University of Technology,
al. Powstancow Warszawy 12, 35-959 Rzeszow, Poland
mjamro@kia.prz.edu.pl

Abstract. Control software performs important roles in various branches of industry. Its complexity and importance are still growing, thus it is crucial to provide engineers with new methods to improve its quality. One of possible solutions is modeling, which could be introduced into the overall development process. The paper proposes an approach to modeling of requirements dedicated to control systems developed according to the IEC 61131-3 standard. Such a solution supports four kinds of requirements. The first group specifies expected behavior of Program Organization Units (POUs, namely programs, function blocks, functions, and classes). The other two present performance requirements oriented towards POU execution and communication between devices in Distributed Control Systems (DCSs). The last type is dedicated to displays in a Human-Machine Interface (HMI) and specifies their expected operation. The proposed approach has been introduced in the CPDev engineering environment for programming various kinds of controllers.

Keywords: control software, IEC 61131-3, modeling, requirements.

1 Introduction

Control systems often perform important roles in industry. Such systems have been used for many years, however, their size, complexity, and importance are still growing [1]. There are several factors that cause this progress. For example, many hardware-based solutions are replaced by their software versions [2], which simplifies configuration. Such a benefit is important, because created systems should be easy to modify after changed requirements, hardware, processes, or features [3,4]. An impact on complexity is also caused by replacing centralized systems by distributed intelligent ones [5]. What is more, control software should be characterized by reliability, availability, maintenance, safety, and security [6].

The above reasons cause that it is necessary to provide engineers with development processes that simplify software creation and allow to improve its quality. Despite this fact, the current methods of control software development contain stages that are performed in an ineffective way and could cause problems [6]. One of possible solutions is to increase the abstraction level by introducing

the Model-Driven Development (MDD) paradigm. It could allow to find errors earlier, decrease costs and development time [7], as well as automatically generate implementation or its parts. The modeling of software is performed using available modeling languages, such as Unified Modeling Language (UML) [8] or Systems Modeling Language (SysML) [9]. The model could present various aspects of the system, including its structure, behavior, and requirements. Each of them is a complex topic, but this paper is focused on the latter.

Requirements specify expectations that should be met by the created system. They can be divided into two groups, namely functional and non-functional. The first defines a way how the system should operate, while the other specifies additional properties, such as performance or usability.

In the paper, the approach to modeling of requirements is presented. Such a solution uses the SysML graphical modeling language and could be integrated with the overall MDD process. First of all, it allows to specify functional requirements regarding behavior of particular software units, namely Program Organization Units (POUs, i.e. programs, function blocks, functions, and classes) from the worldwide IEC 61131-3 standard [10]. The approach also supports modeling of non-functional performance requirements for POU execution and communication between devices in a Distributed Control System (DCS). What is more, requirements for displays of Human-Machine Interface (HMI) are allowed.

The paper is organized as follows. Sec. 2 briefly presents related work in the area of MDD-based processes for control software. To make understanding of the proposed approach easier, Sec. 3 describes the running example shown in the following sections. Sec. 4 explains basic concepts regarding the proposed approach, together with two modeling rules. The next three parts describe particular requirements, namely POU functional (Sec. 5), POU performance (Sec. 6.1), communication performance (Sec. 6.2), as well as related to HMI displays (Sec. 7).

2 Related Work

Many researchers are interested in the topic of control software modeling. Various languages and methods are used for this purpose. Some of them also support modeling of requirements. In this section, a brief information about related work is presented, focused on MDD-based approaches for control systems.

Hastbacka et al. [6] present an approach to improve the modeling phase. It uses a dedicated UML profile and contains a few steps, such as requirement specification, functional design, platform-dependent modeling, and conversion into an executable application. The requirements are modeled using a set of stereotypes that are generalized by «*automationRequirement*», such as «*instrumentationRequirement*», «*controlFunctionRequirement*», and «*safetyRequirement*». The authors also mention a possibility of importing requirements from other sources, such as Piping and Instrumentation Diagrams (P&IDs) and spreadsheets.

Other works cover the topic of MDD-based processes for control software as well. Thramboulidis et al. [11] show the component-based approach for the Model Integrated Mechatronik, which is dedicated to DCSs based on the IEC 61499

standard [12]. It supports generation of implementation models for various execution platforms in an automatic way. In another paper, Zaeh and Poernbacher [13] show the MDD process for developing software for machine tools, including modeling of a system structure and behavior. The interesting approach is also proposed by Laleau et al. [14] who extend the SysML language with concepts from the Knowledge Acquisition in autOMated Specification (KAOS) method for the goal-oriented requirements modeling.

3 Running Example and Supporting Environment

To make understanding of the proposed approach easier, the running example, based on a simplified version from [15], is used in this paper. It represents a simple system that operates on a parking lot with two gates – entrance and exit (Fig. 1). The ticket machine, with the button to print a ticket, is located next to the entrance gate. Similarly, the sentry box for the parking lot service is placed next to the exit gate. When a car is detected next to the entrance gate and the button is pushed, the gate should be open. It should be close if a car is not detected next to the gate for at least 5 seconds. Regarding the exit gate, it should be open when a car is detected next to the gate and the button is pressed in the sentry box. Such a gate should close if a car is no longer detected for at least 5 seconds.

The proposed SysML-based modeling approach has been introduced into the CPDev engineering environment¹ [16]. Such a solution is created in the Department of Computer and Control Engineering at Rzeszow University of Technology (Poland). It allows to program various kinds of controllers and DCSs in the IEC 61131-3 languages. The environment supports modeling [17], a few testing methods [18], creating multi-platform HMI [19], as well as simulation and configuration. CPDev has both industrial and laboratory applications, including the Mega-Guard Ship Automation and Navigation System (Praxis Automation Technology B.V., the Netherlands)². It is also used to program controllers from LUMEL S.A. (Poland)³ and Nauka i Technika Sp. z o.o. (Poland)⁴ companies.

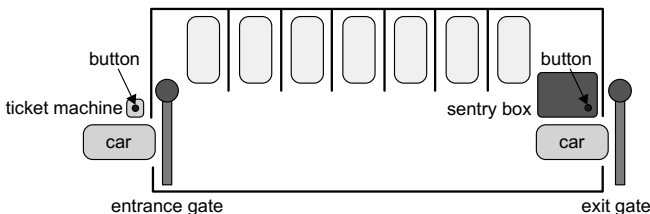


Fig. 1. Overview of the running example

¹ <http://cpdev.kia.prz.edu.pl/>

² <http://www.praxis-automation.com/>

³ <http://www.lumel.com.pl/en/>

⁴ <http://www.nit.pl/>

4 Requirements in IEC 61131-3 Control Systems

For the purpose of this paper, it is assumed that an IEC 61131-3 control system consists of a set of resources (such as controllers), a set of tasks, a set of Programs Organization Units (POUs, namely programs, function blocks, functions, and classes) with control algorithms, as well as a Human-Machine Interface (HMI) with a set of displays. Each element from such a system should meet particular requirements, either functional or non-functional. The proposed approach to modeling supports POU functional requirements, POU performance requirements, communication performance requirements, as well as HMI requirements.

All supported kinds of requirements, both functional and non-functional, are modeled according to the following modeling rule:

1. The model is placed on the requirement diagram from the SysML language. Its name and location are specific to the requirement type (see Sec. 5–7).
2. The diagram contains at least one element representing a requirement, marked with a stereotype extending *«requirement»* (Fig. 2, on the left).
3. A requirement name is specified as a name of a suitable *«requirement»*-derived element. The name should briefly specify aim of the requirement.
4. Each requirement should have a unique identifier set as a value of the *id* property. A format of this property is specific to the requirement type.
5. A content of the requirement is specified as a value of the *text* property.
6. The diagram contains exactly one top-level requirement. Its *allocatedTo* section specifies the element for whom the requirement is defined.
7. The hierarchy of requirements is created by connecting suitable elements via the containment relationship. The parent requirement is met only when all subrequirements are satisfied.

As mentioned by Linhares et al. in [20], requirement diagrams from the SysML language present data in an informal way, which makes verification of requirements more difficult, as well as could be ambiguous while browsing diagrams. To solve this problem, the modeling approach proposed in this paper emphasizes a

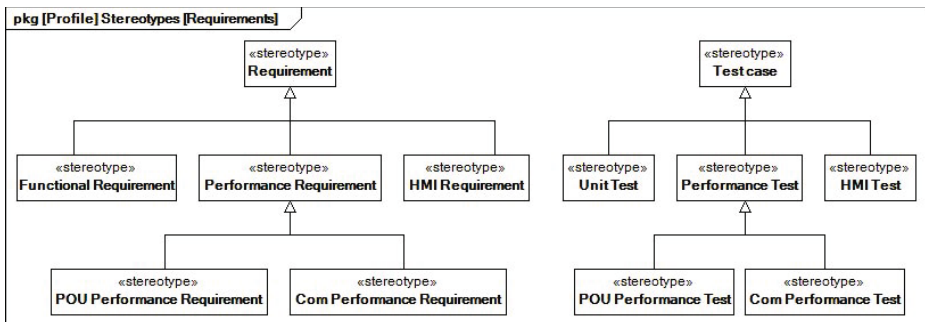


Fig. 2. Available stereotypes for modeling of requirements and tests

role of automated tests that verify requirements. It is assumed that passing all tests assigned to a particular requirement means that such a requirement is successfully verified. A set of tests is modeled on the same diagram as requirements, according to the following modeling rule:

1. Each test is represented by a element with a stereotype extending «*testCase*» (Fig. 2, on the right). Such a stereotype is specific to the requirement type.
2. A test name is specified by a name of a suitable «*testCase*» element.
3. Additional settings for a test are defined as values of properties in a «*testCase*»-derived element. Such properties are specific to the requirement type.
4. Tests are assigned to particular requirements by connecting «*requirement*»-derived and «*testCase*»-derived blocks via the «*verify*» relationship. The arrow should be directed towards a requirement.

The two above modeling rules contain two kinds of statements – general and dependent on a requirement type. The latter are described in details in the following sections of this paper, together with examples and explanations.

5 POU Functional Requirements

The functional requirements oriented towards POU are the first type of requirements supported by the proposed approach. They specify how particular units should operate in various circumstances. The requirements could define expected behavior either in normal conditions, as well as in erroneous scenarios.

Modeling of POU functional requirements is performed according to the modeling rule presented in Sec. 4. The diagram should be placed in the *POU Requirements* package. The diagram name should be set to a name of the unit. Requirements are represented by «*functionalRequirement*» elements, while an identifier is provided in the format *F.N[N]*, where *N* is an integer number. Functional requirements oriented towards POU are verified by a set of unit tests. Each of them is shown as a «*unitTest*» element with the *kind* property equal *Textual* to indicate that tests are created in the CPTest+ test definition language [18].

A part of the POU functional requirements model for the running example is presented in Fig. 3. It contains seven requirements in three-level hierarchy with one top-level requirement (*F.1*). Each of them has a name, a description, and an identifier. The requirements are verified by a set of unit tests. Exemplary three tests for the *ENTRANCE GATE OPENING* requirement are shown in Fig. 3.

6 Performance Requirements

Apart from meeting functional requirements, control systems often need to comply with non-functional ones, especially related to performance. The proposed approach supports requirements related to performance of POU execution and communication between devices in a DCS. Both topics are explained in the following part of this section.

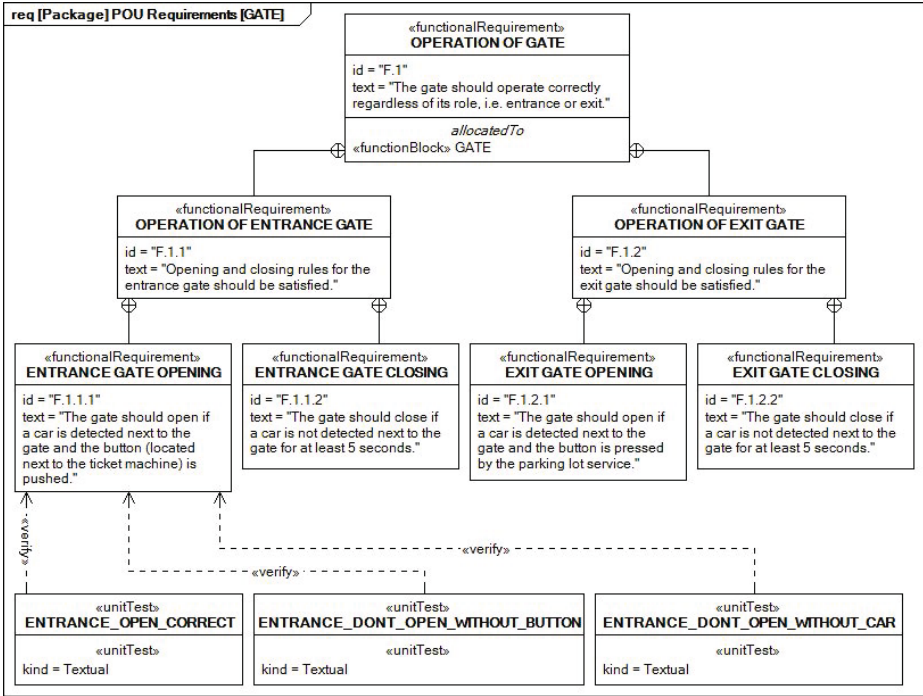


Fig. 3. Functional requirements for the GATE function block

6.1 POU Performance Requirements

Each POU from a control system may have performance restrictions that specify how much time could be spent on its execution. Such requirements should be modeled in SysML and become a part of the overall system model. In the proposed approach, performance requirements are modeled similarly to the functional ones. The approach is based on the preliminary version presented in [21].

The diagram should be located in the *POU Performance Requirements* package. Its name should be set to a name of the unit. Requirements are represented by *«performanceRequirement»* elements. An identifier of each of them should be provided in the format *PP.N[N]*, where *N* is an integer number. The top-level requirement should be allocated to a *«program»*, *«functionBlock»*, or *«function»* block that represents a particular POU. Such requirements are verified using a set of tests represented by *«pouPerformanceTest»* blocks. Each of them has the three following properties to configure the test:

- *mode* – a test mode that specifies the way of calculating a test result, namely:
 - *Always* – all results should be lower or equal to *time* to pass
 - *Average* – an average value of results should not exceed *time* to pass
- *time* – the given time
- *length* – a length of the test

The performance requirement *PP.1* for the *GATE* function block from the running example is presented in Fig. 4 (at the top). It specifies that the maximum execution time should not exceed 15 ms, while the average value of results should not be higher than 10 ms. The requirement is verified by two POU-oriented performance tests, represented by *«pouPerformanceTest»* elements.

6.2 Communication Performance Requirements

Apart from checking performance requirements related to execution of POU, it is necessary to ensure that communication between devices in a DCS is performed within the given time constraints. Such requirements should be defined in the model and verified by a set of dedicated tests.

A way of modeling of communication performance requirements is similar to POU performance ones and is based on the approach from [22]. The diagram is placed in the package named *Communication Performance Requirements*. An identifier of each requirement should be set to *CP.N[N]*, where *N* is an integer number. The top-level requirement should be assigned to a *«comTask»* element that represents a given communication task. Another stereotype is also used to indicate a communication performance test – *«comPerformanceTest»*. It contains four properties to configure the test, namely *check*, *mode*, *time*, and *length*. The first is set as *Successful* or *Finished* and indicates whether the correctness

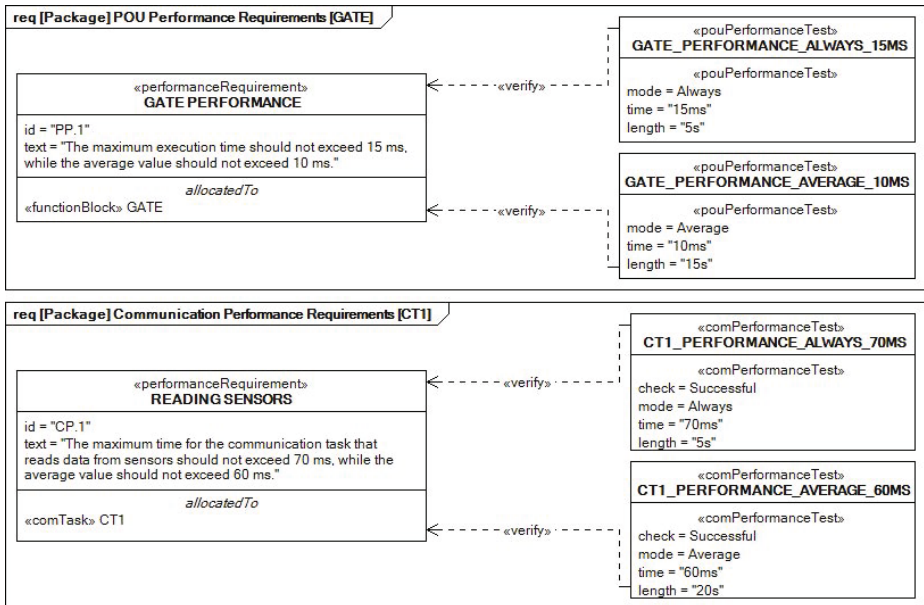


Fig. 4. Performance requirements for the *GATE* function block (at the top) and the *CT1* communication task (at the bottom)

of communication transaction should be verified. The meaning of the remaining three properties is the same as in case of POU performance tests.

It is assumed that the first communication task in the running example is named *CT1*. It reads values from sensors by cyclical execution of a dedicated communication transaction that uses one of available Modbus [23] functions. The associated requirement (Fig. 4, at the bottom) indicates that the process of reading data from sensors should never take more than 70 ms, while the average value should not exceed 60 ms. Such a requirement is verified by two tests.

7 HMI Requirements

An HMI could be an integrated part of a control system, as explained in Sec. 4. In the proposed approach, it is assumed that an HMI consists of a set of displays together with additional programs preparing data for presentation. A way how data are shown on displays should meet a set of requirements. They are modeled in a similar way to other types of requirements mentioned in this paper.

A single diagram is created for each HMI display and is located in the *HMI Requirements* package. The diagram name should be set to a display name. Requirements are represented by *«hmiRequirement»* elements with identifiers provided in the format *H.N[N]*, where *N* is an integer number. Verification of

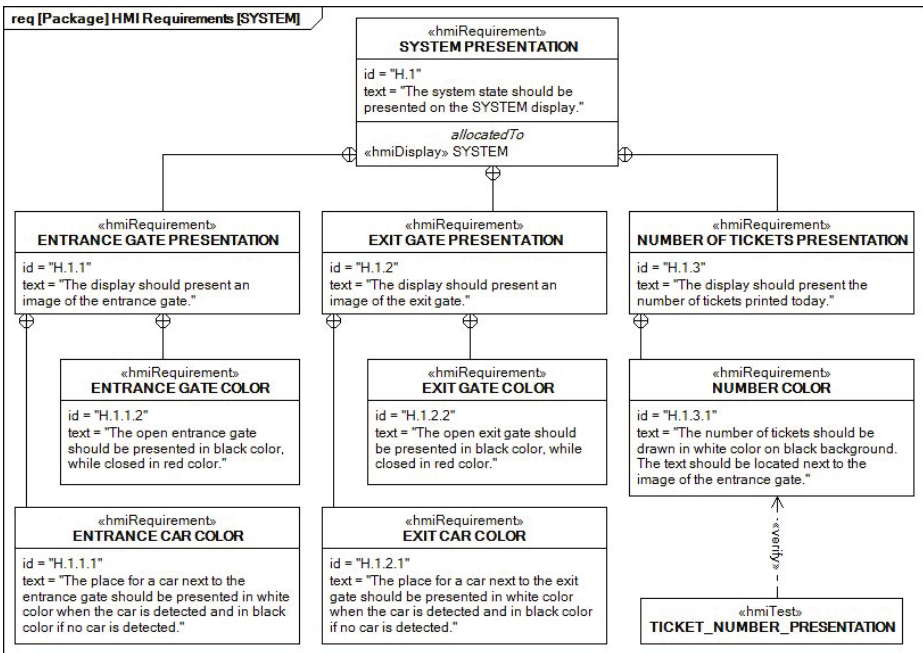


Fig. 5. HMI requirements for the SYSTEM display in the operator interface

such requirements is performed using a set of dedicated tests, which are modeled as «*hmiTest*» elements with names specifying the role of tests.

A part of the HMI requirements for the parking lot system from the running example is presented in Fig. 5. It contains nine requirements organized in a three-level hierarchy. This set of requirements is dedicated to the *SYSTEM* display, as specified by allocation in the top-level requirement and by the diagram name. Such requirements are verified using HMI tests. However, only one test is presented on the diagram, namely *TICKET_NUMBER_PRESENTATION*.

8 Conclusion

The introduction of the MDD approach in a control software development process could allow to move such a process into a higher level of abstraction, as well as to increase the software quality. There are several elements that could be modeled, including structure, behavior, and requirements. This paper is focused on the latter and presents a way of modeling both functional and non-functional requirements using requirement diagrams from the SysML graphical modeling language with a set of dedicated stereotypes.

The proposed approach is based on two general modeling rules that specify a way of requirements and tests modeling. Such rules are particularized for various requirement types, namely functional oriented towards POU's from IEC 61131-3 solutions, performance of POU execution and communication between devices in DCSs, as well as related to HMI displays. Each requirement should be verified by a set of tests, including unit, performance, and HMI ones. The proposed modeling solution could be used in various SysML-based MDD processes, as well as could be extended to support other kinds of requirements and tests.

The modeling functionalities have been introduced into the CPDev engineering environment for programming various kinds of controllers and DCSs.

References

1. Vyatkin, V.: Software Engineering in Industrial Automation: State-of-the-Art Review. *IEEE Transactions on Industrial Informatics* 9, 1234–1249 (2013)
2. Kormann, B., Vogel-Heuser, B.: Automated test case generation approach for PLC control software exception handling using fault injection. In: *IECON 2011 - 37th Annual Conference on IEEE Industrial Electronics Society*, pp. 365–372 (2011)
3. Winkler, D., Hametner, R., Biffel, S.: Automation component aspects for efficient unit testing. In: *IEEE Conference on Emerging Technologies Factory Automation, ETFA 2009*, pp. 1–8 (2009)
4. Wenger, M., Zoitl, A.: Re-use of IEC 61131-3 Structured Text for IEC 61499. In: *2012 IEEE International Conference on Industrial Technology (ICIT)*, pp. 78–83 (2012)
5. Dubinin, V., Vyatkin, V.: Semantics-Robust Design Patterns for IEC 61499. *IEEE Transactions on Industrial Informatics* 8, 279–290 (2012)
6. Hastbacka, D., Vepsäläinen, T., Kuikka, S.: Model-driven development of industrial process control applications. *The Journal of Systems and Software* 84, 1100–1113 (2011)

7. Estevez, E., Marcos, M.: Model-Based Validation of Industrial Control Systems. *IEEE Transactions on Industrial Informatics* 8, 302–310 (2012)
8. OMG: Unified Modeling Language (OMG UML), Infrastructure, V2.4.1 (2011)
9. OMG: Systems Modeling Language (OMG SysML), V1.3 (2012)
10. IEC: IEC 61131-3 - Programmable controllers - Part 3: Programming languages (2013)
11. Thramboulidis, K., Perdakis, D., Kantas, S.: Model driven development of distributed control applications. *The International Journal of Advanced Manufacturing Technology* 33, 233–242 (2007)
12. IEC: IEC 61499-1 - Function blocks - Part 1: Architecture (2005)
13. Zaeh, M., Poernbacher, C.: Model-driven development of PLC software for machine tools. *Production Engineering* 2, 39–46 (2008)
14. Laleau, R., Semmak, F., Matoussi, A., Petit, D., Hammad, A., Tatibouet, B.: A first attempt to combine SysML requirements diagrams and B. *Innovations in Systems and Software Engineering* 6, 47–54 (2010)
15. Jamro, M.: SysML Modeling of POU-Oriented Unit Tests for IEC 61131-3 Control Software. In: 2014 19th International Conference on Methods and Models in Automation and Robotics, MMAR (2014) (to be published)
16. Jamro, M., Rzonca, D., Sadolewski, J., Stec, A., Swider, Z., Trybus, B., Trybus, L.: CPDev Engineering Environment for Modeling, Implementation, Testing, and Visualization of Control Software. In: Szewczyk, R., Zieliński, C., Kaliczyńska, M. (eds.) *Recent Advances in Automation, Robotics and Measuring Techniques*. AISC, vol. 267, pp. 81–90. Springer, Heidelberg (2014)
17. Jamro, M.: Automatic Generation of Implementation in SysML-Based Model-Driven Development for IEC 61131-3 Control Software. In: 2014 19th International Conference on Methods and Models in Automation and Robotics, MMAR (2014) (to be published)
18. Jamro, M., Trybus, B.: Testing Procedure for IEC 61131-3 Control Software. In: 12th IFAC/IEEE International Conference on Programmable Devices and Embedded Systems (PDeS), pp. 192–197 (2013)
19. Jamro, M., Trybus, B.: IEC 61131-3 Programmable Human Machine Interfaces for Control Devices. In: 2013 The 6th International Conference on Human System Interaction (HSI), pp. 48–55 (2013)
20. Linhares, M., de Oliveira, R., Farines, J., Vernadat, F.: Introducing the modeling and verification process in SysML. In: *IEEE Conference on Emerging Technologies and Factory Automation, ETFA*, pp. 344–351 (2007)
21. Jamro, M.: Development and Execution of POU-Oriented Performance Tests for IEC 61131-3 Control Software. In: Szewczyk, R., Zieliński, C., Kaliczyńska, M. (eds.) *Recent Advances in Automation, Robotics and Measuring Techniques*. AISC, vol. 267, pp. 91–102. Springer, Heidelberg (2014)
22. Jamro, M., Rzonca, D.: Measuring, Monitoring, and Analysis of Communication Transactions Performance in Distributed Control System. In: Kwiecień, A., Gaj, P., Stera, P. (eds.) *CN 2014. CCIS*, vol. 431, pp. 147–156. Springer, Heidelberg (2014)
23. MODICON, Inc.: *Modicon MODBUS Protocol Reference Guide* (1996)

Fractional Standard and Positive Descriptor Time-Varying Discrete-Time Linear Systems

Tadeusz Kaczorek

Bialystok University of Technology, Faculty of Electrical Engineering
Wiejska 45D, 15-351 Bialystok
kaczorek@isep.pw.edu.pl

Abstract. The Weierstrass-Kronecker theorem on the decomposition of the regular pencil is extended to the fractional descriptor time-varying discrete-time linear systems. A method for computing the solutions of the fractional systems is proposed. Necessary and sufficient conditions for the positivity of the systems are established.

Keywords: fractional, descriptor, time-varying, positive, discrete-time, solution.

1 Introduction

A dynamical system is called positive if its trajectory starting from any nonnegative initial condition state remains forever in the positive orthant for all nonnegative inputs. An overview of state of the art in positive system theory is given in the monographs [7, 8] and in the papers [9–12]. Models having positive behavior can be found in engineering, economics, social sciences, biology and medicine, etc.

The Laypunov, Bohl and Perron exponents and stability of time-varying discrete-time linear systems have been investigated in [1–6]. The positive standard and descriptor systems and their stability have been analyzed in [8–11]. The positive linear systems with different fractional orders have been addressed in [9, 14] and the singular discrete-time linear systems in [10]. The switched discrete-time systems have been considered in [16–18] and the extremal norms for positive linear inclusions in [15].

The positivity and stability of time-varying discrete-time linear systems have been investigated in [13].

In this paper the Weierstrass-Kronecker decomposition theorem will be applied to fractional descriptor time-varying discrete-time linear systems with regular pencils to find their solutions and necessary and sufficient conditions for the positivity of the systems will be established.

The paper is organized as follows. In section 2 the Weierstrass-Kronecker decomposition theorem is applied to find solutions to standard fractional descriptor time-varying discrete-time linear systems. Necessary and sufficient conditions for the

positivity of the descriptor systems are established in section 3. Concluding remarks are given in section 4.

The following notation will be used: \mathfrak{R} – the set of real numbers, $\mathfrak{R}^{n \times m}$ – the set of $n \times m$ real matrices, $\mathfrak{R}_+^{n \times m}$ – the set of $n \times m$ matrices with nonnegative entries and $\mathfrak{R}_+^n = \mathfrak{R}_+^{n \times 1}$, I_n – the $n \times n$ identity matrix.

2 Standard Fractional Descriptor Systems

Consider the fractional descriptor time-varying discrete-time linear system

$$E(i)\Delta^\alpha x_{i+1} = A(i)x_i + B(i)u_i, \quad i \in Z_+ = \{0, 1, \dots\} \quad (2.1a)$$

$$y_i = C(i)x_i \quad (2.1b)$$

where $x_i \in \mathfrak{R}^n$, $u_i \in \mathfrak{R}^m$, $y_i \in \mathfrak{R}^p$ are the state, input and output vectors and $A(i) \in \mathfrak{R}^{n \times n}$, $B(i) \in \mathfrak{R}^{n \times m}$, $C(i) \in \mathfrak{R}^{p \times n}$ are matrices with entries depending on $i \in Z_+$ and the fractional difference of the order α is defined by

$$\Delta^\alpha x_i = \sum_{j=0}^i (-1)^j \binom{\alpha}{j} x_{i-j} \quad (2.1c)$$

$$\binom{\alpha}{j} = \begin{cases} 1 & \text{for } j=0 \\ \frac{\alpha(\alpha-1)\dots(\alpha-j+1)}{j!} & \text{for } j=1, 2, \dots \end{cases} \quad (2.1d)$$

It is assumed that $\det E(i) = 0$, $i \in Z_+$ and

$$\det[E(i)\lambda - A(i)] \neq 0 \quad (2.2)$$

for some $\lambda \in \mathbb{C}$ (the field of complex numbers) and $i \in Z_+$.

Substituting (2.1c) into (2.1a) we obtain

$$E(i)x_{i+1} = [E(i)\alpha - A(i)]x_i - \sum_{j=2}^{i+1} c_j E(i)x_{i-j+1} + B(i)u_i \quad (2.3a)$$

where

$$c_j = (-1)^{j+1} \binom{\alpha}{j}. \quad (2.3b)$$

It is well-known [11, 15] that if (2.2) holds then there exists a pair of nonsingular matrices $P(i), Q(i) \in \mathfrak{R}^{n \times n}$ such that

$$P(i)[E(i)\lambda - A(i)]Q(i) = \begin{bmatrix} I_{n_1} & 0 \\ 0 & N \end{bmatrix} \lambda - \begin{bmatrix} A_1(i) & 0 \\ 0 & I_{n_2} \end{bmatrix}, \quad i \in Z_+ \quad (2.4)$$

where $u_1 = \deg \det[E(i)\lambda - A(i)]$, $A_1(i) \in \mathfrak{R}^{n_1 \times n_1}$, $N \in \mathfrak{R}^{n_2 \times n_2}$ is the nilpotent matrix with the index μ (i.e. $N^\mu = 0$ and $N^{\mu-1} \neq 0$).

The matrices $P(i), Q(i), A_1(i)$ can be found by for example the use of elementary row and column operations [15].

Premultiplying (2.1a) by the matrix $P(i)$, introducing the new state vector

$$\bar{x}_i = Q^{-1}(i)x_i = \begin{bmatrix} \bar{x}_{1,i} \\ \bar{x}_{2,i} \end{bmatrix}, \quad \bar{x}_{1i} = \begin{bmatrix} \bar{x}_{11,i} \\ \bar{x}_{12,i} \\ \vdots \\ \bar{x}_{1n_1,i} \end{bmatrix}, \quad \bar{x}_{2i} = \begin{bmatrix} \bar{x}_{21,i} \\ \bar{x}_{22,i} \\ \vdots \\ \bar{x}_{2n_2,i} \end{bmatrix} \quad (2.5)$$

and using (2.4) we obtain

$$\bar{x}_{1,i+1} = A_{1\alpha}(i)\bar{x}_{1,i} - \sum_{j=2}^{i+1} c_j \bar{x}_{1,i-j+1} + B_1(i)u_i, \quad (2.6a)$$

$$N\bar{x}_{2,i+1} = (N_\alpha + I_{n_2})\bar{x}_{2,i} - \sum_{j=2}^{i+1} c_j N\bar{x}_{2,i-j+1} + B_2(i)u_i \quad (2.6b)$$

where

$$A_{1\alpha}(i) = A_1(i) + \alpha I_{n_1} \in \mathfrak{R}^{n_1 \times n_1}, \quad P(i)B(i) = \begin{bmatrix} B_1(i) \\ B_2(i) \end{bmatrix}, \quad B_1(i) \in \mathfrak{R}^{n_1 \times m}, \quad B_2(i) \in \mathfrak{R}^{n_2 \times m}. \quad (2.6c)$$

The solution $\bar{x}_{1,i}$ of equation (2.6a) for known initial condition $\bar{x}_{10} \in \mathfrak{R}^{n_1}$ and input $u_i \in \mathfrak{R}^m$, $i \in Z_+$ can be computed iteratively using the formula

$$\bar{x}_{1,i} = A_{1\alpha}(i-1)\bar{x}_{1,i-1} - \sum_{j=2}^i c_j \bar{x}_{1,i-j} + B(i-1)u_j, \quad i \in Z_+ \quad (2.7)$$

where c_j is defined by (2.6b).

To simplify the notation it is assumed that the matrix N in (2.6b) has the form

$$N = \begin{bmatrix} 0 & 1 & 0 & \dots & 0 \\ 0 & 0 & 1 & \dots & 0 \\ \vdots & \vdots & \vdots & \ddots & \vdots \\ 0 & 0 & 0 & \dots & 1 \\ 0 & 0 & 0 & \dots & 0 \end{bmatrix} \in \mathfrak{R}^{n_2 \times n_2}. \quad (2.8)$$

From (2.6b) and (2.8) we have

$$\begin{bmatrix} 0 & 1 & 0 & \dots & 0 \\ 0 & 0 & 1 & \dots & 0 \\ \vdots & \vdots & \vdots & \ddots & \vdots \\ 0 & 0 & 0 & \dots & 1 \\ 0 & 0 & 0 & \dots & 0 \end{bmatrix} \begin{bmatrix} \bar{x}_{21,i+1} \\ \bar{x}_{22,i+1} \\ \vdots \\ \bar{x}_{2n_2,i+1} \end{bmatrix} = \begin{bmatrix} 1 & \alpha & 0 & \dots & 0 \\ 0 & 1 & \alpha & \dots & 0 \\ \vdots & \vdots & \vdots & \ddots & \vdots \\ 0 & 0 & 0 & \dots & \alpha \\ 0 & 0 & 0 & \dots & 1 \end{bmatrix} \begin{bmatrix} \bar{x}_{21,i} \\ \bar{x}_{22,i} \\ \vdots \\ \bar{x}_{2n_2,i} \end{bmatrix}, \quad i \in \mathbb{Z}_+ \quad (2.9)$$

$$+ \sum_{j=2}^{i+1} \begin{bmatrix} 0 & c_j & 0 & \dots & 0 \\ 0 & 0 & c_j & \dots & 0 \\ \vdots & \vdots & \vdots & \ddots & \vdots \\ 0 & 0 & 0 & \dots & c_j \\ 0 & 0 & 0 & \dots & 0 \end{bmatrix} \begin{bmatrix} \bar{x}_{21,i-j+1} \\ \bar{x}_{22,i-j+1} \\ \vdots \\ \bar{x}_{2n_2,i-j+1} \end{bmatrix} + \begin{bmatrix} B_{21}(i) \\ \vdots \\ B_{2n_2}(i) \end{bmatrix} u_i$$

and

$$\begin{aligned} 0 &= \bar{x}_{2n_2,i} + B_{2n_2}(i)u_i, \\ \bar{x}_{2n_2,i+1} &= \bar{x}_{2n_2-1,i} + \alpha \bar{x}_{2n_2,i} + \sum_{j=2}^{i+1} c_j \bar{x}_{2n_2,i-j+1} + B_{2n_2-1}(i)u_i, \\ &\vdots \\ \bar{x}_{22,i+1} &= \bar{x}_{21,i} + \alpha \bar{x}_{22,i} + \sum_{j=2}^{i+1} c_j \bar{x}_{22,i-j+1} + B_{21}(i)u_i \end{aligned} \quad , \quad i \in \mathbb{Z}_+. \quad (2.10)$$

Solving the equations (2.10) with respect to the components of the vector $\bar{x}_{2,i}$ we obtain

$$\begin{aligned} \bar{x}_{2n_2,i} &= -B_{2n_2}(i)u_i, \\ \bar{x}_{2n_2-1,i} &= -B_{2n_2}(i+1)u_{i+1} + \alpha B_{2n_2}(i)u_i + \sum_{j=2}^{i+1} c_j B_{2n_2}(i-j+1)u_{i-j+1} - B_{2n_2-1}(i)u_i, \\ &\vdots \\ \bar{x}_{21,i} &= -B_{2n_2}(i+n_2-1)u_{i+n_2-1} + \alpha B_{2n_2}(i+n_2-2)u_i + \sum_{j=2}^{i+1} c_j B_{2n_2}(i+n_2-j-1)u_{i-j+1} + \dots - B_{21}(i)u_i. \end{aligned} \quad (2.11)$$

The admissible initial conditions for the system (2.6b) are given by (2.11) for $i = 0$.

The solution of the equation (2.6b) for known $u_i \in \mathfrak{R}^m$ and admissible initial conditions $\bar{x}_{20} \in \mathfrak{R}^{n_2}$ is given by (2.11).

The considerations can be easily extended to the case when the matrix N in (2.6b) has the form

$$N = \text{blockdiag}[N_1, \dots, N_q], \quad q > 1 \tag{2.12}$$

and N_k for $k = 1, 2, \dots, q$ has the form (2.7).

Example 2.1. Consider the fractional descriptor time-varying system described by the equation (2.1a) with the matrices

$$E(i) = \begin{bmatrix} 0 & 0 & 0 & \frac{e^{2i}}{\cos(i) + 2} \\ -\frac{(i+2)(\sin(i)+1)}{i+1} & e^i & 0 & -\frac{e^{2i}(e^{-i}+1)}{\cos(i)+2} \\ \frac{i+2}{i+1} & 0 & 0 & 0 \\ 0 & 0 & 0 & 0 \end{bmatrix},$$

$$B(i) = \begin{bmatrix} \frac{1}{\cos(i)+2} & 0 \\ e^{-i} - \frac{e^{-i}+1}{\cos(i)+2} & \frac{2i(i+2)(\cos(i)+1)(\sin(i)+1)}{i+1} - \sin(i)(\sin(i)+1) \\ 0 & \sin(i) - \frac{2i(i+2)(\cos(i)+1)}{i+1} \\ 0 & \frac{2i(i+2)}{i+1} \end{bmatrix}, \tag{2.13}$$

$$A(i) = \begin{bmatrix} 0 & 0 & a_{13}(i) & 0 \\ a_{21}(i) & a_{22}(i) & a_{23}(i) & a_{24}(i) \\ a_{31}(i) & 0 & 0 & a_{34}(i) \\ 0 & 0 & 0 & a_{44}(i) \end{bmatrix},$$

where

$$a_{13}(i) = \frac{1}{\cos(i)+2},$$

$$a_{21}(i) = \frac{(i+2)(i+2\cos(i)+2\sin(i)+i\sin(i)+\cos(i)\sin(i)+3)}{(i+1)(\sin(i)+2)},$$

$$a_{22}(i) = 1 - 2e^i, \quad a_{23}(i) = -\frac{e^{-i}+1}{\cos(i)+2}, \quad a_{24}(i) = \frac{e^{2i}(i+2)(\cos(i)+1)(\sin(i)+1)}{i+1},$$

$$a_{31}(i) = -\frac{i+2}{\sin(i)+2}, \quad a_{34}(i) = -\frac{e^{2i}(i+2)(\cos(i)+1)}{i+1}, \quad a_{44}(i) = \frac{e^{2i}(i+2)}{i+1}.$$

The condition (2.2) is satisfied since

$$\det[E(i)\lambda - A(i)] = -\frac{(i+2)^2(2e^i + \lambda e^i - 1)(2\lambda + i + \lambda \sin(i) + 1)e^{2i}}{(i+1)^2(\cos(i)+2)(\sin(i)+2)} \neq 0. \quad (2.14)$$

In this case

$$P(i) = \begin{bmatrix} 1+e^{-i} & 1 & 1+\sin(i) & 0 \\ 0 & 0 & 1 & 1+\cos(i) \\ 2+\cos(i) & 0 & 0 & 0 \\ 0 & 0 & 0 & \frac{i+1}{i+2} \end{bmatrix}, \quad Q(i) = \begin{bmatrix} 0 & \frac{i+1}{i+2} & 0 & 0 \\ e^{-i} & 0 & 0 & 0 \\ 0 & 0 & 1 & 0 \\ 0 & 0 & 0 & e^{-2i} \end{bmatrix} \quad (2.15)$$

and

$$\begin{bmatrix} I_{n_1} & 0 \\ 0 & N \end{bmatrix} = P(i)E(i)Q(i) = \begin{bmatrix} 1 & 0 & 0 & 0 \\ 0 & 1 & 0 & 0 \\ 0 & 0 & 0 & 1 \\ 0 & 0 & 0 & 0 \end{bmatrix},$$

$$\begin{bmatrix} A_1(i) & 0 \\ 0 & I_{n_2} \end{bmatrix} = P(i)A(i)Q(i) = \begin{bmatrix} e^{-i}-2 & 1+\cos(i) & 0 & 0 \\ 0 & -\frac{i+1}{2+\sin(i)} & 0 & 0 \\ 0 & 0 & 1 & 0 \\ 0 & 0 & 0 & 1 \end{bmatrix}, \quad (2.16)$$

$$\begin{bmatrix} B_1(i) \\ B_2(i) \end{bmatrix} = P(i)B(i) = \begin{bmatrix} e^{-i} & 0 \\ 0 & \sin(i) \\ 1 & 0 \\ 0 & 2i \end{bmatrix},$$

$$(n_1 = n_2 = 2).$$

The equations (2.6) have the form

$$\begin{bmatrix} \bar{x}_{11,i+1} \\ \bar{x}_{12,i+1} \end{bmatrix} = \begin{bmatrix} e^{-i}-2 & 1+\cos(i) \\ 0 & -\frac{i+1}{2+\sin(i)} \end{bmatrix} \begin{bmatrix} \bar{x}_{11,i} \\ \bar{x}_{12,i} \end{bmatrix} + \sum_{j=2}^{i+1} c_j \begin{bmatrix} \bar{x}_{11,i-j+1} \\ \bar{x}_{12,i-j+1} \end{bmatrix} + \begin{bmatrix} e^{-i} & 0 \\ 0 & \sin(i) \end{bmatrix} \begin{bmatrix} u_{1,i} \\ u_{2,i} \end{bmatrix} \quad (2.17a)$$

and

$$\begin{bmatrix} 0 & 1 \\ 0 & 0 \end{bmatrix} \begin{bmatrix} \bar{x}_{21,i+1} \\ \bar{x}_{22,i+1} \end{bmatrix} = \begin{bmatrix} 1 & \alpha \\ 0 & 1 \end{bmatrix} \begin{bmatrix} \bar{x}_{21,i} \\ \bar{x}_{22,i} \end{bmatrix} + \sum_{j=2}^{i+1} c_j \begin{bmatrix} 0 & 1 \\ 0 & 0 \end{bmatrix} \begin{bmatrix} \bar{x}_{21,i-j+1} \\ \bar{x}_{22,i-j+1} \end{bmatrix} + \begin{bmatrix} 1 & 0 \\ 0 & 2i \end{bmatrix} \begin{bmatrix} u_{1,i} \\ u_{2,i} \end{bmatrix}. \quad (2.17b)$$

The solution of (2.17a) is given by (2.7) with the matrices $A_1(i)$ and $B_1(i)$ defined by (2.16).

From (2.17b) we have

$$\begin{aligned} \bar{x}_{22,i} &= -2iu_{2,i}, \\ \bar{x}_{21,i} &= -2(i+1)u_{2,i+1} + \alpha 2iu_{2,i} + \sum_{j=2}^{i+1} c_j 2(i-j+1)u_{2,i-j+1} - u_{1,i}, \quad i \in Z_+. \end{aligned} \quad (2.18)$$

The solution of the equation (2.1a) with (2.13) is given by

$$x(i) = \begin{bmatrix} x_1(i) \\ x_2(i) \\ x_3(i) \\ x_4(i) \end{bmatrix} = Q(i) \begin{bmatrix} \bar{x}_{11,i} \\ \bar{x}_{12,i} \\ \bar{x}_{21,i} \\ \bar{x}_{22,i} \end{bmatrix}, \quad i \in Z_+ \quad (2.19)$$

where $Q(i)$ is defined by (2.14) and the components of the state vector $\bar{x}(i)$ by (2.7) with $A_1(i)$ and $B_1(i)$ defined by (2.16).

3 Positive Systems

Definition 3.1. The fractional descriptor time-varying discrete-time linear system (2.1) is called the (internally) positive if and only if $x_i \in \mathfrak{R}_+^n$ and $y_i \in \mathfrak{R}_+^p$, $i \in Z_+$ for any admissible initial conditions $x_0 \in \mathfrak{R}_+^n$ and all inputs $u_i \in \mathfrak{R}_+^m$, $i \in Z_+$.

The matrix $Q(i) \in \mathfrak{R}^{n \times n}$, $i \in Z_+$ is called monomial if in each row and column only one entry is positive and the remaining entries are zero for $i \in Z_+$.

It is well-known [8] that $Q^{-1}(i) \in \mathfrak{R}_+^{n \times n}$, $i \in Z_+$ if and only if the matrix is monomial.

It is assumed that for the positive system (2.1) the decomposition (2.4) is positive for the monomial matrix $Q(i)$. In this case

$$x_i = Q(i)\bar{x}_i \in \mathfrak{R}_+^n \text{ if and only if } \bar{x}_i \in \mathfrak{R}_+^n, \quad i \in Z_+. \quad (3.1)$$

It is also well-known that premultiplication of the equation (2.1a) by the matrix $P(i)$ does not change its solution x_i , $i \in Z_+$.

From (2.11) it follows that $\bar{x}_{2,i} \in \mathfrak{R}_+^{n_2}$, $i \in Z_+$ for $u_i \in \mathfrak{R}_+^m$, $i \in Z_+$ if and only if

$$-B_2(i) \in \mathfrak{R}_+^{n_2 \times m} \text{ for } i \in Z_+. \quad (3.2)$$

Therefore, the following theorem has been proved.

Theorem 3.1. Let the decomposition (2.4) of the system be possible for a monomial matrix $Q(i) \in \mathfrak{R}_+^{n \times n}$, $i \in Z_+$. The substitution (2.6b) is positive if and only if the condition (3.2) is satisfied.

Theorem 3.2. Let the decomposition (2.4) of the system be possible for a monomial matrix $Q(i) \in \mathfrak{R}_+^{n \times n}$, $i \in Z_+$. The substitution (2.6a) for $0 < \alpha < 1$ is positive if and only if

$$A_1 \alpha(i) \in \mathfrak{R}_+^{n_1 \times n_1}, \quad B_1(i) \in \mathfrak{R}_+^{n_1 \times m}, \quad i \in Z_+. \quad (3.3)$$

Proof. Sufficiency. If $0 < \alpha < 1$ then from (2.3b) and (2.1d) we have

$$c_2 = (-1)^2 \frac{\alpha(\alpha-1)}{2} < 0 \quad (3.4a)$$

and

$$c_{j+1} = (-1)^{j+1} \binom{\alpha}{j+1} = \frac{(j-\alpha)}{j+1} c_j < 0, \quad j = 2, 3, \dots \quad (3.4b)$$

From (2.7) and (3.4) it follows that $\bar{x}_{1,i} \in \mathfrak{R}_+^{n_1}$, $i \in Z_+$ for $x_0 \in \mathfrak{R}_+^n$ and $u_i \in \mathfrak{R}_+^m$, $i \in Z_+$ if the condition (3.3) is satisfied.

The necessity can be shown in a similar way as for standard descriptor systems in [11]. ■

Theorem 3.3. Let the decomposition (2.4) of the system be possible for a monomial matrix $Q(i) \in \mathfrak{R}_+^{n \times n}$, $i \in Z_+$. The system (2.1) for $0 < \alpha < 1$ is positive if and only if:

- 1) the conditions (3.3) are satisfied,
- 2) (3.2) holds,
- 3) $C(i) \in \mathfrak{R}_+^{p \times n}$ for $i \in Z_+$.

Proof. By Theorem 3.2 and 3.1 the solutions (2.6a) and (2.6b) are positive if and only if the conditions (3.2) and (3.3) are met. From (2.1b) and (2.5a) we have

$$y_i = C(i)Q(i)Q^{-1}(i)x_i = \bar{C}(i)\bar{x}_i, \quad i \in Z_+. \quad (3.5a)$$

where

$$\bar{C}(i) = C(i)Q(i). \quad (3.5b)$$

For monomial matrix $Q(i) \in \mathfrak{R}_+^{n \times n}$ from (3.3) we have

$$\bar{C}(i) \in \mathfrak{R}_+^{p \times n}, \quad i \in Z_+ \text{ if and only if } C(i) \in \mathfrak{R}_+^{p \times n}, \quad i \in Z_+ \quad (3.6)$$

and

$$y_i \in \mathfrak{R}_+^p, i \in \mathbb{Z}_+ \text{ if and only if } C(i) \in \mathfrak{R}_+^{p \times n}, i \in \mathbb{Z}_+. \quad (3.7)$$

Example 3.1. Consider the fractional descriptor time-varying system described by the equation (2.1) with the matrices

$$E(i) = \begin{bmatrix} 0 & 0 & 0 & \frac{1}{2\sin(i)+4} \\ -\cos(i)-1 & \frac{1}{\cos(i)+2} & 0 & -\frac{e^{-i}+2}{2\sin(i)+4} \\ 1 & 0 & 0 & 0 \\ 0 & 0 & 0 & 0 \end{bmatrix},$$

$$B(i) = \begin{bmatrix} -\frac{1}{\sin(i)+2} & 0 \\ e^{-i} + \frac{e^{-i}+2}{\sin(i)+2} & -(\cos(i)+1)(e^{-i} + \sin(i)+2) \\ 0 & e^{-i} + \sin(i)+2 \\ 0 & -1 \end{bmatrix}, \quad (3.8)$$

$$C(i) = \begin{bmatrix} 0 & \frac{1}{\cos(i)+2} & 0 & 0.5 \\ \frac{i+2}{i+1} & 0 & \frac{e^{-i}}{e^{-i}+1} & 0 \end{bmatrix},$$

$$A(i) = \begin{bmatrix} 0 & 0 & a_{13}(i) & 0 \\ a_{21}(i) & a_{22}(i) & a_{23}(i) & a_{24}(i) \\ a_{31}(i) & 0 & 0 & a_{34}(i) \\ 0 & 0 & 0 & a_{44}(i) \end{bmatrix},$$

where

$$a_{13}(i) = \frac{1}{(\sin(i)+2)(e^{-i}+1)}, \quad a_{21}(i) = -e^{-i} - \cos(i) - \sin(i) - e^{-i} \cos(i),$$

$$a_{22}(i) = \frac{i+1}{(i+2)(\cos(i)+2)}, \quad a_{23}(i) = -\frac{e^{-i}+2}{(\sin(i)+2)(e^{-i}+1)},$$

$$a_{24}(i) = \frac{(i+2)(\cos(i)+1)(e^{-i}+1)}{2(i+1)},$$

$$a_{31}(i) = e^{-i} + 1, \quad a_{34}(i) = -\frac{(i+2)(e^{-i} + 1)}{2(i+1)}, \quad a_{44}(i) = \frac{i+2}{2(i+1)}.$$

The condition (2.2) is satisfied since

$$\det[E(i)\lambda - A(i)] = \frac{(e^{-i} - \lambda + 1)(i - 2\lambda - \lambda i + 1)}{2(i+1)(\cos(i) + 2)(\sin(i) + 2)(e^{-i} + 1)} \neq 0 \quad (3.9)$$

In this case

$$P = \begin{bmatrix} 2 + e^{-i} & 1 & 1 + \cos(i) & 0 \\ 0 & 0 & 1 & 1 + e^{-i} \\ 2 + \sin(i) & 0 & 0 & 0 \\ 0 & 0 & 0 & \frac{i+1}{i+2} \end{bmatrix}, \quad Q = \begin{bmatrix} 0 & 1 & 0 & 0 \\ 2 + \cos(i) & 0 & 0 & 0 \\ 0 & 0 & 1 + e^{-i} & 0 \\ 0 & 0 & 0 & 2 \end{bmatrix} \quad (3.10)$$

and

$$\begin{aligned} \begin{bmatrix} I_{n_1} & 0 \\ 0 & N \end{bmatrix} &= P(i)E(i)Q(i) = \begin{bmatrix} 1 & 0 & 0 & 0 \\ 0 & 1 & 0 & 0 \\ 0 & 0 & 0 & 1 \\ 0 & 0 & 0 & 0 \end{bmatrix}, \\ \begin{bmatrix} A_1(i) & 0 \\ 0 & I_{n_2} \end{bmatrix} &= P(i)A(i)Q(i) = \begin{bmatrix} \frac{i+1}{i+2} & 1 - \sin(i) & 0 & 0 \\ 0 & 1 + e^{-i} & 0 & 0 \\ 0 & 0 & 1 & 0 \\ 0 & 0 & 0 & 1 \end{bmatrix}, \\ \begin{bmatrix} B_1(i) \\ B_2(i) \end{bmatrix} &= P(i)B(i) = \begin{bmatrix} e^{-i} & 0 \\ 0 & 1 + \sin(i) \\ -1 & 0 \\ 0 & -\frac{i+1}{i+2} \end{bmatrix}, \\ \bar{C}(i) &= C(i)Q(i) = \begin{bmatrix} 1 & 0 & 0 & 1 \\ 0 & \frac{i+2}{i+1} & e^{-i} & 0 \end{bmatrix} \end{aligned} \quad (3.11)$$

The descriptor system is positive since the tree conditions of Theorem 3 are satisfied. The matrix $Q(i)$ defined by (3.10) is monomial, the conditions (3.2) and (3.3) are met

$$-B_2(i) = \begin{bmatrix} 1 & 0 \\ 0 & \frac{i+1}{i+2} \end{bmatrix} \in R_+^{2 \times 2},$$

$$A_1(i) = \begin{bmatrix} \frac{i+1}{i+2} & 1 - \sin(i) \\ 0 & 1 + e^{-i} \end{bmatrix} \in R_+^{2 \times 2} \text{ and } B_1(i) = \begin{bmatrix} e^{-i} & 0 \\ 0 & 1 + \sin(i) \end{bmatrix} \in R_+^{2 \times 2}, \quad i \in Z_+ \tag{3.12}$$

and

$$C(i) = \begin{bmatrix} 0 & \frac{1}{\cos(i)+2} & 0 & 0.5 \\ \frac{i+2}{i+1} & 0 & \frac{e^{-i}}{e^{-i}+1} & 0 \end{bmatrix} \in R_+^{2 \times 4} \text{ for } Z_+. \tag{3.13}$$

The solution to the equation (2.1) with the matrices $E(i)$, $A(i)$, $B(i)$ given by (3.8) can be found in a similar way as in Example 2.1.

4 Concluding Remarks

The Weierstrass-Kronecker theorem on the decomposition of the regular pencil has been extended to the fractional descriptor time-varying discrete-time linear systems. A method for computing the solutions of the fractional systems has been proposed. Necessary and sufficient conditions for the positivity of the systems have been established. The effectiveness of the test are demonstrated on examples. The considerations can be extended to the fractional descriptor time-varying continuous-time linear systems.

Acknowledgments. This work was supported by National Science Centre in Poland.

References

1. Czornik, A., Newrat, A., Niezabitowski, M., Szyda, A.: On the Lyapunov and Bohl exponent of time-varying discrete linear systems. In: 20th Mediterranean Conf. on Control and Automation (MED), Barcelona, pp. 194–197 (2012)
2. Czornik, A., Niezabitowski, M.: Lyapunov Exponents for Systems with Unbounded Coefficients. *Dynamical Systems: an International Journal* 28(2), 140–153 (2013)
3. Czornik, A., Newrat, A., Niezabitowski, M.: On the Lyapunov exponents of a class of the second order discrete time linear systems with bounded perturbations. *Dynamical Systems: an International Journal* 28(4), 473–483 (2013)
4. Czornik, A., Niezabitowski, M.: On the stability of discrete time-varying linear systems. *Nonlinear Analysis: Hybrid Systems* 9, 27–41 (2013)

5. Czornik, A., Niezabitowski, M.: On the stability of Lyapunov exponents of discrete linear system. In: Proc. of European Control Conf., Zurich, pp. 2210–2213 (2013)
6. Czornik, A., Klamka, J., Niezabitowski, M.: On the set of Perron exponents of discrete linear systems. In: Proc. of World Congress of the 19th International Federation of Automatic Control, Kapsztad, pp. 11740–11742 (2014)
7. Farina, L., Rinaldi, S.: Positive Linear Systems; Theory and Applications. J. Wiley, New York (2000)
8. Kaczorek, T.: Positive 1D and 2D systems. Springer, London (2001)
9. Kaczorek, T.: Positive linear systems consisting of n subsystems with different fractional orders. IEEE Trans. Circuits and Systems 58(6), 1203–1210 (2011)
10. Kaczorek, T.: Positive descriptor discrete-time linear systems. Problems of Nonlinear Analysis in Engineering Systems 1(7), 38–54 (1998)
11. Kaczorek, T.: Positive descriptor time-varying discrete-time linear systems
12. Kaczorek, T.: Positive singular discrete time linear systems. Bull. Pol. Acad. Techn. Sci. 45(4), 619–631 (1997)
13. Kaczorek, T.: Positivity and stability of time-varying discrete-time linear systems. Submitted to Conf. Transcomp 2015 (2015)
14. Kaczorek, T.: Selected Problems of Fractional Systems Theory. Springer, Berlin (2012)
15. Kaczorek, T.: Vectors and Matrices in Automation and Electrotechics. WNT, Warszawa (1998) (in Polish)
16. Rami, M.A., Bokharaie, V.S., Mason, O., Wirth, F.R.: Extremal norms for positive linear inclusions. In: 20th International Symposium on Mathematical Theory of Networks and Systems, Melbourne (2012)
17. Zhang, H., Xie, D., Zhang, H., Wang, G.: Stability analysis for discrete-time switched systems with unstable subsystems by a mode-dependent average dwell time approach. ISA Transactions 53, 1081–1086 (2014)
18. Zhang, J., Han, Z., Wu, H., Hung, J.: Robust stabilization of discrete-time positive switched systems with uncertainties and average dwell time switching. Circuits Syst, Signal Process. 33, 71–95 (2014)
19. Zhong, Q., Cheng, J., Zhong, S.: Finite-time H_∞ control of a switched discrete-time system with average dwell time. Advances in Difference Equations 191 (2013)

Decomposition and Parallelization of Linear Programming Algorithms

Andrzej Karbowski

Institute of Control and Computation Engineering,
Warsaw University of Technology

A.Karbowski@elka.pw.edu.pl

NASK, Research and Academic Computer Network, Warsaw, Poland

Abstract. The paper assesses possible approaches to decomposition and parallelization of basic linear programming algorithms, including: Dantzig-Wolfe, Benders, augmented Lagrangian, revised simplex and primal-dual interior point methods. Quite surprisingly, the first three of them - of hierarchical optimization type - exhibit considerable advantages nowadays, in the era of multicore processors and accelerators of any type (GPU, FPGA, Xeon Phi, etc.).

Keywords: linear programming, decomposition, parallel computing, hierarchical optimization, mixed integer programming, GPGPU, multicore calculations.

1 Introduction

In the paper we consider decomposition and parallel processing methods to solve linear programming problems. We assume the general form of such a problem:

$$\min_x c^T x \tag{1}$$

$$Ax = b \tag{2}$$

$$x \geq 0 \tag{3}$$

where $x, c \in \mathbb{R}^n$, $b \in \mathbb{R}^m$, and A is a matrix of size $m \times n$. It is assumed, that the domain is \mathbb{R}^n , but we comment also on the mixed case, when some of the coordinates of the x vector are integer numbers. At the beginning we will briefly present two classical approaches to decomposition of linear programming problems with block-angular structure of constraints matrix: Dantzig-Wolfe method for the case with constraints binding blocks and Benders method for the case with variables binding blocks. In the next part their contemporary significance will be assessed and some suggestions for improvements, as well as alternative approaches, will be presented.

2 Dantzig-Wolfe Method

We consider a linear programming problem of the form [9]:

$$\min_{x_0, x_1, x_2, \dots, x_p} \sum_{i=0}^p c_i^T x_i \tag{4}$$

$$\sum_{i=0}^p F_i x_i = b_0 \tag{5}$$

$$D_i x_i = b_i, \quad i = 1, \dots, p \tag{6}$$

$$x_i \geq 0, \quad i = 0, 1, 2, \dots, p \tag{7}$$

where $x_i, c_i \in \mathbb{R}^{n_i}, b_i \in \mathbb{R}^{m_i}, i = 0, 1, 2, \dots, p; F_i$ is a matrix of size $m_0 \times n_i, i = 1, \dots, p, D_i, i = 1, \dots, p$ is a matrix of size $m_i \times n_i$, where $m_i \leq n_i$.

The number of equations is $\sum_{i=0}^p m_i$, and the number of unknowns is $\sum_{i=0}^p n_i$. The full constraints equation can be summarized as follows:

$$\begin{bmatrix} F_0 & F_1 & F_2 & F_3 & \dots & F_p \\ 0 & D_1 & 0 & 0 & \dots & 0 \\ 0 & 0 & D_2 & 0 & \dots & 0 \\ \vdots & & & & & \\ 0 & 0 & 0 & 0 & \dots & D_p \end{bmatrix} \begin{bmatrix} x_0 \\ x_1 \\ x_2 \\ \vdots \\ x_p \end{bmatrix} = \begin{bmatrix} b_0 \\ b_1 \\ b_2 \\ \vdots \\ b_p \end{bmatrix} \tag{8}$$

that is, in the formulation (1)-(3) we will have:

$$c = \begin{bmatrix} c_0 \\ c_1 \\ c_2 \\ \vdots \\ c_p \end{bmatrix}, \quad x = \begin{bmatrix} x_0 \\ x_1 \\ x_2 \\ \vdots \\ x_p \end{bmatrix}, \quad A = \begin{bmatrix} F_0 & F_1 & F_2 & F_3 & \dots & F_p \\ 0 & D_1 & 0 & 0 & \dots & 0 \\ 0 & 0 & 0 & D_2 & \dots & 0 \\ \vdots & & & & & \\ 0 & 0 & 0 & 0 & \dots & D_p \end{bmatrix}, \quad b = \begin{bmatrix} b_0 \\ b_1 \\ b_2 \\ \vdots \\ b_p \end{bmatrix} \tag{9}$$

Owing to the specific block-angular structure of the constraints coefficient matrix it is possible to design an optimization method consisting in solving problems with the constraints matrices D_1, D_2, \dots, D_p and modified in subsequent iterations performance indices, calculated by a superior - coordination - problem, also called a master problem.

In the basic version of the Dantzig-Wolfe method [9], [11] it is assumed, that the system of equations and inequalities (6), (7), which we will call local constraints of the i -th problem, for $i = 1, \dots, p$, defines a bounded set (if one is not sure, it is sufficient to limit any coordinate by a very large number, greater than realistic values the solutions may take) - polyhedron $S_i, i = 1, \dots, p$. Denote the individual vertices of S_i as $x_i^j, j = 1, \dots, r_i$. Every point of this polyhedron can be represented as a convex combination of vertices:

$$x_i = \sum_{j=1}^{r_i} \alpha_{ij} x_i^j \tag{10}$$

where

$$\sum_{j=1}^{r_i} \alpha_{ij} = 1 \tag{11}$$

$$\alpha_{ij} \geq 0, \quad j = 1, \dots, r_i \tag{12}$$

Substituting (11)-(12) to (5)-(6) and denoting:

$$\sigma_0 = c_0 \tag{13}$$

$$f_{ij} = F_i x_i^j, \quad i = 1, \dots, p; j = 1, \dots, r_i \tag{14}$$

$$\sigma_{ij} = c_i^T x_i^j, \quad i = 1, \dots, p; j = 1, \dots, r_i \tag{15}$$

we obtain the following problem equivalent to problem (4)-(7):

$$\min_{x_0, \alpha} \sum_{i=1}^p \sigma_0^T x_0 + \sum_{j=1}^{r_i} \sigma_{ij} \alpha_{ij} \tag{16}$$

$$F_0 x_0 + \sum_{i=1}^p \sum_{j=1}^{r_i} f_{ij} \alpha_{ij} = b_0 \tag{17}$$

$$\sum_{j=1}^{r_i} \alpha_{ij} = 1, \quad i = 1, \dots, p \tag{18}$$

$$\alpha_{ij} \geq 0, \quad i = 1, \dots, p; j = 1, \dots, r_i \tag{19}$$

The equality constraints matrix in problem (16)-(19) will now take the following form:

$$\begin{aligned} & \begin{bmatrix} F_0 & f_{11} & f_{12} & \dots & f_{1r_1} & f_{21} & f_{22} & \dots & f_{2r_2} & \dots & f_{p1} & f_{p2} & \dots & f_{pr_p} \\ 0 & 1 & 1 & \dots & 1 & & & & & & & & & & \\ 0 & & & & & 1 & 1 & \dots & 1 & & & & & & \\ 0 & & & & & & & & & \ddots & & & & & \\ 0 & & & & & & & & & & & 1 & 1 & \dots & 1 \end{bmatrix} \\ & = \begin{bmatrix} F_0 & f_{11} & f_{12} & \dots & f_{1r_1} & f_{21} & f_{22} & \dots & f_{2r_2} & \dots & f_{p1} & f_{p2} & \dots & f_{pr_p} \\ 0 & e_1 & e_1 & \dots & e_1 & e_2 & e_2 & \dots & e_2 & \dots & e_p & e_p & \dots & e_p \end{bmatrix} \end{aligned} \tag{20}$$

where e_i is the i -th versor of dimension p . Hence, to find a solution of the problem (4)-(7) one can solve the equivalent problem (16)-(19). However, there is a difficulty - we do not know neither column vectors f_{ij} nor coefficients σ_{ij} for $i > 0$. However, we do not need to know all of them! If we use the revised simplex method, just enough for us is to know the inverse of the basis matrix and a column vector that is inserted therein.

Denote a feasible basis in the problem (16)-(19) at a certain stage as A_B , and the corresponding vector of dual variables as $\mu = A_B^{-T} c_B$, where c_B - vector containing the basic prices. The vector entering the basis, labeled with indices (k, t) , is the one for which the minimum value of the reduced price \tilde{c}_{kj} is reached, that is

$$\tilde{c}_{kt} = \min \left\{ \min_{l=1, \dots, n_0} \left(\tilde{c}_{0l} = \sigma_{0l} - \mu^T \begin{bmatrix} f_{0l} \\ 0 \end{bmatrix} \right), \min_{i=1, \dots, p} \left[\min_{j=1, \dots, r_i} \left(\tilde{c}_{ij} = \sigma_{ij} - \mu^T \begin{bmatrix} f_{ij} \\ e_i \end{bmatrix} \right) \right] \right\} \quad (21)$$

where f_{0l} is l -th column of the matrix F_0 . Typically, the reduced prices are calculated for nonbasic columns (variables), but the algorithm is valid also when they are calculated for basic variables, because prices for them are reduced to zero. This does not affect the course of the algorithm, as a new column is inserted into the basis only if its reduced price, a minimum for all columns, is negative. Otherwise, i.e., when $\tilde{c}_{kt} \geq 0$, the solution corresponding to the basis A_B would be optimal [9],[11].

Taking into account the definitions (14), (15) and dividing the vector of multipliers μ in two parts: μ_0 of dimension m_0 (the number of constraints binding subvectors x_i) and μ_1 of dimension p (the number of subvectors x_i for $i > 0$), the part of the formula (21) related to subvectors x_i for $i > 0$ can be written as follows:

$$\min_{i=1, \dots, p} \left[\min_{j=1, \dots, r_i} \left(\sigma_{ij} - \mu^T \begin{bmatrix} f_{ij} \\ e_i \end{bmatrix} \right) \right] = \min_{i=1, \dots, p} \left[\min_{j=1, \dots, r_i} (c_i^T - \mu_0^T F_i) x_i^j - \mu_{1i} \right] \quad (22)$$

Note, that assuming that the problem is not degenerate, i.e., the optimal solutions are the vertices of sets $S_i, i = 1, \dots, p$, every inner minimizations in (22) is equivalent to solving the problem:

$$\min_{x_i} [z_i = (c_i^T - \mu_0^T F_i) x_i] \quad (23)$$

$$D_i x_i = b_i \quad (24)$$

$$x_i \geq 0 \quad (25)$$

Let us denote the optimal value of the objective function in problem (23)-(25) as z_i^* . One iteration of Dantzig-Wolfe algorithm can now be summarized as follows [9]:

1. Solve in parallel p local problems (23)-(25)
2. Calculate

$$\tilde{c}_{kt} = \min \left(\min_{l=1, \dots, n_0} (c_{0l} - \mu_0^T f_{0l}), \min_{i=1, \dots, p} (z_i^* - \mu_{1i}) \right) \quad (26)$$

3. If $\tilde{c}_{kt} \geq 0$, then the current basic solution α_{ij} (where ij are pointers to the set of columns of the basis A_B) is the optimal solution of the problem (16)-(19)

and using the formula (10) the solution of the initial problem (4)-(7) can be determined. Otherwise go to point 4

4. (Column generation) Calculate the vector to be introduced into the basis and the corresponding price σ_{kt} . For $k > 0$ take as the introduced vector:

$$a^* = \begin{bmatrix} f_{kt} \\ e_k \end{bmatrix} \tag{27}$$

$f_{kt} = F_k x_k^t$ and $\sigma_{kt} = c_k^T x_k^t$, and for $k = 0$ introduce to basis the vector

$$a^* = \begin{bmatrix} f_{0t} \\ 0 \end{bmatrix} \tag{28}$$

and take $\sigma_{kt} = c_{0t}$.

5. Determine the vector removed from the basis, new values of variables, and the elements of the inverse matrix, using the standard procedure of the revised simplex method, that is, determining the index $q \in \{1, 2, \dots, m_0 + p\}$, such that

$$\frac{v_{0q}}{v_{Nq}} = \min_{\substack{j=1, \dots, m_0+p \\ v_{kj} > 0}} \frac{v_{0j}}{v_{Nj}} \tag{29}$$

where

$$v_0 = A_B^{-1} \begin{bmatrix} b_0 \\ 1 \\ \vdots \\ 1 \end{bmatrix}, \quad v_N = A_B^{-1} a^* \tag{30}$$

Go to point 1.

3 Benders Method

We consider a linear programming problem of the form¹:

$$\min_{x_0, x_1, x_2, \dots, x_p} \sum_{i=0}^p c_i^T x_i \tag{31}$$

$$G_0 x_0 = b_0 \tag{32}$$

$$G_i x_0 + D_i x_i = b_i, \quad i = 1, \dots, p \tag{33}$$

$$x_i \geq 0, \quad i = 0, 1, 2, \dots, p \tag{34}$$

where $x_i, c_i \in \mathbb{R}^{n_i}, b_i \in \mathbb{R}^{m_i}, i = 0, 1, 2, \dots, p; G_i$ is a matrix of size $m_i \times n_i$, with $m_i \leq n_i, D_i$ is a matrix of size $m_i \times n_i, i = 1, \dots, p$.

The number of equations is $\sum_{i=0}^p m_i$, and the number of unknowns is $\sum_{i=0}^p n_i$.

¹ In the original Benders' paper [1] a mixed discrete-continuous problem was considered, where both the objective and constraints functions were sums of two components: linear, dependent on continuous variables and nonlinear, being a function of discrete variables.

The full constraints equation can be presented as follows:

$$\begin{bmatrix} G_0 & 0 & 0 & \dots & 0 \\ G_1 & D_1 & 0 & \dots & 0 \\ G_2 & 0 & D_2 & \dots & 0 \\ \vdots & & & & \\ G_p & 0 & 0 & \dots & D_p \end{bmatrix} \begin{bmatrix} x_0 \\ x_1 \\ x_2 \\ \vdots \\ x_p \end{bmatrix} = \begin{bmatrix} b_0 \\ b_1 \\ b_2 \\ \vdots \\ b_p \end{bmatrix} \quad (35)$$

Thus, in the formulation (1)-(3):

$$c = \begin{bmatrix} c_0 \\ c_1 \\ c_2 \\ \vdots \\ c_p \end{bmatrix} \quad x = \begin{bmatrix} x_0 \\ x_1 \\ x_2 \\ \vdots \\ x_p \end{bmatrix}, \quad A = \begin{bmatrix} G_0 & 0 & 0 & \dots & 0 \\ G_1 & D_1 & 0 & \dots & 0 \\ G_2 & 0 & D_2 & \dots & 0 \\ \vdots & & & & \\ G_p & 0 & 0 & \dots & D_p \end{bmatrix}, \quad b = \begin{bmatrix} b_0 \\ b_1 \\ b_2 \\ \vdots \\ b_p \end{bmatrix} \quad (36)$$

Since the vector x_0 is present in all constraints, it will be convenient to denote it with a specific symbol; let us take $v \equiv x_0$. Quite often v has discrete coordinates, i.e., $v \in \mathbb{Z}^{n_0}$ and fixing it makes the remaining problem (as continuous) much easier to solve. Because of that it is called the vector of complicating variables [1].

With this notation we get the problem:

$$\min_{x_1, x_2, \dots, x_p, v} \sum_{i=1}^p c_i^T x_i + c_0^T v \quad (37)$$

$$D_i x_i + G_i v = b_i, \quad i = 1, \dots, p \quad (38)$$

$$G_0 v = b_0 \quad (39)$$

$$x_i \geq 0, \quad i = 1, 2, \dots, p, \quad v \geq 0 \quad (40)$$

The constraints equation will now take the form:

$$\begin{bmatrix} D_1 & 0 & \dots & 0 & G_1 \\ 0 & D_2 & \dots & 0 & G_2 \\ \vdots & & & & \\ 0 & 0 & \dots & D_p & G_p \\ 0 & 0 & \dots & 0 & G_0 \end{bmatrix} \begin{bmatrix} x_1 \\ x_2 \\ \vdots \\ x_p \\ v \end{bmatrix} = \begin{bmatrix} b_1 \\ b_2 \\ \vdots \\ b_p \\ b_0 \end{bmatrix} \quad (41)$$

In the case when the vector v is fixed (i.e., it is a parameter), and takes the values for which the constraint (38) is satisfied for some $x_i \geq 0$, the subvectors x_i could be determined by independent solution of p problems:

$$\min_{x_i} c_i^T x_i \quad (42)$$

$$D_i x_i = b_i - G_i v \tag{43}$$

$$x_i \geq 0 \tag{44}$$

Let us denote as $z_i(v)$ the optimal cost in the problem (42)-(44), that is

$$z_i(v) = \min_{x_i} \{c_i^T x_i | D_i x_i = b_i - G_i v, x_i \geq 0\} \tag{45}$$

and as V_0 the set of v for which all local problems (42)-(44) are feasible, that is:

$$V_0 = \{v \in \mathbb{R}^{n_0} | \exists x_i \in \mathbb{R}^{n_i} D_i x_i = b_i - G_i v, x_i \geq 0, i = 1, \dots, p\} \tag{46}$$

The problem (37)-(40) can now be written as the following problem with respect to the vector v :

$$\min_{v \in V_0} \sum_{i=1}^p c_i^T z_i(v) + c_0^T v \tag{47}$$

$$G_0 v = b_0 \tag{48}$$

$$v \geq 0 \tag{49}$$

Due to the fact, that the set V_0 is not known explicitly, while solving the problem (47)-(49) some points out of it can occur, what unfortunately means the inability to solve the problem (42)-(44). Then, it is worth to solve instead the problem dual to it, wherein in the case of infeasibility of the primal problem, the unboundedness appears, which is relatively easy to detect and, as it will be shown later on, constructively use.

The dual problem to the problem (42)-(44) has the form:

$$\max_{\lambda_i} (b_i - G_i v)^T \lambda_i \tag{50}$$

$$D_i^T \lambda_i \leq c_i \tag{51}$$

where $\lambda_i \in \mathbb{R}^{m_i}$. Let us denote as A_i the admissible set with regard to constraints defined by (51), namely:

$$A_i = \{\lambda_i | D_i^T \lambda_i \leq c_i\} \tag{52}$$

We assume, that the polyhedron A_i is not empty and has at least one vertex (extreme point). If it is unbounded, it has also extreme rays, that is nonzero elements in which exactly $\dim \lambda_i - 1$ linearly independent constraints is active. The extreme rays calculated with respect to the vertices form equivalence (abstraction) classes - half-lines. We say that a (finite) set of extreme rays is full, if it contains exactly one representative from every equivalence class. Suppose, that for a set A_i the full set of extreme rays has J_i elements, that is one can select from A_i at most J_i linearly independent extreme rays. We denote as $\lambda_i^k, k = 1, \dots, K_i$ the set of vertices of A_i and as $\tilde{\lambda}_i^j, j = 1, \dots, J_i$ the set containing J_i linearly

independent extreme rays of Λ_i (when the set Λ_i is bounded, we assume $J_i = 0$). The following theorem given by Minkowski and Weyl describes how any point of a polyhedron may be represented:

Theorem 1. *Let*

$$P = \{y \in \mathbb{R}^n \mid Hy \leq s\} \quad (53)$$

be a nonempty polyhedron with at least one extreme point. Let y^1, y^2, \dots, y^K be the extreme points, and let $\{\tilde{y}^1, \tilde{y}^2, \dots, \tilde{y}^J\}$ be a complete set of extreme rays of P . Let

$$Q = \left\{ \sum_{k=1}^K \alpha_k y^k + \sum_{j=1}^J \beta_j \tilde{y}^j \mid \alpha_k \geq 0, \beta_j > 0, \sum_{k=1}^K \alpha_k = 1 \right\} \quad (54)$$

Then, $Q = P$.

Assuming, that the set Λ_i is nonempty, either the dual problem (50)-(51) has an optimal solution and then the value of $z_i(v)$ is finite or it is infinite, in the case when the primal problem (42)-(44) is infeasible [4]. In particular, the value of $z_i(v)$ is finite if and only if:

$$(\tilde{\lambda}_i^j)^T (b_i - G_i v) \leq 0, \quad j = 1, \dots, J_i \quad (55)$$

In this case $z_i(v)$ will be also the optimal value of the performance index in the dual problem, achieved for some extreme point λ_i^{k*} of the set Λ_i , that is,

$$z_i(v) = (\lambda_i^{k*})^T (b_i - G_i v) = \max_{k=1, \dots, K_i} (\lambda_i^k)^T (b_i - G_i v) \quad (56)$$

In other words, $z_i(v)$ is the smallest number z_i , such that

$$(\lambda_i^k)^T (b_i - G_i v) \leq z_i, \quad k = 1, \dots, K_i \quad (57)$$

Using this characteristic of $z_i(v)$ and taking into account the condition (55) the master problem (47)-(49) can be written as follows:

$$\min_{v, z} c_0^T v + \sum_{i=1}^p c_i^T z_i \quad (58)$$

$$G_0 v = b_0 \quad (59)$$

$$(\lambda_i^k)^T (b_i - G_i v) \leq z_i, \quad i = 1, \dots, p, \quad k = 1, \dots, K_i, \quad (60)$$

$$(\tilde{\lambda}_i^j)^T (b_i - G_i v) \leq 0, \quad i = 1, \dots, p, \quad j = 1, \dots, J_i, \quad (61)$$

$$v \geq 0 \quad (62)$$

In practice, in the master problem (58)-(62) obviously not all extreme points in the definition of optimality cuts (60) and not all extreme rays in the definition of

feasibility cuts (61) are used, but a relaxed approach is applied, which takes into account these extreme points or rays that appeared in the course of the algorithm.

The typical iteration of the Benders algorithm can be described in the following way [1],[4]:

1. We solve the relaxed master problem (58)-(62), which takes into account only part of the problem constraints constructed with the use of the extreme points and rays that have emerged in previous iterations, i.e., solutions of the dual problem (50)-(51). The optimal solution (v^*, z^*) of the master problem is calculated.
2. For every $i = 1, \dots, p$ the following local problems are solved in parallel by simplex method:

$$\min_{x_i} c_i^T x_i \tag{63}$$

$$D_i x_i = b_i - G_i v^* \tag{64}$$

$$x_i \geq 0 \tag{65}$$

using the dual formulation.

3. If, for every $i = 1, \dots, p$, the local problem is feasible and the optimal cost is less than or equal to z_i^* , all the constraints are satisfied, we have the optimal solution of the master problem and the initial problem (31)-(34).
4. If the local problem for some i has the optimal solution with the performance index greater than z_i^* , the basic optimal solution λ_i^{k*} of the problem dual to it is remembered. Then it is transferred to the relaxed master problem, to which a cut

$$(\lambda_i^{k*})^T (b_i - G_i v) \leq z_i, \tag{66}$$

is added to constraints.

5. If for some i the local problem is infeasible, the problem dual to it has the infinite performance index, the extreme ray $\tilde{\lambda}_i^{j*}$ is found and stored. It is then passed to the master problem, and used to define the cut:

$$(\tilde{\lambda}_i^{j*})^T (b_i - G_i v) \leq 0, \tag{67}$$

added to the constraints of this problem.

Benders method is treated as dual to Dantzig-Wolfe method. This is due to the fact, that the constraints matrix A of a structure allowing for the use of one of these methods is obtained by transposing the matrix which implies the other. One can choose the type of problem (minimize/maximize), the type of constraint (equality/inequality), the numerical parameters, that exactly the dual problem relative to each other are obtained. Both initial, without decomposition, and decomposed, with coordination. The column generation in the Dantzig-Wolfe method will then correspond to adding cuts in the Benders method.

4 The Usefulness of Dantzig-Wolfe and Benders Methods on the Background of Other Possibilities of Parallelization of Linear Programming Problems

At present Dantzig-Wolfe and Benders methods in the original versions are rarely used for solving large scale continuous linear programming problems. The reason is their too slow convergence. Dantzig-Wolfe algorithm shows fairly quick approaching the optimum in first iterations, but then, in the next, very little progresses. In the Benders method cuts generated in the advanced stage of the algorithm can differ very little from each other. Extending the duration of the successive iterations becomes a problem. One can remedy this by using the approach proposed by Ruszczyński [19], in which a square regularizing proximal component is added to index (58), so we obtain a modified objective:

$$\min_{v,z} c_0^T v + \sum_{i=1}^p c_i^T z_i + \frac{1}{2} \|v - \bar{v}^k\| \quad (68)$$

where \bar{v}^k is the last, or even earlier, point of optimum (this depends on how much the solution has improved compared to the previous one). This is actually the application of the well-known bundle method of nondifferentiable optimization [17] to a linear programming problem. As in the bundle method, a part of inactive cuts of type (66), (67) is eliminated, so that there are no more than $n_0 + p$ of them. Unfortunately, this does not improve Benders algorithm enough, to make it an attractive method of solving large general linear programming problems, although it is very popular to solve mixed integer network problems [12], [20]. In the review [10] Fourer lists only one commercial implementation of this algorithm (AIMMS).

With the Dantzig-Wolfe method it is yet worse - the review [10] does not refer to any commercial implementation! Nevertheless, this approach in combination with branch and bound method (so-called branch and price approach), taking into account extensions like structural dual and primal-dual inequalities and stabilization strategies is used successfully to solve many practical problems of mixed integer (linear) programming [18], [20].

In modern linear programming solvers the revised simplex method in primal or dual version is usually used. The implementations use sparse matrices with many improvements, mainly for the selection of a new variable (column index) introduced into the basis.

Nowadays quite popular is, also using sparse solvers of systems of linear equations based on Cholesky factorization, primal-dual interior point method [10]. This method for most problems is a little faster, but its solutions are not as accurate as that of the simplex method [16], [5]. This is the reason, that to solve discrete and mixed discrete-continuous problems almost exclusively simplex method is used, combined with the branch and bound algorithm [8], [10]. This algorithm can be naturally parallelized - by allocating sequentially arriving branches to different cores [6]. During the calculations the information on the best feasible solution from the discrete/mixed domain (often obtained by using all sorts of heuristics [8], [10]) hitherto found is exchanged globally.

In the last two decades the issue of parallelization of the simplex algorithm was extensively studied [15]. Parallelization was mainly concentrated on operations on nonbasic variables, including the most laborious task of determination of the reduced prices, and the choice of variable entering the basis [7], [15]. Recall, that the reduced prices are calculated from the formula [11]:

$$\tilde{c}_N = c_N - A_N^T A_B^{-T} c_B \quad (69)$$

where A_B - basis matrix, A_N - matrix composed of the remaining columns of constraints (of a problem transformed to the canonical form), c_B - price coefficients for basic variables, c_N - price coefficients for nonbasic variables. The expression (69), in which there are operations of matrix multiplication and subtraction, can be easily parallelized and vectorized: it is sufficient to partition a set N of indices of nonbasic variables and to assign the resulting subsets of nonbasic variables N_1, N_2, \dots, N_p , such that $N_1 \cup N_2 \cup \dots \cup N_p = N$ to different cores. Earlier, before the division of the labor, the vector:

$$\pi_B = A_B^{-T} c_B \quad (70)$$

used by all threads should be calculated. Then, in parallel, one may calculate the coordinates of subvectors $\tilde{c}_{N_i}, i = 1, \dots, p$ of the vector \tilde{c}_N from the expression:

$$\tilde{c}_{N_i} = c_{N_i} - A_{N_i}^T \pi_B \quad (71)$$

The mentioned partition of the set N can be used later on to choose a coordinate to be introduced into the basis. In the simplest version, due to so-called Dantzig criterion, it will be (in the primal minimization problem) the choice of the lowest value of the price. Index q of the introduced variable can be determined using the following decomposition:

$$\tilde{c}_q = \min_{i \in N} \tilde{c}_i = \min \left(\min_{i_1 \in N_1} \tilde{c}_{i_1}, \dots, \min_{i_p \in N_p} \tilde{c}_{i_p} \right) \quad (72)$$

In modern solvers other methods of selection of the variable entering the basis are often used, such as, for example: steepest edge strategy, Devex, hybrid strategies [7], [15]. They also parallelize well, but primarily for dense matrices. Large practical problems usually are, unfortunately, sparse. According to Hall [15], it can be seen, that the parallel implementations of these versions of simplex algorithm, which are more effective as a tool to solve large, sparse linear programming problems, are less successful from the standpoint of acceleration due to parallelization. The biggest speedups demonstrate less powerful versions of the simplex algorithm. For general problems parallelization is advisable to calculation of the reduced prices in the dual simplex algorithm when the number of columns in relation to the number of rows is very large [15].

As it was mentioned earlier, currently the most widely used algorithm to solve continuous linear programming problems that do not require very high accuracy, especially sparse, is based on primal-dual interior point method [13]. It is a general nonlinear programming method [14]. The decomposition of this method exploiting

the structure of the Jacobian matrix while Cholesky factorization was thoroughly described in [13] and [14]. However, it consists actually in writing the full Newton method solver. Moreover, relocating and combining different blocks of the Jacobian in this approach makes it quite elaborated and addressed to rather advanced users.

Because of the above mentioned difficulties, for less advanced users, more attractive may be another general nonlinear programming algorithm, much simpler to implement, namely augmented Lagrangian method, also known as the method of multipliers [2]. It is so attractive, because it allows for the decomposition of a general linear problem (i.e., without the assumption of a special structure of the constraints matrix) until independent scalar optimizations, which can be easily solved analytically.

More precisely, the following problem is considered [3]:

$$\min_x c^T x \tag{73}$$

$$Ax = b \tag{74}$$

$$0 \leq x \leq d \tag{75}$$

where $c, x, d \in \mathbb{R}^n$, $b \in \mathbb{R}^m$ and A is a $m \times n$ matrix. Multipliers method proposed in [3] minimizes augmented Lagrangian of the equivalent problem in the enlarged space of decision variables, so that the constraints binding variables, that cause nonseparability, do not appear in the Lagrangian, they only limit the domain of new variables. The equivalent formulation will have the form:

$$\min_{x,u} c^T x \tag{76}$$

$$a_{ji}x_i = u_{ji}, \quad j = 1, \dots, m, \quad i \in I(j) \tag{77}$$

$$\sum_{i \in I(j)} u_{ji} = b_j, \quad j = 1, \dots, m \tag{78}$$

$$0 \leq x \leq d \tag{79}$$

where $I(j)$ is the set of indices of nonzero coordinates of the j -th row of the matrix A . New values of decision variables x_i^{k+1}, u_{ji}^{k+1} will be determined by minimizing the augmented Lagrangian:

$$L_a(x, u, \mu) = \sum_{i=1}^n c_i x_i + \sum_{j=1}^m \sum_{i \in I(j)} \mu_{ji}^k (a_{ji}x_i - u_{ji}) + \frac{\alpha^k}{2} \sum_{j=1}^m \sum_{i \in I(j)} (a_{ji}x_i - u_{ji})^2 \tag{80}$$

subject to $\sum_{i \in I(j)} u_{ji} = b_j, \quad j = 1, \dots, m$ and $0 \leq x \leq d$. New values of Lagrange multipliers are calculated from the formula:

$$\mu_{ji}^{k+1} = \mu_{ji}^k + \alpha^k (a_{ji}x_i^{k+1} - u_{ji}^{k+1}) \tag{81}$$

where α^k is a suitably chosen step coefficient. The problem with index (80) can already be easily solved analytically, leading, after getting rid of the vector u , to the algorithm:

$$x_i^{k+1} = \left\{ x_i^k - \frac{1}{\alpha^k \|a_i\|_2^2} [c_i + a_i^T (\bar{\mu}^k + \alpha^k w^k)] \right\}_+ \tag{82}$$

where a_i is the i -th column of the matrix A , $\{\cdot\}_+$ is the projection on the interval $[0, d_i]$, and w^k is the vector with coordinates expressed by the formula:

$$w_j^k = \frac{1}{t_j} (a_j^T x^k - b_j) \quad j = 1, \dots, m \tag{83}$$

where t_j is cardinality of the set $I(j)$, that is $t_j = \bar{I}(j)$. The coordinates of the vector $\bar{\mu}^k$ are multipliers characteristic for subsequent constraints (74) of the initial problem, because it is easy to show that:

$$\mu_{ji}^k = \bar{\mu}_j^k \quad \forall k, j = 1, \dots, m, i \in I(j). \tag{84}$$

They are changed iteratively according to the formula:

$$\bar{\mu}_j^{k+1} = \bar{\mu}_j^k + \frac{\alpha^k}{t_j} \left(\sum_{i \in I(j)} a_{ji} x_i^{k+1} - b_j \right), \quad j = 1, \dots, m. \tag{85}$$

It is difficult to propose a simpler algorithm for solving general linear programming problems. This method, owing to the use of the sets $I(j)$ can be attractive for solving very large problems, which tend to be sparse. On the other hand, when solving dense problems, thanks to a scalar, very simple expressions for new primal (82) and dual (85) variables, it can be easily and efficiently implemented in hardware vector and array processing environments (SIMD), e.g., using SSE, AVX, Altivec, GPU.

5 Conclusions

The fundamental in the linear programming world simplex method does not parallelize well when it is used to solve big real-life problems. The decomposition of recently popular primal-dual interior point method is rather a decomposition of the Newton algorithm to solve the set of nonlinear equations, than the decomposed optimization itself. Moreover, this method is not very useful to solve discrete or mixed discrete-continuous problems.

It seems, that the old Dantzig-Wolfe and Benders methods have the highest potential to be used to solve in the modern multicore environment the most important from the practical point of view mixed integer linear programming problems with block-angular constraint matrices.

In the general case of big dense matrices, the most promising seems to be the augmented Lagrangian method, which, owing to its fine grain, allows for even a beginner in mathematical programming to write an efficient linear optimization code, easily ported to modern systems with SIMD accelerators.

References

1. Benders, J.F.: Partitioning procedures for solving mixed-variables programming problems. *Numer. Math.* 4, 238–252 (1962)
2. Bertsekas, D.P.: *Constrained Optimization and Lagrange Multiplier Methods*. Academic Press, Boston (1982)
3. Bertsekas, D.P., Tsitsiklis, J.N.: *Parallel and Distributed Computation: Numerical Methods*. Prentice-Hall, Englewood Cliffs (1989)
4. Bertsimas, D., Tsitsiklis, J.N.: *Introduction to Linear Optimization*. Athena Scientific, Belmont (1997)
5. Bixby, R.E.: Solving Real-World Linear Programs: A Decade and More of Progress. *Operations Research* 50, 3–15 (2002)
6. Bixby, R.E., Cook, W., Cox, A., Lee, E.K.: Computational Experience with Parallel Mixed Integer Programming in Distributed Environment. *Annals of Operations Research* 90, 19–43 (1999)
7. Bixby, R.E., Martin, A.: Parallelizing the Dual Simplex Method. *INFORMS Journal on Computing* 12, 45–56 (2000)
8. Bixby, R.E., Rothberg, E.: Progress in computational mixed integer programming - A look back from the other side of the tipping point. *Annals of Operations Research* 149, 37–41 (2007)
9. Dantzig, G.B., Wolfe, P.: Decomposition Principle for Linear Programs. *Operations Research* 8, 101–111 (1960)
10. Fourer, R.: Linear Programming Software Survey. *OR/MS Today* 40(3) (2013)
11. Gass, S.I.: *Linear programming: methods and applications*. McGraw-Hill, New York (1969)
12. Geoffrion, A.M., Graves, G.W.: Multicommodity Distribution System Design by Benders Decomposition. *Management Science* 20, 822–844 (1974)
13. Gondzio, J., Sarkissian, R.: Parallel interior-point solver for structured linear programs. *Math. Program.* 96, 561–584 (2003)
14. Gondzio, J., Grothey, A.: Exploiting structure in parallel implementation of interior point methods for optimization. *Comput. Manag. Sci.* 6, 135–160 (2009)
15. Hall, J.A.J.: Towards a practical parallelisation of the simplex method. *Computational Management Science* 7, 139–170 (2010)
16. Illés, T., Terlaky, T.: Pivot versus interior point methods: Pros and cons. *European Journal of Operational Research* 140, 170–190 (2002)
17. Kiwiel, K.C.: *Methods of Descent for Nondifferentiable Optimization*. Springer, Berlin (1985)
18. Lübbecke, M.E., Desrosiers, J.: Selected Topics in Column Generation. *Operations Research* 53, 1007–1023 (2005)
19. Ruszczyński, A.: Regularized decomposition and augmented Lagrangian decomposition for angular linear programming problems. In: Lewandowski, A., Wierzbicki, A. (eds.) *Aspiration Based Decision Support Systems. Lecture Notes in Economics and Mathematical Systems*, vol. 331, pp. 80–91. Springer, Berlin (1989)
20. Vanderbeck, F., Wolsey, L.A.: Reformulation and Decomposition of Integer Programs. In: Jünger, M., Liebling, T.M., Naddef, D., Nemhauser, G.L., Pulleyblank, W.R., Reinelt, G., Rinaldi, G., Wolsey, L.A. (eds.) *50 Years of Integer Programming 1958–2008*, pp. 431–502. Springer, Heidelberg (2010)
21. Yarmish, G., Van Slyke, R.: A distributed, scaleable simplex method. *Journal of Supercomputing* 49, 373–381 (2009)

45 Years of Mechatronics – History and Future

Andrzej Milecki

Poznan University of Technology, ul. Piotrowo 3, 60-965 Poznań, Poland
Andrzej.milecki@put.poznan.pl

Abstract. The word of Mechatronics is already 45 years old. This is an occasion to present the definitions of mechatronics, its history and to show current state of the art in this discipline. The article presents a short overview of the literature related to mechatronics. The development of mechatronics is also illustrated along with development of computers and washing machines. Finally the achievements are summarized and some questions related to mechatronics' future are stated.

Keywords: mechatronics, controller, washing machine.

1 Introduction

The word "Mechatronics" was originally created in 1969 by Mr. Tetsuro Mori, from Japanese Corporation Yaskawa Electric that was building mechanical factory equipment. At that time, Yaskawa Electric Corporation started to use electronic features for manufacturing mechanical equipment and wanted to introduce a technical term to name that new technology. Therefore Mori combined the two technical words 'mechanical' and 'electronics' and created the new term "Mechatronics". The Yaskawa Company has applied to make this word a registered brand and has got the rights in 1972 [1]. In the beginning, this term didn't gain much popularity, but after the 1980s this word has received broad acceptance in industry and in academia and, in order to allow its free use, Yaskawa decided to abandon its rights to "Mechatronics" in 1982. During this time the meaning of word has broadened and it is now widely used as a description of almost every application of electronics into mechanical devices. A number of definitions has been proposed in the literature for the wider concept of mechatronics. The most commonly used definitions emphasize mechatronics as the synergistic integration of mechanical engineering with electronics and intelligent computer control in the design and manufacture of products and processes.

Nowadays, the term Mechatronics is 45 years old and within these years significant improvements were introduced in the capacity and capability of the technologies related to mechatronics. There are many devices, which has changed significantly their design concept, parameters and functionality as a result of development of mechatronics.

In the paper a few different definitions of mechatronics are presented. These definitions are also illustrated by figures and schemes. In the next point the brief history of mechatronics is sketched. Its evolution was illustrated with development of washing machines and with research conducted at Poznan University of Technology.

The goal of the paper is to show the history and possible future potential and directions for mechatronics as an engineering discipline. There are still open areas for creation of a scientific background, tools and methods for design of mechatronic devices. Also the definition field is to be further explored for example, a definition of a single overarching structure for mechatronics is still needed.

2 Definitions of Mechatronics

There are several books focusing on mechatronics, for example [2], which includes case studies illustrating the mechatronics concepts applied in such areas as automatic cameras, aerospace parts manufacturing, fly-by-wire systems, and boat autopilot. Other books which can be cited here are: [3–6]. An overview of general aspects are given in the journals: *Mechatronics* [12] and *IEEE/ASME* [13]. Since early 1990s several conferences have been organized e.g., UK Mechatronics Forum (1990, 1992, 1994, 1996, 1998, 2000, 2002), AIM (1999, 2001, 2003), IFAC (2000, 2002, 2004). The mechatronics developments up until now can be found for example in papers [9–13] published in journals and conference proceedings. In the last 10 years more sophisticated control functions have been introduced, e.g., the adaptation of controller parameters, the detection of faults and, the reconfiguration of device elements and controller parameters. Hence, mechatronic systems are evolving into direction which is called intelligent mechatronic systems.

Over the last 45 years several definitions of mechatronics, either as a text, logo or pictures have been proposed. On a web page [14] one may find list of over 20 definitions of mechatronics, which conclude that mechatronics is about the integration of the core disciplines of mechanical engineering (mechanical elements, machines, robot arms etc.), electronics (microelectronics, power electronics, sensors and actuators) and information technology (control and automation, software engineering, artificial intelligence). Probably the most popular definition is given on a web page of a Mechatronics journal: “Mechatronics is the synergistic combination of precision mechanical engineering, electronic control and systems thinking in the design of products and manufacturing processes. It relates to the design of systems, devices and products aimed at achieving an optimal balance between basic mechanical structure and its overall control”. Nowadays, the aim of mechatronics is to improve the functioning of systems and devices by transforming them into one automatic and intelligent system.

Other definitions of the term “mechatronics” emphasize the fact that this discipline is a synergistic blend of its components. In this example mechatronics is: ‘synergistic combination of precision engineering electronic control and systems thinking in the design of products and manufacturing processes’. Industrial Research and Development Advisory Committee of the European Community Mechatronics defines it as: ‘the application of complex decision making to the operation of physical systems’. The term mechatronics is described by many graphics and schemes as shown in Fig. 1. In the design of mechatronic products, interrelations play an important role. This is because the mechanical solution influences the electronic system and the control system has influence on electronic and mechanical parts. In this way simultaneous engineering has to take place, with the goal of designing an integrated system and also creating synergistic effects.

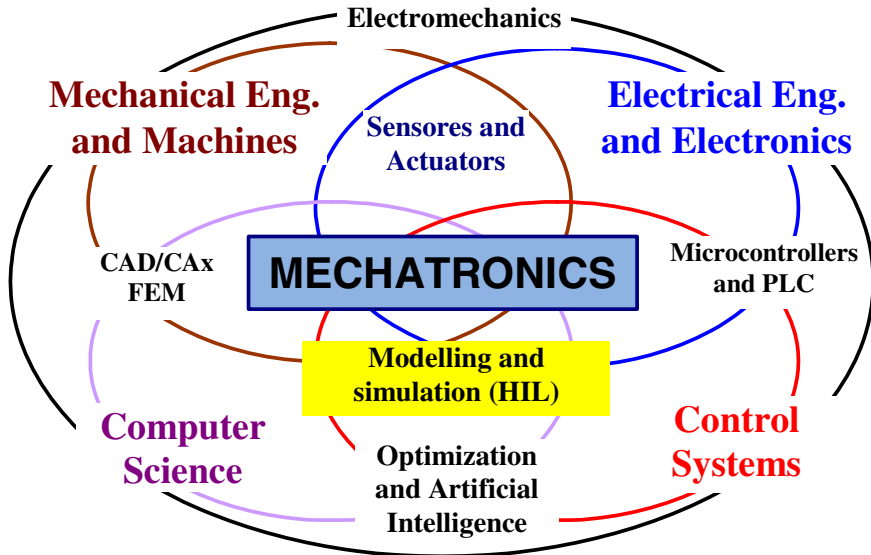


Fig. 1. The graphical definition of mechatronics

Before the 1970s, such products like machine tools, manufacturing equipment, and home appliances were based only on mechanical solutions with only small number of electric elements like switches, relays, electro-valves, motors, lamps etc. In the seventies, several new advanced electronic elements like thyristors and triacs, high power transistors, as well as operational amplifiers and digital integrated circuits occurred on the market, what significantly enlarged the possibilities of implementation of electronics into mechanical products. In parallel the computers became smaller and faster. New programming methods and languages proposed in 1970s facilitated the implementation of computers in control of complicated production processes, NC machine tools, robots and production devices. Engineers and end-users noted and appreciated the benefits of using computers in control. In 1972 a first microcontroller occurred on the market, what facilitated the implementation of computer control into mechanical devices. This was a pure breakthrough in mechatronics development, i.e. in embedding of electronic controllers in mechanical devices. Thanks to the microcontrollers, since the 1980s, the implementation of electronics into mechanical devices become easy and cheap.

Nowadays the application area of mechatronics is extremely broad. It is used in the automation of devices and processes, servo-drives, industrial machines, medical systems, home equipment, energy and power systems, vehicles, military equipment, data communication systems, medicine equipment and many, many others. Google gives almost 26 million results as a response to word search for “mechatronics”. In the 45 years of mechatronics history many improvements have occurred in science and in engineering. The list of these achievements must however also be placed in the context of earlier developments and not only considered a result of “mechatronics” word creation. Nevertheless, the integration of mechanics and electronics is usually

assigned to mechatronics. For example, in manufacturing, the introduction of mass production systems integrated with machine tool and robots technology also supported the underlying concepts of systems integration generally felt to be integral to mechatronics [2]. Mechatronics has also developed issues such as biomechatronics, focused on development of devices which mechanics, work and control is built based on biological entities and micromechatronics, generally associated with MEMS solutions.

3 Control Computers Then and Now

Mechatronic device consists of: mechanical part, electrical part (electromechanic), electronical part and computer technology (control and informatics). The elements of mechatronics systems include sensors, actuators, microcontrollers (or microprocessors) and real-time control software.

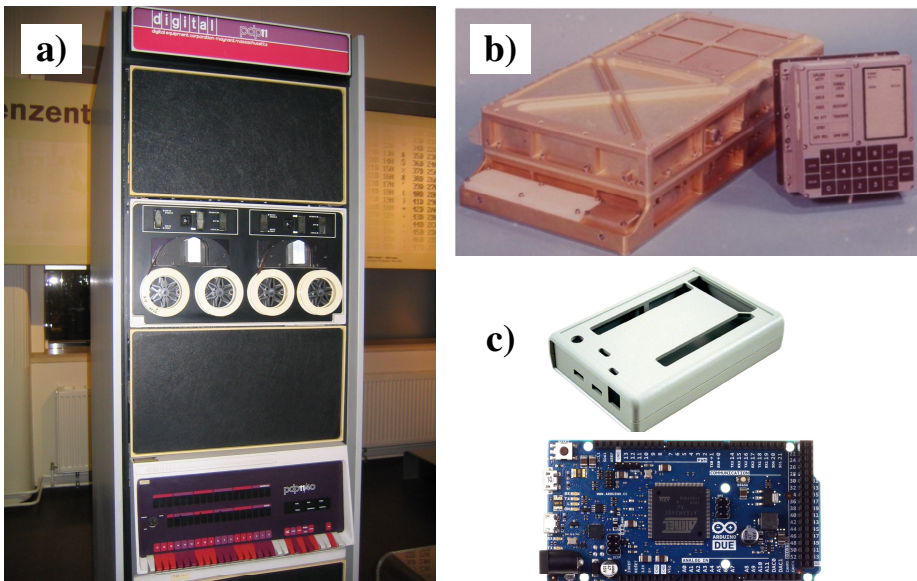


Fig. 2. Computers: a) PDP-11/40 (181×76×54) cm, b) Apollo Guidance Computer and its interface (61×32×17) cm, c) Arduino duo (11×7,7×2,5) cm

The differences between the technical state of the art in 1970s when mechatronics epoch began and now, is illustrated with the parameters of computers used then and presently. In the year 1970 the Digital Equipment Corporation (DEC) introduced the PDP-11, which was a series of 16-bit minicomputers sold until the 1990s. These computers had several innovative features, and were easier to program than their predecessors. The computer allowed to address 4 MB of physical memory segregated onto a private

memory bus and 2 kB of cache memory. The PDP-11 was used in many real-time applications. In total, around 600,000 PDP-11s of all models were sold. Its successor in the mid-range minicomputer niche was the 32-bit VAX-11. Unfortunately, the dimensions of the PDP-11 computer were in range of meters, so it was not possible to embed it into mechanical devices (Fig. 2).

In fact, the only computer from 1970s, which was indeed embedded was Apollo Guidance Computer (AGC). It was installed on a board of Apollo Command Module and Lunar Module. The computer provided computation and electronic interfaces for guidance, navigation, and control of the spacecraft. It had a 16-bit word length, with 15 data bits and one parity bit. Most of its software was stored in a special read-only memory known as “core rope” memory. The IBM PC XT released in 1981, had 8 times more memory than Apollo's Guidance Computer – 16k, vs. the Apollo's 2k and it ran at a clock speed of 4 MHz while AGC was four times slower. The iPhone is so advanced compared to the computer used in Apollo's guidance system that it's really hard to compare the two. The AGC may be compared only with produced today 8-bit microcontroller like for example ATmega 128 (16 MHz). Microcontrollers like 16-bit PIC24 or Arduino have much better parameters than AGC.

4 Mechatronics Development on Example of Washing Machines

The development of mechatronics can be easily observed on example of washing machines. The first washing machine was probably the scrub board invented in 1797. In 1908 the Hurley Machine Company invented a drum type washing machine with a galvanized tub and an electric motor (patent issued in 1910). In the 1940s, the first fully automated, electric washing machine appeared on the market. This type of washing machines strengthened their position on the market in 1970s. In that time, the machines were only electromechanical devices, having not a single electronic piece. The programmer (Fig. 3) used several cams to switch on and off, different elements in the washing machine. This programmer was driven by small AC synchronous motor.

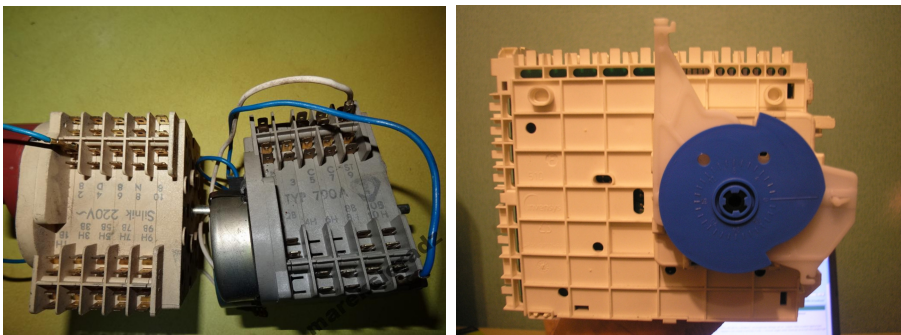


Fig. 3. The photos of washing machine cam controllers

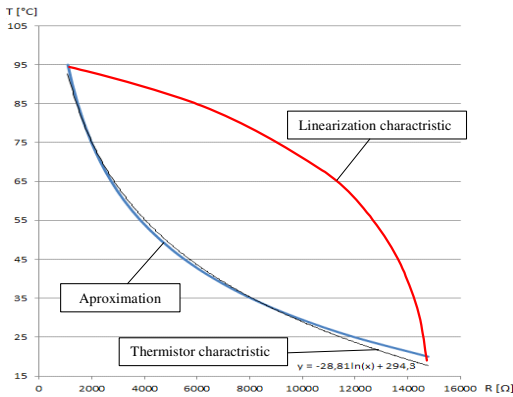


Fig. 4. NTC thermostat characteristic, its approximation (blue) and linearization curves (red)

The sensors used in washing machines produced in that time were switch type, performing only on/off operation. This were only thermostats, which changed the position of switches when the water temperature reached 30 °C, 60 °C and 90 °C and pressostat, which was used for switching off the electro valve when the water level produced assumed pressure. Nowadays on/off thermostat has been replaced by thermistor, which is a semiconductor element with a non-linear characteristic. This characteristic may be approximated by following equation:

$$T = -28.8 \cdot \ln(R) + 294.3 \quad (1)$$

where: T – temperature in °C, R – NTC thermistor resistance in Ohms.

In washing machine controllers currently used, this curve is reversed as shown in Fig. 4, stored in microcontroller's memory and used in linearization.

In the washing machines produced more than 20 years ago the on/off pressure sensors were applied. Nowadays, they are replaced by a linear pressure sensor, in which ferromagnetic core moves inside the coil according to the pressure of water in a drum. The measurement is only possible when microprocessor is used. This enables to fill water according to the washing program or to the weight of the laundry in a drum. In the modern washing machines also MEMS acceleration sensors are used, which enable the measurement of drum oscillations. Thanks to this the balance of laundry in the drum is controlled and the rotational velocity is adjusted accordingly, assuring safe and silent work. In old washing machines the heater could be switched only on/off by a relay, which caused a wear problem, and therefore is now replaced by triac. This low-cost semiconductor element is very durable, and is also used for switching on and off of electro valves and pump motors.

All actuators used in old washing machines were only on/off type. These concern: electro-valve which was switched on for filling the drum by the water, the heater used for heating the water, and the pump which was used for pumping the water out. The main motor was built as three-in-one element, having three coils: first for left rotation, the second for right rotation and the third used for centrifugation. Every motor coil was switched on separately.

In old washing machines usually one phase or two phase inductive motor was used to drive the drum. It posed three coils, which enabled to set only low velocity rotation in the left or right direction or high velocity rotation in the right direction. In many

washing machines produced till now a one phase commutated motor is applied. Using a triac it is possible to control a velocity in a wide range.

In the late 1970s, the first microprocessor-controlled washing machine was designed. This allowed to improve the functionality and achieve great flexibility and effectiveness in laundry machines. Today, all washing machines in the market are controlled by microprocessor. The number and quality of various sensors and mechanisms was improved, which enables the automation of the entire washing process. In the modern washing machines some sensors can measure the parameters, giving analog electrical signals on the outputs. This enables to control the water level, water temperature, spin speed, cycle program, load balancing, child lock systems, and noise reduction systems. Since 1980 the microcontrollers were added to the washing machine design. Nowadays one may find different washer models with LED or LCD displays and buttons for operation. Thanks to the microprocessors the washing machines became "smart", and that made the whole washing process faster and easier. Washers today are energy efficient and environment friendly. Thanks to advanced control algorithms applied in microcontrollers, washers use less electricity to run the machine and also to set the water to the right temperature levels.

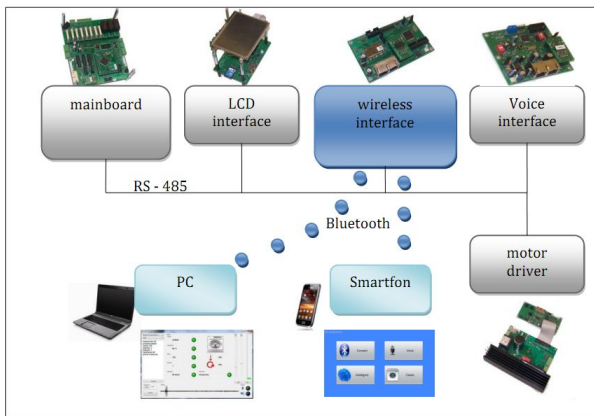


Fig. 5. Washing machine controller communication

much more complicated and time consuming. Also the programming, testing and debugging procedures are almost completely different and more difficult.

Two years ago, at Poznan University of technology a new washing machine controller was designed and built, basing on a 32-bit STM32 microcontroller universal [17]. In order to achieve flexibility we proposed the modular structure, which consisted of:

- main board with CPU type STM32, input sensor module, USB, RS-485 and other communication units (Fig. 5), EEPROM and buzzer module,
- user interfaces: touch-panels (Fig. 6), smartphone, laptop,
- high power board for control of the drum drive and for switching on/off, etc.

In typical washing machines produced nowadays, 8-bit microcontrollers are commonly used. However, today the market offers 32-bit microcontrollers, which are able to perform advanced control tasks but their design is much more complicated [15, 16]. The same concerns the design of printed circuit board (PCB), which requires high experience of the designer. Comparing to 8-bit microcontroller, the start-up process of 32-bit microcontrollers is

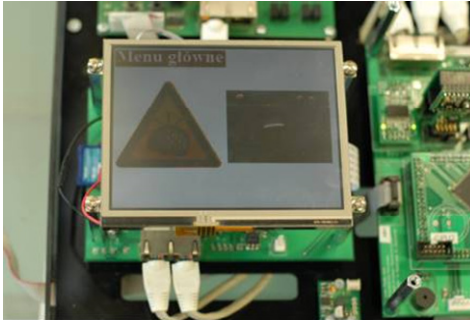


Fig. 6. Controller with touch-panel



Fig. 7. The photo of the controller and connected to it interfaces

All modules communicated together using serial communication networks. In the proposed solution every single module posed its own intelligence, which was an important advantage. Every module could be built as autonomous, self-controlled unit and therefore in a more safe way. Thanks to this, every module could also be designed independently. In this approach, the user had the opportunity to create the controller's structure, abilities and price. Moreover, the same controller could be used in different washing machines but with different types of additional modules, for example user interfaces. Such solution facilitated the testing and certification process.

In the designed washing machine controller three serial busses were implemented: SPI, USB and RS-485, which assured high speed internal communication. The first one was used for programming purposes, setting in motion, debugging and communication with EEPROM. The second bus was used for communication with user interface and high power module i.e. drive controller, relay module. Within the project a few human-washing machine interfaces were designed, built and tested, starting with a mechanical one with rotary switch and LCD displayed and finishing on a color touch-

screen (Fig. 6). The controller was also equipped with a voice interface module which could be used for communication with, for example blind users.

Additionally the wireless communication card was designed and connected to the controller. It enabled the connection with any device using Bluetooth system, for example with PC, smartphone or pager. The special software for smartphone (Samsung S5) and PC (laptop) was written and implemented. It enabled the programming of washing machine using standard programs or the user could create their own washing cycle. Moreover, a so called by us "intelligent programming" method was proposed and implemented. It enabled settling of the washing parameters using questions and answers. This method utilized control methodology based on fuzzy logic. The additional interface was a USB, which enabled the wire communication with PC

based computer and was used for testing and diagnosis of washing machine. In a project our own direct drive controller was designed and built, but almost every washing machine drive system could be used i.e. single phase serial motor with triac, direct drive or synchronous PM motor (Fig. 7).

5 Discussion and Conclusion

The influence of mechatronics as driver of the product and production process development is nowadays unquestionable. The introduction of microprocessors in 1980's brought dynamic advancement resulting in the production of embedded microcontrollers. These developments in computer science and information technology resulted in second generation of mechatronics. In this generation a deeper integration of advanced software enabled the improved functioning of complex mechatronic machines and systems. Thanks to this, the mechatronic devices are characterized with a complex structure and perform many, also intelligent functions. The mechatronics goal for now and for the future is to develop autonomous, self-learning devices.

Mechatronics approach enables to optimize the available mix of technologies in order to establish a high quality and high precision products assuring the obtainment of the features customers demand. Mechatronics is nowadays a must for successful high tech product innovation. Almost 90% of today's innovation in modern drives, house equipment and cars relate to mechatronic systems. The results of research in mechatronics are quite generally applicable. This design strategy in mechatronic devices seems to be dominative for the future; thus it is critical to assure good levels of education in this topic. The development of new, fast and intelligent devices could increase the production performance and benefit customers.

The term "Mechatronics" is already 45 years old. It means that it is now matured enough and its definition is clear and permanent. However, several parallel definitions exist which either only seem to mean the same, or only are compatible. Moreover, the definitions treat mechatronics too wide, which means that almost every device having mechanical part and electronic controller can be regarded as a mechatronic one. Now it is time to define current and future direction and status of mechatronics as an engineering discipline, or maybe also a design philosophy. In the paper [18], David Bradley asked "Does mechatronics still remain significantly different when compared to other approaches to system integration?" As the answer, it seems that the direction of research related to mechatronics should be defined afresh and differences between mechatronics and other disciplines should be clearly indicated.

In the last years one may observe the trend in mechatronics development into creation of devices which are animals- or even human- like. This seems to be a real challenge for the future development of mechatronic devices, which should move like a human, use similar to human senses and could communicate similarly to humans. Therefore the development and implementation of speech recognition and communication systems into mechatronic devices is very important. Also visual system applications in mechatronic devices can bring significant progress in the future. It will be very convenient and nice to

communicate with devices using voice and gestures. In addition, the application of artificial intelligence methods in mechatronic devices is here crucial. Maybe, from these observations and insights a new word like for example “Humantronics” can be a highlight for future mechatronics trends and developments.

To reach this goal, I fully agree with what David Bradley wrote in [18], that next steps of development are, e.g., more intelligent mechatronic systems with learning behavior and decision making, fault-tolerant mechatronic systems for highly reliable and safe systems (e.g., vehicles, production machinery, medical devices and aerospace systems). A further development may be the integration of mechatronic systems with wire-bound and wire-less communication channels (audio nets, internet), e.g., with remote access for software updates, telemonitoring and telediagnosis, maintenance procedures, security measures, etc.

References

1. Japan Trade Registration No. 946594 (1972)
2. Bradley, D., Dawson, D., Burd, D., Loader, A.: *Mechatronics electronics in products and processes*. Chapman & Hall, London (1991)
3. Kitaura, K.: *Industrial mechatronics*. New East Business Ltd. (1986) (in Japanese)
4. McConaill, P., Drews, P., Robrock, K.-H. (eds.): *Mechatronics and robotics*. ICS Press, Amsterdam (1991)
5. Heimann, B., Gerth, W., Popp, K.: *Mechatronik (Mechatronics)*. Fachbuchverlag Leipzig, Leipzig (2001)
6. Bishop, C.: *The mechatronics handbook*. CRC Press, Boca Raton (2002)
7. *Mechatronics, An international journal*. Aims and scope. Pergamon Press, Oxford (1991)
8. *IEEE/ASME Transactions on Mechatronics*, vol. 1(1). IEEE, Piscataway (1996)
9. Schweitzer, G.: *Mechatronics – A concept with examples in active magnetic bearings*. *Mechatronics* 2, 65–74 (1992)
10. Harashima, F., Tomizuka, M.: *Mechatronics – “what it is, why and how?”*. *IEEE/ASME Transactions on Mechatronics* 1, 1–2 (1996)
11. Isermann, R.: *Modeling and design methodology of mechatronic systems*. *IEEE/ASME Transactions on Mechatronics* 1, 16–28 (1996)
12. Gausemeier, J., Brexel, D., Frank, T., Humpert, A.: *Integrated product development*. In: *Third Conference on Mechatronics and Robotics, Germany* (1995)
13. Tomizuka, M.: *Mechatronics: from the 20th to the 21th century*. In: *First IFAC Conference on Mechatronic Systems, Darmstadt, Germany*, pp. 1–10. Elsevier, Oxford (2000)
14. <http://www.mechatronics.colostate.edu/definitions.html> (accessed November 15, 2014)
15. Mallikarjun, S.: *32-bit MCUs offer high integration, high functionality*. *Electronic Products* 49(7), 40–43 (2006)
16. Brown, G.: *Discovering the STM32 Microcontroller* (2012)
17. Milecki, A., Pittner, G.: *Design of 32-bit Washing Machine Controller*. *Solid State Phenomena* 220-221, 463–469 (2015)
18. Bradley, D.: *Mechatronics – More questions than answers*. *Mechatronics* 20, 827–841 (2010)

Analysis and Modelling of Magnetic Circuits in Magnetic Shape Memory Alloy Actuators

Bartosz Minorowicz¹, Cezary Jędrzycka², Frederik Stefański¹, and Amadeusz Nowak¹

¹ Institute of Mechanical Technology, Poznan University of Technology
{bartosz.minorowicz, frederik.stefanski, nowak.amadeusz}@gmail.com

² Institute of Electrical Engineering and Electronics, Poznan University of Technology
cezary.jedryczka@put.poznan.pl

Abstract. Authors presented in article modeling of magnetic circuit for magnetic shape memory alloys. These alloys are a new class of smart materials which can generate strains and force in external magnetic field. Thus that properties MSMA fill gap between classical SMA and magnetostrictive materials. As a drawbacks strong nonlinearities should be mentioned: wide asymmetric hysteresis loop, thermal sensitivity, first cycle effect. Very high flux density need for effective operation over the whole range strongly affects on size of the magnetic circuit. Mathematical modeling does not allow for design optimal shape of core. Authors aided their work by FEA of magnetic flux in core. Computed results were compared with magnetic induction measured on prepared test bench.

Keywords: magnetic shape memory alloys, FEA, MSMA, hysteresis, position regulation.

1 Introduction

Nowadays most of drives in machines are conventional solutions, in which linear (solenoids) and rotary (AC, DC motors, torque motors) motions are generated by the electromagnetic force. Requirements that are placed out in front of positioning systems in the most advanced mechatronic devices (i.e. bioengineering, aerospace engineering, CNC machines), often exceed the capabilities of conventional drives [1]. These requirements can meet of a system in which transducer design is based on application of smart materials technologies. In a group of smart materials with possibility of application in advanced positioning devices should be mentioned: piezoelectric materials, magnetostrictive materials (both – small deformations, high dynamics), as well as thermal activated shape memory alloys (large deformations, weak dynamics, especially when cooling). New very interesting material is magnetic shape memory alloy which combines good dynamics, similar to magnetostrictive terfenol D, and deformations similar to thermally activated SMA. These properties make magnetically controlled SMA (MSMA – Magnetic Shape Memory Alloys) a promising solution for precise and fast positioning systems. However before any engineering

applications it should be well tested [2] and accurate models of MSMA actuators should be developed.

For MSMA as in the case of other shape memory materials the external stimulus is needed to produce the force and strain. Name: "magnetic shape memory alloys" indicates that strain of such materials is controlled by magnetic field. The magnetic field can be excited by energized coils, by permanent magnets or by hybrid solutions. For proper guide of magnetic flux to the material the magnetic core is needed. All magnetic cores used for MSMA actuators have a gap where is MSMA is placed. For design of magnetic circuit typically classical methods based on magnetic circuits theory are used [3]. Due to nonlinearity and hysteresis of the magnetic circuits those methods often are not sufficient accurate for needs of optimal design of magnetic circuit [4]. In the presented approach the 3D finite element model of magnetic circuit of MSMA actuator has been elaborated and used for identification of circuit model parameters.

2 Magnetic Shape Memory Alloys

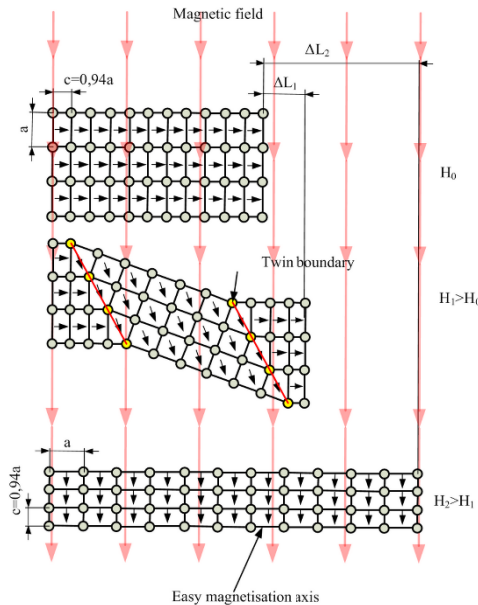


Fig. 1. Reorientation phenomenon in magnetic shape memory alloys

Reorientation phenomenon of crystal lattice and shape change in magnetic field in new class of smart materials were described by Ullakko in 1996 [5]. After improvements in production process and chemical composition, 6% strain was obtained for Ni_2MnGa alloy. It is easy to find in literature strains up to 10%, but this value is achieved only in some experiments [6]. Materials with magnetic shape memory owe their properties to magnetic anisotropy accomplished in production process and present in each tetragonal cell of crystal lattice. These facts are described in [5]. When magnetic field strength H is 0, magnetisation vectors are aligned parallel to shorten side of cell. Growing strength of magnetic field causes that vectors start arrange along this field lines. Energy need for this process is bigger than vector rotation together with the

whole cell. By difference in lengths of cell sides, shape change appears (visible extension – Fig. 1). The magnetic shape memory effect is self-supporting, only applying of external force greater than twinning stress can restore original length. In practice this is a spring, but compressive force generated by it is not sufficient to ensure return of MSMA sample to its original shape, so one of disadvantages is a first cycle effect,

which reduces scope of strain in next cycles. Other disadvantages are significant temperature dependence and wide hysteresis loop distinguished for smart materials. This hysteresis loop is more complicated in modelling because it is distinguished by large asymmetry (Fig. 2) [7].

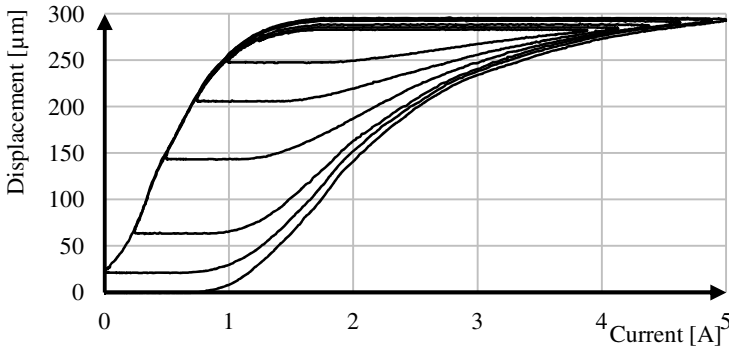


Fig. 2. Example characteristics displacement vs. current (decreasing sine). Clearly visible non-linearities: hysteresis and its asymmetric shape, saturation.

3 Design and Mathematical Modelling of Magnetic Circuit

Analysis and comparison of actuator where magnetic field is generated by coils and by coils with permanent magnets support is placed in [8]. Very interesting solution can be also found in [9]. In this design permanent magnets generate magnetic flux density in air gap which results in small deformation of MSMA. By superposition of magnetic fields it is possible to increase (up to 0.65 T), or decrease (down to 0 T), magnetic flux density in air gap. Circuits with permanent magnets are investigated because this can reduce power consumption of actuator and also limit the impact of magnetic hysteresis of the core. Moreover magnetic shape memory alloy Ni_2MnGa components are produced as cuboids, where in cross section can be noticed that one side is significantly shorter than other one (Fig. 3). This difference is made intentionally because relative permeability of material ($\mu_r = 2$), makes that power needed to produce necessary magnetic flux in air gap rises rapidly with increasing width of MSMA component. Core shape and air gap in actuators design ensure that magnetic field lines passes parallel to this shorter side.

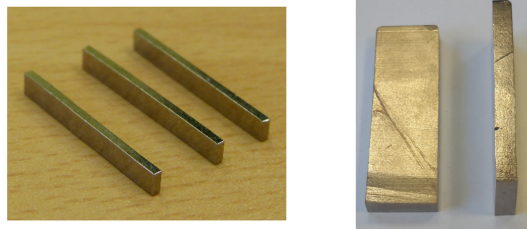


Fig. 3. Samples made of Ni_2MnGa , 1×2.5×20 (left), 3×10×30 (right)

Magnetic cores in MSMA actuators can be made in two ways, as a solid or as a stack of plates made of electrically insulated steel sheets (compound Fe and Si). For applications where high dynamic is major criterion the laminated cores are better because they significantly reduce eddy currents, but if size of actuator is more important it is profit to use solid cores ensuring higher value of saturation flux density. These cores can be made of pure iron [10], ARMCO [11], low carbon steel [12], Fe-Ni and Fe-Co compounds [8, 9]. In Fig. 4 authors show comparison of different magnetic materials, with clearly visible saturations (B-H curves).

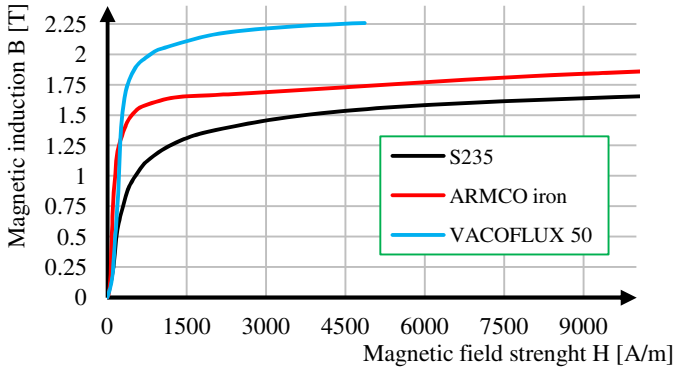


Fig. 4. Magnetization curves for different magnetic materials

In the mathematical modeling approach based on equivalent circuit (Fig. 5), MSMA element placed in gap in magnetic core was treated as air. This is due the fact that its relative magnetic permeability is very close to 1 when material is in state $\epsilon = 0$. For known dimensions of MSMA sample: shape of core, cross section and width of gap were initially designated.

For assumed magnetic flux density equal to 0,65 T, and supply current equal to 4 A the dimensions of magnetic circuit and coils parameters were calculated.

$$\Phi_i = B_i \cdot A_i \tag{1}$$

The magneto-motive force of 2 coils can be written as (Ohm’s law for magnetic circuit):

$$2NI = \sum_{i=1}^n \mathcal{R}_i \cdot \Phi_i \tag{2}$$

where

$$\mathcal{R}_i = \frac{l_i}{\mu_0 \mu_r i A_i} \tag{3}$$

Φ_i is magnetic flux, B_i is magnetic induction, A_i is cross section of magnetic core or air gap, N is coil turns, I is supply current, R_i is reluctance, l_i is length of core part, μ_0 and μ_r are magnetic permeability of vacuum and relative of core part. Subscript i means i -th branch of equivalent circuit (Fig. 5).

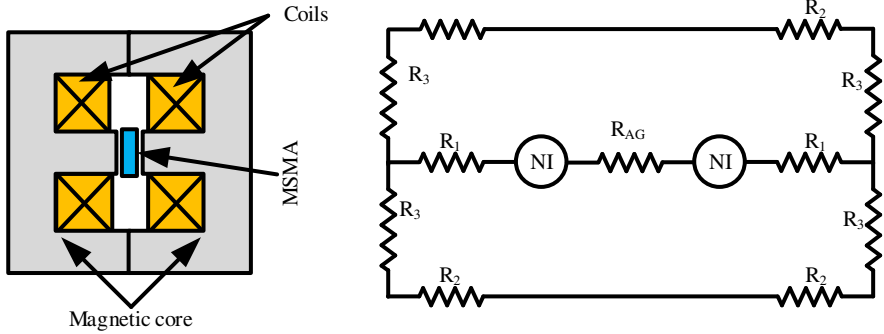


Fig. 5. Shape of magnetic circuit and its equivalent model

As a material for core the low carbon soft magnetic steel type 04J (PN-89/H-84023/02), was selected. This steel is in chemical composition and magnetic properties is very close to pure ARMCO iron. Core parts were heat treated after milling operations. Annealing is performed to decrease magnetic hysteresis and increase relative permeability.

To confront performed analytical calculations the model of magnetic circuit was created in MATLAB/Simulink by using Simscape library: Electrical and Magnetic components. Table 1 summarizes cross sections, core parts lengths and calculated reluctances used in evaluation of magnetic flux density of the MSMA gap.

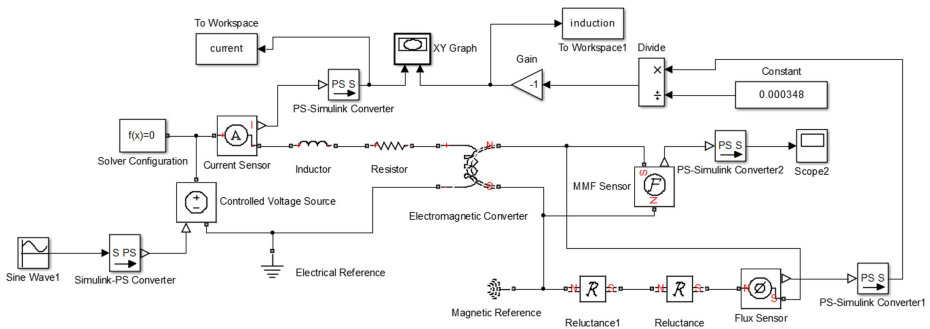


Fig. 6. Model of magnetic circuit in MATLAB/Simulink

Table 1. Magnetic core summary

| Core part | Area [mm ²] | Length [mm] | Reluctance [H ⁻¹] |
|-----------------|-------------------------|-------------|-------------------------------|
| R ₁ | 348 | 21.4 | 12233.9 |
| R ₂ | 348 | 23 | 13148.58 |
| R ₃ | 261 | 64 | 48783.12 |
| R _{AG} | 348 | 3.2 | 7317468.6 |

4 FEM Analysis

In order to determine the magnetic flux density in the considered excitation system and to validate performed analytical calculations 3D the finite element (FE), model has been developed in Ansys Maxwell environment. The considered system consists of two coils connected in parallel to the supply system and ferromagnetic core made of aforementioned material. Each coil has 425 turn wound on bobbin core made of polyamide. Analyzed region has been subdivided into about 151000 tetrahedral elements. View of the applied FE mesh has been shown in Fig. 7. Determined current and magnetic flux densities distribution for supply current equal to 4 A have been shown in Fig. 8 and 9.

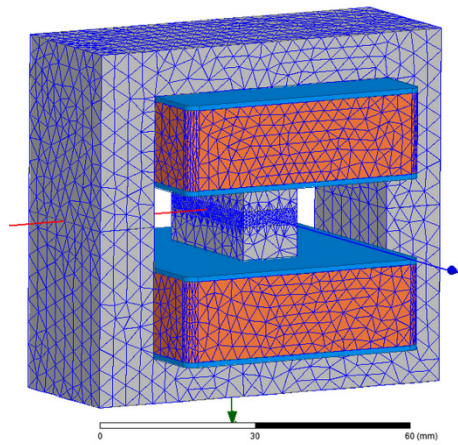


Fig. 7. View of the applied FE mesh (without surrounding air)

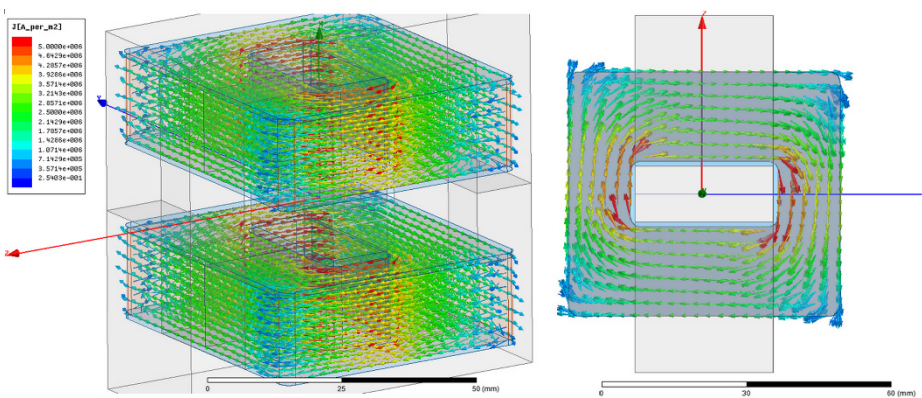


Fig. 8. Distribution of source current density in the coils

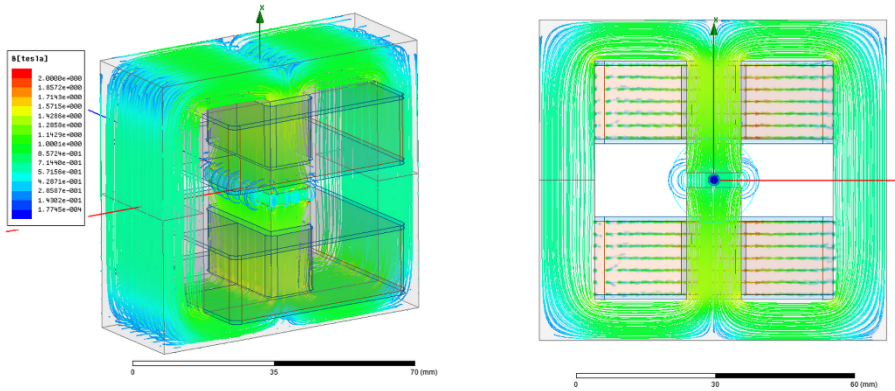


Fig. 9. Determined magnetic flux density distribution for supply current equal to 4 A

5 Research

Test stand for magnetic induction examinations in gap (no 1), is presented in Fig. 10. Measurement of magnetic induction in gap was performed by Hall effect teslameter RX 21-b (no 4). Measuring ranges are: 0–300 mT (resolution 0.01 mT), 300–3000 mT (resolution 0.1 mT), switching between ranges is carried out automatically. This device is equipped by temperature measurement, thus that measured induction can be corrected constantly. Standard transverse probe has 2.2 mm of thickness, for this reason new thinner probe no 2 (1.2 mm), with Hall sensor at its end no 3 was made in cooperation with Resonance Technology desired for magnetic circuits for the thickest MSMA elements (1 mm). Probe was held by magnetic base holder (no 5). Coils were powered by programmable DC power supply EA-PSI 8032-10T (no 6). In Fig. 11 were plotted curves for analytical calculations, FEM analysis and measurement.

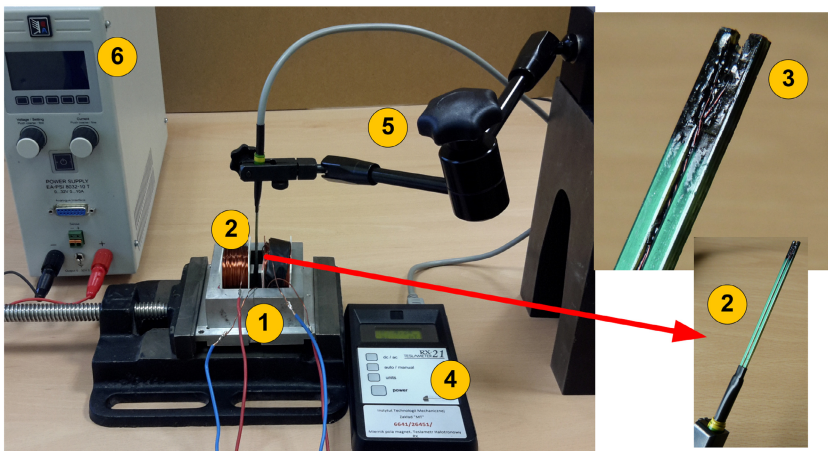


Fig. 10. Test stand for magnetic induction examinations

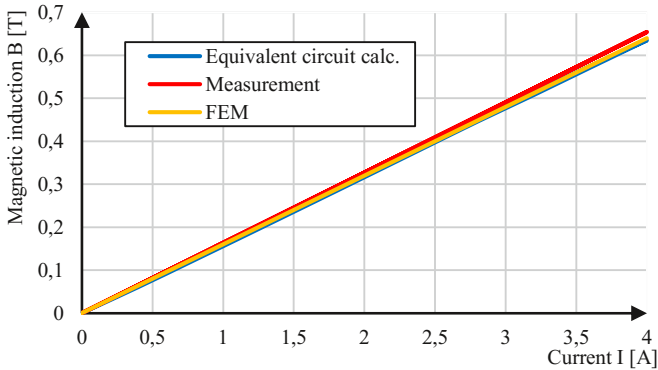


Fig. 11. Magnetic induction vs. current in air gap desired for MSMA 3×10×30 elements

Model for air gap width 3.2 mm is proper and validated. Based on this work another calculations were performed, everything was the same besides air gap width. In Fig. 12 calculations for MSMA widths 1, 2, 3, 4, 5 mm (+0.2 clearance), were presented, other dimensions were kept constant – 10 and 30 mm. Additionally power consumption of two coils (425 turns each), which task is generation of magneto motive force to obtain 0.65 T of magnetic induction in air gap.

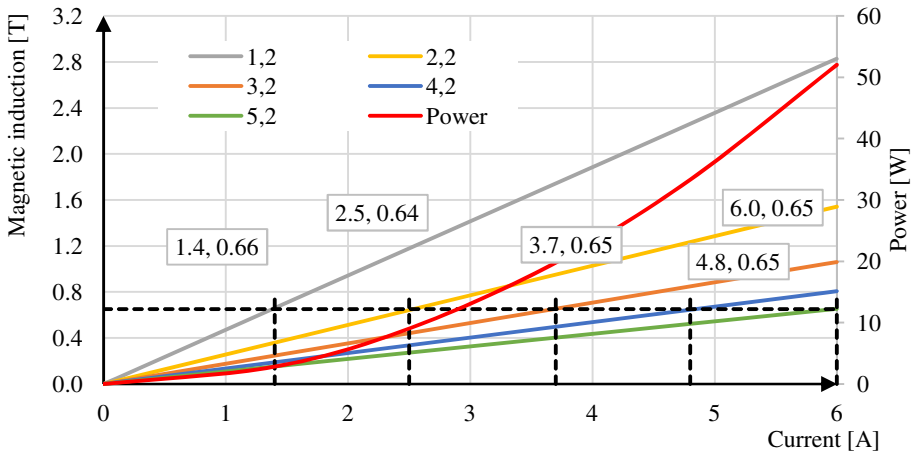


Fig. 12. Magnetic induction for different width of air gap and comparison with power consumption for two coils (turns each) in parallel connection

6 Conclusions

Performed analysis in MATLAB and Ansys have been confirmed by measurements of magnetic induction in gap in magnetic circuit. By changing material for magnetic core magnetic hysteresis and saturation in the gap are significantly reduced, compared to core made of typical construction steel. Next step will be design and analysis circuits with permanent magnets.

Acknowledgements. This article was financially supported within the project "Engineer of the Future. Improving the didactic potential of the Poznan University of Technology" – POKL.04.03.00-00-259/12, implemented within the Human Capital Operational Programme, co-financed by the European Union within the European Social Fund.

References

1. Higuchi, T.: Next generation actuators leading breakthroughs. *Journal of Mechanical Science and Technology* 24(1), 13–18 (2010)
2. Janocha, H.: *Magnetic Field Driven Unconventional Actuators*
3. Suorsa, I., Tellinen, J., Ullakko, K., Pagounis, E.: Voltage generation induced by mechanical straining in magnetic shape memory materials. *Journal of Applied Physics* 95(12), 8054–8058 (2004)
4. Schlüter, K., Holz, B., Raatz, A.: Principle design of actuators driven by magnetic shape memory alloys. *Advanced Engineering Materials* 14(8), 682–686 (2012)
5. Ullakko, K., Huang, J.K., Kantner, C., O’Handley, R.C., Kokorin, V.V.: Large magnetic-field-induced strains in Ni₂MnGa single crystals. *Applied Physics Letters* 69(13), 1966–1968 (1996)
6. Niskanen, A.J.: *Magnetic Shape Memory (MSM) Alloys for Energy Harvesting and Sensing Applications* (2012)
7. Minorowicz, B., Nowak, A., Stefanski, F.: Hysteresis Modelling in Electromechanical Transducer with Magnetic Shape Memory Alloy. *Przegląd Elektrotechniczny* 11, 244–247 (2014)
8. Wegener, K., Blumenthal, P., Raatz, A.: Development of a miniaturized clamping device driven by magnetic shape memory alloys. *Journal of Intelligent Material Systems and Structures* 25(9), 1062–1068 (2014)
9. Schlüter, K., Riccardi, L., Raatz, A.: An Open-Loop Control Approach for Magnetic Shape Memory Actuators Considering Temperature Variations. *Advances in Science and Technology* 78, 119–124 (2013)
10. Tellinen, J., Suorsa, I., Jääskeläinen, A., Aaltio, I., Ullakko, K.: Basic properties of magnetic shape memory actuators, 566–569 (2002)
11. Le Gall, Y., Bolzmacher, C.: Design and characterization of a multi-stable magnetic shape memory alloy hybrid actuator. *Microsystem Technologies* 20(4-5), 533–543 (2014)
12. Schiepp, T., Maier, M., Pagounis, E., Schlüter, A., Laufenberg, M.: FEM-Simulation of Magnetic Shape Memory Actuators. *IEEE Transactions on Magnetics* 50(2), 989–992 (2014)

Share Mode Magnetorheological Dampers for Vibration Attenuation in Domestic Washing Machines

Bartosz Minorowicz, Frederik Stefański, Grzegorz Pittner, and Roman Regulski

Institute of Mechanical Technology, Poznan University of Technology
ul. Piotrowo 3, 61-138 Poznań, Poland

{bartosz.minorowicz, frederik.stefanski}@gmail.com,
grzegorz.pittner@put.poznan.pl,
roman.regulski@doctorate.put.poznan.pl

Abstract. The article presents a new approach for noise reduction of a household washing machine. The noise sources and phenomenon were described. After investigation of a currently used solution, and alternative available solutions, a new approach was presented. Design and tests of a low costs magnetorheological fluid, semi-active damper were presented. The input parameters for the new damper were identified on the base of investigation of a viscous damper, used in washing machines. The described MR damper was applied in a washing machine suspension system. Next, a study of washing machine acceleration RMS for different unbalanced masses and drum rotations, were performed. During this research the new damper was switched on and off, to shows it influence on the acceleration. The end results show that the new designed dampers can strongly reduce the vibrations of the washing machine housing and its plastic components.

Keywords: washing machine, MR dampers, vibrations, magnetorheological fluid, share mode.

1 Introduction

Very well-known source of noise in block of flats are washing machines, especially in the late evenings when other noises are reduced. This annoying noise is created by vibrations of washing machine components. Above 1000 rpm these, mostly plastic components have their resonance frequencies [1]. Washing cycle can be divided into three main stages: washing, rinsing and spin drying. Each is distinguished by different rotary speeds of drum. Laundry in drum is placed unevenly resulting in an unbalance. Rotary speeds at first two stages are too small to cause audible vibrations. The most critical points are: crossing resonance point for drum (about 200 rpm), while acceleration and deceleration, and rotating at rotary speeds above 1000 rpm, when vibration forces affected on frame by suspension [2]. As a result of heavy frame vibrations washing machine can change its position. It is deeply analysed in [3]. In classical design of front loaded washing machine spring-mass-damper configuration can be featured. Household goods manufacturers use the simplest kind of dampers which are

based on viscous friction phenomenon (passive damper). Another known in engineering methods for vibrations reduction are: active and semi active [4]. Additionally in viscous dampers attenuation parameters strongly depends on linear velocity. An ideal solution would be pair of dampers with electrically adjustable damping parameters. These could fulfil damper with magnetorheological fluid. Magnetorheological fluids change their rheological properties under external stimulus in form of magnetic field (from coils or permanent magnets). This field causes that randomly distributed particles create regular chains along field lines, whole process is fully reversible. Particles are made of iron, iron oxide, silicon steel, nickel, cobalt and are not bigger than 10 μm . They are combined with oil, which is carrier, such combination makes that MR fluids are non-Newtonian fluids [5]. Analyzing this topic and available literature it can be stated that ideal solution is fully adjustable damper. A significant disadvantage of this solution is cost, which can exceeds the cost of whole washing machine. It is because fully adjustable damper needs to work in closed loop system with additional sensors and electronics. Authors decided that new dampers should work as on/off device. Damper will be energized when rotary speed passes through mechanical resonance and off when high damping transmits vibration forces on washing machine frame. It is illustrated in Fig. 1.

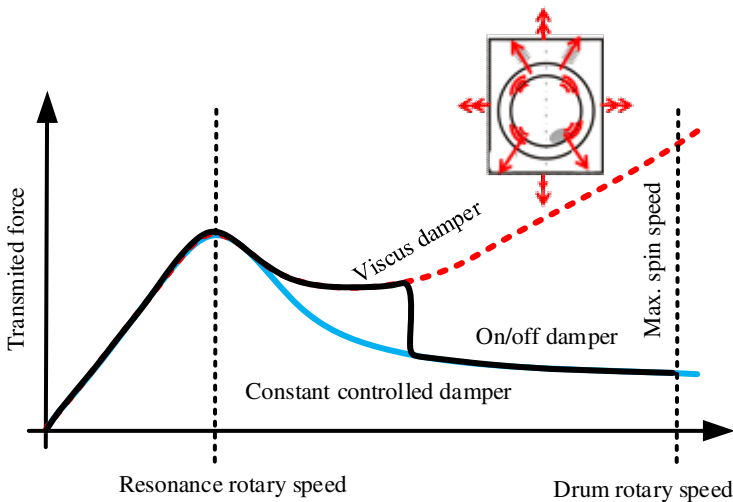


Fig. 1. Comparison of work of three different dampers mounted in washing machine during acceleration to spin speed

At Institute of Mechanical Technology this is another attempt to practical application of devices with MR fluids. Previous research have focused on MR dampers for heavy duty applications [6, 7].

Mechanical example of reduction unwanted vibrations is balancing by moving masses or liquids. Unfortunately in washing machines due to limited space and necessity to install another actuator, such solutions can be considered theoretically or can be applied only in prototypes [2].

2 Domestic Washing Machine

Front loaded washing machines are one of the most popular devices in households in European Union [8]. Other type, top loaded (vertical axis), is also included in study and research but not so often as front loaded [2]. A typical washing machine with direct drive (Fig. 2), consists: plastic casing (1), which holds water. Rubber sealing (11), and closed door seal washing machine from the front, on the opposite side ball-bearings (4, 5), and drive – rotor with motor are sealed by lip sealing placed on shaft (3). Shaft end is connected with drum (2), which is made of stainless steel with densely arranged holes for water free flow. Space inside drum is designated for laundry (10). Laundry soaked with water, placed unevenly on drum circumference can weights a few kilograms which significantly affects on magnitude of unbalance. For effective spinning cycle drum has to rotate from 600 up to 1400 rpm. Aforementioned device has direct drive, distinguishing features of such solution are: high torque generation, no belt pulley and reducing mechanisms, free of backlash, simpler design, better dynamics, cost and noise reduction [3]. Casing has joints for dampers (8), and coil springs (9), which are a part of suspension. Concrete blocks (12) in front part reduce vibrations amplitude by significant mass increase of whole suspended system.

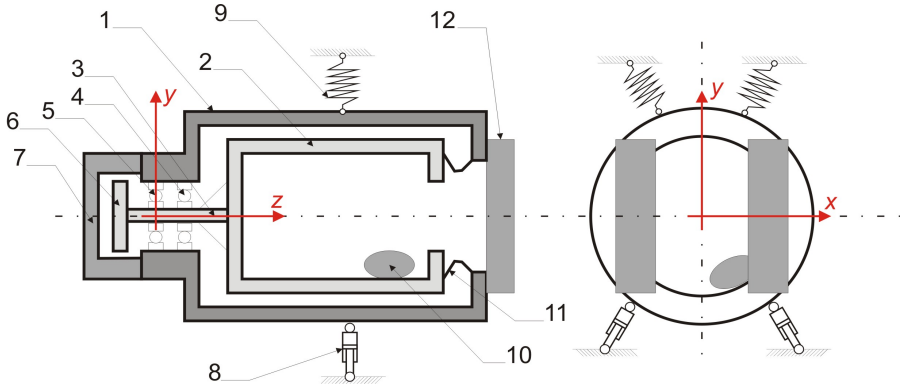


Fig. 2. Direct drive washing machine design

3 Share Mode Magnetorheological Dampers

3.1 Viscous Damper Examinations

After removal from washing machine a classic viscous damper was examined on prepared test stand (Fig. 3), which design is intended for different kinds of dampers examinations. Drive is provided by AC motor which rotary speed is set by inverter. Next in drive is a worm transmission which reduces rotary speed and increases generated torque. Rotary motion is converted to linear by slider crank gear mechanism. Eccentric disk placed in crank enables adjustment of damper stroke. Linear movement

is carried out by roller bearing supported table. Dampers and table were connected by double-acting force transducer (HBM U9B with operating range ± 5 kN). For data acquisition SPIDER 8 was used, which was recording force and displacement (LVDT transducer connected with table). Measured characteristics are plotted in Fig. 4.

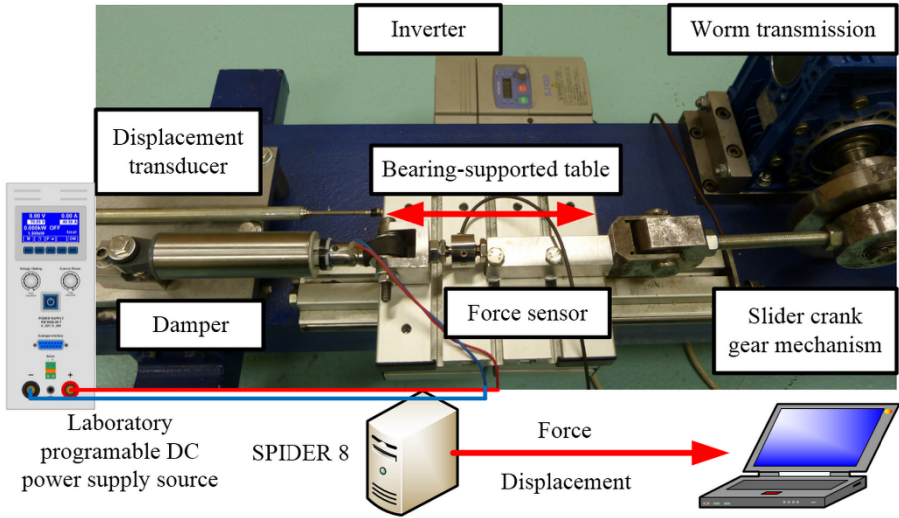


Fig. 3. Test stand configuration

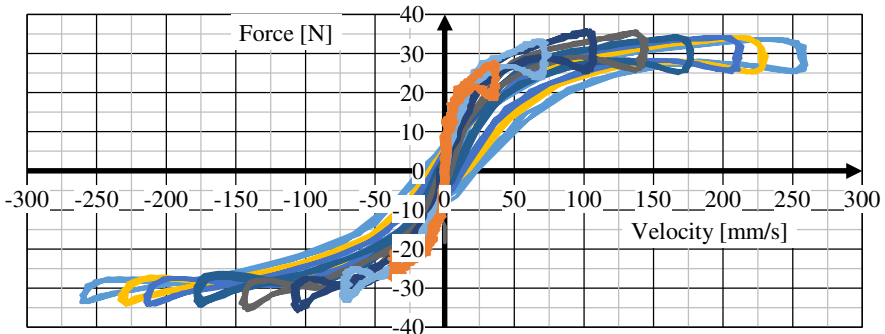


Fig. 4. Force vs. velocity for conventional washing machine viscous damper

3.2 Design of Share Mode Magnetorheological Damper

Incensement of magnetic field makes that yield stress in MR fluid raises. In area of dampers design two operating modes can be considered: valve mode (most popular), and shear mode (Fig. 5). In valve mode growth of chains disturb free flow between chambers. Disadvantages of such design are possibility of leakage, usage of large amount of fluid and obtained damping force significantly exceeds needs for application in washing machines.

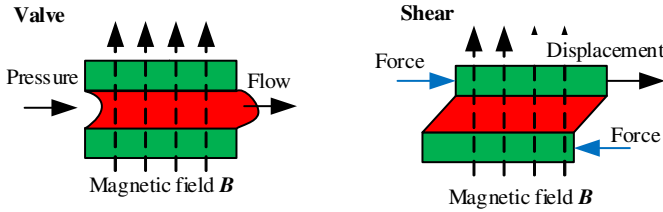


Fig. 5. Comparison of valve and shear operating mode

Based on literature analysis aforementioned above authors decided to develop new dampers which work in share operating mode. For known damping force, shape of magnetic core and size of magnetic poles, necessary coil turns and excitation current were calculated. First step was definition of shear stress which must occur in magnetorheological fluid (equations 1 and 2).

$$F = F_{\eta} + F_{\tau} = \frac{\eta SA}{g} + \tau_y A \quad (1)$$

$$\tau_y = \frac{F}{A} - \frac{\eta SA}{g} \quad (2)$$

where F is expected force, field dependent yield stress τ_y , g is the fluid gap, η is the fluid viscosity, S is the relative pole velocity and A is the shear area.

Resultant shear stress allows for designation strength of magnetic field in MRF-132DG MR based on fluid characteristics. Other calculations were made for verification of magnetic induction in each part of magnetic core. Last thing was coil turns calculation assuming that for 0.5 A damping force is close to 40 N.

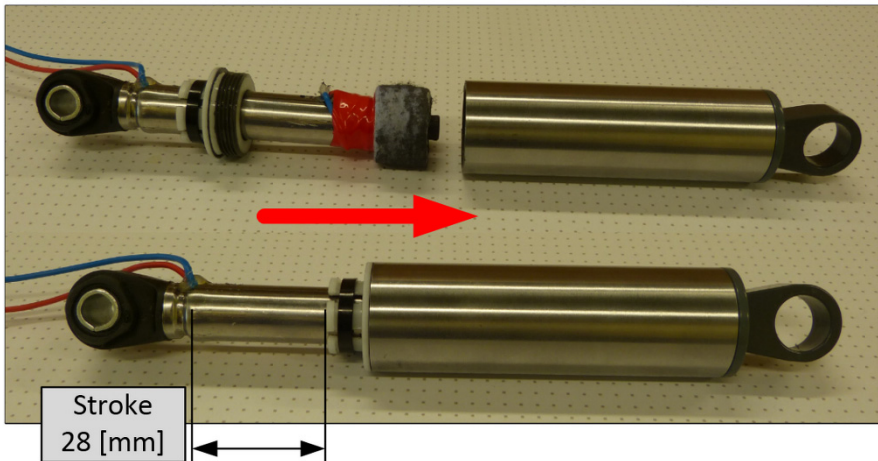


Fig. 6. Design of share mode single coil MR damper

Based on measurements and limitations inside washing machine, shape of new MR damper is very similar to original (Fig. 6). Proposed damper has one coil wound on piston (160 turns). Piston has at its circumference glued fiber which before final assembling was soaked with magnetorheological fluid. Such design allows for significant reduction of use of MR fluid. Piston connected with rod adapted from viscous damper moves in cylindrical tube, which is made of soft magnetic steel. Clearance between piston and cylinder provides enough space for soaked fiber without generating excessive friction force while coil is non-powered. Coil supply wires are placed inside rod which is additionally filled with silicon based material. New damper was examined on aforementioned above test rig. Results: force vs. velocity and force vs. stroke were plotted in Fig. 7 and 8. More details about design can be found in paper [9]. Similar devices are presented by J.D. Carlson in papers [10, 11]. Damper parameters were summarized in Table 1.

Table 1. Comparison of commercial damper RD-1097-01 and new design

| Parameter | RD-1097-01 | Single coil |
|--------------------|----------------------------|----------------------|
| Max. length | 253 mm | 224 mm |
| Min. length | 195 mm | 184 mm |
| Body diam. | 32 mm | 36 mm |
| Weight | 0.48 kg | 0.58 kg |
| Stroke | ± 25 mm | ± 14 mm |
| Coil res. (25 °C) | 20 Ω | 2.0 Ω |
| Coil inductance | No data | 4.65 mH |
| Coil wire diameter | No data | 0.4 mm |
| Magnetic core | No data | Steel S235 |
| Amount of MR fluid | 3 cm ³ [10, 11] | 1 cm ³ |
| Max. force | 100 N; 51 mm/s; 1 A | 90 N; 80 mm/s; 2.5 A |
| Min. force | 9 N; 200 mm/s; 0 A | 7 N; 80 mm/s; 0 A |

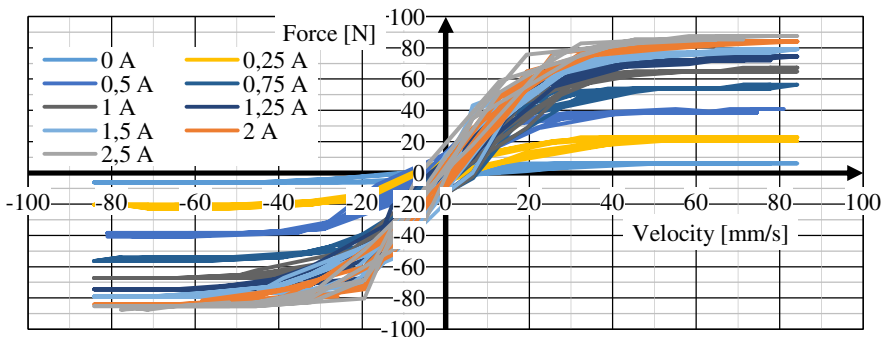


Fig. 7. Force vs. velocity for new MR fibre damper

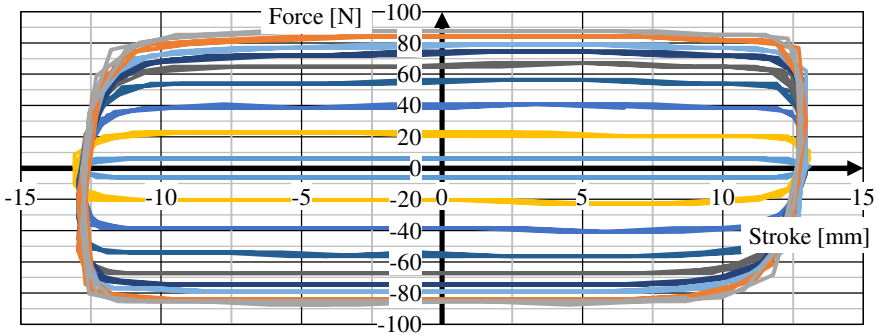


Fig. 8. Force vs. stroke for new MR fibre damper (legend in Fig. 7)

4 Washing Machine with New Dampers – Experimental Study

Original viscous dampers were replaced by pair of new. Dampers were working as on/off devices. When current is off theoretically damping force should be 0 N, but it is not, because of friction in MR fluid and rod guide. To induce vibrations masses were magnetically fixed on circumference of the drum. Four cases were tested for: 0, 0.1, 0.2, 0.3 kg of the masses, each for 400, 800, 1200 rotations of drum. Acceleration RMS was recorded as a result of measurements. Sensors were placed in three different positions on washing machine body. First as close as possible to spring catch, second in the middle of external side panel of washing machine and third as close as possible to damper catch (Fig. 9).

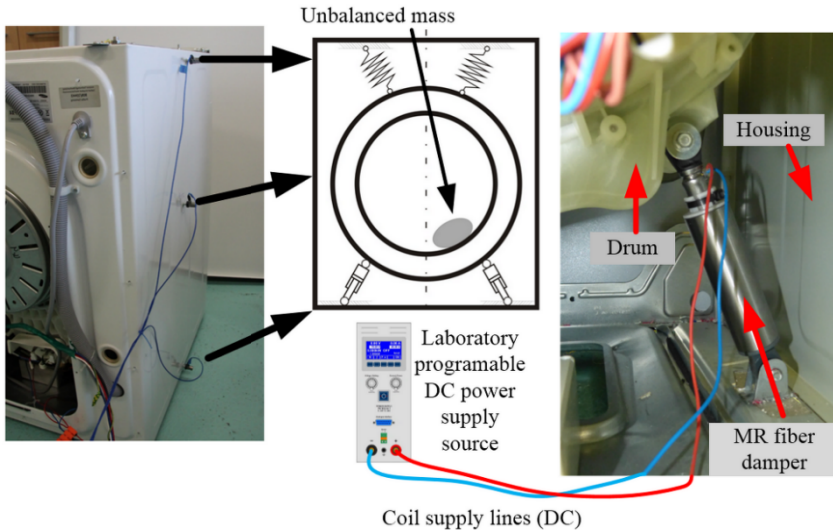


Fig. 9. Washing machine equipped with acceleration sensors and two the same new MR dampers

Results as graphs acceleration RMS vs. rotations for on and off damping were prepared (Fig. 10–12). Results are confirmation that while revolutions are above resonance rotations area, when damping is off, amplitude of acceleration RMS decreases instantaneously, it is shown in Fig. 13.

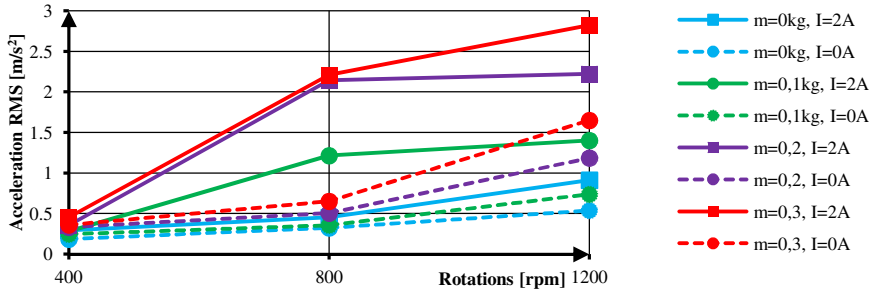


Fig. 10. Acceleration RMS vs. drum rotations in spring measuring point

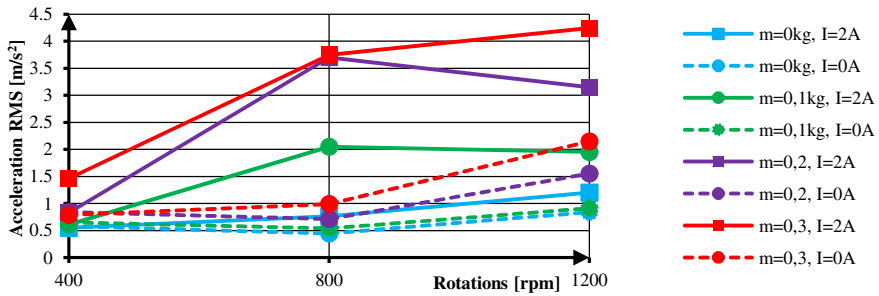


Fig. 11. Acceleration RMS vs. drum rotations in middle measuring point

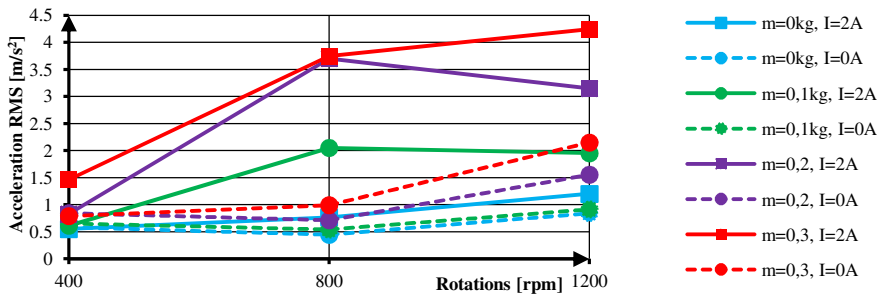


Fig. 12. Acceleration RMS vs. drum rotations in damper mounting measuring point

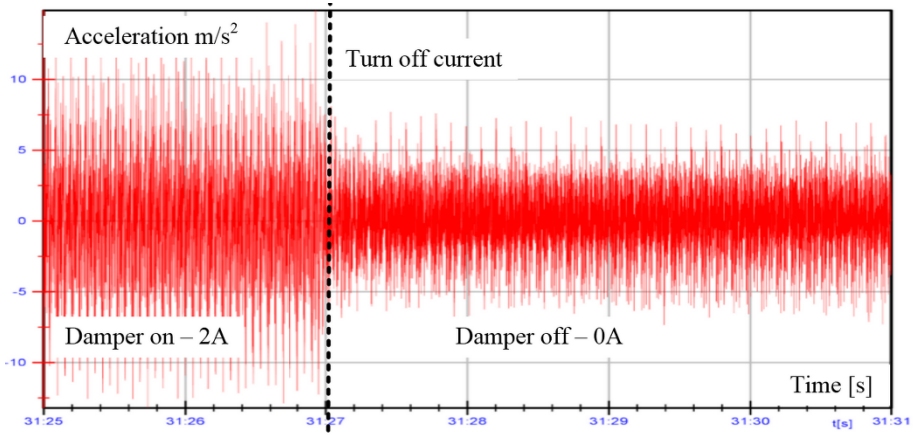


Fig. 13. Comparison of acceleration RMS for ON and OFF damping in damper mounting measuring point

5 Conclusions

New dampers can be easier adapted to design of washing machines because such solution works and it is worth to notice that amount of used MR fluid is reduced significantly. Thus that design can be simpler, there is no need for sealing and replenishment of this smart fluid which is very expensive. Additionally by adding permanent magnets in some cases dampers can work as energy harvesters.

Our research proved that previous theoretical analysis were right and acceleration RMS as a result of this vibrations of external parts can be reduced.

References

1. Nguyen, Q.H., Choi, S.B., Woo, J.K.: Optimal design of magnetorheological fluid based dampers for front loaded washing machines. *Proceedings of the Institution of Mechanical Engineers, Part C: Journal of Mechanical Engineering Science* 228(2), 294–306 (2014)
2. Chen, H.W., Zhang, Q.J.: Stability analyses of a vertical axis automatic washing machine with a hydraulic balancer. *Mechanism and Machine Theory* 46(7), 910–926 (2011)
3. Kalkat, M.: Experimentally vibration and noise analysis of two types of washing machines with a proposed neural network predictor. *Measurement* 47, 184–192 (2014)
4. Świtoński, E., Mężyk, A., Klein, W.: Application of smart materials in vibration control systems. *Journal of Achievements in Materials and Manufacturing Engineering* 24(1), 291–296 (2007)
5. Kciuk, M., Kciuk, S., Turczyn, R.: Magnetorheological characterisation of carbonyl iron based suspension. *Journal of Achievements in Materials and Manufacturing Engineering* 33(2), 135–141 (2009)
6. Milecki, A., Sedziak, D.: The use of magnetorheological fluid dampers to reduce servo drive velocity jumps due to load changes. *Journal of Intelligent Material Systems and Structures* 16(6), 501–510 (2005)

7. Milecki, A., Hauke, M.: Application of magnetorheological fluid in industrial shock absorbers. *Mechanical Systems and Signal Processing* 28, 528–541 (2012)
8. Buśkiewicz, J., Pittner, G., Barczewski, R.: Numerical and experimental vibration analysis of domestic washing machine drum. *International Journal of Applied Mechanics and Engineering* 17, 765–777 (2012)
9. Minorowicz, B., Stefanski, F.: Proposal of a new group of magnetorheological dampers. *Przegląd Elektrotechniczny* 7, 263–267 (2014)
10. Carlson, J.D., Jolly, M.R.: MR fluid, foam and elastomer devices. *Mechatronics* 10(4), 555–569 (2000)
11. Carlson, J.D.: Low-cost MR fluid sponge devices. *Journal of Intelligent Material Systems and Structures* 10(8), 589–594 (1999)

Immune Algorithm for Optimization of Membership Function in Fuzzy Models

Bogumiła Mrozek

Faculty of Physics, Mathematics and Computer Science,
Cracow University of Technology, Poland
bmrozek@pk.edu.pl

Abstract. The immune algorithm based on clonal selection can be used for identification and optimization of the parameters of Sugeno fuzzy model extracted from numerical data. In [5] the rules of fuzzy model were extracted using clonal selection for clustering task, implemented in the MATLAB code. In this paper, the application of the clonal selection has been proposed to solve optimization problems. The algorithm of clonal selection can be used before the clustering version of identification of parameters of the fuzzy model Sugeno-type. Then the same algorithm can be adapted to solve optimization tasks. The results were applied to approximation of a test function.

Keywords: data clustering, optimization, fuzzy model, clonal selection.

1 Introduction

Fuzzy models are able to reproduce the relationship between physical quantities that are difficult to describe by mathematical relationships [1, 3]. They give good approximations of any functions. If it is difficult to create a mathematical model, one can describe fuzzy rules in a qualitative way. The fuzzy models can be identified sequentially. The sequential mode may determine the structure and antecedents by chosen clustering algorithm, and then optimize the consequent and/or antecedent parameters by evolutionary optimization methods [9].

The majority of developed artificial immune system (AIS) algorithms are based on various mechanisms in the biological immune system (IS). Negative selection, immune networks and clonal selection are still the most discussed models. Artificial immune systems can be defined as metaphorical computational system developed using ideas, theories and components extracted from the biological immune system.

The basic clonal selection algorithm have been introduced by de Castro and von Zuben [6, 7]. Several version of this algorithm (ClonAlg or CLONALG) and its applications are proposed, for example in [7, 10]. Over recent years there have been many papers on artificial immune systems (AIS) application for its adaptations in fuzzy models, for example [12–14].

In [12] an immune algorithm was used to tune the membership functions of fuzzy variables used to mine the fuzzy association rules that improve the performance of the intrusion detection system and show the use of immune algorithm in such mining task.

An application the clonal selection algorithm (CLONALG) for optimization parameters of membership function of input and output variables for Mamdani-type fuzzy model is described in [13]. The membership functions parameters with respect to fuzzy variables can be found for a fuzzy system whose rules table and shape of membership functions were given previously.

In [14] an immune approach based on clonal selection and immune network theories for Adaptive Neuro-Fuzzy Inference System (ANFIS) learning is proposed. Additionally a multiantibody model is implemented to perform simultaneous identification of parameters and structure of ANFIS.

It is necessary to remain that ANFIS algorithm is implemented in `anfis` function, which is an element of Fuzzy Logic Toolbox in MATLAB [2]. Using a given input/output data set, the `anfis` function constructs only Sugeno-type fuzzy system [11] whose membership function parameters are adjusted using either a *backpropagation* algorithm alone, or in combination with a *least squares estimation*. This learning method works similarly to that of neural networks. The `anfis` function has many limitation but it offers universal approximation of nonlinear functions which is easy to use in technical application.

The clonal selection algorithm can be applied both for optimization problems as well as in of clustering and pattern recognition [7]. This means that the clonal selection algorithm may be used to automatically generate Sugeno-type fuzzy models, both at the initial stage (by clustering) and at the final tuning (optimization).

In [5] the clonal selection algorithm was used in fuzzy clustering version for identification of parameters of Sugeno fuzzy model extracted from measurement numerical data [1]. In this paper CLONALG algorithm is used in two versions: one for clustering tasks and another for optimization problems. It allows to create an CLONAG implementation which will have smaller limitations than `anfis` function and will be easy to use in technical application.

This paper is organized as follows. Section 2 is a briefly introduction to Sugeno fuzzy models and extracting knowledge from the numerical data. Section 3 describes clonal selection mechanism in versions for optimization, pattern recognition and clustering problems. Section 4 presets application examples. Conclusions and proposals of future work are given in Section 5.

2 Methods for Construction of Sugeno-Type Fuzzy Model

2.1 Fuzzy Models

Based on an input-output data, a fuzzy model may be constructed. It should create rules of inference, generalize knowledge and be robust to data errors. The Sugeno-type fuzzy model is computationally very efficient and works properly in conjunction with methods of adaptation and with algorithms of optimization. It is particularly attractive when applied to modeling and control of nonlinear systems.

A typical fuzzy rule in a Sugeno fuzzy model [8] has the form:

$$\text{If } (x \text{ is } A_j) \text{ and } (y \text{ is } B_j) \text{ then } z_j = f_j(x, y) \quad (1)$$

where A_j and B_j are fuzzy sets in the antecedent of j -th rule, while $z_j = f_j(x, y)$ is a crisp function in consequent of j -th rule. Usually $f_j(x, y)$ is a polynomial of the input variables x and y , but it can be any function as long as it can appropriately describe the output of the model within the fuzzy region specified by antecedent of the rule. Most often $f_j(x, y)$ is a first-order polynomial or a constant (zero-order polynomial). Consequent of j -th rule can be expressed as:

$$z_j = f_j(x, y) = p_j x + q_j y + r_j \quad (2)$$

where p_j, q_j, r_j – polynomial coefficients, in zero-order model: $z_j = r_j$.

Operation of Sugeno type fuzzy model is based on the performance of switching between several optimal linear models. In this way, strongly non-linear objects can be modeled.

2.2 Extracting Knowledge from the Numerical Data

It is very useful if rules base (knowledge base) of fuzzy model can be automatically extracted from the measured data. The most common method of automatic extraction of rules is based on grouping of numerical input-output data, often called clustering. Effective clustering algorithms specify the center of clusters – focus areas of measurement (numerical) data. This involves the determination of parameters of fuzzy model together with the organization of its structure (rule base).

Fuzzy clustering creates assignment in ambiguously. One element of the set of data may belong to several clusters, each of them to a certain extent. The methods of fuzzy clustering are one of the unsupervised learning techniques.

Generally, these methods can be divided into:

- Methods, in which the number of clusters is not known. The user must initially assume the number of clusters and enters this number as a parameter of the algorithm [5].
- Number of clusters may be determined automatically based on a measure of data density in space. Examples of this type algorithms can be *clonal selection* algorithm. The advantage of this algorithm is the independent matching of the optimal clusters number based on the declared cluster radius [5].

The effectiveness of various clustering algorithms may be evaluated using a number of quality indexes such as: partition, entropy, Xie-Bieni or Fukuyamy–Sugeno [5].

2.3 Extraction of Fuzzy Rules Directly from Numerical Data

Chiu presents the method of extracting fuzzy rules from data for function approximation [1]. *Subtractive* or *clonal selection clustering* may be applied to the input space of each group of data individually to extract the rules for identifying each class of data. The clusters found in the data of a given group identify regions in the input

space that map into the associated class. Hence, we can translate each cluster center into a fuzzy rule for identifying the class.

Extracting fuzzy rules for approximation of function from data, clustering is performed in the combined input/output space, i.e., each data point x_i is a vector that contains both input and output values. Each center of cluster is essence of prototypical data point that exemplifies an input/output behavior of the system.

The main task in constructing the model is to determine the fuzzy rule base and the number of fuzzy sets (membership function) assigned to individual inputs and outputs of the model. Subsequently, they are also appropriately selecting algorithms for aggregation of simple premises.

Each cluster center x_i^* is considered as a fuzzy rule that describes the system behavior. This computational model can be used as a fuzzy inference system employing traditional fuzzy **if-then** rules [1, 3, 5]. Each rule has the following form:

$$\text{if } Y_1 \text{ is } A_{i1} \ \& \ Y_2 \text{ is } A_{i2} \ \& \ \dots \ \text{then } Z_1 \text{ is } B_{i1} \ \& \ Z_2 \text{ is } B_{i2} \ \dots \quad (3)$$

where Y_j is the j -th input variable and Z_j is the j -th output variable; A_{ij} is an exponential membership function in the i -th rule associated with the j -th input and B_{ij} is a membership function in the i -th rule associated with the j -th output.

This computational scheme is equivalent to an inference method that uses multiplication as the AND (**&**) operator, weights the consequent of each rule by the rule's degree of fulfillment, and computes the final output value as a weighted average of all the consequents.

Another approach is to let the consequent parameter z_{ij}^* be a linear function of the input variables. That is, it let

$$z_{ij}^* = G_{ij} y + h_{ij} \quad (4)$$

where G_{ij} is an N -element vector of coefficients and h_{ij} is a scalar constant.

The *if-then* rules then become the Sugeno-type. For given a set of rules with fixed premise membership functions, optimization G_{ij} and h_{ij} in all consequent equations is a simple *linear least-squares estimation* problem [1].

2.4 Optimization of Coefficients in Consequent and Premise Fuzzy Rules

Identification method for Sugeno type fuzzy model consist of two steps: (1) find cluster centers to establish number of fuzzy rules and parameters the rules premise and (2) calculate with optimizing the rules consequents parameters. Optimizing only the coefficients in consequent equations allows a significant degree of model optimization to be performed without adding much computational complexity.

If better accuracy of estimation fuzzy model is needed it can be obtained by optimizing the parameters of membership functions with chosen evolutionary algorithm, for example clonal selection method. For new parameters of premise membership functions, the parameters all consequent equations should be recalculated.

3 Biological and Artificial Immune Systems

The *biological immune system* is based on two aspects. The first is detection of the pathogen (infections foreign element) in terms of verifying the molecules that belong to the body and could be harmful. Second aspect is to eliminate the risk that must effectively select the appropriate method depending on the type of pathogen. The system is capable of “remembering” each infection, so that a second exposure to the same pathogen is dealt with more efficiently.

The elements of the immune system are the so-called lymphocytes, who take part in the detection and elimination of the pathogen. They are divided into T-cells and B-cells [6]. T-lymphocytes are responsible for considering the "suspicious" cells. They give a signal to undertake defensive actions. B-lymphocytes are subordinated to the T-lymphocytes. They produce antibodies to eliminate these pathogens and are involved in memorizing these structures which leads to the formation of immunological memory.

Clonal selection theory is used to describe of the immune response to antigenic incentive. It involves the construction of a large number of cell clones responding to an antigen that was found in the body [6]. In response to the first contact with the antigen and under the influence of T-lymphocytes, B-lymphocytes are activated and cloned. This process is proportional to the similarity of the selected antigen - higher the similarity is, more generated B-cells. Then, clones are subject to hypermutation. The process is inversely proportional to the affinity of the antigen cell receptors – higher the affinity, lower intensity of the mutation. The population of the mutant clones is evaluated for the degree of adjustment for the antigen: antigen-binding clones are poorly removed, and the well-binding are included in the immunological memory [6].

3.1 Clonal Selection Algorithm

Clonal selection algorithms are a class of algorithms inspired by the clonal selection theory of acquired immunity that explains how B and T-lymphocytes improve their response to antigens over time called affinity maturation. The *selection* is inspired by the affinity of antigen-antibody interactions, *reproduction* is inspired by cell division, and *variation* is inspired by somatic hypermutation.

Clonal selection algorithms use a mutation operator that is inversely proportional to the fitness (high fitness, low mutation). However, it also makes more, (low mutated) copies of the high fitness solutions. It can fit a population to a fitness function very quickly. The two operations (selection of the best individuals and their cloning) are necessary for correct operation with this algorithm. The literature describes several implementations with the use of *clonal selection algorithms* [10]. It is most commonly used for optimization problems, clustering and pattern recognition tasks.

The clonal selection principles are:

- most stimulated cells will reproduce under a hypermutation scheme (B-cell),
- low affinity clones are eliminated,
- self-reactive clones will be purged from the population.

3.2 Optimization and Clustering Using Clonal Selection Mechanism

The clonal selection algorithm (CLONALG) is used in two versions: one for optimization problems and one for pattern recognition/classification (clustering) tasks [6, 7]. Fig. 1 shows the block diagram of computational procedure for the CLONALG algorithm in version for *global optimization*. The block diagram of the CLONALG adapted to be applied to *pattern recognition* tasks is presented in Fig. 2.

The following notation is used to describe this algorithms [7]: \mathbf{Ab} : available antibody repertoire, $\mathbf{Ab}_{(m)}$: memory antibody repertoire, $\mathbf{Ab}_{(r)}$: remaining antibody repertoire, $\mathbf{Ab}_{(n)}^j$: n antibodies from \mathbf{Ab} with highest affinities to antigen \mathbf{Ag}_j , $\mathbf{Ab}_{(d)}$: set of d new molecules that will replace d low-affinity antibodies from $\mathbf{Ab}_{(r)}$. At the beginning, there is no explicit antigen population to be recognized, but an objective function $\mathbf{g}(\cdot)$ to be optimized (maximized or minimized).

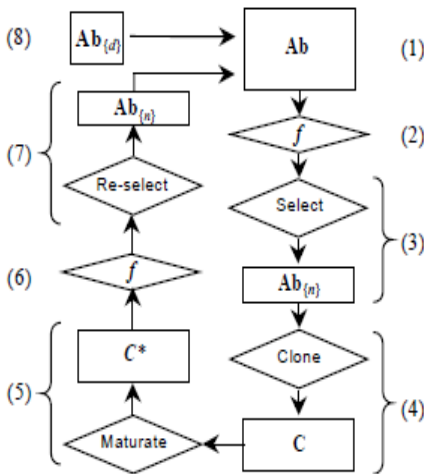


Fig. 1. Computational procedure for the clonal selection algorithm (CLONALG): *global optimization* version [7]

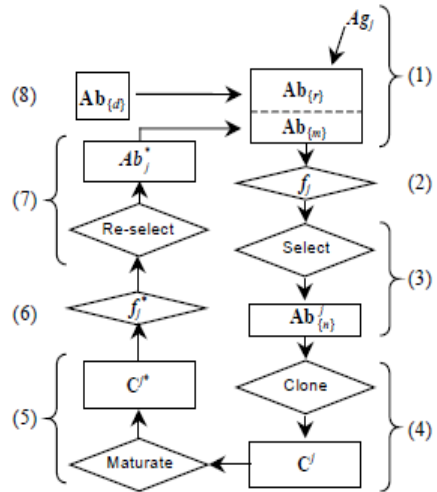


Fig. 2. Computational procedure for the clonal selection algorithm (CLONALG): *pattern recognition* version [7]

The CLONALG algorithm for *optimization tasks* can be described as follows:

- *Step1*, an antibody affinity corresponds to the evaluation of the objective function $\mathbf{g}(\cdot)$ for given antibody: each antibody \mathbf{Ab}_i represents an element of the input space. In addition, as there is no specific antigen population to be recognized, whole antibody population \mathbf{Ab} will compose the memory set and, hence it is no longer necessary to maintain a separate memory set $\mathbf{Ab}_{(m)}$.
- *Step2*, determine the vector \mathbf{f}_j that contains its affinity to all the N antibodies in \mathbf{Ab} .
- *Step3*, select the n highest affinity antibodies from \mathbf{Ab} to create a new set $\mathbf{Ab}_{(n)}$ of high affinity antibodies by relation to population of antigens \mathbf{Ag}_j to be recognized.

- *Step4*, the n selected antibodies will be cloned independently, proportionally to their antigenic affinities and will generate a repertoire \mathbf{C}^j of clones: the higher the antigenic affinity, the higher the number of clones generated for each of n selected antibodies.
- *Step5*, the repertoire \mathbf{C}^j is submitted to an affinity maturation process inversely proportional to the antigenic affinity, generating population \mathbf{C}^{j*} of matured clones: the higher the affinity, the smaller the mutation rate.
- *Step6*, verify the affinity \mathbf{f}_j^* of the matured clones \mathbf{C}^{j*} by relation to antigen $\mathbf{A}\mathbf{g}_j$.
- *Step7*, n antibodies are selected to compose the set $\mathbf{A}\mathbf{b}$, instead of selecting the single best individual $\mathbf{A}\mathbf{b}^*$.
- *Step8* finally replace the d lowest affinity antibodies from $\mathbf{A}\mathbf{b}_{\{r\}}$ (remaining antibodies repertoire), with relation to $\mathbf{A}\mathbf{g}_j$ by new individuals.

The main immune aspects taken into account to develop the CLONAG algorithm were: maintenance of a specific memory set, selection and cloning of the most stimulated antibodies, death of non stimulated antibodies, affinity maturation and reselection of the clones proportionally to their antigenic affinity, generation and maintenance of diversity.

To apply the proposed CLONALG algorithm to *pattern recognition* tasks, a few modifications have to be made in this algorithm (see Fig. 2) [7]. In the *pattern recognition* case, an explicit antigen population $\mathbf{A}\mathbf{g}$ is available for recognition. The CLONALG algorithm modifications can be described as follows:

- *In Step1*, randomly choose an antigen $\mathbf{A}\mathbf{g}_j$ ($\mathbf{A}\mathbf{g}_j \in \mathbf{A}\mathbf{g}$) and present it to all antibodies in the repertoire $\mathbf{A}\mathbf{b}$.
- *In Step7*, from set $\mathbf{A}\mathbf{g}_j$ of mature clones \mathbf{C}^{j*} , re-select the highest affinity one $\mathbf{A}\mathbf{b}_j^*$ with relation to $\mathbf{A}\mathbf{g}_j$ to be a candidate to enter the set of memory antibodies $\mathbf{A}\mathbf{b}_{\{m\}}$. If the antigenic affinity of this antibody with relation to $\mathbf{A}\mathbf{g}_j$ is larger than its respective memory antibody, then $\mathbf{A}\mathbf{b}_j^*$ will replace this memory antibody.

After presenting all the M antigens from $\mathbf{A}\mathbf{g}$ and performing the 8 steps above to all of them, a *generation* has been completed.

Clustering algorithm using clonal selection mechanism is based on the method used for pattern recognition tasks, described in [6, 7]. The algorithm is performing successive iterations. Each section starts assuming initial population representing the downloaded data. Of these, the data pattern is also selected. If the element of the data set representing a pattern is fixed in advance within the cluster, then the other element is selected. The next step is to compare the pattern with all elements of the population.

Calculated similarity is presented in the form of matching vector, which is then sorted according to the value of similarity. Ordered population is cloned in proportion to the degree of alignment and the number of dependent values cloning. This creates a temporary population, which matures in the process of hypermutation. The intensity depends on the ratio hypermutation.

Mature temporary population is re-compared with the pattern and calculates the matching vector. Then it is sorted according to the value of similarity. Best suited element of the temporary population is written to memory as a new center of the

cluster, provided that they are not in the other cluster. Iteration ends up substituting the worst elements of the population with the new matched. The algorithm terminates after a predetermined number of iterations or in the case where all points lie within clusters and it is incapable to determine a new pattern.

4 Application Examples

The immune algorithm for fuzzy models generation was applied to fuzzy modeling problem based from the numerical data. Two testing examples with application clonal selection algorithm used to clustering tasks are described in [5]. Efficient methods for extracting fuzzy rules from the high dimensional numerical data based on cluster estimation have been presented in [1].

The clustering method with clonal selection mechanism implemented in MATLAB was tested in [3, 5]. This method was experienced with *Trip* data (published in [1, 2]) and compare with subtractive, fuzzy C-means, Gustafson–Kessel clustering algorithms. *Trip* data set contains the relationship between the number of automobile trips generated from an area and the area's demographic factors. Demographic and trips data are from 100 traffic zones in New Castle County, Delaware. Five demographic factors are considered: population, number of dwelling units, vehicle ownership, median household income and total employment..

Hence, the model has 5 input variables and 1 output variable. Fuzzy model make estimation of the number of automobile trips generated from an area based on 5 demographics factor from of this area. 75 data points (of 100 available) were selected for extracting fuzzy rules for Sugeno fuzzy model by using 4 clustering algorithms. It means that on base this numerical data the model of traffic patterns in an area was constructed based on the area's demographics data (see Fig. 3).

Trip data sets and results of clustering for 4 methods (fuzzy C-means, Gustafson–Kessel, subtractive and clonal selection methods) are presented and discussed in [5].

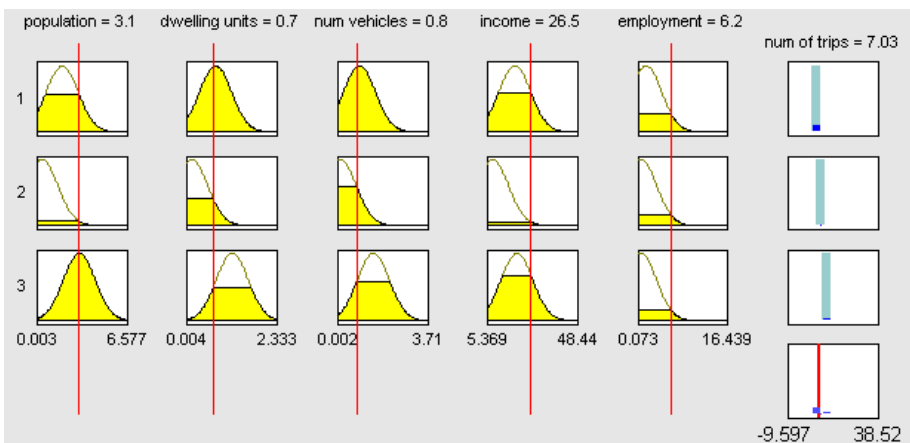


Fig. 3. Rule viewer of fuzzy model extracted from *Trip* data with 5 input and 1 output variables

In [3] and [5] an real technical problem of fire detection in the mine, in its early stages was also presented. The main idea was to created fuzzy model to determine the index of fire risk based on independent, pre-processed analog signals (*DWP* data). Various parameters are controlled using special detectors (carbon monoxide, hydrogen cyanide and smoke).

The proposed fuzzy model describes this problem. The model structure and antecedent parameters were extracted using 4 clustering data methods (same as in *Trip* case) implemented in MATLAB.

Two experiments with *Trip* and *DWP* data indicate that clonal selection clustering algorithm is computationally fast and robust.

Numerical data used to build the fuzzy models have different accuracy. Usually measurement data can have bigger errors than numerical data calculated from formula of selected function. Functions of one or two variables can be also approximated with chosen accuracy from numerical data using some clustering method and algorithm fuzzy rules generation proposed by Chiu [1].

For given set of rules with fixed premise of preferred type membership functions, optimization of coefficients in all consequent equations is a simple linear least-squares estimation problem [1].

For better approximation (with accepted accuracy) use an optimization algorithm for calculate optimal coefficients of membership function in premise may be used. This optimization can be made by *chosen evolutionary algorithm* or *ANFIS*, which is based on classic methods of neural networks learning.

ANFIS is *neuro-adaptive* learning technique [11] incorporated into *anfis* function in Fuzzy Logic Tolbox (MATLAB), which uses a hybrid learning algorithm to identify parameters of Sugeno-type fuzzy inference systems. It applies a combination of the least-squares method and the backpropagation gradient descent method for training fuzzy membership function parameters to emulate a given training data set.

Function *anfis* only supports Sugeno-type fuzzy systems and cannot accept all the customization options that basic fuzzy inference allows. An additional limitations can be find in [2].

There are many types of evolutionary algorithms. Generally they work well but they has many options and its use is complicated. The algorithm of clonal selection, (CLONALG) was adapted to solve global optimization tasks in [4]. This algorithm was compared with evolutionary algorithms, such as: *genetic algorithm*, *direct search* and *simulated annealing*. Current results show that the main immune mechanism of clonal selection with cell suppression can be successfully applied. Using relatively small population of candidate solutions it was able to find global minimum for all tested function.

A preliminary test of approximation was done for tridimensional *peaks* function $z = f(x, y)$,

$$z = 3(1 - x)^2 e^{-x^2 - (y+1)^2} - 10\left(\frac{1}{5}x - x^3 - y^5\right)e^{-x^2 - y^2} - \frac{1}{3}e^{-(x+1)^2 - y^2} \quad (5)$$

where $x, y \in [-3, 3]$.

The function (5) was approximated by fuzzy mode Sugeno type. This model was generated by clonal selection algorithm in version for clustering tasks and then an auxiliary optimization of parameters of membership functions was done. The fuzzy model had 7 rules and Gauss functions were used as membership functions – 7 to each input of fuzzy model. The *RMS Error* was equal 0.0196.

5 Conclusion and Future Work

Fuzzy models allow describing a very complex phenomenon that are difficult to be represented in the form of mathematical formulas. Two experiments with *Trip* and *DWP* data indicate that clonal selection clustering algorithm is computationally fast, robust and useful. The preliminary test of approximation of *peaks* functions (5) show that clonal selection in optimization version work well.

The future works will involve the applications CLONAG implementation which will be easy to use in technical application and which will have small limitation for identification of parameters of Sugeno fuzzy models extracted from numerical data.

References

1. Chiu, S.: Fuzzy model identification based on cluster estimation. *J. of Intelligent and Fuzzy Systems* 2, 267–278 (1994)
2. Fuzzy Logic Toolbox User's Guide, Version 8.2, The MathWorks, Inc. (R2013b)
3. Felka, D.: Metody budowy inteligentnych modeli na bazie danych numerycznych, Innowacyjne rozwiązania w obszarze automatyki, robotyki i pomiarów. In: Kacprzyk, J. (ed.) *Konkurs Młodzi Innowacyjni 2012*, vol. 2012, pp. 75–88. PIAP Warszawa (2012) (in polish)
4. Mrozek, B.: Optimization using the clonal selection and chosen evolutionary algorithm. In: 7th Conference Computer Methods and Systems (CMS 2009), Kraków, pp. 247–252 (2009)
5. Mrozek, B.: Immune algorithm for fuzzy models generation. In: Szewczyk, R., Zieliński, C., Kaliczyńska, M. (eds.) *Recent Advances in Automation, Robotics and Measuring Techniques. AISC*, vol. 267, pp. 187–196. Springer, Heidelberg (2014)
6. de Castro, L.N., von Zuben, F.J.: *Artificial Immune Systems: Part I – Basic Theory and Applications*, Technical Report – RT DCA 01/99 (1999)
7. de Castro, L.N., Von Zuben, F.J.: Learning and Optimization Using the Clonal Selection Principle. *IEEE Transactions on Evolutionary Computation*, Special Issue on Artificial Immune Systems 6(3) (2002)
8. Takagi, T., Sugeno, M.: Fuzzy identification of systems and its application to modeling and control. *IEEE Trans. on Systems, Man & Cybernetics* 15, 116–132 (1985)
9. Wang, H., Zhao, L., Du, W., Qian, F.: A hybrid method for identifying T-S fuzzy models. In: 8th International Conference on Fuzzy Systems and Knowledge Discovery (FSKD), Shanghai, vol. 1, pp. 11–15 (2011)
10. Wong, E., Lau, H.: Advancement in the twentieth century in artificial immune systems for optimization: review and future outlook. In: *IEEE International Conference on Systems, Man, and Cybernetics*, San Antonio, pp. 4195–4202 (2009)

11. Jang, J.-S.R.: ANFIS: Adaptive-Network-based Fuzzy Inference Systems. *IEEE Transactions on Systems, Man, and Cybernetics* 23(3), 665–685 (1993)
12. Mo, H., Zuo, X., Xu, L.: Immune algorithm optimization of membership functions for mining association rules. In: Jiao, L., Wang, L., Gao, X.-b., Liu, J., Wu, F. (eds.) *ICNC 2006*. LNCS, vol. 4222, pp. 92–99. Springer, Heidelberg (2006)
13. Şakiroğlu, A.M., Arslan, A.: Optimization of Fuzzy Membership Function Using Clonal Selection. In: Beliczynski, B., Dzielinski, A., Iwanowski, M., Ribeiro, B. (eds.) *ICANNGA 2007*. LNCS, vol. 4431, pp. 694–701. Springer, Heidelberg (2007)
14. Korablev, N., Sorokina, I.: Immune approach for neuro-fuzzy systems learning using multiantibody model. In: Liò, P., Nicosia, G., Stibor, T. (eds.) *ICARIS 2011*. LNCS, vol. 6825, pp. 395–405. Springer, Heidelberg (2011)

Characteristics of the Improved Magnetic Shape Memory Alloy Actuator Test Stand

Amadeusz Nowak¹, Bartosz Minorowicz¹, Frederik Stefański¹, and Zoran Pandilov²

¹ Institute of Mechanical Technology, Poznan University of Technology, Poznan, Poland
{bartosz.minorowicz, nowak.amadeusz,
frederik.stefanski}@gmail.com

² Faculty of Mechanical Engineering, University “Sv. Kiril i Metodij”, Skopje, Macedonia
panzo@mf.edu.mk

Abstract. The article describes improved magnetic shape memory alloy actuator (MSMA actuator) test stand and the previously made stand. There are pointed weak sides of the first stand and the improvements in the new one. Several quasi-static measurements were performed and results were compared between both measurement stands. The MSMA actuator characterises with significant hysteresis loop, but improved test stand allowed to reduce its width. The increased rigidity of the stand excluded influence of stand deformations on the results. The described stand resulted with similar but improved measurements of the MSMA actuator characteristics, which also proved the correctness of the previous results.

Keywords: magnetic shape memory alloys, MSMA, hysteresis, test stand, smart material.

1 Introduction

Demand of finding new actuator designs resulted in many applications of materials from group called “smart materials” or “active materials”. Aims of the new actuators is to use benefits of the materials and enhance their structures. One of the youngest “smart material” is Magnetic Shape Memory Alloy, commonly named MSMA. Its properties was described first merely 18 years ago by Ullakko [1]. The material indicates shape memory behavior induced by applying external magnetic field. The alloys are included to the same group as widely known Shape Memory Alloys (SMA, e.g. Terfenol-D). Ordinary SMA are activated thermally and in order to distinguish both groups of materials with shape memory, it is proposed to use names and abbreviations: TSMA for thermally activated alloys and MSMA for magnetically activated ones [4, 5, 12]. When external magnetic field is applied to the MSMA material sample, it elongates or contracts, accordingly to the direction of the magnetic field vector and initial state of the sample. After reducing the field, the material preserves its final shape until it is deformed by different magnetic field or external force. The phenomenon bases on that it is needed less energy to deform crystallographic structure of the material than rotate magnetic domains. Although the sense of the magnetic vector is

not relevant, elongating field direction must be perpendicular to contracting field, which complicates design of the magnetically stimulated only actuator. This is one of the main disadvantages of the material. What is more, the relative permeability of the material changes during its elongation from 65 to 2, which makes the material harder to contract magnetically than elongate. Therefore the mostly used actuator design contains electrical coil to produce elongating magnetic flux and spring to produce mechanical contraction and initial pretension. Another important disadvantage is occurrence of wide asymmetric hysteresis loop in static characteristic of MSMA actuators, similar to other “smart materials” based designs. This is general problem in precise displacement control and regulation. Many researchers recorded measurements of the MSMA hysteresis. The hysteresis shapes varies because they depend on actuators designs and individual material samples properties. In order to prepare proper hysteresis model, the actuator or test stand design should provide repeatable results. Small scale fabrication of the MSMA samples for research purposes only should be taken into consideration by comparing the measurements, but noticeable are differences between results achieved by different research teams [2–12].

2 Motivation for the Test Stand Improvement

2.1 General Description of the Problem

In order to check MSMA actuator, simple test stand was designed and built [10]. The main purposes were to initially obtain several the parameters of MSMA actuator and general properties of MSMA samples and to easily reconfigure the test stand. The stand gives possibility to measure force generated by MSMA and pushing rod displacement at the same time, what was useful in first calibrations of the actuator [11, 12]. During first measurements authors recognized several problems with the test stand. There were some problems with repeatability of the results, so the first gathered information were treated as uncertain. After several simple modifications in structure, obtained results were satisfactory. Nonetheless, the problems which were met by the first measurement attempt motivated to design new improved test stand of the MSMA actuator.

2.2 Description of Previous Test Stand Version

As mentioned, first measurement stand was designed to be universal, easy in modifications and easy to access elements. The consequence of that choice is less rigidity of the stand, which was very problematic in the first study phase, especially in position regulation with PID controller. The general view of the system is presented in the Fig. 1. The stand consists of base plate supported on four supports (no 1 in the figure), table with micrometer screw that allow precise calibration (2), optical displacement sensor Philtec Fiberoptic D47, which was later replaced with HBM LVDT type sensor (3). Number 4 points to pushing rod with return spring, where the rod is pushed directly by the magnetic shape memory alloy. Magneto motive force source parts of

assembly are two identical coils (5), magnetic poles with MSMA sample placed in gap (6). Last element is force transducer (7), which allows measuring force generated by MSMA.

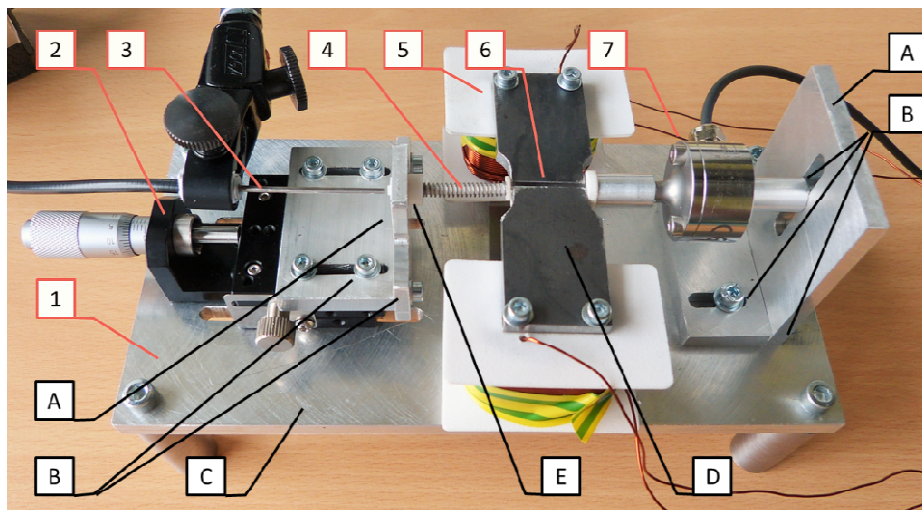


Fig. 1. General view of the previous test stand: 1 – base, 2 – micrometer screw table, 3 – optical displacement sensor, 4 – pushing rod with return spring, 5 – actuator coils, 6 – MSMA material inside magnetic poles, 7 – force transducer

The same Fig. 1 presents several weak points of the initial test stand. First of all the rigidity of the elements may not be sufficient (indicator A). This is necessary especially for precise measurements in micrometric scale. Second important matter is the relatively big amount of threaded connections (B). Every connection of elements could result in additional rigidity loss and even some backlashes. In the stand 3 screw connections between parts exist on each side (micrometer table not counted). Another problem is unstable placement of the stand on supports and flexibility of the base plate (C). Deflections of the base or whole stand were observed and only placement on very rigid, additional beam helped solving this problem. One of the last important notification is the fact of magnetic circuit deflection during the current increase (D). The magnetic core elements thank to the threaded connections are not rigid sufficiently. Electromagnetic force pulls in the magnetic poles, contracting the magnetic gap, modifying the magnetic circuit properties and in extreme situation pressing the MSMA sample. The all mentioned issues impede the results repeatability and reliability, but the last one could reason also in hysteresis enlargement. The imperfection may appears in pushing rod – driving guide connection (E). Every additional friction force existing by the actuator's end movement will worsen its work and could increase the width of the hysteresis loop. Due to the potential friction occurrence in rod-guide pair it is not sure whether current hysteresis shape origins only from MSMA properties. Further part of the article describes these problem in more details.

3 Improved Magnetic Shape Memory Alloy Test Stand

Next research phase assumed the improvement of the initially built test stand. The mechanical structure of the stand was modified in order to improve the reliability of the results. Measurement configuration is presented in the Fig. 3. Whole stand with sensors was mounted to a rigid table (1). Sensor's arm was placed on the micrometer screw table (2). Optical displacement sensor Philtec Fiberoptic D47 is presented in the figure, but the second used sensor was HBM LVDT type displacement transducer (3). Next number points the pushing rod and driving guide pair with return spring (4). One of the most important change is the mounting frame, which was fabricated from single part of aluminum based alloy plate to achieve better rigidity of the stand (5). Another significant change was adding rigid bar above the magnetic poles and MSMA material, which prevented from deflecting of the magnetic circuit elements (6). Additional screw (7) was used for fixing the MSMA sample and assembling stand (7). Number (8) is first of two electrical coils, the second is not visible. These are energized by special controllable current supplier. The last are two base plates for mounting the MSMA actuator (9). These are thicker than previous base plate and placed rigidly. The stand became more compact, and rigid. Tests showed that during MSMA material extension, deformation of the frame (5) is not recorded by used displacement sensor, therefore its rigidity is sufficient for the measurements. Threaded connections were also reduced to minimum – stand contains only one screw connection supporting the MSMA sample. The new stand version was designed for displacement measurements only.

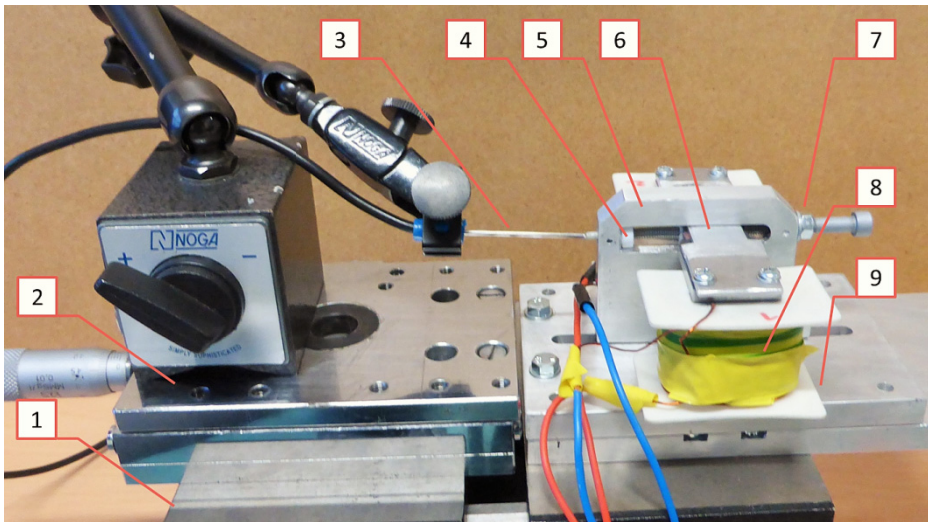


Fig. 2. View of the improved test stand: 1 – rigid base, 2 – micrometer screw table, 3 – displacement sensor, 4 – pushing rod-guide with return spring, 5 – rigid actuator frame, 6 – plate preventing from magnetic circuit deflections and MSMA sample below, 7 – supporting screw for MSMA, 8 – electrical coil, 9 – base plate for MSMA actuator and test stand

4 Measurements and Comparison to Previous Results

In the first study phase occurred many problems in achieving repeatable and sure results. Example one are presented in the Fig. 3 and these are compared to the data acquainted with the improved test stand. The violet line is measured input current, which shape was sinus with decreasing amplitude and bias equaling 2.5 A and frequency 0.1 Hz. Supply current range is 0–5 A for parallel coils connection 2.5 A for each. Acquisition and control was performed with use of dSPACE system with sampling period 1 ms. The green line origins from the stand number one with wider magnetic gap, when the orange represents the situation when magnetic gap width was reduced. The red line is displacement output from improved test stand. The hysteresis effect prevents from displacement change for lower amplitude current variations. Noticeable are drift of the steady value and additional peaks after the current local maximums. Other comparisons are presented in Fig. 4 and Fig. 5, where are quasi-static displacement characteristics. Data presented in article [12] were acquainted on previous test stand with some minor improvements and these are in the mentioned figures marked with blue line. The red line are results from current improved stand to make comparison of the stands available. Maximum displacements achieved by the MSMA actuator differs about 30 μm , but this could be result of different pretensions of return spring. In order to better compare the hysteresis loop shapes, the measurements from improved stand were scaled to similar displacement range as in the previous tests, which is shown in the Fig. 5. Character of displacement change for increasing current is very similar, almost identical, but when input current decreases, the MSMA actuator's pushing rod displacement changes in a different way. Results from improved test stand show faster response to current decrease, which means that blocking forces in the MSMA actuator structure are smaller. Elongation of the MSMA material is active process induced by increase of magnetic induction in gap, while contraction is passive process resulted by spring relaxation. Therefore return action is more dependent to any disturbance forces, like e. g. friction forces. One of the properties of MSMA materials, which allows shape memory effect to exist, is "twinning stress". This is value of stress that must be applied to elongated material to shorten it. The effect results additional blocking force treated as internal friction of the MSMA material. This may be advantage of the material application as self-supporting effect, but when the actuator is designed in the return-spring variant, this force distorts the actuator's work. Moreover, there always may exists friction in pushing rod-guide connection. In both stands there were used parts fabricated from PTFE based material to make the friction force smaller. In second stand the pushing rod was even little polished to ensure low friction work, therefore the hysteresis origins mainly from the magnetic shape memory alloy material's properties. Authors initially hoped to achieve significantly different hysteresis shape, but on the other hand the new results confirmed the correctness of the MSMA actuator previous measurement and repeatability of the results. It is sure that the rigidity of the new test stand is improved and it does not have influence on the results. In addition, tests of the improved test stand were repeated with use of optical contactless sensor, but these were not presented in the article, because were practically identical as these achieved with LVDT type transducer. This excluded eventual errors from use of particular transducer type.

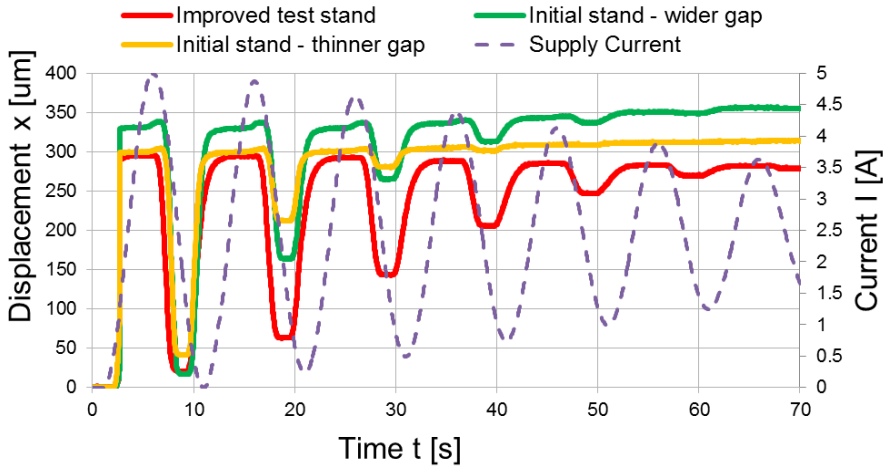


Fig. 3. Displacements of the pushing rod under different test stand configurations, but with the same input current signal, noticeable errors of actuator responses

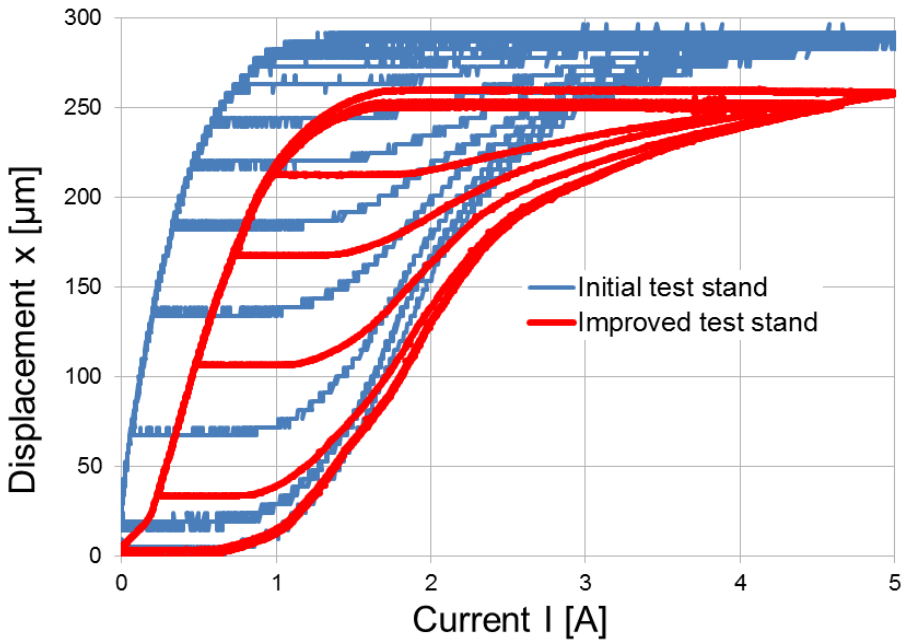


Fig. 4. Comparison between previous test stand results and improved test stand results – quasi-static displacement characteristics

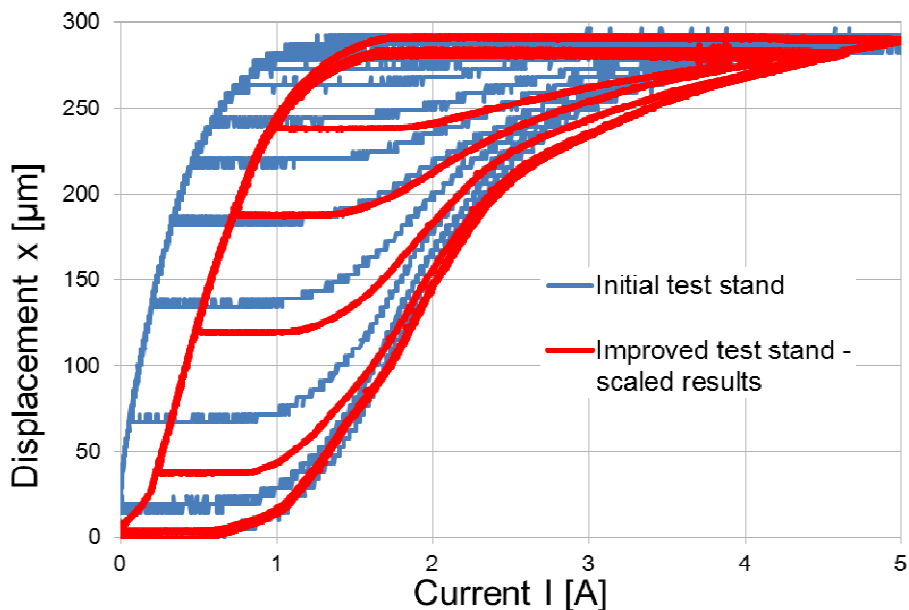


Fig. 5. Comparison between previous test stand results and improved test stand results – quasi-static displacement characteristics with the second hysteresis scaled

5 Conclusions

Modifications of test stand for MSMA actuator was done and the test stand was compared to the previous one. Quasi-static characteristic of the actuator was acquainted and significant hysteresis loop occurs. The results obtained on both stands were compared. The main improvement of the new test stand is much increase of the stand mechanical rigidity. Possible existence of additional friction force could be the minor reason of the wider hysteresis of the MSMA actuator. The differences between hysteresis shapes achieved by scientists could be reasoned by differences between designs of actuators, as well as differences between magnetic shape memory samples' individual properties. Further research will focus on MSMA actuator modeling task, especially hysteresis effect and force hysteresis generated by MSMA measurements. Eventually it could be considered research under hysteresis compensation in control and environmental parameters change influence on its shape.

Acknowledgments. This article was financially supported within the project "Engineer of the Future. Improving the didactic potential of the Poznan University of Technology" – POKL.04.03.00-00-259/12, implemented within the Human Capital Operational Programme, co-financed by the European Union within the European Social Fund.

References

1. Ullakko, K., Huang, J.K., Kantner, C., O'Handley, R.C., Kokorin, V.V.: Large magnetic field induced strains in Ni_2MnGa single crystals. *Applied Physics Letters* 69(13), 1966–(1968)
2. Jaaskalainen, A., Aaltio, I., Suorsa, I., Tellinen, J., Ullakko, K.: Basic properties of magnetic shape memory actuators. In: Published in 8th International Conference ACTUATOR 2002, Bremen, Germany, June 10-12 (2002)
3. Schlüter, K., Riccardi, L., Raatz, A.: An Open-Loop Control Approach for Magnetic Shape Memory Actuators Considering Temperature Variations. *Advances in Science and Technology* 78, 119–124 (2012)
4. Holtz, B., Riccardi, L., Janocha, H., Naso, D.: MSM Actuators: Design Rules and Control Strategies. *Advanced Engineering Materials* 14(8), 668–681 (2012)
5. Schlüter, K., Holz, B., Raatz, A.: Principle Design of Actuators Driven by Magnetic Shape Memory Alloys. *Advanced Engineering Materials* 14(8), 682–686 (2012)
6. Sadeghzadeh, A., Asua, E., Feuchtwanger, J., Etxebarria, V., García-Arribas, A.: Ferro-magnetic Shape memory alloy actuator enabled for nanometric position control using hysteresis compensation. *Sensors and Actuators A: Physical* 182, 122–129 (2012)
7. Flaga, S., Oprzędkiewicz, I., Sapiński, B.: Characteristics of an Experimental MSMA-Based Actuator. *Solid State Phenomena* 198, 283–288 (2013)
8. Flaga, S., Sapiński, B.: The Properties of the Magnetic Shape Memory Alloy Actuator, Active Noise and Vibration Control Methods, Krakow-Wojanow, Poland, pp. 259–264 (June 2011)
9. Flaga, S., Sioma, S.: Characteristics of Experimental MSMA-Based Pneumatic Valves. In: Proceedings of SMASIS-2013, ASME Conference on Smart Materials, Adaptive Structures and Intelligent Systems, Paper No. SMASIS2013-3323, V001T04A016, p. 6 pages (2013)
10. Minorowicz, B.: Design of Test Stand for Magnetic Shape Memory Alloys Samples and Representation of Obtained Results. *Solid State Phenomena*, Vols 221, 633–639 (2015) (in press)
11. Minorowicz, B., Nowak, A.: Force Generation Survey in Magnetic Shape Memory Alloys. *Archives of Mechanical Technology and Automation* 33(1), 37–46 (2013)
12. Minorowicz, B., Nowak, A., Stefański, F.: Position regulation of magnetic shape memory actuator. *Journal of Achievements in Materials and Manufacturing Engineering* 61(2), 216–221 (2013)

Control of an Oriented PV System with the Use of a Discrete, Robust, Fractional Order PID Controller

Krzysztof Oprzedkiewicz

AGH University, Faculty of Electrotechnics, Automatics,
Informatics and Biomedical Engineering,
Dept. of Automatics and Biomedical Engineering
A. Mickiewicza 30, 30-059 Krakow, Poland
kop@agh.edu.pl
<http://www.agh.edu.pl>

Abstract. In the paper the proposition a fractional order, robust, discrete PID controller dedicated to minimum-energy control an interval - parameter, oriented PV system is presented. A tuning of robust controller with use of different cost function is also proposed. Results are by an example depicted.

Keywords: robust control, fractional order PID, oriented PV system, minimal-energy control.

1 An Introduction

An application of fractional order calculus in modeling and control of dynamic systems has been considered by many Authors, for example Podlubny (see [13],[14]) , Das (see [3]), Kaczorek [4], Pan and Das [11].

In many situations the use of non integer order controller assures the better control performance, than integer order control. It is caused by the fact, that fractional orders of integration and derivative actions are additional tuning parameters of controller, which allow us to precisely tune the power of both control actions. The use of fractional order controllers has been considered by many Authors, for example by Podlubny in [13] or Petras in [12].

In this paper a proposition of use a fractional order, discrete PID controller to control the elevation angle in the moving part of an experimental oriented PV system will be presented. The control plant is described with the use of interval transfer function. The use of interval model is determined by the fact, that the PV works all the year outdoor in extremally different atmospheric conditions.

It is well known, that an important control problem for oriented PV systems is a minimal energy control. Generally, for integer order control this problem has been considered by many Authors for years, classic solutions of it are well known, but the use of fractional order controllers generates a number of new problems, particularly for uncertain-parameter systems.

In the paper the following problems will be discussed:

- An oriented PV system and its interval model,
- A fractional order PID controller and its discrete approximation,
- A digital closed-loop control system,
- Tuning method for the considered controller
- An Example

2 An Oriented PV System and Its Interval Model

Let us consider a moving part of an oriented PV system shown in figure 2. The most simple scheme of this plant is a DC motor with gearbox, considered by many Authors, for example Athans and Falb in [1], Petras [12], p. 121). The simplified scheme of it is shown in figure 1.

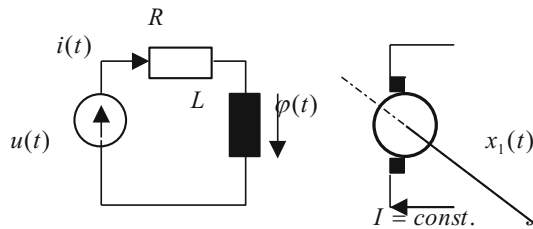


Fig. 1. A DC electric drive as a model of moving part of the oriented PV system

The exact description of the plant we deal with can be found in [8], [5], [6], [7]. Exact parameters of the PV presented in figure 2 are given in paper [9]. The most simple model of the plant shown in figure 1 has the form of an interval transfer function:

$$G(s, q) = \frac{q}{s} \quad (1)$$

where: q denotes interval parameter of the PV, defined as follows:

$$q = [q_l; q_h] \subset I(\mathbb{R}) \quad (2)$$

Vector q describes parameters of the plant, changing during work of the system outdoor in extremely different atmospheric conditions (summer and winter, with and without snow, etc.). Additionally - these parameters have different values for moving up and moving down the PV. Exemplary values of this parameter are given in the example.



Fig. 2. An experimental oriented PV system

3 A Fractional Order PID Controller and Its Discrete Approximation

A continuous fractional order PID controller is described with the use of the following, continuous, fractional order transfer function:

$$G_c(s, p) = k_P + k_I s^\alpha + k_D s^\beta \quad (3)$$

where k_P , k_I and k_D denote coefficients of proportional, integral and derivative actions of the controller, α and β denote fractional orders of the integral and derivative actions. All these parameters can be assembled in a vector p :

$$p = [k_P, k_I, k_D, \alpha, \beta] \quad (4)$$

All the vectors p build the set of permissible controller parameters P , defined as underneath:

$$P = \{p = [k_P, k_I, k_D, \alpha, \beta] : k_P, k_I, k_D > 0, -1 < \alpha < 0, 0 < \beta < 1\} \subset \mathbf{R}^5 \quad (5)$$

The discrete, fractional order PID controller can be obtained after discretization of time-continuous controller described by (3). The translation can be done with the use of the elementary dependence between continuous and discrete Laplace transforms (see for example [12]):

$$(\omega(z^{-1}))^\gamma = \left(\frac{1+a}{T_s}\right)^\gamma \left(\frac{1-z^{-1}}{1+az^{-1}}\right)^\gamma = \left(\frac{1+a}{T_s}\right)^\gamma CFE\{\dots\} \quad (6)$$

In (6) a is the coefficient depending on approximation type, T_s denotes the sample time, $CFE\dots$ is a Continuous Fraction Expansion:

$$CFE_\gamma\left\{\frac{1-z^{-1}}{1+az^{-1}}\right\} = \frac{v_{\gamma 0} + v_{\gamma 1}z^{-1}}{w_{\gamma 0} + w_{\gamma 1}z^{-1}} \quad (7)$$

Coefficients of discrete transfer function (7) are equal:

$$v_{\gamma 0} = w_{\gamma 0} = \frac{2}{a + \gamma + \gamma a - 1}; \quad v_{\gamma 1} = \frac{a - \gamma - \gamma a - 1}{a + \gamma + \gamma a - 1}; \quad w_{\gamma 1} = 1 \quad (8)$$

In (8) the value of the coefficient a depends on the approximation type, for example, $a = 1$ for Tustin approximation, $a = 0$ for Euler approximation. In further consideration the Euler approximation will be applied. This implies, that coefficients (8) turn to the following simpler form:

$$v_{\gamma 0} = w_{\gamma 0} = \frac{2}{\gamma - 1}; \quad v_{\gamma 1} = \frac{-\gamma - 1}{\gamma - 1}; \quad w_{\gamma 1} = 1 \quad (9)$$

In (9) $\gamma = \alpha$ for integral part of the controller and $\gamma = \beta$ for derivative part respectively. Consequently, the discrete fractional order PID controller can be described with the use of the following discrete transfer function $G_c^+(z^{-1}, p)$, which is also a function of vector p defined by (4):

$$G_c^+(z^{-1}, p) = k_P + k_I \left(\frac{1}{T_s} \right)^\alpha CFE_\alpha + k_D \left(\frac{1}{T_s} \right)^\beta CFE_\beta \quad (10)$$

In (10) k_P , k_I , k_D denote gain of proportional, integral and derivative actions of the controller, $\alpha < 0$ denotes the non integer order of integration, $\beta > 0$ denotes the non integer order of the derivation, CFE_\cdot is described by (8) and (9). Notice, that the controller (10) can be directly implemented at each digital platform (PLC or microcontroller).

$$G_c^+(z^{-1}, p) = \frac{a_2 + a_1 z^{-1} + a_0 z^{-2}}{b_2 + b_1 z^{-1} + b_0 z^{-2}} \quad (11)$$

where:

$$\begin{aligned} a_0 &= k_P w_{\alpha 1} w_{\beta 1} + k_I v_{\alpha 1} w_{\beta 1} + k_D p_{\beta 1} w_{\alpha 1} \\ a_1 &= k_P (w_{\alpha 0} w_{\beta 1} + w_{\alpha 1} w_{\beta 0}) + k_I (v_{\alpha 0} w_{\beta 1} + v_{\alpha 1} w_{\beta 0}) + k_D (v_{\beta 0} w_{\alpha 1} + v_{\beta 1} w_{\alpha 0}) \\ a_2 &= k_P w_{\alpha 0} w_{\beta 0} + k_I v_{\alpha 0} w_{\beta 0} + k_D v_{\beta 0} w_{\alpha 0} \end{aligned} \quad (12)$$

$$\begin{aligned} b_0 &= w_{\alpha 1} w_{\beta 1} \\ b_1 &= w_{\alpha 0} w_{\beta 1} + w_{\alpha 1} w_{\beta 0} \\ b_2 &= w_{\alpha 0} w_{\beta 0} \end{aligned} \quad (13)$$

The whole closed loop control system containing both plant and controller will be described in the next section.

4 A Digital Closed-Loop Control System

The digital closed loop control system for the plant we deal with is shown in figure 3. The uncertain-parameter plant is described by (1)-(2), the digital fractional order PID controller is described by (10). The problem during tuning the

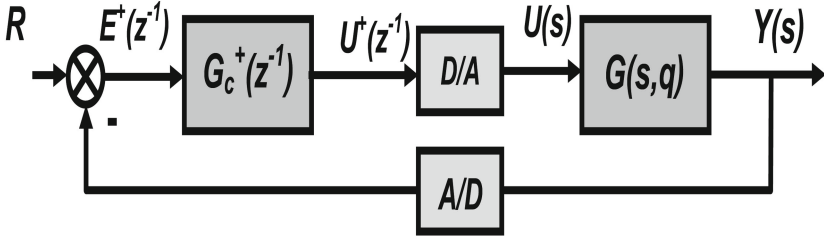


Fig. 3. A digital closed-loop control system

considered control system we deal with is to find such a vector $p_0 \in P$ for which the energy consumption will be minimal or close to minimal in the whole interval q , defined by (2). The transfer function of the whole closed-loop control system $G_{cl}^+(z) = \frac{Y^+(z)}{R^+(z)}$ is described by (14).

$$G_{cl}^+(z) = \frac{G_c^+(z)G^+(z)}{1 + G_c^+(z)G^+(z)} \quad (14)$$

where $G_c^+(z^{-1})$ denotes the discrete transfer function of the controller, described with the use of (10)-(13) and $G^+(z^{-1})$ denotes the discrete transfer function of the plant with the zero-order hold at the input:

$$G^+(z^{-1}, p, q) = c \frac{z^{-1}}{1 - z^{-1}} \quad (15)$$

where:

$$c = qT_s \quad (16)$$

Finally, with respect to (11) and (15) the discrete, closed-loop transfer function (14) is equal:

$$G_{cl}^+(z^{-1}, p, q) = \frac{c(a_2z^{-1} + a_1z^{-2} + a_0z^{-3})}{b_2 + (b_1 - b_2 + ca_0)z^{-1} + (b_0 - b_1 + ca_1)z^{-2} - (b_0 + ca_0)z^{-3}} \quad (17)$$

where $a_{...}$, $b_{...}$ and c are described by (12), (13) and (16) respectively.

Furthermore, the relationship between z' transform of control signal $U^+(z^{-1})$ and z' transform of a reference signal R can be also given. It has the following form:

$$U^+(z^{-1}) = \frac{G_c^+(z^{-1})}{1 + G_c^+(z^{-1})G^+(z^{-1})} R \quad (18)$$

After any elementary transformations the equation (18) turns to the following form:

$$U^+(z^{-1}) = \frac{a_2 + (a_1 - a_2)z^{-1} + (a_0 - a_1)z^{-2} - a_0z^{-3}}{b_2 + (b_1 - b_2 + ca_2)z^{-1} + (b_0 - b_1 + ca_1)z^{-2} + (ca_0 - b_0)z^{-3}} R \quad (19)$$

Consequently, the discrete control signal, calculated as inverse z transform from $U^+(z^{-1})$ described by (19) is equal:

$$u^+(n) = Z^{-1} (U^+(z^{-1})) \quad (20)$$

Notice, that:

- The parameters of the transfer function (17) are interval numbers, because the coefficient c is the interval number (see (2), (16)),
- The discrete transfer function (17) is the integer order transfer function, because non integer orders α and β were replaced by integer order approximation CFE.

The both above remarks allow us to test the properties of the considered digital control system with the use of approach dedicated to discrete, interval, integer order systems.

5 Tuning Method for the Considered Controller

The main goal of use the proposed controller is to minimize an energy consumption during moving the PV from initial to final position.

The energy consumption during moving the PV is described by the following cost function:

$$I(p, q) = T_s \sum_{n=n_0}^{N_f} (u^+)^2(n) \quad (21)$$

where T_s denotes the sample time, $u^+(n)$ denotes the discrete control signal described by (20), n_0 and N_f denote the initial and final time moments of moving the PV system.

In the considered case the problem of optimal tuning the considered fractional order, discrete, robust PID controller consists in finding such a vector $p_0 \in P$ (where P denotes the set of permissible controller parameters described by (5) which keeps the cost function (21) minimal or close to minimal in the whole interval q .

The vector p_0 can be found with the use of the following algorithm:

1. We calculate vectors p minimizing the cost function (21) for both border values of q separately. Denote these vectors by p_{0_l} and p_{0_h} , respectively. These vectors can be calculated with the use of MATLAB.

2. We calculate values of cost function (21) for each value q_l, q_h and both vectors $p_{..}$ calculated in step 1. Denote these values as $I(p_{..}, q_{..})$ respectively. It is easy to notice, that total number of all combinations is equal 4. We collect all values of $I(p_{..}, q_{..})$ in a table: rows of the table are associated to vertices $q_{..}$ and columns are associated to vectors $p_{0..}$.
3. Finally, as the vector p_0 we select such a vector $p_{..}$, which minimizes one of the following, additional cost functions:
 - (a) The average minimal energy consumption:

$$I_{av}(p, q) = 0.5 \sum_q I(p_{..}, q), \quad q \in \{q_l, q_h\} \tag{22}$$

- (b) The maximal robustness of control system:

$$I_r(p, q) = | \max(I(p_{..}, q)) - \min(I(p_{..}, q)) | \quad q \in \{q_l, q_h\} \tag{23}$$

- (c) The minimum from maximal energy consumption:

$$I_{max}(p, q) = \min_q \max I(p_{..}, q), \quad q \in \{q_l, q_h\} \tag{24}$$

Selection of certain criterion depends on particular situation during control. The use of the proposed will be shown in the next section.

6 An Example

As an example let us consider the control system described above. We deal with the control of the elevation angle for experimental, oriented PV system shown in figures 1 and 2. The interval parameters of the control plant are equal:

$$q = [0.7746; 1.1228].$$

The identification method for these parameters was exactly discussed in paper [9]. During simulations the sample time in the system was equal 1[s].

The parameters of robust controller were calculated with the use of the algorithm proposed in the previous section. The 1'st step of algorithm (The values of vectors $p_{0..}$ and suitable values of cost function 21) are presented in the table 1 and marked in bold.

The results associated to the 2'nd step of algorithm are also presented in the table 1.

Table 1. The 1'st and 2'nd steps of the algorithm

| vectors $p_{..}, q_{..}$. Cost function (21) | $p_{0l} = [0.85, 0.03, 0.05, -0.5, .05]$ | $p_{0h} = [0.7, 0.02, 0.05, -0.4, 0.9]$ |
|--|--|---|
| $q_l = 0.7746$ | 0.9461 | 0.6915 |
| $q_h = 1.1228$ | 0.8791 | 0.5944 |

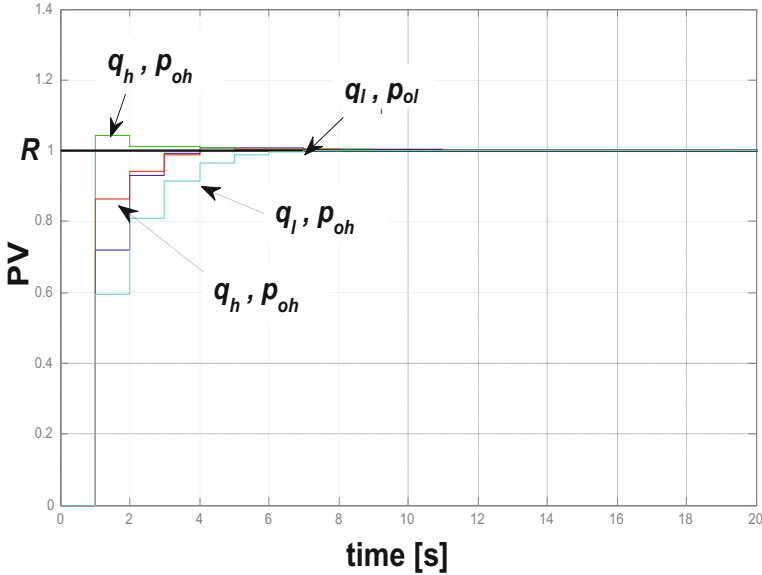


Fig. 4. The step responses of control system for both boundary values of the vector q and both vectors p shown in table 1

Next the vectors of controller parameters p_0 optimal in the sense of cost functions (22), (23) and (24) can be find with the use of table 1. It is easy to see, that:

1. The minimum of cost function (22) describing the minimum average energy consumption is achieved for vector p_{0_h} , the cost function is equal: $I_{av}(p_{0_h}, q)=0.6430$.
2. The maximal robustness of the control system, described by cost function (23) is achieved for vector p_{0_l} , the cost function is equal: $I_r(p_{0_l}, q)= 0.0670$.
3. The minimum value of cost function (24) is achieved for vector p_{0_h} , the cost function is equal: $I_{max}(p_{0_h}, q)=0.6915$.

The set of step responses of the control system with controller parameters assembled in the both vectors p_{0_h} and p_{0_l} and both boundary vectors q_l and q_h describing the plant are shown in figure 4.

Notice, that the set of controller parameters assures the good control performance in sense another cost functions also: the step response does not have any overshooting and the settling time is resonable.

7 Final Conclusions

Final conclusions from the paper can be formulated as follows:

- Results of simulations show, that the proposed robust, fractional order, discrete PID controller assures the good control performance for the considered uncertain parameter oriented PV system.
- The presented approach can be easily generalised at another classes of uncertain parameter control plants (more complex plants with number of uncertain parameters greater than one),
- The proposed controller can be easily implemented at each digital platform (microcontroller, PLC/PAC). The proposed in this paper fractional order PID controller is recently implemented at SIEMENS PLC, results will be presented soon.
- An another important problem is to propose the analytical method of tuning the proposed PID controller. This also will be considered.

Acknowledgments. This paper was sponsored by NCN grant no 6693/B/T02/2011/40.

References

1. Athans, M., Falb, P.L.: Optimal Control. An Introduction to the Theory and Its Applications. Dover (2007)
2. Caponetto, R., Dongola, G., Fortuna, L., Petr, I.: Fractional Order Systems: Modeling and Control Applications. In: Chua, L.O. (ed.), New Jersey, London. Series on Nonlinear Science, vol. 72, pp. 1–178 (2010)
3. Das, S.: Functional Fractional Calculus for System Identification and Control. Springer, Berlin (2010)
4. Kaczorek, T.: Selected Problems of Fractional Systems Theory. Springer, Berlin (2011)
5. Mitkowski, W., Oprzedkiewicz, K.: Optimal control for an uncertain parameters, second order plant with the use of discrete controller. Journal of Mathematics and System Science 2(4), 258–263 (2012)
6. Mitkowski, W., Oprzedkiewicz, K.: Fractional-order $P2D^\beta$ controller for uncertain parameter DC motor. In: Mitkowski, W., Kacprzyk, J., Baranowski, J. (eds.) Theory & Appl. of Non-integer Order Syst. LNEE, vol. 257, pp. 249–259. Springer, Heidelberg (2013)
7. Mitkowski, W., Oprzedkiewicz, K.: Tuning of the half-order robust PID controller dedicated to oriented PV system. LNEE. Springer (2014)
8. Oprzedkiewicz, K.: A robust suboptimal PD servo controller for an oriented PV system, vol. 16(1), pp. 59–71 (2012), <http://journals.bg.agh.edu.pl/AUTOMAT/2012.16.1/automat.2012.16.1.59.pdf> ISSN 1429-3447
9. Oprzedkiewicz, K., Glowacz, W., Zaczyk, M., Teneta, J., Wieckowski, L.: An identification of interval model an elevation angle in oriented PV system. In: Electrotechnical Review 2014, vol. 8, pp. 243–247. Sigma-NOT (2014)
10. Padula, F., Visioli, A.: Tuning rules for optimal PID and fractional-order PID controllers. Journal of Process Control 21, 69–81 (2011)

11. Pan, I., Das, S.: Intelligent Fractional Order Systems and Control. An Introduction. Studies in Computational Intelligence, vol. 438. Springer, Berlin (2013)
12. Petr, I.: Fractional-Order Feedback Control of a DC Motor. J. of Electrical Engineering 60(3), 117–128 (2009)
13. Podlubny, I.: Fractional Differential Equations. Academic Press, San Diego (1999)
14. Podlubny, I.: Fractional - order systems and controllers. IEEE Trans. on Automatic Control 44(1), 208–214 (1999)

Production System Designing with the Use of Digital Factory and Augmented Reality Technologies

Dariusz Plinta¹ and Martin Krajčovič²

¹ University of Bielsko-Biala, Production Engineering Department,
Bielsko-Biala, Poland

dplinta@ath.bielsko.pl

² University of Zilina, Industrial Engineering Department,
Zilina, Slovakia

martin.krajcovic@fstroj.uniza.sk

Abstract. Current requirements for continuous reduction of products, processes and systems life cycles increase the need of rapid design of “lean” and “flexible” production systems. This means that classical approaches of production systems design have to be extended by the application of advanced technologies and methods, such as digital factory, virtual and augmented reality, computer simulation, reverse engineering, etc. The article describes design, optimization and visualization of the production layout using a combination of conventional design approaches and modern computer technologies, like VisTable software and augmented reality.

Keywords: Production systems, digital factory, augmented reality.

1 Designing Production Systems

Layouts and temporal structure optimization of manufacturing requires application of a multi-criteria approach in designing production systems, especially in arranging production machines and workstations. We must take into account economical, technical, logistic, personal and other parameters of the proposed system [4].

From the perspective of spatial arrangement optimization, the most important decision criteria include minimization of transport activities and costs, simple material flow, suitable connection between external logistics chains, minimizing the need for space, minimizing inventories and production cycles, fulfilling the requirements regarding health and safety at work, flexibility and possibility of future changes.

For the above mentioned reasons, production layout design requires implementation of a few basic steps, which are described in this article in more detail:

1. collection, processing and analysis of input data,
2. designing an ideal layout,
3. constraints specification and creation of a real system and its evaluation,
4. visualization of the proposed layout.

2 Collection, Processing and Analysis of Input Data

Preparation and analysis of input data significantly affect the final quality of the proposed variant of the designed production system. The main problem of collecting, processing and evaluating input data for the designing process is to ensure comprehensiveness, completeness, accuracy and timeliness of necessary information [6, 7]. The proposed solution has to meet the requirements of the current, but also the future production, and an essential part of the input data analysis is forecasting basic future parameters (range of products, demand structure, cost structure, etc.). The forecasting horizon must be adapted to the lifecycle of individual elements of the production system (structural elements, energy facilities, production equipment, handling equipment, etc.) The basic source of information for designing is a database for technical preparation of production. Data for production layout preparation should contain information about products, which will be produced in the production system (products types, parts lists, product parameters, the planned production volumes, etc.), production processes (manufacturing and assembly, technologies, standards time, etc.) and resources which will be used (machines, equipment, tools, personnel, etc.).

Analysis of the input data we should help us obtain the following information:

- an overview of the planned material flow in the analysed production system – for summarizing and further use of this information in designing optimal production layout it seems that the checkered table of transport relations is the right tool for such analyses (Fig. 1)
- total needs of different types of resources, which are necessary for realization of the planned production – the needs for production resources can be calculated by capacitive sizing of production system (Fig. 2)
- technological and time relations and time requirements of individual operations in the manufacturing process.

This data constitute the basis for the correct layout (optimal allocation of machines with respect to material flow) and time structure (balancing workplaces) of the future production system.

| | 1 | 2 | 3 | 4 | 5 | 6 | 7 | 8 | 9 | 10 | 11 |
|----|-----------------|-----------|----------|---------|---------------|---------------|----------------|-----------------|--------|-------|----------|
| 1 | C K Úalej | Ergonomic | SV 18 RA | TNC 20N | GBL 25 tyč | BUA 28x630 | SUI 50/1000 | INDEX GU 600 | PF 150 | GAC | Kontrola |
| 2 | Ergonomic | 0 | 10000 | 15000 | 0 | 0 | 5000 | 0 | 0 | 0 | 0 |
| 3 | SV 18 RA | 0 | 0 | 10000 | 0 | 0 | 0 | 0 | 0 | 0 | 0 |
| 4 | TNC 20N | 0 | 0 | 0 | 0 | 15000 | 0 | 0 | 0 | 0 | 10000 |
| 5 | GBL 25 tyč | 0 | 0 | 0 | 0 | 15000 | 0 | 0 | 0 | 10000 | 0 |
| 6 | BUA 28x630 | 0 | 0 | 0 | 0 | 0 | 0 | 0 | 0 | 0 | 45000 |
| 7 | SUI 50/1000 | 0 | 0 | 0 | 0 | 0 | 0 | 5000 | 8000 | 0 | 0 |
| 8 | INDEX GU 600 | 0 | 0 | 0 | 0 | 5000 | 0 | 0 | 0 | 0 | 0 |
| 9 | PF 150 | 0 | 0 | 0 | 0 | 0 | 0 | 0 | 0 | 0 | 8000 |
| 10 | GAC | 0 | 0 | 0 | 0 | 10000 | 0 | 0 | 0 | 0 | 0 |
| 11 | Kontrola | 0 | 0 | 0 | 0 | 0 | 0 | 0 | 0 | 0 | 0 |

Fig. 1. The checkered table with transport relations

| Workplace type | Product | | | | | | Calculated total number of machines | Real total number of machines |
|----------------|---------|------|------|------|------|------|-------------------------------------|-------------------------------|
| | P1 | P2 | P3 | P4 | P5 | P6 | | |
| Ergonomic | 0.24 | | 0.15 | 0.12 | | | 0.51 | 1 |
| SV 18 RA | 0.15 | | | | | | 0.15 | 1 |
| TNC 20N | 3.24 | | 2.18 | | | | 5.41 | 6 |
| GBL 25 | | 1.81 | | | | 0.73 | 2.54 | 3 |
| BUA 28x630 | | 0.36 | 0.36 | 0.39 | | 0.34 | 1.45 | 2 |
| SUI 50/1000 | | | | 0.24 | 1.16 | | 1.40 | 2 |
| INDEX GU 600 | | | | 1.33 | | | 1.33 | 2 |
| PF 150 | | | | | 2.32 | | 2.32 | 3 |
| GAC | | | | | | 0.97 | 0.97 | 1 |
| Inspection | 0.05 | 0.02 | 0.03 | 0.09 | 0.04 | 0.02 | 0.25 | 1 |

Fig. 2. Capacitive calculation of necessary workplaces

3 The Proposal of the Ideal Layout

The processed input data is used to design the ideal layout of workplaces. At this stage, the proposal will not be considered with real work space requirements, input-output points of the production system or other constraints (e.g. space restrictions). Creating the ideal arrangement is performed using heuristic optimization algorithms. Figure 5 presents a description of the chosen heuristic algorithm, which optimizes the layout of workplaces used as the objective function the total transport capacity calculated as the sum of the products of the Euclidean distance and intensity of traffic between all workplaces:

$$\min. p_v = \sum_{i=1}^n \sum_{j=i+1}^n I_{ij} * l_{ij} \tag{1}$$

where:

- p_v - collective material flow between workplaces,
- I_{ij} - intensity of transport between workplaces i and j ,
- l_{ij} - Euclidean distance between workplaces i and j ,

$$l_{ij} = \sqrt{(x_i - x_j)^2 + (y_i - y_j)^2} \tag{2}$$

where:

- x_i, x_j - x-coordinate position of workplaces i and j ,
- y_i, y_j - y-coordinate position of workplaces i and j .

This algorithm does not consider the real need for surfaces for particular workplaces and its output is a location of workplaces in the square grid (Fig. 3).

Taking into account manufacture processes of products, the proposed arrangement of workplaces introduces the complicated material flows, which are realized in different directions. But due to the close distance between workplaces, where the largest quantities of materials are transferred, the total length of material flows for individual products are shorter.

| | 11 | 12 | 13 | 14 | 15 | 16 | 17 | 18 |
|----|----|----|-----------|-------------|-------------|------------|------------|----|
| 11 | | | | | | | | |
| 12 | | | | INDEX GU600 | INDEX GU600 | | | |
| 13 | | | SV 18RA | SUI 50/1000 | SUI 50/1000 | PF 150 | | |
| 14 | | | Ergonomic | TNC 20N | TNC 20N | TNC 20N | PF 150 | |
| 15 | | | GBL 25 | TNC 20N | TNC 20N | TNC 20N | PF 150 | |
| 16 | | | GBL 25 | GBL 25tyc | BUA 28/630 | BUA 28/630 | Inspection | |
| 17 | | | GAC | | | | | |

Fig. 3. Ideal layout of workplaces

The algorithm is divided into three phases:

1. Initialization procedure: basic input data for the algorithm is information about material flow between different workplaces (checked table). The table is transformed into a triangular shape by summing up the intensity of transport between workplaces, regardless of the transport direction. Basing on the checked table, a ranking of all pairs of workplaces is prepared (pairs from highest to lowest intensity). Furthermore, the selected pair of workplaces with the highest intensity will be placed side by side in the middle square grid.
2. The workplace selection procedure: the next workplace, which will be placed on the layout, is next in the ranking of pairs of workplaces and one of them was placed on the layout in previous steps. When several pairs of workplaces have the same intensity, we should take into account an additional decision criterion, for example total volume transport through the workplace.
3. The workplace placements procedure: to identify the best position on the layout, the so-called weight position is used, which is given as the sum of the products of the intensities of traffic between new workplaces and the other workplaces, which are placed in the layout and contiguity coefficient, which is determined as follows:
 - if the considered location of a new workplace has a common border with the placed workplace, the coefficient $K_p = 1$
 - if the considered location of a new workplace has a common point with the placed workplace, the coefficient $K_p = 0.5$
 - if the considered location of a new workplace has no common border or point, the coefficient $K_p = 0$

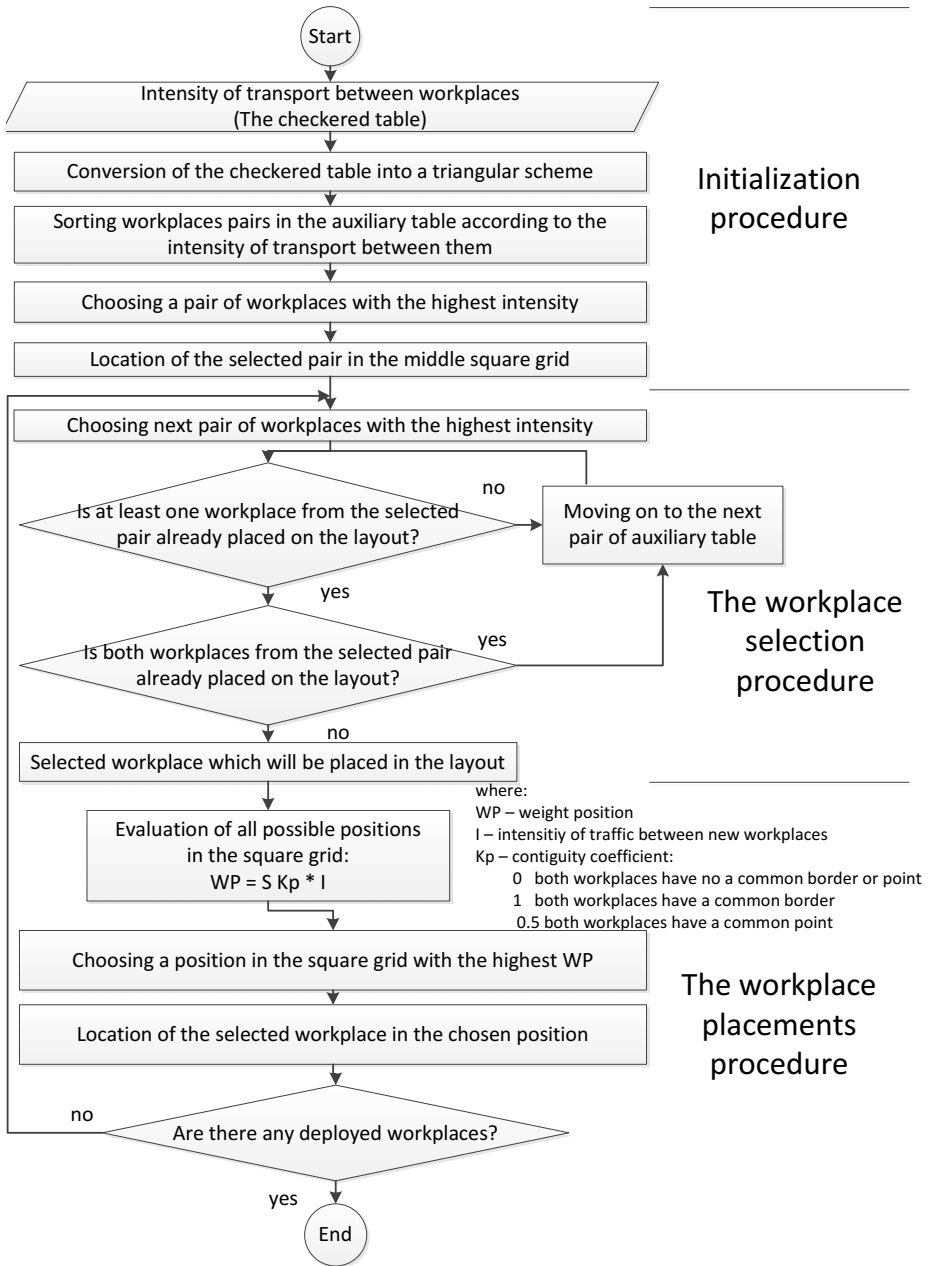


Fig. 4. The algorithm of the ideal layout creation

4 Creation of a Real Production System and Its Evaluation in Virtual Reality Environment

The next stage of the proposal is realized for example with VisTable software, which allows for interactive design of 2D/3D layouts of production systems and also provides basic tools for analysis and optimization of material flows [8, 11].

Real layout design in the VisTable environment implementation requires the following steps:

1. Preparation of 2D/3D objects – can be performed as follows:
 - (a) Usage of libraries of 2D/3D objects from the VisTable software. Current objects of the library can be further complemented and expanded to new categories as well as new objects.
 - (b) Acquiring new 3D models using reverse engineering methods, DMU (Digital Mock Up) and FMU (Mock Up Factory) models. Creating new 3D models of factory buildings can be aided by 3D laser scanning technology.
 - (c) Creating new models using CAD applications (AutoCAD, Microstation, CATIA, etc.). Compared with the application of 3D scanning method, this method is more labour-intensive to obtain new objects.
2. Modelling of the production system – this phase comprises:
 - (a) Saving objects from the library on the projection surface.
 - (b) Defining transport relations between objects.
 - (c) Designing transport lanes and transport networks.
3. Layout optimization – VisTable software allows for optimization of the proposed layout and has some basic analytical tools:
 - (a) Sankey diagram,
 - (b) I - D diagram (Intensity – Distance diagram),
 - (c) calculation of the overall transport performance,
 - (d) triangular method,
 - (e) safety work analysis.
4. Visualization of the production system – 2D or 3D layout of the production system, which may be presented as classic visualization by computer monitor, using a projection table, or using virtual technology and augmented reality.

The transformation of the ideal layout from the previous step occurs by performing the following activities:

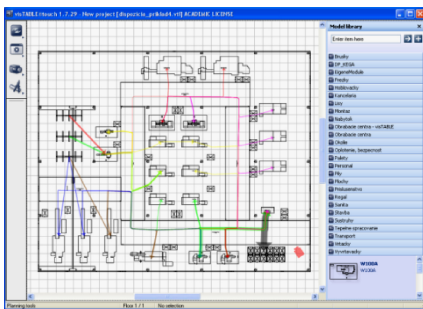
- replacement of dimensionless workplaces by objects with real shapes and dimensions of machines/workplaces,
- tethering the required number and particular types of machines/workplaces according to the results of capacity calculations.

Earlier deployment mock-ups of machines and workplaces respond to the ideal arrangement, which was the result of the procedure realized in the previous step. This initial deployment is supplemented by transport links between machines visualized by means of the Sankey diagram (Fig. 5a).

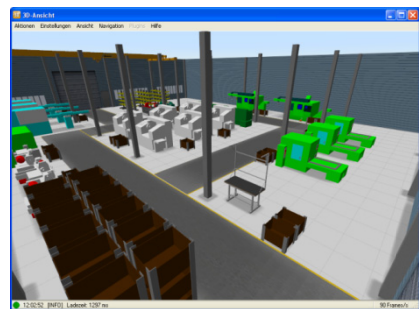
The initial deployment is further modified taking into account:

- service areas of workplaces,
- material flow in the production hall and between halls (input, output, location of storage buffers),
- needs of transportation and material handling (handling units in production, transport network, etc.),
- building structures (columns, walls) and permanent fittings (electricity, industrial gas stations, etc.).

The result is a realistic layout of workplaces, which respects all the existing constraints in production presented in 2D or 3D view (Fig. 5).



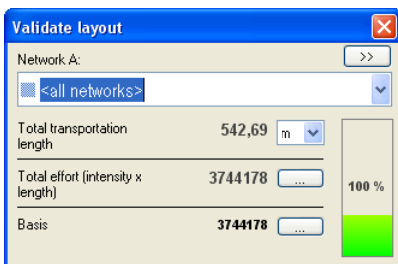
a) 2D layout



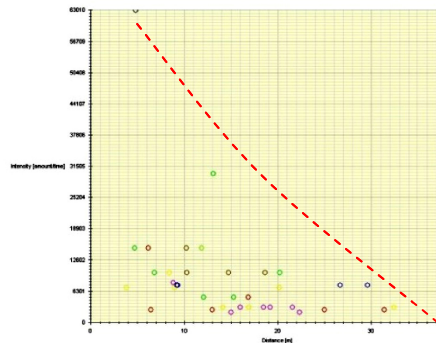
b) 3D model

Fig. 5. The real layout of workplaces

The VisTable software also allows for evaluation and optimization of the designed production systems. The basic tools include the Sankey diagram, calculation of the length of material flows and the overall transport performance (Fig. 6a), and the "distance – intensity" diagram (DI diagram, Fig. 6b).



a) The length of transport and traffic performance



b) Diagram "distance – intensity"

Fig. 6. Evaluation of Production Layout

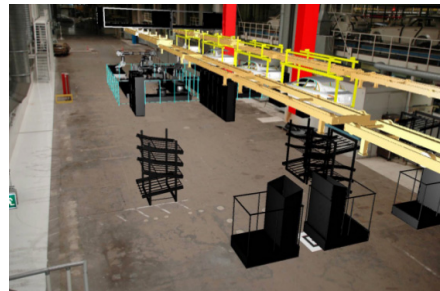
5 Layout Visualization with Augmented Reality

In our departments at universities in Bielsko-Biala and Zilina, the concept of Digital Factory is currently being developed with progressive approaches to visualization of digital information [3, 9, 12]. It seems appropriate to apply augmented reality AR technologies for design and visualization of production systems [2].

The basis of augmented reality is the ability to combine different elements of the real and virtual worlds into a single view [1]. Augmented reality is a technology, which is supported by human visual perception. Appropriate combination of real and virtual objects makes it possible to provide a large amount of additional information, but there has to be direct contact with the user's real environment. Unlike virtual reality, where all modelled objects are created by computer, augmented reality does not replace the real world, but it only adds the selected virtual elements. The view can be realized by camera and monitor using the HMD (Head Mounted Display) equipment placed on the head.



Virtual reality – computer-modelled environment



Augmented Reality – a combination of the real environment and virtual objects

Fig. 7. The difference between the virtual and augmented reality

Research on the use of AR in designing manufacturing and logistics systems is currently focused on the application of augmented reality systems based on real scene and identification tags (markers) in the camera recorded scenes, which define user position and orientation [5, 10].

5.1 The Application of Augmented Reality with the Planning Table

This example is concerned with the concept of interactive projection system created at the University in Zilina, which is based on the projection on the planning table. The current version of this system uses 3D visualization layout of the production system presented on a monitor screen or a wall using a data projector. It is a projection of the 3D model to 2D view.

By using augmented reality in designing with the planning table, there is an extended visualization in which 3D models are placed directly on the planning table. 3D models emerge from the layout and, thanks to this, a designer has a perfect view of the designed production system (Fig. 8). Using the aforementioned imaging, it is not necessary to use additional data projector displaying the projected production system.

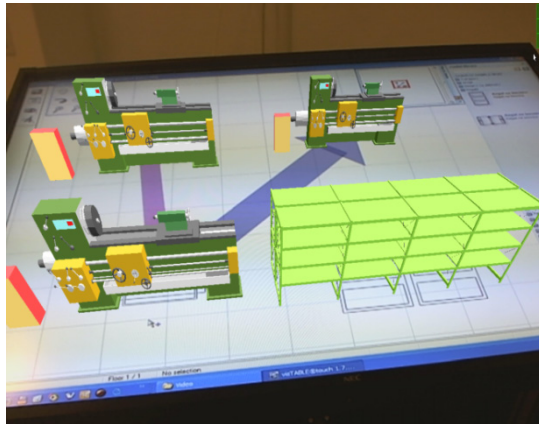


Fig. 8. Layout visualization using augmented reality technology on the projection planning table

This system uses labels (markers) to identify the position and type of the 3D object, which are displayed above them, and also to determine the position and orientation of the user's viewpoint (camera) in the observed scene (the projection area of the table).

5.2 The Usage of AR in Visualization of Production Systems in Real Environment

The designed production system, which is created using, for example, the planning table can be placed by means of augmented reality in the real environment of the production hall. Locating virtual objects in a real environment allows for identification and evaluation of the impact of additional boundary conditions, which may affect the final position of particular workplaces in production halls and which were not visible enough in previous design phases, such as possible collision with the building blocks of the hall, the location of power devices, machinery and equipment for power distribution, interconnection of production machinery and equipment with the current transportation and handling system, potential problems with installing new machinery and equipment, etc.

The main problem which needs be solved in relation with the application of AR is establishing sufficient mobility for the system in augmented reality.

6 Conclusions

The contribution shows a possibility of linking traditional approaches and methods of production design (preparation and analysis of input data, the use of optimization algorithms) with new technologies of digital data processing (the VisTable software, augmented reality technology) and methodology for designing and visualizing production systems.

Possibilities for application of advanced digital technologies constitute the subject of research within the frame of „digital factory“ concept.

References

1. Azuma, R.T.: A Survey of Augmented Reality. *Teleoperators and Virtual Environments* 6, 355–385 (1997)
2. Bajana, J.: Innovative presentation of information using augmented reality. In: *Advanced Industrial Engineering*, pp. 155-170, FCNT, Bielsko-Biala (2013)
3. Bohušová, B., Hnát, J., Gregor, M.: DELMIA – Tool of Digital factory. In: *TRANSCOM 2007 – 7-th European Conference of Young Research and Science Workers, EDIS-ŽU, Žilina* (2007)
4. Furmann, R., Krajčovič, M.: Interactive 3D Design of Production Systems. In: *Digital Factory 2009 – Workshop Handbook, SLCP, Žilina* (2009)
5. Gabajova, G.: Picking process using augmented reality. In: *Advanced Industrial Engineering, FCNT, Bielsko-Biala*, pp. 41–66 (2013)
6. Gregor, M., et al.: Virtual reality technology as a support for competitiveness and productivity improvement. Research project, No.: APVT-20-026304, University of Zilina (2004)
7. Gregor, M., Medvecký, Š., Mičieta, B., Matuszek, J., Hřečková, A.: *Digital Factory. KRUPA print, Žilina* (2007)
8. Gregor, M., Plinta, D., Furman, R., Štefánik, S.: Digital factory – 3d laser scanning, modelling and simulation of production processes. In: *Metody i techniki zarządzania w inżynierii produkcji, Bielsko-Biała* (2011)
9. Haas, W.: *AK-Digitale Fabrik. Bericht Roadmap. Audi, Ingolstadt* (2004)
10. Mirandová, G., Gabaj, I.: Use of augmented reality in storing and picking components from warehouse. In: *Metody i techniki zarządzania w inżynierii produkcji, Bielsko-Biała* (2011)
11. Štefánik, A., Furmann, R.: Computer simulation – aided designing of production and logistics systems (in Slovak). *AI magazine – Journal About the Automotive Industry, Mechanical Engineering and Economics* 4(2), 46–47 (2011)
12. Westkaemper, E., Bischoff, J., Von Biel, R., Duerr, M.: *Factory Digitalizing – An adapted approach to a digital factory planning in existing factories and buildings. Werkstattstechnik*, 91 (2001)

Monitoring and Prediction of Time Series Based on Fuzzy Cognitive Maps with Multi-step Gradient Methods

Katarzyna Poczęta and Alexander Yastrebov

Kielce University of Technology,
al. Tysiąclecia Państwa Polskiego 7, 25-314 Kielce, Poland
{k.piotrowska,a.jastriebow}@tu.kielce.pl
<http://kzi.tu.kielce.pl>

Abstract. Fuzzy cognitive map FCM is a useful tool for modeling systems for time series monitoring and prediction in various fields. This paper is devoted to the analysis of the application of FCM with multi-step learning algorithms based on gradient method and Markov model of gradient for multivariate time series monitoring and prediction. Real data from a monitor system mounted in a domotic house were used in learning and testing process. The comparative analysis of two-step method of Markov model of gradient, multi-step gradient method and one-step gradient method from the point of view of the obtained prediction error was performed.

Keywords: fuzzy cognitive map, multi-steps algorithms, gradient method, Markov model of gradient, monitor system, time series prediction.

1 Introduction

Fuzzy cognitive map FCM [7] is a universal tool for modeling complex decision support systems for classification [5], prediction [6,16,10] or control process [20]. FCM can be used for time series monitoring and prediction in various fields, e.g. water demand [1], stock [2,8,18], enrollment [8,18] and etc. Researchers have presented diverse approaches of time series prediction based on fuzzy cognitive maps. In [8] fuzzy c-means clustering was used to develop fuzzy information granules from historical data, convert original time series into granular time series and establish the structure of prediction model. A novel time series modeling based on fuzzy information granules to construct fuzzy granular model of time series which can realize prediction at the granular level is proposed in [9]. In [4] authors model and forecast time series with the use of fuzzy cognitive maps and moving window approach. Implementation of FCM based on neural network is presented in [3,17].

This paper presents a new approach of multivariate time series monitoring and prediction based on fuzzy cognitive map with multi-step supervised learning algorithms. Multi-step gradient method [21] and Markov model of gradient [14,22]

were used to develop a model with the use of real data from a monitor system mounted in a domotic house [23]. The aim of the analysis is the current state monitoring and the next state prediction. The comparative analysis of two-step method of Markov model of gradient, multi-step gradient method and one-step gradient method from the point of view of the obtained prediction error was performed. Simulations were done with the use of ISEMK (Intelligent Expert System based on Cognitive Maps) software tool.

The paper is structured as follows. Section 2 describes fuzzy cognitive maps. Section 3 presents the multi-step supervised learning algorithms for FCMs based on gradient method and Markov model of gradient. Section 4 describes the basic features of ISEMK software tool. Section 5 presents selected results of simulation analysis of monitoring and prediction of time series. Section 6 contains a summary of the paper.

2 Fuzzy Cognitive Maps

The structure of FCM is based on a directed graph:

$$\langle X, R \rangle, \quad (1)$$

where $X = [X_1, \dots, X_n]^T$ is the set of the concepts; $X_i(t)$ is the value of the i -th concept form the interval $[0, 1]$, $i = 1, 2, \dots, n$, n is the number of concepts; $R = \{r_{j,i}\}$ is relations matrix, $r_{j,i}$ is the relation weight between the j -th concept and the i -th concept, value from the interval $[-1, 1]$. With increasing of imprecision of the input data fuzzy relations [15,16] or grey numbers [13] can be applied.

In this paper a nonlinear dynamic model described by the equation (2) was used [12].

$$X_i(t+1) = F \left(X_i(t) + \sum_{j \neq i} r_{j,i} \cdot X_j(t) \right), \quad (2)$$

where t is discrete time, $t = 0, 1, 2, \dots, T$, T is end time of simulation; $F(x)$ is stabilizing function, which can be chosen in the form:

$$F(x) = \frac{1}{1 + e^{-cx}}, \quad (3)$$

where $c > 0$ is a parameter.

FCMs have the ability to learn the relations matrix R with the use of unsupervised [6,20], supervised [21] or evolutionary [10,19] algorithms. The idea of multi-step supervised learning algorithms for fuzzy cognitive maps is presented below.

3 Multi-step Learning Algorithms

The characteristic feature of the multi-step learning algorithms for FCMs is the estimation of a current value of the relations matrix elements on the basis of a few previous estimations. Simulation analysis of multi-step learning algorithms for fuzzy cognitive maps was made with the use of the gradient method [21] and the Markov model of gradient [22].

3.1 Gradient Method

Multi-step supervised learning based on gradient method is described by the equation [21]:

$$r_{j,i}(t+1) = P_{[-1,1]} \left(\sum_{k=0}^{m_1} \alpha_k \cdot r_{j,i}(t-k) + \sum_{l=0}^{m_2} (\beta_l \cdot \eta_l(t) \cdot (Z_i(t-l) - X_i(t-l)) \cdot h_{j,i}(t-l)) \right), \quad (4)$$

where $\alpha_k, \beta_l, \eta_l$ are learning parameters, which are determined using experimental trial and error method, $k = 1, \dots, m_1; l = 1, \dots, m_2$, m_1, m_2 are the number of the steps of the method; t is a time of learning, $t = 0, 1, \dots, T$, T is end time of learning; $h_{j,i}(t)$ is a sensitivity function; $X_i(t)$ is the value of the i -th concept (predicted value), $Z_i(t)$ is the reference value of the i -th concept (monitored value); $P_{[-1,1]}(x)$ is an operator of design for the set $[-1,1]$, in the paper hyperbolic tangent was used.

Sensitivity function $y_{j,i}(t)$ is described as follows:

$$h_{j,i}(t+1) = (h_{j,i}(t) + X_j(t)) \cdot F'(X_i(t) + \sum_{j \neq i} r_{j,i} \cdot X_j(t)), \quad (5)$$

where $F'(x)$ is derivative of the stabilizing function.

Learning parameters $\alpha_k, \beta_l, \eta_l$ have to satisfy the conditions (6)–(10) to reach the convergence of the multi-step gradient method [21].

$$\sum_{k=0}^{m_1} \alpha_k = 1, \quad (6)$$

$$0 < \eta_l(t) < 1, \quad (7)$$

$$\eta_l(t) = \frac{1}{\lambda_l + t}, \quad (8)$$

$$\lambda_l > 0, \quad (9)$$

$$\beta_l \geq 0. \quad (10)$$

A special case of multi-step gradient method is the one-step algorithm, which modifies the relations matrix according to the formula:

$$r_{j,i}(t+1) = P_{[-1,1]}(r_{j,i}(t) + \beta_0 \cdot \eta_0(t) \cdot (Z_i(t) - X_i(t)) \cdot h_{j,i}(t)). \quad (11)$$

3.2 Markov Model of Gradient

Another example of multi-step algorithms is the two-step method based on Markov model of gradient [14]. Modification of the relation weight is described by the formula [22]:

$$r_{j,i}(t+1) = P_{[-1,1]}(r_{j,i}(t) - y_{j,i}(t)), \quad (12)$$

where: $y_{j,i}$ is the Markov model of gradient, described as follows:

$$y_{j,i}(t+1) = a \cdot y_{j,i}(t) - \beta_0 \cdot \eta_0(t) \cdot (Z_i(t) - X_i(t)) \cdot h_{j,i}(t) . \quad (13)$$

where a is a learning parameter, $a \in (0, 1)$.

Termination criterion for the presented methods can be expressed by the formula:

$$J(t) = \frac{1}{n} \sum_{i=1}^n (Z_i(t) - X_i(t))^2 < e , \quad (14)$$

where $J(t)$ is a learning error function; e is a level of error tolerance.

4 ISEMK System

ISEMK is a computer software, which is a universal tool for modeling phenomena based on FCM [11]. ISEMK realizes [11]:

- the implementation of fuzzy cognitive map based on expert knowledge and historical data;
- reading and writing of FCM parameters with the use of .xml files;
- supervised learning based on multi-step algorithms and real data;
- unsupervised learning based on Hebbian algorithms;
- the analysis of learned FCMs by determining the accuracy of prediction based on testing data;
- exporting data of learning and FCM analysis to .csv files;
- proper visualizations of done research.

Figure 1 shows an exemplary visualization of the results of learning based on multi-step gradient method and real data.

5 Simulation Results

The analysis of the application of FCM with multi-step learning algorithms based on Markov model of gradient and gradient method for time series monitoring and prediction was performed. FCM was initialized, learned and tested on the basis of real data taken from the UCI Machine Learning Repository. The dataset is collected from a monitor system mounted in a domotic house. The data was sampled every minute, computing and uploading it smoothed with 15 minute means [23]. The data from 7 days were used in learning process and the data from the next 2 days were used in testing process.

The aim of the analysis is the prediction of future values of the system based on currently monitored values. This approach could be a support for the management of all located in the domotic house installations and could increase the functionality, comfort and safety of use of the building.

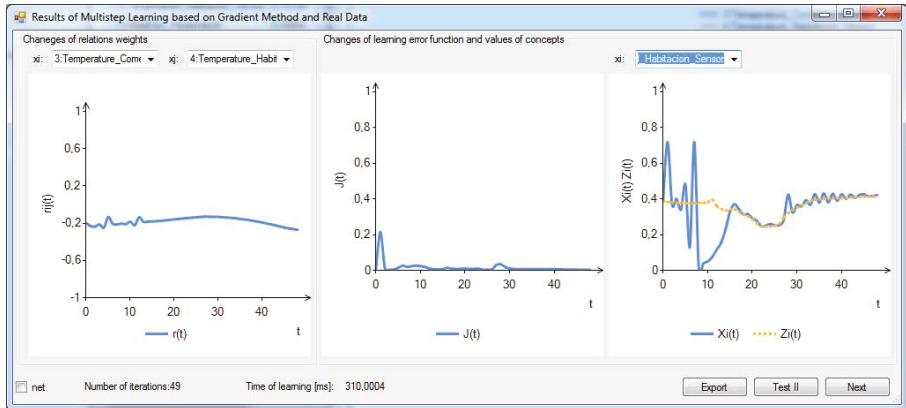


Fig. 1. Sample results of FCM learning

The map with the following concepts was analyzed [23]:

- X_1 – indoor temperature (dinning-room);
- X_2 – indoor temperature (room);
- X_3 – weather forecast temperature;
- X_4 – carbon dioxide (dinning room);
- X_5 – carbon dioxide (room);
- X_6 – relative humidity (dinning room);
- X_7 – relative humidity (room);
- X_8 – lighting (dinning room);
- X_9 – lighting (room);
- X_{10} – rain, the proportion of the last 15 minutes where rain was detected;
- X_{11} – sun dusk;
- X_{12} – wind;
- X_{13} – sun light in west facade;
- X_{14} – sun light in east facade;
- X_{15} – sun light in south facade;
- X_{16} – sun irradiance;
- X_{17} – enthalpic motor 1, 0 or 1 (on-off);
- X_{18} – enthalpic motor 2, 0 or 1 (on-off);
- X_{19} – enthalpic motor turbo, 0 or 1 (on-off);
- X_{20} – outdoor temperature;
- X_{21} – outdoor relative humidity;
- X_{22} – day of the week, 1=Monday, 7=Sunday.

The relations matrix was initialized with random values from the interval $[-0.2, 0.2]$. The structure of the initialized map is presented in Fig. 2.

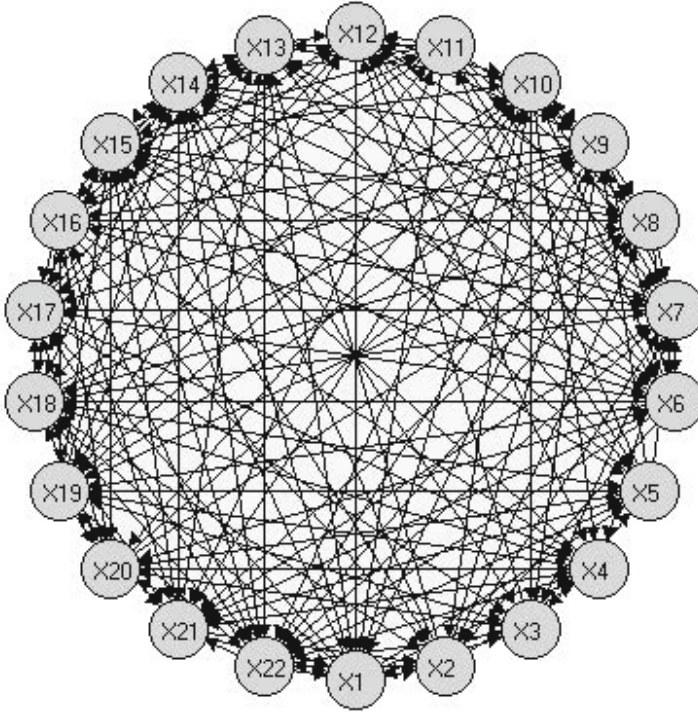


Fig. 2. Structure of the initialized map

One-step, multi-step gradient method and Markov model of gradient were used to learn the initialized fuzzy cognitive map. The learning process was carried out for various parameters in order to minimize the prediction error described by the formula:

$$J_P = \frac{1}{n_t - 1} \sum_{t=1}^{n_t} \left(\frac{1}{n} \sum_{i=1}^n (Z_i(t) - X_i(t))^2 \right) \cdot 100\%, \quad (15)$$

where t is a time of testing, $t = 1, \dots, n_t$, n_t is the number of the testing records; $X_i(t)$ is the predicted value of the i -th concept; $Z_i(t)$ is the reference (monitored) value of the i -th concept, $i = 1, 2, \dots, n$, n is the number of concepts.

Figure 3 shows the exemplary results of learning. Obtained results corroborate convergence of the presented methods of FCM learning. Figure 4 presents selected results of testing.

Table 1 presents the results of the comparative analysis of one-step gradient method, multi-step gradient method and Markov model of gradient.

The application of fuzzy cognitive map with multi-step gradient method, one-step gradient method or Markov model of gradient allows to obtain the model that correctly performs the task of predicting of the next values based on the currently monitored values of the monitor system in the domotic house. The

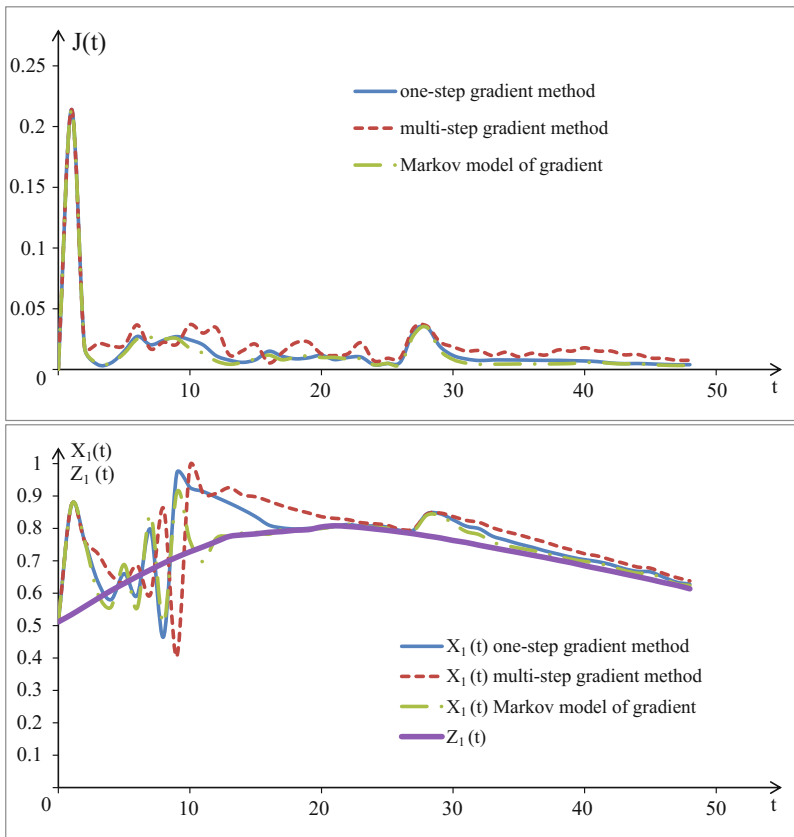


Fig. 3. Selected results of learning, obtained values of $J(t)$ and $X_1(t)$

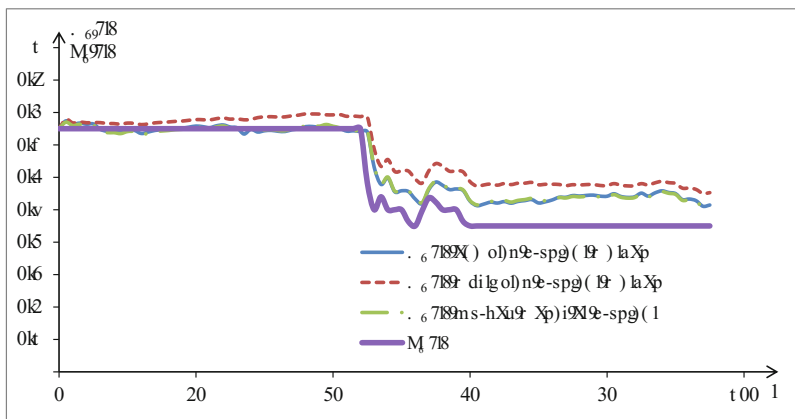


Fig. 4. Selected results of testing, obtained values of $X_3(t)$

Table 1. Chosen results of the analysis of the multi-step supervised learning for: $e = 0.00001$, $c = 3$

| Method type | $\alpha_k, k = 0, 1, 2$ | $\beta_l, l = 0, 1, 2$ | $\lambda_0 = \lambda_1 = \lambda_2$ | J_P [%] |
|----------------------------|-------------------------|------------------------|-------------------------------------|---------------|
| one-step gradient method | 1 | 50 | 100 | 3.0563 |
| multi-step gradient method | 0.7 0.3 0 | 50 0 0 | 100 | 2.799 |
| multi-step gradient method | 0.5 0.3 0.2 | 50 0 0 | 100 | 2.61 |
| multi-step gradient method | 1 0 0 | 30 20 0 | 100 | 3.179 |
| multi-step gradient method | 1 0 0 | 20 20 10 | 100 | 3.2356 |
| Markov model $a = 0.2$ | – | 50 | 100 | 3.2494 |
| Markov model $a = 0.5$ | – | 50 | 100 | 3.6687 |
| one-step gradient method | 1 | 30 | 100 | 2.8837 |
| multi-step gradient method | 0.7 0.3 0 | 30 0 0 | 100 | 2.5359 |
| multi-step gradient method | 0.5 0.3 0.2 | 30 0 0 | 100 | 2.1937 |
| multi-step gradient method | 1 0 0 | 20 10 0 | 100 | 2.8947 |
| Markov model $a = 0.2$ | – | 30 | 100 | 3.0038 |
| Markov model $a = 0.5$ | – | 30 | 100 | 3.3348 |
| one-step gradient method | 1 | 10 | 10 | 2.675 |
| multi-step gradient method | 0.7 0.3 0 | 10 0 0 | 10 | 2.3643 |
| multi-step gradient method | 0.5 0.3 0.2 | 10 0 0 | 10 | 2.0327 |
| multi-step gradient method | 1 0 0 | 7 3 0 | 10 | 2.6723 |
| multi-step gradient method | 0.5 0.3 0.2 | 5 3 2 | 10 | 2.124 |
| Markov model $a = 0.2$ | – | 10 | 10 | 2.811 |
| Markov model $a = 0.5$ | – | 10 | 10 | 3.141 |

minimum of prediction error function $J_P = 2.0327\%$ was obtained for the multi-step gradient method for the following parameters: $\alpha_0 = 0.5$, $\alpha_1 = 0.3$, $\alpha_2 = 0.2$, $\beta_0 = 10$, $\lambda_0 = 10$.

6 Conclusions

This paper presents the proposed method of multivariate time series monitoring and prediction based on fuzzy cognitive map with multi-step supervised learning algorithms. FCM, multi-step gradient method and Markov model of gradient were described. The comparative analysis of two-step method of Markov model of gradient, multi-step gradient method and one-step gradient method from the point of view of the obtained prediction error was performed with the use of real data from a monitor system mounted in a domestic house. It could be stated that the application of fuzzy cognitive map with multi-step supervised learning algorithms based on gradient method and Markov model of gradient allows to predict the next values based on the currently monitored values of the system with a satisfactory degree of accuracy.

References

1. Ahmadi, S., Alizadeh, S., Forouzideh, N., Yeh, C., Martin, R., Papageorgiou, E.I.: ICLA Imperialist Competitive Learning Algorithm for Fuzzy Cognitive Maps to Water Demand Forecasting. In: 2014 IEEE International Conference on Fuzzy Systems (FUZZ-IEEE), Beijing, China, July 6–11, pp. 1041–1048 (2014)
2. Froelich, W., Wakulicz-Deja, A.: Learning Fuzzy Cognitive Maps from the Web for Stock Market Decision Support System. In: Węgrzyn-Wolska, K.M., Szczepaniak, P.S. (eds.) *Adv. in Intel. Web, ASC*, vol. 43, pp. 106–111. Springer, Heidelberg (2007)
3. Hengjie, S., Chunyan, M., Roel, W., Zhigi, S., Catthoor, F.: Implementation of Fuzzy Cognitive Maps based on Fuzzy Neural Network and Application in Numerical Prediction of Time Series. *IEEE Trans. Fuzzy Systems* 18, 233–250 (2010)
4. Homenda, W., Jastrzębska, A., Pedrycz, W.: Modeling Time Series with Fuzzy Cognitive Maps. In: IEEE International Conference on Fuzzy Systems (FUZZ-IEEE), Beijing, China, July 6–11, pp. 2055–2062 (2014)
5. Kannappan, A., Papageorgiou, E.I.: A new classification scheme using artificial immune systems learning for fuzzy cognitive mapping. In: IEEE International Conference on Fuzzy Systems (FUZZ), pp. 1–8 (2013)
6. Kannappan, A., Tamilarasi, A., Papageorgiou, E.I.: Analyzing the performance of fuzzy cognitive maps with non-linear hebbian learning algorithm in predicting autistic disorder. *Expert Systems with Applications* 38, 1282–1292 (2011)
7. Kosko, B.: Fuzzy cognitive maps. *Int. J. Man-Machine Studies* 24, 65–75 (1986)
8. Lu, W., Yang, J., Liu, X., Pedrycz, W.: The modeling and prediction of time series based on synergy of high-order fuzzy cognitive map and fuzzy c-means clustering. *Knowledge-Based Systems* 70, 242–255 (2014)
9. Lu, W., Pedrycz, W., Liu, X., Yang, J., Li, P.: The modeling of time series based on fuzzy information granules. *Expert Systems with Applications* 41, 3799–3808 (2014)
10. Papageorgiou, E.I., Froelich, W.: Multi-step prediction of pulmonary infection with the use of evolutionary fuzzy cognitive maps. *Neurocomputing* 92, 28–35 (2012)
11. Piotrowska, K., Poczęta, K.: Intelligent expert system based on cognitive maps. *Studia Informatica* 332A(105), 605–616 (2012) (in Polish)
12. Roberts, F.S.: Discrete models with applications in the social, biological and ecological problems. Science, Moscow (1986) (in Russian)
13. Salmeron, J.L.: Modelling grey uncertainty with Fuzzy Cognitive Maps. *Expert Systems with Applications* 37, 7581–7588 (2010)
14. Shilman, S.V., Yastrebov, A.I.: Convergence analysis of some class of multi-step stochastic optimization algorithms. *Automation and Telemekhanics* 8 (1976) (in Russian)
15. Słoiń, G.: The use of fuzzy numbers in the process of designing relational fuzzy cognitive maps. In: Rutkowski, L., Korytkowski, M., Scherer, R., Tadeusiewicz, R., Zadeh, L.A., Zurada, J.M. (eds.) *ICAISC 2013, Part I. LNCS*, vol. 7894, pp. 376–387. Springer, Heidelberg (2013)
16. Słoiń, G.: Application of Models of Relational Fuzzy Cognitive Maps for Prediction of Work of Complex Systems. In: Rutkowski, L., Korytkowski, M., Scherer, R., Tadeusiewicz, R., Zadeh, L.A., Zurada, J.M. (eds.) *ICAISC 2014, Part I. LNCS*, vol. 8467, pp. 307–318. Springer, Heidelberg (2014)
17. Song, H.J., Miao, C.Y., Shen, Z.Q., Roel, W., Maja, D.H., Francky, C.: Design of fuzzy cognitive maps using neural networks for predicting chaotic time series. *Neural Networks* 23, 1264–1275 (2010)

18. Stach, W., Kurgan, L., Pedrycz, W.: Numerical and Linguistic Prediction of Time Series With the Use of Fuzzy Cognitive Maps. *IEEE Transactions on Fuzzy Systems* 16, Issue 1, 61–72 (2008)
19. Stach, W., Kurgan, L., Pedrycz, W., Reformat, M.: Genetic learning of fuzzy cognitive maps. *Fuzzy Sets and Systems* 153(3), 371–401 (2005)
20. Stylios, C.D., Papageorgiou, E.I.: Fuzzy Cognitive Maps. In: Pedrycz, W., Skowron, A., Kreinovich, V. (eds.) *Handbook of Granular Computing*, pp. 755–774. John Wiley & Son Ltd, Publication Atrium (2008)
21. Yastrebov, A., Piotrowska, K. (Poczęta, K.): Simulation Analysis of Multistep Algorithms of Relational Cognitive Maps Learning. In: Yastrebov, A., Kuźmińska-Sołśnia, B., Raczyńska, M. (eds.) *Computer Technologies in Science, Technology and Education. Institute for Sustainable Technologies - National Research Institute*, pp. 126–137. Radom (2012)
22. Yastrebov, A., Poczęta, K.: Application of fuzzy cognitive map with two-step learning algorithm based on Markov model of gradient for time series prediction. *Logistyka* 6/2014, – in Polish (2014)
23. Zamora-Martinez, F., Romeu-Guallart, P., Pardo, J.: UCI Machine Learning Repository. Universidad CEU Cardenal Herrera (2014), <http://archive.ics.uci.edu/ml>

Multichannel High Voltage Amplifier for Piezo Actuators

Roman Regulski, Amadeusz Nowak, Bartosz Minorowicz, and Frederik Stefański

Institute of Mechanical Technology, Poznan University of Technology
ul. Piotrowo 3, 60-965 Poznań, Poland
{roman.regulski, amadeusz.nowak}@doctorate.put.poznan.pl,
{bartosz.minorowicz, frederik.stefanski}@gmail.com

Abstract. This paper describes investigations of a low cost high voltage amplifier, which was based on specialized operational amplifiers. The purpose of the amplifier is to control piezoelectric actuators with many electrodes, such as bimorph benders, piezoelectric tubes, ring and disc benders. Proposed amplifier has two independent channels which can be configured for the specific research aim. Every channel of the device can works in inverted or non inverted mode. Also the voltage gain and current limit can be set separately.

Keywords: high voltage amplifier, piezoelectric actuator, bimorph bender, piezo tube, multichannel amplifier.

1 Introduction

Nowadays piezoelectric actuators are widely used in many applications. Their advantages lead to finding novel approach of their usage [1, 2]. Drawback which limits the application of piezo transducers are requirements for their power supply. Due to the fact that piezo materials require high voltages to control, it is necessary to search for new solutions of high voltage amplifiers. In recent years there have been research on various issues related to the design and improvement of properties of such devices. We can find examples of different high-voltage amplifiers in [3–7]. Some solutions are equipped with a microcontroller devices and can be digitally controlled. Also the high-voltage operational amplifiers are used [8, 9]. Commercially available high voltage piezoelectric amplifiers are usually one channel solution, are expensive and have fixed limitations.

The main goal of the research was to obtain the performance of designed high voltage amplifier and show the way to build cheap multichannel high voltage amplifier. The scope of the research includes voltage and current tests. Frequency response for driving different loads under different voltage were conducted.

2 Piezoelectric Actuators Supplying

The cited above papers doesn't describe in detail the basic problems of supply circuits from electronic point of view, which one can meet in design of high power and low

cost amplifier for piezoelectric benders. No specific research about the current, its limitation in amplifier and influences of user parameters are discussed. Therefore we decided to focus our research on amplifiers, which are cheap and available on the market and on electrical elements behaviors.

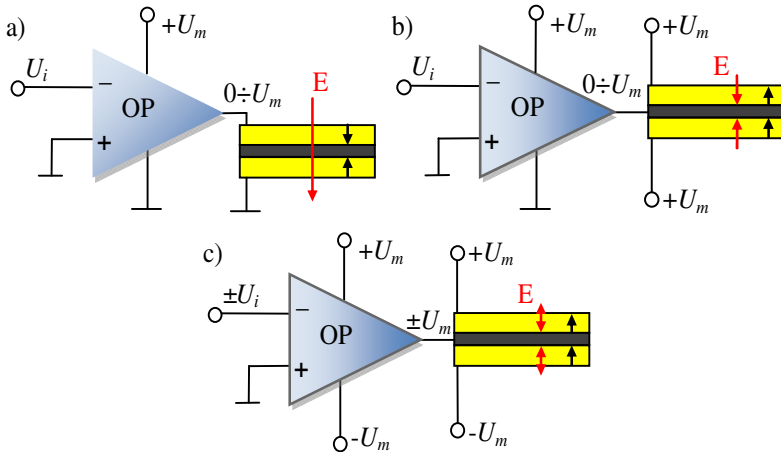


Fig. 1. Single source drive methods with operational amplifier (OP): a) series connection – unipolar, b) parallel connection with one supply voltage – bipolar, c) parallel connection with symmetrical supply voltage

There are a number of methods for supplying piezo actuators. According to the principle of inverse piezoelectric phenomena, applying an electric field to piezoelectric material, results in extraction or contraction of dimensions. In piezoelectric bimorph actuators both of these effects are utilized in common. In Fig. 1 three configurations with the use of one operational amplifier to control piezo actuator. These connections are applicable to every type of bimorph piezo such as bender or disc. We may have different combinations of the direction of polarization in PZT material, and in general two wire and three wire bimorph actuators can be found. Having regard to this, amplifier is connected electrically in parallel or series with the electrodes of the bimorph. The first (Fig. 1a), shows the concept of serial connection, where the electric field E is applied through the two electrodes and the poling direction of each piezoelectric layer is opposite. In this case the application of the electric field creates opposing strains in the two layers which results in bending. The second (Fig. 1b) concept shows the parallel configuration, in which the centre electrode is connected to the amplifier output, while a positive voltage is applied to the outer two electrodes. In this case, instead of opposite polarizations, the field orientation creates opposite strains. The series configuration requires twice the voltage to obtain the same field. The method on Fig. 1c, called ‘simultaneous drive,’ comprises of a constant high-voltage applied across the actuator and a unipolar drive stage connected to the central electrode.

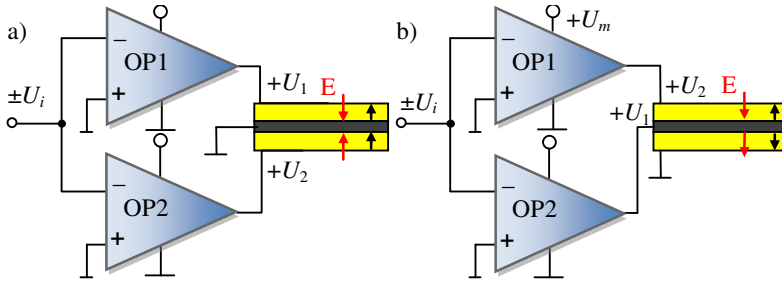


Fig. 2. Drive methods with dual source high voltage amplifier a) alternating, b) simultaneous

The dual source drive schematics are shown in Fig. 2. The method presented on Fig. 2a, called ‘alternating drive,’ comprises of two unipolar operational amplifiers connected to the outer electrodes and operated 180° out of phase, with a common ground on the central electrode. In general, every amplifier can be controlled by different input signals, giving by this way broaden possibilities. The second option shown in Fig 2b, is called “the simultaneous drive”. In this case the amplification of every amplifier is different.

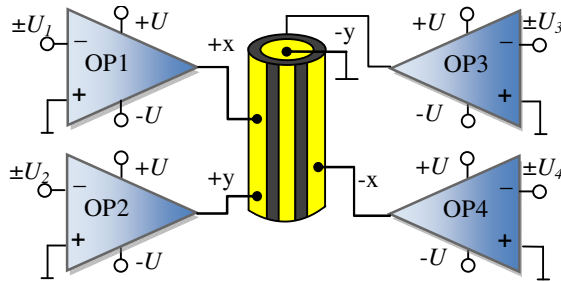


Fig. 3. Drive method options for piezoelectric actuator (tube) with independent control of each electrode

Bimorph actuators requires one or two channel high voltage amplifier. Piezo tubes or other piezo drives with more than two electrodes can be fully controlled only when each electrode has independent supply (Fig. 3). Applying control signal from different sources, complex movement of the bending element can be achieved. For example, piezoelectric tube requires four sources. Most of the commercially available amplifiers are equipped with one channel, which disqualifies them the ability to easily use with these kind of actuators.

3 High Voltage Circuit

High voltage amplifier has two independent channels based on PA91 [10]. PA91 is a specialized high voltage operational amplifier. The circuit scheme of one channel is

shown in Fig. 4. Voltage gain, as in inverting opamp, is set by R1–R4 resistors. Due to the high voltage in feedback loop and low breakdown voltage of resistors, multiple feedback resistors in series configuration were used. D1 and D2 are additional input protection clamp diodes to prevent a damage of input transistors in case of large differential input voltages. D3 and D4 are Zener diodes to protect the circuit in case of power supply overvoltage. C1 and R5 are forming external phase compensation circuit. C4 is a optional feedback capacitor to compensate phase lag due to the capacitive loading.

The output current limit can be set by resistor R9. The input voltage is in a range ± 10 V and the maximum output voltage was in a range ± 225 V. However in our investigations only ± 150 V was used. In the supplier toroidal transformer, diode rectifier, filter, electronic controller and stabilizer were used. The photo of the build by us piezo bender actuator supply unit is shown in Fig. 6d. In this device two high voltage amplifiers type PA91 and their supplier were installed. Electronic is placed in shielded vented box. Each amplifier is equipped with suitable heat sink.

On the developed amplifier, series of investigations was conducted. For the purpose of the investigations the voltage gain was set to 20 V/V, and output current limit was set to 65 mA with 10Ω output resistor according to formula from application note. These values can be manipulated to the specific application. Also a non inverting mode is a possible configuration by changing the internal connection with additional jumpers and wires. One channel of these circuit can be easily multiplied. Rear and front panel in our construction were adapted to specific laboratory needs. For the testing purposes in the front panel, the circuit for discharge the high voltage outputs was installed. The discharge circuit consist of appropriate resistor load with push button. In future development, upgrades are available.

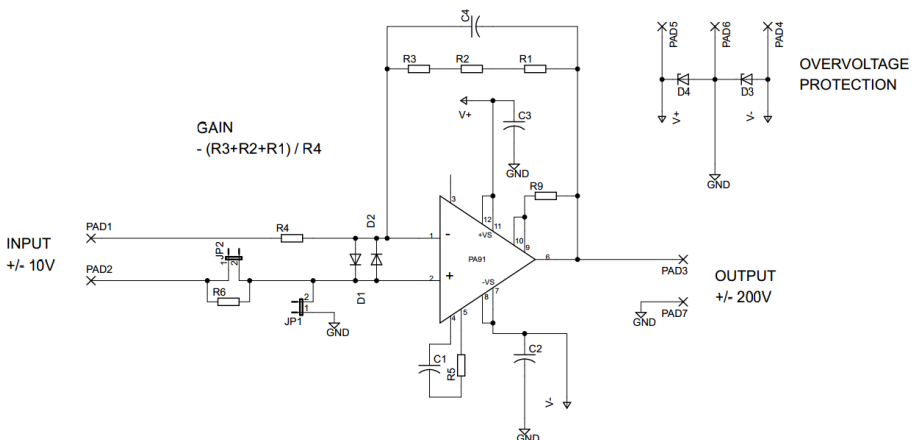


Fig. 4. Circuit scheme of one channel of high voltage amplifier

4 Performance

Electrically, the piezoelectric actuators behave as a nonlinear capacitive load. Due to this fact high voltage amplifiers for piezo must withstand this kind of load. To obtain the performance of developed amplifier measuring stand was prepared. The measuring scheme is shown in Fig. 5. It consist of an oscilloscope to measure the voltage and current signal. Current is measured via voltage drop on small value resistor and through the RMS milliamp meter. In this circuit amplifier can be loaded with two capacitors which capacitance are equivalent to piezoelectric benders. In our investigations film capacitors and PI Ceramic type PL112.11 bimorph bender were used.

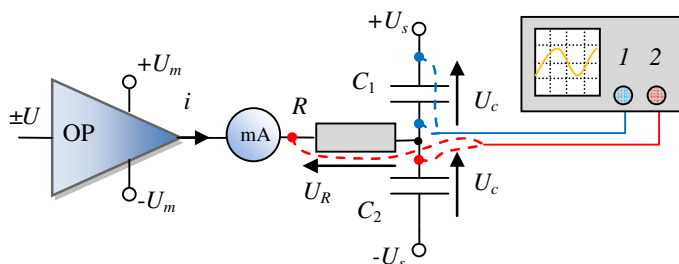


Fig. 5. Measuring scheme of PA91 amplifier with load: piezo bender type PL112.11 or capacitors $2 \times 1.1 \mu\text{F}$, $U_m = \pm 150 \text{ V}$, $U_s = \pm 30 \text{ V}$

In Fig. 6 recorded output voltage (blue) and current (red) sinusoidal signals are shown. These results were obtained when the amplifier PA91 was burdened with piezoelectric bender PL112.11. The input signal was a sine wave with fixed amplitude from generator. During the experiment frequency of the signal was slowly increased. In Fig 6a signal frequency reaches 500 Hz and there is no deformation in output wave of voltage and current. In Fig. 6b the recorded output voltage and current sinusoidal signals were in this area of operation disturbed. It is easy to note that current limit occurs. In Fig. 6c. current is strictly cut off and the sinusoidal voltage signal become triangular.

Frequency characteristics of output peak to peak voltage is shown in Fig. 7. Both axes are scaled logarithmically. These characteristics were measured for different output voltages of sinusoidal signals of amplitude equal to: 20 Vpp, 50 Vpp, 100 Vpp and 200 Vpp and different load of capacitors $C = 1 \mu\text{F}$ and $C = 100 \text{ nF}$. In this case one can notice that the operating area of amplifier depends directly on output current limitation which limits the operating bandwidth. When the current limit occurs the amplitude of output voltage is decreased. According to these characteristics, maximum load and operating frequency can be defined. It is very important, due to that different piezo actuators are capable of operating with different maximum frequencies.

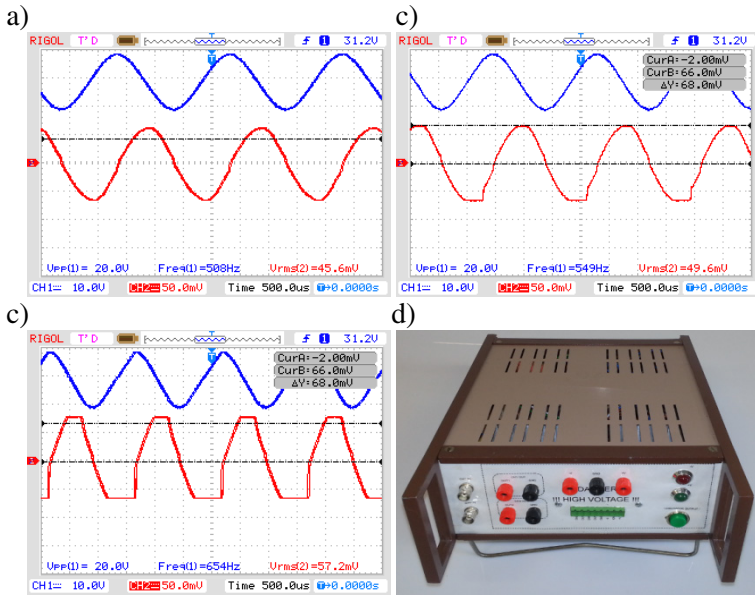


Fig. 6. PA91 oscillograms under driving PIEZO PL112.11, Output Signal: 20 Vpp Sine, $U_m = \pm 150$ V, $U = \pm 30$ V a) $f = 500$ Hz, $I_{rms} = 45$ mA, b) $f = 550$ Hz, $I_{rms} = 50$ mA, c) $f = 650$ Hz, $I_{rms} = 57$ mA, d) developed high voltage amplifier

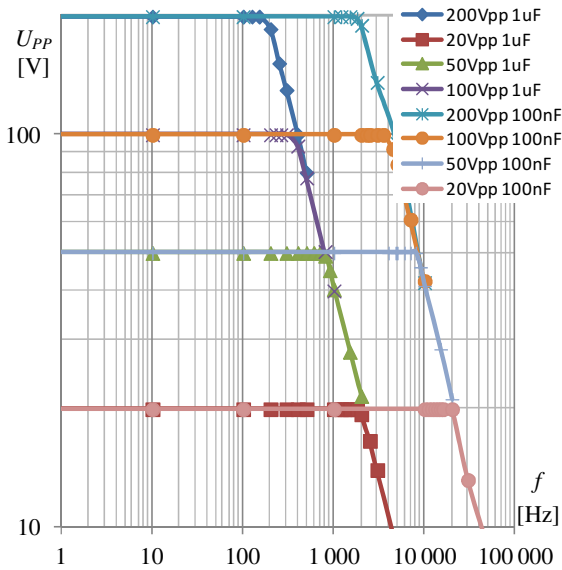


Fig. 7. Frequency response – the peak to peak output voltage under different capacitive loads

5 Conclusions

Nowadays wide accessibility to integrated circuits allows researchers, constructors to find new solutions of supplying piezoelectric actuators. In the paper, multichannel control circuit for supplying of piezo actuators based on high voltage power amplifier dedicated for piezo bender actuators is presented and described.

This circuit was used for control of piezo bender actuator. The investigation results are presented and discussed. The amplifier PA91 is devoted for supplying of piezo actuators. It is capable to operate up to voltages reaching ± 225 V. The minimum supply voltage is equal to ± 40 V. This amplifier is alternative to commercial solutions because its cost is about 100 Euro.

References

1. Sibiela, M.: Optimal controller for vibration isolation system with controlled hydraulic damper by piezoelectric stack. *Mechanical Systems and Signal Processing* 36, 118–126 (2013)
2. Mazeika, D., Vasilijev, P.: Optimal controller for vibration isolation system with controlled hydraulic damper by piezoelectric stack. *Mechanical Systems and Signal Processing* 36, 118–126 (2013)
3. Colclough, M.S.: A fast high-voltage amplifier for driving piezoelectric positioners. *Review of Scientific Instruments* 71 (2000)
4. Horn, T., Melbert, J.: A Linear 10 kV Power Amplifier for Piezo Actuators, CIPS 2010, Nuremberg, Germany (2010)
5. Fleming, A.J.: A megahertz bandwidth dual amplifier for driving piezoelectric actuators and other highly capacitive loads. *Review of Scientific Instruments* 80 (2009)
6. Wallenhauer, C., Gottlieb, B., Zeichfußl, R., Kappel, A.: Efficiency-Improved High-Voltage Analog Power Amplifier for Driving Piezoelectric Actuators. *IEEE Transactions on Circuits and Systems* 57 (2010)
7. Shyr-Long, J., Yung-Cheng, T.: A Multicell Linear Power Amplifier for Driving Piezoelectric Loads. *IEEE Transactions on Industrial Electronics* 55 (2008)
8. Koçum, C.: Digitally gain controlled linear high voltage amplifier for laboratory applications. *Review of Scientific Instruments* 82 (2011)
9. Flaxer, E.: Multichannels high voltage programmable driver for piezoelectric transducer. *Review of Scientific Instruments* 79 (2008)
10. PA91 Datasheet (Apex Microtechnology), <http://www.apexanalog.com>

Modelling of Electrohydraulic Drive with a Valve Controlled by Synchronous Motor

Dominik Rybarczyk¹, Dariusz Sędziak¹, Piotr Owczarek¹, and Adam Owczarkowski²

¹Institute of Mechanical Technology, Poznan University of Technology,
Piotrowo 3, 60-965 Poznań, Poland

²Institute of Control and Information Engineering,
Poznan University of Technology,
Piotrowo 3, 60-965 Poznań, Poland

{Dominik.Rybarczyk, Dariusz.Sedziak,
Piotr.Owczarek}@put.poznan.pl,

Adam.Owczarkowski@doctorate.put.poznan.pl

Abstract. The article describes modelling of electrohydraulic servo drive. In the drive a new type of proportional valve with a synchronous motor controlled by dedicated power electronics is used. The model of the electrohydraulic servo drive prepared in Matlab-Simulink is described. The study included the examination of the basic characteristics such as step response.

Keywords: electrohydraulic servo drive, proportional valve, synchronous motor.

1 Introduction

Electrohydraulic servo drives are commonly used in a large amount of practical applications. Wide industrial applicability of such drives is a result of their many advantages. They require small power input signals, to precisely control very big forces at output. Electrohydraulic servo drives are highly non-linear devices. Much of the current written publications related to the electrohydraulic servo drives focuses on improving the properties of existing drive, by implementation of modern forms of control, overseeing the work of these devices, as well as finding of new ways to provide movement of valve moving parts [3]. In proportional valves as the spool driving actuator most frequently proportional electromagnets are used. Following this path, it is advisable to search for set point actuators with better dynamic properties and positioning accuracy. In following article Permanent Magnet Synchronous Motors (PMSM) is proposed as control actuator for such task [3].

In the article the Authors describes the modelling of the electrohydraulic servo drive with proportional valve controlled by modern low power synchronous motor, which can be used in loop of the controller.

2 Electrohydraulic Drive with Synchronous Motor – Simulation and Modeling

2.1 Proportional Valve with Synchronous Motor

Modern synchronous motors ensure high positioning accuracy with high dynamics. In the proposed proportional valve spool is actuated by a low-power Permanent Magnet Synchronous Motor (PMSM) [4].

In the literature many attempts to use of variable types of motors in hydraulic valves are described. Publication [2] described the use of a stepping motor in the valve, to obtain a very small velocity of electrohydraulic drive. Article [3] describes the use of servo motor for control of the proportional valve for high range of flow. In article [1, 6] Author presented the study of the use of a stepping motor in linear electrohydraulic drive.

2.2 Modeling of the Electrohydraulic Servo Drive

The motor (1) was connected to the spool 3 by flexible coupling bellow 2 (Fig. 1). Applying the electrical power to the motor causes rotation and simultaneously axial translation of the spool in the valve body 4. Control edge openings x are proportional to the angular motor position and to the pitch of used thread 5. Direction of rotation determines direction of spool translation and opening or closing of valve gaps x . The proportional valve 1 is connected to the hydraulic cylinder 2 as shown on Fig. 2. Servo drive is equipped with internal position sensor 3, measuring the actual position of cylinder piston.

In the valve, Authors used PMSM motors type B&R 8LVA23. Its basic parameters are: the rated speed 3000 rev/min, rated current 2,9 A and stall torque 0,68 Nm. The motor was equipped with an absolute encoder type EnDat, providing a continuous information about the current position, even after a power failure, which assures a very high positioning accuracy and safe operation.

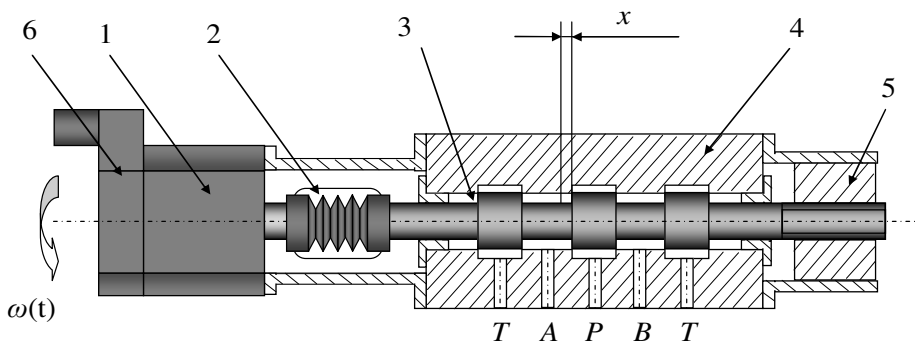


Fig. 1. Scheme of electrohydraulic proportional valve with PMSM motor

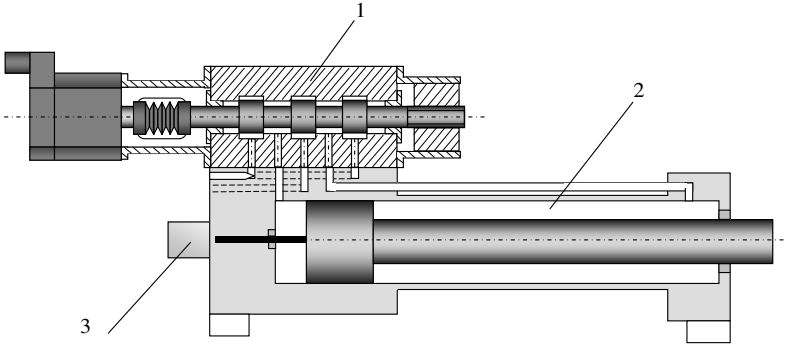


Fig. 2. Electrohydraulic servo drive with proportional valve with PMSM motor

Model of electrohydraulic servo drive (Fig. 3) was based on the graphical simplification of real system.

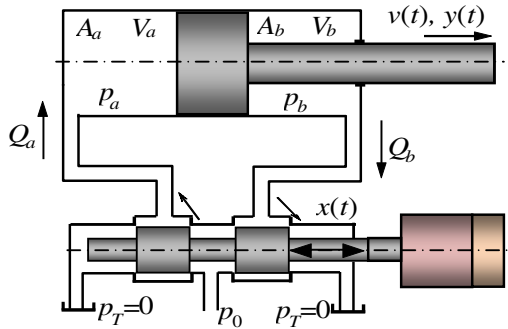


Fig. 3. Schema of the four edge electrohydraulic amplifier with PMSM motor and hydraulic actuator

The set of equations describing the electrohydraulic servo drive model can be specified as follows:

$$Q_a(t) = Q_{sa}(t) + Q_{ha}(t) + Q_v(t) \tag{1}$$

$$Q_b(t) = Q_{sb}(t) + Q_{hb}(t) + Q_v(t) - Q_{vb}(t) \tag{2}$$

$$Q_b(t) = K_{Qp}x(t) - K_l p_b(t) \tag{3}$$

$$Q_{ha}(t) = A \frac{dy(t)}{dt} \tag{4}$$

$$Q_{hb}(t) = aA \frac{dy(t)}{dt} \tag{5}$$

$$Q_{sa}(t) = \frac{V_a}{E_o} \frac{dp_a(t)}{dt} \quad (6)$$

$$Q_{sb}(t) = -\frac{V_b}{E_o} \frac{dp_b(t)}{dt} \quad (7)$$

$$Q_v(t) = K_v[p_a(t) - p_b(t)] \quad (8)$$

$$Q_{vb}(t) = K_{vb}p_b(t) \quad (9)$$

$$m \frac{d^2 y(t)}{dt^2} + D \frac{dy(t)}{dt} = A[p_a(t) - ap_b(t)] \quad (10)$$

where: Q_a, Q_b – flow, Q_{ha}, Q_{hb} – absorption of the actuator chambers, Q_{sa}, Q_{sb} – flow of the covering losses due to compressibility, Q_{vb} – leakage flow on the piston rod, p_a, p_b – the pressure in the chambers of the actuator, A_a, A_b – active surfaces of the piston, V_a, V_b – the volume of liquid in the chambers of the actuator.

Unknown model parameters such as capacity of the hydraulic pipes and the flow rate has been identified with used of the Kalman filter.

The present set of equations (1–10) allows to determine transfer function, representing the change in velocity of the piston transforms $Y(s)$ as a function of changes position of the slider amplifier transform $X(s)$ (taking into account the zero loading force F_{obc}):

$$G(s) = \frac{sY(s)}{X(s)} = \frac{k_s \omega_s^2}{s^2 + 2\zeta_s \omega_s s + \omega_s^2} \quad (11)$$

where:

- gain:

$$k_s = \frac{K_{Qp} \left(\frac{1}{V_A} + \frac{a}{V_B} \right)}{A \left(\frac{1}{V_A} - \frac{a^2}{V_B} \right)}, \quad (12)$$

- pulsation:

$$\omega_s = \sqrt{\frac{c_s}{m}}, \quad (13)$$

- damping:

$$\zeta_s = \frac{D_w}{2m \sqrt{\frac{c_s}{m}}}, \quad (14)$$

- stiffness of the actuator:

$$c_s = E_0 A^2 \left(\frac{1}{V_A} - \frac{a^2}{V_B} \right). \tag{15}$$

3 Simulation

Simulation model was built based on the equations (1–10). In Fig. 4 the simulation model of the electrohydraulic servo drive with PMSM based valve is shown. Its structure is typical for single piston side cylinders, where non-symmetric designs of the cylinders requires separate block chains for each cylinder chamber [1, 4].

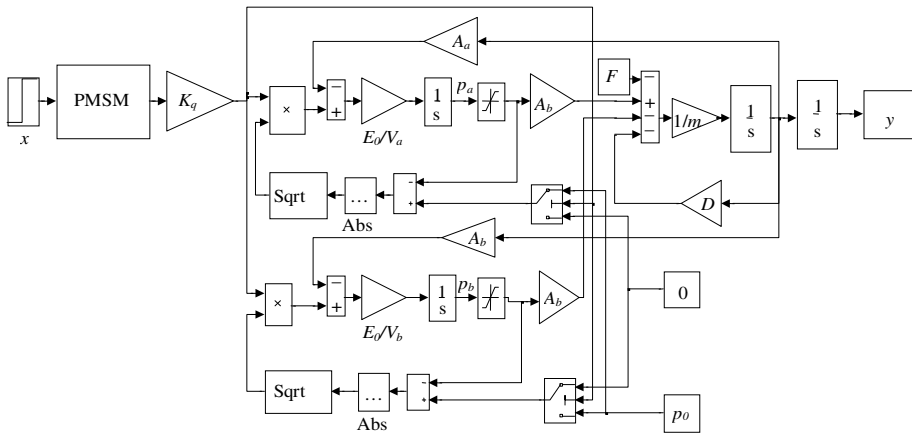


Fig. 4. Model of the electrohydraulic servo in Matlab Simulink software

The stroke of the hydraulic actuator was 200 mm. The diameters of the piston and the piston rod respectively, were $A = 40$ mm and $Aa = 63$ mm. The simulation includes linear stiffness and a linear coefficient of kinetic friction coulomb rate of $D = 29000$ [N·s/m]. The value of the reduced mass was $m = 20.2$ kg (mass of the piston and piston rod). The modulus of elasticity was $E_0 = 1.2 \cdot 10^9$ N/m². The values of the coefficients occurring in equations (6) (in the middle position of the piston) amounted to $E_0/V_a = 3.82 \cdot 10^{11}$ Pa/m³ and $E_0/V_b = 5.96 \cdot 10^{11}$ Pa/m³.

Model of the electrohydraulic servo drive was tested by used of the step response signals. Figures 5 shows the simulation results, with the displacement of the piston rod as the result of the valve opening. The simulation was performed for the supply pressure p_0 amounting to 5 MPa and 15 MPa.

Figure 6 shows the impact of the load on the drive system for a supply pressure $p_0 = 15$ MPa.

Figure 7 shows the displacement of the piston relative to the valve opening valve (with coincidence character).

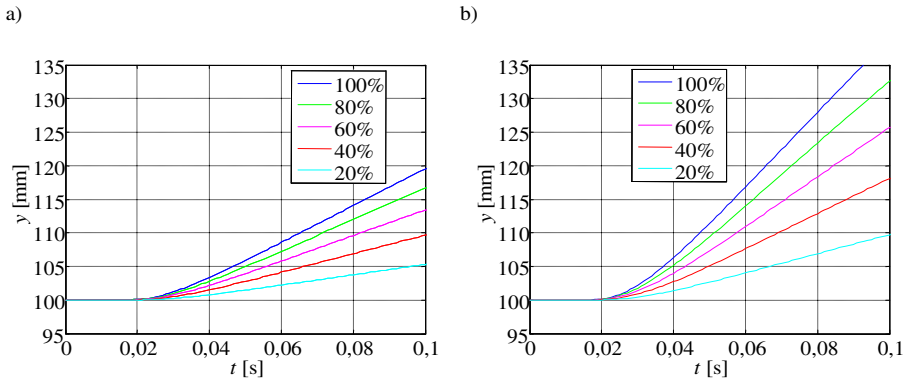


Fig. 5. Displacement of the piston rod for a supply pressure of 5 MPa (a) and 15 MPa (b)

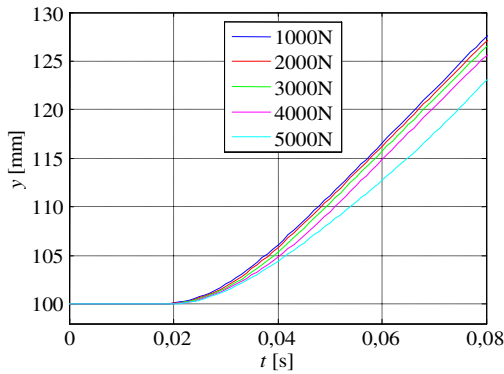


Fig. 6. Load impact on the electrohydraulic servo drive

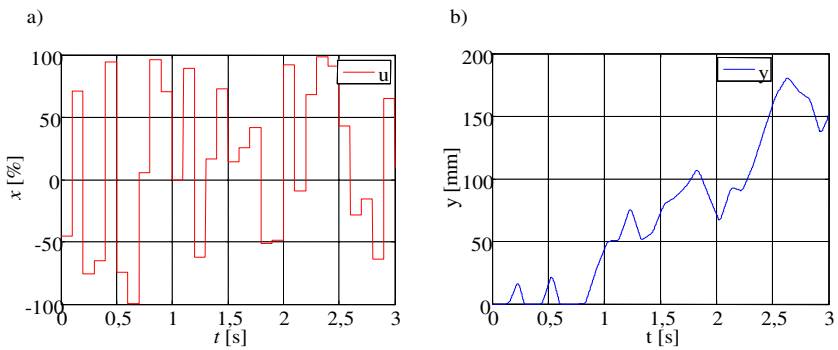


Fig. 7. Servo drive response (b) on given valve command signal (a)

4 Experimental Research

Modelling were allowed to the testing drive based on proposed here valve. The test stand (Fig. 8) consist of a hydraulic cylinder with stroke range 200 mm combined with a proportional valve controlled by synchronous motor. The cylinder was equipped with a magnetostrictive type of position sensor.

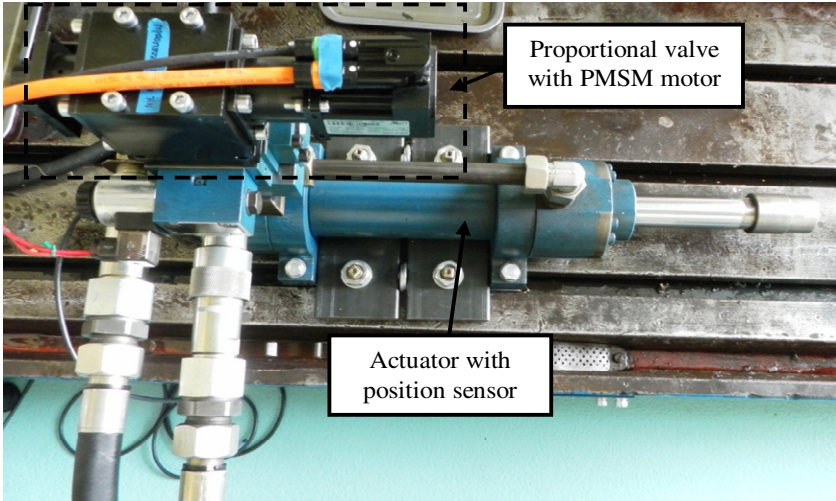


Fig. 8. Test stand

The drive was tested with step response signal. Based on the step response characteristic of the model and the real object can be state that the model accurately reflects the real object (Fig. 9). Position error between model and the real object, in extreme cases, was 2 mm.

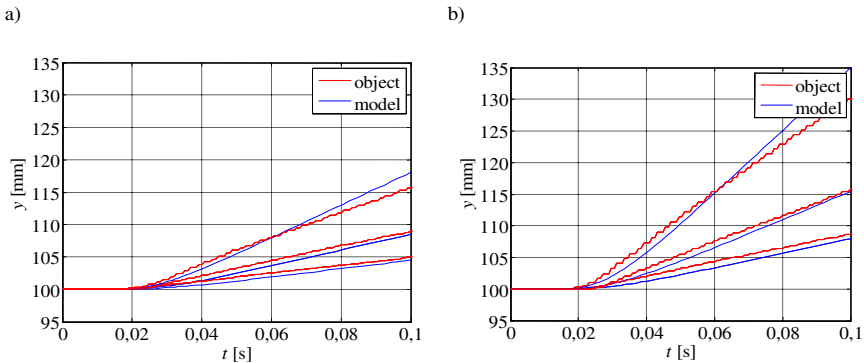


Fig. 9. Displacement of the piston rod for model and the object, for selected supply pressures: a) 5 MPa, b) 15 MPa

5 Conclusion

Article presents the basic equations describing the electrohydraulic drive. On the basis of this equations, simulation model was built. The electrohydraulic drive is equipped with the proportional valve controlled by PMSM motor. To compare the results of simulation with the real object, dedicated test stand was built. Based on these results can be state that the model accurately reflects the real object.

Performed drive model can be used as a reference model in adaptive control systems. The currently ongoing studies are aimed at implement it in the Model Following Control system.

Acknowledgements. The work described in this paper was funded from 02/22//DSPB/1145 project (Nowe techniki w urządzeniach mechatronicznych).

References

1. Milecki, A.: Modelling of an electrohydraulic servo drive unit with a servo valve, Archives of Mechanical Technology and Automation, vol. 21, pp. 165–170 (February 2001)
2. Milecki, A., Myszkowski, A.: - Modelling of electrohydraulic servo drive used in very low velocity applications. Int. J. Modelling, Identification and Control 7(3) (2009)
3. Milecki, A., Rybarczyk, D.: Modeling and Control of Proportional valve with Synchronous Motor. In: The 9-th International Conference Mechatronic Systems and Materials, MSM 2013 (2013)
4. Milecki, A., Rybarczyk, D., Owczarek, P.: Application of the MFC method in electrohydraulic servo drive with a valve controlled by synchronous motor. In: Advances in Intelligent Systems and Computing, ISI Proceedings. seria 267, Springer International Publishing, ISSN 2194-5357, ISBN 978-3-319-05352-3
5. Murrenhoff, H.: Trends in Valve Development, Ölhydraulik und Pneumatik, Niemcy, vol. 46(4) (2003)
6. Ławniczak, A., Milecki, A.: Influence of hydraulic amplifier gain coefficient on dynamic properties of electrohydraulic servo drive with stepping motor as an input element, Colloquium Dynamics of Machines 1998, pp. 3–4 (1998)
7. Wiegandt, M.: Development of a servomotor driven proportional valve. In: 7 the International Fluid Conference Aachen 2010 (2010)

Object-Oriented Approach to I/O Handling in Control Programs

Dariusz Rzońca, Jan Sadolewski, and Bartosz Trybus

Rzeszow University of Technology,
Department of Computer and Control Engineering,
al. Powstańców Warszawy 12, 35-959 Rzeszów, Poland
drzonca@prz-rzeszow.pl
<http://kia.prz.edu.pl/>

Abstract. The paper shows how new object-oriented features introduced in IEC 61131-3:2013 can be used for handling inputs and outputs. The new extensions such as classes, interfaces or inheritance are first characterized. Then, an UML model of I/O handling with diagrams for peripherals, universal data type and board capabilities is given. Finally, a practical example of model implementation is shown with portions of ST code accessing three different types of I/O boards.

Keywords: distributed control system, IEC 61131-3, function block, object oriented programming, UML.

1 Introduction

IEC 61131-3:2013 standard [2] supports object-oriented paradigm introducing extensions like classes, interfaces, inheritance and polymorphism. Such an approach is a novelty for control software. Object-oriented programming simplifies creating universal, more portable code. This paper discusses interfacing control programs with I/O peripherals in the scope of the new revision of the IEC 61131-3 standard, especially within CPDev engineering environment [4].

Handling I/O signals in control program depends on hardware. An additional mechanism which will interface controller inputs and outputs with program variables is necessary. Generally two approaches are possible, namely program-dependent and program-independent, as described in [6]. The first one requires direct referencing of inputs and outputs in control programs, which makes the program tied to a particular hardware. Another solution involves an logical assignment which is independent from programming, so the same program is portable and may be used in various hardware platforms. Such separation of program and hardware layers, is typical for multi-module PLCs and DCSs (Distributed Control Systems). Usually it involves additional configuration step, where a configuration tool connects program variables with inputs and outputs, or communication interfaces.

Object-oriented extensions make another solution possible. A control program may be written in a way to use general interfaces or classes and call abstract

methods, independent of target hardware. Specific implementation of methods related to hardware is made in final classes, derived from base ones. In this approach porting a control program to another hardware platform requires just replacing derived, hardware-dependent classes. Therefore portability of control software is greatly enhanced.

2 Object-Oriented Features in IEC-61131-3:2013

Current revision (2013) of IEC 61131-3 standard [2] introduces many object-oriented extensions. Semantics of the control languages defined in the previous revision have been enhanced to support classes, interfaces, inheritance and polymorphism. Such features are common in general purpose programming languages, but until now were rarely used in control programs. This section will briefly describe new possibilities and their impact on control software development process.

Classes in IEC 61131-3:2013 are specific Program Organization Units (POUs) designed for object oriented programming. Classes consist of data structures and methods. Data are partitioned into public and internal variables. Methods (algorithms) are performed upon the variables. An instance of a class has to be created before its methods can be called or its variables can be accessed.

Inheritance of classes allows for developing general base classes which are later extended by derived specific classes. In particular it is possible to create an *abstract class* intended to be a base type of other classes to be used for inheritance. A class is abstract if at least one of its methods is abstract, i.e. not yet implemented. Such an abstract class cannot be instantiated, and non-abstract class derived from it should include actual implementations of all inherited abstract methods.

Numerous different classes may extend a single base class. Such process may be repeated multiple times, however so-called *multiple inheritance* i.e. extending more than one parent class is not supported. The derived class inherits all variables from its base class as well as all methods except those declared as `PRIVATE`, or `INTERNAL` outside the namespace. Such a derived class typically extends the base (parent) class by adding its new own methods and variables in addition to the inherited ones, thus creating a new functionality. Moreover, implementation of methods in derived class may override existing methods in the base class.

IEC 61131-3:2013 standard introduces also the concept of *interfaces* to provide for separation of the interface specification from its implementation as a class. Thus different implementations of a common interface specification is possible. An interface contains a set of method prototypes. Such a prototype consists of the method name, `VAR_INPUT`, `VAR_OUTPUT` and `VAR_IN_OUT` variables and the method result, however it does not contain any algorithm. A class may implement one or more interfaces, so in contrary to multiple inheritance of classes, multiple implementation of interfaces is indeed possible. Final derived class should include actual implementation of all inherited abstract methods.

Inheritance of the interfaces is also possible. A derived interface may extend one or more already defined base interfaces and provide new functionality. Such a derived interface inherits all method prototypes from its parent interfaces, and may contain additional method prototypes.

An interface may be also used as the type of a variable. Such a variable will be used as a reference to an instance of a class implementing this interface. The variable has to be assigned to an instance of a class before it can be used.

Function blocks are also enhanced to support the object-oriented paradigm, similarly as defined for classes. They can use methods, implement interfaces and inherit from other function block or base class. Both function block body and methods are optional, so three variants are possible. In the first one, a function block will contain only a body, without any methods, as in previous revision (IEC 61131-3:2003). In the second variant, a function block consists of both function block body and methods. In the third one, a function block will contain only methods, without a function block body, so such a function block can be also declared as a class.

Polymorphism in the scope of IEC 61131-3:2013 standard is possible in four cases. First one is related to an interface. Interfaces cannot be instantiated, so if an interface is used as the type of a variable, such variable will hold a reference to an instance of a class implementing this interface, as mentioned earlier. Therefore, calls of methods using an interface reference requires dynamic (late) binding. Second case is related to `VAR_IN_OUT` variables. Such a variable may be assigned to an instance of a derived function block type, so the calls of a function block and their methods also requires dynamic binding.

Third case mentioned in the IEC 61131-3:2013 standard involves polymorphism with reference. An instance of a derived type may be assigned to a reference to a base class, as well as a variable with a type may be assigned to a reference to a derived function block type. Therefore, the calls of a function block and their methods via a dereferentiation of a reference are also cases where dynamic binding takes place.

The last case where polymorphism is necessary involves usage of the keyword `THIS`. It may be a reference to the current function block type or to one of its derived function block types, so the calls of a function block method using `THIS` also requires dynamic binding.

3 Proposed Model of I/O Class Hierarchy

Object-oriented approach can be used to develop universal class and interface model hierarchy which allows to express all common I/O devices. UML is well-known notation of interfaces and classes [1]. Limited capability of class inheritance which allows only for one class to be derived, and multiple interfaces to be implemented (see section 2), leads to introducing interfaces instead of classes in the model. Interface inheritance could be elaborated for three aspects: board peripheries, value type and board capabilities.

3.1 Peripherals

Interfaces for an input board can be organized as depicted at Fig. 1. At the top of the figure the most general interface **BoardIO** is presented. It consists of the method **GetIO_OID** which is an acronym of *Get Input/Output Object Identifier*. The method is responsible for returning a unique identifier which can be used to distinguish all I/Os on the board.

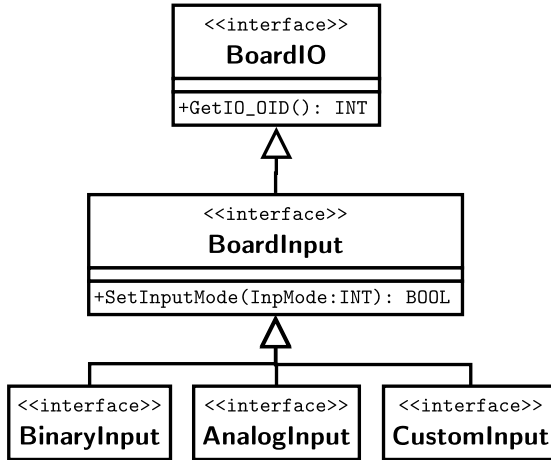


Fig. 1. Interface hierarchy of inputs

The second interface **BoardInput** derives from **BoardIO** and restricts all board I/Os to inputs only. It consists of **SetInputMode** method which allows to apply different modes on I/O channels. Switching between i.e. Schmitt input, counter, and normal I/O can be used to select the mode. Method is assumed to be virtual, which allows to redefine it in further inheritance.

The remaining three interfaces introduce the board inputs with more detail. The first one, **BinaryInput** should be implemented in those classes which are responsible for board channels with binary input capabilities. The second interface **AnalogInput** should describe all channels which are capable to return various numbers. The third one **CustomInput** is considered to provide description for those inputs which are not mentioned by the interfaces **BinaryInput** and **AnalogInput**.

Similar inheritance has been designed for board outputs. It is presented at Fig. 2. Like in the previous inheritance diagram, **BoardOutput** derives from the same **BoardIO** interface (internals are collapsed for brevity). Interface **BoardOutput** introduces the method **SetOutputMode** which is responsible for changing output capabilities like PWM, range output, etc. The remaining interfaces introduce board outputs with more detail. Interface **BinaryOutput** is responsible for denoting binary outputs in various modes, **AnalogOutput** can represent output

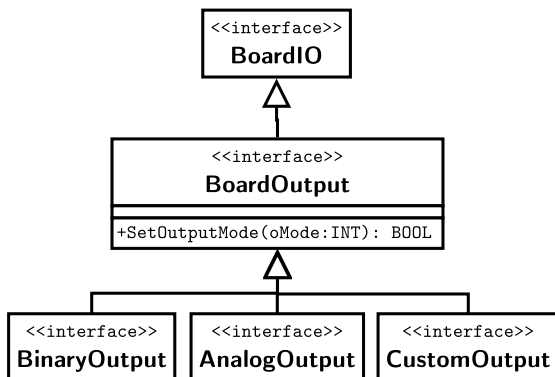


Fig. 2. Interface hierarchy of outputs

board with numeric values, and `CustomOutput` is considered to provide description for those outputs which are not handled by the previous ones. All input and output values can be represented by the *Universal Value Type*, described below.

3.2 Universal Value Type

Nowadays boards may contain a large number of inputs and outputs, often with some advanced capabilities. Commonly a control program will change outputs in dependence on inputs values. To achieve universality and flexibility, a script may be considered allowing to customize input and output handling without modifying the control program. Since such a script should process input and output in a generic way, we will introduce *Universal Value Type* for representing the processed values.

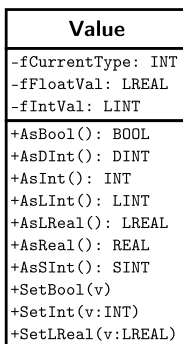


Fig. 3. Class for representing universal number type

Class diagram for the universal type is presented at Fig. 3. It can be noticed that the field `fCurrentType` is responsible for selecting representation form and mandatory conversions. The field `fFloatVal` stores floating-point values, whereas `fIntVal` stores all integers and Boolean values. Similar idea of data storing has been implemented in the language Lua [3]. Value access in particular type can be obtained by methods `AsBool`, `AsSInt`, `AsInt`, `AsDInt`, `AsLInt`, `AsReal`, `AsLReal`. They allow to obtain the value type as the script writer wants. Storing various values can be achieved by methods like `SetBool`, `SetSInt`, `SetInt`, `SetDInt`, `SetLInt`, `SetReal`, `SetLReal`. Using the `As` and `Set` methods may seem a bit difficult at first, so let us consider the expression `Z := X + Y`; as an example. The expression takes the following form, when using the universal value type:

```
VAR
  X, Y, Z : Value;
END_VAR
...

Z.SetReal(X.AsInt() + Y.AsInt());
```

This approach makes implementation of script much easier. Such universal value can be used in both operations – acquiring inputs and storing outputs, regardless of their types. The universal value type is used in the board capability interfaces described below.

3.3 Board Capabilities

Manufactures produce different boards which are equipped with various combination of input and output channels. An interface hierarchy is proposed here to generalize the capabilities of the boards. The model is presented at Fig. 4.

`BinaryInputBoard` interface has been designed for boards equipped with binary inputs. It consists of two methods: `EnumBinaryInputs` which returns an array of all binary inputs attached to the board, as instances of `BinaryInput` interface from Fig. 1. The second method `GetBinaryInput` acquires the universal type value described in 3.2. The input of the method is one element of array returned by `EnumBinaryInputs`.

Similar approach can be seen in `BinaryOutputBoard` interface. `EnumBinaryOutputs` returns an array of `BinaryOutput` instances (Fig. 2). The method `SetBinaryOutput` can be used to set value of the output. It requires two parameters: `BinaryOutput` instance and universal value to set. As the result, value of type `BOOL` can be returned to indicate success or failure.

Boards equipped with analog inputs implement the `AnalogInputBoard` interface. As in its binary counterpart, it provides method for enumerating all analog inputs on the board (`EnumAnalogInput`), and `GetAnalogInput` which provides the value acquired from analog input. `AnalogOutputBoard` interface covers boards with analog outputs. Similarly, it provides method `EnumAnalogOutputs`

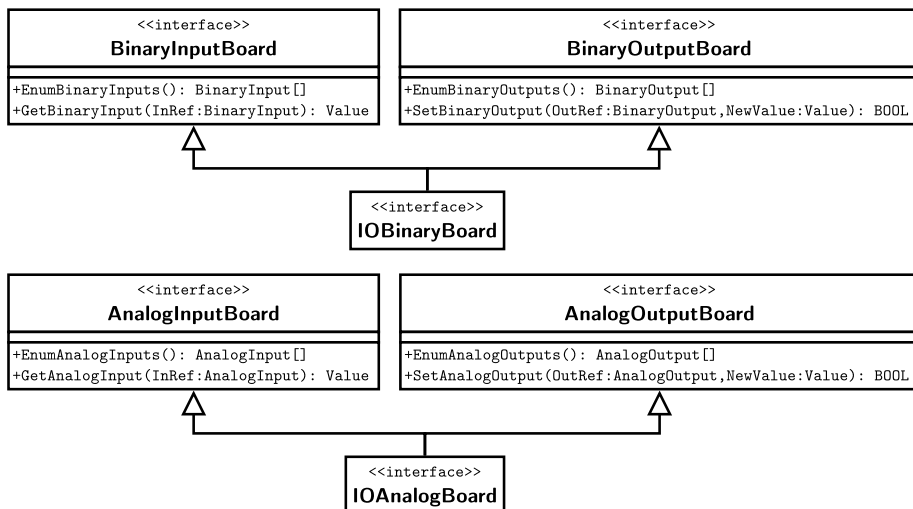


Fig. 4. Hierarchy interfaces of I/O boards

and `SetAnalogOutput`. Quite commonly, boards are equipped in both binary inputs and binary outputs. For such scenario, `IOBinaryBoard` interface has been prepared, which inherits from the two parent interfaces. Similar `IOAnalogBoard` interface exists for analog inputs and analog outputs on a single board.

4 Implementation Example

As a practical example we will now show how the proposed object model has been implemented in the CPDev engineering environment. CPDev is a tool for creating and executing IEC 61131-3 control software, with debugging and testing capabilities [4]. The object-oriented I/O handling has been prototyped in CPDev to demonstrate the new approach for IEC programming.

4.1 Execution Platform

CPDev control programs can be run on multiple hardware platforms via the virtual machine, being a portable interpreter of binary code produced by the compiler [8]. The runtime environment for the prototype implementation of the object I/O model is a PC computer running a version of Windows operating system (e.g. Windows Embedded). In this case, the CPDev virtual machine is built into a software module called WinController creating an executing environment for control programs. Main concepts of WinController resemble CPCtrl soft controller [7] handling I/O boards [5], but with some advanced enhancements. For example, it allows to utilize multiple virtual PLC controllers, each running a separate task. WinController is run as the operating system service, meaning it is constantly online. During development the user can use direct connection between CPDev IDE and WinController for program uploading and monitoring.

4.2 I/O Boards

WinController interfaces external inputs and outputs via dedicated external modules. The modules handle specific I/O hardware and connects it with CPDev virtual machine. WinController is able to connect to more than a single module at the same time, thus making the system scalable and flexible. For demonstration purposes, we will present here a sample setup with three external I/O modules, i.e.:

- RT-DAC USB data acquisition card from Inteco,
- NI-DAQ USB 6008 from National Instruments,
- generic GPS module with NMEA protocol.

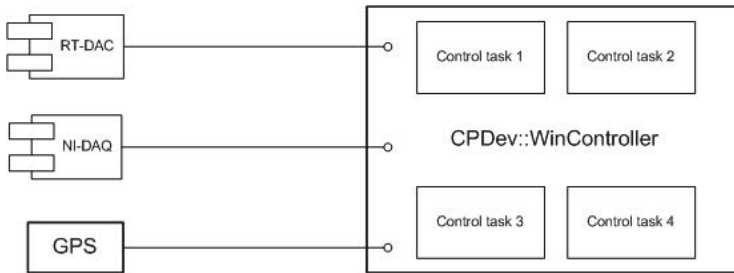


Fig. 5. CPDev WinController with three external I/O modules

The overall structure of the setup is shown in Fig. 5. The first two modules are data acquisition cards with several binary and analog inputs and outputs. Their vendors provide software libraries which have been used to interface the cards with WinController. The latter module generates a stream of text data with GPS readouts. As shown in Fig. 5, WinController can run multiple control task simultaneously, however for simplicity we will consider here a single task only.

4.3 Code Example

The sample CPDev project with object I/O involves three global variables defined as follows:

```
VAR_GLOBAL
  IOBOARD1 : RTDAC;
  IOBOARD2 : NIDAQ;
  GPS_SOURCE : GPS_NMEA;
END_VAR
```

The two IOBOARD variables are object instances of the types RTDAC and NIDAQ respectively, while GPS_SOURCE instantiates the type GPS_NMEA. The types used are object types implementing the model interfaces described in section 3. For example, RTDAC is defined as:

```
CLASS RTDAC IMPLEMENTS IOBinaryBoard, IOAnalogBoard
...
END_CLASS
```

Since the RT-DAC board involves both binary and analog inputs and outputs, the class implements two interfaces modeled in Fig. 4 (NIDAQ class is defined similarly). Implementation of the interface methods, such as `GetBinaryInput` or `SetAnalogOutput` depend on the vendor's card libraries. For example, RTDAC uses C++ library with low-level configuration and communication functions. The functions are called from IEC 61131-3 ST language via the CPDev native function block mechanism [8].

The control code can refer to the I/O objects e.g. in the following way:

```
VAR
  SIGNAL : Value;
END_VAR

SIGNAL := IOBOARD1.GetBinaryInput(IOBOARD1.EnumBinaryInputs()[1]);
IOBOARD2.SetBinaryOutput(IOBOARD2.EnumBinaryOutputs()[3], SIGNAL);
```

The code transfers a Boolean value stored in the SIGNAL variable of the universal type from the first binary input of IOBOARD1 (i.e. RTDAC) to the third output of IOBOARD2 (NIDAQ). It can be seen, that using the interface functions makes the code universal, so it does not depend on the particular setup. One can switch the cards or use a card from another manufacturer by changing the types of global variables only.

The GPS_NMEA is a class-based implementation of the GPS example shown previously in [6]. By using the object-oriented features, the code for accessing GPS data can now take the form of a class:

```
CLASS GPS_NMEA IMPLEMENTS AnalogInputBoard
...
  LONGITUDE_INPUT : REAL_ANALOG_INPUT;
  METHOD PUBLIC GET_LONGITUDE : REAL
  VAR w : VALUE; END_VAR
    w := THIS.GetAnalogInput(LONGITUDE_INPUT);
    GET_LONGITUDE := w.AsReal();
  END_METHOD
...
END_CLASS
```

The GPS module is a kind of analog input board, with three basic inputs: longitude, latitude, altitude (real numbers). Since the class implements `AnalogInputBoard` interface, one can access them via the generic function `GetAnalogInput`, but for convince extra public methods i.e `GET_LONGITUDE`, `GET_LATITUDE`, `GET_ALTITUDE` are available (only the first one is shown in the code above), giving the values in a simpler way, e.g.:

```
LON := GPS_SOURCE.GET_LONGITUDE();
```

5 Summary

The new object-oriented features of IEC 61131-3:2013 provide the user with a high-level concept of programming available so far in general-purpose languages such as Java or C#. Object orientation can be a challenge and uncommon for IEC engineers accustomed to classical programming scheme. In the paper we have presented a possible way of how the object approach can be applied to input and output handling. The given concept uses a set of new code constructions such as interfaces and classes. A practical example shows implementation of the UML object model adding a possibility to handle I/O modules from different vendors.

References

1. Bennet, S., McRobb, S., Farmer, R.: *Object-Oriented Systems Analysis and Design Using UML*. McGraw-Hill Education. Maidenhead (2006)
2. IEC 61131-3:2013 standard. *Programmable controllers - Part 3: Programming languages*. IEC (2013)
3. Ierusalimsky, R.: *Programming in Lua*. Lua.org. Rio de Janeiro (2013)
4. Jamro, M., Rzonca, D., Sadolewski, J., Stec, A., Swider, Z., Trybus, B., Trybus, L.: CPDev engineering environment for modeling, implementation, testing, and visualization of control software. In: Szewczyk, R., Zieliński, C., Kaliczyńska, M. (eds.) *Recent Advances in Automation, Robotics and Measuring Techniques*. AISC, vol. 267, pp. 81–90. Springer, Heidelberg (2014)
5. Rzońca, D., Sadolewski, J., Trybus, B.: Coloured Petri-nets models of CPDev soft controller with I/O boards. *Przegląd Elektrotechniczny (Electrical Review)* 9, 170–173 (2010)
6. Rzonca, D., Sadolewski, J., Trybus, B.: Interfacing inputs and outputs with IEC 61131-3 control software. In: Szewczyk, R., Zieliński, C., Kaliczyńska, M. (eds.) *Recent Advances in Automation, Robotics and Measuring Techniques*. AISC, vol. 267, pp. 229–238. Springer, Heidelberg (2014)
7. Sadolewski, J.: Programmable soft controller with data acquisition cards. *CMS 2009 Computer Methods and Systems*, pp. 385–389 (2009)
8. Trybus, B.: Development and Implementation of IEC 61131-3 Virtual Machine. *Theoretical and Applied Informatics* 23(1), 21–35 (2011)

Solution of the State Equation of Descriptor Fractional Continuous-Time Linear Systems with Two Different Fractional

Łukasz Sajewski

Białystok University of Technology, Faculty of Electrical Engineering
Wiejska 45D, 15-351 Białystok
l.sajewski@pb.edu.pl

Abstract. The descriptor fractional continuous-time linear systems with two different fractional orders are considered. The Drazin inverse of matrices is applied to find the solutions of the state equations. Some additional changes to classical Drazin approach for finding solution of the state equation of descriptor systems is proposed. An equality defining the set of admissible initial conditions for given inputs is derived.

Keywords: descriptor, fractional, different order, solution.

1 Introduction

Descriptor (singular) linear systems have been considered in many papers and books [1–3, 5, 6, 8, 10, 15, 16, 20, 28, 29]. The first definition of the fractional derivative was introduced by Liouville and Riemann at the end of the 19th century [22, 23] and another one was proposed in 20th century by Caputo [24]. This idea has been used by engineers for modeling different processes [7, 9]. Mathematical fundamentals of fractional calculus are given in the monographs [19, 21–24]. The positive fractional linear systems have been investigated in [13, 14, 19].

The positive linear systems with different fractional orders have been addressed in [17, 18].

Stability of fractional continuous-time linear systems consisting of n subsystem with different fractional orders [3]. The reachability and minimum energy control problem for systems with two different fractional orders in [25–27].

Drazin inverse matrix method for fractional descriptor continuous-time and discrete-time linear systems have been proposed in [11, 12].

In this paper solution to the state equation of descriptor fractional positive continuous-time linear systems with two different fractional orders will be formulated and solved.

The paper is organized as follows. In section 2 the basic definitions and theorems of the descriptor fractional continuous-time linear systems are recalled. Section 3 gives the problem formulation for systems with two different fractional orders. Solution to the state equation is given in section 4. Concluding remarks are given in section 5.

The following notation will be used: \mathfrak{R} – the set of real numbers, $\mathfrak{R}^{n \times m}$ – the set of $n \times m$ real matrices, I_n – the $n \times n$ identity matrix.

2 Descriptor Fractional System

Consider the fractional descriptor continuous-time linear system

$$E {}_0D_t^\alpha x(t) = Ax(t) + Bu(t), \quad n-1 < \alpha < n, \quad n \in W, \tag{2.1}$$

where α is fractional order, $x(t) \in \mathfrak{R}^n$ is the state vector $u(t) \in \mathfrak{R}^m$ is the input vector, $E, A \in \mathfrak{R}^{n \times n}$, $B \in \mathfrak{R}^{n \times m}$ and

$${}_0D_t^\alpha x(t) = \frac{d^\alpha x(t)}{dt^\alpha} = \frac{1}{\Gamma(n-\alpha)} \int_0^\infty \frac{f^{(n)}(\tau)}{(t-\tau)^{\alpha+1-n}} d\tau, \quad f^{(n)}(\tau) = \frac{d^n f(\tau)}{d\tau^n} \tag{2.2}$$

where $n-1 < \alpha < n$, $n \in W = \{1, 2, \dots\}$ is the Caputo definition of $\alpha \in \mathfrak{R}$ order derivative of $x(t)$ and

$$\Gamma(\alpha) = \int_0^\infty e^{-t} t^{\alpha-1} dt \tag{2.3}$$

is the Euler gamma function.

It is well known [19] that the Laplace transform (\mathcal{L}) of (2.1) is given by the formula

$$\mathcal{L} \left[\frac{d^\alpha f(t)}{dt^\alpha} \right] = \int_0^\infty \frac{d^\alpha f(t)}{dt^\alpha} e^{-st} dt = s^\alpha F(s) - \sum_{k=1}^n s^{\alpha-k} f^{(k-1)}(0+), \quad n-1 < \alpha < n, \quad n \in W, \tag{2.4}$$

where $F(s) = \mathcal{L}[f(t)]$ and $n-1 < \alpha < n$, $n \in W$.

It is assumed that $\det E = 0$ but the pencil (E, A) of (2.1) is regular, i.e.

$$\det[Es - A] \neq 0 \text{ for some } s \in \mathbb{C} \text{ (the field of complex numbers)}. \tag{2.5}$$

Assuming that for some chosen $c \in \mathbb{C}$, $\det[Ec - A] \neq 0$ and premultiplying (2.1) by $[Ec - A]^{-1}$ we obtain

$$\bar{E} {}_0D_t^\alpha x(t) = \bar{A}x(t) + \bar{B}u(t), \tag{2.6a}$$

where

$$\bar{E} = [Ec - A]^{-1}E, \quad \bar{A} = [Ec - A]^{-1}A, \quad \bar{B} = [Ec - A]^{-1}B. \tag{2.6b}$$

Note that the equations (2.1) and (2.6a) have the same solution $x(t)$.

Definition 2.1. The smallest nonnegative integer q is called the index of the matrix $\bar{E} \in \mathfrak{R}^{n \times n}$ if [4, 16]

$$\text{rank } \bar{E}^q = \text{rank } \bar{E}^{q+1}. \tag{2.7}$$

Definition 2.1. [4, 16] A matrix \bar{E}^D is called the Drazin inverse of $\bar{E} \in \mathfrak{R}^{n \times n}$ if it satisfies the conditions

$$\bar{E}\bar{E}^D = \bar{E}^D\bar{E}, \tag{2.8a}$$

$$\bar{E}^D\bar{E}\bar{E}^D = \bar{E}^D, \tag{2.8b}$$

$$\bar{E}^D\bar{E}^{q+1} = \bar{E}^q, \tag{2.8c}$$

where q is the index of \bar{E} defined by (2.6).

The Drazin inverse \bar{E}^D of a square matrix \bar{E} always exists and is unique [4, 16]. If $\det \bar{E} \neq 0$ then $\bar{E}^D = \bar{E}^{-1}$.

Lemma 2.1. [4, 16] The matrices \bar{E} and \bar{A} defined by (2.5b) satisfy the following equalities

$$1. \bar{A}\bar{E} = \bar{E}\bar{A} \text{ and } \bar{A}^D\bar{E} = \bar{E}\bar{A}^D, \bar{E}^D\bar{A} = \bar{A}\bar{E}^D, \bar{A}^D\bar{E}^D = \bar{E}^D\bar{A}^D, \tag{2.9a}$$

$$2. \ker \bar{A} \cap \ker \bar{E} = \{0\}, \tag{2.9b}$$

$$3. \bar{E} = T \begin{bmatrix} J & 0 \\ 0 & N \end{bmatrix} T^{-1}, \bar{E}^D = T \begin{bmatrix} J^{-1} & 0 \\ 0 & 0 \end{bmatrix} T^{-1}, \bar{A} = T \begin{bmatrix} A_1 & 0 \\ 0 & A_2 \end{bmatrix} T^{-1} \tag{2.9c}$$

$\det T \neq 0$, $J \in \mathfrak{R}^{n_1 \times n_1}$, is nonsingular, $N \in \mathfrak{R}^{n_2 \times n_2}$ is nilpotent, $n_1 + n_2 = n$,

$$4. (I_n - \bar{E}\bar{E}^D)\bar{A}\bar{A}^D = I_n - \bar{E}\bar{E}^D \text{ and } (I_n - \bar{E}\bar{E}^D)(\bar{E}\bar{A}^D)^q = 0. \tag{2.9d}$$

The solution to the equation (2.1) is given by

$$x(t) = \Phi_0(t)\bar{E}\bar{E}^D v + \bar{E}^D \int_0^t \Phi(t-\tau)\bar{B}u(\tau)d\tau + (\bar{E}\bar{E}^D - I_n) \sum_{k=0}^{q-1} (\bar{E}\bar{A}^D)^k \bar{A}^D \bar{B}u^{(k\alpha)}(t), \tag{2.10a}$$

where

$$\Phi_0(t) = \sum_{k=0}^{\infty} \frac{(\bar{E}^D\bar{A})^k t^{k\alpha}}{\Gamma(k\alpha+1)}, \Phi(t) = \sum_{k=0}^{\infty} \frac{(\bar{E}^D\bar{A})^k t^{(k+1)\alpha-1}}{\Gamma[(k+1)\alpha]}, \tag{2.10b}$$

$$u^{(k\alpha)}(t) = {}_0D_t^{k\alpha} u(t) \tag{2.10c}$$

and the vector $v \in \mathfrak{R}^n$ is arbitrary [12].

3 Systems with Two Different Fractional Orders

Consider a fractional linear system with two different fractional orders $\alpha \neq \beta$ described by the equation [18, 26]

$$\begin{bmatrix} \frac{d^\alpha x_1(t)}{dt^\alpha} \\ \frac{d^\beta x_2(t)}{dt^\beta} \end{bmatrix} = \begin{bmatrix} A_{11} & A_{12} \\ A_{21} & A_{22} \end{bmatrix} \begin{bmatrix} x_1(t) \\ x_2(t) \end{bmatrix} + \begin{bmatrix} B_1 \\ B_2 \end{bmatrix} u(t), \tag{3.1}$$

and $p-1 < \alpha < p; q-1 < \beta < q; p, q \in W$ where $x_1(t) \in \mathfrak{X}^{n_1}$, $x_2(t) \in \mathfrak{X}^{n_2}$, $u(t) \in \mathfrak{X}^m$ and $y(t) \in \mathfrak{X}^p$ are the state, input and output vectors respectively, $A_{ij} \in \mathfrak{X}^{n_i \times n_j}$, $B_i \in \mathfrak{X}^{n_i \times m}$; $i, j = 1, 2$.

Initial conditions for (3.1) have the form

$$x_1(0) = x_{10}, x_2(0) = x_{20} \text{ and } x_0 = \begin{bmatrix} x_{10} \\ x_{20} \end{bmatrix}. \tag{3.2}$$

It is well-known [17, 18] that the solution of the equation (3.1) for $0 < \alpha < 1; 0 < \beta < 1$ with initial conditions (3.2) has the form

$$\begin{bmatrix} x_1(t) \\ x_2(t) \end{bmatrix} = \Phi_0(t) \begin{bmatrix} x_{10} \\ x_{20} \end{bmatrix} + \int_0^t \Phi_1(t-\tau) \begin{bmatrix} B_1 \\ 0 \end{bmatrix} u(\tau) d\tau + \int_0^t \Phi_2(t-\tau) \begin{bmatrix} 0 \\ B_2 \end{bmatrix} u(\tau) d\tau \tag{3.3a}$$

where

$$T_{k,l} = \begin{cases} I_n & \text{for } k=l=0 \\ \begin{bmatrix} A_{11} & A_{12} \\ 0 & 0 \end{bmatrix} & \text{for } k=1, l=0 \\ \begin{bmatrix} 0 & 0 \\ A_{21} & A_{22} \end{bmatrix} & \text{for } k=0, l=1 \\ T_{10}T_{k-1,l} + T_{01}T_{k,l-1} & \text{for } k+l > 0 \end{cases} \tag{3.3b}$$

$$\Phi_0(t) = \sum_{k=0}^{\infty} \sum_{l=0}^{\infty} T_{k,l} \frac{t^{k\alpha+l\beta}}{\Gamma(k\alpha+l\beta+1)},$$

$$\Phi_1(t) = \sum_{k=0}^{\infty} \sum_{l=0}^{\infty} T_{k,l} \frac{t^{(k+1)\alpha+l\beta-1}}{\Gamma[(k+1)\alpha+l\beta]}, \quad \Phi_2(t) = \sum_{k=0}^{\infty} \sum_{l=0}^{\infty} T_{k,l} \frac{t^{k\alpha+(l+1)\beta-1}}{\Gamma[k\alpha+(l+1)\beta]}. \tag{3.3c}$$

Now let consider the fractional descriptor continuous-time linear system with different fractional orders

$$E \begin{bmatrix} \frac{d^\alpha x_1(t)}{dt^\alpha} \\ \frac{d^\beta x_2(t)}{dt^\beta} \end{bmatrix} = A \begin{bmatrix} x_1(t) \\ x_2(t) \end{bmatrix} + Bu(t), \tag{3.4}$$

and $p-1 < \alpha < p; q-1 < \beta < q; p, q \in W$, where $E = \begin{bmatrix} E_1 & 0 \\ 0 & E_2 \end{bmatrix} \in \mathfrak{R}^{(n_1+n_2) \times (n_1+n_2)}$,

$$A = \begin{bmatrix} A_{11} & A_{12} \\ A_{21} & A_{22} \end{bmatrix} \in \mathfrak{R}^{(n_1+n_2) \times (n_1+n_2)}, B = \begin{bmatrix} B_1 \\ B_2 \end{bmatrix} \in \mathfrak{R}^{(n_1+n_2) \times m}.$$

It is assumed that $\det E = 0$ but the pencil (E, A) of (3.4) is regular, i.e.

$$\det \left[\begin{bmatrix} E_1 & 0 \\ 0 & E_2 \end{bmatrix} \begin{bmatrix} s^\alpha & 0 \\ 0 & s^\beta \end{bmatrix} - \begin{bmatrix} A_{11} & A_{12} \\ A_{21} & A_{22} \end{bmatrix} \right] \neq 0 \text{ for some } s^\alpha, s^\beta \in \mathbb{C} \tag{3.5}$$

where \mathbb{C} is the field of complex numbers.

Similar as for (2.1) assuming that for some chosen $c_1, c_2 \in \mathbb{C}$,

$\det[E \text{diag}(c_1, c_2) - A] \neq 0$ and premultiplying (3.4) by $[E \text{diag}(c_1, c_2) - A]^{-1}$ we obtain

$$\bar{E} \begin{bmatrix} \frac{d^\alpha x_1(t)}{dt^\alpha} \\ \frac{d^\beta x_2(t)}{dt^\beta} \end{bmatrix} = \bar{A} \begin{bmatrix} x_1(t) \\ x_2(t) \end{bmatrix} + \bar{B}u(t), \tag{3.6a}$$

where

$$\begin{aligned} \bar{E} &= [E \text{diag}(c_1, c_2) - A]^{-1} E = \begin{bmatrix} \bar{E}_{11} & \bar{E}_{12} \\ \bar{E}_{21} & \bar{E}_{22} \end{bmatrix}, \\ \bar{A} &= [E \text{diag}(c_1, c_2) - A]^{-1} A = \begin{bmatrix} \bar{A}_{11} & \bar{A}_{12} \\ \bar{A}_{21} & \bar{A}_{22} \end{bmatrix} = \bar{T}_{10} + \bar{T}_{01}, \\ \bar{B} &= [E \text{diag}(c_1, c_2) - A]^{-1} B = \begin{bmatrix} \bar{B}_1 \\ \bar{B}_2 \end{bmatrix} = \bar{B}_{10} + \bar{B}_{01}, \\ \bar{T}_{10} &= \begin{bmatrix} \bar{A}_{11} & \bar{A}_{12} \\ 0 & 0 \end{bmatrix}, \bar{T}_{01} = \begin{bmatrix} 0 & 0 \\ \bar{A}_{21} & \bar{A}_{22} \end{bmatrix}, \bar{B}_{10} = \begin{bmatrix} \bar{B}_1 \\ 0 \end{bmatrix}, \bar{B}_{01} = \begin{bmatrix} 0 \\ \bar{B}_2 \end{bmatrix}. \end{aligned} \tag{3.6b}$$

Note that the equations (3.4) and (3.6a) have the same solution $x(t)$.

In case of system with two different fractional order the Definition 2.1 takes the form:

Definition 3.1. The smallest nonnegative integer $q_i, i = 1, 2$ is called the index of the matrix $\bar{E}_{ii} \in \mathfrak{R}^{n_i \times n_i}$ if

$$\text{rank } \bar{E}_{ii}^{q_i} = \text{rank } \bar{E}_{ii}^{q_i+1} \tag{3.7}$$

and $q = q_1 + q_2$ is the index of \bar{E} .

Remark 3.1. According to system (3.6), condition $\alpha \neq \beta$ and formulation of solution (3.3) of the state equation (3.1) (case of the system (3.6) with $\det E \neq 0$), impose additional conditions to Lemma 2.1.

4 Solution to the State Equation by the Use of Drazin Inverse

In this section the solution to the state equation (3.6) will be presented by the use of the Drazin inverses of the matrices \bar{E} and \bar{A} .

Assumption 4.1. For system with two different fractional orders the first condition of the Lemma 2.1 takes the form $\bar{T}_{k,l}\bar{E} = \bar{E}\bar{T}_{k,l}$ and $\bar{T}_{k,l}^D\bar{E} = \bar{E}\bar{T}_{k,l}^D, \bar{E}^D\bar{T}_{k,l} = \bar{T}_{k,l}\bar{E}^D, \bar{T}_{k,l}^D\bar{E}^D = \bar{E}^D\bar{T}_{k,l}^D$.

Theorem 4.1. If the Assumption 4.1 is true then the solution to the equation (3.6) is given by

$$\begin{aligned} x(t) = & \Phi_0(t)\bar{E}\bar{E}^D v + \bar{E}^D \int_0^t [\Phi_1(t-\tau)B_{10} + \Phi_2(t-\tau)B_{01}]u(\tau)d\tau \\ & + (\bar{E}\bar{E}^D - I_{n_1+n_2}) \sum_{k=0}^{q_1-1} \sum_{l=0}^{q_2-1} \bar{E}^{k+l} \bar{T}_{k,l}^D \bar{A}^D \bar{B} u^{(k\alpha+l\beta)}(t) \end{aligned} \tag{4.1a}$$

where

$$\bar{T}_{k,l} = \begin{cases} I_n & \text{for } k=l=0 \\ \begin{bmatrix} \bar{A}_{11} & \bar{A}_{12} \\ 0 & 0 \end{bmatrix} & \text{for } k=1, l=0 \\ \begin{bmatrix} 0 & 0 \\ \bar{A}_{21} & \bar{A}_{22} \end{bmatrix} & \text{for } k=0, l=1 \\ \bar{T}_{10}\bar{T}_{k-1,l} + \bar{T}_{01}\bar{T}_{k,l-1} & \text{for } k+l > 0 \end{cases} \tag{4.1b}$$

$$\Phi_0(t) = \sum_{k=0}^{\infty} \sum_{l=0}^{\infty} (\bar{E}^D)^{k+l} \bar{T}_{k,l} \frac{t^{k\alpha+l\beta}}{\Gamma(k\alpha+l\beta+1)},$$

$$\Phi_1(t) = \sum_{k=0}^{\infty} \sum_{l=0}^{\infty} (\bar{E}^D)^{k+l} \bar{T}_{k,l} \frac{t^{(k+1)\alpha+l\beta-1}}{\Gamma[(k+1)\alpha+l\beta]},$$

$$\Phi_2(t) = \sum_{k=0}^{\infty} \sum_{l=0}^{\infty} (\bar{E}^D)^{k+l} \bar{T}_{k,l} \frac{t^{k\alpha+(l+1)\beta-1}}{\Gamma[k\alpha+(l+1)\beta]} \quad (4.1c)$$

$$u^{(k\alpha+l\beta)}(t) = {}_0D_t^{k\alpha+l\beta} u(t) \quad (4.1d)$$

and the vector $v = \begin{bmatrix} v_1 \\ v_2 \end{bmatrix} \in \mathfrak{R}^{n_1+n_2}$ is arbitrary.

Proof. Proof will be accomplished by showing that (4.1a) satisfies the equation (3.6a).

Since the system (4.1) is linear then we can split proof on two cases:

1) For $u(t) = 0$ we have $\bar{E} {}_0D_t^\alpha x(t) = \bar{A}[\Phi_0(t)\bar{E}\bar{E}^D v]$ since

$$\begin{aligned} \bar{E} {}_0D_t^\alpha x(t) &= \bar{E} {}_0D_t^\alpha [\Phi_0(t)\bar{E}\bar{E}^D v] = \\ &= \bar{E} {}_0D_t^\alpha \left[\bar{E}\bar{E}^D v + \sum_{k=0}^{\infty} \sum_{l=0}^{\infty} (\bar{E}^D)^{k+l} \bar{T}_{k,l} \frac{t^{k\alpha+l\beta}}{\Gamma(k\alpha+l\beta+1)} \bar{E}\bar{E}^D v \right] = \\ &= \sum_{k=0}^{\infty} \sum_{l=0}^{\infty} \bar{E} (\bar{E}^D)^{k+l+1} \bar{T}_{k+1,l+1} \frac{t^{k\alpha+l\beta}}{\Gamma(k\alpha+l\beta+1)} \bar{E}\bar{E}^D v, \\ \bar{A}[\Phi_0(t)\bar{E}\bar{E}^D v] &= \bar{A} \sum_{k=0}^{\infty} \sum_{l=0}^{\infty} (\bar{E}^D)^{k+l} \bar{T}_{k,l} \frac{t^{k\alpha+l\beta}}{\Gamma(k\alpha+l\beta+1)} \bar{E}\bar{E}^D v = \\ &= \bar{T}_{10} \sum_{k=0}^{\infty} \sum_{l=0}^{\infty} (\bar{E}^D)^{k+l} \bar{T}_{k,l} \frac{t^{k\alpha+l\beta}}{\Gamma(k\alpha+l\beta+1)} \bar{E}\bar{E}^D v + \\ &\quad + \bar{T}_{01} \sum_{k=0}^{\infty} \sum_{l=0}^{\infty} (\bar{E}^D)^{k+l} \bar{T}_{k,l} \frac{t^{k\alpha+l\beta}}{\Gamma(k\alpha+l\beta+1)} \bar{E}\bar{E}^D v = \\ &= \sum_{k=0}^{\infty} \sum_{l=0}^{\infty} (\bar{E}^D)^{k+l} \bar{T}_{k+1,l} \frac{t^{k\alpha+l\beta}}{\Gamma(k\alpha+l\beta+1)} \bar{E}\bar{E}^D v + \\ &\quad + \sum_{k=0}^{\infty} \sum_{l=0}^{\infty} (\bar{E}^D)^{k+l} \bar{T}_{k,l+1} \frac{t^{k\alpha+l\beta}}{\Gamma(k\alpha+l\beta+1)} \bar{E}\bar{E}^D v = \\ &= \sum_{k=0}^{\infty} \sum_{l=0}^{\infty} \bar{E} (\bar{E}^D)^{k+l+1} \bar{T}_{k+1,l+1} \frac{t^{k\alpha+l\beta}}{\Gamma(k\alpha+l\beta+1)} \bar{E}\bar{E}^D v \end{aligned} \quad (4.2)$$

with

$$\begin{aligned}
 {}_0D_t^\alpha \overline{E} \overline{E}^D v &= 0, \quad \overline{E} (\overline{E}^D)^{k+l+1} \overline{T}_{k+l+1} = \overline{T}_{k+l+1} (\overline{E}^D)^{k+l}, \quad \overline{A} = \overline{T}_{10} + \overline{T}_{01}, \\
 \Phi_1(t) &= \sum_{k=0}^{\infty} \sum_{l=0}^{\infty} (\overline{E}^D)^{k+l} \overline{T}_{k,l} \frac{t^{(k+1)\alpha+l\beta-1}}{\Gamma[(k+1)\alpha+l\beta]} = \\
 &= \frac{t^{\alpha-1}}{\Gamma(\alpha)} + \sum_{k=0}^{\infty} \sum_{l=0}^{\infty} (\overline{E}^D)^{k+l+1} \overline{T}_{k+l,l} \frac{t^{(k+2)\alpha+l\beta-1}}{\Gamma[(k+2)\alpha+l\beta]}, \tag{4.3} \\
 \Phi_2(t) &= \sum_{k=0}^{\infty} \sum_{l=0}^{\infty} (\overline{E}^D)^{k+l} \overline{T}_{k,l} \frac{t^{k\alpha+(l+1)\beta-1}}{\Gamma[k\alpha+(l+1)\beta]} = \\
 &= \frac{t^{\beta-1}}{\Gamma(\beta)} + \sum_{k=0}^{\infty} \sum_{l=0}^{\infty} (\overline{E}^D)^{k+l+1} \overline{T}_{k,l+1} \frac{t^{k\alpha+(l+2)\beta-1}}{\Gamma[k\alpha+(l+2)\beta]}
 \end{aligned}$$

and (2.9d) holds.

2) For $v = 0$ we have

$$\begin{aligned}
 \overline{E} {}_0D_t^\alpha x(t) - \overline{A}x &= \overline{E}^D \overline{B}u(t) + (\overline{E} \overline{E}^D - I_{n_1+n_2}) \sum_{k=0}^{q_1-1} \sum_{l=0}^{q_2-1} \overline{E}^{k+l+1} \overline{T}_{k+l+1}^D \overline{B}u^{(k\alpha+l\beta+1)}(t) \\
 - \overline{A}(\overline{E} \overline{E}^D - I_{n_1+n_2}) &\sum_{k=0}^{q_1-1} \sum_{l=0}^{q_2-1} \overline{E}^{k+l} \overline{T}_{k,l}^D \overline{A}^D \overline{B}u^{(k\alpha+l\beta)}(t) = \overline{B}u(t). \tag{4.4}
 \end{aligned}$$

In general, substituting (4.1a) in the left side of the equation (3.6a), using (4.1b), (4.1c), Definition 2.2 and Assumption 4.1 we obtain

$$\begin{aligned}
 \overline{E} \begin{bmatrix} \frac{d^\alpha x_1(t)}{dt^\alpha} \\ \frac{d^\beta x_2(t)}{dt^\beta} \end{bmatrix} &= \overline{E} \begin{bmatrix} \frac{d^\alpha}{dt^\alpha} \left[\Phi_0(t) \overline{E} \overline{E}^D v + \overline{E}^D \int_0^t [\Phi_1(t-\tau) B_{10} + \Phi_2(t-\tau) B_{01}] u(\tau) d\tau \right. \\ \left. + (\overline{E} \overline{E}^D - I_{n_1+n_2}) \sum_{k=0}^{q_1-1} \sum_{l=0}^{q_2-1} \overline{E}^{k+l} \overline{T}_{k,l}^D \overline{A}^D \overline{B}u^{(k\alpha+l\beta)}(t) \right] \\ \frac{d^\beta}{dt^\beta} \left[\overline{E} \overline{E}^D v + \sum_{k+l \geq 1}^{\infty} (\overline{E}^D)^{k+l} \overline{T}_{k,l} \frac{t^{k\alpha+l\beta}}{\Gamma(k\alpha+l\beta+1)} \right. \\ \left. + \overline{E}^D \int_0^t \left[\frac{(t-\tau)^{\alpha-1}}{\Gamma(\alpha)} \overline{B}_{10} + \frac{(t-\tau)^{\beta-1}}{\Gamma(\beta)} \overline{B}_{01} \right] u(\tau) d\tau \right] \\ \frac{d^\alpha}{dt^\alpha} \left[\overline{E} \overline{E}^D v + \overline{E}^D \int_0^t \left[\sum_{k+l \geq 1}^{\infty} (\overline{E}^D)^{k+l+1} \overline{T}_{k+l,l} \frac{t^{(k+2)\alpha+l\beta-1}}{\Gamma[(k+2)\alpha+l\beta]} \overline{B}_{10} \right. \right. \\ \left. \left. + \sum_{k+l \geq 1}^{\infty} (\overline{E}^D)^{k+l+1} \overline{T}_{k,l+1} \frac{t^{(k+2)\beta+k\alpha-1}}{\Gamma[(l+2)\beta+k\alpha]} \overline{B}_{01} \right] u(\tau) d\tau \right] \\ \left. + (\overline{E} \overline{E}^D - I_{n_1+n_2}) \sum_{k=0}^{q_1-1} \sum_{l=0}^{q_2-1} \overline{E}^{k+l} \overline{T}_{k,l}^D \overline{A}^D \overline{B}u^{(k\alpha+l\beta)}(t) \right] \\
 &= \sum_{k=0}^{\infty} \sum_{l=0}^{\infty} \overline{E} (\overline{E}^D)^{k+l+1} \overline{T}_{k+l+1} \frac{t^{k\alpha+l\beta}}{\Gamma(k\alpha+l\beta+1)} \overline{E} \overline{E}^D v + \overline{E}^D \overline{B}u(t) \\
 &+ \overline{E}^D \int_0^t \left[\overline{T}_{10} \Phi_1(t-\tau) B_{10} + \overline{T}_{01} \Phi_2(t-\tau) B_{01} \right] u(\tau) d\tau + (\overline{E} \overline{E}^D - I_{n_1+n_2}) \sum_{k=0}^{q_1-1} \sum_{l=0}^{q_2-1} \overline{E}^{k+l+1} \overline{T}_{k+l+1}^D \overline{B}u^{(k\alpha+l\beta+1)}(t). \tag{4.2}
 \end{aligned}$$

Therefore, the solution (4.1a) satisfies the equation (3.6a). \square

From (4.1a) for $t = 0$ we have

$$x(0) = \overline{EE}^D v + (\overline{EE}^D - I_{n_1+n_2}) \sum_{k=0}^{q_1-1} \sum_{l=0}^{q_2-1} \overline{E}^{k+l} \overline{T}_{k,l}^D \overline{A}^D \overline{B} u^{(k\alpha+l\beta)}(0). \quad (4.6)$$

Therefore, for given admissible $u(t)$ the consistent initial conditions should satisfy the equality (4.6). In particular case for $u(t) = 0$ we have $x_0 = \overline{EE}^D v$ and $x_0 \in \text{Im}(\overline{EE}^D)$ where Im denotes the image of \overline{EE}^D .

5 Concluding Remarks

The descriptor fractional continuous-time linear systems with two different fractional orders has been considered. The Drazin inverse of matrices has been applied to find the solutions of the state equations of the considered system. Some additional changes to classical Drazin approach for finding the solution of the state equation of descriptor systems is proposed. An equality defining the set of admissible initial conditions for given inputs has been derived.

Acknowledgments. This work was supported by National Science Centre in Poland.

References

1. Bru, R., Coll, C., Romero-Vivo, S., Sanchez, E.: Some problems about structural properties of positive descriptor systems. LNCIS, vol. 294, pp. 233–240. Springer, Berlin (2003)
2. Bru, R., Coll, C., Sanchez, E.: About positively discrete-time singular systems, System and Control: theory and applications. Electr. Comput. Eng. Ser. World Sci. Eng. Soc. Press, Athens, 44–48 (2000)
3. Buśłowicz, M.: Stability analysis of continuous-time linear systems consisting of n subsystem with different fractional orders. Bull. Pol. Ac. Tech. 60(2), 279–284 (2012)
4. Campbell, S.L., Meyer, C.D., Rose, N.J.: Applications of the Drazin inverse to linear systems of differential equations with singular constant coefficients. SIAMJ Appl. Math. 31(3), 411–425 (1976)
5. Dai, L.: Singular control systems. LNCIS. Springer, Berlin (1989)
6. Dodig, M., Stosic, M.: Singular systems state feedbacks problems. Linear Algebra and its Applications 431(8), 1267–1292 (2009)
7. Dzielinski, A., Sierociuk, D., Sarwas, G.: Ultracapacitor parameters identification based on fractional order model. Proc ECC, Budapest (2009)
8. Fahmy, M.M., O'Reill, J.: Matrix pencil of closed-loop descriptor systems: infinite-eigenvalues assignment. Int. J. Control 49(4), 1421–1431 (1989)

9. Ferreira, N.M.F., Machado, J.A.T.: Fractional-order hybrid control of robotic manipulators. In: Proc. 11th Int. Conf. Advanced Robotics, Coimbra, Portugal. ICAR, pp. 393–398 (2003)
10. Guang-Ren, D.: Analysis and Design of Descriptor Linear Systems. Springer, New York (2010)
11. Kaczorek, T.: Application of Drazin inverse to analysis of descriptor fractional discrete-time linear systems with regular pencils. *Int. J. Appl. Math. Comput. Sci.* 23(1), 29–33 (2013)
12. Kaczorek, T.: Drazin inverse matrix method for fractional descriptor continuous-time linear systems. *Bull* 62(3), 409–412 (2014), doi:10.2478/bpasts-2014-0042.
13. Kaczorek, T.: Fractional positive continuous-time systems and their reachability. *Int. J. Appl. Math. Comput. Sci.* 18(2), 223–228 (2008)
14. Kaczorek, T.: Fractional positive linear systems. *Kybernetes: The International Journal of Systems & Cybernetics* 38(7/8), 1059–1078 (2009)
15. Kaczorek, T.: Infinite eigenvalue assignment by output-feedbacks for singular systems. *Int. J. Appl. Math. Comput. Sci.* 14(1), 19–23 (2004)
16. Kaczorek, T.: Research Studies Press J, vol. 1. Wiley, New York (1992)
17. Kaczorek, T.: Positive linear systems consisting of n subsystems with different fractional orders. *IEEE Trans. Circuits and Systems* 58(6), 1203–1210 (2011)
18. Kaczorek, T.: Positive linear systems with different fractional orders. *Bull. Pol. Ac. Tech.* 58(3), 453–458 (2010)
19. Kaczorek, T.: Selected Problems in Fractional Systems Theory. Springer, Berlin (2011)
20. Kucera, V., Zagalak, P.: Fundamental theorem of state feedback for singular systems. *Automatica* 24(5), 653–658 (1988)
21. Miller, K.S., Ross, B.: An Introduction to the Fractional Calculus and Fractional Differential Equations. Wiley, New York (1993)
22. Nishimoto, K., Fractional Calculus. Decartess Press, Koriama (1984)
23. Oldham, K.B., Spanier, J.: The Fractional Calculus. Academic Press, New York (1974)
24. Podlubny, I.: Fractional Differential Equations. Academic Press, San Diego (1999)
25. Sajewski, Ł.: Reachability of fractional positive continuous-time linear systems with two different fractional orders. In: Szewczyk, R., Zieliński, C., Kaliczyńska, M. (eds.) Recent Advances in Automation, Robotics and Measuring Techniques. AISC, vol. 267, pp. 239–250. Springer, Heidelberg (2014)
26. Sajewski, Ł.: Reachability, observability and minimum energy control of fractional positive continuous-time linear systems with two different fractional orders. *Multidim. Syst. Sign. Process* 25, doi:10.1007/s11045-014-0287-2
27. Sajewski, Ł.: Minimum energy control of fractional positive continuous-time linear systems with two different fractional orders and bounded inputs. In: Latawiec, K.J., Łukaniszyn, M., Stanisławski, R. (eds.) Advances in Modeling and Control of Non-integer Order Systems. LNEE, vol. 320, pp. 171–181. Springer, Heidelberg (2015)
28. Van Dooren, P.: The computation of Kronecker’s canonical form of a singular pencil. *Linear Algebra and its Applications* 27, 103–140 (1979)
29. Virnik, E.: Stability analysis of positive descriptor systems. *Linear Algebra and its Applications* 429, 2640–2659 (2008)

A Hybrid Approach to Sustainable Supply Chain Optimization

Paweł Sitek

Department of Control and Management Systems,
Kielce University of Technology, Poland
sitek@tu.kielce.pl

Abstract. This paper describes the hybrid approach to optimization of decision problems in sustainable supply chain (SSC). The hybrid approach proposed here combines the strengths of mathematical programming (MP) and constraint logic programming (CLP), which leads to a significant reduction in the search time necessary to find the optimal solution, and allows solving larger problems. The hybrid method appears to be not only as good as either of its components used independently but in most cases it is much more effective. The simplified models of cost optimization presented in the article illustrate the advantages of the approach. For these models, the use of hybrid approach allows obtaining optimal solutions ten times faster.

Keywords: constraint logic programming, mathematical programming, optimization, sustainable supply chain, decision support.

1 Introduction

Modern supply chains have evolved into highly complex structures with multiple layers of sourcing, planning levels, multimodality and extended information exchange at every link of the chain. The principal challenge of supply chain management is to maintain a regular and uninterrupted flow of goods, services, information, and financial resources while minimising costs. Along with complexity, enormous numbers of constraints relating to resources, time, production capacity, distribution capacity, transportation, etc. characterize today's supply chains. Until recently, the businesses had to contend with those challenges and constraints mainly in terms of short-term profits. Nowadays, given the new constraints related to the availability of non-renewable resources (coal, petroleum, natural gas, etc.), enterprises are more than ever obliged to rethink their strategies to ensure the sustainability of their operations. Another group of new constraints results from novel research areas dealing with the actions related to one or more phases of the product life cycle such as product design [6], production planning and control for remanufacturing [10], product recovery [7], reverse logistics and carbon emissions reduction [16]. Sustainable development means the interdependence between three aspects: the economic, the environmental, and the social performance of an enterprise. An integrated approach that links supply chain decisions to the three key elements of sustainability is the ultimate goal of sustainable

supply chain management (SSCM) [13]. Aggregation of the new challenges and re-definition of management goals and objectives have to result in the modification and expansion of decision and optimization models. Most decision and optimisation models for solving problems in supply chain management (SCM) [12] and in sustainable supply chain management are derived from the operations research (OR) areas, mathematical programming (MP) in particular. Due to a variety of constraint types and logical interdependencies between them, the constraint programming (CP) environment [1, 14, 3] can offer a very good framework for representing the knowledge and information needed for the decision support in SCM and SSCM.

The main contribution is to propose a hybrid approach (mixed MP and CP) with the transformation of the problem in the context of SSCM. In addition, showing the versatility and effectiveness of the hybrid approach to optimize the SSCM problems using Hybrid Solution Platform (HSP). At the end, the use of HSP in modeling and optimization of hybrid models is presented.

The remainder of the article is organized as follows. Research methodology and motivation are provided in Section 2. In Section 3 the hybrid solution platform is described and the implementation aspects discussed. Optimisation models presented as illustrative examples are provided in Section 4. Computational examples and tests of the implementation platform are presented in Sub-section 4.4. The possible extensions of the proposed approach as well as the conclusions are included in Section 5.

2 Methodology and Motivation

Based on numerous studies and our own experience, we strongly believe that the constraint-based environment [1, 14, 2, 20, 17], offers a very good framework for representing the knowledge, information and methods needed for the decision support. The central issue for a constraint-based environment is a constraint satisfaction problem (CSP), which is a mathematical problem defined as a set of elements whose states must satisfy a number of constraints. CSP represents the entities in a problem as a homogeneous collection of finite constraints over variables, which is solved using constraint satisfaction methods.

Constraint satisfaction problems on finite domains are typically solved using a form of search. The most widely used techniques include variants of backtracking, constraint propagation, and local search. Constraint propagation embeds any reasoning that consists in explicitly forbidding values or combinations of values for some variables of a problem because a given subset of its constraints cannot be satisfied otherwise [18]. Effective search for the solution in CSP problems depends considerably on the effective constraint propagation, which makes it a key method of the constraint-based approach. Constraint logic programming (CLP) is a form of constraint programming (CP), in which logic programming is extended to include concepts from constraint satisfaction. A constraint logic program contains constraints in the body of clauses. Constraints can also be present in the goal. These environments are declarative. The declarative approach and the use of logic programming provide incomparably greater possibilities for decision problems modelling than the pervasive approach based on mathematical programming (MP).

Based on [5, 8, 9] and our previous work [15, 21, 19], we observed some advantages and disadvantages of these environments. An integrated approach of constraint programming (CP) and mixed integer programming (MIP) can help to solve optimisation problems that are intractable with either of the two methods alone [4, 11].

Both MIP and finite domain CP/CLP involve variables and constraints. However, the types of the variables and constraints that are used, and the ways the constraints are solved are different in the two approaches [4].

In both MIP and CP/CLP, there is a group of constraints that can be solved with ease and a group of constraints that are difficult to solve. The easily solved constraints in MIP are linear equations and inequalities over rational numbers.

Integrity constraints are difficult to solve using mathematical programming methods and often the real problems of MIP make them NP-hard. In CP/CLP, domain constraints with integers and equations between variables are easy to solve. The system of such constraints can be solved over integer variables in polynomial time. The inequalities between variables, general linear constraints, and symbolic constraints are difficult to solve in CP/CLP (NP-hard). This type of constraints reduces the strength of constraint propagation. Both approaches, CLP and MP, use various layers of the problem (methods, the structure of the problem, data) in different ways. The MP approach focuses mainly on the methods of optimization and, to a lesser degree, on the structure of the problem. The data, however, is completely outside the model. The same model without any changes can be solved for multiple instances of data. In the CLP approach, due to its declarative nature, the methods are already in place. The data and structure of the problem are used for its modelling.

Observations above together with the knowledge of the properties of CLP and MP systems enforce the integration. The integration called hybridization consists in the combination of both systems and the transformation of the modelled problem.

The motivation underlying this research was to implement this approach as a hybrid solution platform to support managers in the modelling and optimization of decision problems in SSCM. This solution is better than using MP or CLP separately. What is difficult to solve in one environment can be easy to solve in the other. The hybrid approach allows the use of all layers/dimensions of the problem to solve it.

3 A Hybrid Approach – Concept and Implementation

The hybrid approach to modelling and optimization of decision problems in SSCM is able to bridge the gaps and eliminate the drawbacks that occur in both MP and CLP approaches. To support this concept, we propose the hybrid solution implementation platform (HSP), where:

- knowledge related to the sustainable supply chain can be expressed as linear and logical constraints;
- the novel method of constraint propagation is introduced (obtained by transforming the decision model to explore its structure);

- constrained domains of decision variables (domain solution), new constraints and values for some variables are transferred from the CLP into the MP system in order to optimize;
- efficiency of finding solutions to larger size problems is increased.

Linking various types of constraints in one environment and using the best and already proved problem optimization and transformation methods constitute the base of the hybrid solution platform architecture. The concept and architecture of this platform with its CLP-predicates and MP-procedures is presented in Fig. 1.

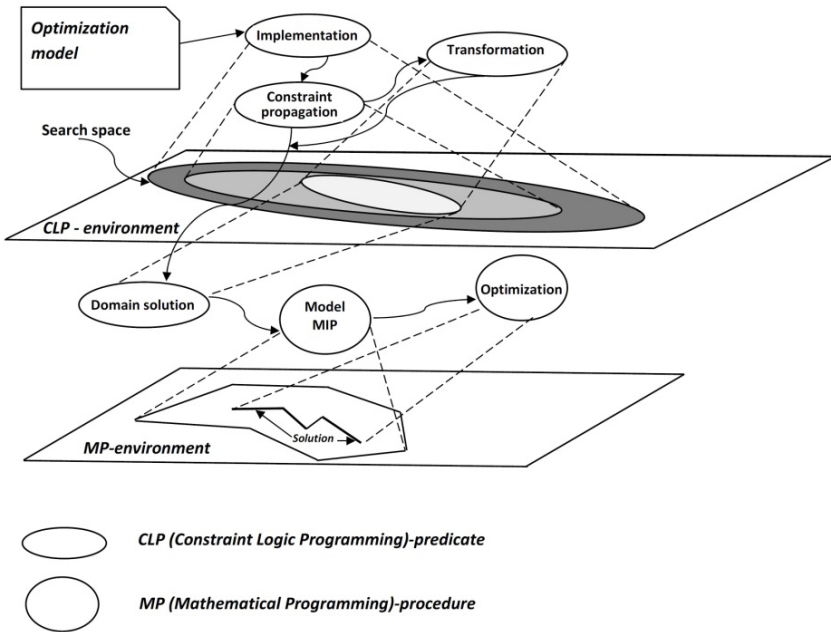


Fig. 1. Detailed scheme of the hybrid solution platform (HSP)

From a variety of tools for the implementation of CLP techniques in the hybrid solution platform, ECLⁱPS^c software [23] was selected. ECLⁱPS^c is an open-source software system for the cost-effective development and deployment of constraint programming applications. Environment for the implementation of MP in HSE was LINGO by LINDO Systems [22].

4 Illustrative Example

The HSP proposed was verified and tested for the illustrative example, which is the authors' original model of cost optimization for the supply chain with multimodal transportation and recycling.

The proposed model is the cost model taking into account different types of parameters, i.e., space (area/volume occupied by the product, distributor capacity and capacity of transportation unit, recycling centre capacity), time (duration of delivery and service by distributor, etc.) and a transportation mode. Multimodality in this example is understood as the possibility of using different modes of transportation: railway, commercial vehicles, heavy trucks, etc. It is a simplified SSCM problem in which financial and environmental dimensions are included. The environmental dimensions refer to both transportation and recycling. The introduced environmental costs of the use of the given transportation means are constant and dependent on the transportation means type. The additional environmental costs are hidden in the transportation costs and depend on the route followed and on the quantity of the goods transported. The simplified structure of the sustainable supply chain network for this example has been shown at the Fig. 2. The all parameters, indices, decision variables for illustrative model have been presented.

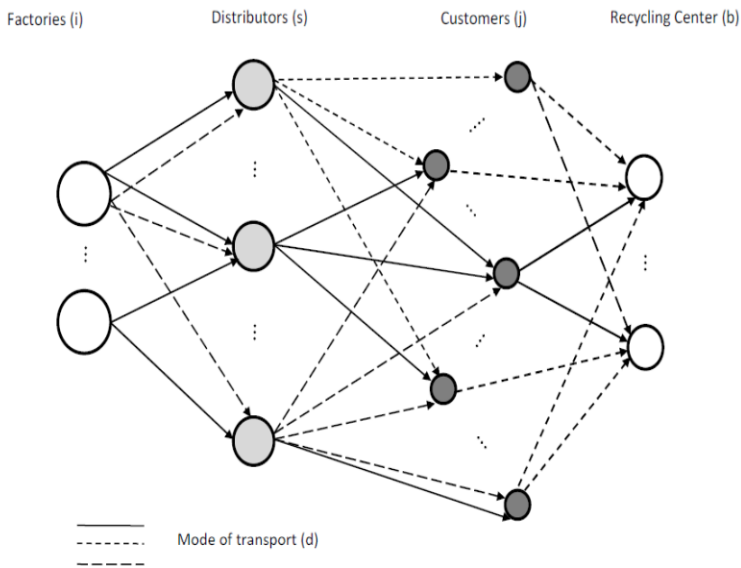


Fig. 2. The simplified structure of the sustainable supply chain network

4.1 Objective Function

The objective function (1) defines the aggregate costs of the entire chain and consists of nine elements. The first element comprises the fixed costs associated with the operation of the distributor involved in the delivery (e.g. distribution centre, warehouse, etc.). The second and eighth elements correspond to environmental costs of using various means of transportation. Those costs are dependent on the number of courses of the given means of transportation, and additionally, on the environmental levy, which in turn may depend on the use of fossil fuels and carbon-dioxide emissions. The third

component determines the cost of the delivery from the manufacturer to the distributor. Another component is responsible for the costs of the delivery from the distributor to the end user (the store, the individual client, etc.). The next component of the objective function determines the cost of manufacturing the product by the given manufacturer. The sixth component determines the fixed costs associated with recycling. The seventh component of the objective function represents the profit earned from the sale of products after recycling as the raw material for producers or suppliers. There is a minus sign next to it because the remaining components of the objective function are cost components, and the profit reduced the costs. The last component defines the costs of the product delivery from customers to the recycling centres.

$$\begin{aligned}
 & \sum_{s=1}^E (F_s \cdot Tc_s) + \sum_{d=1}^L Od_d \left(\sum_{i=1}^N \sum_{s=1}^E Xb_{i,s,d} + \sum_{s=1}^E \sum_{j=1}^M Yb_{j,s,d} \right) + \sum_{i=1}^N \sum_{s=1}^E \sum_{d=1}^L Koa_{i,s,d} + \\
 & \sum_{s=1}^E \sum_{j=1}^M \sum_{d=1}^L Kog_{s,j,d} + \sum_{i=1}^N \sum_{k=1}^O (C_{ik} \cdot \sum_{s=1}^E \sum_{d=1}^L X_{i,s,k,d}) + \sum_{b=1}^U (Fr_b \cdot Tb_b) - \tag{1} \\
 & \sum_{b=1}^U \sum_{k=1}^O (Cb_{bk} \cdot \sum_{j=1}^M \sum_{d=1}^L Zr_{j,b,k,d}) + \sum_{d=1}^L Od_d \left(\sum_{b=1}^U \sum_{j=1}^M Zb_{j,b,d} \right) + \sum_{j=1}^M \sum_{b=1}^U \sum_{d=1}^L Kr_{j,b,d} \cdot Zb_{j,b,d}
 \end{aligned}$$

4.2 Constraints

The model was based on constraints (2)–(23). Constraint (2) specifies that all deliveries of product k produced by the manufacturer i and delivered to all distributors s using mode of transportation d do not exceed the manufacturer’s production capacity. Constraint (3) covers all customer j demands for product k ($Z_{j,k}$) through the implementation of delivery by distributors s (the values of decision variables $Y_{j,s,k,d}$). The flow balance of each distributor s corresponds to constraint (4). The possibility of delivery is dependent on the distributor’s – constraint (5a) and recycling centres’ – (5b) technical capabilities. Time constraint (6) ensures the terms of delivery are met. Constraints (7a), (7b), (7c), (8) guarantee deliveries with available transportation taken into account. Constraints (9a), (9b), (10a), (10b), (10c), (11) set values of decision variables based on binary variables Tc_s , $Xa_{i,s,d}$, $Ya_{s,j,d}$, $Za_{j,b,d}$, Tb_b . The remaining constraints (14)–(23) arise from the nature of the model (MILP). Constraint (24) allows the distribution of exclusively one of the two selected products in the distribution centre s . Similarly, constraint (25) allows the production of exclusively one of the two selected products in the factory i . Similar constraint (26) prevents the simultaneous recycling of selected pairs of products. Those constraints result from technological, marketing, sales or safety and environmental reasons. Therefore, some products cannot be distributed and/or produced together. The constraint can be re-used for different pairs of product k and for some of or all distribution centres s , factories i and recycling centres b . A logical constraint like this cannot be easily implemented in a MILP model. Only declarative application environments based on constraint satisfaction problem (CSP) make it possible to implement constraints such as (24), (25), (26). Adding this type of constraints changes the model class. It is a hybrid model (1)–(26).

$$\sum_{s=1}^E \sum_{d=1}^L X_{i,s,k,d} R_{s,k} \leq W_{i,k} \text{ for } i = 1..N, k = 1..O \quad (2)$$

$$\sum_{s=1}^E \sum_{d=1}^L (Y_{s,j,k,d} \cdot R_{s,k}) \geq Z_{j,k} \text{ for } j = 1..M, k = 1..O \quad (3)$$

$$\sum_{i=1}^N \sum_{d=1}^L X_{i,s,k,d} = \sum_{j=1}^M \sum_{d=1}^L Y_{s,j,k,d} \text{ for } s = 1..E, k = 1..O \quad (4)$$

$$\sum_{k=1}^O (P_k \cdot \sum_{i=1}^N \sum_{d=1}^L X_{i,s,k,d}) \leq Tc_s \cdot V_s \text{ for } s = 1..E \quad (5a)$$

$$\sum_{k=1}^O (P_k \cdot \sum_{j=1}^M \sum_{d=1}^L Zr_{j,n,k,d}) \leq Tb_b \cdot Vb_b \text{ for } b = 1..U \quad (5b)$$

$$Xa_{i,s,d} \cdot Tf_{i,s,d} + Xa_{i,s,d} \cdot Tp_{s,k} + Ya_{s,j,d} \cdot Tm_{s,j,d} \leq Tc_{j,k} \quad (6)$$

for $i = 1..N, s = 1..E, j = 1..M, k = 1..O, d = 1..L$

$$Ra_{i,s,d} \cdot Xb_{i,s,d} \cdot Pt_d \geq X_{i,s,k,d} \cdot P_k \text{ for } i = 1..N, s = 1..E, k = 1..O, d = 1..L \quad (7a)$$

$$Rb_{s,j,d} \cdot Yb_{s,j,d} \cdot Pt_d \geq Y_{s,j,k,d} \cdot P_k \text{ for } s = 1..E, j = 1..M, k = 1..O, d = 1..L \quad (7b)$$

$$Zb_{j,b,d} \cdot Pt_d \geq Z_{j,b,k,d} \cdot P_k \text{ for } b = 1..U, j = 1..M, k = 1..O, d = 1..L \quad (7c)$$

$$\sum_{i=1}^N \sum_{s=1}^E Xb_{i,s,d} + \sum_{j=1}^M \sum_{s=1}^E Yb_{j,s,d} + \sum_{j=1}^M \sum_{b=1}^U Zb_{j,b,d} \leq Zt_d \text{ for } d = 1..L \quad (8)$$

$$\sum_{i=1}^N \sum_{d=1}^L Xb_{i,s,d} \leq CW \cdot Tc_s \text{ for } s = 1..E \quad (9a)$$

$$\sum_{j=1}^M \sum_{d=1}^L Zb_{j,b,d} \leq CW \cdot Tb_b \text{ for } b = 1..U \quad (9b)$$

$$Xb_{i,s,d} \leq CW \cdot Xa_{i,s,d} \text{ for } i = 1..N, s = 1..E, d = 1..L \quad (10a)$$

$$Yb_{s,j,d} \leq CW \cdot Ya_{s,j,d} \text{ for } s = 1..E, j = 1..M, d = 1..L \quad (10b)$$

$$Zb_{j,b,d} \leq CW \cdot Za_{j,b,d} \text{ for } b = 1..U, j = 1..M, d = 1..L \quad (10c)$$

$$\sum_{b=1}^U \sum_{d=1}^L (Zr_{j,b,k,d} \cdot Rb_{b,k}) = Z_{j,k} \text{ for } j = 1..M, k = 1..O \quad (11)$$

$$Koa_{i,s,d} = A_{i,s,d} \cdot Xb_{i,s,d} + \sum_{k=1}^O (Ka_{i,s,k,d} * X_{i,s,k,d}) \text{ for } i = 1..N, s = 1..E, d = 1..L \quad (12)$$

$$Kog_{s,j,d} = G_{s,j,d} \cdot Yb_{j,s,d} + \sum_{k=1}^O Kb_{s,j,k,d} \cdot Y_{s,j,k,d} \text{ for } s = 1..E, j = 1..M, d = 1..L \quad (13)$$

$$X_{i,s,k,d} \geq 0 \text{ for } i = 1..N, s = 1..E, k = 1..O, d = 1..L \quad (14)$$

$$Xb_{i,s,d} \geq 0 \text{ for } i = 1..N, s = 1..E, d = 1..L \quad (15)$$

$$Yb_{s,j,d} \geq 0 \text{ for } s = 1..E, j = 1..M, d = 1..L \quad (16)$$

$$X_{i,s,k,d} \in C \text{ for } i = 1..N, s = 1..E, k = 1..O, d = 1..L, \quad (17)$$

$$Xb_{i,s,d} \in C \text{ for } i = 1..N, s = 1..E, d = 1..L \quad (18)$$

$$Y_{s,j,k,d} \in C \text{ for } s = 1..E, j = 1..M, k = 1..O, d = 1..L \quad (19)$$

$$Yb_{s,j,d} \in C \text{ for } s = 1..E, j = 1..M, d = 1..L \quad (20)$$

$$Xa_{i,s,d} \in \{0,1\} \text{ for } i = 1..N, s = 1..E, d = 1..L \quad (21)$$

$$Ya_{s,j,d} \in \{0,1\} \text{ for } s = 1..E, j = 2..M, d = 1..L \quad (22)$$

$$Tc_s \in \{0,1\} \text{ for } s = 1..E \quad (23)$$

$$\text{ExclusionD}(X_{i,s,k,d}, X_{i,s,l,d}, s) \text{ for } k \neq l, s = 1..E \quad (24)$$

$$\text{ExclusionP}(X_{i,s,k,d}, X_{i,s,l,d}, i) \text{ for } k \neq l, i = 1..N \quad (25)$$

$$\text{ExclusionR}(Zr_{j,b,k,d}, X_{i,b,l,d}, b) \text{ for } k \neq l, b = 1..U \quad (26)$$

Table 1. Summary indices, parameters and decision variables

| Symbol | Description |
|----------------|---|
| <i>Indices</i> | |
| N | number of manufacturers/factories |
| M | number of customers |
| E | number of distributors |
| O | number of product types |
| L | number of mode of transportation |
| U | number of recycling centres |
| k | product type k = 1..O |
| j | delivery point/customer/city j = 1..M |
| i | manufacturer/factory i = 1..N |
| s | distributor /distribution centre s = 1..E |
| d | mode of transportation d = 1..L |
| b | recycling center b = 1..U |

Table 1. (continued)

| Input parameters | |
|---------------------------|--|
| F_s | the fixed cost of distributor/distribution center s |
| P_k | the area/volume occupied by product k |
| V_s | distributor s maximum capacity/volume |
| Vr_b | recycling center b maximum capacity/volume |
| $W_{i,k}$ | production capacity at factory i for product k |
| $C_{i,k}$ | the cost of product k at factory i |
| $R_{s,k}$ | if distributor s can deliver product k then $R_{s,k} = 1$, otherwise $R_{s,k} = 0$ |
| $Tp_{s,k}$ | the time needed for distributor s to prepare the shipment of product k |
| $Tc_{j,k}$ | the cut-off time of delivery to the delivery point/customer j of product k |
| $Z_{j,k}$ | customer demand/order j for product k |
| Zt_d | the number of transportation units using mode of transportation d |
| Pt_d | the capacity of transportation unit using mode of transportation d |
| $Tf_{i,s,d}$ | the time of delivery from manufacturer i to distributor s using mode of transportation d |
| $Ka_{i,s,k,d}$ | the variable cost of delivery of product k from manufacturer i o distributor s using mode of transportation d |
| $Ra_{i,s,d}$ | if manufacturer i can deliver to distributor s using mode of transportation d then $Ra_{i,s,d} = 1$, otherwise $Ra_{i,s,d} = 1$ |
| $A_{i,s,d}$ | the fixed cost of delivery from manufacturer i to distributor s using mode of transportation d |
| $Tm_{s,j,d}$ | the time of delivery from distributor s to customer j using mode of transportation d |
| $Kb_{s,j,k,d}$ | the variable cost of delivery of product k from distributor s to customer j using mode of transportation d |
| $Rb_{s,j,d}$ | if distributor s can deliver to customer j using mode of transportation d then $Rb_{s,j,d} = 1$, otherwise $Rb_{s,j,d} = 1$ |
| $G_{s,j,d}$ | the fixed cost of delivery from distributor s to customer j using mode of transportation d |
| Od_d | the environmental cost of using mode of transportation d |
| Fr_b | the fixed cost of recycling centre b |
| $Cb_{b,k}$ | the value of product k at recycling centre b |
| $Rc_{j,b,d}$ | if customer j can deliver to recycling centre b using mode of transportation d then $Rc_{j,b,d} = 1$, otherwise $Rc_{j,b,d} = 1$ |
| $Kr_{j,b,d}$ | the fixed cost of delivery from customer j to recycling centre b using mode of transportation d |
| $Rb_{b,k}$ | if recycling centre b can deliver product k then $Rb_{b,k} = 1$, otherwise $Rb_{b,k} = 0$ |
| $Ud_{j,k}$ | percentage coefficient of products number k delivered for recycling by customer j |
| Decision variables | |
| $X_{i,s,k,d}$ | delivery quantity of product k from manufacturer i to distributor s using mode of transportation d |
| $Y_{s,j,k,d}$ | delivery quantity of product k from distributor s to customer j using mode of transportation d |
| $Xa_{i,s,d}$ | if delivery is from manufacturer i to distributor s using mode of transportation d then $Xa_{i,s,d} = 1$, otherwise $Xa_{i,s,d} = 1$ |
| $Xb_{i,s,d}$ | the number of courses from manufacturer i to distributor s using mode of transportation d |
| $Ya_{s,j,d}$ | if delivery is from distributor s to customer j using mode of transportation d then $Ya_{s,j,d} = 1$, otherwise $Ya_{s,j,d} = 0$ |
| $Yb_{s,j,d}$ | the number of courses from distributor s to customer j using mode of transportation d |
| Tc_s | if distributor s participates in deliveries, then $Tc_s = 1$, otherwise $Tc_s = 0$ |
| Tb_b | if recycling centre b participates in deliveries, then $Tb_b = 1$, otherwise $Tb_b = 0$ |
| $Zr_{j,b,k,d}$ | delivery quantity of product k from customer j to recycling centre b using mode of transportation d |
| $Za_{j,b,d}$ | if delivery is from customer j to recycling centre b using mode of transportation d then $Za_{j,b,d} = 1$, otherwise $Za_{j,b,d} = 0$ |
| $Zb_{j,b,d}$ | the number of courses from customer j to recycling centre b using mode of transportation d |
| values calculated | |
| $Koa_{i,s,d}$ | the total cost of delivery from manufacturer i to distributor s using mode of transportation d |
| $Kog_{s,j,d}$ | the total cost of delivery from distributor s to customer j using mode of transportation d |
| Cw | arbitrarily large constant, for instance, the sum of all orders |
| Vx_s | the value corresponds to the distributor's real uptake capacity |

4.3 Model Transformation

The transformation is an important and inseparable part of the hybrid approach (see Fig. 1). Due to the nature of the decision and optimization problems in SCM, SSCM (adding up decision variables and constraints involving a lot of variables), the constraint propagation efficiency decreases dramatically. The idea was to transform the problem by changing its representation without changing the very problem. At the stage of transformation, the structure of, and maximum knowledge about the problem have to be used, including the knowledge about the orders, technical capacity of the producers, distributors and recycling centres. All permissible routes were first generated based on the fixed data and a set of orders, then the specific values of parameters i, s, k, d, b were assigned to each of the routes. In this way, only decision variables X and Z_r (deliveries) had to be specified. This transformation fundamentally improved the efficiency of the constraint propagation and reduced the number of backtracks and decision variables. This is due to the simple fact that it should be set-values for the two decision variables instead of seven. A route model is a name adopted for the models that underwent the transformation.

4.4 Numerical Experiments

In order to verify and evaluate the proposed approach, many numerical experiments were performed for the illustrative example. All the experiments relate to the supply chain with two manufacturers ($i = 1..2$), three distributors ($s = 1..3$), five customers ($j = 1..5$), three modes of transportation ($d = 1..3$), two recycling centres ($b = 1..2$), twenty types of products ($k = 1..20$), and five sets of orders (E1(5), E2(10), E3(15), E4(20), E5(25), (n) – the number of orders in set E). In order to compare the results and effectiveness of the HSP, the model was also implemented in mathematical programming environment (LINGO). The experiments were conducted to optimise examples E6(25), E7(25), which were the implementations of the hybrid model (with logical constraints) in the HSF.

Table 2. Results of numerical examples for both approaches

| E(No) | MILP-LINGO | | | | MILP-HSF | | | |
|------------|---|----------|------------|----------|-----------|----------|-----------|----------|
| | <i>Fc</i> | <i>T</i> | <i>V</i> | <i>C</i> | <i>Fc</i> | <i>T</i> | <i>V</i> | <i>C</i> |
| E1(5) | 8199 | 67 | 3485(2711) | 2297 | 8199 | 7 | 827(200) | 434 |
| E2(10) | 22558 | 84 | 3485(2711) | 2567 | 22558 | 9 | 889(256) | 440 |
| E3(15) | 32103 | 219 | 3485(2711) | 2837 | 32103 | 9 | 919(280) | 446 |
| E4(20) | 52691* | 900** | 3485(2711) | 3107 | 52547 | 45 | 946(304) | 452 |
| E5(25) | 54215* | 900** | 3485(2711) | 3371 | 53950 | 134 | 1018(376) | 452 |
| P(No) | Hybrid-HSF | | | | | | | |
| | <i>Fc</i> | <i>T</i> | <i>V</i> | <i>C</i> | | | | |
| E7(25) | 54129 | 195 | 1024(392) | 476 | | | | |
| E8(25) | 54322 | 201 | 1036(402) | 482 | | | | |
| Fc | the optimal value of the objective function | | | | | | | |
| T | solution search time | | | | | | | |
| V/C | the number of integer variables/constraints | | | | | | | |
| * | the feasible value of the objective function after the time T | | | | | | | |
| ** | calculation was stopped after T=900s | | | | | | | |

In example E6, the implementation of logical constraints for the hybrid model was as follows: product $k = 2$ cannot be distributed with product $k = 11$; product $k = 2$ cannot be distributed with product $k = 12$, and these products cannot be produced and recycling together. In example E7, the implementation of logical constraints for the hybrid model was as follows: product $k = 2$ cannot be shipped with product $k = 11$ and product $k = 2$ cannot be shipped with product $k = 12$.

The results of these experiments are shown in the Table 2. The use of the HSF helped achieve high efficiency at reduced computing time. For the sets with a smaller number of orders, E1(5), E2(10), E3(15), the optimal answer was found nine to twenty four times faster than when using LINGO. For larger sets, only the HSP was capable of finding optimal answers within acceptable time (below 900 s).

5 Conclusion

This paper provides a robust and effective hybrid approach to modelling and optimization of SSCM problems, implemented with the hybrid solution platform (HSP) which incorporates two environments (i) mathematical programming (LINGO) and (ii) constraint logic programming (ECLIPSe). The models presented as examples are transformed using the HSP, which results in the new representation of the problem. The application of this hybrid leads to a substantial reduction in (i) number of decision variables (up to four times), (ii) number of constraints (up to seven times) (iii) computing time (up to twenty four times). The proposed solution method with HSP is recommended for decision-making problems whose structure is similar to that of the presented models (Section 4). This structure is characterized by (i) constraints and the objective function in which decision variables are added up and (ii) logical constraints which are difficult to implement in mathematical programming-based models. In the versions to follow, implementation is planned of other supply chain layers such as remanufacturing, reverse logistic, etc. and agile supply chain [24].

References

1. Apt, K., Wallace, M.: Constraint Logic Programming using Eclipse. Cambridge University Press, Cambridge (2006)
2. Bocewicz, G., Nielsen, I., Banaszak, Z.: Iterative multimodal processes scheduling. *Annual Reviews in Control* 38(1), 113–132 (2014)
3. Bocewicz, G.: Robustness of Multimodal Transportation Networks. *Eksploatacja i Niezawodność – Maintenance and Reliability* 16(2), 259–269 (2014)
4. Bockmayr, A., Kasper, T.: A Framework for Combining CP and IP, Branch-and-Infer. *Constraint and Integer Programming: Toward a Unified Methodology Operations Research/Computer Science Interfaces* 27, 59–87 (2014)
5. Dang, Q., Nielsen, I., Steger-Jensen, K., Madsen, Q.: Scheduling a Single Mobile Robot for Part-Feeding Tasks of Production Lines. *Journal of Intelligent Manufacturing* (2004), doi:10.1007/s10845-013-0729-y
6. Hugo, A., Pistikopoulos, E.N.: Environmentally conscious long-range planning and design of supply chain networks. *Journal of Cleaner Production: Recent advances in Industrial Process Optimisation* 13(15), 1471–1491 (2005)

7. Jayaraman, V.: Production planning for closed-loop supply chains with product recovery and reuse: an analytical approach. *Intern. Journal of Production Research* 44(5), 981–998 (2006)
8. Kanyalkar, A.P., Adil, G.K.: An integrated aggregate and detailed planning in a multi-site production environment using linear programming. *International Journal of Production Research* 43, 4431–4454 (2005)
9. Lang, J.C.: *Production and Operations Management: Models and Algorithms, Production and Inventory Management with Substitutions*. Lecture Notes in Economics and Mathematical Systems 636, 9–79 (2010)
10. Luo, Y., Zhou, M., Caudill, R.J.: An integrated E-supply chain model for agile and environmentally conscious manufacturing. *IEEE/ASME Transactions on Mechatronics* 6(4), 377–386 (2001)
11. Milano, M., Wallace, M.: Integrating Operations Research in Constraint Programming. *Annals of Operations Research* 175(1), 37–76 (2010)
12. Mula, J., Peidro, D., Diaz-Madroneo, M., Vicens, E.: Mathematical programming models for supply chain production and transportation planning. *European Journal of Operational Research* 204, 377–390 (2010)
13. Seuring, S., Müller, M.: From a Literature Review to a Conceptual Framework for Sustainable Supply Chain Management. *Journal of Cleaner Production* 16, 1699–1710 (2008)
14. Sitek, P., Wikarek, J.: *New Frontiers in Applied Artificial Intelligence: A Declarative Framework for Constrained Search Problems*. LNCS(LNAD), vol. 5027, pp. 728–737. Springer, Heidelberg (2008)
15. Sitek, P., Wikarek, J.: A hybrid approach to modelling and optimization for supply chain management with multimodal transport. In: *International Conference on Methods and Models in Automation & Robotics – MMAR*, pp. 777–782 (2013)
16. Ramudhin, A., Chaabane, A., Paquet, M.: Carbon market sensitive sustainable supply chain network design. *International Journal of Management Science and Engineering Management* 5(1), 30–38 (2010), doi:10.1080/17509653.2010.10671088
17. Relich, M., Muszyński, W.: The Use of Intelligent Systems for Planning and Scheduling of Product Development Projects. *Procedia Computer Science* 35, 1586–1595 (2014)
18. Rossi, F., Van Beek, P., Walsh, T.: *Handbook of Constraint Programming (Foundations of Artificial Intelligence)*. Elsevier Science Inc., New York (2006)
19. Wikarek, J.: Implementation aspects of hybrid solution framework. In: Szewczyk, R., Zieliński, C., Kaliczyńska, M. (eds.) *Recent Advances in Automation, Robotics and Measuring Techniques*. AISC, vol. 267, pp. 317–328. Springer, Heidelberg (2014)
20. Sitek, P., Wikarek, J.: A Hybrid Approach to the Optimization of Multiechelon Systems, *Mathematical Problems in Engineering*, vol. 2015, Article ID 925675, 12 pages (2015), doi:10.1155/2015/925675
21. Sitek, P., Wikarek, J.: Hybrid Solution Framework for Supply Chain Problems. In: Omatu, S., Bersini, H., Corchado Rodríguez, J.M., González, S.R., Pawlewski, P., Bucciarelli, E. (eds.) *Distributed Computing and Artificial Intelligence 11th International Conference*. AISC, vol. 290, pp. 11–18. Springer, Heidelberg (2014)
22. Lindo Systems INC., LINDO™ Software for Integer Programming, Linear Programming, Nonlinear Programming, Stochastic Programming, Global Optimization, <http://www.lindo.com> (accessed August 12, 2014)
23. Eclipse, Eclipse – The Eclipse Foundation open source community website, <http://www.eclipse.org> (accessed august 12, 2014)
24. Grzybowska, K., Kovács, G.: Developing Agile Supply Chains – system model, algorithms, applications, Springer, Agent and Multi-Agent Systems. In: Jezic, G., et al. (eds.) *Technologies and Applications*. LNCS, pp. 576–585. Springer, Heidelberg (2012)

New Approach to Automation and Robotics Vocational Education in Support of Europe Reindustrialization

Michał Smater and Jacek Zieliński

Industrial Research Institute for Automation and Measurements PIAP,
Warsaw, Poland
{msmater, jzielinski}@piap.pl

Abstract. The post-industrial Europe cannot effectively fight the economic crisis. The Europa 2020 strategy goal is the advancement of the European Union economy which would be impossible without re-industrialisation. To reverse the declining role of industry, the re-industrialisation will notably be based on SMEs in which the production processes are not automated enough. In result the existing, as well as new companies will invest significant efforts in Automation and Robotisation (A&R) to minimise costs by eliminating manual work. The article presents the approach for preparation of the new generation vocational courses tailored especially to meet the needs and expectations of small and medium enterprises connected with introduction of new technologies, especially connected with Automation and Robotisation.

Keywords: automation, robotisation, e-learning, vocational training, reindustrialisation, SME.

1 Introduction

Reindustrialization of the European economy is a must. More and more people come to this conclusion, more and more new voices announces that there is no other way. The service based economy was a great mistake. There is no other way of strengthening the economy than creating goods the real one not virtual.

The Europe still suffers from economic crisis and if there will be no immediate actions performed to change the situation the crisis can last for a long time. One of the main reasons for that is based on a fact that the current, post-industrial, based on services, model of European economy does not have strong enough basement to fight the crisis efficiently. To overcome that one of the Europe 2020 strategy key priorities envisages advancement of the European economy. This was perceived by European Commission which in October 2012 announced communication to, among others, European Parliament 'A Stronger European Industry for Growth and Economic Recovery'. With the renewed industrial strategy outlined in this Communication, the Commission seeks to reverse the declining role of industry in Europe from its current level of around 16% of GDP to as much as 20% by 2020.

To achieve that goals the Europe must enter the path of sustainable development characterized by social inclusion and innovation which has to be supported by a

reindustrialization of Europe economies. This approach was remarked by the Report on EU competitiveness [1].

The reindustrialization will notably be based on manufacturing companies, especially SMEs and the main rationale for strengthening the manufacturing sector in Europe is rooted in evidence that the sector is the locus of significant innovation, which in turn also provide opportunities for growth in the service sector as well (in particular business services) [2]. The manufacturing sector can be still treated as the engine for modern economies because development in manufacturing has a multiplier effect on the growth of the economy [3]: a general increase in productivity of the manufacturing sector makes a contribution to the growth of GDP that is four times higher than that of other inputs.

The reindustrialization process requires new skills (in quantitative and qualitative terms) to support changes in technology and organizational models (within the companies and in their networks) [2] especially in SMEs where in comparison to large industrial enterprises, the production processes are not automated enough. These new skills can be nurtured in workplaces or their development can be incorporated in the educational pathway (beginning from the secondary level). New skills are also needed by the labour force already employed or seeking employment, and both the companies and training organizations, until now devoted to the adult training, can be better integrated with the general education system.

All of this means that, in near future, the market demand for high qualified specialists for different industry branches will explode.

Unfortunately, European education and training systems still do not provide proper skills for people employability. Moreover, there is no cooperation with business or employers to make the learning experience closer to the reality of working environment [4]. The education system changes are necessary and foreseen. However, it will be rather long time process; evolution not a revolution. There is still a place for smaller independent of the system initiatives providing focused on skills vocational trainings. The advantage of such initiatives is that they require much shorter time to appear and less efforts to sustain and with utilization of modern ICT technologies their impact is over national [5]. Over one year ago a consortium of several institutions from different European countries seeing the necessity of increasing skills for employability in reindustrialized Europe launched such initiative to elaborate vocational training system for automation and robotisation education for small and medium enterprises [6].

SMEs (small and medium-sized enterprises) represent 99% of all businesses in Europe and account in average for more than 60% of the employment and turnover figures (Source: European Small Business Survey, 2012). However only 24% of SMEs provide vocational education and training compared to 80% of large enterprises (employing over 250 people). SMEs play a key role in generating employment and creating economic wealth, but skill deficiencies in SMEs are adversely affecting their ability to reach their growth potential. Today more than ever before, the skills, motivation and activation of employees are crucial preconditions for the sustainable success, productivity and innovation of enterprises. However, the situation of SMEs with regard to training is characterized by a paradox. On the one hand, continuous training

and lifelong learning (both for workers and managerial staff) are regarded as crucial elements of competitiveness against the backdrop of globalization. On the other hand however, statistics show that continuous training and qualifications are less likely to be available to employees working in SMEs than to those in large companies [7]. By their very nature, SMEs are small, constrained by time and budget and reluctant to engage in learning/training programs.

2 Building the Concept

The main initial assumption for new vocational education platform was that it will be based entirely on an e-learning solution. To assure as much as possible system functionalities and education content matching requirements of current skills demand the consortium adopted one of agile software development methodologies for the system development where close collaboration with stakeholders and potential end-users is one of the significant priority. The initial, general system concept required polishing and enrichment with details. At the beginning the end-users needs and requirements research was done.

Consortium partners have elaborated and distributed among project target groups a detailed questionnaire for requirements gathering and needs analysis regarding the way to plan and improve skills and professional knowledge for SMEs.

A total of 103 questionnaires were filled by the target groups: SMEs managers, employees, trainers and consultants involved in automation and manufacturing jobs. The answers were distributed among the partner countries as follows: 36 from Bulgaria, 25 from Italy and 42 from Poland. The answers collected at the end of survey analysis allowed achieving a good level of knowledge about SMEs needs in the automation and robotics training field.

The results of the survey illustrate how professional associations and consultants may contribute to the use of e-learning technologies for SMEs. It also shows that – besides significant cost savings – there are further advantages that make the use of e-learning technologies attractive. In fact online learning can provide several good opportunities to SMEs in overcoming part of their technological, environmental, organizational, and managerial inadequacies.

Savings of travel or hotel costs are an obvious advantage of e-learning compared to face-to-face seminars. There are, however, also a number of other benefits, which are less easy to express in numbers but that have been also frequently reported by the target groups' feedback:

- Time independence. Learning activities can be carried out in the evening or during the weekend. Thus, managers and employees are not inhibited in their daily work routine.
- Focus. In their daily work, managers and employees are used to focusing on the essentials. This working style is better supported by e-learning than by face-to-face seminars. Participants can concentrate on the specific Automation learning goals, in which they are interested.
- Learning at one's own pace. Participants of e-learning courses can take the time they need to assimilate learning material. By contrast, during seminars participants

are often reluctant to ask several times about the same problem, even if they have not yet understood it.

- Advanced learning culture in SMEs. The application of e-learning as part of the learning opportunities in a SME company leads to developing new learning culture. Compared to face-to-face seminars, e-learning allows for a prompt realization of the knowledge acquired. Consultants therefore interact more often and exchange information more frequently than was the case when attending face-to-face seminars.

The responders expressed their expectations for the future online course. They were based on their preferences and supported by a real assessment of the possibilities for course participation. First of all they expect flexible time and place for conduction for the course supported by well-structured materials on interesting and useful topics.

Simulations, good practices and exercises were also expected. Participants requested that the information presented will be practical and specific and not general. What respondents wanted as a result of the course was to improve their qualification and to widen their worldview. Maximum interactivity and availability of links to other sites was also recommended. There should be no excessive audio and visual effects, and still the information has to be detailed enough, if necessary there should be graphs (pictures) and video clips. Respondents also expect the course to be practically oriented, to present different case studies and to encourage the application of the learned in the production process, not to be only theoretical. The course has to be conducted with a real lecturer but in virtual environment, in real time in order to follow the results of the training, as well as online training with video materials.

From the analysis of the ARIALE questionnaires on end users requirements, several interesting conclusions can be drawn:

- The target group involvement in competence development and learning contents improvements can have a very positive effect on the individual SME's competitiveness and performance.
- Formal methods of teaching and learning are not necessarily the most appropriate way of engaging, motivating and transferring knowledge to SMEs workforce. So formal training is not the best way of learning for SMEs. Instead, non-formal and informal learning can constitute the most important way of acquiring and developing the skills and competencies required at work.
- Training activities have to be focused on the specific needs of the SMEs for example giving the possibilities to assemble the learning contents available in the platform. An active learning approach focuses on solving real problems and the employees' needs.
- The SMEs' heads frequently own a negative attitude to change and learning. In many cases, time devoted to learning activities is considered as lost time. When employees are involved in the learning process dealing with issues of relevance to their careers they become motivated learners. To get effective motivation the learner should be put in the centre of learning.
- SMEs are driven primarily by profit and they are focused especially on bottom line. The role of promotion is very essential. No matter how good the training and

support material, it has to be carefully promoted from the head and delivered to be effective. It must go to considerable lengths to highlight the commercial benefits of business improvement (non-commercial benefits can be promoted as secondary benefits once the main commercial message has been thought).

- Learning for many SMEs' heads has seen unfortunately as a cost, and they do not always consider it as an investment for the future. The curricula should have a measurable impact within the organisation and should be affordable and value for money.
- SMEs use a short-term approach; they only set up a training action plan on Automation or Robotics only when they face meet problems. Approaches to learning, training and development in small firms needs to take account of the shorter planning time frames they use by relating learning opportunities and benefits to these shorter periods.
- Some of the advantages of e-learning directly address the needs of SME's: flexibility, cost benefits, location is not a barrier, freedom to work at own pace, less disruption to work schedules.
- An informal environment should be built to aid networking. The network should provide a forum for exploring ideas with peers, and give support to individuals. Network learning broadens access and participation of SMEs in real-life learning environments. Network technology offers the opportunity to facilitate, strengthen and connect SMEs in order to build and enhance networks of business at the regional, national, or international level [8].

The user requirements survey results was also used to specify e-learning system shape and features. Answers was grouped in three categories: course delivery and organization, communication in the course, course content. It is very interesting that despite the survey was done in three such a different countries the answers were very similar In most questions only small, negligible differences were observed only for some questions differences were noticeable but still answers were very similar.

Most respondents prefer web forms or e-mails for course registration. Fax or telephone were not very popular answer. It can be concluded that such way of communication seems rather old fashioned and not very convenient nowadays. Trainees should have possibility to assess their knowledge level before attending to the course to check if the new knowledge is appropriate for them. Minor differences were observed between countries regarding way of knowledge assimilation assessment. However most respondents prefer test questions after each lessons. Very important for the questioned potential end-users was overall system functionality and user friendly interface of the e-learning system. It should be simple, easy to learn its logic and to navigate. Respondents opt for clear introduction to the course explaining benefits for learner, scope of the knowledge and logical structure of learning modules and lessons. Each lesson should also have short introductory description. Access to entire course should not be restricted in any way, learner should have possibility to stop learning any lesson at any time and start another module/lesson. At the end of the course a certificate of course completion should be issued, but only for students who achieved at least 80% of proper answers for test questions. The system should have the possibility to provide courses for organized groups of students with supervision of the teacher/instructor.

Such events should have an introductory presentation given by the teacher. All respondents were interested in obtaining course materials off-line e.g. On CD-ROM. Practical tasks, e-tasks or out-of-class work were also considered as highly useful and helpful in the learning process.

For the communication channel between learners and between learners and teachers the online discussion forum and e-mails were chosen. Only for Italy respondents prefer the videoconferencing. Very important were e-participation, e-collaboration and virtual classroom. The system should allow such functionality. The learning process should be supported by teacher/instructor. It was not considered as necessary to have such support on-line. Just e-mail contact is satisfactory. But an online discussion functionality should be assured by the system. Teachers should have possibility to monitor course participants progress.

Regarding the course content answers in each country were most consistent. Course content must be arranged in clear and logical order. Learning goals and objectives should be clearly presented at the beginning of each lesson. Course content should contain as much as possible practical knowledge. The questionnaire presented proposed course structure and thematic scope. It was considered by the respondents as highly usable and should be followed in further development.

3 Prototype Implementation

At the early stage of the initiative the hardware server was carefully selected. The basic condition for it was to ensure high level of data safety. The installed server hardware contains 3 hard disks configured in RAID 5 array. Such configuration ensures very high data security with reasonable storage area management in comparison to other RAID arrays levels. In case of one disk failure the entire array work without interruption and all the data is continuously available. Only read/write performance of the array is decreased during the time of new disk replacement. Other server hardware specifications were at secondary importance, however it was considered that the server should ensure comfortable work in moderate internet connection load.

The server was installed at PIAPs premises and connected to the Internet by the local PIAP-LAM network.

As the operating system Linux Debian distribution was chosen. The open source solutions allows to decrease overall server costs. Debian is one of the most stable and secure Linux distributions available. The complete software configuration necessary to establish e-learning system comprises:

- operating system Debian Wheezy (last, most stable release)
- web server Apache 2
- data base MySQL
- script language interpreter PHP
- Moodle LCMS

All software components are continuously monitored and upgraded to the last, most stable and safe releases.

Then based on above mentioned identified target audience needs and requirements the first prototype instance of an e-learning system with chosen training materials was developed. A set of learning objects was implemented to newly established e-learning platform. The vast range of knowledge related to automation and robotics was divided and grouped in six major thematic modules:

- ICT based means for automation and innovation
- Sensors in industrial automation
- Actuators in industrial automation
- Application of PLC in industrial automation
- Industrial networks and interfaces in industrial automation systems
- Industrial robots in automation systems

The main goal of technical development was to establish initial version of the e-learning system containing lessons in English language and to prepare the system for testing by end-users.

The screenshot shows the ARIALE system front page. At the top, there is a green header with the ARIALE logo and navigation options like "Theme colours" and "Log in". Below the header is a large image of an industrial robot arm in a factory setting. A green banner below the image contains the text: "Robotics: Industrial robots allow to perform tasks often impossible to be done by humans. Robots can carry heavy loads, work in extremely adverse environment like welding/cutting with plasma, painting with toxic chemicals, etc. while keeping high accuracy and work pace." To the left of the main content is a navigation sidebar with "Home" and "Courses" links, a welcome message, and a calendar for November 2014. The main content area is titled "Available courses" and lists three course categories: "Automatisation and Robotisation for SME (Workers)", "Automatisation and Robotisation for SME (Trainers and Consultants)", and "Automatisation and Robotisation for SME (Managers)". Each category has a brief description of the course content.

Fig. 1. ARIALE system front page

The ARIALE system front page presents list of available courses for three target groups:

- SME managers,
- SME workers,
- Trainer and consultants.

The access to each course is restricted only for authorized users. Once the visitor chooses a course he is redirected to the login page.

Fig. 2. Course structure

At the top of the page there is an area where news from discussion forum are presented. The user has access to the discussion forum where users can exchange opinions on the topics related to the course. On the left side of the page there is navigation menu allowing user to navigate through entire course content. This menu is also available in the lesson presentation pages.

The final version of the course will offer flexible array of activities including forums, glossaries, resources, chats and workshops. Students will be able to participate in those activities, contacting teachers or other students on- and off-line and this kind of a collaboration provides a way for experienced individuals to learn and share their knowledge. Some tools as discussion boards will also be capable of capturing knowledge and also will function as document repositories for storing files and searching for information and files.

Together with the e-learning system accompanying methodology is developed based on the previous approaches researched and successfully used by project partners in similar cases. Elaborated methodology comprises of detailed instructions

necessary to create and adapt course content, establish the ICT system and implement the content as well as to organise and execute the course.

4 Conclusions

The overall conclusion of the survey on SMEs was that it is possible to involve successfully them by using an engagement strategy that communicates needs and addressing their current automation problems. The combination of face-to-face and virtual action learning (blended learning) can work well, and help to encourage the SMEs to join online courses. The need for a clear structure of the curricula was underestimated and in the future, more attention should be given to informing potential participants on the structure, tasks and the expectations of their involvement.

There is also a need of tutors and/or facilitators to be in communication almost on a daily basis and use a flexible style to motivate the participants.

At present times vocational education of automation and robotics needs to be fast and efficient and shall maintain a balance between theory and practice tailored especially for chosen target audience. The solution which is being developed will be an answer to those requirements. The system shall now be tested by end-users for the compliance with requirements research done at the beginning.

Acknowledgements. Project “Automatization, Robotization for New Reindustrialized Europe (acronym ARIALE)” has been funded with support from the European Commission under the Lifelong Learning Programme. This publication reflects the views only of the authors, and the Commission cannot be held responsible for any use which may be made of the information contained therein.

References

1. European Commission. Directorate-General for Enterprise and Industry: European Competitiveness Report. Towards Knowledge-Driven Reindustrialisation, Commission Staff Working Document SWD (2013)
2. Mengoli, P., Russo, M.: Innovation in education and re-industrialisation in Europe. DEMB Working Paper Series, vol. 35 (July 2014)
3. Berger, S.: Making in America. From Innovation to Market. MIT Press, Cambridge, Mass (2013)
4. Communication from the Commission to the European Parliament, the Council, the European Economic and Social Committee and the Committee Of The Regions, Rethinking Education: Investing in skills for better socio-economic outcomes (2012)
5. Słowikowski, M., Zieliński, J.: Dissemination and support the implementation of innovative solutions in automation and robotics through the application of innovative solutions and training methods. *Pomiary Automatyka Robotyka (PAR)* 5, 144–147 (2014), ISSN 1427-9126

6. Information about project: Automatization, Robotization for New Reindustrialized Europe, ARIALE (2014), <http://www-ariale.eu>
7. 2009Guide for Training in SMEs, <http://ec.europa.eu/social/BlobServlet?docId=3074&langId=en>
8. Casalino, N., Gaspari, C., Taranto, G.: Public Report on Manufacturing SMEs Requirements with respect to Training of Automation. Robotisation (2014), <http://www.ariale.eu>

Ship Maneuvering Model for Autopilot Simulator

Andrzej Stec

The Faculty of Electrical and Computer Engineering
Rzeszow University of Technology, Rzeszow, Poland
astec@kia.prz.edu.pl

Abstract. The paper presents a ship maneuvering model which can be used in autopilot simulators for testing new algorithms. The ship model implements both ship dynamics and waves. The motion response amplitude operator (RAO) is used for calculating motion disturbances.

Keywords: ship maneuvering model, waves model, Motion RAO, autopilot.

1 Introduction

At the design stage, using of plant simulators is a very reasonable idea. It allows us to test software algorithms, especially in case of lacking the real plant, or speeding up the process of its creation. It is also a good solution when experiments take a lot of time or due to security aspects. By using the simulator you do not need to worry about causing physical damage of the plant, which can have serious financial consequences.

If you create specialized or unusual solutions, you often do not have the plant model ready to use. Sometimes, it is possible to find a similar project, but without the possibility of its customization. Advanced commercial solutions are powerful, but often too expensive. Hardware or software constraints of the target device may also be an issue.

The paper presents a ship maneuvering model used to help in creation of the autopilot software [1] developed as a result of cooperation with Praxis Automation Technology B.V. from the Netherlands. The target device is based on the ARM7 microcontroller and programmed in the IEC 61131-3 ST language of CPDev software [2]. The model has been implemented as a part of this software for plant simulation or wave motion filtering.

2 Ship Dynamics

The motion of a ship is usually considered in six degrees-of-freedom. Three of them are in horizontal plane (surge, sway, and heave), while the remaining ones (roll, pitch, and yaw) describe orientation. To derive the motion equations, two coordinate systems are considered: inertial (the North-East-Down frame) and body-fixed (Fig. 1). The first is defined relative to the earth's reference ellipsoid, while the other is connected with ship-fixed coordinates. The position $[x \ y \ z]^T$ and orientation $[\varphi \ \theta \ \psi]^T$ of

the ship are usually described in the inertial frame. Linear velocities $[u \ v \ w]^T$ and angular velocities $[\varphi \ \theta \ \psi]^T$ are most often expressed in body-fixed frame. There is also a transformation matrix which relates both frames with each other.

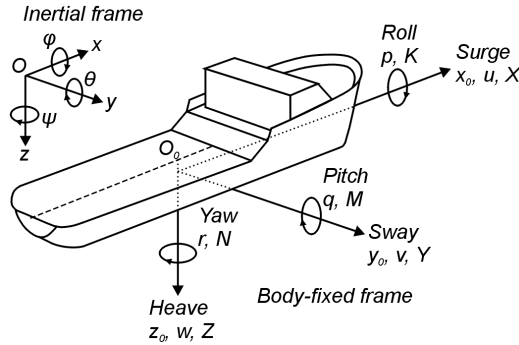


Fig. 1. Coordinate system (SNAME 1950)

The full nonlinear model of motion is described by six equations, and each of them represents a mass-damper-spring system. These equations can also be expressed in matrix-vector form (1) [3]

$$\mathbf{M}\dot{\mathbf{v}} + \mathbf{C}(\mathbf{v})\mathbf{v} + \mathbf{D}(\mathbf{v})\mathbf{v} + \mathbf{g}(\boldsymbol{\eta}) + \mathbf{g}_0 = \boldsymbol{\tau} + \boldsymbol{\tau}_{\text{wind}} + \boldsymbol{\tau}_{\text{wave}} \tag{1}$$

where

- \mathbf{v} – generalized velocity $[u \ v \ w \ p \ q \ r]^T$
- $\boldsymbol{\eta}$ – position and Euler angles $[x \ y \ z \ \varphi \ \theta \ \psi]^T$
- $\mathbf{M} = \mathbf{M}_{RB} + \mathbf{M}_A$ – system inertia matrix (*rigid-body + added mass*)
- $\mathbf{C}(\mathbf{v}) = \mathbf{C}_{RB}(\mathbf{v}) + \mathbf{C}_A(\mathbf{v})$ – Coriolis and centripetal matrix
- $\mathbf{D}(\mathbf{v})$ – damping matrix
- $\mathbf{g}(\boldsymbol{\eta})$ – gravitational/buoyancy forces
- \mathbf{g}_0 – ballast control
- $\boldsymbol{\tau}$ – control forces
- $\boldsymbol{\tau}_{\text{wind}}, \boldsymbol{\tau}_{\text{wave}}$ – wind and wave forces

When the sea currents are considered, same modifications of (1) are needed.

The large number of matrix coefficients in Eq. (1) causes that such a model is very complicated. Some of the coefficients may be obtained from sea trials, some of them may be estimated from experiment for the physical model (e.g. scale 1:70) in the pool. Another very reasonable solution is to use advanced software (e.g. VERES or WAMIT) analyzing the shape of the hull and basic parameters of the ship. Unfortunately, the software is usually very expensive, and used mainly by companies involved in ship designing. Models available in publications usually describe only

selected aspects of the problem. Without the knowledge about all of the factors, it is difficult to compare the results with others.

One of the advanced, complete and opened projects involving many aspects of marine technology is Marine Systems Simulator [4]. Authors of the project provide detailed data for ship models, library tools and sample programs in Matlab/Simulink. One of the models, after some modifications and added functionalities, is used for the presented work.

The ship maneuvering models usually ignore heave and pitch motion. It allows reducing the number of degrees of freedom to four (4-DoF). When the roll motion is ignored as well, the model becomes the 3-DoF model, which in most cases is good enough.

The ship dynamics model from (1) is generally nonlinear, and is often replaced by a linear one. For ship maneuvering, the most important relation involves yaw angle (or yaw rate) and rudder angle. Assuming some simplifying assumptions, such a relation can be reduced to a transfer function (2) [5].

$$\frac{r}{\delta} = \frac{K(T_3s+1)(s^2 + 2\eta\omega_0s + \omega_0^2)}{(T_1s+1)(T_2s+1)(s^2 + 2\xi\omega_n s + \omega_n^2)} \quad (2)$$

Quadratic factors represent the coupling effect from the roll mode on the yaw rate. The zero (T_3s+1) and the pole (T_2s+1) are due to the coupling effect from the sway mode on the yaw dynamics. If the roll mode is neglected, equation (2) can be further reduced to the following form.

$$\frac{r}{\delta} = \frac{K(T_3s+1)}{(T_1s+1)(T_2s+1)} \quad (3)$$

Equation (3) is known as the 2nd order Nomoto model in which K is the static yaw rate gain, while T_1 , T_2 and T_3 are time constants. Because the pole term (T_2s+1) and the zero term (T_3s+1) in (3) nearly cancel each other, a further simplification is allowed to give the 1st order Nomoto model.

$$\frac{r}{\delta} = \frac{K}{(Ts+1)} \quad (4)$$

where $T=T_1+T_2-T_3$ is called the effective yaw rate time constant. To derive the yaw angle ψ , the yaw rate ($r=d\psi/dt$) needs to be integrated. Finally, the relation can be presented in the following form.

$$\frac{\psi}{\delta} = \frac{K}{s(Ts+1)} \quad (5)$$

The gain and the time constant of (4) can be derived from standard zig-zag or circle tests. They are done during sea trials, and from time to time during normal maneuvers of the ship. However, the transfer function parameters change with speed of

the ship, so it is necessary to alter them continuously while sailing. It is a common practice in commercial autopilots.

In fact, there are two implementations of the ship dynamics presented in the solution. The first is the nonlinear model of the S-175 container, based on data from [6], [4], and the second one which is based on (5), i.e. the 1st order Nomoto model. Parameters of the second model are obtained from the zig-zag test of the container ship model. The gain and time constant are as follows: $K = 0045$, $T = 19$ sec. Implementation of the autopilot's function block is supplemented by a simple steering machine model, which restricts rudder rate and angle to proper limits.

3 Sea Waves

The main distort acting on the vessel are waves. Their height depends on the strength of the wind and its duration. The impact on the ship depends on the vessel characteristics (e.g. dimensions and weight), but also on its speed. The wave angle of attack is also important (Fig. 2).

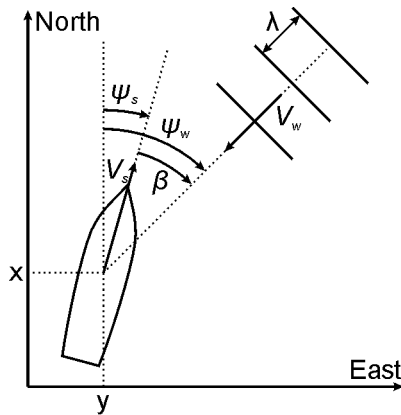


Fig. 2. Considered wave-ship headings

The long-crested wave elevation under assumption of zero speed can be written as a sum of N components.

$$\zeta(t) = \sum_{k=1}^N \zeta_k \sin(\omega t + \varepsilon) \tag{6}$$

In case of the ship moving at forward speed V , the encounter frequency of incident wave changes its value according to (7). It is also shown in Fig. 3.

$$\omega_e = \omega + \frac{\omega^2 V}{g} \cos(\beta) \tag{7}$$

where β is a wave angle of attack.

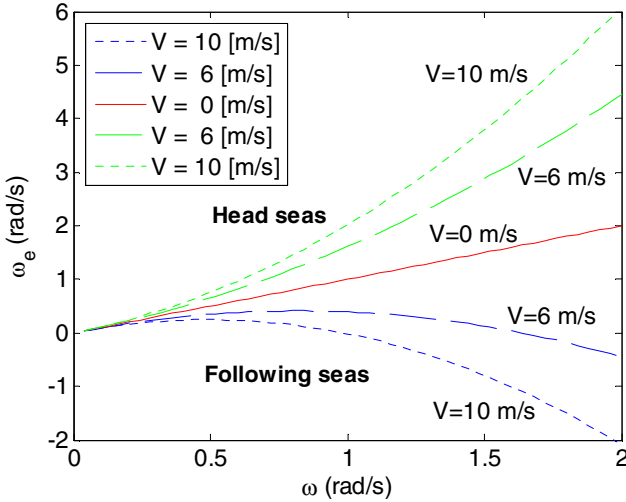


Fig. 3. Encounter frequency vs. wave frequency

Equation (7) assumes that the ship changes its position only due to forward speed without heading change. The more general equation takes into account any position in the wave area regardless of the ship’s speed and orientation

$$\zeta(x, y, t) = \sum_{k=1}^N \zeta_k \sin(\omega t + kx \cos(\beta) + ky \sin(\beta) + \varepsilon) \tag{8}$$

where $k=\omega^2/g$ is the wave number, and x, y are coordinates of the ship position moving through the water.

According to the Modified Pierson-Moskowitz wave spectrum, recommended by ITTC for a fully developed sea, the wave energy can be calculated as

$$S(\omega) = \frac{A}{\omega^5} \exp\left(-\frac{B}{\omega^4}\right), \quad A = 173 \frac{H_s^2}{T_1^4}, \quad B = \frac{691}{T_1^4} \tag{9}$$

where T_1 is the average wave period. A relation between wave spectrum and significant wave height (H_s) is shown in Fig. 4.

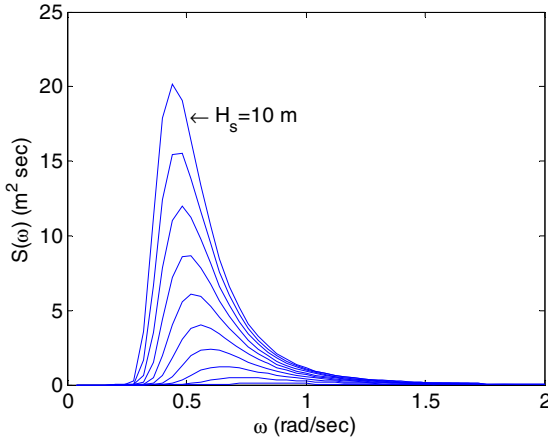


Fig. 4. Wave spectrum vs. wave frequency and significant wave height

The wave elevation for long-crested sea receives the form

$$\zeta(x, y, t) = \sum_{n=1}^N \sqrt{2S(\omega_n)\Delta\omega} \cos(\omega_n t + \varepsilon_n + k_n(x \cos(\beta) + y \sin(\beta))) \quad (10)$$

The main task for the autopilot is to maintain a constant heading angle (yaw angle) while external conditions may vary. This is obtained by rapid rudder deflections in response to waves or wind. To prevent unnecessary deflections of the rudder, yaw signal must be filtered out. However, the encounter frequency varies with the speed and waves direction. It is important to adjust the filter parameters to the encounter frequency.

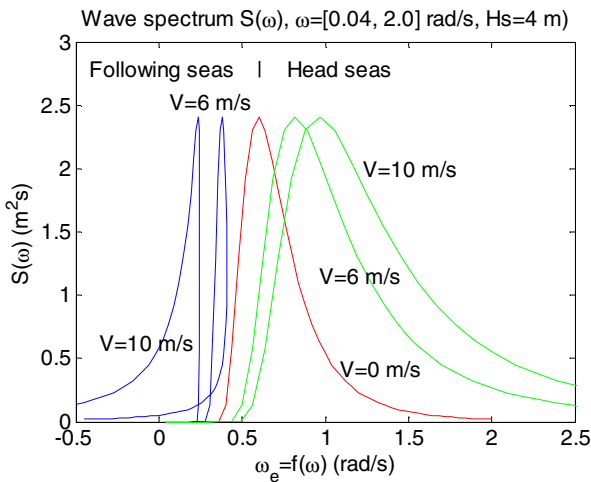


Fig. 5. Wave spectrum vs. encounter frequency

Figure 5 shows dependence of the spectral density as a function of encounter frequency, for a few speeds of the ship. Positive values ω_e mean head seas, while negative – following seas. It should be noted that the encounter frequency of the following seas may change into head seas as the speed of the ship increases.

4 Response Amplitude Operators

There are two kinds of Response Amplitude Operators (RAOs), namely Wave Force RAO and Motion RAO. The first relates wave amplitude with forces acting on the hull of the ship, while the other relates wave amplitude with motions of the hull. Force RAO permits computing both the 1st order wave-induced forces (wave frequency forces) and the 2nd order wave drifts. Motion RAO allows to compute only the 1st order wave-induced positions (wave frequency motions). Those RAOs can be computed by special hydrodynamic programs with results usually returned as data tables [7]. The user receives six tables (one for each degree-of-freedom) for wave frequency (WF) forces and motions, and three tables for wave drift (WD) [8]. Values in tables for forces and motions depend on wave frequency, wave attack angle and ship's speed. Values are proportional to wave amplitude.

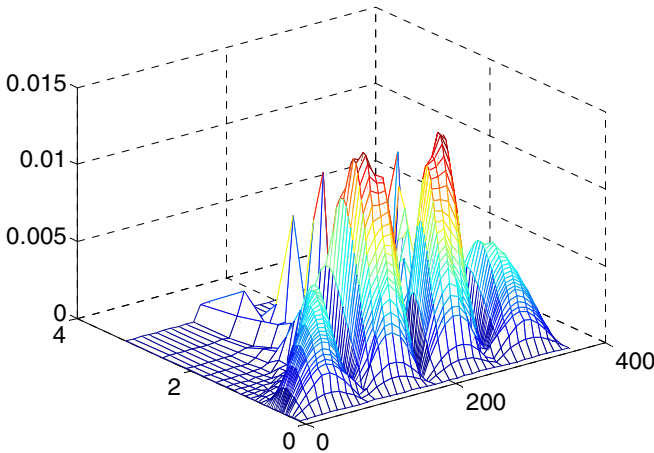


Fig. 6. Motion RAO table for S-175 ship model as 3D chart (velocity 10.3 m/s)

The presented model of the ship implements functionality of the Motion RAO for yaw angle only, which is the most important for control purposes. Because of hardware constraints and small software resources of the autopilot, the model calculates wave-induced yaw disturbances basing on simple equations, which approximate the Motion RAO table. Instead of complicated and time consuming calculations or large-size tables, a few equations similar to (11) are proposed.

$$\psi_{RAO} = \frac{k\omega_n^2\omega}{\sqrt{(\omega_n^2 - \omega^2)^2 + (2\xi\omega_n\omega)^2}} (1 - \tanh(V_s/6)\cos(\beta)) \tag{11}$$

In case of S-175 container values of the coefficients are as follows: $k = 0.16$, $\omega_n = 0.6$, $\xi_n = 0.5$. Figure 7 shows the result of calculations for the same ship model as in Fig. 6. In similar way, values for other velocities can be computed.

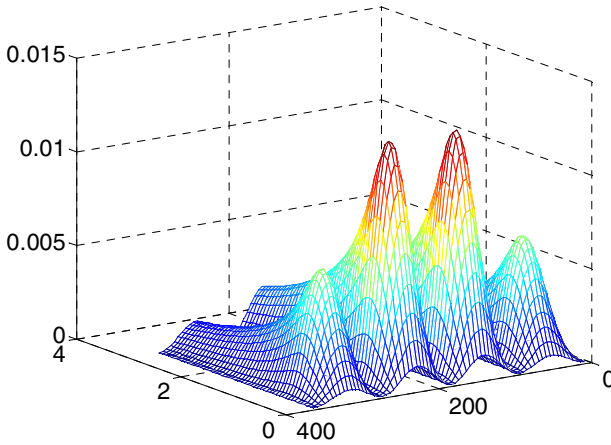


Fig. 7. Motion RAO table for S-175 ship model calculated with (11)

5 Ship Model with Waves

The function block diagram for control purposes with maneuvering ship model is shown in Fig. 8. The main blocks are: ship dynamics, waves model and motion RAO.

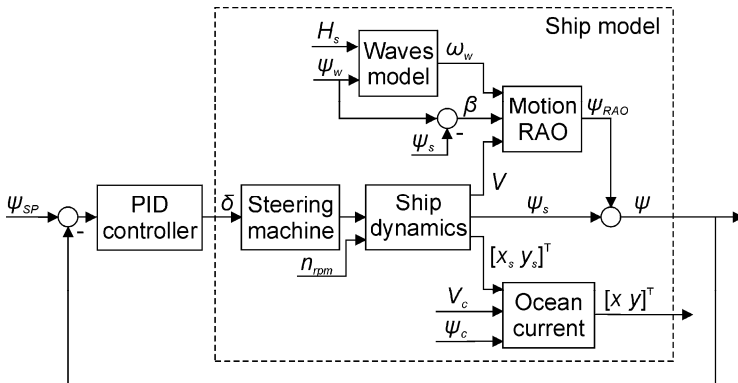


Fig. 8. Function block diagram with maneuvering ship model

Time responses of yaw rate (rate of turn, ROT) and yaw angle (heading) for step rudder deflection are presented in Fig. 9. As can be seen both S-175 and Nomoto response in similar way. It should be noted that the answers depend on speed of the ship. Gain and time constant of Nomoto model have to be corrected.

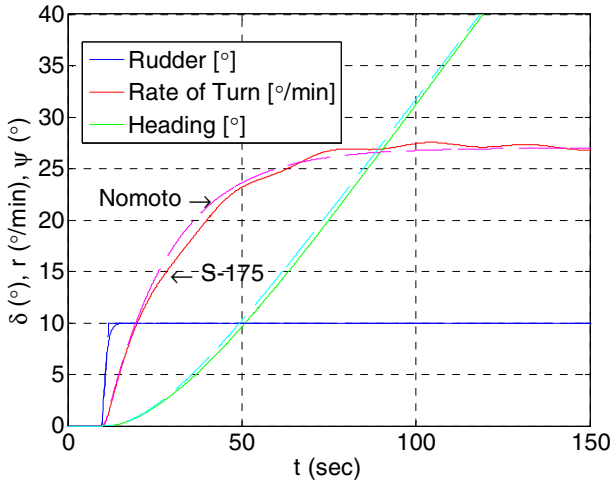


Fig. 9. Step responses of S-175 and Nomoto models

Figure 10 presents the influence of sea waves on measured signal. The waves are 4 m height and the angle of attack is equal to 45 degrees. The influence seems to be small, but cannot be neglected as the rate of change is quite significant.

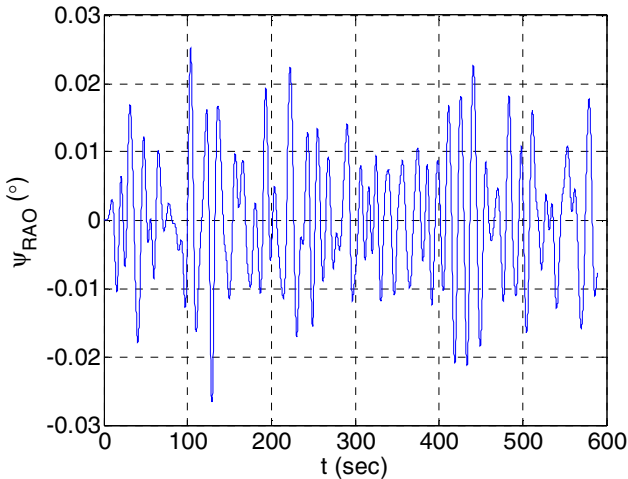


Fig. 10. The influence of sea waves on the ship

6 Summary

The paper presents the maneuvering ship model that could be integrated with the autopilot software. Two algorithms for the dynamics have been implemented. The first is a nonlinear 4-DoF model of the S-175 container, while the other is its 1st order Nomoto model. The nonlinear 4-DoF model is mainly intended for plant simulation, while the 1st order Nomoto model can be built into sea wave filter of the autopilot to estimate the position and orientation of the ship, e.g. Kalman filter. In addition to the ship dynamics, yawing motion caused by wave oscillation is modeled. In this case, simple equations for modelling of Motion RAO are used instead of large-size tables. The ship's position can also be changed under the sea currents interactions.

References

1. Trybus, L., Swider, Z., Stec, A.: Tuning Rules of Conventional and Advanced Ship Autopilot Controllers. This conference
2. Jamro, M., Rzonca, D., Sadolewski, J., Stec, A., Swider, Z., Trybus, B., Trybus, L.: CPDev engineering environment for modeling, implementation, testing, and visualization of control software. In: Szewczyk, R., Zieliński, C., Kaliczyńska, M. (eds.) Recent Advances in Automation, Robotics and Measuring Techniques. AISC, vol. 267, pp. 81–90. Springer, Heidelberg (2014)
3. Fossen, T.I.: Handbook of Marine Craft Hydrodynamics and Motion Control. Wiley, Chichester (2011)
4. MSS. Marine Systems Simulator, Viewed 23.11 (2010), <http://www.marinecontrol.org>
5. Tzeng, C.Y., Chen, J.F.: Fundamental properties of linear ship steering dynamic models. Journal of Marine Science and Technology 7(2), 79–88 (1999)
6. Son, K.H., Nomoto, K.: On the Coupled Motion of Steering and Rolling of a High-speed Container Ship. Naval Architect of Ocean Engineering 20, 73–83 (1982); From J.S.N.A., Japan, Vol. 150, pp. 232–244 (1981)
7. Fathi, D.: ShipX Vessel Responses (VERES). MARINTEK report, Norwegian Marine Technology Research Institute (MARINTEK), <http://www.marintek.sintef.no>
8. Perez, T.: Ship Motion Control. Course Keeping and Roll Stabilisation Using Rudder and Fins. Springer-Verlag London Ltd (2005)

Research of Basic Parameters of Piezoelectric Tube Actuator

Roman Regulski, Frederik Stefański, Bartosz Minorowicz, and Dariusz Sędziak

Institute of Mechanical Technology, Poznan University of Technology
ul. Piotrowo 3, 61-138 Poznań, Poland

roman.regulski@doctorate.put.poznan.pl
{frederik.stefanski,bartosz.minorowicz}@gmail.com,
dariusz.sedziak@put.poznan.pl

Abstract. The article present basic research of the piezoelectric tube actuator. In this study the actuator was tested for various DC voltages. Further hysteresis and creep effect of the piezo ceramic material were presented. The next point of this research was positioning control of tube under closed loop control. For this purpose classic PID control algorithm was applied, with a negative feedback from laser displacement sensor. The control software was developed under Matlab Simulink and dSPACE control system, which allows fast modification and testing.

Keywords: piezoelectric tube, PID control, hysteresis, creep.

1 Introduction

Piezoelectric actuators are commonly used for high precision positioning applications, because of their high positioning resolution and fast response time. However the piezoelectric actuators exhibit strong hysteresis behaviour which rises with an increase of the intensity of applied electric field. The same material properties cause in creep effect – unwanted displacement of the actuator over time with unchanged control voltage. This nonlinearities have a strong influence in reducing the expected positioning accuracy in an open loop control system [1–3]. The applicability of the actuator is determined by capability to remove this disadvantages during the control process. Because of this many efforts were made to minimalized this effects, by applying different control strategies.

Among different control methods, these effects can be eliminated by a closed loop control system in an effective way. This paper presents research of the basic piezoelectric tube properties and investigation of a closed loop control with use of a classical proportional integral derivative (PID) control algorithm.

2 Piezoelectric Tube Actuator

The researched PT230 tube was developed by PI Ceramic. The investigated piezoelectric tube actuator has unique features comparing to others piezoelectric actuators.

The tube can elongate along the longest axis, change its radius dimension or bend the free end, depending on the electrical connection and electrodes configuration. The piezoelectric tube actuator is made of ferroelectrically soft ceramic material (PIC151 type), based on Lead Zirconate Titanate (PZT) [8]. This material uses the inverse piezoelectric effect discovered by Jacques and Pierre Curie, which describes that piezoelectric material exposed to an electric potential changes its shape. The lateral motion of the free end of the tube will be under investigation in this paper. The actuators are used as transducers *inter alia* in scanning tunnelling microscopy, scanning probe microscopy, as fibre stretchers and in microdosing applications [4, 5, 8].

The tube has five electrodes, one inner and four distributed on the outer surface (circumference of the tube), used for motion control of the free end of the actuator. For the purpose of this research only two outer opposite electrodes were energized, while the remaining electrodes are connected to ground. The fifth electrode located on the inner side of the tube was connected to ground. The electrical connection is shown in Fig. 1b. In this configuration the free end of the tube will bend along the x axis (Fig. 1a). The geometrical parameters of the tube are length $L = 40$ mm, outer diameter $d_o = 3.2$ mm, inner diameter $d_i = 2.2$ mm. The piezoelectric charge constants for the actuator $d_{31} = -210 \times 10^{-12}$ C/N, and the maximal operating voltage is ± 250 V.

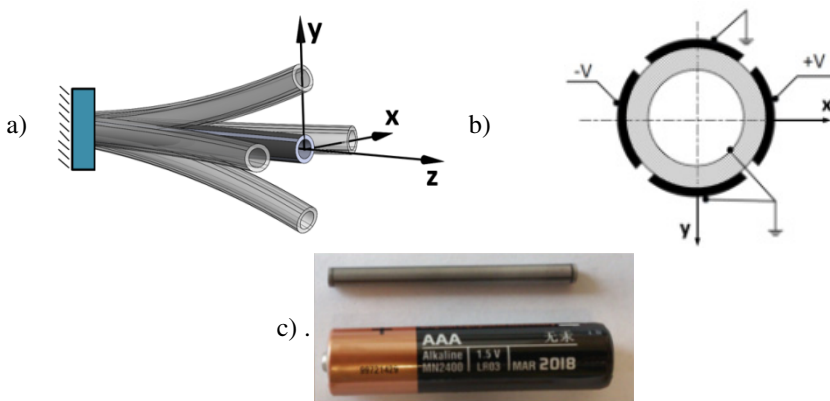


Fig. 1. Piezoelectric tube actuator a) bending directions, b) cross-section of the actuator and power connection configuration, c) PT230 tube

3 Test Bench

For the purpose of this research a test rig was designed and is presented in the Fig. 2. The investigated PZT tube was electrically isolated and glued in the mounting bracket (no. 1). To control of the piezoelectric tube actuator a high voltage amplifier was designed (no. 2). The device consists of: AC transformer, DC rectifier with filtering, and two power amplifier modules based on PA91 (APEX). Every channel normally works in inverting mode, with option to work in non-inverting mode. The gain of each channel can be set separately. For the purpose of this work the gain was set to 20, due to the ratio of input and desired output signal.

4 Piezo Tube Research

In order to study the basic properties of the actuator, a number of studies were performed on the aforementioned test stand. The first test concern about the hysteresis behaviour of this material. The Fig. 4 shows that the relationship between voltage and displacement is not linear. The test material also exhibits a symmetric hysteresis of approximately 20% – the ratio of the extreme difference in the displacement for 0 V, to the maximum displacement.

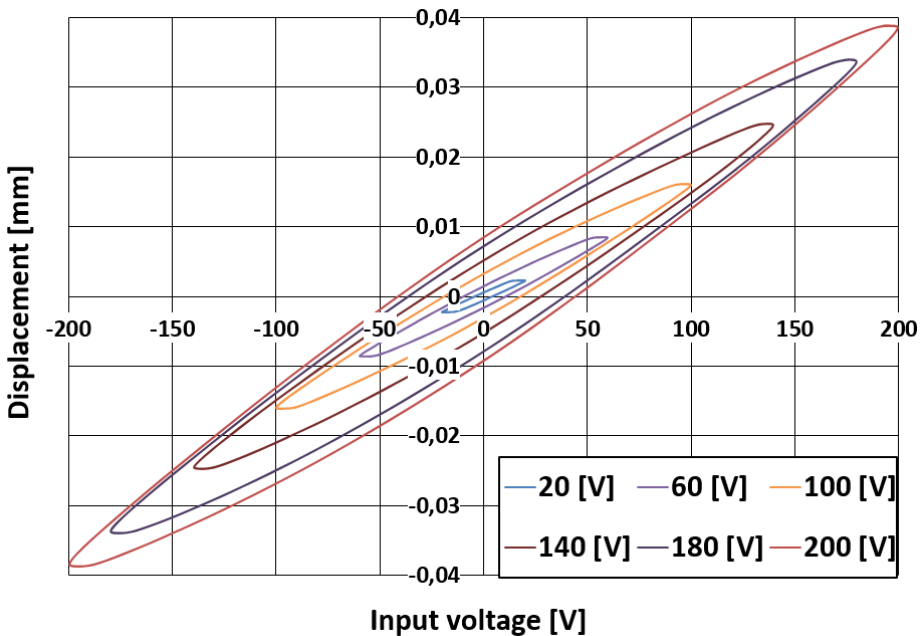


Fig. 4. The results of displacement for different supply voltage for 3 Hz sinus input signal

The next test was performed to show the change of the hysteresis loops for a decreasing input signal $v(t) = \cos(2\pi/6 t)$. The amplitude of the control signal was from -1 VDC to 1 VDC, what stands for a piezo input signal from -190 VDC to 190 VDC. The results were presented in the figure 5, shows the main and minor hysteresis loops.

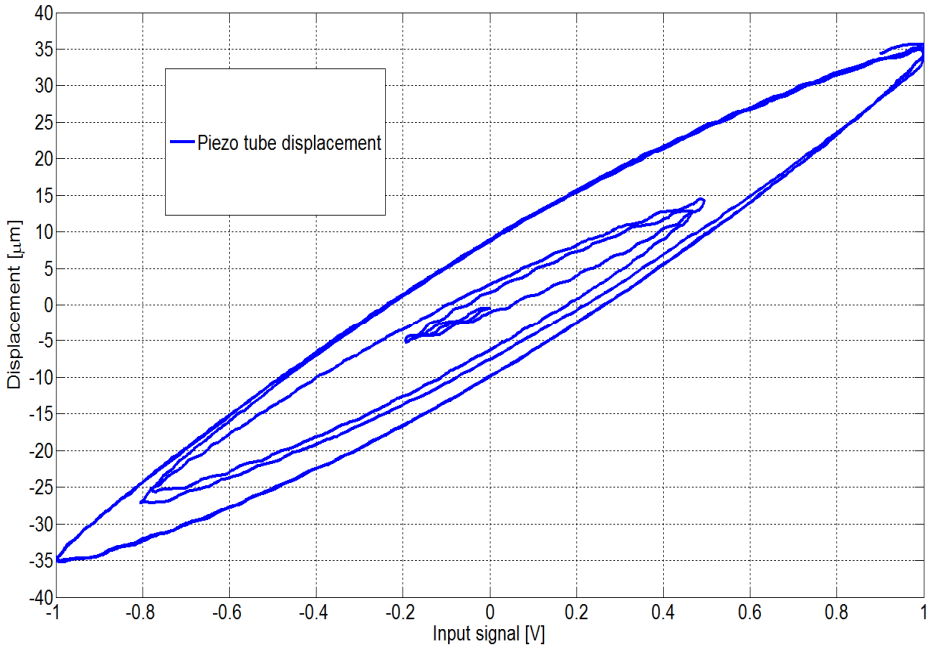


Fig. 5. Piezoelectric tube displacement response for a decreasing input signal

The creep effect was researched next. This effect is defined as unwanted displacement of the actuator over time at unchanged control voltage [6]. This phenomenon was tested and shown in Fig. 6. The study was performed for step response input signal and continued for over one hundred seconds.

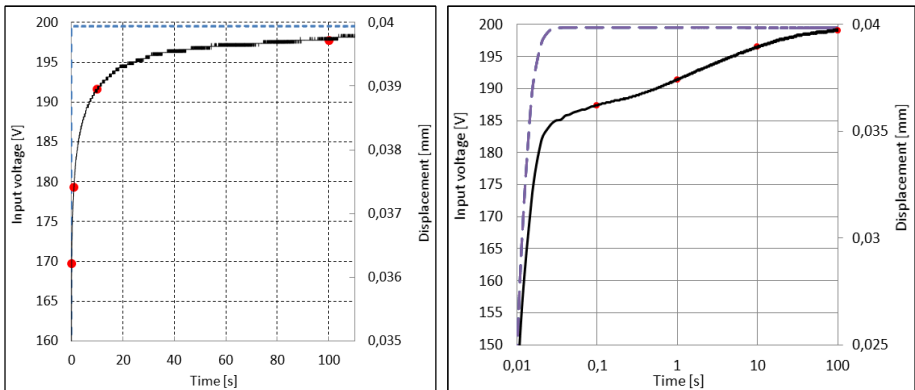


Fig. 6. Creep test results in normal and logarithmic scale

5 PID Displacement Control

In this paragraph results of PID closed loop position control of the PZT tube were presented. The aim of this was to reduce the influence of the hysteresis behaviour on positioning. The proportional-integral-derivative (PID) controller was implemented in Simulink model. During testing the PID control algorithm was tuned using manually tuning method under real time work in dSPACE software Control Desk.

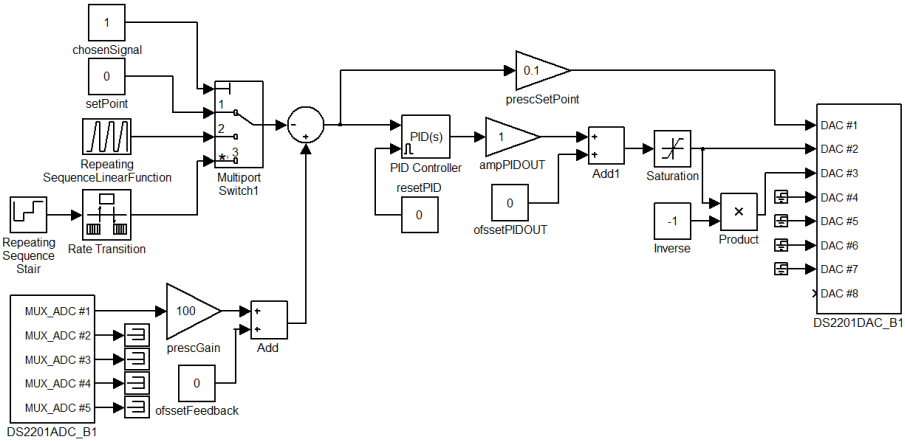


Fig. 7. Simulink model with PID controller

The Simulink model is presented in Fig. 7. The step response of the regulator and result of control is shown in Fig. 8. Controller parameters during the test were $P = 0.1$, $I = 2$, $D = 0.0004$. On the Fig. 9 tracing error and the piezo displacement under PID control in time were presented.

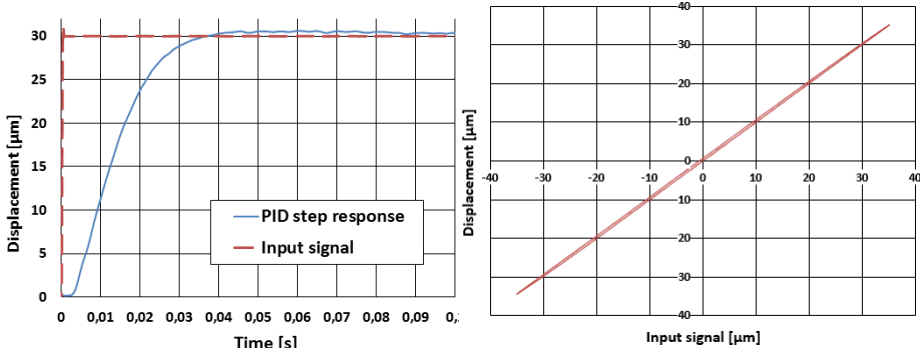


Fig. 8. Step response of PID regulator and displacement under control of sinusoidal input signal

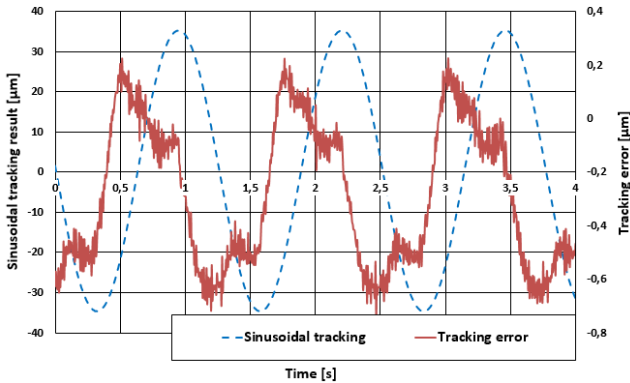


Fig. 9. Control error and piezo displacement under PID control

6 Conclusions

Performed basic researches have shown that the piezo actuator exhibit a symmetric hysteresis of approximately 20% of width. The creep effect was also recognized and it shows that the piezo tube continues to change its position at unchanged control voltage. These material properties make the tube not suitable for open loop positioning without an additional controller. The authors used basic closed loop control to minimize the influence of hysteresis on positioning accuracy. The applied classical PID controller was effective and allowed to reduce the tracking error under $1 \mu\text{m}$. The next step of research will be piezo tube positioning control under different input signal frequencies.

References

1. Yang, M., Gu, G., Zhu, L.: Parameter identification of the generalized Prandtl-Ishlinskii model for piezoelectric actuators using modified particle swarm optimization. *Sensors and Actuators A: Physical* 189, 254–265 (2013)
2. Hassani, V., Tjahjowidodo, T.: Integrated Rate and Inertial Dependent Prandtl-Ishlinskii Model for Piezoelectric Actuator. In: 2nd International Conference on Instrumentation, Control and Automation, Bandung (November 2011)
3. Qin, Y., Tian, Y., Zhang, D., Shirinzadeh, B.: A Novel Direct Inverse Modeling Approach for Hysteresis Compensation of Piezoelectric Actuator in Feedforward Applications. *ASME Transactions on Mechatronics* 18(3) (2013)
4. Bihikkaj, B., Yong, Y.K., Mahmood, I.A., Moheimani, S.O.R.: Diagonal control design for atomic force microscope piezoelectric tube nanopositioners
5. Bhikkaji, B., Moheimani, S.O.R.: Fast scanning using piezoelectric tube nanopositioners: A negative imaginary approach. In: IEEE/ASME International Conference on Advanced Intelligent Mechatronics, Singapore (2009)
6. Osamah, M., Kamal, Y.: Modeling of Piezoelectric Tube Actuators. *Innovation in Manufacturing Systems and Technology* (2004)
7. Baek-Ju, S., Eun-Woong, L., In-Su, K.: Displacement Control of piezoelectric Actuator using the PID Controller and System Identification Method. In: Power System Technology and IEEE Power India Conference (2008)
8. PI Ceramic GmbH, <http://piceramic.com>

Hysteresis Modelling of a Piezoelectric Tube Actuator

Frederik Stefański, Bartosz Minorowicz, and Amadeusz Nowak

Institute of Mechanical Technology, Poznan University of Technology
ul. Piotrowo 3, 61-138 Poznan, Poland
{frederik.stefanski,bartosz.minorowicz,
nowak.amadeusz}@gmail.com

Abstract. The article concerns about a piezoelectric tube actuator hysteresis. The actuator can bend in two directions and application of this piezo elements can entail new features and capabilities of mechatronic devices. Unfortunately as other smart materials, piezoelectric materials are distinguished by hysteresis phenomenon. Authors present result of displacement measurement, which was performed for decreasing amplitude cosine input signal. Based on this result phenomenological generalized Prandtl-Ishlinskii model was matched. The results of the piezoelectric tube and the model displacement were compared.

Keywords: piezoelectric tube, generalized Prandtl-Ishlinskii model, hysteresis.

1 Introduction

Actuators based on piezoelectric materials have been widely used in high precision systems, for instance scanning probe microscopes, micro-positioning devices [1–3]. It is because of their high positioning resolution, very fast frequency response and small size. Despite their advantages, piezoelectric materials exhibit strong nonlinearities such as hysteresis and creep. Because hysteresis cause inaccuracies in the system positioning, many efforts have been made to eliminate these properties [4–6].

One of the proposed solutions to reduce the hysteresis effect is the inverse compensation applied in a controller design, which uses an inversed hysteresis model [7–9]. To describe the hysteresis phenomenon, many different models are proposed in the literature. This approaches can be divided into physics based models [10] and phenomenological models [11–13].

The generalized Prandtl-Ishlinskii model (GPI) model as well as classical Prandtl-Ishlinskii model (PI) are well-known phenomenological hysteresis models. The PI model and his modification were proposed to characterize symmetric hysteresis properties, similarly to piezoceramic materials [14–17]. The GPI model allow to model asymmetric hysteresis loops and their saturation. Thus the GPI model is more sufficient for modeling of transducers based on magnetostrictive or shape memory alloys. Despite that, GPI model can be used for symmetric hysteresis actuators and provide even better results than the classical PI model [18]. Therefore, in this publication a generalized Prandtl-Ishlinskii model was used to describe the hysteresis of piezoceramic tube actuator.

1.1 Generalized Prandtl-Ishlinskii Hysteresis Model

The generalized Prandtl-Ishlinskii uses a generalized play operator, which is nonlinear comparing to the classical play operator (Fig. 1).

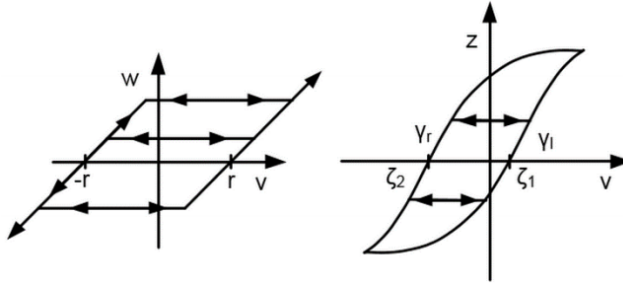


Fig. 1. Classical PI play operator (left), generalized PI play operator (right)

The classical play operator F_r behaves like backlash block in Simulink. Backlash block represents equal proportional change in output for raising input. Implicitly in backlash when threshold equals 0 output value is given by $f(x) = x$ function. This discontinuity works when input changes its direction of change, then decreasing input does not change output value. Output value F_r can be described as formulation (1) for input function $v(t)$ which is monotone in each subinterval $[t_i \leq t_{i+1}]$ and satisfies conditions (2), (3). These conditions are also true for generalized output G_r . Dependence between input and output value of this model is represented by equation (4). Each output of single play operator is multiplied by $p(r)$ which is non-negative density function determined from measured input-output transducer characteristics [18].

$$F_r[v](t) = \begin{cases} \max(v(t) - r, w(t_i)), & \text{for } v(t) > v(t_i) \\ \min(v(t) + r, w(t_i)), & \text{for } v(t) < v(t_i) \\ w(t_i), & \text{for } v(t) = v(t_i) \end{cases} \quad (1)$$

$$t_i < t \leq t_{i+1} \quad (2)$$

$$0 < i \leq N - 1 \quad (3)$$

$$Y_p(t) = \omega(v)[t] + \int_0^R p(r)F_r[v](t)dr \quad (4)$$

In generalized operator output value G_r increases along function defined as γ_l and decreases along other γ_r (5). This combination helps in description of asymmetric behavior.

$$G_r[v](t) = \begin{cases} \max(\gamma_l(t) - r, z(t_i)), & \text{for } v(t) > v(t_i) \\ \min(\gamma_r(t) + r, z(t_i)), & \text{for } v(t) < v(t_i) \\ z(t_i), & \text{for } v(t) = v(t_i) \end{cases} \quad (5)$$

For description of generalized play operator two envelop functions are used. Because the hysteresis loops of piezoelectric actuator are symmetric, the envelop functions are linear [18].

$$\gamma_r = a_0 v + a_1 \tag{6}$$

$$\gamma_l = b_0 v + b_1 \tag{7}$$

Density function is different for each play operator and depends on threshold value. Value of r_j is always positive and N is number of generalized play operators. In this case eight operators were used.

$$p(r_j) = \rho e^{-\tau r_j} \tag{8}$$

$$r_j = \alpha j \tag{9}$$

$$j \in \langle 1; N \rangle \tag{10}$$

Sum of integral generalized operator and value of function $\Omega[v](t)$ (11) is an output of model. Described integral can be also represented by sum of finite number of generalized play operators (12).

$$Y_{p\gamma}(t) = \Omega[v](t) + \int_0^R p(r) G_{lr}^\gamma[v](t) dr \tag{11}$$

$$Y_{p\gamma}(t) = \Omega[v](t) + \sum_{j=1}^N p(r_j) G_{l_j r_j}^\gamma[v](t) dr \tag{12}$$

Function $\Omega[v](t)$ consists of single linear functions, which act for increasing and decreasing input signal. More precise analyses can be found in papers [18].

$$\Omega[v](t) = c_0 v + c_1 \tag{13}$$

2 Experimental Setup and Data Acquisition

In this research, PT230 piezoelectric tube developed by PI Ceramic was used (Fig. 2). The geometrical parameters of the tube are: length $L = 40$ mm, outer diameter $d_o = 3.2$ mm, inner diameter $d_i = 2.2$ mm. The piezoelectric charge constant is $d_{31} = -180e-12$ C/N and the maximal operating voltage is ± 250 VDC. The tube has five electrodes, one inner and four distributed on the outer surface. The four equal electrodes allow to move the free end of the tube on the z-y plane (Fig. 2 c)). For the purpose of this paper, two opposite electrodes were connected to supply voltage, and the inner electrode to the common ground – presented on the Fig. 2 c). In this electrical configuration, when voltages with equal magnitude, but opposite polarity are applied to the two opposite electrodes, the tube bends towards the z axis positive direction. It is because one side of the tube extends and the opposite side retracts, depending on the polarity of applied voltage.

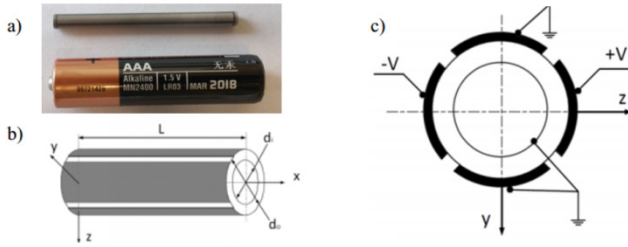


Fig. 2. Piezoelectric tube a) PT230, b) dimensions, c) electric connection schematic

The main parts of the test bench showed on the figure 3 are: piezoceramic tube actuator (no. 1), PHILTEC Fibreoptic D47 displacement sensor (no. 2), solid metal mounting (no. 3), high voltage power supply (no. 4), AC transformer (no. 5), PC with Matlab-Simulink (no. 6) and a dSPACE DS2201 ADC/DAC converter card (no. 7).

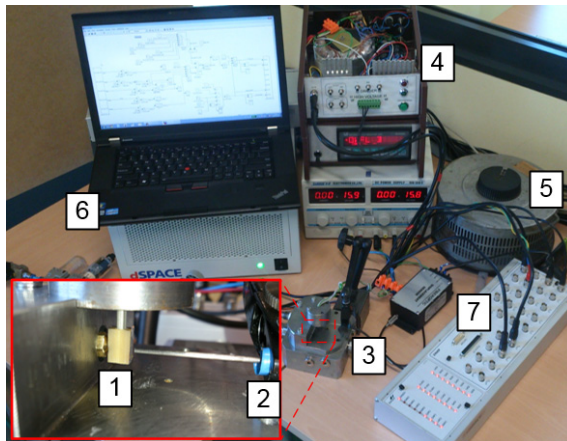


Fig. 3. Test rig and an enlargement of the piezo tube

The piezo tube was electrically isolated and glued in the metal mounting. A light cuboid was glued on the free end of the tube to create a good flat reflect surface for the fibre optic sensor. The supply power for the piezoelectric tube actuator was delivered by a high voltage amplifier designed for purpose of this research. This amplifier consists of: AC transformer, DC rectifier with filtering, and two PA91 (APEX) high voltage and power amplifier modules. The amplifier was supplied by an autotransformer connected to the power grid.

Created system works in real time mode under Control Desk dSPACE software, where all parameters from Matlab-Simulink model can be changed continuously. The model was used to generate signals and get measurement data. Output signals from DAC card were directly connected to voltage amplifier. One of the signals was inverted in order to obtain two voltages supply signals with opposite polarity. ADC card was used to collect and register signal from displacement sensor. The figure 4 shows the schematic of the test bench configuration.

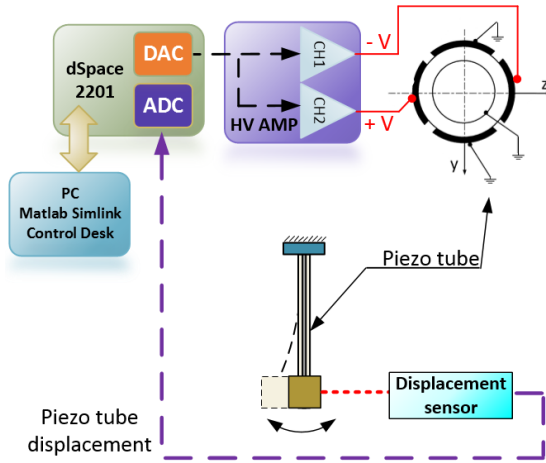


Fig. 4. Scheme of the test rig

3 Experimental Results

The generalized Prandtl-Ishlinskii model parameters need to be estimated on the base on a characteristic gathered from a modelled object. The response characteristic of the piezo tube was based on decreasing input signal $v(t) = \cos(2\pi/6 t)$, with a maximal amplitude from -1 VDC to 1 VDC.

Tests of the piezoelectric tube were performed on the aforementioned test bench. The input signal is proportional to the voltage generated by the amplifier. The amplitude -1 VDC to 1 VDC of the input signal stand for 190 VDC to -190 VDC supply voltage. The input signal was shown in the Fig. 5 and output characteristics of the piezoceramic tube was presented on the Fig. 6. Thanks to applying of decreasing cosine function major and minor hysteresis loop could be evaluate.

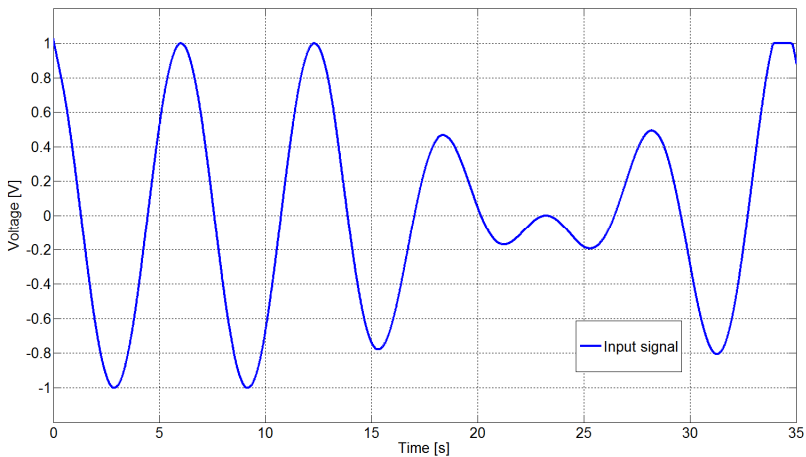


Fig. 5. Input signal for the piezo tube hysteresis characterization

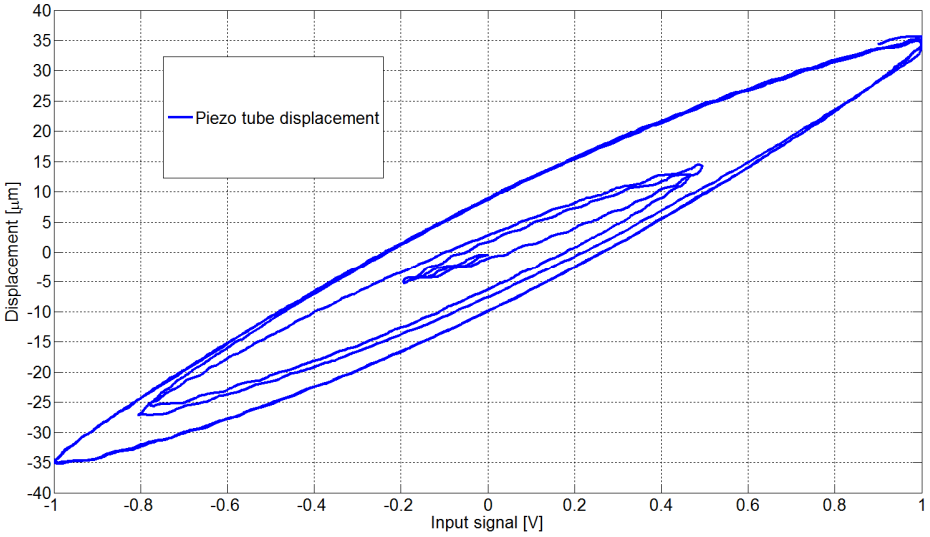


Fig. 6. Piezoelectric tube displacement response for the input signal

The GPI model parameters were identified through a minimization of an error squared function, using the Matlab-Simulink Optimization Toolbox. The obtained parameters of the model were presented in the Table 1.

Table 1. Estimated GPI model values

| Parameter | Estimated values [dimensionless] |
|-----------|-------------------------------------|
| α | 0.1577 |
| ρ | 0.92697 |
| τ | -1.40379 |
| a_0 | 0.78482 |
| a_1 | 0.24793 |
| b_0 | 0.76125 |
| b_1 | -0.92390 |
| c_0 | -1.14128 |
| c_1 | -23.95506 |

3.1 Generalized Prandtl-Ishlinskii Model Results

After model parameters estimation, the model was tested for the same $v(t)$ input signal like the piezo tube. The comparison of the piezo and GPI model displacement response for the input signal in time were plotted in the Fig. 7. In the Fig. 8 the shape of

the major and minor hysteresis loop generated by the GPI model was compared to the piezo displacement results. The last Fig. 9 present the GPI modelling error, calculated as a difference between the measured and modelled displacement.

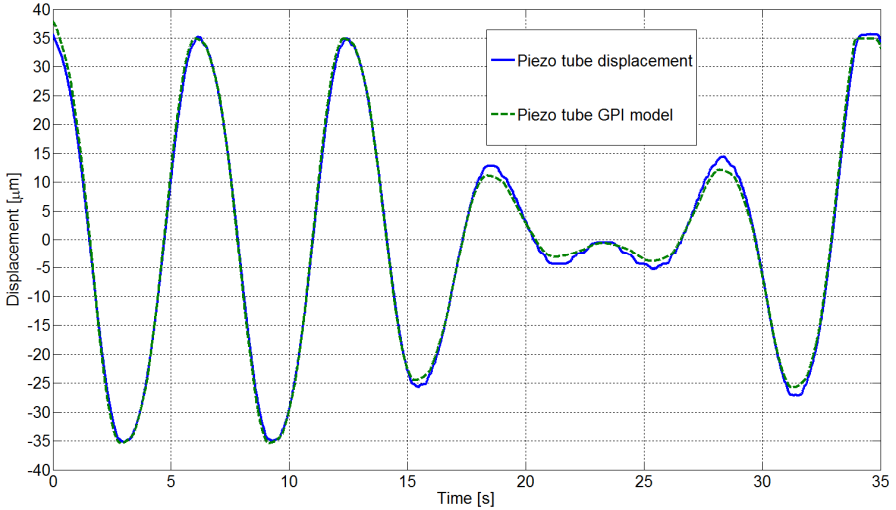


Fig. 7. Comparison of the piezoelectric tube and GPI model displacement response in time

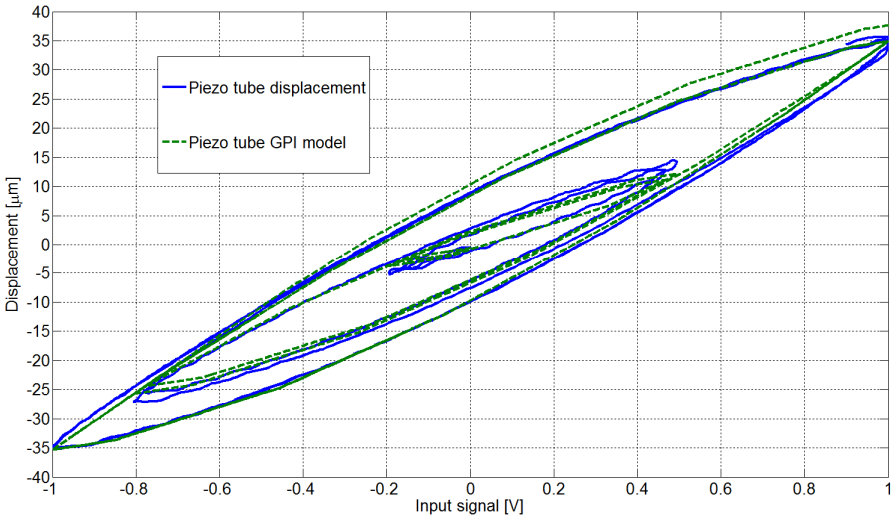


Fig. 8. Comparison of the piezo tube and GPI model displacement response versus input signal

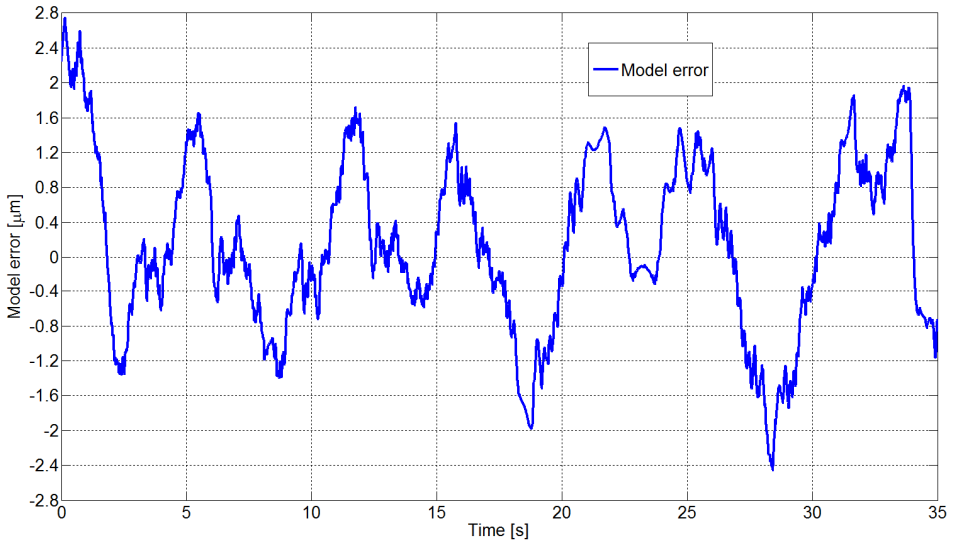


Fig. 9. Generalized Prandtl-Ishlinskii model error

4 Conclusions

The results show that the generalized Prandtl-Ishlinskii model can provide an effective hysteresis model of the piezoelectric tube. The Fig. 7 and Fig. 8 shows that the model follows with a good precision the shape of the major as well as minor hysteresis loops. The biggest model error can be noticed at the start and around the minor hysteresis loops. However, the model error presented on the Fig. 9 shows that the peak error of the modelled displacement is approximately 3.3% relative the whole displacement range. The model accuracy is sufficient, and will be used in the future to prepare an inverse hysteresis model.

Acknowledgments. This article was financially supported within the project "Engineer of the Future. Improving the didactic potential of the Poznan University of Technology" – POKL.04.03.00-00-259/12, implemented within the Human Capital Operational Programme, co-financed by the European Union within the European Social Fund.

References

1. Bihikkaj, B., Yong, Y.K., Mahmood, I.A., Moheimani, S.O.R.: Diagonal control design for atomic force microscope piezoelectric tube nanopositioners.
2. Heamawatanachi, S., Bamberg, E.: Design and characterization of PZT driven micromachining tool based on single-point tool tip geometry. *Precision Engineering* 33, 387–394 (2008); *Review of Scientific Instruments* 84 (2013)
3. Salapaka, S., Salapaka, M.: Scanning probe microscopy. *IEEE Control Systems* 28, 65–83 (2008)

4. Yang, M., Gu, G., Zhu, L.: Parameter identification of the generalized Prandtl-Ishlinskii model for piezoelectric actuators using modified particle swarm optimization. *Sensors and Actuators A: Physical* 189, 254–265 (2013)
5. Hassani, V., Tjahjowidodo, T.: Integrated Rate and Inertial Dependent Prandtl-Ishlinskii Model for Piezoelectric Actuator. In: 2nd International Conference on Instrumentation, Control and Automation, Bandung (November 2011)
6. Qin, Y., Tian, Y., Zhang, D., Shirinzadeh, B.: A Novel Direct Inverse Modeling Approach for Hysteresis Compensation of Piezoelectric Actuator in Feedforward Applications. *ASME Transactions on Mechatronics* 18(3) (2013)
7. Xu, Q., Li, Y.: Dahl model-based hysteresis compensation and precise positioning control of an XY parallel micromanipulator with piezoelectric actuation. *Journal of Dynamic Systems, Measurement, and Control* 132(4) (2010)
8. Gu, G., Yang, M., Zhu, L.: Real-time inverse hysteresis compensation of piezoelectric actuators with a modified Prandtl-Ishlinskii model. *Review of Scientific Instruments* 86(6) (2012)
9. Janaideh, M., Mao, J., Rakheja, S., Xie, W., Su, C.: Generalized Prandtl-Ishlinskii Hysteresis Model: Hysteresis Modelling and Its Inverse for Compensation in Smart Actuators. In: *Proceedings of the 47th IEEE Conference on Decision and Control, Cancun, Mexico* (2008)
10. Smith, R.C.: *Smart Material System: Model Development*. Society for Industrial and Applied Mathematics (2005)
11. Galinaities, W.: Two methods of piezoceramic and shape memory alloy hysteresis. Ph.D. dissertation, Dept. Math., Blacksburg, Virginia, USA (1999)
12. Song, G., Zhao, J., Zhou, X., Aberu-Garcia, J.A.D.: Tracing control of a piezoceramic actuator with hysteresis compensation using inverse Preisach model. *IEEE Transactions on Mechatronics* 10(2), 198–209 (2005)
13. Huhhes, D., Wen, J.: Preisach modelling of piezoceramic and shape memory alloy hysteresis. *Smart Materials and Structures* 6, 287–300 (1997)
14. Brokate, M., Sprekels, J.: *Hysteresis and Phase Transitions*. Springer, New York (1996)
15. Krejci, P., Kuhnen, K.: Inverse control of systems with hysteresis and creep. In: *IEEE Proc. Control Theory Application*, vol. 148, pp. 185–192
16. Janocha, H., Kuhnen, K.: Real-time compensation of complex hysteretic non-linearities. *Control* 9, 407–418
17. Al Janaideh, M., Rakheja, S., Su, C.: A generalized Prandtl-Ishlinskii model for characterizing the hysteresis and saturation nonlinearities of smart actuators. *Smart Materials and Structures* 18 (2009)

Application of Jiles-Atherton Model for Modelling Magnetization Characteristics of Textured Electrical Steel Magnetized in Easy or Hard Axis

Roman Szweczyk

Industrial Research Institute for Automation and Measurements
Al. Jerozolimskie 202, PL-02-486, Warsaw, Poland
szweczyk@mchtr.pw.edu.pl

Abstract. Paper presents the results of application of extended Jiles-Atherton model for modeling of the magnetic hysteresis loops of anisotropic, grain oriented Unisil M130-27s silicon electrical steel. During the modeling both anisotropy of the magnetic material as well as changes of average energy required to break pinning site were considered. Moreover, equation determining anisotropic anhysteretic magnetization was corrected to be coherent with isotropic model. Parameters of the model were determined during the evolutionary strategy-based optimization process simultaneously considering six hysteresis loops measured for different value of amplitude of magnetizing field as well as for magnetization in direction of the easy and hard axis of the magnetic material. Source code for this process is available at the web page. High level of agreement between experimental results and results of modeling was achieved and confirmed by the value of coefficient of determination. Simultaneous determination of Jiles-Atherton model parameters based on six hysteresis loops enables successful assessment of average anisotropy energy density during the optimization process. Moreover, set of nine Jiles-Atherton model's parameters is suitable to model functional characteristics of the magnetic core made of silicon electrical steel necessary for numerical optimization of construction of electric and electronic devices.

1 Introduction

Grain oriented electrical steels [1] and other anisotropic materials, such as amorphous [2] and nanocrystalline [3] alloys, are commonly used in electric and electronic industry as material for cores of inductive components, especially for transformers or choke coils. However, numerical optimization of parameters of such devices require numerical models of magnetic hysteresis loops which can successfully operate in wide range of amplitudes of magnetizing fields and consider anisotropic properties of electrical steels as well. One of the most suitable models for this purpose is Jiles-Atherton model presented by Jiles and Atherton [4, 5] and developed by Andrei [6]. It should be highlighted, that this model connect specific physical properties of the magnetic material, such as average anisotropy energy density [7–9], with technical properties of the material determined by its magnetic hysteresis loops.

On the other hand, one set of original Jiles-Atherton model parameters enable effective modeling only for single hysteresis loop. For this reason extension of this model was proposed by [10]. As a result wide range of hysteresis loops during the magnetizing in both easy and hard axis of material may be modelled. However, results of such modeling for anisotropic electrical steel, where one set of parameters is determined for magnetization in the easy and hard axis, were still not presented. This paper is going to fill this gap and provide effective tool for modeling magnetic hysteresis of cores of grain oriented steel-based inductive components.

2 Tested Material

Experiments were carried out on grain oriented Unisil M130-27s silicon electrical steel. Silicon content in such steel is 3.1 %, its density is 7.65 kg/dm^3 whereas resistivity about $48 \mu\Omega\text{cm}$. For grain oriented electrical steel testing, the Magnite-S heat resistant insulation coatings were applied to both sides of the sample strips. The coatings are approximately $3 \mu\text{m}$ thick per side.

Three sets of strips for Epstein frame were cut: (1) in rolling direction, (2) perpendicularly to rolling direction, (3) in angle equal 55° to rolling direction. Cutting direction accuracy was better than 1° .

3 Magnetic Measurements

For magnetic measurements three Epstein frames, accordingly to methods described in IEC 60404-2, were produced. Each frame consist of 48 strips cut in specific direction. Frames were wound with 400 turns of magnetizing windings and 400 turns of sensing windings accordingly to IEC 60404-2.

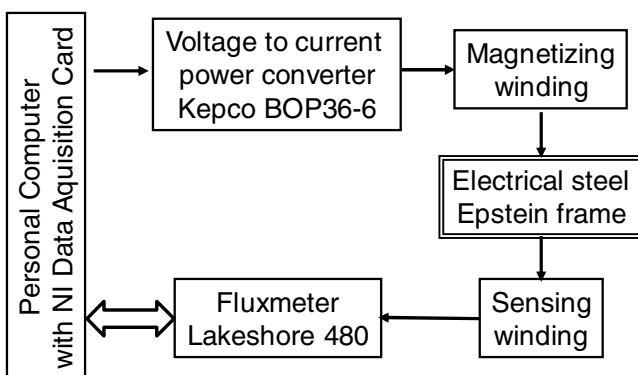


Fig. 1. Schematic block diagram of digitally controlled hysteresis graph

Measurements of B-H hysteresis loops were carried out with use of digitally controlled hysteresis graph presented in Fig. 1. Magnetizing winding was connected to

the output of BOP36-6 high power voltage-current converter produced by Kepco, whereas sensing winding was connected to input of type 480 fluxmeter produced by Lakeshore. Whole system was controlled by personal computer equipped with data acquisition card produced by National Instruments. Measuring process was controlled by special software developed in LabVIEW environment.

To reduce dynamic effects, the measurements were carried out in quasi-static mode. For this reason frequency of magnetizing current was reduced to 0.5 Hz. This reduction was important from the results of the modeling interpretation point of view.

Results of measurements of $B(H)$ hysteresis loops of grain oriented Unisil M130-27s silicon electrical steel are presented in Fig. 2 as dotted lines. As it was expected, for strips of material magnetized perpendicularly to the rolling direction, lower values of flux density B are achieved (for given value of amplitude of magnetizing field H) than for material cut in the rolling direction. However, for material, which was cut in angle equal 55° to rolling direction, the same shape of hysteresis loop was achieved as for material cut perpendicularly to rolling direction. As a result, to simplify the modeling of magnetic properties, uniaxial anisotropy of Unisil M130-27s silicon electrical steel was assumed.

4 Jiles-Atherton Model for Anisotropic Materials and Proposed Extension of This Model

The Jiles-Atherton (J-A) model enables modeling the $B(H)$ hysteresis loops of soft magnetic materials. This model of magnetization process is based on the analysis of the total free energy of the magnetic material [4, 5] accordingly to following fundamental equations:

$$A = G + \mu_0 \cdot H \cdot M \quad (1)$$

$$G = U - T \cdot S + \frac{3}{2} \sigma \cdot \lambda \quad (2)$$

$$U = \frac{1}{2} \alpha \cdot \mu_0 \cdot M^2 \quad (3)$$

where A is Helmholtz free energy, G – Gibbs free energy, U – is internal energy, S – entropy, M – magnetization, α – interdomain coupling accordingly to Bloch model and T , σ , λ are temperature of material, stresses and magnetostrictive strain respectively.

Effective strength of magnetic field H_e , which influence the magnetization process may be calculated directly from total free energy equations as:

$$H_{eff} = \frac{1}{\mu_0} \left(\frac{\partial A}{\partial M} \right)_T = H + \alpha \cdot M + \frac{3}{2} \sigma \cdot \left(\frac{\partial \lambda}{\partial M} \right)_T \quad (4)$$

Above equation reduces to $H_{eff} = H + \alpha M$ for materials which are not subjected to the influence of stresses σ .

First step of modeling with use of Jiles-Atherton model is calculation of anhysteretic magnetization M_{an} . In general form, for anisotropic materials, this magnetization is given as by Ramesh [7] and corrected [11] to following form:

$$M_{aniso} = M_s \left[\frac{\int_0^\pi e^{\frac{E(1)+E(2)}{2}} \sin \theta \cdot \cos \theta \cdot d\theta}{\int_0^\pi e^{\frac{E(1)+E(2)}{2}} \sin \theta \cdot d\theta} \right] \quad (5)$$

where θ is the integration parameter and $E(i)$ is given by following dependence [7]:

$$E(i) = \frac{H_{eff}}{a} \cos \theta - \frac{K_{an}}{M_s \cdot \mu_0 \cdot a} \sin^2 \phi_i \quad (6)$$

where M_s is saturation magnetization, a quantifies domain walls density, K_{an} is anisotropic energy density, and $\phi_1 = \psi - \theta$ as well as $\phi_2 = \psi + \theta$, where ψ is an angle between the easy axis of the material and the magnetizing field direction. Unfortunately, functions in equation (2) don't have any known antiderivatives. As a result, M_{aniso} has to be calculated numerically.

In the case of magnetization of isotropic magnetic materials M_{iso} , due to the absence of K_{an} , equation (5) reduces to the Langevin equation [5]:

$$M_{iso} = M_s \left[\coth \left(\frac{H_{eff}}{a} \right) - \left(\frac{a}{H_{eff}} \right) \right] \quad (7)$$

It should be indicated, that in the original equation (5) in Jiles-Atherton model for anisotropic materials, presented by Ramesh [7], sum of energies $E(1)$ and $E(2)$ is not divided by 2. As a result anhysteretic anisotropic magnetization M_{aniso} is not coherent with M_{iso} , given by equation (7), for K_{an} equal zero. Equation (5) presented in this paper is corrected. This form is coherent with isotropic magnetization M_{iso} as well as is physically judged.

According to Jiles-Atherton model, the total value of anhysteretic magnetization M_{an} can be calculated as a weighted sum of anisotropic magnetization M_{aniso} and isotropic magnetization M_{iso} [7] in the real material:

$$M_{an} = t \cdot M_{aniso} + (1-t) \cdot M_{iso} \quad (8)$$

where t is the weight coefficient, describing a participation of anisotropic phase in the material [7].

In the Jiles-Atherton model the irreversible magnetization M_{irr} can be calculated from following equation:

$$\frac{dM_{irr}}{dH} = \delta_M \frac{M_{an} - M_{irr}}{\delta \cdot k} \quad (9)$$

taking into account the parameter k , which quantifies average energy required to break pinning site. In this equation parameter $\delta = +1$ for $\frac{dH}{dt} > 0$ and $\delta = -1$ for $\frac{dH}{dt} < 0$.

Additional parameter $\delta_M = 0$ when $\frac{dH}{dt} < 0$ and $M_{an} - M > 0$ as well as when $\frac{dH}{dt} \geq 0$ and $M_{an} - M < 0$. In other cases $\delta_M = 1$. Parameter δ_M guarantees the avoidance of unphysical stages of the Jiles-Atherton model for minor loops, in which incremental susceptibility becomes negative [8].

Reversible magnetization M_{rev} in the Jiles-Atherton model can be calculated from equation Jiles and Atherton [4, 5]:

$$M_{rev} = c \cdot (M_{an} - M_{irr}) \quad (10)$$

where c describes magnetization reversibility. Total magnetization M is given as the sum of reversible magnetization M_{rev} and irreversible magnetization M_{irr} [4, 5].

$$M = M_{rev} + M_{irr} \quad (11)$$

The most significant limitation of original Jiles-Atherton model is the fact, that it can give quite good agreement between experimental hysteresis loop and results of the modeling, but only for single hysteresis loop [10]. This limitation is especially important from practical point of view. As a result it is problematic to use Jiles-Atherton model in case of changing amplitude of magnetizing field.

To overcome this problem it should be taken into account, that the Jiles-Atherton model parameter k changes during the magnetization process [4, 5]. These changes are connected with changes of the average energy required to break pinning site [12]. As a result model's parameter k should be connected with the magnetic state of the material.

In the previous attempts, this state was described by the magnetizing field H [13]. However, from physical point of view, the magnetic state of the material should be described by magnetization M . To describe the changes of parameter k , the following equation was proposed [10]:

$$k = k_0 + \frac{e^{k_2 \cdot (1-|M|/Ms)} - 1}{e^{k_2} - 1} \cdot (k_1 - k_0) \quad (12)$$

where parameters k_0 , k_1 and k_2 describe shape of function determining k .

Conception of extension of Jiles-Atherton model presented above was verified for both isotropic [14] and anisotropic [15] magnetic materials. However, verification was focused only on magnetizing field H parallel to the easy axis of magnetization. This creates problems with determination of average anisotropy energy density K_{an} in the material.

5 Determination of Model's Parameters

Unfortunately, there is no clearly stated methodology of determination of Jiles-Atherton model's parameters. As a result, on the base of experimental $B(H)$ hysteresis loops, values of the extended Jiles-Atherton model's parameters were calculated during the optimization process. However, for proper determination of extended Jiles-Atherton model's parameters, the set of three hysteresis loops (for each magnetizing field direction) measured for the different value of magnetizing field have to be used [10]. In these measurements amplitudes of magnetizing field should cover areas of both reversible magnetization for amplitude in the range of coercive field H_c , as well as range of domain walls movements, for the amplitude about $10 H_c$.

Moreover, for proper determination of value of average anisotropy energy density Kan in Unisil M130-27s silicon electrical steel, two such sets of three hysteresis loops were used: one for strips of material magnetized perpendicularly to the rolling direction, and the second for material cut perpendicularly to rolling direction.

The target function G for optimization process was given by the following equation:

$$G = \sum_{i=1}^n (B_{J-A}(H_i) - B_{meas}(H_i))^2 \quad (13)$$

where B_{J-A} were the results of the modelling and B_{meas} were the results of the experimental measurements, both for the value H_i of magnetizing field. As a result in presented research the Jiles-Atherton model's parameters were determined simultaneously for six $B-H$ hysteresis loops measured for different value of magnetizing field H provided in two perpendicular angles.

Target function G exhibits many local minima but is continuous on the intervals. For this reason, in the case of minimization of the target function, the evolutionary cognitive methods [16, 17] such as strategy $(\mu+\lambda)$ together with simulated annealing [18] in the first step, and then the gradient optimization in the second step, were applied.

In opposite to the (μ, λ) evolutionary strategy, $(\mu+\lambda)$ is especially suitable for this kind of optimization due to the fact, that it can't lose the best results, once they are achieved. In $(\mu+\lambda)$ strategy the population (group) of vectors of the nine Jiles-Atherton model's parameters (individuals) was subjected to iterative mutation (random value changes of each parameter in vector) and crossing-over exchange of parameters between vectors, as well as to the selection accordingly with the best value of target function.

In presented investigation the population of $N = 900$ vectors (individuals) was used. During the crossing-over operation, the group of $\mu = 3$ parents vectors was able to generate during the crossing-over exchange $\lambda = 12$ descendant vectors. These descendant vectors were subjected to mutations. The mutation had a normal distribution with initial standard deviation $\sigma = 0.04$ of initial value of each parameter. The value of σ decreased to its 96% in each iteration of evolutionary strategy, which is in line with the idea of the simulated annealing.

Finally, twenty of vectors connected with the lowest value of optimization function G were subjected to gradient descent optimization. Gradient descent was realized only for limited total changes of parameters, which minimized risk connected with local minimis.

To enable verification and further development of software for calculation according to Jiles-Atherton model, all MATLAB scripts used in presented research, together with results of experimental measurements of $B(H)$ hysteresis loops of Unisil M130-27s silicon steel are available at: <http://zsisp.mchtr.pw.edu.pl/JASmodel/M130/>

6 Results of Modeling

The set of Jiles-Atherton model's parameters calculated on the base of experimental results is presented in Table 1. The Fig. 2 presents both experimental results of measurements of $B(H)$ hysteresis loops of grain oriented Unisil M130-27s silicon electrical steel as well as the results of calculation of these loops on the base of parameters presented in table 1. The same set of parameters was used for calculation of hysteresis loops measured for magnetizing field perpendicular and parallel to rolling direction of this steel.

Table 1. Estimated parameters of Jiles-Atherton model for grain oriented Unisil M130-27s silicon electrical steel

| Parameter | Description | Value |
|-----------|---|------------------------|
| M_s | Saturation magnetization | $1.476 \cdot 10^6$ A/m |
| a | Quantifies domain walls density | 96.11 A/m |
| k_0 | Maximal value of k | 15.48 A/m |
| k_1 | Minimal value of k | 7.20 A/m |
| k_2 | Shape parameter of function determining k | -0.774 |
| c | Magnetization reversibility | 0.962 |
| α | Interdomain coupling | $1.089 \cdot 10^{-4}$ |
| t | Participation of anisotropic phase | 0.243 |
| K_{an} | Magnetic anisotropy energy density | 5266 J/m ³ |

It should be indicated, that very good agreement was achieved between experimental and simulation results. This good agreement was confirmed by high level of coefficient of determination R^2 , which exceeds 0.99.

Presented results indicate that one set of expended Jiles-Atherton model parameters enable modelling of the magnetic hysteresis loops of anisotropic materials in wide range of amplitude of magnetization field H as well as for different value of angle between the rolling direction of anisotropic steels. These are the significant advantages of extended

model, which are especially important from technical point of view. As a result one set of nine parameters presented in Table 1 is suitable to model functional characteristics of the magnetic core made of M130-27s silicon electrical steel necessary for numerical optimization of construction of electric and electronic devices.

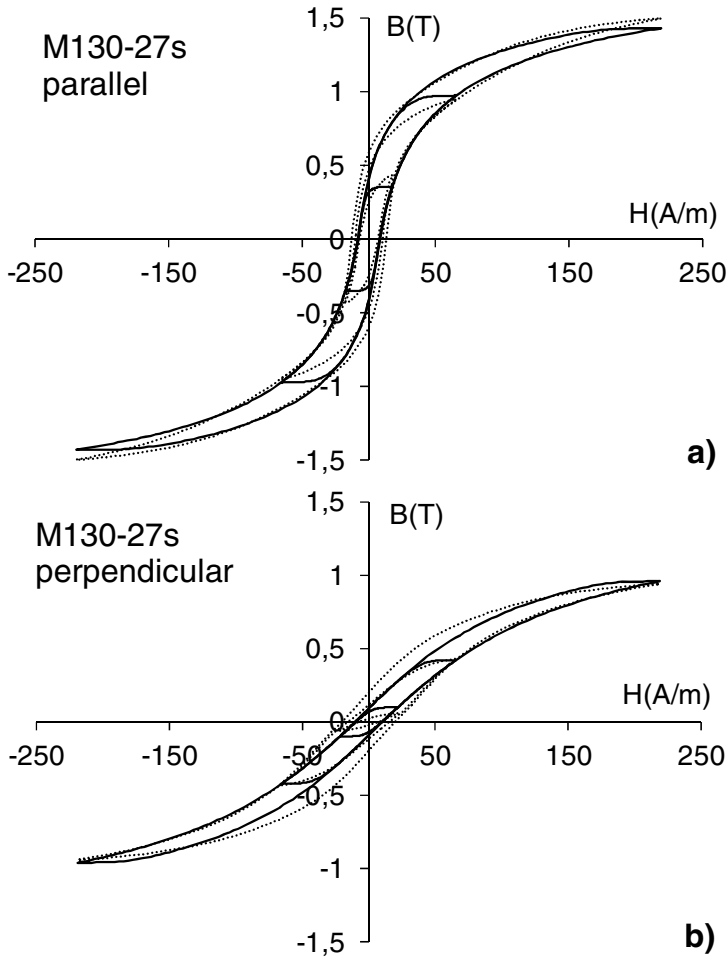


Fig. 2. $B(H)$ magnetic hysteresis loop of grain oriented Unisil M130-27s silicon electrical steel measured for magnetizing field H : a) parallel to the rolling direction, b) perpendicularly to the rolling direction. Experimental result: dotted line, results of modeling: solid line

7 Conclusions

Presented results confirm possibility of application of extended Jiles-Atherton model for modeling the magnetic characteristics of anisotropic, textured materials, such as Unisil M130-27s silicon electrical steel. Due to considering the changes of parameter

k during the magnetization process, extended model enables modeling the set of magnetic hysteresis loops measured for different values of amplitude of magnetizing field H . Moreover, the same set of parameters is suitable for the magnetic hysteresis loops modeling during the magnetization in the easy and hard axis direction.

High level of agreement between experimental results and results of modeling was achieved. This good agreement was confirmed by the value of coefficient of determination, which exceeds 99%.

Simultaneous determination of Jiles-Atherton model parameters based on six hysteresis loops enables successful assessment of average anisotropy energy density K_{an} during the optimization process. Such determination of K_{an} gives more unequivocal results when is carried out on the base of hysteresis loops measured parallel and perpendicularly to the steel rolling direction.

Acknowledgments. Calculations for the modelling were made in the Interdisciplinary Centre for Mathematical and Computational Modelling of Warsaw University, within grant G36-10.

References

1. Fryskowski, B.: Experimental evaluation of magnetic anisotropy in electrical steel sheets. *Journal of Magnetism and Magnetic Materials* 320, 515–522 (2008)
2. Wang, J., Wang, Z., Jia, Y., Shi, R., Wen, Z.: High temperature soft magnetic properties of $(\text{Fe}_{1-x}\text{Co}_x)_{73.5}\text{Cu}_1\text{Mo}_3\text{Si}_{13.5}\text{B}_9$ ($x=0.5, 1$) alloys. *Journal of Magnetism Magnetic Materials* 328, 62–65 (2013)
3. Kolano-Burian, A., Varga, L.K., Kolano, R.: High-frequency soft magnetic properties of Finemet modified with Co. *Journal of Magnetism Magnetic Materials* 316, E820–E822 (2007)
4. Jiles, D.C., Atherton, D.L.: Theory of ferromagnetic hysteresis. *Journal of Applied Physics* 55, 2115–2120 (1984)
5. Jiles, D.C., Atherton, D.L.: Theory of ferromagnetic hysteresis. *Journal of Magnetism Magnetic Materials* 61, 48–60 (1986)
6. Andrei, P., Caltun, O., Stancu, A.: Differential phenomenological models for the magnetization processes in soft MnZn ferrites. *IEEE Transactions on Magnetics* 34, 231–241 (1998)
7. Ramesh, A., Jiles, D.C., Roderik, J.: A model of anisotropic anhysteretic magnetization. *IEEE Transactions on Magnetics* 32, 4234–4236 (1999)
8. Chwastek, K., Szczygłowski, J.: Identification of a hysteresis model parameters with genetic algorithms. *Mathematics and Computers in Simulation* 71, 206–211 (2006)
9. Baghel, A.P.S., Kulkarni, S.V.: Hysteresis modeling of the grain-oriented laminations with inclusion of crystalline and textured structure in a modified Jiles-Atherton model. *Journal of Applied Physics* 113, 43908–43908 (2013)
10. Szewczyk, R.: Extension for the model of the magnetic characteristics of anisotropic metallic glasses. *Journal of Physics D: Applied Physics* 40, 4109–4113 (2007)
11. Szewczyk, R.: Validation of the Anhysteretic Magnetization Model for Soft Magnetic Materials with Perpendicular Anisotropy. *Materials* 7, 5109–5116 (2014)

12. Forster, H., Suess, D., Schrefl, T., Fidler, J., Scholz, W.: Micromagnetic simulation of domain wall pinning and domain wall motion. *Computational Materials Science* 25, 540–546 (2002)
13. Lederer, D., Igarashi, H., Kost, A., Honmat, T.: On the parameter identification and application of the Jiles-Atherton hysteresis model for numerical modelling of measured characteristics. *IEEE Transactions on Magnetics* 35, 1211–1214 (1999)
14. Szewczyk, R.: Modelling of the magnetic and magnetostrictive properties of high permeability Mn-Zn ferrites. *Pramana – Journal of Physics* 67, 1165–1171 (2006)
15. Szewczyk, R.: Modelling of the magnetic characteristics of isotropic and anisotropic materials for sensor applications. *Acta Physica Polonica A* 113, 67–70 (2008)
16. Jackiewicz, D., Szewczyk, R., Salach, J.: Modelowanie charakterystyk magnesowania stali konstrukcyjnych. *Pomiary Automatyka Robotyka* 2, 552–555 (2012) (in Polish)
17. Szewczyk, R.: Reliability and Efficiency of Differential Evolution Based method of determination of Jiles-Atherton model parameters for X30CR13 corrosion resisting martensitic steel. *Journal of Automation, mobile robotics and intelligent systems* 8(4), 63 (2014)
18. Schwefel, H.P.: *Evolution and optimum seeking*. Wiley, New York (1995)

Tuning Rules of Conventional and Advanced Ship Autopilot Controllers

Leszek Trybus, Zbigniew Świder, and Andrzej Stec

The Faculty of Electrical and Computer Engineering
Rzeszów University of Technology, Rzeszów, Poland
{ltrybus, swiderzb, astec}@prz-rzeszow.pl

Abstract. Ship autopilots are divided into conventional, capable of keeping desired course, and advanced which can track the path connecting waypoints on the route. The paper presents tuning rules for PID controller of conventional autopilot and for PI or state-space controller of advanced one. Single design parameters determining closed-loop dynamics are specified for each of them. The rules are implemented in software of autopilot prototype developed jointly with a Dutch company.

Keywords: ship autopilot, PID controller, tuning rules, state observer.

1 Introduction and Motivation

Automatic control of ship course is executed by conventional autopilots which correct the actual course by means of the rudder to bring it back to desired reference. Gyroscope or magnetic compass measure the course. Adaptive autopilot adjusts controller settings to ship speed. The rudder should not be affected by wave-induced yaw motions of the ship.

Advanced autopilots not only keep the desired course but are also able to track a path connecting waypoints on the route. It requires a GPS-based navigation system which determines deviation from the path due to sea current or wind, and corrects the course. Advanced autopilot is in fact a cascade system with track controller acting as primary, and course controller as secondary. Well established companies like Sperry Marine, Raytheon, Kongsberg and a few others offer both conventional and advanced autopilots with adaptive features.

Since a few years Rzeszów University of Technology has been cooperating with Praxis Automation Technology B.V. in the Netherlands on implementation of CPDev package [5] for programming ship monitoring and navigation systems manufactured by Praxis. Several months ago joint development of autopilot prototype has been initiated, with Rzeszów responsible for control software. Preliminary version of such software implemented on PC and ARM microcontroller has been completed recently.

Tuning rules of the autopilot controllers were one of the problems encountered at the beginning, since well regarded textbooks [2,3,4] are not sufficiently specific in this respect. For practical reasons, we have been looking for such rules, which apart

from no oscillations and no overshoot requirements, are able to determine dynamics of course and track control loops by means of single design parameters. The dynamics depend on ship construction and sea state.

Outline of development of such rules for PID course controller and PI or state-space track controller is presented in this paper. They have been tested on 4-DOF model of a container ship [6],[8]. We begin with overview of the autopilot structures to show major components of control software.

2 Structure of the Autopilots

Structure of conventional adaptive autopilot, based on the guidelines from [2,3], is shown in Fig.1. ψ_{ref} and ψ are reference and actual course, respectively, δ denotes rudder angle. ψ_L , ψ_H are low- and high-frequency components of ψ , the latter induced by waves as yaw motions. The observer generates estimates $\hat{\psi}_L$, $\hat{\psi}_H$, of which $\hat{\psi}_L$ is used by course feedback. This limits reaction of the rudder to waves. The observer can be implemented either as Kalman filter or Luenberger observer. ARMAX identifier determines wave frequency ω_n which is a coefficient in observer equations. Note that ω_n depends on sea state and direction of the wind in relation to ship course. Rate limiter eliminates overshoot after step change of ψ_{ref} . Settings of the PID controller are adapted to ship speed V .

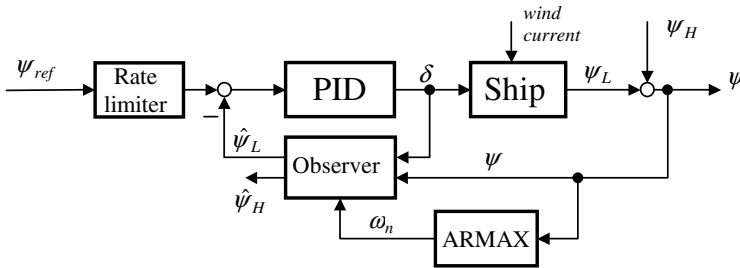


Fig. 1. Structure of the course autopilot

Cascade structure of the track autopilot is shown in Fig.2. If deviation y of the ship from reference path is detected, track controller (primary) corrects reference ψ_{ref} by $\Delta\psi_{ref}$, so the sum $\psi_{ref} + \Delta\psi_{ref}$ becomes set-point for the course controller (secondary). Track controller can be implemented as state-space or PI. Track-keeping settling time can be specified for the former and not for the latter. Naturally, all state variables, and not just y as in Fig.2, are needed to implement state feedback. Kinematics equations involving GPS position, speed V and course ψ (or $\Delta\psi = \psi - \psi_{ref}$) determine forward displacement x and perpendicular deviation y .

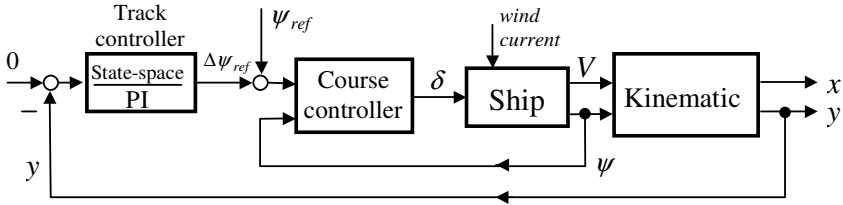


Fig. 2. Structure of the track-keeping autopilot

3 PID Course Controller

An integral with time constant

$$\frac{k}{s(Ts+1)} = \frac{\psi(s)}{\delta(s)} \tag{1}$$

called Nomoto model [2,3,4] is a simple description of the way according to which rudder angle δ affects the ship course angle ψ . The gain k depends directly and time constant T inversely on the ship speed V , i.e.

$$k = k_0 \frac{V}{V_0}, \quad T = T_0 \frac{V_0}{V} \tag{2}$$

The reference three $\{k_0, T_0, V_0\}$ is assumed known from zig-zag maneuvers during sea trials or after leaving the port. k_0, T_0 also include dynamics of the steering machine.

Course control is implemented by means of the PID controller

$$k_p \left(1 + \frac{1}{T_i s} + T_d s\right) = k_p \frac{(T_i s + 1)(T_2 s + 1)}{T_i s} \tag{3a}$$

$$T_i = T_1 + T_2, \quad T_d = \frac{T_1 T_2}{T_1 + T_2} \tag{3b}$$

Tuning specifications are as follows:

- (a) no oscillations of the transient responses
- (b) closed-loop time constant given by

$$T_d = \frac{T}{r}, \quad r > 1 \tag{4}$$

- (c) no overshoot to step changes of set-point.

The condition (b) requires the time constant T_{cl} to be r -times smaller than the ship time constant T . r is a design parameter. By choosing large r one can make the loop arbitrarily "fast" (theoretically).

To determine controller settings k_p , T_i , T_d , we apply time constant cancellation by taking

$$T_2 = T \quad (5)$$

Then the open-loop and closed-loop transfer functions become

$$G_{open}(s) = K \frac{T_1 s + 1}{s^2} \quad (6a)$$

$$G_{loop}(s) = \frac{K(T_1 s + 1)}{s^2 + K T_1 s + K} \quad (6b)$$

with

$$K = \frac{k_p k}{T_i} \quad (6c)$$

The condition (a) is satisfied if determinant of G_{loop} 's denominator equals zero, what gives

$$K = \frac{4}{T_1^2} \quad (7)$$

Then the double root is

$$s_{1,2} = -\frac{K T_1}{2} = -\frac{2}{T_1} \quad (8)$$

The condition (b) requires the closed-loop time constant $T_{cl} = 1/|s_{1,2}| = T_1/2$ to be equal to T/r . From this we get

$$T_1 = \frac{2T}{r} \quad (9)$$

Now PID settings follow from (3b), (6c) (7) and (9), so

$$k_p = \frac{r^2}{kT} \frac{r+2}{r}, \quad T_i = T \frac{r+2}{r}, \quad T_d = T \frac{2}{r+2} \quad (10)$$

Note that due to (2), the settings depend on the ship speed V . Sensitivity tests have revealed that the settings should be modified only if speed change exceeds 20%.

The system involving PID controller only will exhibit overshoot due to the term T_1s+1 in the numerator of G_{loop} . To eliminate this we can use the set-point filter $1/(T_1s+1)$, as shown in Fig.3. The transfer function of the system becomes

$$G_{cl}(s) = \frac{1}{(T_{cl}s+1)^2} = \frac{\psi(s)}{\psi'_{ref}(s)} \quad (11)$$

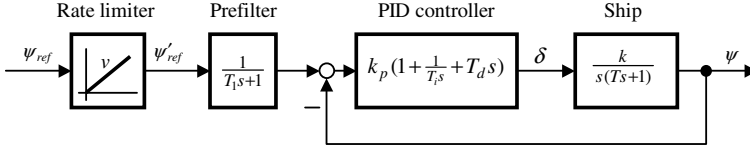


Fig. 3. Course control system for controller design

4 Set-Point Rate Limiter

Since the rudder angle δ cannot exceed certain rudder limit δ_M

$$|\delta| < \delta_M, \quad (12)$$

so the prefilter $1/(T_1s+1)$ does not suffice for to avoid overshoot for step changes of ψ'_{ref} (typically $\max \delta_M = 35^\circ$). Besides, helmsman may adjust δ_M to ship speed V . As in some process control systems where overshoot is not allowed, the autopilot must be provided with a set-point rate limiter, which limits rate of ψ'_{ref} change to some value v .

Let $\psi'_{ref} = v \cdot t$. Using (11), one can write an expression for the rudder angle

$$\delta(s) = \frac{1}{k} \frac{s(T_s+1)}{(T_{cl}s+1)} \frac{v}{s^2} = \frac{1}{k} \frac{T_s+1}{(T_{cl}s+1)^2} \frac{v}{s} \quad (13)$$

Its time representation $\delta(t)$ has a maximum for $T_{cl} < T$ ($r > 1$). From the condition

$$\max \delta(t) \leq \delta_M \quad (14)$$

and using $T_{cl} = T/r$ one can find

$$r \leq \frac{k}{f(r)} \delta_M \quad (15)$$

where the function $f(r)$ is shown in Fig.4. As seen, the smaller rudder limit δ_M and larger design parameter r (i.e. the smaller required T_{cl}), the smaller rate v of the set-point change allowed by the limiter.

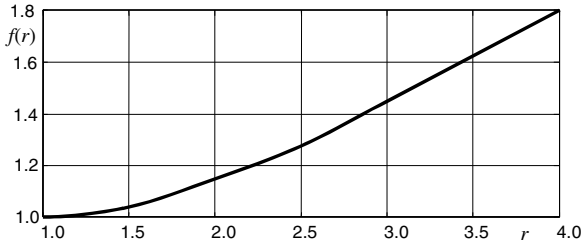


Fig. 4. Function $f(r)$ for set-point rate limiter

5 Limitation of PI Track Controller

Suppose we are given a reference path to be followed by the ship. Let ψ_{ref} denotes the course along this path. GPS navigation system determines perpendicular deviation y from the path. As shown in [2], for small course error $\Delta\psi = \psi - \psi_{ref}$, deviation y is a speed-weighted integral of $\Delta\psi$, i.e.

$$y(s) = \frac{V}{s} \Delta\psi(s) \tag{16}$$

($\Delta\psi$ in radians). Applying standard PI controller we consider the system of Fig.5.

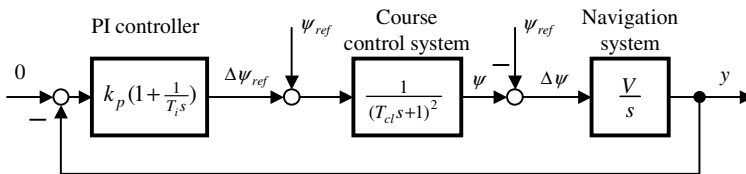


Fig. 5. Track-keeping system with standard PI controller

Specifications are the following:

- (a) no oscillations of the transient responses
- (b) short settling time (as far as possible).

The problem can be solved by applying root locus design [1],[7].

The two requirements will be satisfied if we find such controller zero $1/T_i$ for which the closed-loop system has a triple real pole (unique in this case). After some Matlab trials one can find such pole at $s_{tr} = -0.16/T_{cl}$ for

$$T_i = 15 T_{cl} \quad (17)$$

Then the root locus magnitude condition yields

$$k_p = 0.2 \frac{1}{T_{cl} V} \quad (18)$$

Settling time of the track-keeping is

$$t_{tr} \cong \frac{4}{|s_{tr}|} = 25 T_{cl} \quad (19)$$

Note that such settling time is over 6 times longer than settling time of the course control ($4 T_{cl}$). Besides, for typical data k_p turns out to be very small and T_i large. So, as may be expected from [1], we have got a low-gain PI controller.

6 State-Space Track Controller

If slow dynamics of the standard PI track-keeping is not satisfactory, state-space controller may be a solution. Deviation y , course error $\Delta\psi$ and its derivative $\Delta\dot{\psi}$ are state variables, with $\Delta\dot{\psi}$ obtained either from direct measurement (rate-of-turn) or by differentiation of $\Delta\psi$ (with some smoothing). To compensate steady-state disturbances we have to add an integral of y as the fourth variable. Thus the state vector consists of

$$x_I = \int y dt, \quad x_1 = y, \quad x_2 = \psi, \quad x_3 = \Delta\dot{\psi} \quad (20)$$

Output of the controller is generated by

$$\Delta\psi_{ref} = -(K_I x_I + K_1 x_1 + K_2 x_2 + K_3 x_3) \quad (21)$$

Building a state-space description $\{A, b, c\}$ for the "plant" composed of $1/(T_{cl}s + 1)^2$ and V/s is straightforward, so omitted here.

To get analytical results quickly, assume that specification has the form of quadruple closed-loop pole

$$p = \frac{\sigma}{T_{cl}} \quad (22)$$

related to course control time constant T_{cl} , with some design parameter σ . By choosing $\sigma = 1$ one can make settling time of track-keeping comparable to that of course control ($4T_{cl}$). This may be, however, too ambitious, so values $\sigma \leq 0.5$ are rather recommended.

Having the state-space description $\{A, b, c\}$ and the closed-loop characteristic equation $(s + p)^4$ with $p = \sigma/T_{cl}$ one can find the following gains

$$K_I = \frac{\sigma^4}{T_{cl}^2} \frac{1}{V}, \quad K_1 = 4 \frac{\sigma^3}{T_{cl}} \frac{1}{V}, \quad K_2 = 6\sigma^2 - 1, \quad K_3 = 2T_{cl}(2\sigma - 1) \quad (23)$$

Note how the gains depend on σ and T_{cl} .

Simulation of track-keeping for a container ship [6],[8] is shown in Fig.6. Dashed and continuous line denote reference and actual path, respectively. Small overshoot indicates that some improvement may still be needed.

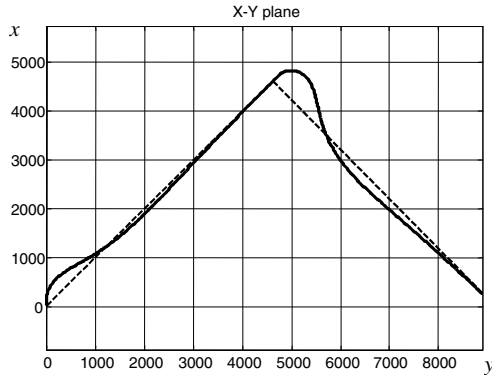


Fig. 6. Track-keeping plot with a change of reference path

7 Conclusions

Tuning rules for PID controller of conventional autopilot and for PI or state-space track controller of advanced autopilot have been presented. Single design parameters to determine closed-loop dynamics are required for each of them. Hence autopilot behavior can be easily adjusted to ship construction or sea state. Controller settings depend on ship speed. Set-point rate limiter eliminates overshoots by automatic adjustment of the rate to rudder limit and course controller design parameter.

The rules are applied in control software of autopilot prototype. Service screen of the preliminary interface is shown in Fig.7. The following operating modes are available: Heading Control (HDG_C, i.e. course control), TRACK Control, Turn Radius, Turn ROT (rate-of-turn).

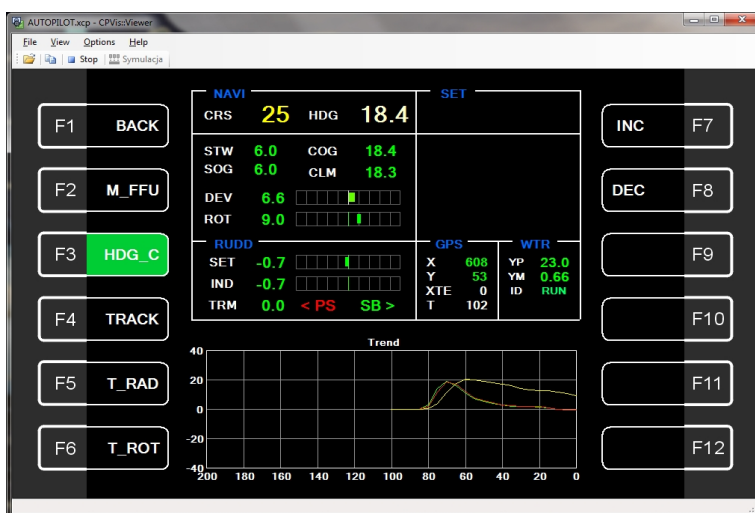


Fig. 7. Service screen of the prototype interface

References

1. Dorf, R.C., Bishop, R.M.: Modern Control Systems, 11th edn. Prentice Hall, Upper Saddle River (2008)
2. Fossen, T.I.: Guidance and Control of Ocean Vehicles, 4th edn. Wiley, Chichester (1999)
3. Fossen, T.I.: Marine Control Systems. Marine Cybernetics, Trondheim (2002)
4. Lisowski, J.: Ship as Automatic Control Plant. Wyd. Morskie, Gdańsk (1981) (in Polish)
5. Jamro, M., Rzonca, D., Sadolewski, J., Stec, A., Swider, Z., Trybus, B., Trybus, L.: CPDev Engineering Environment for Modeling, Implementation, Testing, and Visualization of Control Software. In: Szewczyk, R., Zieliński, C., Kaliczyńska, M. (eds.) Recent Advances in Automation, Robotics and Measuring Techniques. AISC, vol. 267, pp. 81–90. Springer, Heidelberg (2014)
6. Stec, A.: Ship Maneuvering Model for Autopilot Simulator. This conference
7. Trybus, L.: Control Theory. Ofic. Wyd. PRz., Rzeszów (2007) (in Polish)
8. <http://www.marinecontrol.org/Tutorial.html>

A Novel Approach to Optimization of Jobs in Groups

Jarosław Wikarek

Department of Control and Management Systems,
Kielce University of Technology, Poland
j.wikarek@tu.kielce.pl

Abstract. This study deals with scheduling groups of jobs, their arrival and delivery, and individual processing of each of them. All jobs in a group should be delivered at the same time after processing. The objective of the problem is to minimize the average delivery time of the group containing that job (waiting period). The authors present a novel way of modeling the optimization problem – a hybrid approach to modeling. This approach includes the design and implementation of the optimization model in the MILP (Mixed-Integer Linear Programming) environment, an iterative algorithm for solving the model under the dynamic emergence of new orders as well as transformation and linearization of the model in CLP/MILP environments. In addition, the paper proposes new functionalities based on the CLP (Constraint Logic Programming) environment and illustrative models for service providers (a restaurant).

Keywords: mathematical programming, constraint logic programming, optimization, decision support systems, group work.

1 Introduction

A very good illustration of the handling of jobs in groups is the process of preparing and serving food in a restaurant [1]. Guests enter the restaurant in different groups at different moments. Each group chooses a table and all orders of the group members are taken simultaneously. After the accomplishment of these processes, all meal items ordered by a group are served simultaneously. The quality of service and the rate of customer satisfaction are raised if a meal item is served as soon as it is ready. In a restaurant, a group of meal items ordered by guests sitting at a table should be delivered together. Thus, the cooked meal items for a specific group have to wait until the last item of that group is cooked and is ready to be served.

The proposed research problem finds many applications in industrial companies, including but not limited to food, ceramic tile, textile production industries, distributions, supply chain, installation of bulky equipment, manufacturing of complex devices, etc. It can be noticed in many production and logistic industries that have different customers. Assume that each customer has different orders. Each order has a different process function and resources, but all items ordered by a customer or group of customers should be delivered at the same time in one package to reduce the transportation costs, subsequent processing steps time and costs or/and assure proper quality of the product/service and customer satisfaction.

The remainder of the article is organized as follows. Section 2 presents a literature review. Problem statement, research methodology, mathematical model and contribution are provided in Section 3. Computational examples, tests of the implementation platform and discussion are presented in Section 4. Possible extensions of the proposed approach as well as the conclusions are included in Section 5.

2 Literature Review

To best meet customers' expectations (Section 1), multiple decision problems have to be solved. These include processes of food preparation and delivery, proper arrangements of customers at the tables, etc. Due to the number and character of the problems (multimodal, asynchronous, parallel) as well as constraints related to resources, time, etc., they are considered at different decision making levels. At the strategic level, problems of optimal configuration of the order processing/handling environment occur. In the case of a restaurant, these include the selection, configuration and arrangement of tables, known as the Table Mix Problem (TMP) [1, 2]. The "best" table mix is influenced by several factors such as: the expected number of each size party that will be potential customers; the expected meal duration of each party; the dimensions and the layout of the restaurant, which limit the number and type of tables that can be used, and the possibility of combining tables of different dimensions. Once the TMP is solved, i.e. the number of tables, their size, etc. are decided, it is necessary to assign tables to customers in the most profitable way. Operational decisions are mainly concerned with the most profitable assignment of customers to specific tables. The "Parties Mix Problem" consists of deciding on accepting or denying a booking request from different groups of customers, with the aim of maximizing the total expected revenue [3]. The revenue management RM problem is dealt with in multiple papers as the overarching question [3, 4]. Scheduling methods for optimal and simultaneous provision of service to groups of customers are proposed most often in the flexible flow-shop system (FFS). In the FFS system, processing is divided into several stages with parallel resources at least in one stage. All of the tasks should pass through all stages in the same order (preparing meals) [5, 6]. The exemplified objectives of the problem [6] are minimizing the total amount of time required to complete a group of jobs and minimizing the sum of differences between the completion time of a particular job in the group and the delivery time of this group containing that job (waiting period).

Our motivation was to develop a method that allows modeling and optimization decisions for problems handling incoming orders in groups with the same date of completion for various forms of organization. Development of decision-making models, whose implementation using the proposed method will allow obtaining quick answers to key questions asked by a service manager. The method takes into account the dynamics resulting from the coming of new groups of orders while previous orders are handled.

3 Problem Statement and Methodology

The majority of models presented in the literature (Section 2) refer to a single problem and optimization according to the set criterion. Fewer studies are devoted to multiple-criteria optimization by operations research (OR) methods [6]. One paper [7] applies constraint programming, but it is used only to solve the static problem of restaurant configuration. Declarative environments such as CP/CLP facilitate problem modeling and introduction of logical and symbolic constraints [8–12]. Unfortunately, high complexity of decision-making models and their integer nature contribute to poor efficiency of modeling in OR methods and inefficient optimization in CLP. Therefore, a novel approach to modeling and solving these problems was developed. A declarative environment was chosen as the best structure for this approach [8, 11, 13]. Mathematical programming environment was used for problem optimization [14]. This mixed and integrated approach is the basis for the creation of the implementation environment to support managers. In addition to optimizing particular decision making problems connected with groups of orders, such environment allows asking various questions while processing the orders.

The main contribution on our part is the new method for the modeling and optimization of decision-making problems for handling orders in groups. It is based on the integration of CLP and MP environments (section 3.3). The objective function of the constructed decision model is to minimize the average service/waiting time for each group. The linearization model of decision-making was built using the CLP environment. Based on the proposed method and model, we designed the environment that allows managers to ask questions and get fast answers in the process of handling groups of orders. The iterative algorithm proposed enables dynamic use of this method. The algorithm is designed in such a way that allows you to run framework in subsequent periods in which there are orders. The algorithm also updates every period the availability of resources.

3.1 Problem Description

This problem can be stated as follows (Fig. 1). Orders ($j = 1..M$) enter the system in groups at different periods ($h = 1..V$). Each order should be processed by specific resources, including parallel resources ($k = 1..E$). The orders ($j = 1..M$) in each group should be delivered. It is assumed that all processors in the last stage are eligible to process all jobs. This assumption is valid due to the fact that processors in the last stage (waiters at restaurants who deliver meals or packers in a factory, or quality control) are the same in most of the application areas of the proposed problem. Special points at which orders are submitted and then delivered are introduced (e.g. tables) ($i = 1..N$). (These points can be aggregated in groups $b = 1..W$). The problem does not cover configuration of the points but relates to handling orders, as many orders may come from one customer (orders several items from the menu). Each order may be processed by a different resource set in any order.

The objective function is stated as the minimization of the average delivery time for each group. Possible questions for this model are:

- What is the minimum average waiting time in each group? (Q1)
- Can the order be delivered within g period? (Q2)
- Which order (meal item) cannot be delivered in each group of orders within g period? (Q3)
- Which order (meal item) can be prepared in the number of M within g period for points i ? (Q4)
- With the specified number of resources Rzt (waiters), is it possible to deliver orders to all groups within N time? (Q5)
- Is it possible to deliver orders of all groups with resources $d_1, d_2, ..d_k$ within g period? (Q6)

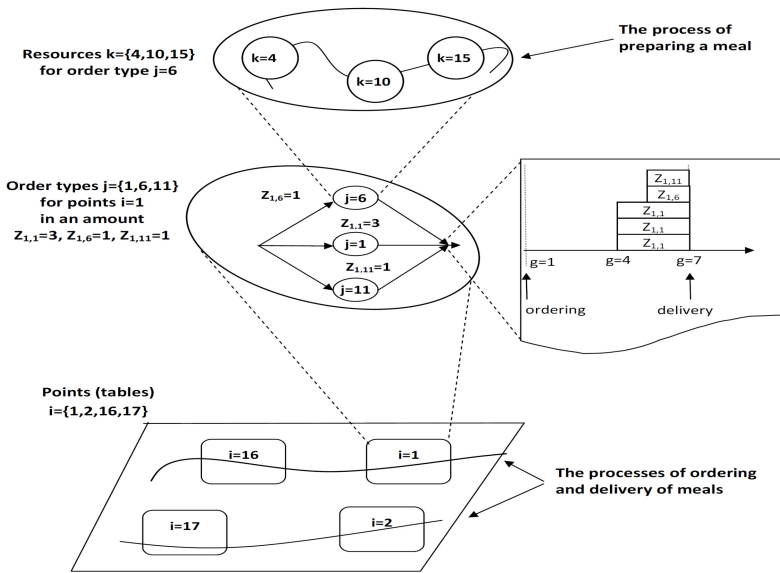


Fig. 1. Scheme for the problem of handling orders in a restaurant

3.2 Mathematical Model

A mathematical model is developed for the research problem. The sets, indices, parameters, decision variables are presented in Table 1.

Objective Function

Minimization of average waiting time at each point i (1).

Constraints

Constraint (2) specifies the starting time of handling order j from point i . Delivery/processing/handling of order j cannot start before moment St , at which demand appears (3). Only available number of resources k can be used in any period of time

(4). When order j for point i is delivered using resource k in period g , the resources have to be reserved for a period of time (5). Determining the end times for resource jobs – constraints (6), (7) ensure the value of variable $Y_{i,j,k,g}$ and continuous handling/processing of the order. All orders j for point i should end at the same moment (8). Constraint (9) binds variable $X_{i,j,k,g}$ (setting its value to be 1 where index g takes values ranging from $S_{i,j}$ to Tkp_i) (9). Constraint (10) specifies the number of different type of resources. Constraint (11) is responsible for the binarity of selected decision variables.

Table 1. Summary indices, parameters and decision variables

| Sets | |
|--|-----------------|
| Set of points (tables) | N |
| Set of orders | M |
| Set of resources | E |
| Number of periods | U |
| Number of periods in which orders can be entered | V |
| Indices | |
| Points (tables) | $i = 1..N$ |
| Orders | $j = 1..M$ |
| Resources | $k = 1..E$ |
| Period | $g = 1..U$ |
| Period in which orders can be entered | $h = 1..V$ |
| parameters | |
| Time for execution of order j | t_j |
| Available number of resources k | d_k |
| Number of k resources needed for execution of order j | $R_{i,k}$ |
| The number of resources of different type (waiters) | Rzt |
| Number used to convert periods to moments (for connecting index g with variable $S_{i,j}$, if $S_{i,j}=7$ then index $g=7$) | pp _g |
| Inputs | |
| The number of orders j at point i during period g | $Z_{g,i,j}$ |
| Decision variables | |
| If the execution of order j for point i uses resource k in period g then $X_{i,j,k,g}=1$, otherwise $X_{i,j,k,g}=0$ | $X_{i,j,k,g}$ |
| If g is the last period in which resource k is used in the execution of order j for point i then $Y_{i,j,k,g}=1$, otherwise $Y_{i,j,k,g} = 0$ | $Y_{i,j,k,g}$ |
| If g is the last period in which orders are executed for point i then $W_{i,g}=1$, otherwise $W_{i,g}=0$ | $W_{i,g}$ |
| Calculated number of periods g (using pp_g) delivery of all orders for point i . | Tkp_i |
| Calculated number of periods g (using pp_g) starting time of order j delivery for point i . | $S_{i,j}$ |

$$Fc_1 = \min \frac{1}{N} \sum_{i=1}^N Tkp_i \tag{1}$$

$$S_{i,j} + t_j = Tkp_i \text{ for } i = 1..N, j = 1..M, z_{i,j} > 0$$

$$S_{i,j} = 0 \text{ for } i = 1..N, j = 1..M, z_{i,j} = 0 \tag{2}$$

$$S_{i,j} \geq St \text{ for } i = 1..N, j = 1..M, \tag{3}$$

$$\sum_{i=1}^N \sum_{j=1}^M (X_{i,j,k,g} \cdot R_{j,k} \cdot z_{i,j}) \leq dk_{k,g} \text{ for } k = 1..E, g = 1..U \tag{4}$$

$$\sum_{i=1}^N \sum_{j=1}^M (X_{i,j,k,g} \cdot R_{j,k} \cdot z_{i,j}) = p_{-zaj_{k,g}} \text{ for } k = 1..E, g = 1..U$$

$$\sum_g^U X_{i,j,k,g} = t_j \text{ for } i = 1..N, j = 1..M, k = 1..E, z_{i,j} > 0, l_{j,k} > 0$$

$$X_{i,j,k,g} = 0 \text{ for } i = 1..N, j = 1..M, k = 1..E, z_{i,j} = 0 \tag{5}$$

$$X_{i,j,k,g} = 0 \text{ for } i = 1..N, j = 1..M, k = 1..E, l_{j,k} = 0$$

$$\sum_g^U Y_{i,j,k,g} = 1 \text{ for } i = 1..N, j = 1..M, k = 1..E, z_{i,j} > 0, R_{j,k} > 0 \tag{6}$$

$$X_{i,j,k,g-1} - X_{i,j,k,g} \leq Y_{i,j,k,g-1} \text{ for } i = 1..N, j = 1..M, k = 1..E, g = 2..U, z_{i,j} > 0, R_{j,k} > 0$$

$$Y_{i,j,k,g} = 0 \text{ for } i = 1..N, j = 1..M, k = 1..E, g = U \tag{7}$$

$$Y_{i,j,k,g} = 0 \text{ for } i = 1..N, j = 1..M, k = 1..E, g = 1$$

$$Y_{i,j,k1,g} = Y_{i,j,k2,g} \text{ for } i = 1..N, j = 1..M, k1, k2 = 1..E, g = 1..U, z_{i,j} > 0, R_{j,k} > 0 \tag{8}$$

$$X_{i,j,k,g} = \begin{cases} 1 & \text{for } i = 1..N, j = 1..M, k = 1..E, g = 1..U, g \geq S_{i,j}, g \leq Tkp_i \\ 0 & \text{otherwise} \end{cases} \tag{9}$$

$$\sum_{i=1}^N \sum_{j=1}^M \sum_{k=1}^E Y_{i,j,k,g} \leq Rzt \text{ for } g = 1..U \tag{10}$$

$$X_{i,j,k,g} = \{0,1\} \text{ for } i = 1..N, j = 1..M, k = 1..E, g = 1..U$$

$$Y_{i,j,k,g} = \{0,1\} \text{ for } i = 1..N, j = 1..M, k = 1..E, g = 1..U \tag{11}$$

3.3 Linearization of the Model

The mathematical model presented in 3.2 is non-linear. To linearize this model, an ancillary variable was used, $W_{i,g} = \{0, 1\}$, determined according to formula 12 (where coefficients/factors pp_g are determined by the CLP). Additional constraints (13), (14) and (15) were introduced to replace constraint (9). After the linearization, the model was formulated in the form of the mixed integer linear programming (MILP) problem.

$$Tkp_i = \sum_{g=1}^U pp_g \cdot W_{i,g} \text{ for } i = 1..N, \tag{12}$$

$$Y_{i,j,k,g} = W_{i,g} \text{ for } i = 1..N, j = 1..M, k = 1..E, g = 1..U, z_{i,j} \geq 0, R_{j,k} \geq 0 \tag{13}$$

$$\sum_{g=1}^U W_{i,g} \leq 1 \text{ for } i = 1..N \tag{14}$$

$$W_{i,g} = \{0,1\} \text{ for } i = 1..N, g = 1..U \tag{15}$$

3.4 A Novel Integrated Approach to Modeling, Solving and Optimization

The idea of integrating CLP and MILP environments outlined in Section 3 idea was expanded into the framework, as in Fig. 2. It can be used to implement specific decision models (Section 3.2) as well as ask questions related to these models. The questions and the additional constraints are implemented in the form of CLP predicates. Examples of question that can be asked are presented in Section 3. The CLP environment is used to model the problem, linearize and transform it. It is also effective in terms of receiving answers to general questions, such as *Is it possible...? Is it enough...?* For optimization and specific questions, such as *What is the minimum ...? What is the shortest time ...?*, after the initial “domain” solving, the problem is finally solved in the MP environment.

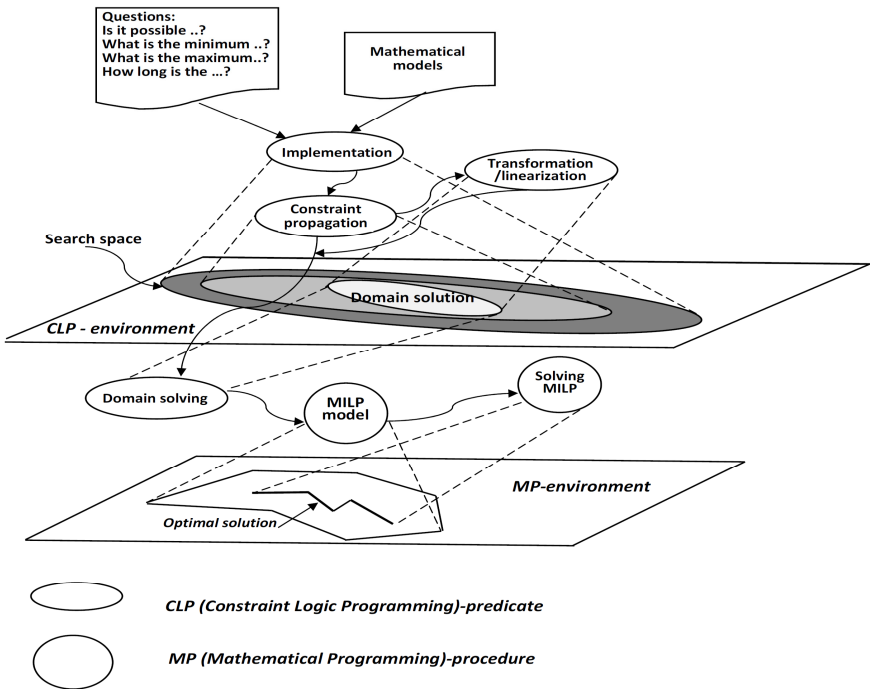


Fig. 2. The scheme of the integrated implementation framework

4 Numerical Experiments

In order to verify and evaluate the proposed approach, many numerical experiments were performed for the illustrative example. All the experiments relate to the restaurants with twenty points (tables) ($i = 1..20$), twenty five order types ($j = 1..25$), fifteen resource types ($k = 1..15$), twenty time periods ($g = 1..20$) and twenty eight orders $Z_{g,i,j}$. Computational experiments consisted in asking questions Q1..Q6 for the model (Section 3.2) implemented in the framework (Section 3.3) iteratively run with interactive algorithm. Orders are ordered in groups of $h_1 = 1, h_2 = 3, h_3 = 6$ periods. Figure 3 shows the implementation schedule of all orders for this example while minimizing the average waiting time. The answer to question Q1, ie. the minimum waiting time for each order of period h_1 is from $Tpk = 3$ to $Tpk = 4$, for the period h_2 is from $Tpk = 3$ to $Tpk = 8$, and for the period h_3 respectively from $Tpk = 2$ to $Tpk = 5$.

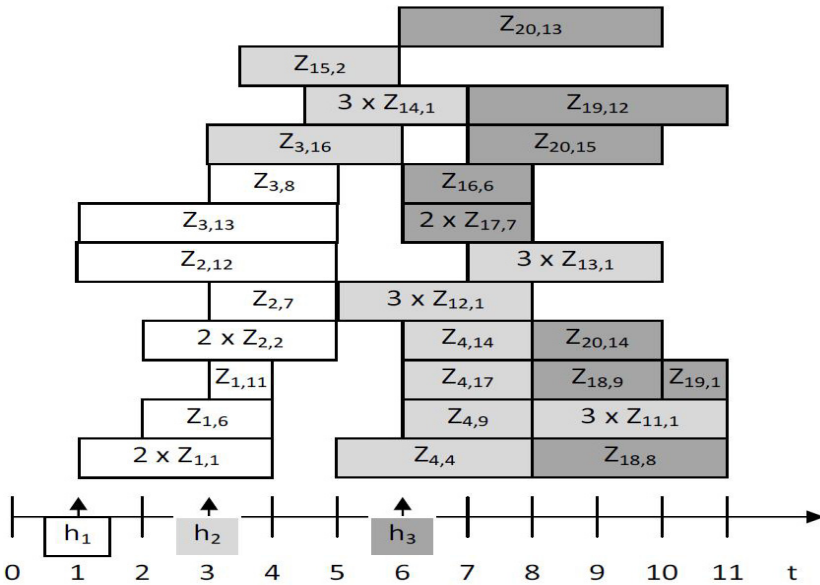


Fig. 3. Gantt chart for illustrative example ($Z_{i,j}$)

The answer to the question Q2 for ordering h_1 period is for $g = 1, g = 2, g = 3, g = 4$ No, but for $g = 5$ Yes. For the remaining periods of order h_2 and h_3 response can be read from the schedule (Fig. 3). For the h_1 period if we take $g = 4$ the answer to Q3 is that it is impossible to achieve groups of orders from the $i = 2, i = 3$ points and can be from the point $i = 1$. Table 2 shows the possible answers to the question Q4 with the following parameters: What order (item meal can be prepared in a number of 20 within $g = 10$ period to five points i ?

Table 2. Answers to the question Q4 for illustrative example

| j | Answer | g | j | Answer | g | j | Answer | g |
|---|--------|----|----|--------|----|----|--------|----|
| 1 | Yes | 10 | 10 | Yes | 4 | 18 | No | -- |
| 2 | Yes | 10 | 11 | Yes | 4 | 19 | No | -- |
| 3 | Yes | 10 | 12 | Yes | -- | 20 | No | -- |
| 4 | Yes | 10 | 13 | Yes | -- | 21 | Yes | 10 |
| 5 | Yes | 10 | 14 | Yes | 7 | 22 | Yes | 10 |
| 6 | Yes | 7 | 15 | Yes | 10 | 23 | Yes | 10 |
| 7 | Yes | 7 | 16 | No | -- | 24 | Yes | 10 |
| 8 | Yes | 7 | 17 | No | -- | 25 | Yes | 10 |
| 9 | Yes | 7 | | | | | | |

For questions Q5 if we assume that $Rzt = 2$ and period $g = 11$, the answer is No. However, if $Rzt = 5$ $g = 11$ the answer is Yes.

For questions Q6 with the number of resources (d_k) of respectively 5, 6, 7, 8, 9, 4, 5, 6, 7, 8, 8, 7, 6, 5, 4 at the $g = 11$ the answer is No, and period $g = 18$, the answer is Yes.

5 Conclusion

The proposed approach to the optimization processes for the reference problem of handling orders in a restaurant can be used in many areas. Similar issues exist wherever there are a variety of customer orders, the handling of which requires processes and additionally, both are ordered and executed jointly with a single delivery deadline. In practice, such an approach to group order handling occurs in manufacturing, services, logistics and project management. The presented framework, which is an implementation of the proposed approach, enables effective planning, design and management of the processes by a manager. This allows the implementation of decision-making models with different objective functions and the introduction of the models already implemented with additional constraints. It also provides the opportunity to ask two types of questions and obtain answers. General questions may require domain solution, which in practice determines the availability of resources to execute orders. The wh-questions will in practice define the best, fastest, cheapest or the most expensive of the possible solutions. To obtain answers, optimization is necessary. The illustrative example shows only part of the framework’s potential. Further work will consist in the implementation of more complex models such as a decision-making model covering operations. Introduction of precedence constraints to operations and orders, uncertainty, fuzzy logic etc. is considered. New questions will be implemented to broaden the scope of decision support.

References

1. Guerriero, F., Miglionico, G., Olivito, F.: Strategic and operational decisions in restaurant revenue management. *European Journal of Operational Research* 237, 1119–1132 (2014)
2. Thompson, G.M.: Optimizing restaurant table configuration: Specifying combinable tables. *Cornell Hotel and Restaurant Administration Quarterly* 44, 53–60 (2003)

3. Chiang, W.C., Chen, J.C.H., Xu, X.: An overview of research on revenue management: Current issues and future research. *International Journal of Revenue Management* 1, 97–128 (2007)
4. Thompson, G.M.: Restaurant profitability management, The evolution of restaurant revenue management. *Cornell Hospitality Quarterly* 51, 308–322 (2010)
5. Ribas, I., Leisten, R., Framinan, J.: Review and classification of hybrid flow shop scheduling problems from a production system and a solutions procedure perspective. *Comput. Oper. Res.* 37, 1439–1454 (2010)
6. Tadayon, B., Salmasi, N.: A two-criteria objective function flexible flowshop scheduling problem with machine eligibility constraint. *The International Journal of Advanced Manufacturing Technology* 64(5-8), 1001–1015 (2013)
7. Vidotto, A., Brown, K.N., Beck, J.C.: Managing Restaurant Tables using Constraints. *Knowledge Based Systems* 20(2), 160–169 (2007)
8. Apt, K., Wallace, M.: *Constraint Logic Programming using Eclipse*. Cambridge University Press, Cambridge (2006)
9. Sitek, P., Wikarek, J.: A Hybrid Approach to the Optimization of Multiechelon Systems, *Mathematical Problems in Engineering*, vol. 2015, Article ID 925675, 12 pages (2015), doi:10.1155/2015/925675
10. Sitek, P., Wikarek, J.: A hybrid approach to modeling and optimization for supply chain management with multimodal transport. In: *Proceedings of the 18th International Conference on Methods and Models in Automation and Robotics (MMAR 2013)*, pp. 777–782 (2013)
11. Sitek, P., Wikarek, J.: Hybrid Solution Framework for Supply Chain Problems. In: Omatu, S., Bersini, H., Corchado Rodríguez, J.M., González, S.R., Pawlewski, P., Bucciarelli, E. (eds.) *Distributed Computing and Artificial Intelligence*, 11th International Conference. AISC, vol. 290, pp. 11–18. Springer, Heidelberg (2014)
12. Sitek, P.: A hybrid CP/MP approach to supply chain modelling, optimization and analysis. In: *Proceedings of the 2014 Federated Conference on Computer Science and Information Systems*, pp. 1345–1352 (2014), doi:10.15439/2014F89
13. Sitek, P.: A Hybrid Approach to the Two-Echelon Capacitated Vehicle Routing Problem (2E-CVRP). In: Szewczyk, R., Zieliński, C., Kaliczyńska, M. (eds.) *Recent Advances in Automation, Robotics and Measuring Techniques*. AISC, vol. 267, pp. 251–264. Springer, Heidelberg (2014)
14. Schrijver, A.: *Theory of Linear and Integer Programming*. John Wiley & Sons, New York (1998)
15. LINDO Systems INC, 2014, LINDO™ Software for Integer Programming, Linear Programming, Nonlinear Programming, Stochastic Programming, Global Optimization (2014), <http://www.lindo.com> (accessed August 12)
16. Eclipse, Eclipse - The Eclipse Foundation open source community website (2014), <http://www.eclipse.org> (accessed August 12)

Multiple File Server with the Implemented Mechanism ACL

Marian Wrzesień and Piotr Ryszawa

Industrial Research Institute for Automation and Measurements PIAP,
Warsaw, Poland
{mwrzesien, pryszawa}@piap.pl

Abstract. Presented – implemented and made available to users in the PIAP – a multi-access file server, whose functionality is achieved by implementing Access Control List ACL in the operating system Linux OS. Discusses the methodology for configuring the server constituting condition for achieving this objective. Analyzed the server implementation which allows the use of the ACL. The implementation of this mechanism was preceded by modifying a standard file system on the server to the version that supports Extended Attributes EA. In the Linux server has been implemented Samba server in which are located defined resources. Discussed the process of setting up a Samba server. To manage the obtained functionality has been developed and presented a method to allocate permissions for individual users to specific resources and proposed solutions for managing access ACL. Discussed the resource size constraints on the disk based on the properties `usrquota` and `grpquota` of the file system.

Keywords: File Server, Samba, Access Control List, Extended Attributes.

1 Introduction

In everyday practice, while computer data processing, are used a variety of server solutions, of which Novell NetWare server is already a classic solution. It allows the establishment of rights to information resources [SRWCEMFA] [Supervisor, Read, Write, Create, Erase, Modify, File scan, Access control]. Despite the clarity of functionality OS NetWare, there are some imperfections such as small management capabilities, its questionable stability and well-known among users ABEND (abnormal termination or stop functioning of the program), and at the end, the language barrier and lack of openness of the system.

Differently from the NetWare OS is Linux OS – selected for use while research on the issues discussed in the presented article. During the research, the authors used the version of CentOS Linux distribution, which is characterized by transparency, high stability, user friendly interface, resources security, and above all, is easy to integrate the system in a network environment LAN PIAP of Institute, where Windows 7 OS is used, and where the backups are performed on servers running CentOS.

Access to IT resources in the standard CentOS system is implemented as follows:

```
[u [g [o [a]]] [+ - =] [r [w [x]]]
```

which means that the rights to read (r), write (w) and execute (x) are being added (+) subtracted (-) or replaced (=) to the user or to group or to others. This solution implies a limit the setting of the rights to one user and one group. Delegating access to other users can be accomplished only by categorizing users in groups, causing quite a stir when assigning accesses.

The aim of this study was to:

- Server implementation, that allows the use of ACLs,
- The use of existing mechanisms in the Samba server, which are used to share specified resources,
- Developing a method for assigning access rights to specific IT resources for an individual user.

It was proposed solutions to manage the list of ACLs from the server.

2 The Server with ACL Mechanism

The implementation of the server with the privileges of the ACL includes:

- Modification of the file system which enables the use of ED (Extended Attributes) to store the rights in the ACL,
- Implementing a Samba server which is designed for storing and sharing computer data.

After completion of the server deployment, have been designed and launched the tools for managing the ACL access rights.

2.1 Implementation of the ACL Server

The Server Software

The server uses CentOS Linux operating system. During the implementation of the system, the modules outside of this version of the distribution have not been applied.

Server ACL Configuration

The condition to obtain the functionality of the ACL was to modify the file system /home partition, which is intended to be the location of shared IT resources. This was done during the implementation of the server by entering in the configuration file /etc/fstab – shown in Fig. 1 – beyond-standard file system modifications.

```

#
#/etc/fstab
# Created by anaconda on Wed May 14 11:00:35 2014
#
# Accessible filesystems, by reference, are maintained under '/dev/disk'
# See man pages fstab(5), findfs(8), mount(8) and/or blkid(8) for more info
#
UUID=74323e03-7607-4989-be2a-7c58bbae8b1d /          ext4 defaults          1 1
UUID=ac4b9e6d-6eb1-4ecf-beb4-bcf0c6736e68 /back    ext4 defaults          1 2
UUID=fcb92ac6-3e56-4f04-b25f-db6e6e0be349 /home    ext4 defaults,usrquota,grpquota,user_xattr,acl 1 2
UUID=23f24be5-3263-403a-80d2-1cebd10bbfa6 swap     swap defaults           0 0
tmpfs    /dev/shm tmpfs defaults           0 0
devpts   /dev/pts  devpts gid=5,mode=620        0 0
sysfs    /sys      sysfs defaults            0 0
proc     /proc     proc  defaults               0 0

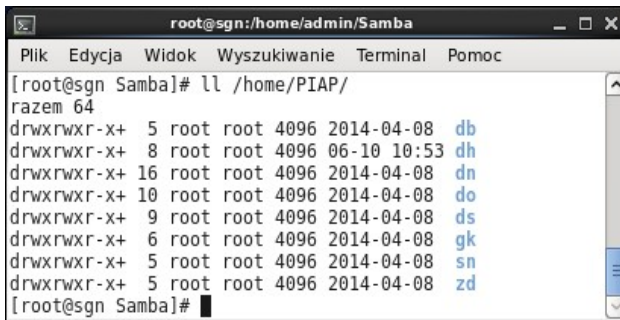
```

Fig. 1. Extract from the configuration file `/etc/fstab`

Entries in the `/home` partition cause inclusion of the following mechanisms:

- the limits for disk resources (usrquota, grpquota),
- EA (usr_xattr),
- ACL (ACL).

EA and ACL entries allow to store ACLs defined in the NTFS file system, in the metadata included in the inodes which point the file or directory with EA functionality. Graphic illustration of the functionality of the ACL of the server is a "+" in the chain provides for access to individual files or directories, as shown on the Fig. 2 below.



```

root@sgn:/home/admin/Samba
Plik  Edycja  Widok  Wyszukiwanie  Terminal  Pomoc
[root@sgn Samba]# ll /home/PIAP/
razem 64
drwxrwxr-x+  5 root root 4096 2014-04-08 db
drwxrwxr-x+  8 root root 4096 06-10 10:53 dh
drwxrwxr-x+ 16 root root 4096 2014-04-08 dn
drwxrwxr-x+ 10 root root 4096 2014-04-08 do
drwxrwxr-x+  9 root root 4096 2014-04-08 ds
drwxrwxr-x+  6 root root 4096 2014-04-08 gk
drwxrwxr-x+  5 root root 4096 2014-04-08 sn
drwxrwxr-x+  5 root root 4096 2014-04-08 zd
[root@sgn Samba]#

```

Fig. 2. Implementation of the `usr_xattr` and `acl` in the directory

The implementation of server functionality which implements ACL, can start the Samba server implementation.

2.2 Implementing a Samba Server

The primary role of the Samba server is sharing server disk resources to users in local network. In the server Linux Centos 6.6 installed software `samba-3.6.23-12.el6.x86_64`. During the implementation of work has been developed server configuration and automatic configuration of the user accounts.

Server Configuration

Samba server settings are contained in the `/etc/samba/smb.conf` configuration file. This file is divided into sections, as defined by the headers placed in square parentheses. The most important section is the `[global]`, which contains the basic server settings. The most important server settings are as below:

- Choosing the type of the database containing user identity attributes

`passdb backend = tdbsam`

(trivial database functionally integrated out of the SAM database – used to store the attributes of the Windows users).

- Protection of the shared resources at the user level

`security = user.`

- Settings that allow to mirror Windows ACL rights in the Samba server:
 - `vfs objects = acl_xattr,`
 - `map acl inherit = yes,`
 - `store dos attributes = yes`

The rules for providing users the home directories was defined in the `[homes]` section. To provide the access to home directories one should follow the appropriate SELinux policy. SELinux is the security enhancement in Linux which allows users and administrators for more control of the access policy. To achieve this, should be set the `samba_enable_home_dirs` parameter as 1.

The configuration file contains also other sections whose entries are responsible for providing the resources for group work. In the present embodiment is shown configuration of the resources (InfoX) provided for group work.

[InfoX]

```
path = /home/APPS/InfoX
security mask = 0700
force group = InfoX
guest ok = no
directory security mask = 0700
writable = yes
```

In the configuration section [InfoX] were used the minimum number of parameters required to share a resource with defined ACL permissions.

In the server also is installed GUI Samba Web Administration Tool so-called SWAT. This interface is used only to monitor the Samba server however the modifying the server configuration is done by editing the configuration file from the console.

User Accounts

The request create an account in the Samba server is preceded by the creation of a user account on the Linux server. The user account is localized in the specified directory by the organizational structure of the Institute. The account is not authorized to login to the server Linux. The account which is created on Linux server is used to assign user ACL rights to the resource. The Samba server account is being mapped to Linux system account. User authentication (login to the server) is based on the Samba account, while an authorization (access to specific resources, with defined rights ACL) based on access rights Linux system account. For the automate the process of creating user accounts on the server, has been designed the script (Fig. 3), the essence of which action is shown in the UML activity diagram (Fig. 4).

```
# ! /bin/bash
#
SambaUsers="/home/admin/Users/Data/ListaUserowSamba"
SambaUsersTxt="/home/admin/Users/Data/ListaUserowSamba.txt"
HomePath="/home/PIAP/"
KO="$1"
USER="$2"
GROUP="users"
HOMEDIR="$HomePath$KO/$USER"
PASSWORD=$(pwgen 10 -s -B -N 1 | tr a-z A-Z)
if ( [ $1 ] && [ $2 ] ); then
    echo "Add to $SambaUsers"
    if [ $( cat $SambaUsers | grep -c ${USER} ) == 0 ]; then
        echo $USER $GROUP $HOMEDIR $PASSWORD >> $SambaUsers
    else
        echo "User ${USER} is on the list"
    fi
    cat $SambaUsers | grep ${USER} | while read USER GROUP
        HOMEDIR PASSWORD; do
        if [ $(pdbedit -L | grep -c ${USER} ) == 0 ]; then
            mkdir -p ${HOMEDIR}
            useradd -g ${GROUP} -d ${HOMEDIR} ${USER}
            mkdir ${HOMEDIR}/Links"
            usermod -L ${USER}
            /usr/sbin/edquota -p DefaultUser ${USER}
            chown -R ${USER}:${GROUP} ${HOMEDIR}
            chmod -R 700 ${HOMEDIR}
            /home/admin/Users/bin/sambouser ${USER} ${PASSWORD}
            printf %-20s%20s "\n" `cat $SambaUsers |
                awk '{print $1"\t"$4}'` > $SambaUsersTxt
        else
            echo "User ${USER} is registered"
        fi
    done
else
    echo -ne "\n\tNo user ID parameter
    The call parameters :
    =====
    \${1}: directory in /home e.g.: \t\tdb/oup
    \${2} identifier e.g.: \t\takowalski
    bye, bye...\n"
fi
```

Fig. 3. Script to create user accounts

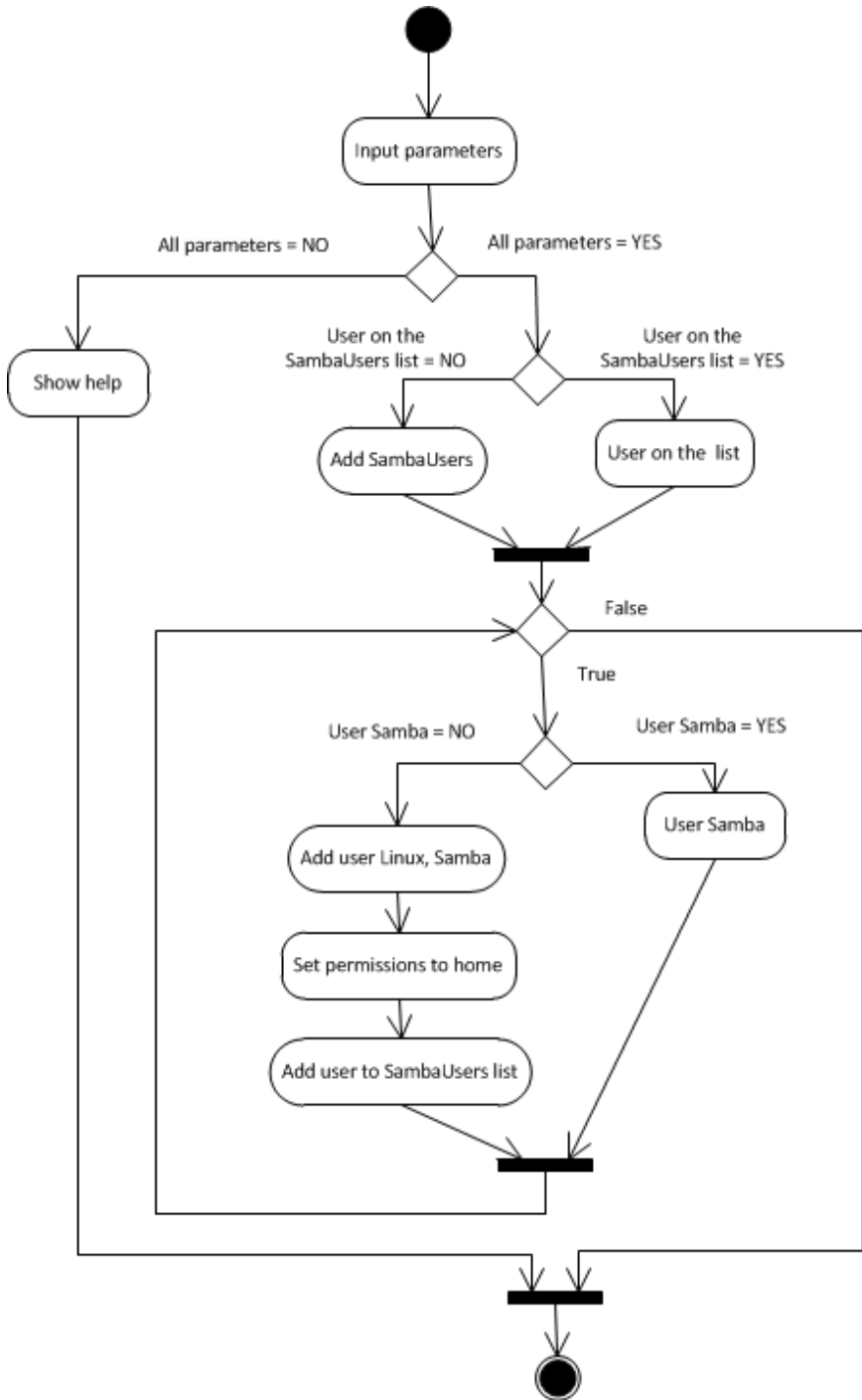


Fig. 4. UML diagram: Process of creating user accounts

To create, lock or unlock the Samba user account is used command `smbpasswd`:

- `smbpasswd -a [user]` – adding an Unix user to Samba
- `smbpasswd -d [user]` – locking a Samba account
- `smbpasswd -e [user]` – unlocking a previously locked Samba account

Limitation of the Samba Server Disk Resources

Disk limitations are implemented by the quota mechanism. Enabling the quota mechanism requires the appropriate parameters (`usrquota`, `grpquota`) which are assigned in the `/home` partition and defined in the file `/etc/fstab`. To limit the number and space of home directories, the `usrquota` for each individual user has been applied. Linux system does not allow to set limits on the disk shared resources (group work), as it is implemented in Windows Server. In order to obtain the functionality available in the Windows Server disk quotas system, was used on Linux `grpquota` mechanism. The names of the user groups created in Linux, are named according to the names of network shares. The created groups have been granted ownership of the shared resources. The groups were deprived of the right to resources in order to enable access control which are assigned to users and are based on ACL attributes only. Changing the group permissions results in a change of the mask permissions. Removing of the group permission causes that the mask has the following form

```
mask:---.
```

In this case mask suspends permissions to the resource despite of the fact that the user is granted privileges to it, as shown in the example below:

```
user:jkowalski:r-x          #effective:---
```

In order to solve the above problem which concern mask permissions, the mask has been modified as shown below.

```
setfacl -R -m m::rwx
```

As a result of the above changes were obtained following form masks

```
mask:rwx.
```

Thus defined mask does not limit user rights.

```
user:jkowalski:r-x          #effective:r-x
```

3 ACL Access Rights Management

ACL access control mechanism has been developed to increase access to files, directories for multiple users and multiple groups. The standard mechanism allows assign rights only for the one user and one group. This mechanism works in the simple cases with the few users. The system described in this article can support more than 200 users and groups.

ACL mechanism allows user to create masks for permissions. Effective permissions on the file (directory), are the sum of the bit of the mask and of the user right. To read the effective permissions, one should use `getfacl -e` command.

When granting permissions, need to be remembered that the standard permissions are prevail for the ACL, e.g. the user has only the ACL right to read, but Linux belongs to a group that has permission to read and write – which means that user has the right to read and write.

While starting the Samba server are defined the resources which are made available by the server. Rights to individual directories should allow the user to, respectively, read (R), write (W), execution (X), inheritance. Here were defined the following access rights defined by the following rules that are shown in Fig. 5.

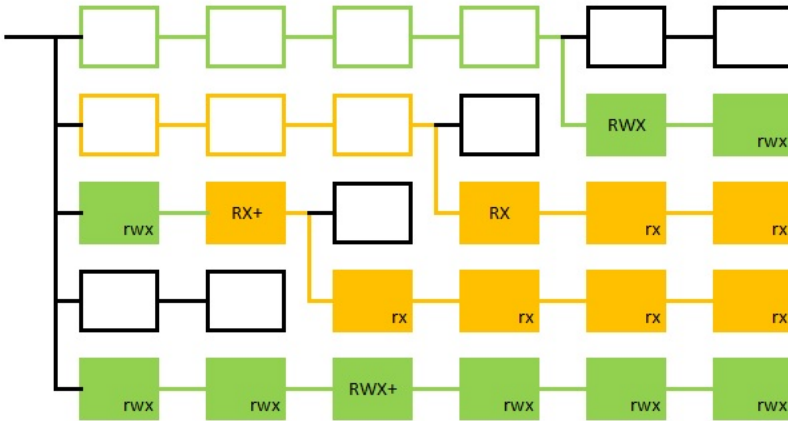


Fig. 5. Interpretation of the access rights ACL

| | | |
|-------|---------------------------|-------------------------------|
| RWX | ancestor: the transition, | a descendant: inheritance RWX |
| RX | ancestor: the transition, | a descendant: inheritance RX |
| RWX + | ancestor: RWX, | a descendant: inheritance RWX |
| RX + | ancestor: RWX, | a descendant: inheritance RX |

3.1 Assign Permissions to Directories

Defined during the implementation of the Samba server resources should be assigned access rights in accordance with the requirements of their respective owners. For this purpose was developed SetAclSamba tool used for each directory falling within the defined resources. Below (Fig. 6) shows a sample script used for broadcasting rights in the resource ACL "Katalog01" contains subdirectories presented. ACL rights as defined above, are allocated to the user (user01, ..., user12)

In this script, the nomenclature used in accordance with the previously accepted meanings rights. The definitions of the various functions contained in the script attached to the script which confers the right (Fig. 7.).

```

# ! /bin/bash
#
Zasoby=(
    "/Katalog01" # 0
    "/Katalog01/Katalog02" # 1
    "/Katalog01/Katalog02/Katalog_A" # 2
    "/Katalog01/Katalog02/Katalog_B" # 3
    "/Katalog01/Katalog02/Katalog_C" # 4
    "/Katalog01/Katalog02/Katalog_D" # 5
    " "
)
. /home/admin/Samba/bin/SetAclFunkcje
CheckPath
#
g=0)
while [ ${Zasoby[$g]} ]; do
    case ${Zasoby[$g]} in
        ${Zasoby[0]})
            ustawFKK "user01 user02"
            ;;
        ${Zasoby[1]})
            ustawFKK "user01 user02"
            ;;
        ${Zasoby[2]})
            ustawFKK "user01 user02 user03 user04"
            ;;
        ${Zasoby[3]})
            ustawFKK "user06 user08"
            ustawFKK+ "user01 user02 user03 user04"
            ustawFKK "user07 user09 user08 user10"
            ;;
        ${Zasoby[4]})
            ustawFKK+ "user01 user02 user03 user04"
            ustawFKK "user07 user09 user10"
            ustawFKK "user08 user11"
            ;;
        ${Zasoby[5]})
            ustawFKK+ "user02 user03 user04 user05"
            ustawFKK "user11 user07 user09 user10"
            ustawFKK+ "user01 user03"
            ustawFKK "user08 user12"
            ;;
        *)
            ;;
    esac
    ((g++))
done

```

Fig. 6. Script to allocate permissions ACL

```

#!/bin/bash
#
ACLsPath="/home/admin/Samba/ACLs${Zasoby[0]}"
function CheckPath {
    echo $ACLsPath
    if [ ! -d $ACLsPath ]; then
        mkdir $ACLsPath
    fi
}
pat0="/home/APPS"
function resetACLs {
    for k in $!; do
        setfacl -R -x u:$k,d:u:$k $pat0${Zasoby[0]}
    done
    setfacl -R -m d:g::- ,g::- $pat0${Zasoby[0]}
    chown -R root:root $pat0${Zasoby[0]}
    chmod -R 770 $pat0${Zasoby[0]}
}
function ustawRX {
    pat=$pat0
    for f in $(echo ${Zasoby[$g]} | sed 's/\// /g'); do
        pat=$pat/$f
        for k in $!; do
            setfacl -m u:$k:rx $pat
        done
    done
    for k in $!; do
        setfacl -R -m u:$k:rx,d:u:$k:rx $pat0${Zasoby[$g]}
    done
}
function ustawRWX {
    pat=$pat0
    for f in $(echo ${Zasoby[$g]} | sed 's/\// /g'); do
        pat=$pat/$f
        for k in $!; do
            setfacl -m u:$k:rx $pat;
        done
    done
    for k in $!; do
        setfacl -R -m u:$k:rwx,d:u:$k:rwx $pat0${Zasoby[$g]}
    done
}
function ustawRX+ {
    pat=$pat0
    for f in $(echo ${Zasoby[$g]} | sed 's/\// /g'); do
        pat=$pat/$f
        for k in $!; do
            setfacl -m u:$k:rwx $pat;
        done
    done
    for k in $!; do
        setfacl -R -m u:$k:rx,d:u:$k:rx $pat0${Zasoby[$g]}
    done
}
function ustawRWX+ {
    pat=$pat0
    for f in $(echo ${Zasoby[$g]} | sed 's/\// /g'); do
        pat=$pat/$f
        for k in $!; do
            setfacl -m u:$k:rwx $pat;
        done
    done
    for k in $!; do
        setfacl -R -m u:$k:rwx,d:u:$k:rwx $pat0${Zasoby[$g]}
    done
}
}

```

Fig. 7. Script that defines the functions fit right ACL

4 Summary

As a result of research work has been implemented a file server that provides controlled access to IT resources for multiple users and multiple groups. This was achieved by implementing a server that allows the user to use the Access Control List ACL and by using mechanisms Samba server that contains specific IT resources.

Friendly use of this solution is ensured thanks to the developed method for allocating access to IT resources for each individual user, as well as through the proposed approach to the access ACL management.

Authors prepared also vector faxing system based on USB modems (modems FM). In this approach, USB modems successfully replaced solutions based on large-scale, stand-alone fax machines, the size of which significantly hampered the construction of tens-line fax system environment PSTN (Public Switched Telephone Network) – necessary for the proper functioning of a large company business [5].

References

1. Eckstein, R., Collier-Brown, D., Kelly, P.: Samba. Leksykon kieszonkowy. Helion, Warszawa (2001)
2. Sharpe, R., Potter, T., Morris, J.: Samba dla każdego. Helion, Warszawa (2002)
3. Schroder, C.: Linux. Receptury. Receptury. Helion, Warszawa (2005)
4. Terpstra, J.H.: Samba-3 By Example, 2nd edn. Prentice Hall (2006)
5. Wrzesień, M., Ryszawa, P.: Multiline Faxing System. *Pomiary Automatyka Robotyka* 19(1), 80–87 (2015) (in Polish)

Predictive Control of a Multivariable Neutralisation Process Using Elman Neural Networks

Antoni Wysocki and Maciej Lawryńczuk

Institute of Control and Computation Engineering,
Warsaw University of Technology
ul. Nowowiejska 15/19, 00-665 Warsaw, Poland
A.T.Wysocki@stud.elka.pw.edu.pl, M.Lawrynczuk@ia.pw.edu.pl

Abstract. This paper presents development and simulation results of a computationally efficient predictive control algorithm based on a recurrent Elman neural network. The considered process is a multivariable neutralisation reactor. Process modelling and control issues are thoroughly discussed. In particular, the discussed computationally efficient predictive control algorithm with on-line trajectory linearisation and quadratic optimisation is compared to the truly nonlinear scheme with nonlinear optimisation repeated of each sampling instant on-line.

Keywords: Process control, Model predictive control, Elman neural networks.

1 Introduction

The core idea of Model Predictive Control (MPC) algorithms is to use on-line a dynamic model of the process to calculate predicted control errors and to minimise a predefined cost-function which defines the future control quality [1,10,14]. Different variants of MPC algorithms are nowadays successfully used in thousands of industrial applications [13]. It is due to advantages of MPC:

- a) the ability to take into account constraints imposed on input and output variables (or state variables) in a systematic way,
- b) the ability to control multi-input multi-output processes,
- c) very good control quality.

As a result, the MPC technique is a sound alternative to the classical Proportional-Integral-Derivative (PID) controller, which may turn out to be useful in the simplest case of single-input single-output not delayed processes with no constraints.

For modelling of dynamic processes neural networks are often used [4]. In most cases, the perceptron with one hidden layer (Multi-Layer Perceptron – MLP) is used, the Radial Basis Functions (RBF) network is less popular. Both MLP and RBF structures are static approximators. In the discrete-time dynamic model the dynamics is realised by delivering the input and output signals from some

previous sampling instants to the inputs of the network. Interesting alternatives are recurrent neural networks [4,11], which are inherently dynamic models. One example of a recurrent network structure is the Elman neural network [2,4,11]. Elman networks are used in various applications: eg. in approximation of phenol concentration [12], in short-term temperature forecasts [5], in modelling of the flow of passengers in subway [6], in identification of the grammatical structure of literary works [7], in air pressure control supplied to the disc drill subway tunnel under a river [15], where, unfortunately, a heuristic optimisation is used for on-line optimisation, with no guarantee of finding a solution.

This paper shows development and simulation results of computationally efficient predictive control algorithm in which the recurrent Elman network is used as a model of the controlled process. A multivariable neutralisation reactor as considered process is chosen. Process modelling and control problems are thoroughly discussed. The discussed computationally efficient predictive control algorithm with linearisation around the trajectory (MPC-NPLT) is compared to the truly nonlinear scheme with nonlinear optimisation (MPC-NO) repeated of each sampling instant on-line.

2 Description of Neutralisation Process

A multivariable neutralisation process (pH reactor) with two manipulated and two controlled variables is considered. Control of pH is of crucial importance in many chemical and biochemical processes. It exhibits severe nonlinear behaviour and therefore cannot be controlled by simple MPC algorithms based on constant linear models or PI controllers. The process with one input and one output is usually considered [3], the multivariable one is researched less frequently [9].

The reactor is shown schematically in Fig. 1. Acid HNO_3 , base NaOH and buffer NaHCO_3 are mixed in the tank. From the modelling point of view the process has two manipulated inputs (q_1, q_3) and two controlled outputs (h, pH). The fundamental model of the process consists of differential equations

$$\begin{aligned} \frac{dW_{a_4}(t)}{dt} &= \left(\frac{W_{a_1} - W_{a_4}(t)}{Ah(t)} \right) q_1(t) + \left(\frac{W_{a_2} - W_{a_4}(t)}{Ah(t)} \right) q_2(t) + \left(\frac{W_{a_3} - W_{a_4}(t)}{Ah(t)} \right) q_3(t) \\ \frac{dW_{b_4}(t)}{dt} &= \left(\frac{W_{b_1} - W_{b_4}(t)}{Ah(t)} \right) q_1(t) + \left(\frac{W_{b_2} - W_{b_4}(t)}{Ah(t)} \right) q_2(t) + \left(\frac{W_{b_3} - W_{b_4}(t)}{Ah(t)} \right) q_3(t) \\ \frac{dh(t)}{dt} &= \frac{q_1(t) + q_2(t) + q_3(t) - C_V \sqrt{h(t)}}{A} \end{aligned}$$

and the algebraic equation

$$W_{a_4}(t) + 10^{pH(t)-14} - 10^{-pH(t)} + W_{b_4}(t) \frac{1 + 2 \times 10^{pH(t)-pK_2}}{1 + 10^{pK_1-pH(t)} + 10^{pH(t)-pK_2}} = 0$$

where $pK_1 = -\log_{10}K_{a_1}$, $pK_2 = -\log_{10}K_{a_2}$.

The nominal operating point and the parameters of the fundamental model are given in Table 1. The discussed neutralisation reactor is characterised by a highly non-linear properties. Fig. 2 presents the static characteristics of the process.

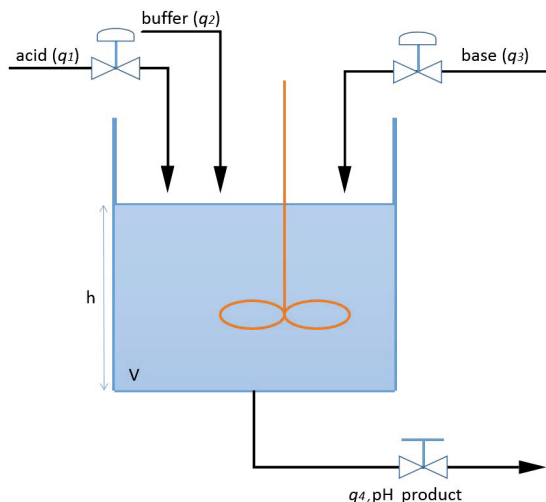


Fig. 1. Neutralisation reactor

3 Computationally Efficient MPC of the Neutralisation Process Based on the Elman Neural Network

3.1 MPC Algorithm with Linearisation around the Trajectory (MPC-NPLT)

The process has two inputs and two outputs, the input and output vectors are: $u = [u_1 \ u_2]^T$, $y = [y_1 \ y_2]^T$, respectively. In MPC algorithms [10,14] at each consecutive sampling instant $k, k = 0, 1, 2, \dots$, a set of future control increments

$$\Delta \mathbf{u}(k) = \begin{bmatrix} \Delta u(k|k) \\ \Delta u(k+1|k) \\ \dots \\ \Delta u(k+N_u-1|k) \end{bmatrix}$$

is calculated, where $\Delta u(k+p|k) = u(k+p|k) - u(k+p-1|k)$. It is assumed that $\Delta u(k+p|k) = 0$ for $p \geq N_u$, where N_u is the control horizon. The objective is to minimise differences between the reference trajectory $y^{\text{ref}}(k+p|k)$ and predicted

Table 1. The operating point and the parameters of a fundamental model of the reactor

| | | |
|---|--|--|
| $q_{1_0} = 16.6 \text{ ml/s}$ | $q_{2_0} = 0.55$ | $q_{3_0} = 15.6 \text{ ml/s}$ |
| $pH_0 = 7.0255$ | $h = 14.009 \text{ cm}$ | $K_{a_1} = 4.47 \times 10^{-7}$ |
| $K_{a_2} = 5.62 \times 10^{-11}$ | $W_{a_1} = 3 \times 10^{-3} \text{ mol}$ | $W_{b_1} = 0 \text{ mol}$ |
| $W_{a_2} = -3 \times 10^{-2} \text{ mol}$ | $W_{b_2} = 3 \times 10^{-2} \text{ mol}$ | $W_{a_3} = -3.05 \times 10^{-3} \text{ mol}$ |
| $W_{b_3} = 5 \times 10^{-5} \text{ mol}$ | $C_V = 8.75 \text{ ml/cm s}$ | $A = 207 \text{ cm}^2$ |

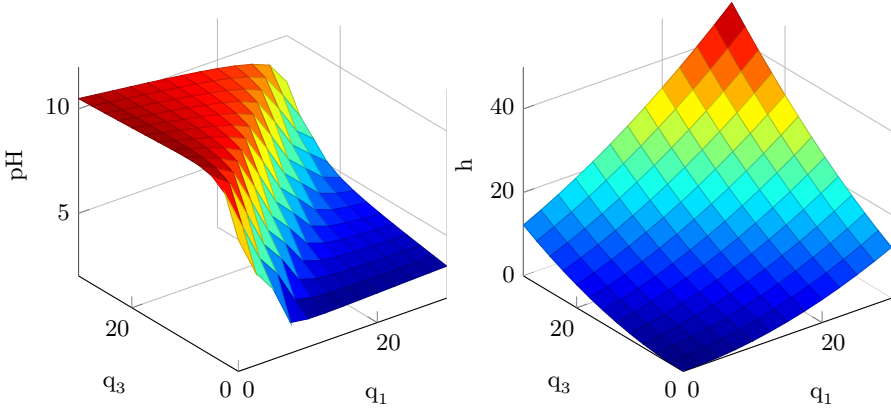


Fig. 2. Static characteristics of the neutralisation reactor

values of the output $\hat{y}(k + p|k)$ over the prediction horizon $N \geq N_u$. Hence, the future control increments are determined from the following MPC optimisation task

$$\begin{aligned} & \min_{\Delta \mathbf{u}(k)} \{ J(k) = \|\mathbf{y}^{\text{ref}}(k) - \hat{\mathbf{y}}(k)\|_M^2 + \|\Delta \mathbf{u}(k)\|_\Lambda^2 \} \\ & \text{subject to} \\ & \mathbf{u}^{\min} \leq \mathbf{u}(k) \leq \mathbf{u}^{\max} \\ & -\Delta \mathbf{u}^{\max} \leq \Delta \mathbf{u}(k) \leq \Delta \mathbf{u}^{\max} \end{aligned}$$

where

$$\begin{aligned} \mathbf{y}^{\text{ref}}(k) &= \begin{bmatrix} \mathbf{y}^{\text{ref}}(k) \\ \vdots \\ \mathbf{y}^{\text{ref}}(k) \end{bmatrix}, \quad \hat{\mathbf{y}}(k) = \begin{bmatrix} \hat{y}(k + 1|k)(k) \\ \vdots \\ \hat{y}(k + N|k)(k) \end{bmatrix} \in \mathbb{R}^{n_y N} \\ \mathbf{u}^{\min} &= \begin{bmatrix} u^{\min} \\ \vdots \\ u^{\min} \end{bmatrix}, \quad \mathbf{u}^{\max} = \begin{bmatrix} u^{\max} \\ \vdots \\ u^{\max} \end{bmatrix}, \quad \Delta \mathbf{u}^{\max} = \begin{bmatrix} \Delta u^{\max} \\ \vdots \\ \Delta u^{\max} \end{bmatrix} \in \mathbb{R}^{N_u N_u} \end{aligned}$$

Only the first two elements of the calculated sequence is applied to the process. At the next sampling instant, $k + 1$, the output signal is measured and updated, and the whole procedure is repeated.

The general straightforward idea of reducing computational burden of nonlinear MPC is to calculate on-line a linear approximation of the model and use it for prediction [8,14]. In more advanced approaches not the model, but the predicted trajectory is linearised on-line [8]. In this study the MPC algorithm with Nonlinear Prediction and Linearisation around the Trajectory (MPC-NPLT) is considered and derived for the neural Elman network. At each sampling instant

of the MPC-NPLT algorithm the predicted output trajectory ($\hat{\mathbf{y}}(k)$) is linearised along the future control sequence

$$\mathbf{u}^{\text{traj}}(k) = \begin{bmatrix} u^{\text{traj}}(k|k) \\ \dots \\ u^{\text{traj}}(k + N_u - 1|k) \end{bmatrix}$$

Using the Taylor’s series expression, the linearised trajectory is

$$\hat{\mathbf{y}}(k) = \hat{\mathbf{y}}^{\text{traj}}(k) + \mathbf{H}(k)(\mathbf{u}(k) - \mathbf{u}^{\text{traj}}(k)) \tag{1}$$

where the output trajectory

$$\hat{\mathbf{y}}^{\text{traj}}(k) = \begin{bmatrix} \hat{y}^{\text{traj}}(k + 1|k) \\ \dots \\ \hat{y}^{\text{traj}}(k + N|k) \end{bmatrix}$$

corresponds to the assumed input trajectory $\mathbf{u}^{\text{traj}}(k)$ and is calculated from a model of the process,

$$\mathbf{H}(k) = \left. \frac{d\hat{\mathbf{y}}(k)}{d\mathbf{u}(k)} \right|_{\substack{\hat{\mathbf{y}}(k)=\hat{\mathbf{y}}^{\text{traj}}(k) \\ \mathbf{u}(k)=\mathbf{u}^{\text{traj}}(k)}} = \begin{bmatrix} \frac{\partial \hat{y}^{\text{traj}}(k+1|k)}{\partial u^{\text{traj}}(k|k)} & \dots & \frac{\partial \hat{y}^{\text{traj}}(k+1|k)}{\partial u^{\text{traj}}(k+N_u-1|k)} \\ \vdots & \ddots & \vdots \\ \frac{\partial \hat{y}^{\text{traj}}(k+N|k)}{\partial u^{\text{traj}}(k|k)} & \dots & \frac{\partial \hat{y}^{\text{traj}}(k+N|k)}{\partial u^{\text{traj}}(k+N_u-1|k)} \end{bmatrix}$$

is a matrix of dimensionality $n_y N \times n_u N_u$, and the vector

$$\mathbf{u}(k) = \begin{bmatrix} u(k|k) \\ \dots \\ u(k + N_u - 1|k) \end{bmatrix}$$

corresponds to the decision variables of the MPC algorithm $\Delta \mathbf{u}(k)$.

Thanks to using the prediction equation (1), the optimisation problem becomes the quadratic programming task

$$\begin{aligned} \min_{\Delta \mathbf{u}(k)} \{ & \mathbf{J}(k) = \|\mathbf{y}^{\text{ref}}(k) - \mathbf{H}(k)\mathbf{J}\Delta \mathbf{u}(k) - \hat{\mathbf{y}}^{\text{traj}}(k) \\ & - \mathbf{H}(k)(\mathbf{u}(k - 1) - \mathbf{u}^{\text{traj}}(k))\|_{\mathbf{M}}^2 + \|\Delta \mathbf{u}(k)\|_{\mathbf{A}}^2 \} \\ \text{subject to} & \\ \mathbf{u}^{\text{min}} \leq & \mathbf{J}\Delta \mathbf{u}(k) + \mathbf{u}(k - 1) \leq \mathbf{u}^{\text{max}} \\ -\Delta \mathbf{u}^{\text{max}} \leq & \Delta \mathbf{u}(k) \leq \Delta \mathbf{u}^{\text{max}} \end{aligned}$$

where $\mathbf{A} = \text{diag}(\lambda, \dots, \lambda)$, \mathbf{J} is the all ones lower triangular matrix of dimensionality $2N_u \times 2N_u$.

Selection of the future input trajectory $\mathbf{u}^{\text{traj}}(k)$ affects the linearisation accuracy and quality of control. The control signal calculated at the previous sampling instant are used

$$\mathbf{u}^{\text{traj}}(k) = \begin{bmatrix} u(k - 1) \\ \vdots \\ u(k - 1) \end{bmatrix}$$

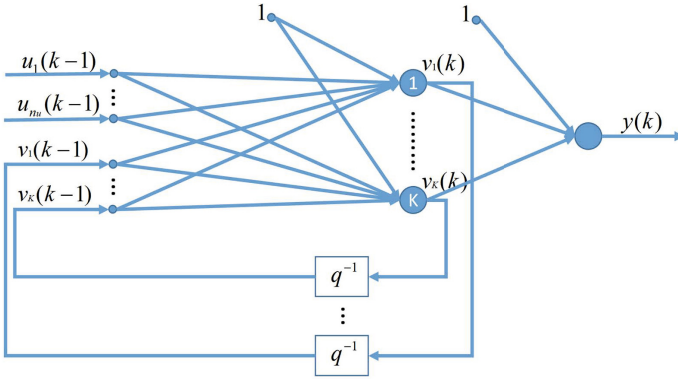


Fig. 3. The Elman neural network

3.2 Elman Neural Network

Fig. 3 shows the structure of the Elman neural network. The network has n_u inputs associated with input signals of the process $u_1(k-1), \dots, u_{n_u}(k-1)$, K hidden neurons with nonlinear activation function $\varphi : R \rightarrow R$, one neuron (adder) and one output $y(k)$. Output signals of hidden layer ($v_1(k), \dots, v_K(k)$) are entered through delay blocks to the inputs of the network, which means that the network has $n_u + K$ inputs $u_1(k-1), \dots, u_{n_u}(k-1), v_1(k-1), \dots, v_K(k-1)$. The output of the Elman neural network model is

$$y(k) = w_0^{(2)} + \sum_{i=0}^K w_i^{(2)} \varphi(w_{i,0}^{(1)} + \sum_{j=1}^{n_u} w_{i,j}^{(1)} u_j(k - \tau_j) + \sum_{j=1}^K w_{i,j+n_u}^{(1)} v_j(k - 1)) \quad (2)$$

where $w_i^{(2)}$ are weights of the second layer of the network (for $i = 0, \dots, K$), whereas the signal $v_0(k) = 1$ is bias. Output signals of each hidden neuron ($i = 1, \dots, K$) are calculated from the formula

$$v_i(k) = \sum_{j=0}^{n_u+K} w_{i,j}^{(1)} X_j(k - 1)$$

where $w_{i,j}^{(1)}$ are weight of the first layer of the network (for $i = 0, \dots, K, j = 0, \dots, n_u + K$) and

$$X_j(k - 1) = \begin{cases} 1 & \text{for } j = 0 \\ u_j(k - 1) & \text{for } 1 \leq j \leq n_u \\ v_j(k - 1) & \text{dla } n_u < j \leq n_u + K \end{cases}$$

3.3 Implementation of the MPC-NPLT Algorithm for the Elman Neural Network

For the considered process with two inputs ($n_u = 2$) and two outputs, the model consists of two Elman networks. From Eq. (2), the output trajectory corresponding to the input sequence $\mathbf{u}^{\text{traj}}(k)$ is

$$\hat{y}^{m,\text{traj}}(k+p|k) = w_0^{(2,m)} + \sum_{j=1}^{K^m} w_j^{(2,m)} \varphi(z_i^{m,\text{traj}}(k+p|k)) + d^m(k)$$

where the index $m = 1, 2$ indicates the output and

$$\begin{aligned} z_i^{m,\text{traj}}(k+p|k) &= w_0^{(1,m)} + \sum_{j=1}^{n_u} w_j^{(1,m)} u_j^{\text{traj}}(k-1+p|k) \\ &+ \sum_{j=1}^{K^m} w_{j+n_u}^{(1,m)} v_j^{m,\text{traj}}(k-1+p|k) \end{aligned}$$

where $v_i^{m,\text{traj}}(k+p|k) = \varphi(z_i^{m,\text{traj}}(k+p|k))$. The unmeasured disturbance is the difference between the measured output signal and the model output

$$\begin{aligned} d^m(k) &= y^m(k) - w_0^{(2,m)} \sum_{i=1}^{K^m} w_i^{(2,m)} \varphi \left(w_{i0}^{(1,m)} + \sum_{j=1}^{n_u} w_{ij}^{(1,m)} u_j(k-1) \right. \\ &\quad \left. + \sum_{j=1}^K w_{ij+n_u}^{(1,m)} v_j^m(k-1) \right) \end{aligned}$$

A linear approximation of the nonlinear output trajectory (Eq. (1)) is determined by a matrix $\mathbf{H}(k)$, each element of which is a 2×2 submatrix

$$\frac{\partial \hat{y}^{\text{traj}}(k+p|k)}{\partial u^{\text{traj}}(k+r|k)} = \begin{bmatrix} \frac{\partial \hat{y}^{1,\text{traj}}(k+p|k)}{\partial u^{1,\text{traj}}(k+r|k)} & \frac{\partial \hat{y}^{1,\text{traj}}(k+p|k)}{\partial u^{2,\text{traj}}(k+r|k)} \\ \frac{\partial \hat{y}^{2,\text{traj}}(k+p|k)}{\partial u^{1,\text{traj}}(k+r|k)} & \frac{\partial \hat{y}^{2,\text{traj}}(k+p|k)}{\partial u^{2,\text{traj}}(k+r|k)} \end{bmatrix}$$

Its entries are calculated according to the formula

$$\frac{\partial \hat{y}^{m,\text{traj}}(k+p|k)}{\partial u^{n,\text{traj}}(k+r+1|k)} = \sum_{i=1}^{K^m} w_i^{(2,m)} \frac{\partial v_i^{m,\text{traj}}(k+p|k)}{\partial u^{n,\text{traj}}(k+r+1|k)}$$

where $p = 1, \dots, N$ and $r = 0, \dots, N_u - 1$. The partial derivatives are

$$\begin{aligned} \frac{\partial v_i^{m,\text{traj}}(k+p|k)}{\partial u^{n,\text{traj}}(k+r+1|k)} &= (1 - \tanh^2(z_i^{m,\text{traj}}(k+p|k))) \left(\frac{\partial u^{i,\text{traj}}(k+p|k)}{\partial u^{n,\text{traj}}(k+r+1|k)} \right. \\ &\quad \left. + \frac{\partial z_i^{m,\text{traj}}(k+p|k)}{\partial u^{n,\text{traj}}(k+r+1|k)} \right) \end{aligned}$$

where the partial derivatives $\frac{\partial u^{i,\text{traj}}(k+p|k)}{\partial u^{n,\text{traj}}(k+r+1|k)}$ have a non-zero value $w_{i,n+1}^{1,m}$ only if $p = r + 1$ or ($p > r + 1$ and $r = N_u - 1$) (otherwise they are 0) and

$$\frac{\partial z_i^{m,\text{traj}}(k+p|k)}{\partial u^{n,\text{traj}}(k+r+1|k)} = \sum_{j=1}^{K^m} w_{i,j+N_u}^{1,m} \frac{\partial v_j^{m,\text{traj}}(k-1+p|k)}{\partial u^{n,\text{traj}}(k+r+1|k)}$$

Table 2. The comparison of the number of parameters (LP) and accuracy ($E_{\text{tr}}(\mathbf{w})$ – for training data set, $E_{\text{val}}(\mathbf{w})$ – for the validation data set, $E_{\text{test}}(\mathbf{w})$ – for test data set) of the recurrent Elman neural network as a model for the neutralisation reactor

| Model for h | LP | $E_{\text{tr}}(\mathbf{w})$ | $E_{\text{val}}(\mathbf{w})$ | $E_{\text{test}}(\mathbf{w})$ |
|----------------------------|-----|-----------------------------|------------------------------|-------------------------------|
| $K = 1$ | 6 | 5.2389×10^{-3} | 1.0194×10^{-2} | – |
| $K = 2$ | 13 | 1.7783×10^{-3} | 8.0903×10^{-3} | – |
| $K = 3$ | 22 | 7.8891×10^{-4} | 2.5322×10^{-3} | – |
| $K = 4$ | 33 | 5.4332×10^{-5} | 1.3425×10^{-4} | 2.5823×10^{-4} |
| $K = 5$ | 46 | 3.1090×10^{-5} | 8.7833×10^{-4} | – |
| $K = 6$ | 61 | 3.7831×10^{-6} | 2.4245×10^{-3} | – |
| $K = 7$ | 78 | 2.4416×10^{-6} | 6.0560×10^{-4} | – |
| Model for pH | LP | $E_{\text{tr}}(\mathbf{w})$ | $E_{\text{val}}(\mathbf{w})$ | $E_{\text{test}}(\mathbf{w})$ |
| $K = 7$ | 78 | 8.2390×10^{-2} | 1.1845×10^{-1} | – |
| $K = 8$ | 97 | 3.0902×10^{-2} | 7.4531×10^{-2} | – |
| $K = 9$ | 118 | 6.4925×10^{-3} | 3.0987×10^{-2} | – |
| $K = 10$ | 141 | 1.7612×10^{-3} | 8.7009×10^{-3} | 1.2311×10^{-2} |
| $K = 11$ | 166 | 1.2254×10^{-3} | 2.5698×10^{-2} | – |
| $K = 12$ | 193 | 8.4389×10^{-4} | 1.4761×10^{-2} | – |
| $K = 13$ | 222 | 8.1113×10^{-4} | 4.1230×10^{-2} | – |

4 Simulation Results

Because the process has two outputs, two Elman networks are used. Because ranges of input and output variables are different, the signals are scaled: $u_1 = (q_1 - q_{1_0})/15$, $u_2 = (q_3 - q_{3_0})/15$, $y_1 = (h - h_0)/35$ and $y_2 = (pH - pH_0)/4$.

At first the network with different number of hidden nodes are evaluated. As far as the first output of the process is considered (the first network), Elman structures with $K = 1, \dots, 7$ nodes are compared, as far as the second output is considered (the second network), the structures with $K = 7, \dots, 13$ nodes are compared. For each of the structures 10 independent experiments are performed (the weights are initialised randomly). Table 2 presents for each structure of the Elman network errors obtained for training, validation and test data sets, the best models are chosen.

For the output h the structure of the recurrent Elman neural network with 4 hidden neurons is chosen, and for the output pH the structure with 10 hidden neurons is chosen. Those networks provides good quality modelling and good generalisation.

Fig. 4 and fig. 5 show a comparison of operation of the MPC-NO algorithm with nonlinear optimisation and the MPC-NPLT algorithm with on-line linearisation around the trajectory and with quadratic optimisation for two types of set-point (reference) trajectory. The great advantage of the MPC-NPLT algorithm is the fact that the obtained trajectories are very similar to those obtained in the MPC-NO scheme.

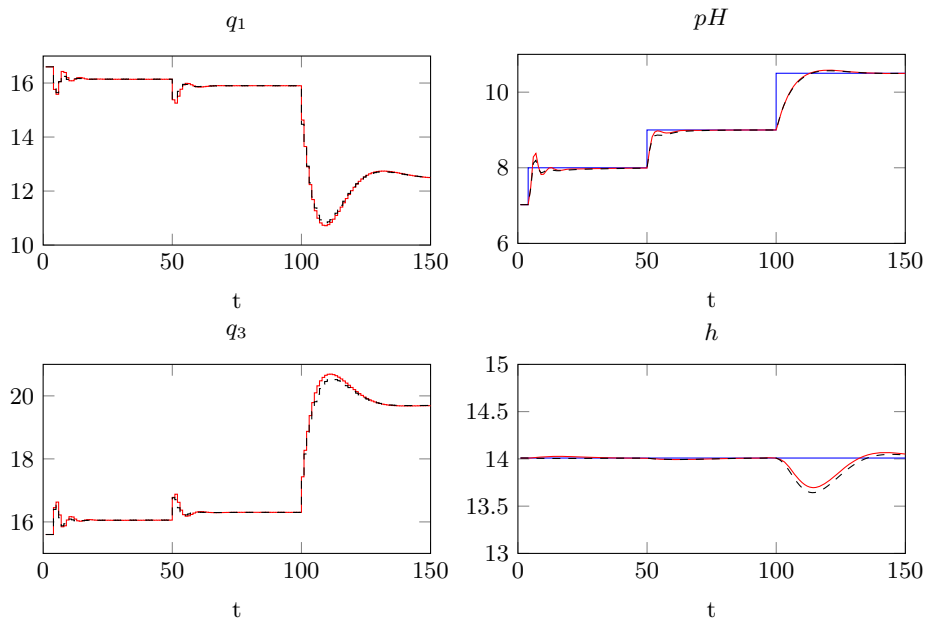


Fig. 4. Simulation results: MPC-NO (dashed line) and MPC-NPLT (solid line) algorithms

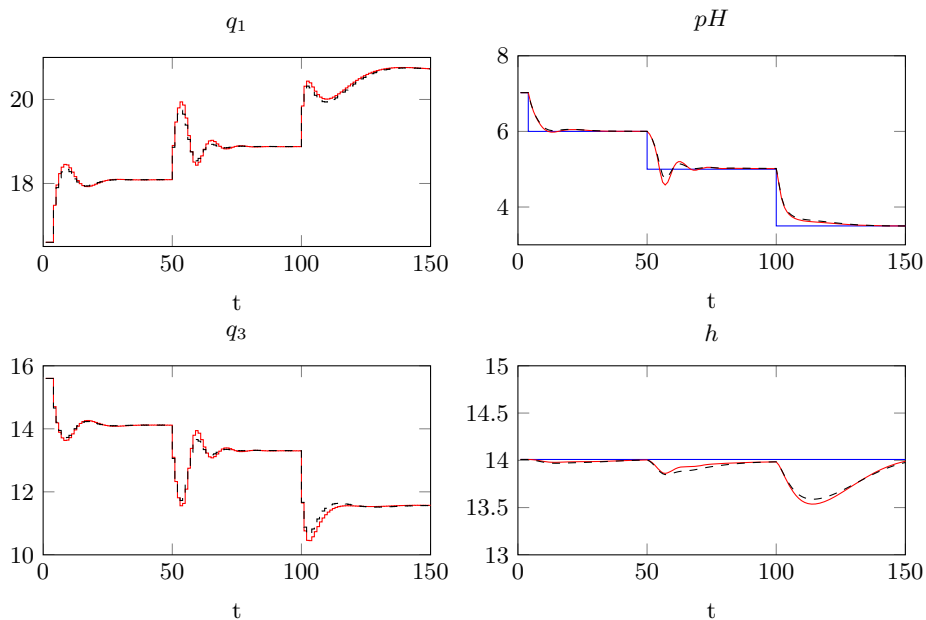


Fig. 5. Simulation results: MPC-NO (dashed line) and MPC-NPLT (solid line) algorithms

5 Summary

This paper describes predictive control of the multivariable neutralisation process. The recurrent Elman neural network is used as the model of the reactor. For predictive control the future output trajectory is linearised on-line, which makes it possible to use computationally simple quadratic optimisation. It is demonstrated that the algorithm gives control accuracy comparable with that possible in MPC with on-line nonlinear optimisation.

References

1. Camacho, E.F., Bordons, C.: *Model Predictive Control*. Springer, London (1999)
2. Elman, J.L.: Finding Structure in Time. *Cognitive Science* 14 (1990)
3. Gómez, J.C., Jutan, A., Baeyens, E.: Wiener model identification and predictive control of a pH neutralisation process. *IEE Proc.-Control Theory Appl.* 151(3) (2004)
4. Haykin, S.: *Neural networks—a comprehensive foundation*. Prentice Hall, Upper Saddle River (2008)
5. Li, P.: Application of a hybrid quantized Elman neural network in short-term load forecasting. *International Journal of Electrical Power and Energy Systems* 55 (2014)
6. Li, Q.: Prediction of urban rail transit sectional passenger flow based on Elman neural network. *Applied Mechanics and Materials* 505-506 (2014)
7. Liou, J.-W.: Distributed representation of word by using Elman network. *International Journal of Intelligent Information and Database Systems* 7(4) (2013)
8. Lawryńczuk, M.: *Computationally Efficient Model Predictive Control Algorithms: A Neural Network Approach*. SSSC, vol. 3. Springer, Heidelberg (2014)
9. Lawryńczuk, M., Marusak, P., Tatjewski, P.: Economic efficacy of multilayer constrained predictive control structures: an application to a MIMO neutralisation reactor. In: *Proceedings of the 11th IFAC/IFORS/IMACS/IFIP Symposium on Large Scale Systems: Theory and Applications*, Gdańsk, Poland, CD-ROM, paper no. 93 (2007)
10. Maciejowski, J.M.: *Predictive control with constraints*. Prentice Hall, Harlow (2002)
11. Mandic, D.: *Recurrent neural networks for prediction*. John Wiley & Sons, Chichester (2001)
12. Pławiak, P., Tadeusiewicz, R.: Approximation of phenol concentration using novel hybrid computational intelligence methods. *International Journal of Applied Mathematics and Computer Science* 24, 165–181 (2014)
13. Qin, S.J., Badgwell, T.A.: A survey of industrial model predictive control technology. *Control Eng. Pract.* 11, 733–764 (2003)
14. Tatjewski, P.: *Advanced control of industrial processes, Structures and algorithms*. Springer, London (2007)
15. Zhou, C., Ding, L.Y., He, R.: PSO-based Elman neural network model for predictive control of air chamber pressure in slurry shield tunneling under Yangtze River. *Automation in Construction* 36 (2013)

Evaluation of Automatic Identification Systems According to ISO 50001: 2011

Pawel Zajac

Wroclaw University of Technology, Faculty of Mechanical Engineering
pawel.zajac@pwr.edu.pl

Abstract. The basic techniques of automatic identification (auto-id) in logistics systems are presented in brief. Auto-id technologies are described with attention given to the existing criteria of their evaluation. A new approach to auto-id system evaluation is proposed. It consists in taking into account the interaction of the automatic identification subsystem with logistics system functional components. Also system energy consumption is taken account in accordance with [2] since this paper continues the series of papers [6–8]. A case illustrating the use of the new method of evaluating auto-id systems is presented. Conclusions are drawn and the direction of further research in this field is indicated.

Keywords: logistics warehousing system, energy consumption, automatic identification.

1 Introduction

Automatic identification systems (auto-id systems) constitute a subsystem of logistics systems. According to [1], a logistics system is defined as the efficient transfer of cargoes (or persons), accompanied by the flow of information. A peculiar characteristic of the logistics system is that at any process time t it can be defined by an ordered pair of numbers representing the state of a cargo unit and information about it. Therefore a properly functioning system of transmitting information about goods being transferred in a logistical chain, characterized by short times, reliability, faultlessness and automation, is vital. Information is conveyed through tags readable and understandable by automatic systems. The information is used to identify a commodity, a document and a person (biometric identification). The information read from a tag can be full, i.e. not requiring verification in a database, but in practice information from a barcode needs to be processed by a computer system and then further processed within the database at the particular workstations. This is referred to as the interaction of the auto-id system with the database system. For the purposes of paper-free information interchange in the whole logistics system the auto-id system exports data to electronic data interchange (EDI) systems, i.e. the information from tags is put into electronic documents covering administration, trade and transport [3], and vice versa. When the application of logistics is extended to areas where the human being is the system subject (mass or cultural events, hotel or tourist services, hospitals, education),

the identification of persons becomes necessary. This special identification (verification) is based on the analysis of human biometric or anthropometric characteristics. Auto-id systems create conditions for, among other things, the automatic sorting of goods during their quick transfer. Auto-id systems are increasingly commonly used owing to:

- increasing personnel costs,
- decreasing costs of information processing in computer systems,
- the growing production rate and difficulties in keeping information transfer through conventional channels up with it,
- the increasingly widespread use of electronic data interchange and common databases, contributing to collaboration between clients and suppliers,
- a reduction in errors caused by the human factor,
- information can be obtained in real time, i.e. at the same moment at which the event (process) occurs.

The main determinants of the auto-id system, having a bearing on system operating costs, are information transfer time and faultlessness.

Research carried out by the US Defence Department [5] shows that about 10 000 and 3000 errors occurred per 3 million characters entered using respectively the keyboard and the OCR technique, whereas only one wrong reading occurred when reading barcodes in the Code 39 symbology. This results have been corroborated by other independent American studies, which show that only 4 errors occurred per 13 million barcode code 39 readings. This confirms the enormous efficiency of automatic identification systems. The speed of entering data from the keyboard is 300–400 characters per minute, while the speed of automatic reading is measured in KB per second. Tests of transponders have been carried out in the Wrocław University of Technology Lab and their results are reported in [6, 11].

From the information carrier point of view the following auto-id technologies can be distinguished:

- **Barcodes.** Over 400 different varieties of barcodes are distinguished today, some of them have already fallen into disuse while other are gaining recognition and are increasingly often used. As regards their structure, barcodes are divided in four groups: linear (1D), stacked, composite and matrix. Moreover, a new group of “special” (single- and two-state) barcodes, i.e. farmacodes and postal barcodes, is forming. All of them are graphic characters applied to the substrate using printing, engraving and etching techniques. Information coding through barcodes consists in contrastingly printing code symbology and then reading it by an optical system. Optical signals reflected from the background with the symbology are analyzed by a photo-electronic system which decodes the information.
- **Transponders** (tags, RFID tags, electronic product codes (EPC)). These are devices interchanging information over a distance through radio waves. As regards their structure and properties, they are divided into active and passive transponders, depending on how they are powered. Passive transponders are powered through radio waves and the receiving system. Active transponders are powered from a

battery or from the mains through a power supply unit. Today passive transponders have a range from a few centimetres to 13 meters. The range of active transponders reaches several hundred meters. Transponders assume the form of: discs, labels, ID badges, capsules, belts, clip-ons, rings, etc.

- **Perforated cards and tapes.** Information was recorded on them in the form of round, square or rectangular holes. A hole represented an on-bit while no hole meant an off-bit. The ASCII code (among other codes) was used to record a character (a digit, a letter or other graphic character).
- **Magnetic tapes, cards, bands** and other magnetic carriers contained information coded in the magnetic coating, read by readers with magnetic heads.
- **Electronic contact cards.** Information is stored in a magnetic memory with high information concentration and read by a microprocessor. The information can be processed and encrypted.
- **Human biometric or anthropometric characteristics** are identified by determining characteristic points and an algorithm of measuring biometric or anthropometric characteristics, and comparing the latter with a reference, such as a fingerprint, and image of the face, the hands, the iris or the retina. Also human gait and signature dynamics are currently being tested.
- **The electronic signature** is one of the latest technologies emulating one of the oldest methods of identifying the author of a given text. In Poland it has been implemented pursuant to the Electronic Signature Act of 2002 [4, 5].
- **Other systems,** occurring in many niche applications in the economy, e.g. a machine vision system for object size and machining tool recognition, etc.

Currently the following criteria are used to evaluate auto-id system: the type of information, the structure of the information, the space available for marking on the object wall, the environmental hazards (temperature, dust, moisture, solar radiation, wear, etc.) to the information carrier, reading speed, the possibility of information multiplication, ergonomics (easy information reading not necessitating any manipulations by the servicing personnel), the cost of implementing a selected system with accessories, system operating costs, system reliability, the reading method and reading system flexibility.

These are both determinate and indeterminate factors. In order to select the proper system one can use one of the commonly known methods, e.g. the point method, but one should be aware that it is based on the experience of experts who determine the weights of the parameters.

Table 1. Comparison of area taken up by barcodes [own study]

| | 6-digit code | 10-digit code | 18-digit code |
|------------|--------------|---------------|---------------|
| Code 2/5 | 9 | 7 | 6 |
| Code 28 | 9 | 6 | 6 |
| Code 39 | 14 | 12 | 10 |
| DataMatrix | 1 | 1 | 1 |

An analysis of the practices used in the industry and in the firms supplying it with software and auto-id equipment shows that the users evaluate the latter using an index of reliability understood as error-free reading. In the case of barcodes there is an element of self-checking consisting in comparing the result read from the carrier with the value calculated according to a specified algorithm (modulo). In this way the system is protected against entering false information. The causes of errors include: poor quality of barcode printing, dirt, non-conformance with scale requirements, etc. In the case of RFID tags, an incorrect readout can be caused by environmental interference, substrate interactions and the interactions of other tags. Therefore protocols of collision-free data transmission by radio are used. They make possible the simultaneous reading of from a few to tens of tags.

In this case, the reliability of an auto-id system is expressed by a ratio of incorrect readouts to all the readouts performed by the system. In the case of biometric systems of automatic identification, the evaluation measures are the false acceptance rate (FAR) and the false reject rate (FRR) [11].

The subject of comparisons are the dimensions of a biometric characteristic. Because of the different measurement conditions, the measurements have a probabilistic character. For this reason the investigated characteristic is verified for a set tolerance. If the tolerance is narrow the FRR of the system will be high while its FAR will be low. If the tolerance is wide, the FRR will be low while the FAR will be high. In both cases, undesirable effects occur. If as the measure of system quality one assumes the total system errors (FAR + FRR), the minimum of this function will be in point “c” (Fig. 10) and the condition $FRR = FAR$ will be satisfied.

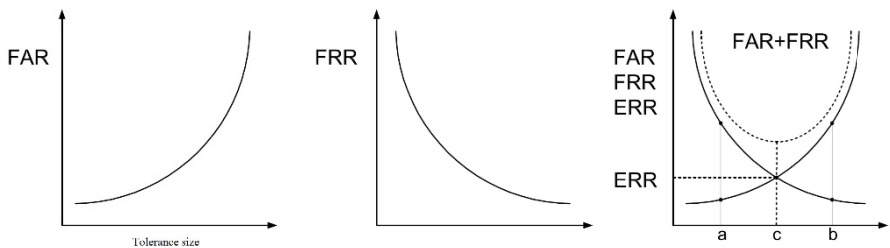


Fig. 1. Effect of measured quantity tolerance size on FAR and FRR [4]

The causes of errors can be disturbances [8]:

- in reading, caused by the human factor,
- caused by external factors,
- caused by internal errors of the reading and processing system,
- caused by a defect in the reading method or in the identification of significant code characteristics,
- caused by a deliberate human action,
- caused by the improper sensitivity of the identification system.

2 Assessment of Auto-id System Energy Consumption

In the design and operation of logistics systems one comes across such topics as zero-energy facilities, energy recovery and system energy consumption. Auto-id systems include sets of devices for reading tags, e.g. (radio) barcodes, printing (in the case of RFID recording), applying codes and creating codes directly on the wall of the tagged object, and computers with proper database software and optionally, a computer system aiding logistics system management, such as WMS, MPR, etc.

It has been observed that because of the economic crisis and savings sought by companies the time between reporting a defect of an auto-id system and restoring its full functionality is a major consideration in the selection of an auto-id system. A faulty auto-id system servicing cargo units, cash registers, etc. causes a halt of the acceptance/release/groupage/sale processes.

Hence the questions arise: when one should purchase a new reader and when a second-hand one?, and is operating intensity a consideration (a scanner used more intensively is more exposed to damage)? The costs of new readers and second-hand readers are much different. They also depend on the type of reader, considering that an industrial device works in harder conditions. In the case of a reader intended for continuous operation, its resistance to accidental dropping and impact and its maximum reading range are important.

An analysis of the situation in enterprises will show approximately how many and what readers are needed for a small storehouse of 100–150 m² in size and how many for a warehouse of up to 400 m² in size. Their cost can range from about 1000 Euros to 1500 Euros. For facilities of about 400 m² in size, the equipment cost will amount to about 7000 Euros.

It appears from the above that the persons selecting an auto-id system do not pay attention to its energy consumption. Most probably the purchaser thinks that a few scanners, a barcode printer and a PC consume very little energy. Calculations made for real facilities indicate that the energy consumption of an auto-id system for a 400 m² warehouse amounts to about 830 KW/year for three-shift operation, i.e. it is small in comparison with the energy consumption of, e.g., the lighting of the facility.

However, as demonstrated in [7] for a “manual” system versus a terminal with an electronic data interchange the difference in the costs of purchasing and operating the auto-id system amounts to 30%, whereas the annual energy consumption of the systems differs by 150%. Therefore when selecting an auto-id system one should consider not only its cost, but also the energy consumption of the whole logistics system. In such cases ISO 50001:2011 should be taken into account.

2.1 ISO 50001:2011 Can Serve as Evaluating Tool

Standard PN-EN 50001: 2011 deals with energy management systems. It was developed mainly to protect the environment through rational energy management. The Standard helps firms to improve their energy efficiency. By defining energy utilization indices and energy consumption indices it enables them to determine the energy utilization level which will guarantee the proper energy result. By implementing the

Standard an organization contributes to an improvement in the energy policy in the whole sector and to a reduction in the emission of greenhouse gases. The main purpose of the Standard is to support organizations in the generation of processes and systems needed to improve the energy results. It is based on the well-known continuous improvement principle: Plan-Do-Check-Action.

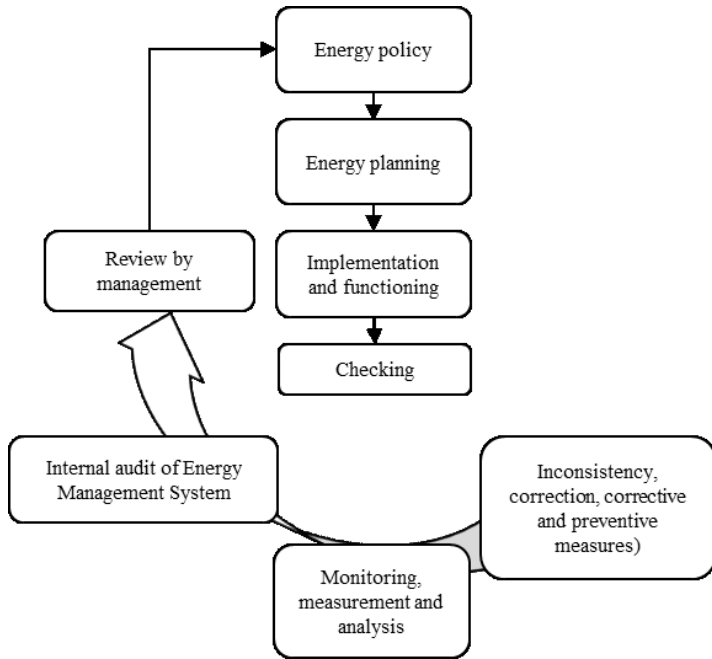


Fig. 2. Procedure for evaluating system on basis of [2]

Plan means prepare goals, tasks and actions to maximally improve the energy result, do – implement the plan, check – supervise the particular processes and produce a report, and action – take concrete steps to improve the energy result. The Standard says that action plans must include above all measures through which the set goals will be reached. Also a method of verifying the energy result should be specified. In the first step for a system which has it peculiar requirements one must define its boundaries (the immediate and further environment), which must be defined for each process and operation through their short description including the characteristic parameters. In the second step one should establish, introduce, maintain and improve an energy management system. All these actions are necessary. Finally, an organization must describe in what way it will satisfy the Standard requirements in order for the energy result to be increasingly better. The auto-id system processes for any logistics system can be presented as in Fig. 3. The latter can be even treated as an algorithm for the preliminary selection of an auto-id system for any case [7].

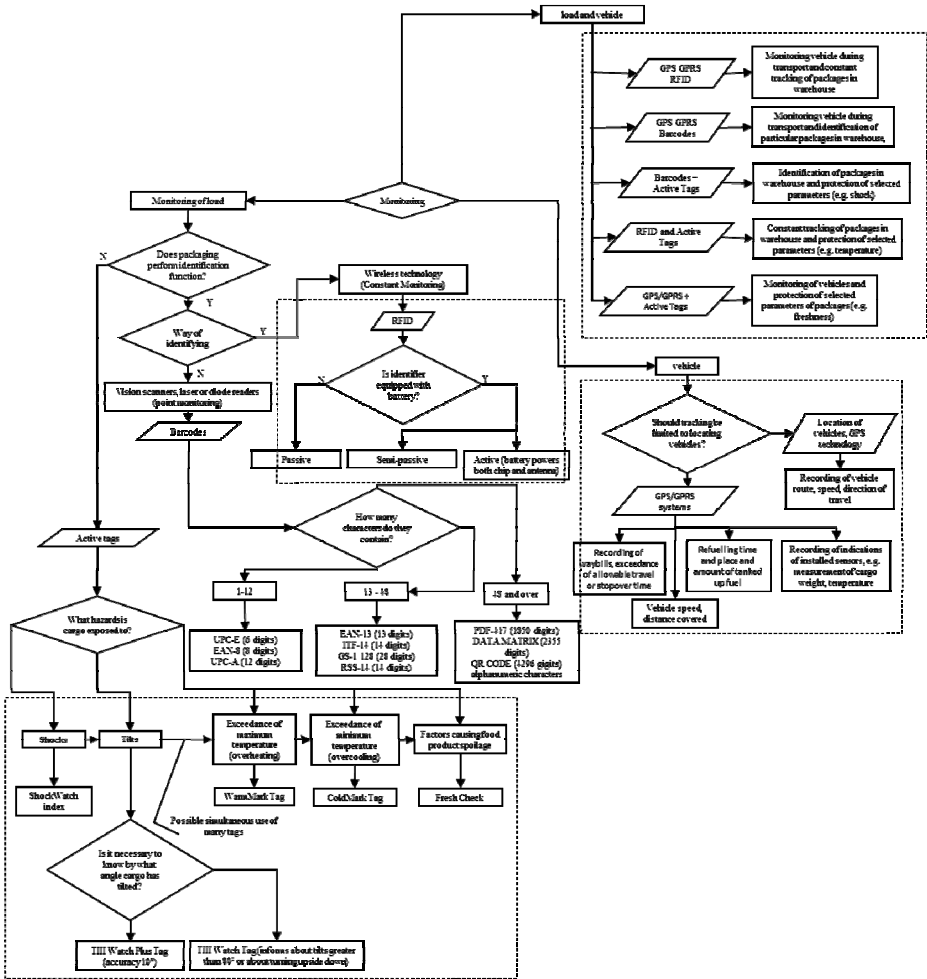


Fig. 3. Algorithm for preliminary check of auto-id system choice (own study)

2.2 Determination of Energy Consumption

Energy consumption of auto-id systems in logistics systems to a large extent depends on the utilitarian value of the information, which is affected by several factors differing in their character, whereby attempts to present them in the scalar form are not practicable. Therefore an attempt was undertaken at the vector description of the utilitarian value of information, assuming its key characteristics to be: up-to-dateness, relevancy, completeness, assimilability and reliability. The characteristics were assigned numerical measures in such a way that for statistically independent pieces of information the utilitarian value of information satisfies the additivity condition in a five-dimensional vector space. The particular characteristics are defined as follows.

The up-to-dateness of information is described by a monotonically non-increasing function of delay with which the information reaches the decision-maker. Delay t_x is counted from the instant at which the event described by this information occurred and it is referred to standard (permissible) value t_0 . The measure of information up-to-dateness is up-to-dateness coefficient k_a expressed by the following formula

$$k_a = 1 - t_x/t_0, t_0 > 0 \quad (1)$$

The relevancy of information expresses its conformity with the user's need. It is defined by a ratio of information units describing information essential for the decision-maker (I_r) to total number of information units I_c (e.g. bits).

$$k_r = I_r/I_c \quad (2)$$

The completeness of information is a ratio of relevant information I_r received by the decision-maker to the amount of relevant information I_c which ideally he/she would obtain fully utilizing the information capacity of the supervised object.

$$k_k = I_r/I_c \quad (3)$$

The assimilability of information is a characteristic expressing its suitability for the direct use by the decision-maker. It is the higher, the lower the anticipated expenditures (costs, time, etc.) necessary to process the received information to a desirable form. If the incurred expenditure amounts to N_x and the standard (allowable) expenditure is N_0 , the assimilability coefficient will amount to

$$k_p = 1 - N_x/N_0, N_0 > 0 \quad (4)$$

The reliability of information is a characteristic expressing its agreement with the object state described by it. It is described by a monotonically non-increasing function of the error with which the function reflects the actual object state. If the information error amounts to δ_x and its allowable value is δ_0 , the information reliability coefficient is described by the formula

$$k_w = 1 - \delta_x/\delta_0, \delta_0 > 0 \quad (5)$$

This means that a negative value of the reliability coefficient indicates information unreliability. Thus the utilitarian value of information can be described by the vector

$$V = [k_a, k_r, k_k, k_p, k_w] \quad (6)$$

Since all the components of this vector are dimensionless quantities it is possible to semi-order the vector space by means of multicriterial optimization, assuming the method of subordinating the defined vector with weight coefficients

$$c = [c_a, c_r, c_k, c_p, c_w] \quad (7)$$

where the vector components express the weight assigned to the particular characteristics of information and satisfy the condition:

$$c_a + c_r + c_k + c_p + c_w = 1 \tag{8}$$

where each of the weights is contained in closed interval $<0, 1>$.

Under such assumptions it is possible to compare the utilitarian values of the particular pieces of information with regard to energy consumption

$$V' > V'' \text{ then and only then when } (c, V') > (c, V'') \tag{9}$$

where (c, V) is a scalar product of the vectors

$$(c, V) = c_a V_a + c_r V_r + c_k V_k + c_p V_p + c_w V_w \tag{10}$$

The above criterion provides the rational basis for the selection of the best auto-id system with logistics system energy consumption taken into account.

3 Example of Method Application

Models of the press distribution processes in a certain firm are presented below [10]. The original press distribution (Fig. 4) consisted of: press distribution for dispatching, advice note acceptance, returns procedure acceptance, the acceptance of newspaper packages into a storage facility, drawing up a delivery specification and plan, specification printing, the physical distribution of the newspapers, the delivery of the press and the collection of returns, entering data from plans of returns, invoicing, printing of invoices, sending invoices, receiving payment, filling in return documents for the press distribution storage facility, sending documents to the distribution storage facility, end. The model was corrected by removing processes 5, 8 and 10 as a result of auto-id system reorganization through the introduction of changes in the form barcodes solely into the auto-id system, consisting in the direct interchange of information between the distributor and the particular retail outlets and enabling electronic interchange of data about the demand for the press, the circulation and daily returns, corrections of delivery specifications and invoices. Both models have one common subprocess, i.e. delivery check A.

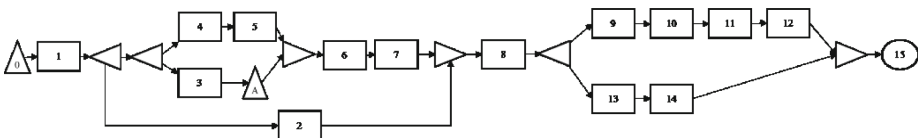


Fig. 4. Press distribution model for dispatching needs (own study)

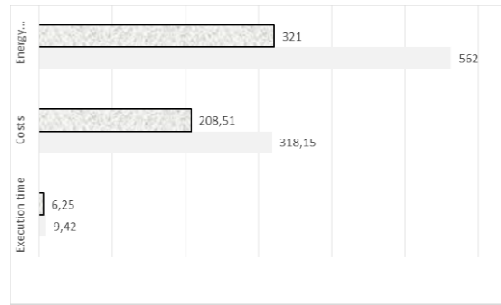


Fig. 5. Comparative results for models before and after auto-id system revitalization

4 Conclusion

The presented algorithm was used to evaluate existing logistics systems. The preliminary results of the evaluation of existing auto-id systems show that the latter met the expectations of their buyers (Fig. 5), providing higher performance (see Sect. 2) while reducing the energy needed to operate the logistics system. It would be interesting to check the model for other facilities performing a similar function. Such parameters as energy consumption and costs can be analyzed in terms of time windows (sometimes important from the customer service point of view). Moreover, using the presented diagrams one can approximately determine the CO₂ emission resulting from the use of the auto-id system. The reduction in the logistics system energy consumption deserves attention. In the considered case, the revitalization of the auto-id system resulted in a cost reduction, but this is not always the case. Attention should be paid to this aspect.

This paper continues the series of papers [6–8], focusing on auto-id systems in the design and operation of logistics systems [2]. In the author's opinion, in the next step one should take into account short- and long-term environmental effects [2].

The proposed concept is a comprehensive one, making it possible to analyze, eliminate and select auto-id system solutions before introducing changes in the logistics system.

References

1. Gudehus, T.: "Logistik 1" Grundlagen, Verfahren, und Strategien. Springer, Berlin (2006)
2. ISO 50001:2011
3. ISO 9735
4. Jamroziak, K., Bocian, M., Kulisiewicz, M.: Energy consumption in mechanical systems using a certain nonlinear degenerate model. *Journal of Theoretical and Applied Mechanics* 51(4), 827–835 (2013)
5. Kwasniowski, T., Zajac, P. (eds.): Automatic identification in logistics systems. Wroclaw University of Technology Publishing House, Wroclaw (2004) (in Polish)
6. Kwasniowski, S., Zajac, P.: Tracing and tracking using RFID tags in logistic systems of transport and storage. *Archives of Transport System Telematics* 6(4) (November 2013)

7. Kierzkowski, A., Zajac, M.: Analysis of the reliability discrepancy in container transshipment. In: 11th International Probabilistic Safety Assessment and Management Conference and the Annual European Safety and Reliability Conference 2012, PSAM11 ESREL 2012, vol. 1, pp. 826–831 (2012)
8. Bujak, A., Zajac, P.: Monitoring of cargo in logistic systems of transport and storage. In: Mikulski, J. (ed.) TST 2013. CCIS, vol. 395, pp. 361–369. Springer, Heidelberg (2013)
9. Bujak, A., Zajac, P.: Can the increasing of energy consumption of information interchange be a factor that reduces the total energy consumption of a logistic warehouse system? In: Mikulski, J. (ed.) TST 2012. CCIS, vol. 329, pp. 199–210. Springer, Heidelberg (2012)
10. Rusiński, E., Moczko, P., Pietrusiak, D., Przybyłek, G.: Experimental and numerical investigations of the jaw crusher supporting structure fatigue failure. *Strojnicki Vestnik - Journal of Mechanical Engineering* 59(9), 556–563 (2013), doi:10.5545/sv-jme.2012.940
11. Zajac, M., Kierzkowski, A.: Uncertainty assessment in semi Markov methods for Weibull functions distributions. In: *Advances in Safety, Reliability and Risk Management – Proceedings of the European Safety and Reliability Conference, ESREL 2011*, pp. 1161–1166 (2012)

Author Index

- Banaszak, Zbigniew 11
Bocewicz, Grzegorz 11
Busłowicz, Mikołaj 1
Bzdyra, Krzysztof 11
- Chaber, Patryk 23
Chechliński, Łukasz 53
- Domański, Paweł D. 33
- Fularz, Michał 43
- Harasymowicz-Boggio, Bogdan 53
Hryniów, Krzysztof 63, 73
- Jakubowski, Arkadiusz 85
Jamro, Marcin 91
Jędryczka, Cezary 137
- Kaczorek, Tadeusz 101
Karbowski, Andrzej 113
Kasiński, Andrzej 43
Kraft, Marek 43
Krajčovič, Martin 187
Kubacki, Arkadiusz 85
- Ławryńczuk, Maciej 23, 335
- Makarewicz, Adam 1
Markowski, Konrad Andrzej 63, 73
Milecki, Andrzej 127
Minorowicz, Bartosz 85, 137, 147, 169,
207, 275, 283
Mrozek, Bogumiła 157
- Nowak, Amadeusz 85, 137, 169, 207, 283
- Oprzedkiewicz, Krzysztof 177
Owczarek, Piotr 215
Owczarkowski, Adam 215
- Pandilov, Zoran 169
Pittner, Grzegorz 147
Plinta, Dariusz 187
Poczęta, Katarzyna 197
- Regulski, Roman 147, 207, 275
Ruszewski, Andrzej 1
Rybarczyk, Dominik 215
Ryszawa, Piotr 323
Rzońca, Dariusz 223
- Sadolewski, Jan 223
Sajewski, Łukasz 233
Schmidt, Adam 43
Sędziak, Dariusz 215, 275
Siemiątkowska, Barbara 53
Sitek, Paweł 243
Smater, Michał 255
Stec, Andrzej 265, 303
Stefański, Frederik 137, 147, 169, 207,
275, 283
Świder, Zbigniew 303
Szewczyk, Roman 293
- Trybus, Bartosz 223
Trybus, Leszek 303

Więclawski, Marcin 33
Wikarek, Jarosław 313
Wrzesień, Marian 323
Wysocki, Antoni 335

Yastrebov, Alexander 197
Zajac, Pawel 345
Zieliński, Jacek 255